An *in vitro* iPSC-corneal epithelial cell model for the study of TGFBI corneal dystrophies and development of an antisense oligonucleotide treatment

Farah Olivia Rezek

Supervised by Prof. Alison Hardcastle and Dr Alice Davidson

Thesis submitted for the degree of Doctor of Philosophy

June 2023

UCL Institute of Ophthalmology
Faculty of Brain Sciences
University College London

Declaration

I, Farah Olivia Rezek, confirm that the work presented in this thesis is my own. Where information has been derived from other sources, I confirm that this has been indicated in the thesis.

_____

Acknowledgements

Firstly, I would like to thank my PhD supervisor Alison Hardcastle, for giving me the opportunity to do this PhD, enabling me to learn, develop skills and giving me the freedom to be creative. I am so grateful for your support and guidance over the past few years. Thank you for welcoming me into the amazing lab and work environment that you have nurtured.

Thank you to my secondary supervisor, Alice Davidson, for your enthusiasm and drive. Thank you to Stephen Tuft, for collaborating with us and making this work possible, and for your efforts in bringing science and the clinic together. Thank you to Mike Cheetham, for your advice, perspectives and high standards that help further our work. You and Alison have built such a warm and lovely team that I am grateful to be a part of. Thank you to Jacqui van der Spuy, for your support and guidance during our time working together. Thank you to our lab manager Naheed Kanuga, the super glue that holds this lab together, even when things feel disastrous and chaotic you are there to support us and provide the best outcome that you can. We appreciate you so much!

Thank you to the whole MCN team, past and present members that have helped me and taught me. Amanda, you kept me sane through the difficult times and I am so happy to have met you and shared this journey with you. To my friends Rowan and Hannah, I'm so lucky to have worked with you both. To my USA (Mississippi) team, Davide, Rosellina and Christina, thank you for the lifelong memories and amazing experiences we shared, plus all the support and laughter you have given me over the years. To Bea, thank you for setting up this project and for being the confident and great scientist you are. Thank you to the other current and past members of the lab, with who I have shared many great conversations and moments, Amy, Erika, Anita, Julio, Nihar, Kwan, Nathan, Hali, Michael, Josh, Kelly, Jim and NZ as well as my current office buddies, Jess, Owen, Di and Freddie.

Thank you to Moorfields Eye Charity for funding this project, I am very grateful to have had this opportunity. Thank you to the TGFBI corneal dystrophy patients who agreed to take part in this study, I really hope this work can contribute to the development of an effective treatment.

To my mother, you are my biggest inspiration and I cannot express the gratitude and admiration I have for you. Thank you for the countless sacrifices you have made for us and for being the most incredible mother I could ask for; I am so lucky and proud that you are my mum. Thank you to my dad for your support and for teaching me the

importance of education, I love you. Thank you to my little sister, I love you. Thank you to my Teta Nadera and Jido Ahmad, I love you and miss you so much, I hope you are happy to know I submitted! Thank you to my best cousin Charlotte, you have always believed in me. Thank you to my Teta Watfe and the rest of my family for your support, I love you so much.

To my best friend, Jordan, I miss you so much. Your vehement belief in me still keeps me going on the hard days. I wish I could talk to you even just about a fraction of the past few years. Thank you for being such a light in my life, you are still with me every day and you have influenced me more than you could ever know.

To the lovely Bickita and Jaleela, I am so lucky to have such inspirational and strong women as my friends. I also have to express gratitude to my cats Blueb and Shroom for brightening up my day, every day.

To Wahaaj, thank you for always being there, supporting me and telling me it’s going to be okay and thank you for riding out this journey with me. I am really looking forward to the next chapter we have together.

Last but not least, to my beloved homeland, Palestine, and to my Palestinian people, this thesis is dedicated to you. You are always in my heart.

Abstract

TGFBI corneal dystrophies (CDs) are autosomal dominant inherited diseases with distinctive phenotype-genotype correlations, however, the underlying mechanism of these conditions are poorly understood. TGFBI CDs are characterised by the accumulation of TGFBI positive protein deposits in the sub-epithelial, Bowman and/or stromal layers of the cornea, presenting with painful corneal erosions and visual impairment. Current surgical treatments do not target the underlying genetic cause of the disease and symptoms commonly reoccur; therefore, alternative therapeutic approaches are required. In order to facilitate the investigation of *TGFBI* CD pathogenesis and provide an appropriate platform for therapeutic screening, patient-derived *in vitro* models offer a compelling approach.

A genetic study of TGFBI CD cases at the Moorfields Eye Hospital patient cohort (n=120) demonstrated that around 1/3 of cases have mutations at the p.R124 hotspot of the *TGFBI* gene. Fibroblasts from four individuals with heterozygous p.R124C or p.R124H mutations, presenting with Lattice Corneal Dystrophy I and Granular Corneal Dystrophy II, respectively, were obtained and reprogrammed into iPSC. Wild type (WT) and a CRISPR/Cas9-edited *TGFBI* knockout iPSC cell lines were cultured in parallel. The endogenous expression of the pluripotency markers Oct4, Nanog, SSEA4 and Tra-1-81 was confirmed in all iPSC lines. All iPSC lines were differentiated to corneal epithelial-like cells and characterised for the transcript and protein expression of corneal epithelial markers such as K14, K3, P63 and PAX6 throughout key differentiation time points. Bulk RNA sequencing was carried out on day 21 of differentiation to investigate potential mechanisms of dysregulated transcription underlying disease, and provided insight into potential disease mechanisms.

Antisense oligonucleotides (ASOs) were designed to specifically reduce the expression of *TGFBI* in a mutant-specific manner by triggering RNase H-mediated degradation of the mutant transcript. ASO treatment resulted in a 20-40% decrease of total *TGFBI* transcript levels. Targeted next generation sequencing demonstrated allele specificity of the ASOs and confirmed their efficacy.

In summary, patient-derived iPSC-derived corneal epithelial-like models have been developed and characterised for the investigation of molecular mechanisms underlying TGFBI CDs and to test therapeutic approaches. ASOs targeting the p.R124 hotspot mutations effectively reduced the expression of the mutant allele of *TGFBI*, therefore, representing a promising targeted therapeutic approach for TGFBI CDs.

Impact statement

TGFBI corneal dystrophies (CDs) make up a group of autosomal dominant CDs that affect the corneal epithelium and stroma, manifesting with symptoms during the first and second decades of life. Missense mutations in the *TGFBI* gene cause the progressive accumulation of the TGFBI protein in the anterior cornea, and at least 78 different pathogenic variants have been reported. TGFBI CD patients experience corneal opacification, leading to visual impairment, often accompanied with painful corneal erosions. Currently available treatments do not target the underlying genetic cause of disease thus, symptoms reoccur.

Through the recruitment and genetic screening of TGFBI CD patients to the current study, the patient profiles presented underscore the necessity for a preventative treatment that targets the underlying genetic cause of disease. Complimentary to clinical examination, genetic screening of the patients highlights the importance of providing individuals with a correct diagnosis, appropriate disease management and family counselling. Further, common surgical procedures for the correction of ocular refractive errors are contraindicated for some forms of TGFBI CD, thus, the implementation of routine genetic screening prior to such procedures can help avoid unnecessary complications and vision deterioration. Genetic confirmation of the TGFBI CD-causative mutation also provides the basis for the development of a patient-tailored gene-directed therapeutic.

There is a lack of knowledge on the function of TGFBI in CD and non-CD contexts. This is likely due to the clear interspecies differences in *TGFBI* expression between humans and the commonly used mouse models. Previously developed mouse models of TGFBI CD do not present with comparable symptoms to those observed in humans. In order to address this limitation and complement existing TGFBI models reported in the literature, somatic cells from patients harbouring two of the most common CD-causative mutations, p.R124C and p.R124H, were obtained, enabling the generation of a patient-derived *in vitro* induced pluripotent stem cell (iPSC)-corneal epithelial cell-like model.

This model enabled CD-mutant vs wild type comparisons of transcriptomic signatures in a relevant genetic and cellular context. These comparisons not only demonstrated the utility of such models in the elucidation of potential disease-related pathways, but also provided critical insights into the study's limitations, thereby facilitating the optimisation of experimental setups. The data presented in this study raises crucial questions regarding the pathogenesis of TGFBI CDs and provides a clear direction for future

experiments aiming to understand the underlying dysfunction of TGFBI in these conditions.

Finally, the development of a gene-directed antisense oligonucleotide therapeutic, demonstrated to be effective in reducing the expression of the *TGFBI* gene in an allele-specific manner using the *in vitro* corneal epithelial cell-like model, represents an advance in the development of a practical therapeutic that holds promise for TGFBI CD patients. Currently available treatments consist of laser ablation of protein deposits located in the anterior cornea, or corneal transplantation for the treatment of deposits located deeper into the stroma. Corneal transplantation is subject to tissue availability, requires significant recovery time and can result in complications such as graft rejection. Further, recurrence of disease symptoms is commonly noted following such treatments. By specifically targeting the CD-causative genetic mutation, the ASOs developed have the potential to prevent the deterioration of vision for affected patients, enhancing their quality of life. This would also reduce the need for surgical intervention and the associated complications, easing the medical burden posed by these treatments. The implementation of ASO treatment for TGFBI CDs can facilitate the acceleration of research by paving the way for similar approaches in other genetic disorders. This advancement can contribute to broader advancements in precision medicine and personalised treatments, benefiting patients with various genetic conditions beyond TGFBI CDs.

Contents

List of figures

List of tables

List of abbreviations

2’-OMe – 2’-OMethyl

6-FAM – carboxifluorescein

ABCB5 – ATP Binding Cassette Subfamily B Member 5

ABCG2 – ATP Binding Cassette Subfamily G Member 2

ALK – Activin receptor–like kinase

ANOVA – analysis of variance

ASO – antisense oligonucleotide

BMP – bone morphogenic protein

BP – biological processes

BSA – bovine serum albumin

CC – cellular compartments

CD – corneal dystrophy

cDNA – complementary deoxyribonucleic acid

CEpi – corneal epithelial like

CKO – CRISPR knockout

CNV – copy number variation

CpG – cytosine-guanine

CRISPR – clustered, regularly interspaced short palindromic repeats

CROPT – cysteine-rich domain of periostin and TGFBIp

DAPI – 4′,6-diamidino-2-phenylindole

DALK – deep anterior lamellar keratoplasty

DEG – differentially expressed gene

DPBS – Dulbecco's phosphate-buffered saline

DSB – double strand break

E8F – essential 8 Flex media

EB – embryoid body

E-CAD – E-cadherin

ECM – extracellular matrix

ELISA – enzyme-linked immunosorbent assay

ER – endoplasmic reticulum

ERK – extracellular signal-regulated kinase

ESC – embryonic stem cell

FACIT – fibril associated collagens with interrupted triple helicies

FACS – fluorescence activated cell sorting

FBS – fetal bovine serum

FDA – food and drug administration
FAK – focal adhesion kinase
FAS1 – fasciclin 1
FDR – false discovery rate
FECD – Fuchs endothelial corneal dystrophy
GA – golgi apparatus
GAG – glycosaminoglycan
GCD – granular corneal dystrophy
GCDII – granular corneal dystrophy 2
GDF – growth and differentiation factors
gDNA – genomic deoxyribonucleic acid
GO – gene ontology
gRNA – guide ribonucleic acid
HDF – human dermal fibroblast
HDR – homology directed repair
HEK293 – human embryonic kidney 293
hPSC – human pluripotent stem cell
HTRA1 – high temperature requirement A serine peptidase 1
HTRA3 – high temperature requirement A serine peptidase 3
IC3D – international committee for classification of corneal dystrophies
ICC – immunocytochemistry
iPSC – induced pluripotent stem cell
JNK – c-Jun amino terminal kinase
K12/KRT12 – keratin 12
K14/KRT14 – keratin 14
K3/KRT3 – keratin 3
K5/KRT5 – keratin 5
KO – knockout
LCA – Leber congenital amaurosis
LASIK – laser-assisted in situ keratomileusis
LCD – lattice corneal dystrophy
LCDI – lattice corneal dystrophy 1
LFC – log2 fold change
LNC – limbal niche cell
lncRNA – long non-coding ribonucleic acid
LPC – limbal progenitor cell
LSC – limbal stem cell

LSCD – limbal stem cell deficiency
LSCN – limbal stem cell niche
MAPK - mitogen-activated protein kinase
MECD – Meesman epithelial corneal dystrophy
MEH – Moorfields Eye Hospital
MF – molecular function
miRNA – micro ribonucleic acid
MMP – matrix metalloproteinases
NGS – next generation sequencing
NHEJ – non-homologous end joining
NSCLC – non-small cell lung cancer
NT – non-treated
PAM – protospacer adjacent motif
PCA – principal component analysis
PCR – polymerase chain reaction
PG – proteoglycan
PI3K – phosphoinositide 3-kinase
PK – penetrating keratoplasty
PS – phosphorothioate
PTK – phototherapeutic keratectomy
qPCR – quantitative polymerase chain reaction
RA – retinoic acid
RAE – random monoallelic expression
RBCD - Reis Bücklers corneal dystrophy
RGD - Arg-Gly-Asp binding motif
RNA – ribonucleic acid
RNAseq – ribonucleic acid sequencing
R-SMADs – receptor-activated SMADs
RT – room temperature
RT-PCR – reverse transcription polymerase chain reaction
SCR – scrambled
scRNAseq – single cell ribonucleic acid sequencing
siRNA – small interfering RNA
SNP – single nucleotide polymorphism
SSO – splice switching oligonucleotide
TAC – transit amplifying cell
TBCD – Thiel-Behnke corneal dystrophy

TGFBI – transforming growth factor-beta induced

TGFBIp – transforming growth factor-beta induced protein

TGFβ – transforming growth factor-beta

TIMP – tissue inhibitor of metalloproteinase

TKR - tyrosine kinase receptor

UMAP – Uniform Manifold Approximation and Projection

UMI – unique molecular identifier

UPR – unfolded protein response

UTR – untranslated region

UV – ultraviolet

WT – wild type

Chapter 1: Introduction

1.1 The human cornea

The cornea, classically described as the window of the eye, is the transparent avascular tissue positioned at the outermost ocular surface. It is a vital component of the visual system, providing 2/3rd of the refractive power of the eye, whilst also functioning as a structural barrier and providing protection against the environment and infection (DelMonte & Kim, 2011). The cornea, sitting in front of the iris and pupil, is located in the anterior segment of the eye (Figure 1.1A). The anterior portion of the cornea, the corneal epithelium, is connected to the conjunctiva which lines the sclera and the inner surface of the eyelids. The posterior portion of the cornea is continuous with the sclera. The border of the cornea, where it meets the conjunctiva and sclera, is called the limbus.

Maintaining the clarity of the cornea is dependent on the precise balance of cellular components and extracellular matrix factors that altogether, enable light to travel through the eye to stimulate the photoreceptor cells of the retina. As the cornea is avascular, it absorbs oxygen and nutrients through direct contact with the tear film and aqueous humour. It is one of the most densely innervated tissues in the human body (Marfurt et al., 2010). The abundance of sensory neurons in the cornea work to protect the eye by eliciting a palpebral reflex which shuts the eyelids in response to various thermal, mechanical, and chemical stimuli. Corneal nerves also work to release trophic substances essential for maintaining the integrity of the corneal epithelium and wound healing, such as, neuropeptides, neurotrophins, and growth factors (T. Nishida, 2005).

The human cornea is made up of 5 distinct layers, comprised of 3 cellular layers: the epithelium, stroma and endothelium; and 2 acellular layers: Bowman's layer and Descemet membrane (Figure 1.1B). The cornea can also be divided into a central portion and a peripheral portion.

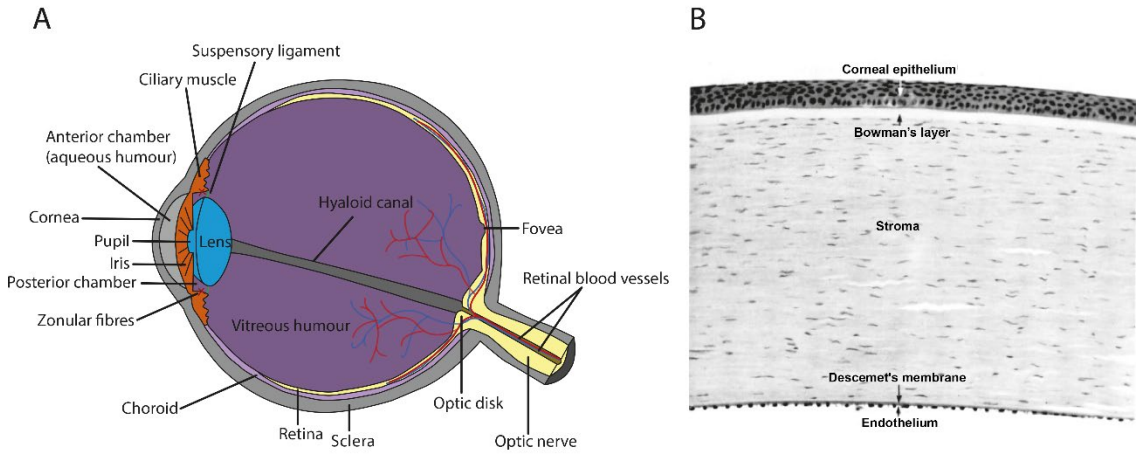

Figure 1.1 Anatomy of the eye and the cornea. A) The eye is divided into a posterior segment which includes the retina, sclera, choroid, fovea and optic nerve; and an anterior segment which includes the cornea, pupil and iris. **B)** A histological section of a healthy human adult cornea displaying its five layers. The epithelium, Bowman's layer, stroma and its sparse keratocytes, Descemet membrane and the single layer of endothelium are shown (adapted from Hogan & Zimmerman pg. 278, 1953).

1.1.1 Corneal epithelium

The epithelium is the anterior-most layer of the cornea, leaving it directly exposed to the pathogens and irritants of the external environment, as well as desiccation. It is a lipoidal tissue consisting of 5-6 cellular layers of nonkeratinized stratified squamous epithelia, which are bathed in tear film produced by conjunctival goblet cells. The epithelium represents slightly less than 10% of the cornea's total thickness and is comprised of three types of epithelial cells: basal, suprabasal and superficial cells (Figure 1.2). The corneal epithelium undergoes a continuous process of cell renewal, superficial epithelial cells eventually desquamate and are shed, being replaced by younger terminally differentiated cells.

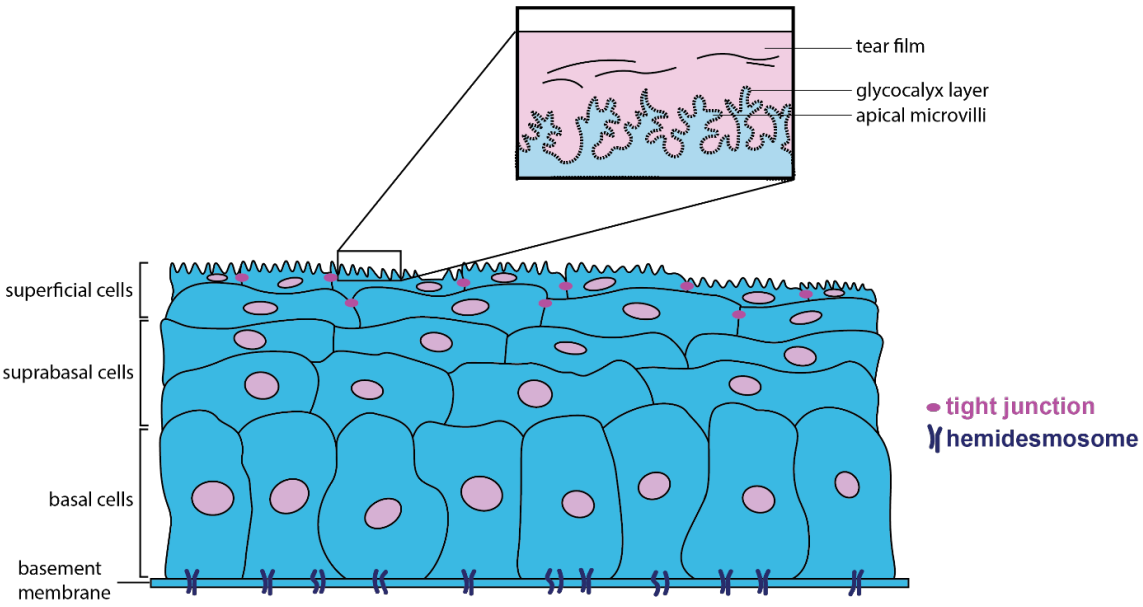

Figure 1.2 Illustration of the corneal epithelium and components of the human ocular surface epithelium. The superficial cells of the corneal epithelium are arranged in 2-3 layers that are connected by tight junctions. On their apical cell membrane are microvilli protrusions which secrete and are bathed in charged glycocalyx. The suprabasal cells of the corneal epithelium are arranged in 2-3 layers. The basal cells of the corneal epithelium are arranged in a single layer and are connected to the basement membrane through hemidesmosomes.

The outermost superficial epithelial cells, organised in 2-3 layers, are flat (squamous) and polygonal, on their apical cell membrane they are bordered by tight junctions and have microvilli protrusions which increase their cellular surface area and secrete charged glycocalyx. The carbohydrate enriched glycocalyx coating of these cells closely interacts with the hydrophilic tear film, enabling the spreading of the film with each blink to allow for normal vision (Sridhar, 2018).

Directly posterior to the superficial cell layer is the suprabasal cell layer, they are also polygonal in shape and are composed of 2-3 layers of cells.

Basal cells make up the posterior-most layer of the corneal epithelium, they have a columnar morphology and are anchored by hemidesmosomes to the basement membrane. The epithelial basement membrane is an acellular, highly specialised extracellular matrix positioned posterior to the basal epithelial cells and anterior to Bowman's layer. The primary components of the corneal epithelial basement membrane are collagens, laminins, heparan sulfate proteoglycans and nidogens (Tuori et al., 1996).

1.1.2 Bowman's layer

Bowman's layer is an acellular non-regenerating extracellular matrix (ECM) layer, located between the corneal epithelium and stroma. It is made up of randomly interwoven collagen fibrils, with its smooth anterior surface positioned towards the epithelial

basement membrane, and its posterior surface integrated into the collagen lamellae of the corneal stroma. This layer is around 8-12μm thick in the adult and becomes thinner with age (Worthen, 1972).

1.1.3 Corneal stroma

The corneal stroma is a tough, collagenous tissue which sits posterior to Bowman's layer and anterior to Descemet's membrane. It is a mesenchymal tissue that originates from the periocular neural crest. The stroma provides the cornea with its mechanical stability and contributes to its transparency. The stroma accounts for around 90% of the human cornea thickness, and mostly consists of an ECM comprised of around 200 organised lamellae of tightly packed collagen fibrils, made up of type I and V heterodimers, as well as glycoproteins and highly sulfated proteoglycans, such as decorin, lumican, mimecan and keratocan (Torricelli & Wilson, 2014). Collagen type V is situated at the centre of the collagen fibrils and type I coats the fibril surface (Ehlers, & Hjortdal, 2005). Proteoglycan turnover appears to take several months, with collagen taking even longer. Lesions of the stromal collagen and of Bowman's layer never regain their original structure (Ehlers & Hjortdal, 2005).

The orderly arrangement of stromal collagen is necessary for corneal transparency (Figure 1.3). Lamellae arrangement in the stroma differs from its anterior portion to its posterior portion. Lamellae in the anterior stroma are dense and highly interwoven, with most appearing to protrude into Bowman's layer (Morishige et al., 2006; Radner et al., 1998). Lamellae in the posterior stroma are less interlaced and are more hydrated than in the anterior portion. The collagen fibrils which are packed into bundles, cross at right angles in the posterior region of the stroma, whereas those in the anterior portion cross at oblique angles (Ehlers, & Hjortdal, 2005). The precise lattice-like structure of the stroma is thought to cause minimal light scattering, enabling the cornea to refract and transmit light to the lens and retina.

Evenly distributed between collagen lamellae are flat keratocytes (corneal stromal cells) which make up around 3-5% of stromal volume and are responsible for secreting the components of the extracellular matrix (DelMonte & Kim, 2011; Torricelli & Wilson, 2014). Following birth, the number of keratocytes undergoing mitosis decreases in rats, and at the time of eyelid opening, keratocytes have withdrawn from the cell cycling process and become quiescent (Zieske, 2004). Keratocytes have slim processes which form gap junctions with neighbouring cell surfaces, enabling communication (Ehlers, & Hjortdal, 2005). The majority of keratocytes are found in the anterior stroma, and key to their function is their expression of water-soluble crystallin proteins which maintain corneal

transparency (Jester et al., 1999). Corneal stromal stem cells have been identified in the corneas of mice, rabbits and humans (Amano et al., 2006; Du et al., 2005, 2009; Yoshida et al., 2006). These cells likely reside in the stromal portion of the limbus and are speculated to be identical to the so called limbal niche cells (Pinnamaneni & Funderburgh, 2012; see Section 1.1.6: Peripheral cornea (limbus). These cells are thought to function to support the potency of limbal stem cells and have also shown the capacity to differentiate into functional corneal stromal cells (Du et al., 2009; J. Wu et al., 2012).

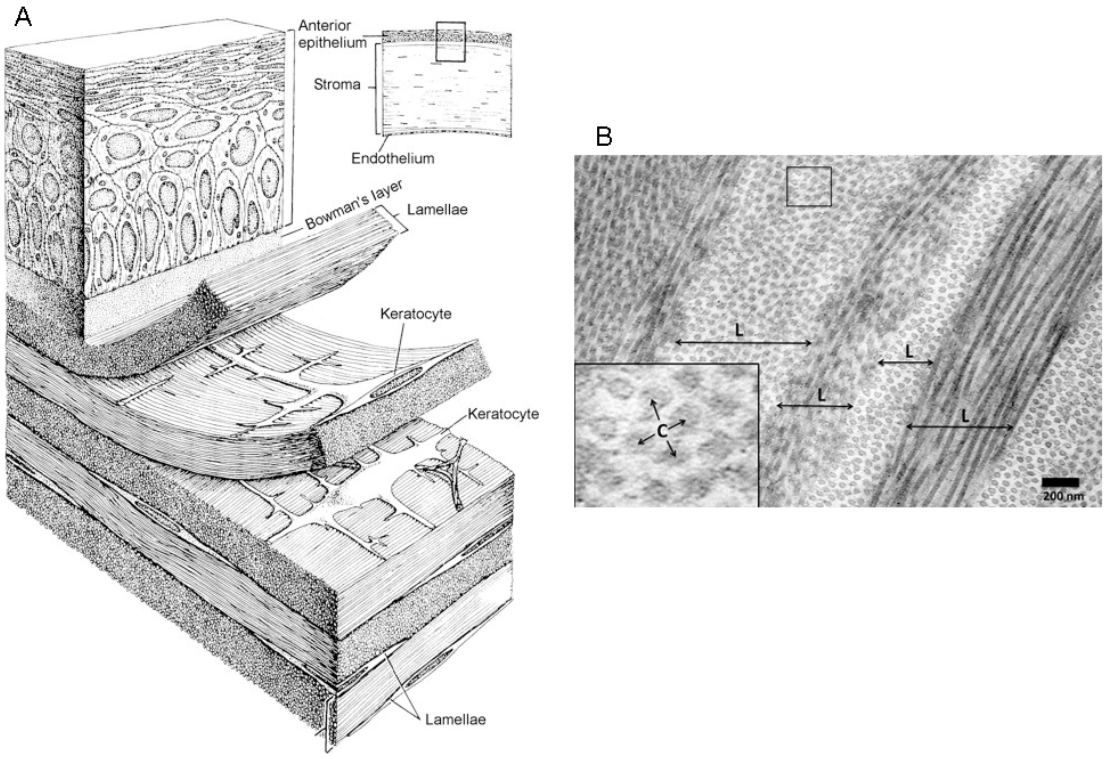

Figure 1.3 Block diagram and transmission electron micrograph of the corneal stroma. A) Block diagram of the cornea illustrating stromal lamellae arranged orthogonally and flat keratocytes (Ehlers, & Hjortdal, 2005). **B)** Transmission electron micrograph of a miniature swine corneal stroma at high magnification. Stacks of lamella (L) are displayed, within which, collagen fibres (C) are orientated orthogonally to the adjacent lamellae (Abhari et al., 2018).

1.1.4 Descemet membrane

The acellular Descemet membrane, found posterior to the corneal stroma and anterior to the endothelium, forms the basement membrane of the corneal endothelium. This membrane is made up of two layers: an anterior banded layer, composed of collagen types VIII and IV, and a posterior nonbanded layer which is secreted by the endothelium (Levy et al., 1996; Murphy et al., 1984). The corneal endothelium and Descemet membrane have a bidirectional relationship, with the health of the endothelium reliant on

a functional, intact Descemet membrane, and healthy endothelial cells required for the secretion of the Descemet membrane (M. Ali et al., 2016). Descemet membrane plays an important role in supporting the corneal endothelium following endothelial injury (J. Chen et al., 2017; Medeiros et al., 2019).

1.1.5 Corneal endothelium

The corneal endothelium is a monolayer of flat, polygonal, mitochondria-rich cells, which line the posterior surface of the cornea and face the anterior chamber of the eye. The main functions of this layer are to maintain the clarity and health of the stroma through control of stromal hydration levels (stromal deturgescence), while remaining permeable to nutrients and other molecules found in the aqueous humour of the anterior chamber (Bourne, 2003). Corneal endothelial cells are very metabolically active in order to support their water transportation function; however, they lack the capacity to regenerate *in vivo* and cell loss due to aging leads to stromal edema and corneal opacification.

1.1.6 Peripheral cornea (limbus)

The corneal limbus resides at the border between the clear cornea and the conjunctiva/sclera. It is a transitional zone that contains numerous components, including blood vessels and nerves along with limbal stem cells (LSCs) in the basal layer and other cell types, which make up the limbal stem cell niche (LSCN) (Figure 1.4). LSCs are quiescent cells that have the ability to differentiate into mature corneal epithelial cells (discussed in detail in Chapter 4, Section 4.1.2), thus they play a vital role in the repair, maintenance and homeostasis of the cornea.

The microenvironment of the limbus is different to that of the central cornea, one of the most striking differences being the presence of blood vessels in the limbus. Furthermore, while the structure of the central cornea is arranged in a flat and uniform manner, enabling light refraction, the limbus contains a series of vertical ridges called the palisades of Vogt. The blood vessels form an undulating network within the palisades of Vogt, providing the stem cells with oxygen and nutrients. Apart from LSCs, the LSCN contains melanocytes which provide UV protection (Davanger & Evensen, 1971; Higa et al., 2005), antigen presenting Langerhan's cells (Baum, 1970) and neural crest-derived limbal niche cells (LNCs) (Polisetti et al., 2023) which function to support LSCs and prevent them from differentiating (G. G. Li et al., 2012; Y. Li et al., 2014).

Research has shown that substrate stiffness can influence stem cell differentiation (Engler et al., 2006) and that the limbus is substantially less rigid than the central cornea (Gouveia et al., 2019) indicating that specific biomechanics also contribute to the microenvironment of the LSCN. Substrate stiffness has also been shown to affect cell

movement, fibroblasts move from soft substrates towards stiffer ones, a concept known as durotaxis (Lo et al., 2000). In the same way, the unidirectional movement of the cells of the limbus to the central cornea may be influenced by the substrate stiffness gradient (Eberwein & Reinhard, 2015).

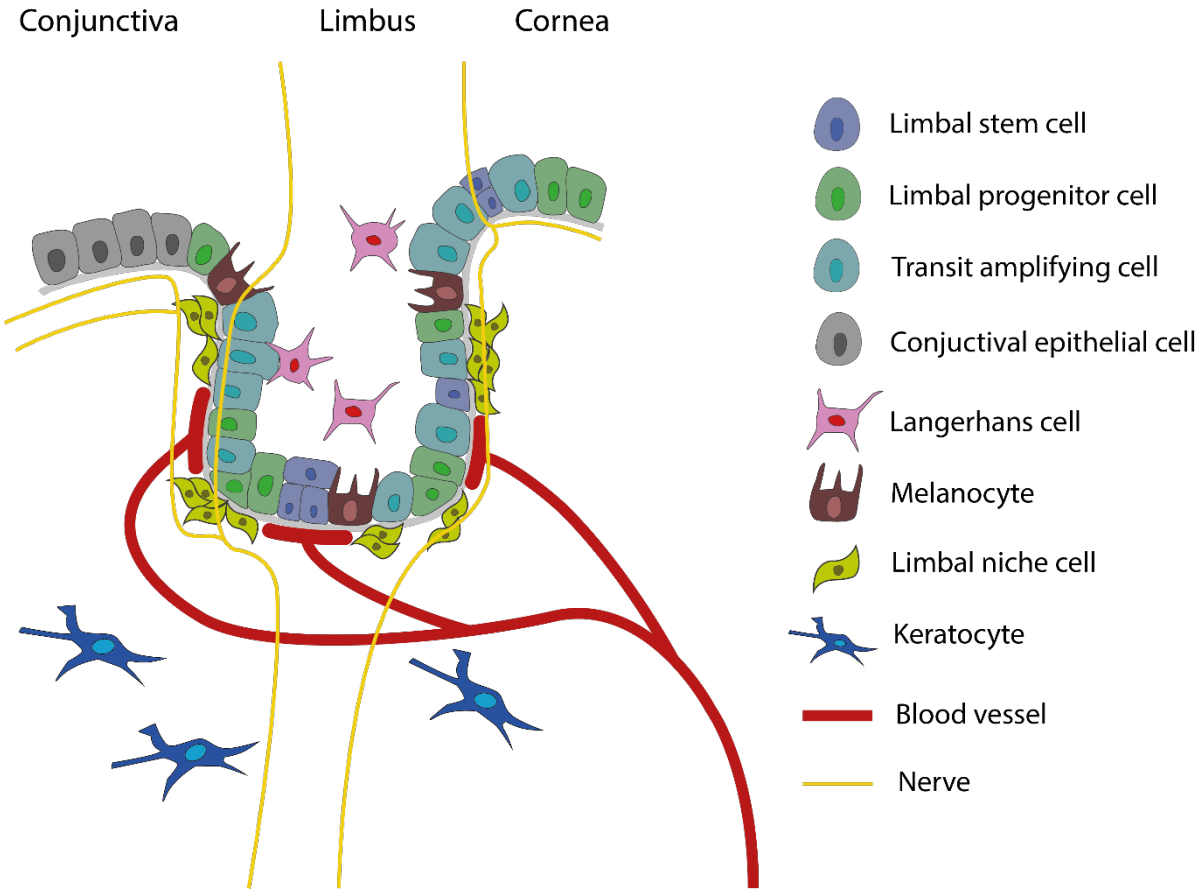

Figure 1.4 The limbal stem cell niche. The limbus resides between the conjunctiva and the cornea. The limbal stem cell niche (LSCN) is localised to the basal layer of the limbus and is comprised of multiple cell types. Limbal stem cells divide and give rise to limbal progenitor cells which give rise to transit amplifying cells that migrate centripetally to the central cornea, dividing along the way, giving rise to cells of the corneal epithelium. Other cell types in the LSCN include antigen-presenting Langerhans cells, melanocytes which provide UV protection and neural crest-derived limbal niche cells – all of which contribute to the microenvironment of the LSCN. Blood vessels are also located in the LSCN, allowing nutrient and metabolic waste transfer, along with nerve projections. Additionally, stromal keratocytes are present in the stromal limbus, which synthesise and secrete the limbal ECM.

1.1.7 Development of the cornea

The development of the cornea is directly coordinated with the development of other ocular anterior structures. During vertebrate embryonic development, the morphogenesis of the cornea occurs through a coordinated multistage process comprised of cellular interactions between different ectodermal-derived tissues, specifically, between the surface and neural ectoderm and the periocular mesenchyme derived from the neural crest. Failure of these interactions results in ocular defects.

At around day 32 of human gestation, interactions between the surface ectoderm and the underlying optic vesicle of the neural ectoderm cause the surface ectoderm to thicken and form the lens placode. The lens placode and optic vesicle invaginate in coordination, resulting in the detachment of the lens placode from the surface ectoderm and the joining together of the lateral ends of the lens placode to form the lens vesicle. The lens vesicle subsequently forms the lens and the optic vesicle forms the optic cup, while the overlying surface ectoderm forms the presumptive corneal epithelium (Figure 1.5).

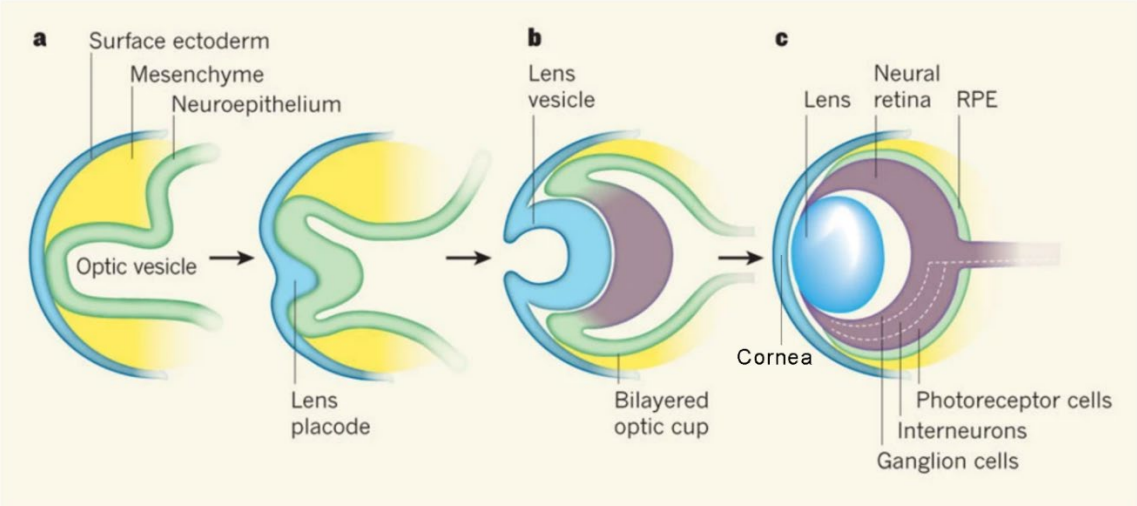

Figure 1.5 Illustration depicting the embryology of the eye. A) During early stages of eye development, the interactions between the surface ectoderm and the underlying optic vesicle of the neural ectoderm cause the surface ectoderm to thicken and form the lens placode. **B)** The lens placode and optic vesicle invaginate in coordination, resulting in the detachment of the lens placode from the surface ectoderm and the joining together of the lateral ends of the lens placode to form the lens vesicle. The optic vesicle forms the optic cup which is made up of two connected crescent shaped layers. **C)** The lens vesicle subsequently forms the lens and the overlying surface ectoderm is the presumptive corneal epithelium. Neural crest cells migrate to meet the presumptive corneal epithelium to form stromal and endothelial layers of the cornea. The inner layer of the optic cup gives rise to the neural retina and the outer layer gives rise to the retinal pigmented epithelium (RPE). Image adapted from R. R. Ali & Sowden (2011).

This process is tightly regulated by transcription factors essential for the proper morphogenesis of the eye, with each event allowing the initiation of the next. For instance, surgical removal of the pre-lens ectoderm results in failure of optic vesicle invagination (Hyer et al., 2003).

Bone morphogenic proteins (BMPs) are essential for lens specification and differentiation. BMP4 and BMP7 are activated sequentially before and at the time of lens placode induction, respectively, but are then completely excluded from the imminent successive stages of lens formation (Dudley & Robertson, 1997; Furuta & Hogan, 1998). The retinal homeobox protein Rx (Rax), is essential for optic cup development. From E9, Rax null mice do not undergo optic cup development and are born without visible eye

structures (Mathers et al., 1997). Six3 is vital for lens formation, early conditional deletion of the gene encoding this protein in the presumptive lens ectoderm results in reduced lens size or absence of the lens, as well as defective optic vesicle morphogenesis (W. Liu et al., 2006). During this developmental stage, expression of the master regulator of the eye, Pax6, is regulated by Six3, and conditional removal of Six3 from the presumptive lens ectoderm prevents the activation of Pax6 resulting in its downregulation (W. Liu et al., 2006).

Both the lens vesicle and the overlying ectoderm express PAX6, which functions to regulate the expression of many transcription factors essential for ocular development and remains prominently expressed in the adult corneal epithelium (Collinson et al., 2003; Koroma et al., 1997). Following its formation, the lens vesicle and the overlying ectoderm press together, with the anterior ectoderm becoming the presumptive corneal and conjunctival epithelium. Committed corneal epithelial cells express the keratin protein pair keratin 3 and keratin 12 (K3/K12), with evidence suggesting that PAX6 stimulates the activity of the K12 promoter (Chaloin-Dufau et al., 1990; J. J. Liu et al., 1999).

During the 7th week of human gestation, multipotent mesenchymal neural crest cells derived from the fused together lateral tips of the neural tube following neurulation, migrate into the space between the lens and primitive corneal epithelium. This subsequently forms the corneal stroma, endothelium, iris and trabecular meshwork. In human corneal development, the mesenchymal cell migration occurs in three waves: the first gives rise to the corneal and trabecular meshwork endothelium; the second wave to the stromal keratocytes; and the third to the development of the iris (Eghrari et al., 2015).

Transforming growth factor beta (TGFβ) signalling is essential for the development of ocular structures derived from neural crest cells. Tissue-specific inactivation of TGFβ2 signalling in mice resulted in the development of corneas that lack an endothelial layer and have abnormal formation of the stroma (Ittner et al., 2005). Furthermore, expression of PITX2 is required for the specification of the endothelium and stromal cell fates, and for establishing the angiogenic privilege of the cornea (Gage et al., 2014).

The mature corneal epithelium does not develop until the opening of the eyelids, at approximately week 24 of gestation in humans (Pansky, 1982). At this point, the posterior basal epithelial cells change from flattened ovoid shapes, into cuboidal shapes arranged in a columnar formation. These cells migrate anteriorly, while differentiating and forming the wing cell layer and the anterior superficial layer of the cornea.

1.1.8 Regeneration and maintenance of the corneal epithelium

The corneal epithelium is the only component of the cornea that undergoes both maintenance and injury-induced regeneration (Stocum, 2006). Maintenance of the ocular surface epithelium is necessary for proper vision. Cells of the corneal epithelium are continually sloughed off the tissue surface into the tear film and must be replaced to ensure cellular homeostasis. Under normal regenerative maintenance conditions in the mammalian corneal epithelium, its renewal takes 14-21 days (Haddad, 2000). The corneal epithelial mass remains constant under normal circumstances; therefore, it is expected that the rate of cellular addition must equal that of cellular loss (Sharma & Coles, 1989). As applications of genetic therapies in the treatment of monogenic diseases of the corneal epithelium progress, it is important to understand the population of cells that provide the tissue with its cellular integrity. This allows us to effectively target the correct population of precursive corneal epithelial cells, appropriately facilitating the prevention of corneal opacification and deterioration.

Long-term labelling experiments using tritiated thymidine identified slow-cycling cells in the limbus which appeared to be responsible for maintaining the constant cellular mass of the corneal epithelium (Cotsarelis et al., 1989; Lehrer et al., 1998). In comparison to cells of the basal corneal epithelium, cells of the basal limbus are more diverse, with its LSC subpopulation being smaller in size and euchromatin-rich, with a high nucleus to cytoplasm ratio (Z. Chen et al., 2004; D. Q. Li et al., 2021; Romano et al., 2003). LSCs are slow-cycling, quiescent cells that remain out of the cell cycle but have a high proliferation potential (D. Q. Li et al., 2021).Single cell RNA sequencing (scRNAseq) and quantitative lineage tracing of the murine limbal epithelium has allowed for a distinction between the two different LSC populations of the inner and outer limbus. LSCs of the outer limbus are quiescent and participate in wound healing, while LSCs of the inner peri-corneal limbus are more mitotically active and are responsible for maintaining corneal epithelial homeostasis (Altshuler et al., 2021).

The trajectory from LSC to differentiated corneal epithelial is not completely clear, however a single cell RNA sequencing (scRNAseq) study that analysed cells of the corneal limbus, indicated that LSCs give rise to limbal progenitor cells (LPCs) which give rise to highly proliferative transit amplifying cells (TACs) (D. Q. Li et al., 2021; J. M. Li et al., 2021) (see Chapter 4, Section 4.1.2). The TACs would rapidly divide and eventually give rise to post-mitotic and then terminally differentiated corneal epithelial cells. Tamoxifen-inducible, CreER-loxP lineage tracing mouse studies have demonstrated that cells originating from the corneal limbus, likely TACs, migrate centripetally while dividing along the way (Di Girolamo et al., 2015; Dorà et al., 2015).

It is generally recognised that LSCs and their progenies are responsible for the cellular maintenance of the corneal epithelium. However, this has been a topic of debate, as some evidence indicated that the central cornea of several species contains highly proliferative cells. Surgical transplantation experiments in mice demonstrated that following the transplantation of labelled limbal epithelial tissue in the limbus of immunocompromised mice, labelled clones only appeared in the cornea if the host cornea had been excised (Majo et al., 2008). This implied that the LSCs were not active during normal maintenance of the cornea as no labelled clones appeared in the cornea in the absence of wounding. Additionally, the rabbit central cornea is able to survive for months following separation or removal of the limbus (Huang & Tseng, 1991; Kawakita et al., 2011). Further, a study that employed a K15-GFP transgene lineage tracing murine model demonstrated that 48 hours following the removal of the K15-GFP+ limbal epithelium, the limbus appeared healed but it did not express K15-GFP. Although, by day 30 post-injury, remarkable recovery of the K15-GFP pattern was evident in the limbus. However, following the removal of both the limbal and corneal epithelium, pathological healing of the cornea occurred, overall, indicating that cells of the corneal epithelium are able to migrate backwards to repair the limbus and then dedifferentiate into LSCs (Nasser et al., 2018). Reports of some patients with total LSC deficiency have demonstrated retention of central islands of the normal corneal epithelium for several years. These studies indicate that, in humans, the central cornea is able to maintain itself to a certain extent upon elimination of the limbus, implying that some cells of the central corneal epithelium retain mitotic properties and are able to act as progenitors. Although the cells of the corneal epithelium do appear to have a latent proliferative potential, it does not dispute that the limbus contains a suitable source of stem cells for corneal epithelial maintenance (J. D. West, 2015). On this basis, genetic therapies targeting diseases of the corneal epithelium, should not only be administrated to the central cornea, but also the corneal limbus to ensure gene expression is modified before the initiation of pathogenesis in terminally differentiated cells.

1.2 The extracellular matrix

Tissues of the body have their own unique and specialised ECM components and organisation, allowing each ECM to carry out tissue-specific roles. The ECM has essential roles in the regulation of development, function and homeostasis of all eukaryotic cells (P. Lu et al., 2011; Mecham, 2012; Rozario & DeSimone, 2010; H. Wang et al., 2022). As well as providing mechanical support, the ECM is actively involved in the establishment, separation, maintenance and nourishment of tissues and organs. Essential molecular ECM components are shared across tissues, yet the complex

structures they form and their unique modifications are highly tissue specific. The diverse functions of different ECM tissues are accomplished through its complex and tissue specific chemical composition and organisation (Naba et al., 2012). ECM components provide dynamic tissue organisation and are also signalling molecules in their own right. In the cornea, the epithelial basement membrane, Bowman's layer, stroma and Descemet membrane all make up distinct ECM forms in the cornea, each with their own unique structural, compositional and functional characteristics. There are two main forms of ECM: the interstitial matrix and the basement membrane (Figure 1.6). The interstitial matrix is located under the basement membrane and found in the spaces between cells such as fibroblasts and other connective tissue cells. In contrast, basement membranes are specialised thin sheet-like structures that underlie polarised epithelia and endothelia.

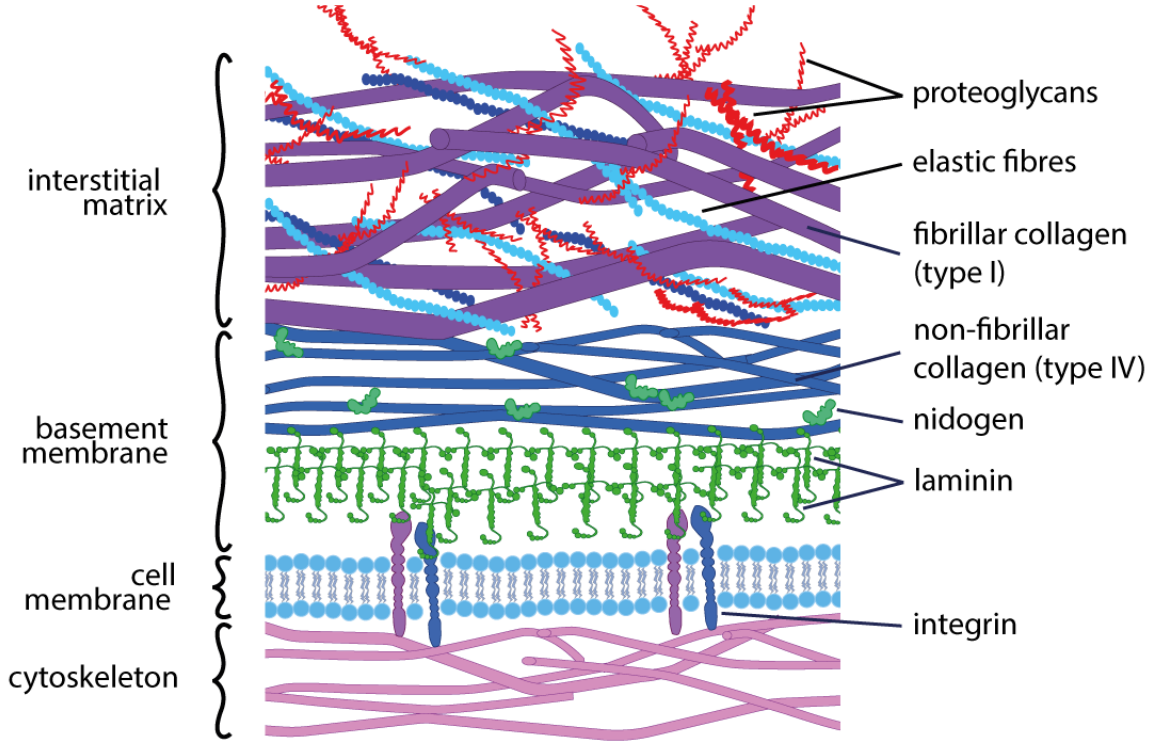

Figure 1.6 The interstitial matrix and basement membrane components of the extracellular matrix (ECM). The ECM is composed of various macromolecules, with fibrillar collagens, elastic fibres and proteoglycans being the main components of the interstitial matrix and collagen type IV, nidogens and laminins being major constituents of the basement membrane. Integrins are transmembrane receptors comprised of two subunits that connect the ECM to the cell cytoskeleton, enabling cells to sense and respond to their environment.

Cells of the tissue are bound to the surrounding ECM structure by **integrins**, which are transmembrane receptors linked intracellularly to the cytoskeleton. They are comprised of an α and β subunit to form a heterodimer. Several genes code for different integrin isoforms. The RGD motif was identified as a general integrin binding motif, but individual integrins are also able to bind to specific protein domains. In addition to their roles as

cell-ECM anchors, integrins transmit signals into the cell, influencing processes such as migration, survival, differentiation and motility (Harburger & Calderwood, 2009).

The fibrous proteins of the ECM, including collagens, fibronectins, laminins, and elastin, primarily play a structural role and are crucial for the appropriate functioning and integrity of various tissues throughout the body, including the human cornea.

Collagens are the most abundant protein form in mammals accounting for ~30% of total protein mass (Baccetti, 1985). The collagen superfamily comprises 28 members. They are comprised of three polypeptide strands called α chains that are twisted together to form a left-handed triple helix structure and undergo processing in the formation of a functional collagen molecule. The diversity of the collagen family is accounted for by α chains of different sizes, several molecular isoforms and supramolecular structures for a single type of collagen, as well as different alternative promoters and alternative splicing (Ricard-Blum, 2011). Based on their structure and supramolecular architecture, collagens are grouped into fibrillar collagens, fibril associated collagens with interrupted triple helices (FACIT) and non-fibrillar types (Michelacci, 2003). Fibrillar collagens are the most common type, and are arranged in striated fibrils. FACIT collagens connect collagen fibrils to other ECM components or cells. Whereas non-fibrillar collagens form specific structures depending on tissue type. The most abundantly expressed collagens in the human cornea are type I, V, VI, XII, XIII, XIV and XXIV (Dyrlund et al., 2012; Meek, 2009).

The **glycoprotein** family is a large and diverse group of proteins that are modified with carbohydrate (glycan) molecules. There are many types of glycoproteins found within the ECM. Laminin and nidogen are abundant glycoproteins of basement membranes. **Laminins** are comprised of three disulfide-linked polypeptides – the α, β and γ chains, which are arranged in a cruciform-like structure with three short arms and one long arm (Macdonald et al., 2010). Laminins interact with cell surface receptors such as integrins and bind to other ECM components to provide structural support and tissue stability.

Elastic fibres are ECM macromolecules that comprise an **elastin** core surrounded by glycoprotein **fibrillin** microfibrils which are responsible for providing tissues with deformability and recoil properties (Kielty et al., 2002). Elastin is encoded by the *ELN* gene, whereas human fibrillin proteins are encoded by three different genes, *FBN1*, *FBN2* and *FBN3*. In the human cornea, elastin microfibril bundles are found within the corneal limbus and the posterior central stroma, with an especially high concentration immediately anterior to Descemet membrane (Lewis et al., 2016; White et al., 2017).

Fibronectin is a large glycoprotein that can exist in various forms, including a soluble plasma form and an insoluble form that is incorporated into the ECM. In the cornea, fibronectin is found in both forms, and its deposition and organization are tightly regulated to maintain corneal transparency and stability (Espana & Birk, 2020; Zollinger & Smith, 2017). Fibronectin interacts with various ECM components and cell surface receptors, including integrins, which mediate cell adhesion and signalling (Labat-Robert, 2012; Zollinger & Smith, 2017). In the cornea, fibronectin helps to anchor corneal epithelial cells to the underlying basement membrane (Kimura et al., 2010; Torricelli et al., 2013). In addition to its structural role, fibronectin is also important for corneal wound healing and is shown to be upregulated during the healing process (Basu et al., 2014; Kadler et al., 2008; M. Nakamura et al., 1994).

Proteoglycans (PGs) are heavily glycosylated protein that are made up of a 'core protein' bound to one or more glycosaminoglycan (GAG) chains. The GAG chains are highly negatively charged enabling them to attract and bind to positively charged ions and water molecules (Casale & Crane, 2019). This results in the formation of a hydrated gel-like substance that helps to cushion and support cells and tissues under mechanical stress. There are various types of PGs such as, small leucine-rich PGs, such as decorin, lumican, keratocan and biglycan; large aggregating PGs such as, aggrecan, versican, and brevican and cell surface proteoglycans such as, syndecans and glypicans. In the human cornea, highly expressed PGs include decorin, lumican, keratocan and biglycan (Dyrlund et al., 2012).

Matrix metalloproteinases (MMPs) are a diverse group of calcium- and zinc-dependent endopeptidases involved in the degradation and remodelling of ECM components. MMPs are subcategorised into groups depending on their substrate specificity, with one group incorporating collagenases (MMP1, 8, 13) (Kaya et al., 2021). Some MMPs are also able to cleave non-ECM molecules such as growth factors and integrins (Page-McCaw et al., 2007). Much of the research of MMPs in the cornea is focused on wound healing, although collagenases are expressed in small amounts during corneal homeostasis (Gabison et al., 2005). MMP expression is upregulated in response to penetrating corneal damage and is essential for wound healing (Couture et al., 2016; Sivak & Fini, 2002).

1.3 Protein folding and aggregation

Following translation from mRNA, proteins begin on a ribosome as a linear chain of amino acids. The linear sequence folds into its specific native conformation and this process is determined by the amino acid chain sequence and is guided by various

molecular regulatory mechanisms such as molecular chaperones. Native protein states usually always conform to structures that are the most thermodynamically stable under physiological conditions (Dobson et al., 1998). However, there are many possible folding conformations accessible to a polypeptide chain (Dill & Chan, 1997; Dobson et al., 1998; Wolynes et al., 1995). Incorrectly folded proteins are detected by quality control mechanisms and can be directed along a pathway such as the unfolded protein response, where they are marked by ubiquitination and degraded in the cytoplasm by proteosomes (Dobson, 2003). In some cases, proteins with a high propensity to misfold, likely due to mutational variants or environmental stresses, can escape the quality control mechanisms and give rise to intractable aggregates either within the cell or more commonly, in the extracellular space.

Protein mis- or unfolding, leading to the formation and deposition of intracellular or extracellular insoluble supramolecular aggregates, is implicated in many types of human pathology. Many of the conformational changes of abnormally folded proteins are due to various types of Mendelian disease-causing mutations, which induce either a toxic gain of activity or loss of function of the encoded protein

Protein aggregates can either have an amorphous or amyloid fibrillar morphology. All amyloid fibrils, even if derived from proteins without any similarity in sequence and conformation, share common morphological features. Amyloid fibrils are ordered aggregates composed of several thousand copies of relatively small proteins or shorter peptides arranged in a repeating cross-β-sheet structure (Sunde & Blake, 1997). Amorphous aggregates, also referred to as disordered aggregates, are composed of misfolded, non-organised, full- or close to full-length proteins.

Many conditions are associated with the deposition of amyloid protein aggregates. Alzheimer's disease is the most common neurodegenerative disorder and is characterised by the accumulation of extracellular beta-amyloid peptides which triggers neuronal degeneration (Kadowaki et al., 2005; Yao et al., 2005). Various other neurodegenerative conditions are caused by the deposition of proteins that have formed amyloid aggregates, such as alpha-synuclein in Parkinson's disease and huntingtin in Huntington's disease. Amyloidosis can also occur in other parts of the body, such as amyloid light-chain amyloidosis, which is caused by the accumulation of an immunoglobulin light chain protein and can affect a wide range of organs and in particular, the liver (Hasib Sidiqi & Gertz, 2021; G. Li et al., 2019; Merlini et al., 2018).

Proteins that have amyloid fibril forming propensities can also form amorphous aggregates. Some protein aggregation pathologies only present with amorphous

aggregates, but this form of pathogenesis has not received much interest as it was previously thought not to be associated with disease. Amorphous aggregation of mutant superoxide dismutase (SOD1) causes amyotrophic lateral sclerosis (Rosen et al., 1993), whereas, crystallins expressed in the lens can form amorphous aggregates, causing cataracts (Boatz et al., 2017).

Corneal dystrophies caused by mutations in *TGFBI* can present with amyloid deposits, amorphous deposits or a mixture of both.

1.4 Corneal Dystrophies

Corneal dystrophies (CDs) are a group of phenotypically heterogenous disorders, usually caused by genetic mutations that affect the production or function of key proteins in the cornea resulting in corneal opacification and visual impairment.

The International Committee for Classification of Corneal Dystrophies (IC3D) was published in 2008 by experts in the field of corneal disease, who established a classification system of CD based on their genetic basis, clinical appearance and histopathological features (Weiss et al., 2008). CDs are defined by the anatomic level predominately affected and are further classified based on evidence for how well defined they are, with category 1 being a well-defined CD caused by known mutations, and category 4 being a 'suspected' dystrophy that is not yet genetically defined. A revised version of the IC3D was published in 2015 to include updated genetic, clinical and histopathological information (Weiss et al., 2015).

CD diagnosis is typically based on the clinical appearance of the cornea observed by slit-lamp biomicroscopy examination, in addition to consideration of ophthalmologic family history (Lisch & Seitz, 2011). Well-defined CDs with known genetic causes can be precisely diagnosed by clinicopathological correlations. The majority of CDs are due to missense mutations that have an autosomal dominant inheritance pattern, though some have autosomal recessive or X-linked inheritance patterns. The monogenic nature of CDs, along with the accessibility of the cornea and its immune privilege, make those with a known pattern of inheritance ideal for the application of gene-based therapeutics.

Although many CD-causative genes and mutations have been identified, the disease mechanisms underlying the conditions are not fully defined. One such example lies in the relatively common CD, Fuchs' endothelial dystrophy, characterised by corneal endothelial dysfunction resulting in guttate formation on the inner corneal surface and corneal opacification. Fuchs' is a slow progressing condition that usually doesn't substantially impair vision until patients reach their 50s and 60s. The condition is slightly

more common in women than men, and prevalence varies between ethnic groups, with the Icelandic population showing a higher prevalence (11% for females, 7% for males) (Zoega et al., 2006) compared to the Japanese population (5.5% for females, 1.5% for males) (Kitagawa et al., 2002). Observations of disease heritability led to the identification of different genetic causes for Fuchs'. Missense mutations in *COL8A2* are associated with early onset Fuchs' (Biswas et al., 2001). Additionally, a trinucleotide repeat expansion in the *TCF4* gene has been shown to increase the risk of developing Fuchs' by 89% (Zarouchlioti et al., 2018).

Macular corneal dystrophy is a rare autosomal recessive condition caused by mutations in the carbohydrate sulfotransferase gene (*CHST6*) which results in abnormal proteoglycan synthesis. The condition presents early in life with superficial white/grey opacities in the central stroma, which progress towards the periphery and throughout the stroma during aging, leading to severe visual impairment (Dang et al., 2009).

Meesmann's corneal dystrophy is a rare autosomal dominant condition caused by heterozygous mutations in the corneal epithelial specific genes *KRT3* and *KRT12*. These mutations affect the corneal epithelium specifically, resulting in intraepithelial microcysts that appear within the first few years of life; however, symptoms are usually mild and vision is not usually affected (Corden et al., 2000).

Although not defined as a corneal dystrophy, limbal stem cell deficiency (LSCD) is a corneal pathology, characterised by the absence or impairment of LSCs and the LSC niche, resulting in conjunctivalisation of the corneal epithelium, where conjunctival epithelial cells spread to the corneal epithelium. LSCD can result from a variety of causes, including chemical or thermal burns, autoimmune diseases, infections, genetic disorders, and ocular surgeries (Elhusseiny et al., 2022).

1.4.1 Epithelial-Stromal TGFBI corneal dystrophies

Several CDs affecting the anterior layers of the cornea can be attributed to missense mutations in the gene transforming growth factor-beta induced (*TGFBI)* with phenotypic heterogeneity and an autosomal dominant inheritance pattern. These CDs are collectively referred to as epithelial-stromal TGFBI dystrophies. In these CDs, pathological deposits containing the *TGFBI* protein (TGFBIp) accumulate within the epithelial, Bowman's and/or stromal layers of the cornea.

TGFBI-linked epithelial-stromal CDs can be broadly divided into two categories: lattice CDs (LCDs) and granular CDs (GCDs). Amyloid deposits are characteristic of LCDs, whereas aggregates are more varied in morphology between the different forms of GCDs

which include: Reis-Bücklers corneal dystrophy/Thiel-Behnke corneal dystrophy and GCD type I and type II.

Specific mutations in TGFBIp result in particular phenotypes of CD, with different missense mutations at the same residue causing distinct patterns of protein deposition (Munier et al., 1997). Accordingly, a genotype-phenotype correlation between mutations at the TGFBIp amino acid residues Arginine 124 (p.R124) and Arginine 555 (p.R555) and various forms of phenotypically distinct CDs has been established (Evans et al., 2016; Figure 1.7). Mutations at the p.R124 and p.R555 hotspots, located in exons 4 and 12, respectively, are the most common cause of TGFBI CDs, with six missense mutations at these residues reported in total (Evans et al., 2016). Conversely, different mutations in *TGFBI* can also lead to a similar phenotype.

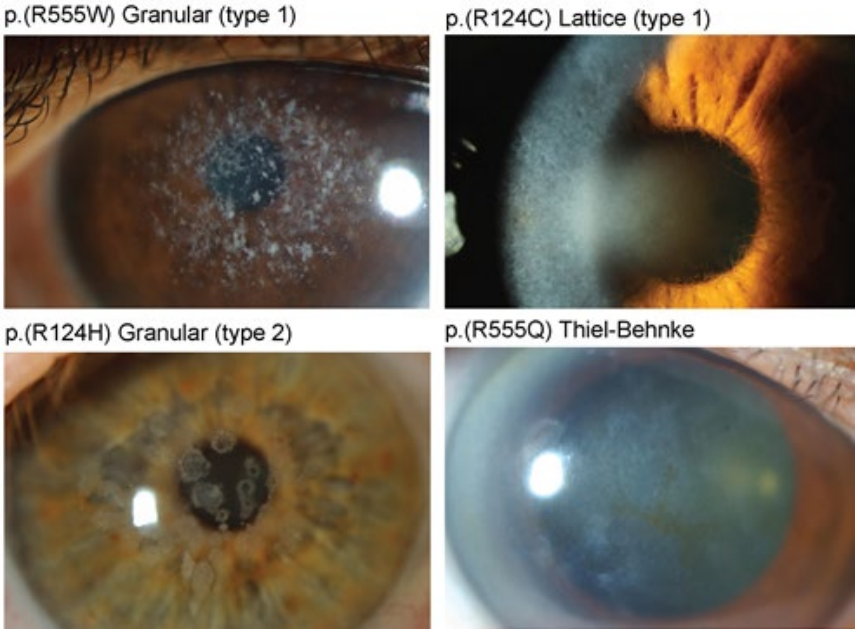

Figure 1.7 Genotype-phenotype correlation of missense mutations in TGFBI hotspots p.R124 and p.R555 (Evans et al., 2016). GCD type I, most commonly caused by the p.R555W TGFBI mutation, presents with 'crumb-like' opacities in the anterior to mid stroma of the central cornea, which progress to the peripheral cornea with disease progression. LCD type I, most commonly caused by the p.R124C TGFBI mutation, presents with a fine network of linear opacities in the epithelium and anterior stroma of the central cornea which eventually advance peripherally. GCD type II, caused by the p.R124H TGFBI mutation, initially presents with round deposits in the anterior stroma. As the disease progresses, amyloid deposits may form within the mid to posterior stroma. TBCD, caused by the p.R555Q TGFBI mutation, presents with honeycomb opacities in Bowmans's layer.

1.4.2 Discovery of *TGFBI* mutations as causative of CD

Two years following the discovery of TGFBIp, the *TGFBI* gene was mapped to the long arm of chromosome 5 at position q31 (Skonier et al., 1994). Shortly after, three phenotypes of CD were reported in eight families and linked to chromosome 5q,

providing the first links between *TGFBI* and CD (Stone et al., 1994). In 1997, Munier et al. constructed a contig covering the chromosome region associated with different CD phenotypes and identified four heterozygous missense mutations occurring at either the p.R124 or p.R555 hotspots of TGFBIp, each causative of clinically distinct forms of epithelial-stromal CD (Munier et al., 1997). In the following year, more CD-causative mutations in *TGFBI* were discovered and linked to CD phenotypes (Munier et al., 2002). Since, multiple genotype-phenotype studies have been carried out establishing a strict correlation between mutations in *TGFBI* and their clinical presentation (Dighiero et al., 2001; Evans et al., 2016; Paliwal et al., 2010; Zenteno et al., 2009). To date, at least 78 CD-causative mutations in *TGFBI* have been identified (Table 9.1, Appendix B), most of which are single missense mutations, but deletions, insertions, frameshift mutations and bi-allelic mutations have also been reported. The p.R124 and p.R555 hotspots located in exon 4 and 12 of *TGFBI* respectively, are responsible for the majority of CD cases in different populations.

1.4.3 Reis Bücklers Corneal Dystrophy

Reis Bücklers corneal dystrophy (RBCD) is a CD that affects the Bowman's layer, first described by Reis in 1917 and then later in more detail by Bücklers in 1949. This disorder presents with confluent, irregular geographic opacities of Bowman's layer and anterior stroma, with onset occurring during early childhood (Liang et al., 2014; Tanhehco et al., 2006). Patients experience painful recurrent corneal erosions and ocular discomfort (Weiss et al., 2015). When analysed by light microscopy, Bowman's layer of RBCD-corneas is replaced by a sheet-like layer of granular Masson trichome-red deposits which may extend to the anterior stroma (Figure 1.8) (Liang et al., 2014). Excised RBCD-corneal samples examined using transmission electron microscopy, display TGFBIp positive rod-shaped bodies lining Bowman's layer which are absent in the normal cornea (Liang et al., 2014; Weiss et al., 2015).

RBCD is predominately caused by the c.317G>T; p.(R124L) mutation in exon 4 of *TGFBI* (M. Okada et al., 1998). This mutation is generally inherited, however, de novo mutations have been reported (Tanhehco et al., 2006). Rarer mutations c.1868G>A; p.(G623D) and c.1618_1620delTTT; p.(F540del) have also been reported as causative of the dystrophy (Afshari et al., 2001; Rozzo et al., 1998). Based on clinical symptoms, it is difficult to distinguish between **Thiel-Behnke corneal dystrophy** (TBCD), another dystrophy of the Bowman's layer, and RBCD. A definitive distinction between these conditions can only be made by either transmission electron microscopy on excised corneas, or genetic analysis. The prognosis of RBCD has been reported to be significantly worse than TBCD (Ellies et al., 2002), thus, a precise genetic diagnosis may

influence treatment regime, although other reports suggest that RBCD and TBCD are indistinguishable.

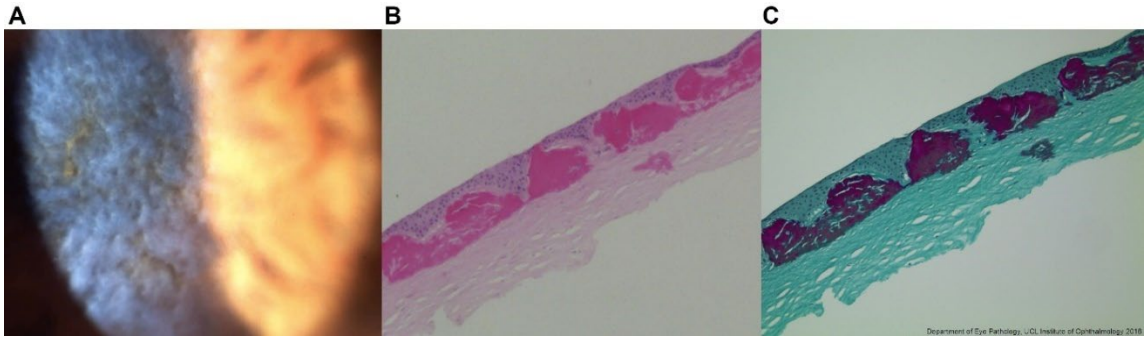

Figure 1.8 Clinical image and histological section of RBCD corneas. A) The RBCD phenotype presents with confluent, irregular geographic opacities of Bowman's layer and the anterior stroma (image provided by Prof Stephen Tuft). **B)** Hematoxylin and eosin stain of a RBCD-cornea. Lumpy bright pink (eosinophilic) deposits are observed in the subepithelial and anterior stromal region (image provided by Dr Caroline Thaung). **C)** The lumpy RBCD deposits stain bright red with Masson trichrome (images B-C provided by Dr Caroline Thaung).

1.4.4 Thiel-Behnke Corneal Dystrophy

TBCD was first described by Thiel and Behnke in 1967. TBCD, like RBCD is a CD affecting Bowman's layer of the cornea, with an onset in early childhood. TBCD is characterised by symmetrical subepithelial honeycomb opacities in the central cornea which can progress to the stromal layers and peripheral cornea (Ridgway et al., 2000). Patients experience painful recurrent corneal erosions and ocular discomfort (Cho et al., 2012). Analysis by light microscopy shows irregular thickening and thinning of the epithelial layer, with areas of vacuolation and separation of some basal cells from the underlying substratum (Ridgway et al., 2000). Furthermore, Bowman's layer is largely obliterated by a superficial fibrocellular scar (Ridgway et al., 2000; Weiss et al., 2015). Observations of TBCD-corneas by transmission electron microscopy displays the presence of curly collagen fibres which is an important distinguishing feature between TBCD and RBCD (Ridgway et al., 2000).

TBCD is caused by the c.1664G>A; p.(R555Q) mutation in exon 12 of *TGFBI* (Y. J. Chen et al., 2010; Cho et al., 2012). The c.1877A>C; p.(H626P) mutation has been reported as causing a TBCD-RBCD mixed phenotype (Wheeldon et al., 2008).

1.4.5 Lattice Corneal Dystrophy

Lattice corneal dystrophies (LCDs) caused by mutations in *TGFBI* are characterised by linear branching structures that form a lattice pattern in the cornea. LCD clinical phenotypes are classified as type I, type IIIA, intermediate type I/IIIA and type IV. LCD type I (LCDI) is the classic form of LCD and is a cornea-specific amyloidosis. LCD type II is not a true corneal dystrophy and is not associated with mutations in TGFBI, rather,

it is a systemic amyloidosis syndrome known as Meretoja syndrome caused by mutations in the gelsolin gene (Kiuru, 1998). Disease manifestations of LCD usually occur bilaterally but unilateral cases have also been observed (Aldave et al., 2006; Raj et al., 2017; Sridhar et al., 2001).

1.4.5.1 Classic lattice corneal dystrophy (LCDI)

LCDI is classed as the classic form of lattice corneal dystrophy. The most common causative genetic variant of LCDI is the exon 4 c.370C>T; p.(R124C) mutation of *TGFBI* (Munier et al., 1997). Translucent narrow lattice lines in the anterior central stroma and/or subepithelial whitish ovoid dots usually appear during the first decade of life, which eventually spread deeper into the stroma and towards the periphery (Kheir et al., 2019). The deposits lead to recurrent corneal erosions and irregularity of the corneal surface (Figure 1.9). As the condition develops, a dense diffuse stromal haze may appear that affects visual acuity. Observation of LCD corneas through light microscopy show epithelial atrophy and degeneration of basal epithelial cells (Weiss et al., 2015; Zechner et al., 1986). Histologically, the deposits can be seen within Bowman's layer and the stroma as an accumulation of eosinophilic, filamentous, and branching structures that stain with Congo red and exhibit apple-green birefringence under polarized light (Dighiero et al., 2001; Stix et al., 2005) (Figure 1.9D). By transmission electron microscopy, extracellular masses of fine electron-dense fibrils characteristic of amyloid material are observed (Dighiero et al., 2001). p.R124C mutations in *TGFBI* have also been reported to cause RBCD-like (Q. N. Yang et al., 2011) or TBCD-like (Chang et al., 2009) phenotypes (Figure 1.9B). Many other missense mutations in *TGFBI*, the majority of which are in the fourth FAS1 domain (see Section 1.5), have been reported to cause LCDI, however, these have been disputed as causative of classic LCDI and are instead thought to represent other LCD variants (K. E. Han et al., 2016). These include the mutations p.V505D (X. Tian et al., 2005), p.L509P (Niel-Butschi et al., 2011), p.L518P (Endo et al., 1999), p.I522N (C. Zhang et al., 2009), p.T538P (C. Zhang et al., 2009) and p.V539D (Chakravarthi et al., 2005).

1.4.5.2 Variants of lattice corneal dystrophy

LCD types other than the classic LCDI are mostly caused by mutations in the FAS1-4 domain of TGFBIp (see Section 1.5, Figure 1.13; Table 9.1, Appendix B). LCD variants are categorised as LCDIII, IIIA, I/IIIA and IV based on deposit location, age of onset, and the lattice line characteristics (Klintworth, 1999). These phenotypes have a later onset compared to LCDI. LCDIII and IIIA phenotypes can present with thick lattice lines that extend from limbus to limbus in the mid stroma. LCDIII has an autosomal recessive inheritance pattern and patients do not usually develop erosions. LCDIIIA has an

autosomal dominant inheritance pattern and patients can present with corneal erosions and is caused by p.P501T (Mashima et al., 2000), p.F540S (Stix et al., 2005), p.A546T (Dighiero et al., 2000), p.A620P (Jung et al., 2014), p.T621P (J. Lee et al., 2016) and p.N622K (Munier et al., 2002) missense mutations. LCDIV presents with a late onset and deep stromal amyloid deposits and is caused by the p.L527R mutation (Munier et al., 2002). LCDI/IIIA is classed as an intermediate form of LCDI and IIIA, and is caused by p.L518R mutations (Munier et al., 2002).

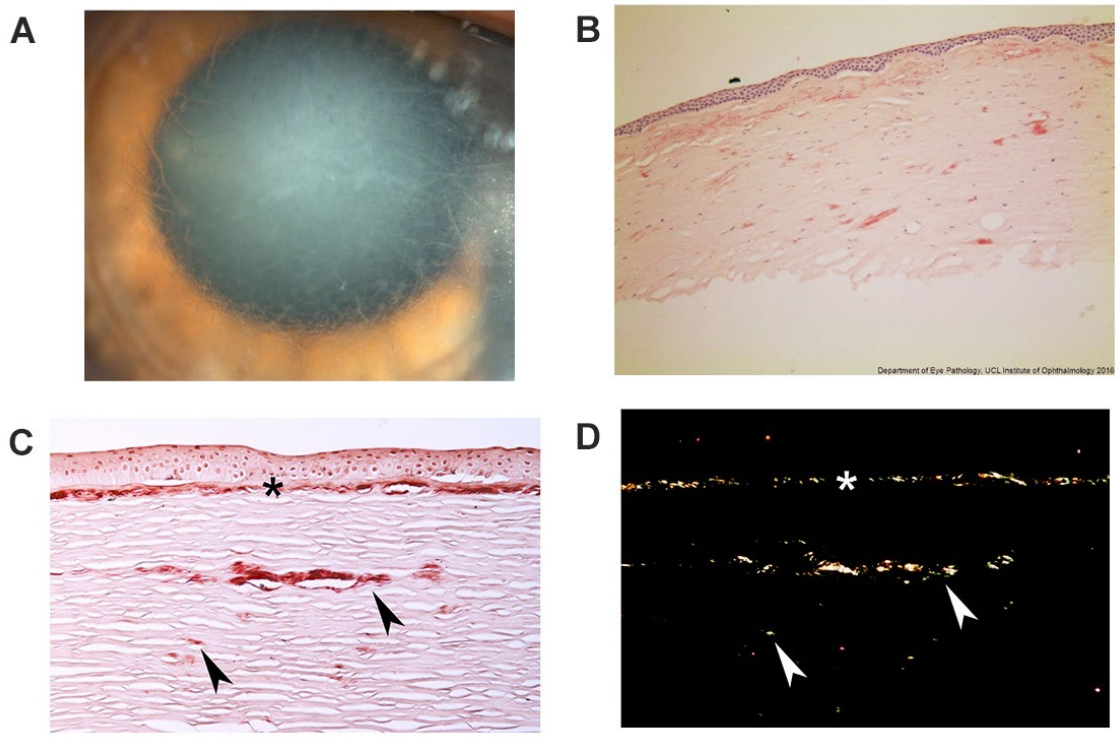

Figure 1.9 Clinical and histological presentation of lattice corneal dystrophy 1 (LCDI). A) LCD presents with a fine network of linear opacities and a continuous haze in the stroma of the central cornea which gradually progress to the periphery (image provided by Prof Stephen Tuft). **B)** Stromal amyloid deposits are positive for Congo red. A lumpy dense subepithelial band, negative for Congo red and Masson's trichrome was also apparent, therefore, this case was labelled as a combined LCD and TBCD phenotype (image provided by Dr Caroline Thaung). **C)** A p.R124C patient cornea shows a continuous layer of subepithelial amyloid (asterisk) and intrastromal amyloid deposits (arrowheads) that are positive for Congo red. **D)** The same section as image C viewed with polarised light confirms the deposits are birefringent and red-green dichroic and thus, amyloid. Images C-D were obtained from (Weiss et al., 2015).

1.4.6 Granular Corneal Dystrophy type I

Granular corneal dystrophy (GCD) type I (GCDI) is characterised by grey-white, well-defined granular opacities in the anterior to mid stroma of the central cornea, which advance to the posterior stroma as the condition progresses (Figure 1.10). Depositions of hyaline material that stains for Masson trichrome are observed in the corneal stroma histologically (Pantanelli et al., 2014). Through transmission electron microscopy,

electron-dense rod-shaped bodies are observed (Møller, 1990). The age of onset usually occurs within the first decade, with patients appearing asymptomatic until the deposits begin to coalesce and cause visual impairment, diagnosis is typically delayed until this point (Weiss et al., 2015). Recurrent erosions are frequently observed (Møller, 1990).

The most common causative genetic variants of GCDI are the c. 1663C>T; p.(R555W) or c.370C>A; p.(R124S) *TGFBI* hotspot mutations (Munier et al., 1997; Stewart et al., 1999).

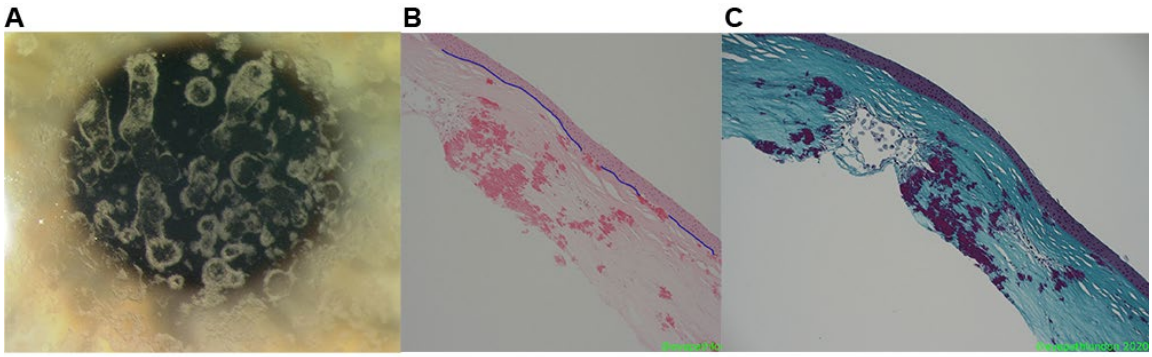

Figure 1.10 Clinical image and histological section of GCDI corneas. A) GCDI presents with grey-white, well-defined granular opacities in the anterior to mid stroma of the central cornea, which advance to the posterior stroma as the condition progresses (image provided by Prof Stephen Tuft). **B)** Hematoxylin and eosin stain shows deposits with sharp outlines and a 'crumb-like' morphology throughout the stroma. Bowman's layer, marked in blue, is interrupted by the deposits. Epithelial thickness appears irregular. C) Masson's trichrome staining shows red deposits, indicative of hyaline material (images B-C provided by Dr Caroline Thaung).

1.4.7 Granular dystrophy type II

GCD type II (GCDII), previously known as Avellino CD or combined granular-lattice CD, is characterised by the deposition of both hyaline and amyloid materials in the corneal stroma. Electron-dense rod-shaped bodies are observed in the anterior stroma by transmission electron microscopy. Onset in heterozygous patients usually occurs during the second decade of life with subsequent slow progression of the dystrophy. Initially, the dystrophy presents as small grey-white dots in the superficial stroma, as progression occurs, the opacities expand in size and amyloid deposition in the deeper stroma can occur, forming lattice lines. Some older patients develop superficial, diffuse anterior stromal haze. Individuals homozygous for the causative GCII mutation have been reported, these patients demonstrate an onset during childhood and a more rapid progression of the condition (Moon et al., 2007). GCDII is caused by the c.371G>A; p.(R124H) mutation in exon 4 of *TGFBI* (Munier et al., 2002). In comparison to GCDI, GCDII typically presents with fewer granular deposits and a less severe phenotype. Histologically, granular deposits in the anterior stroma stain with Masson's trichrome and lattice deposits in the deeper stroma stain with Congo red, indicating hyaline and amyloid

deposits respectively (Figure 1.11). In Japan and South Korea, GCDII caused by heterozygous p.R124H mutations are the most common cause of TGFBI CDs (Fujiki et al., 2001; J. E. Park et al., 2021). Although the p.R124H mutation is almost exclusively the cause of GDCII, some other mutations have also been reported to cause a similar phenotype, including, p.L509P (Gruenauer-Kloevekorn et al., 2009), p.L550P (R. et al., 2011; Zenteno et al., 2009) and p.M619K (Aldave et al., 2008).

A distinct phenotype of the homozygous p.R124H mutation shows a reticular pattern of greyish confluent opacities in the anterior stroma that are interspersed by translucent spaces, this specific pattern is known as a ‘type II opacity’ and has been reported in Japan (Tsujikawa et al., 2007; H. Watanabe et al., 2001). However, homozygous patients presenting with the conventional ‘type I opacity’ have also been reported (Figure 1.12; Watanabe et al., 2001). Surprisingly, due to the translucent spaces separating the deposits, patients with type II opacities demonstrated better best-corrected visual acuity than those of type I opacities (H. Watanabe et al., 2001). Interestingly, lattice-shaped deposits are not observed in the corneas of homozygous patients (K. E. Han et al., 2016).

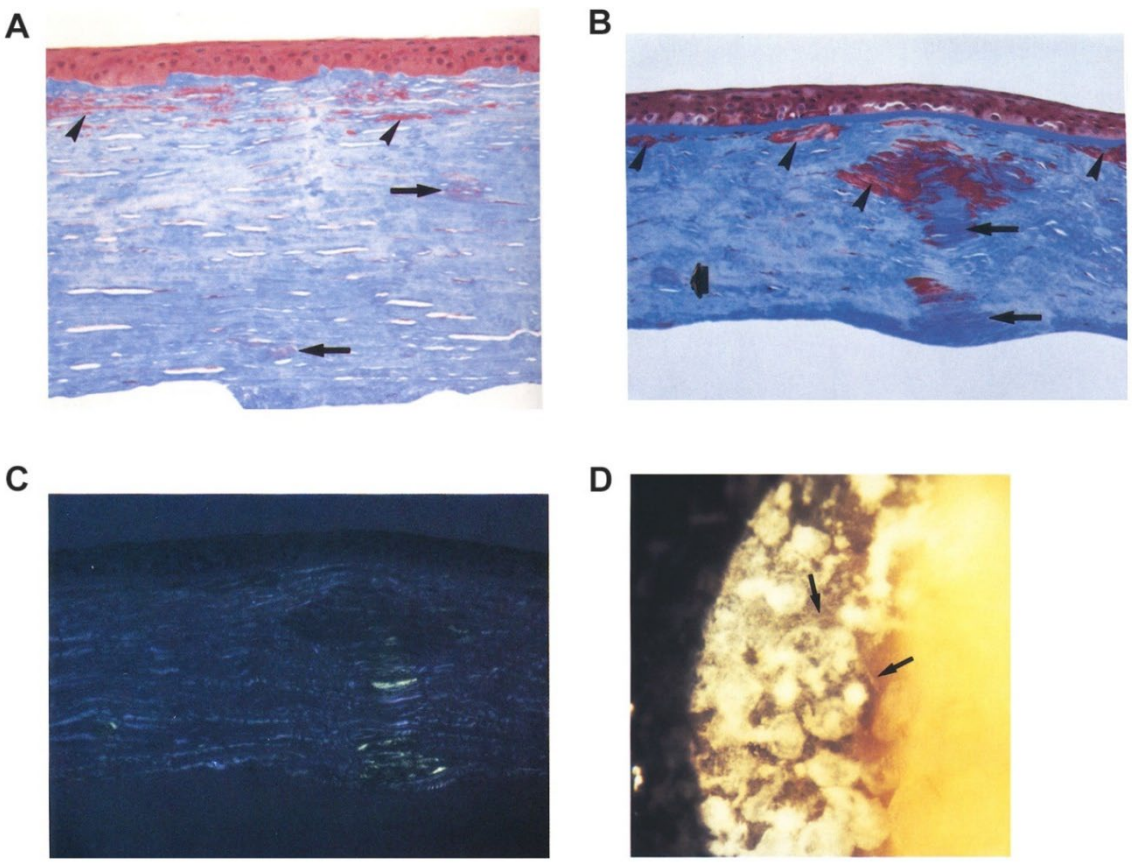

Figure 1.11 Clinical and histological presentation of granular corneal dystrophy II (GCDII). **A)** Recurrent GCDII following a previous superficial kerectomy in a corneal specimen obtained from a 79-year-old woman stained with Masson's trichrome. Superficial, sheet-like granular deposits are observed in the subepithelium and anterior stroma (arrowheads), whereas lattice-like deposits are observed in the mid and deep stroma (arrows). **B)** A corneal specimen obtained from a 49-year-old man with GCDII stained with Masson's trichrome shows granular deposits in the superficial and midstroma (arrowheads) in close proximity to amyloid (arrows) and lattice-like (short arrow) deposits. **C)** Congo red staining demonstrates amyloid deposits (from the same sample as image B) that display green birefringence under polarised light. **D)** Slit lamp biomicroscopy of the same patient presented in images B-C display prominent granular deposits, with some indistinct lattice-like deposits (arrows) observed via retroillumination. Images obtained from Santo et al. (1995).

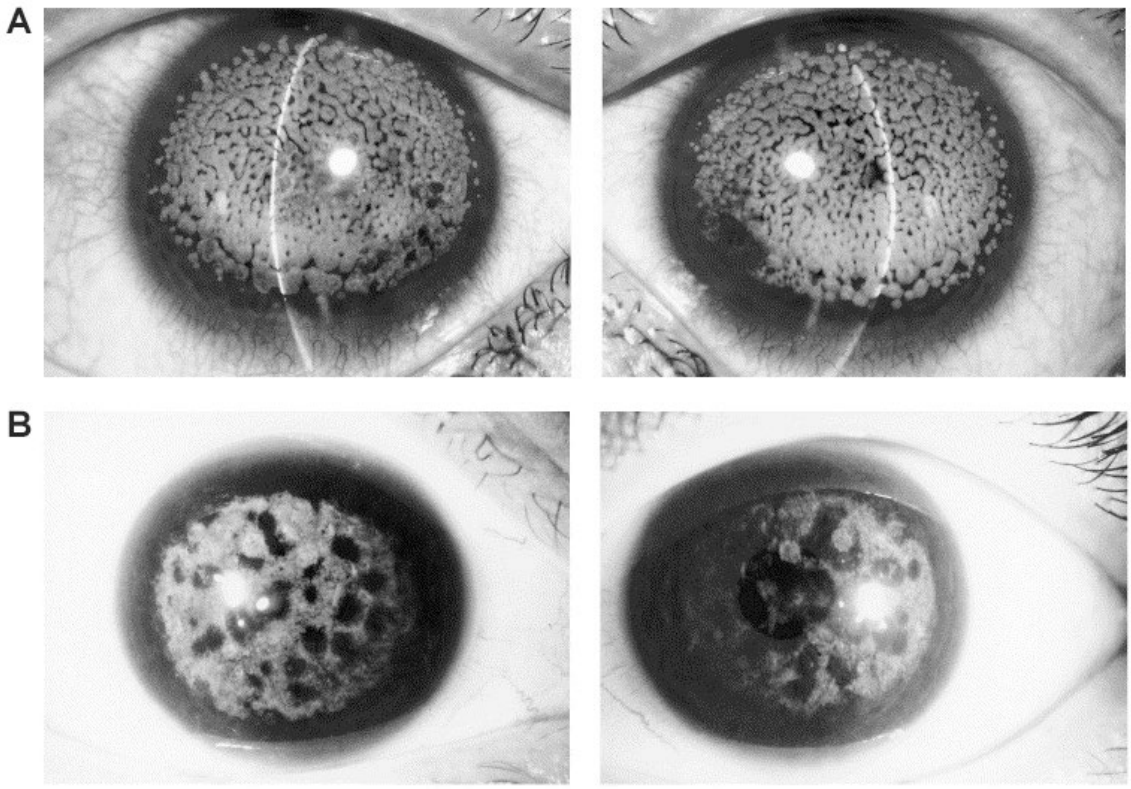

Figure 1.12 Two patterns of GCDII opacity caused by homozygous p.R124H mutations in *TGFBI*. A) A 35-year-old man presents with a conventional type I GCDII opacity, with confluent yet discrete grey/white spot-like opacities observed in the anterior stroma covering the central and paracentral regions of the cornea. Left, right eye. Right, left eye. **B)** A 28-year-old woman presents with a type II GCDII opacity, with reticular grey/white diffuse opacities interspersed with round translucent spaces observed in the anterior corneal stroma. Left, right eye. Right, left eye. Images and patient information obtained from Watanabe et al. (2001).

1.5 The transforming growth factor-β-induced gene and protein

The transforming growth factor-β-induced protein (TGFBIp), encoded by the transforming growth factor beta induced gene (*TGFBI*), was originally referred to as βig-H3 (TGFβ induced gene human clone 3), due to its discovery through induction of its expression following TGFβ administration in a human lung adenocarcinoma cell line (Skonier et al., 1992). In the literature it has also been referred to as keratoepithelin (Becker et al., 2006), collagen fibre associated protein (RGD-CAP) (Hashimoto et al., 1997) and MP78/70 (Gibson et al., 1997).

Human *TGFBI* maps to chromosome 5 in the region 5q31 and is a 34,924-nucleotide genomic gene sequence with only one isoform containing 17 exons which, following processing, becomes a 2,052-nucleotide coding sequence transcript encoding a 683 amino acid residue protein including a 23 residue N-terminal secretory signal peptide. TGFBIp is a secreted ECM protein. Its secreted form has a predicted molecular mass of 68kDa. Following cleavage of the signal peptide, the protein comprises an N-terminal

cysteine-rich domain of periostin and TGFBIp (CROPT) domain followed by four tandem fasciclin 1 (FAS1) domains (FAS1-1, FAS1-2, FAS1-3 and FAS1-4) and a C-terminal Arg-Gly-Asp (RGD) integrin-binding motif (Figure 1.13). The CROPT domain was previously referred to as an EMI domain due to sequence similarities. However, multiple sequence alignment revealed key differences between the now termed CROPT domain and an EMI domain, including a 29-residue long deletion, misalignment of two conserved cysteine residues and a four-read insertion into the EMI consensus motif (Lukassen et al., 2016). The 3D structure of TGFBIp resembles an elongated banana-like shape with the FAS1 domains arranged like beads on a string (Figure 1.14).

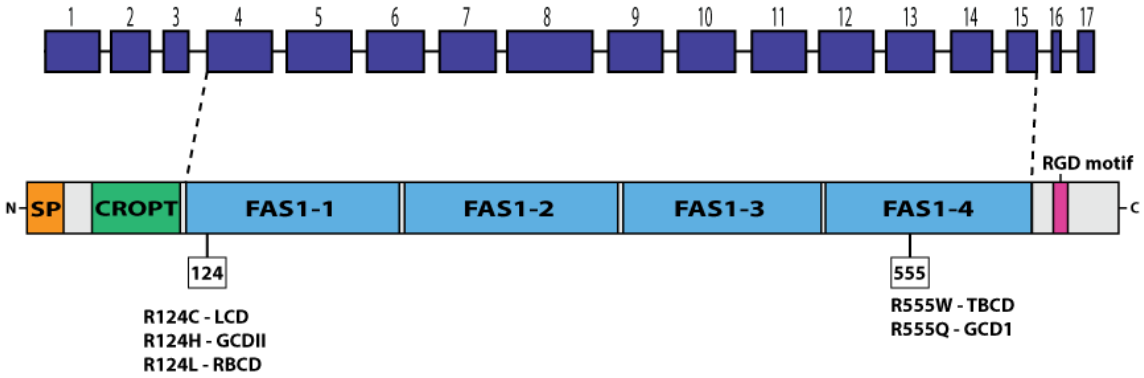

Figure 1.13 Schematic diagram of the *TGFBI* gene and TGFBIp structure displaying positions of selected reported CD-causing mutations and their associated phenotypes. TGFBIp is comprised of a 23 residue N-terminal secretory signal peptide (SP) domain followed by four tandem fasciclin 1 (FAS1) domains and a C-terminal Arg-Gly-Asp (RGD) integrin-binding motif. Exons have been drawn to scale; introns are not drawn to scale but are included to illustrate exon–intron boundaries. Transcript shown is NM_000358.

TGFBI is widely expressed in several human tissues and organs, including, the placenta, leukocytes, heart, ovaries, skin, intestine, prostate, testes, breast, spleen, thymus, liver, pancreas, lung and kidneys (Ivanov et al., 2008). In mice, *Tgfbi* is expressed during embryogenesis and development (Schorderet et al., 2000). Following birth, TGFBIp is produced by epithelial and stromal cells of the cornea (Escribano et al., 1994; Korvatska et al., 1999; Lisch & Seitz, 2014; Wittebol-Post et al., 1987). TGFBIp is expressed in all the layers of the human cornea and is the first and second most abundant protein in the corneal endothelium and stroma, respectively (Dyrlund et al., 2012). TGFBIp expression in the human cornea increases by around 30% between the ages of 6 and 14 (Karring et al., 2010).

TGFBIp is involved in numerous physiological processes, including cell adhesion, migration, wound healing, morphogenesis and inflammation (Gratchev et al., 2001; Thapa et al., 2005). The function of TGFBIp is not very well understood, though it is recognised that it acts as a linker protein, connecting various matrix molecules to each

other and facilitating cell-ECM interactions (Billings et al., 2002; Hanssen et al., 2003; Reinboth et al., 2006). Approximately 60% of TGFBIp is covalently bound to insoluble components of the ECM in human corneas through a disulfide bridge (Andersen et al., 2004). TGFBIp binds to type I, II, IV, VI and XII collagens, as well as various integrins, fibronectin and the proteoglycans biglycan and decorin (Billings et al., 2002; Hanssen et al., 2003; J. E. Kim, Jeong, et al., 2002; Reinboth et al., 2006; Runager et al., 2013; Son et al., 2013). However, the precise function of TGFBIp, particularly the role it plays in the cornea where it is highly expressed compared to other tissues, is still poorly understood.

1.5.1 Posttranslational modifications and multimerization of TGFBIp

TGFBIp has been reported to undergo several posttranslational modifications. Ser37 of TGFBIp undergoes phosphorylation (Bian et al., 2014). In addition, several TGFBIp cysteine residues form disulfide bridges (Figure 1.14). Wild type (WT) TGFBIp contains 11 cysteine residues, six of which are in the CROPT domain, one in the FAS1-1 domain and two in each of the FAS1-2 and FAS1-3 domains. Five disulfide bridges in TGFBIp have been identified. The CROPT domain encompasses two intradomain disulfide bridges (C49-C85 and C84-C97) and one interdomain disulfide bridge to FAS1-2 (C74-C339) (Lukassen et al., 2016). The cysteine residues in FAS1-3 (C473 and C478) form an intradomain disulfide bridge and the remaining cysteine residues in FAS1-1 and Fas1-2 (C214-C317) form an interdomain disulfide bridge (Lukassen et al., 2016). FAS1-4 is the only FAS1 domain of TGFBIp that is not stabilised by an interdomain or intradomain disulfide bond (Basaiawmoit et al., 2011). The majority of CD-causative mutations in TGFBIp are located throughout the fourth FAS1 domain, and its lack of disulfide bonds may be a contributing factor of pathogenicity for disease associated variants.

The CROPT domain residue C65 is not bound to another TGFBIp cysteine residue but is protected by a cysteinylation, implicating C65 as the candidate for the reducible cross-link between TGFBIp and XII collagen (Lukassen et al., 2016). No difference in the disulfide bond pattern of recombinant R124C-TGFBIp has been observed, rather it is cysteinylated (Lukassen et al., 2016), however, this has not yet been verified in the mutant protein’s endogenous form.

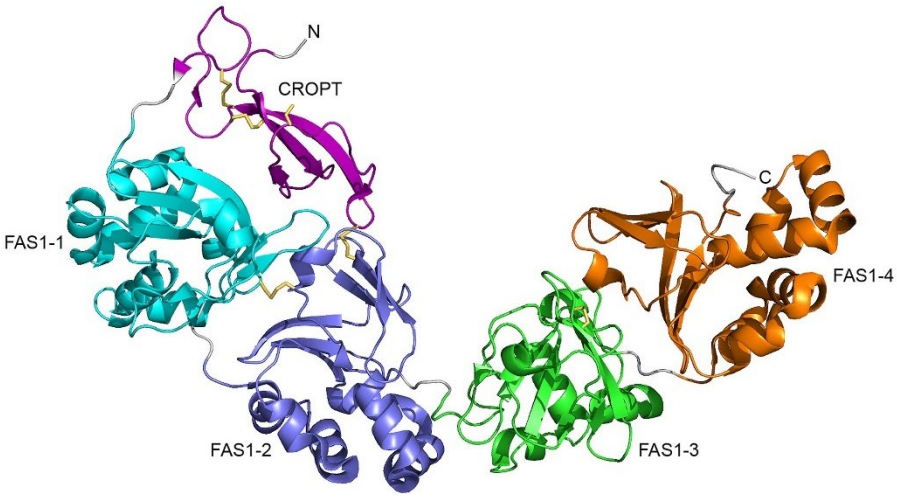

Figure 1.14 Ribbon plot of TGFBIp (residues 43-637). CROPT = magenta, FAS1-1 = cyan, FAS1-2 = blue, FAS1-3 = green and FAS1-4 = orange. Disulfide bridges and the unbound Cy65 are depicted in yellow. As the N-terminus and C-terminus of TGFBIp are highly flexible, the structure of these regions has not been determined. Adapted from Nielsen et al. (2020).

The most abundant form of TGFBIp in the mammalian cornea is truncated after residue A657, consequently removing 26 C-terminal residues, leaving the RGD motif exposed to allow for physiological interactions such as integrin binding (Andersen et al., 2004). This C-terminal cleavage of TGFBIp appears to occur following secretion and initiates the release of a C-terminal peptide containing the RGD sequence which induces apoptosis (J. E. Kim et al., 2003).

Multimerisation of TGFBIp has been observed at increased concentrations through a small-angle X-ray scattering model (Basaiawmoit et al., 2011). As TGFBIp is highly concentrated in the human cornea (Poulsen et al., 2018a) it is likely that TGFBIp exists in multimerised forms.

1.5.2 The TGFBIp paralog periostin

The gene *POSTN,* which encodes for the protein periostin, is considered to belong to the *TGFBI* gene family, along with *TGFBI.* Periostin is a glycoprotein of up to 93kDa and a paralog of TGFBIp, sharing a 47.97% sequence identity. Both TGFBIp and periostin are TGFβ-induced, secreted, integrin-binding ECM proteins that are expressed during cardiac development and are implicated in certain epithelial cancers (Conway & Molkentin, 2008; Ruan et al., 2009). The role of periostin in the development of bones, teeth and cartilage has also been documented (Hamilton, 2008; Kruzynska-Frejtag et al., 2004; Oshima et al., 2002).

TGFBIp and periostin have a similar domain structure (Figure 1.15) with a few main exceptions:

1. *TGFBI* has 17 exons compared to 23 exons in *POSTN.*
2. TGFBIp is shorter and lacks the C-terminal region that undergoes alternative splicing in *POSTN*.
3. *POSTN* lacks the RGD motif (Horiuchi et al., 1999). With the C-terminal region of periostin and TGFBIp being the major difference between the two, it is likely to be the main determinant of functional differences between the proteins. TGFBIp and periostin reportedly interact with each other through their CROPT domains (B. Y. Kim et al., 2009).

It is not known whether periostin plays a role in the pathogenesis of TGFBI CDs. In adult WT mouse corneas, *Postn* mRNA is not expressed and is therefore, not co-expressed with *Tgfbi* in this context (Poulsen et al., 2018b). However, periostin appears to be expressed in human corneal-derived cell lines and primary corneal fibroblasts and is also observed in TGFBIp+ GCDII deposits (B. Y. Kim et al., 2009). In *Tgfbi*$^{-/-}$ mouse corneas, no significant increase in *Postn* expression was observed in comparison to WT mice, indicating that periostin does not compensate for TGFBIp deficiency in the cornea and they are not interchangeable (Poulsen et al., 2018b). The GCDII-causative p.R124H mutation reportedly impairs the binding of periostin to TGFBIp (B. Y. Kim et al., 2009). This finding demonstrates that mutations in TGFBIp can impair its binding to other proteins and that impaired binding of periostin may be involved in the pathophysiology of GCDII.

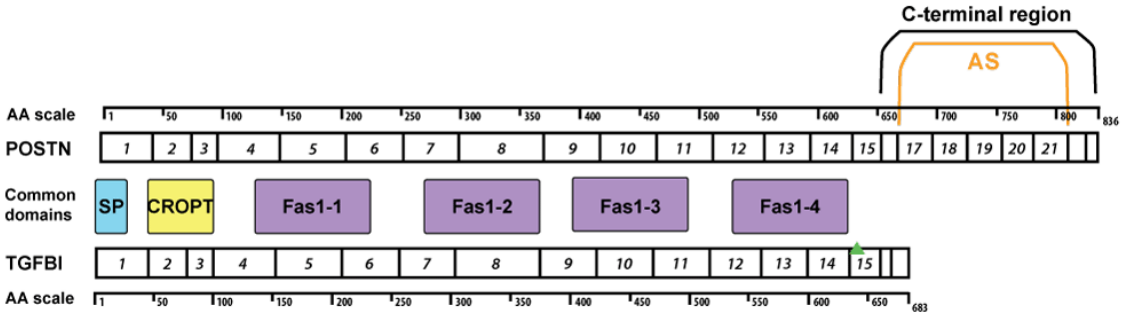

Figure 1.15 Comparison of *POSTN* and *TGFBI* exons and domain structure. *POSTN* and *TGFBI* exons (numbered) depicting the coding sequence are displayed to scale. Amino acid (AA) position scales for each protein are displayed above and below the exon structures of *POSTN* and *TGFBI*, respectively. Domains in common are displayed in the middle: SP = signal peptide, a CROPT domain and four FAS1 domains. The green triangle depicts the TGFBIp integrin binding site. The *POSTN* region between exons 16 and 22 is marked as subject to widespread alternative splicing (AS).

1.5.3 Mouse models of TGFBI dysfunction

Animal models of *Tgfbi*-linked CDs and *Tgfbi* dysfunction have been generated in order to aid the elucidation of CD pathophysiology. Bustamante et al., (2008) used a lentiviral

vector to generate a transgenic mouse model overexpressing *Tgfbi* containing the p.R555W mutation which causes GCDI. Although the mutation was successfully expressed by the mice, no corneal phenotype was observed. Transgenic p.R124H mutant mice have been established that display corneal opacities, with granular and lattice deposits observed in 45% of homozygous and 19.4% of heterozygous mice (Yamazoe et al., 2015). However, the model did not accurately depict the complexity of the human GCDII phenotype (Yamazoe et al., 2015). Additionally, a later publication using the same p.R124H transgenic mouse model reported no observations of deposits, suggested to be due to decreased expression of TGFBIp in mutant mice compared to WT (Lukassen et al., 2020).

Tgfbi p.R124C homozygous and heterozygous mutant mice have recently been generated using CRISPR/Cas9 technology (Kitamoto et al., 2020). At 20 weeks of age, 71.8% of homozygous mice displayed corneal opacity, whereas no corneal opacity was observed in the heterozygous mice under 24 weeks of age. In the corneas of *Tgfbi* p.R124C homozygous mice, significant TGFBIp expression was observed in all layers of the cornea, whereas in WT mice, only the corneal epithelium displayed significant TGFBIp staining. *Tgfbi* mRNA expression levels were also higher in homozygous mice compared to heterozygous and WT mice. These findings indicate dysfunction of p.R124C *Tgfbi* clearance in the mice and abnormal TGFBIp turnover. Deposits were amorphous in nature and amyloid deposition was not observed in this model. Therefore, the complexity of human LCD-causative p.R124C mutation in *TGFBI* is not accurately represented, either due to species differences or that sufficient time was not given for amyloid deposition to occur.

Interestingly, *Tgfbi*$^{-/-}$ mice did not exhibit structural or histological differences in the cornea in comparison to WT control (Poulsen et al., 2018). Minor changes in collagen fibril diameter and interfibrillar spacing of *Tgfbi*$^{-/-}$ mouse corneal stromas was observed in comparison to WT controls. Differential expression of 11 proteins in *Tgfbi*$^{-/-}$ mice was noted in comparison to WT controls, six of which are involved in the assembly of the collagen scaffold and cell adhesion to the ECM (Poulsen et al., 2018). These findings suggest that depletion of TGFBIp in the cornea would not be detrimental and could be a feasible method of treating *TGFBI*-linked CDs.

In mice it seems that TGFBIp is only robustly expressed in the corneal epithelium, suggesting continuous secretion and deposition of TGFBIp from the corneal epithelium into the stroma (Poulsen et al., 2018). This led to the assumption that expression

followed a similar pattern in the human cornea. It is also apparent that TGFBIp is 10-fold more abundant in the human cornea than in mice (Poulsen et al., 2018).

It is important to note discrepancies between the mouse and human corneas when extrapolating mouse models of corneal disease to humans. Mouse corneas are thicker in the centre than in the periphery, whereas human corneas are thinner in the centre and thicker in the periphery (Henriksson et al., 2009). These interspecies differences in morphology perhaps indicate differences in functional mechanisms between human and mouse corneas. Furthermore, the mouse corneal epithelium constitutes ~30% of total corneal thickness with the stroma making up ~70%. In contrast, the corneal epithelium constitutes ~10% and the stroma ~90% of total thickness of the human cornea (Henriksson et al., 2009). The discrepancies in cellular make up between the mouse and human cornea could imply differences in the corneal aggregation process of TGFBIp in these tissues between species.

Collectively, these findings indicate that we cannot fully extrapolate findings in mouse models of TGFBIp expression and dysfunction to human context. It is apparent that human CD-causative mutations in *TGFBI* do not result in a comparably severe phenotype in mice, with predominately homozygous animals demonstrating a phenotype. A model more relevant to human TGFBI CDs is required to gain valuable information of the pathogenesis of the disease.

1.5.4 TGFBI in development

The *TGFBI* gene is conserved in vertebrates (X. Song et al., 2014) and its spatiotemporal expression has been investigated during the embryogenesis of several species. *Tgfbi* knockout (KO) mice are viable, but have reduced skeletal size due to defective periosteal bone formation, indicating that its expression is important for the development of skeletal tissues and the cartilage matrix (J. M. Lee et al., 2015; H. Yu et al., 2012). During mouse embryogenesis, predominant *Tgfbi* expression is observed in mesodermal, collagen-rich connective tissue (Ferguson, Mikesh, et al., 2003). In the mouse eye, *Tgfbi* expression is first observed during the development of the mesenchymal tissue surrounding the optic cup, where it then extends towards the sclera and eventually reaches the cornea (Schorderet et al., 2000).

During chicken embryogenesis, *Tgfbi* expression is also predominantly expressed in mesodermal tissues, including the developing heart (Norris et al., 2004). During zebrafish embryogenesis, *Tgfbi* is extensively expressed (Hirate et al., 2003) in particular, its importance in the formation of proper linkage of the ECM to the cytoskeleton of muscle fibres has been demonstrated (H. R. Kim & Ingham, 2009). Similarly in the developing

Xenopus, *Tgfbi* is widely expressed, and its depletion resulted in a phenotype similar to that caused by canonical Wnt pathway inhibition and was accordingly identified as a regulator of the canonical Wnt pathway (F. Wang et al., 2013). *TGFBI* was observed to be more highly expressed in cells of the developing human heart than in cells obtained from the adult heart (Chan et al., 2003), further demonstrating its importance during development.

1.5.5 TGFBIp in the ECM

TGFBIp is a component of the ECM of various tissues including bone marrow (Klamer et al., 2018), skin (LeBaron et al., 1995), cartilage (Brachvogel et al., 2013; Ohno et al., 2002), kidney (S. H. Lee et al., 2003) and muscle (Ferguson, Thoma, et al., 2003). TGFBIp interacts with a diverse array of integral ECM components, with approximately 60% of the protein being covalently bound to the insoluble portion of the ECM in both human and porcine corneas (Andersen et al., 2004).

Integrins are the primary receptors used by animal cells for cell-ECM binding. TGFBIp is recognised to bind to cell surfaces through several forms of integrin receptors on fibroblasts (J. E. Kim et al., 2000; Ohno et al., 1999), epidermal cells (Bae et al., 2002), endothelial cells (M. Liu et al., 2021; Son et al., 2013), corneal stromal cells (S. Il Choi et al., 2015) and corneal epithelial cells (J. E. Kim et al., 2000). The integrins αVβ3 and αVβ5 are the most studied in relation to TGFBIp binding, with only integrin αVβ5 being expressed in the cornea (S. Il Choi et al., 2015; J. E. Kim, Jeong, et al., 2002; J. O. Nam et al., 2003; Rayner et al., 1998; Son et al., 2013; Thapa et al., 2005). Interactions between integrins and TGFBIp are dependent on the RGD motif in several cases, although the repeated FAS1 domains of TGFBIp also have binding affinity (S. Il Choi et al., 2015; J. O. Nam et al., 2003; Ohno et al., 1999; Son et al., 2013).

TGFBIp is also reported to interact with various ECM proteins, including its paralog periostin through their CROPT domains (B. Y. Kim et al., 2009). TGFBIp also binds to other ECM proteins including fibronectin (Billings et al., 2002), laminin (J. E. Kim, Park, et al., 2002) and the small leucine-rich PGs biglycan and decorin (Reinboth et al., 2006).

Collagens have been identified as TGFBIp interaction partners in several contexts. Collagen XII belongs to the FACIT group of collagens and has been associated with the assembly of the corneal matrix and maintenance of corneal stability (Marchant et al., 2002; Young et al., 2002). TGFBIp and collagen XII are reported to bond in the human and porcine cornea at a stochiometric ratio of 2:1 (Runager et al., 2013). Collagen XII is bound to straited collagen fibres of the ECM, therefore, its interaction with TGFBIp is expected to form a cell anchor to the ECM through integrin-bound TGFBIp (Runager et

al., 2013) (Figure 1.16). Collagen VI is a fibrillar collagen that is highly expressed in the human cornea (Zimmermann et al., 1986). TGFBIp and collagen VI have been reported to interact in the rabbit cornea (Rawe et al., 1997) and bovine ligament (Hanssen et al., 2003). TGFBIp has also been shown to interact with the fibrillar collagen types I, II and IV in porcine cartilage (Hashimoto et al., 1997).

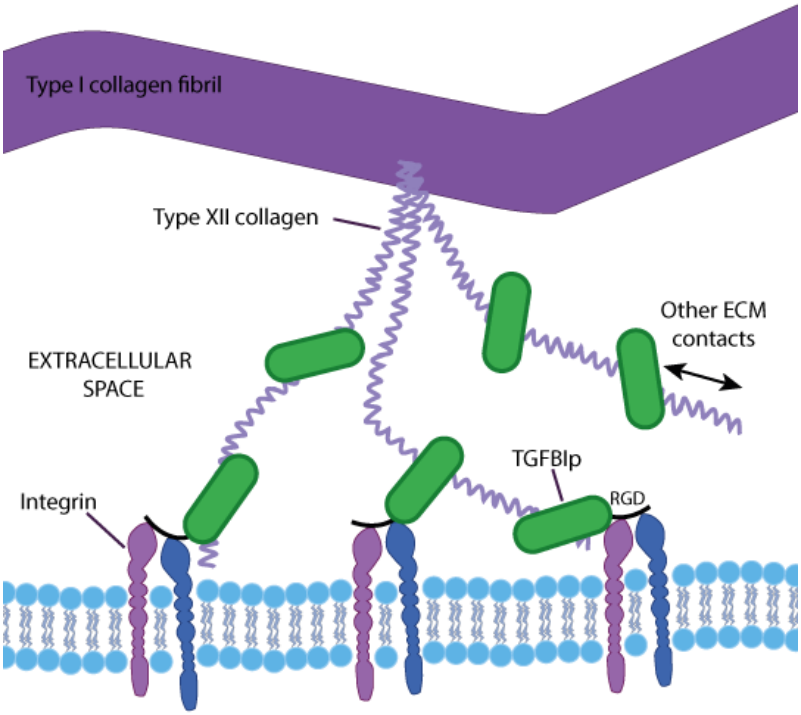

Figure 1.16 Proposed mechanism of TGFBIp-type XII collagen interactions in the cornea. TGFBIp binds to cell surfaces through integrin binding. In the corneal ECM, TGFBIp interacts with collagen XII, which has been shown to interact with type I collagen fibres. Figure based on Runager et al. (2013).

1.5.6 TGFBIp in tumorigenesis

Aside from its role in numerous phenotypes of corneal dystrophy, TGFBIp has been reported to play a dual role in cancer as both a suppressor and promoter of tumorigenesis (Ween et al., 2012). The expression and role of TGFBIp in cancerous cells appears to be specific to cell type and is influenced by TGFBIp processing and concentration.

TGFBIp has been shown to be downregulated in ovarian cancer with evidence suggesting that it plays a tumour suppressor role by supporting ovarian cancer cell death (Ween et al., 2012). Hypermethylation of *TGFBI* has been observed in ovarian, lung and prostate cancer cells, implicating *TGFBI* gene silencing as a carcinogenic process (Kang et al., 2010; Shah et al., 2008). Chemotherapy-resistant ovarian cancer cells treated with TGFBIp demonstrated restoration of chemotherapy sensitivity through integrin-dependent microtubule stabilisation (Ahmed et al., 2007). Similarly, non-small cell lung

cancer (NSCLC) cells also demonstrated an improved response to chemotherapy that was positively correlated with TGFBIp expression (Irigoyen et al., 2010). TGFBIp-mediated induction of apoptosis NSCLC cells occurred through TGFBIp-proteolytic fragment binding to αvβ3 integrin, but not through binding of the full-length protein, demonstrating the effect of proteolytic processing in the role of TGFBIp in cancer (Irigoyen et al., 2010). Other studies have reported TGFBIp as a tumour suppressor in cancer of various tissues such as lung, bone, prostate and breast (Shao et al., 2006; Wen, Partridge, et al., 2011; Zamilpa et al., 2009). These findings are supported by Tgfbi$^{-/-}$ mice that are predisposed to spontaneous tumour development (Y. Zhang et al., 2009).

In contrast, TGFBIp has been reported to promote cancer cell invasion and metastasis, linking elevated TGFBIp expression to tumour aggression (Guo et al., 2011; M. O. Kim et al., 2003; C. Ma et al., 2008; Sasaki et al., 2002; Tang et al., 2007; Zajchowski et al., 2001). The role of TGFBIp as a promoter of tumorigenesis has been observed in cancers of the lung, pancreas, brain and colon (Corona & Blobe, 2021). TGFBIp has also been found to be highly expressed by peritoneal cells, this can work to promote the metastatic behaviour of ovarian cancer cells by promoting their attachment to peritoneal cells (Ween et al., 2011). Overall, the effect of TGFBIp expression in cancer appears to depend on the tumour microenvironment.

1.5.7 TGFBI regulation

Regulation of *TGFBI*/TGFBIp expression is not very well understood and yet to be defined. As with most pleiotropic proteins, TGFBIp is expected to be regulated in a cell- and tissue-specific manner.

1.5.7.1 TGFβ signalling

As TGFBIp was first discovered via its induction following TGFβ1 treatment (Skonier et al., 1992), understanding of the evolutionarily conserved TGFβ signalling pathway is important.

The human TGFβ family is comprised of 33 related homodimeric or heterodimeric ligands and includes three TGFβ isoforms (TGFβ1, 2 and 3), activins, nodal, bone morphogenetic proteins (BMPs), and growth and differentiation factors (GDFs) (Morikawa et al., 2016). TGFβ family ligands bind to three classes of cell surface receptors, TGFβR1, TGFβR2, TGFβR3 and are able to induce the canonical (SMAD-dependent) and non-canonical (SMAD-independent) pathways.

The canonical TGFβ signalling pathway is activated upon TGFβ ligand binding to the serine/threonine kinase receptor TGFβR2 receptor, which then recruits and activates the

TGFβR1 receptor (also known as activin receptor–like kinases (ALKs)). This activation leads to the phosphorylation of receptor-activated SMADs (R-SMADs) SMAD2/3 (for TGFβ/2/3, activins and NODAL ligands) or SMAD1/5/8 (for BMP and GDF ligands), which then form a complex with the common mediator SMAD (Co-SMAD), SMAD4, and translocate into the nucleus where they regulate target gene transcription (Massagué & Wotton, 2000; S. Ross & Hill, 2008). In the nucleus, the R-SMADs and Co-SMAD complex bind to DNA and interact with various transcription factors, co-activators, and co-repressors to regulate target gene expression. This canonical pathway is involved in several cellular processes, including cell proliferation, differentiation, apoptosis, and extracellular matrix production (Blank & Karlsson, 2011; Clayton et al., 2020; B. Song et al., 2009; Ueberham & Arendt, 2013).

The non-canonical TGFβ signalling pathway does not rely on the SMAD proteins but involves various other signalling pathways such as the mitogen-activated protein kinase (MAPK) pathway which includes the extracellular signal-regulated kinases (ERKs), c-Jun amino terminal kinase (JNK) and p38 MAPK pathways; and the phosphoinositide 3-kinases (PI3Ks) pathway. In the context of TGFβ signalling, these pathways are known as the non-SMAD pathways and can be activated through the TGFβ receptors leading to activation of the tyrosine kinase receptors (TKRs). The non-SMAD transducers Erk, JNK, p38 MAPK and PI3K can mediate signalling as independent pathways or in conjunction with SMADs (Y. E. Zhang, 2017). The non-canonical pathway is involved in various cellular processes, including epithelial to mesenchymal transition, cell migration, apoptosis and cytoskeletal rearrangement (Moustakas & Heldin, 2005).

1.5.7.2 Regulation of *TGFBI* expression

Regulation of *TGFBI* expression is complex, poorly understood and likely to differ in different tissue-specific contexts. It is known that TGFβ is able to induce *TGFBI* expression and this has been demonstrated in multiple cell types, including corneal epithelial cells (M. X. Wang et al., 2002; Yellore et al., 2011), corneal stromal cells (S. Il Choi et al., 2016), dermal fibroblasts (LeBaron et al., 1995) and pancreatic cancer cells (Schneider et al., 2002).

The promoter region of *TGFBI* was investigated by Yuan et al. (2004), who initially located a 5’ region 1 Kb upstream of the gene in a human adenocarcinoma cell line and went on to verify the region in a number of other cell types, including primary corneal epithelial cells. Numerous putative transcription factor-binding sequences and five SMAD binding elements were also identified within this region, elucidating a potential regulatory mechanism of TGFBIp expression via TGFβ signal transduction. Another

study found that although TGFBIp expression was upregulated following TGFβ administration in an epidermal cell line, this effect was abolished following treatment with the protein synthesis inhibitor cycloheximide, indicating that TGFBIp is not a direct target of TGFβ and that the synthesis of other proteins is required for its induction (Akiyoshi et al., 2001). Additionally, iPSCs derived from patients with mutations in ribosomal protein coding genes, causative of Diamond Blackfan Anemia, demonstrated an upregulation of *TGFBI* and other TGFβ target genes, along with an increase in the non-canonical TGFβ signalling pathway mediator p-JNK and a decrease in the canonical TGFβ mediator SMAD4 in comparison to WT iPSCs (J. Ge et al., 2015). This is supported by a study that demonstrated that activation of the JNK pathway increased TGFBIp expression (Nie et al., 2020). However, reduction of the canonical TGFβ signalling pathway has also been shown to reduce *TGFBI* expression in lymphoblastoid cell lines (Wood et al., 2007). Altogether, the data indicates that *TGFBI* induction may occur through the canonical and non-canonical TGFβ pathways and this is likely to be context dependent.

Other than TGFβ-dependent induction of TGFBIp, other factors have been shown to upregulate *TGFBI* expression, such as, IL-4 in activated macrophages (Gratchev et al., 2001), retinoic acid in breast carcinoma cells (Dokmanovic et al., 2002) and IL-1β and TNF-α in fibroblast-like synoviocytes (E. J. Nam et al., 2006).

miRNA regulation of *TGFBI* expression has also been demonstrated, specifically, miR-9, miR-21 and miR-181a have been shown to downregulate *TGFBI* expression in corneal stromal cells (S. Il Choi et al., 2016), with evidence suggesting that miR21 directly regulates TGFBIp expression at the 3' untranslated region (UTR) of the *TGFBI* gene (C. Liu et al., 2011). Interestingly, previous reports have indicated that miR-21 and miR-181a expression is upregulated by TGFβ (S. Il Choi et al., 2016; Taylor et al., 2013), which potentially represents a feedback loop where TGFβ is able to positively and negatively regulate *TGFBI* expression. Through activation of miR-21, TGFβ has been shown to inhibit the SMAD2/3 inhibitor SMAD7, by direct binding of the *SMAD7* 3' UTR (Q. Li et al., 2013), potentially indicating that miR-21 can inhibit *TGFBI* expression through binding of its 3' UTR and increase expression of *TGFBI* through activation of TGFβ signalling by reducing the association of SMAD 2/3 with SMAD7. Altogether, the complexities of *TGFBI* regulation are clear, and there is much still to be elucidated on this topic.

Specific integrin receptors, such as, αVβ5, αVβ6, and αVβ8, can bind to latent TGFβ which results in its activation (Van Caam et al., 2020). Immunoprecipitation experiments have demonstrated that TGFBIp is able to indirectly regulate TGFβ signalling through

competition of TGFβ1 and TGFBIp for integrin binding (Bissey et al., 2018). Accordingly, TGFBIp has also been shown to regulate the non-canonical TGFβ PI3K/Akt pathway in a mesothelium cell line, as PI3K/Akt signalling was more active following *TGFBI* depletion (Wen, Hong, et al., 2011). Therefore, TGFBI may be able to regulate the TGFβ signalling pathway through a feedback loop mechanism.

1.5.8 Hypermutability of the p.R124 and p.R555 hotspots

Many of the same proteins and signalling pathways exist in diverse cell types and tissues where they perform specialised functions (Schaefer et al., 2014). TGFBIp appears to fit into this category of proteins as it plays a role in a variety of processes within different cell types and tissues and interacts with a range of other proteins. TGFBIp sequence motifs are highly conserved across vertebrates (X. Song et al., 2014). Positive selection sites in the evolutionary history of *TGFBI* have been identified, indicating that the gene architecture of *TGFBI*, including its domain losses and duplications, could correlate with its positive selection (X. Song et al., 2014).

The p.R124 and p.R555 hotspots of TGFBIp are hypermutable and although TGFBIp is widely expressed in human tissues, these mutations only display a phenotype in the cornea. It has been suggested that the p.R124 and p.R555 mutational hotspots are a product of survivorship bias, as it is likely that few other nonsynonymous *TGFBI* mutations are mild enough to survive germ cell differentiation, maturation, fertilisation and embryogenesis – processes in which TGFBIp is reportedly involved (N. S. Nielsen et al., 2020). Other mutations in *TGFBI* with more detrimental effects are likely to have been filtered out of the human genome by negative selection.

Haplotype analysis of 10 families harbouring either p.R124 or p.R555 missense mutations determined that these mutations have arisen independently numerous times in several ethnic groups and that they are not derived from a common founder (Korvatska et al., 1998). This finding indicates that these mutations arose *de novo* in independent families, demonstrating the mutable propensity of these hotspots.

It is not a coincidence the two mutations representing the majority of TGFBI CDs, p.R124 and p.R555, both undergo substitutions at arginine codons containing cytosine-guanine (CpG) dinucleotides. Arginine is the most commonly substituted amino acid, underlying 20% of all pathogenic single-nucleotide variants (Landrum et al., 2016; Schulze et al., 2020). This is likely because arginine is the only amino acid to contain CpG dinucleotides at the first and second codon positions. The number of nonsynonymous single-nucleotide variants affecting arginine are extraordinary relative to other amino acids (Schulze et al., 2020). Arginine substitutions are most frequently cytosine to thymine

(C>T) and guanine to adenine (G>A) transitions (Schulze et al., 2020), this is mirrored in *TGFBI*-linked CDs with the most common missense p.R124 and p.R555 mutations undergoing these transitions.

CpG dinucleotides have particularly hypermutable propensities in vertebrate genomes. This tendency is due to the deamination of methylated cytosine to yield thymine, in the instance this occurs in germlines, heterozygous mutant alleles are introduced in offspring. It is probable that this is how the *TGFBI* p.R124 and p.R555 hotspots emerged.

1.6 Thesis aims

Pathogenic missense mutations in *TGFBI* cause the accumulation of extracellular protein deposits in the cornea. This pathogenesis occurs in the highly tissue-specific context of the human cornea, and cannot be properly recapitulated by mouse models. The tissue-specific functions of TGFBI in the cornea and the different underlying molecular mechanisms leading to the different phenotypes of TGFBI CD pathogenesis are not understood.

In order to build on the currently known insights into TGFBI CD pathology and facilitate the screening of a therapeutic that targets the underlying genetic cause of disease in an appropriate genomic and cellular context, the development of a novel, patient-derived *in vitro* model is necessary. In the generation of this model, TGFBI CD patient-derived iPSC lines were established and differentiated into corneal epithelial-like (CEpi) cells. The current study aimed to utilise this model in the identification of TGFBI CD molecular disease mechanisms by transcriptomic analysis.

Furthermore, the development of new treatments that target the underlying genetic cause of TGFBI CD is urgently required. The current study aimed to utilise the *in vitro* CEpi model system to demonstrate proof-of-concept of antisense oligonucleotide (ASO)-induced reduction of *TGFBI* in a mutant allele-specific manner. The objective of the prospective antisense ASO treatment is to offer a highly effective preventative gene-directed therapeutic approach for TGFBI CD.

To summarise, the primary aims of the thesis were:

1. To establish induced pluripotent stem cell (iPSC) lines from TGFBI CD patients harbouring two of the most common heterozygous pathogenic mutations in *TGFBI*.
2. To generate and characterise the corneal epithelial cells differentiated from patient and control iPSCs.
3. To compare the transcriptome of patient and control corneal epithelial-like cells in order to identify possible mechanisms of disease.
4. To develop an antisense oligonucleotide-based therapy that reduces *TGFBI* expression in an allele-specific manner.

Chapter 2: Materials and Methods

All materials and consumables are listed in Appendix A.

2.1 General laboratory methods

2.1.1 Genomic DNA (gDNA) extraction

Total gDNA from cell samples was extracted using the Wizard gDNA Purification Kit (Promega) following the manufacturer's guidelines. Briefly, cells were first washed with Dulbecco's phosphate buffered saline (DPBS; Gibco) and lysed using the SV buffer kit component. DNA purification of the samples was carried out using Wizard SV Mini columns and wash buffers by centrifugation at 13,000 g for 1 minute per step. 250 µl of nuclease-free water was used for gDNA elution and was subsequently quantified by spectrophotometry using a Nanodrop 2000 (Thermo Fisher).

2.1.2 RNA extraction and cDNA synthesis

Total RNA was extracted using either the RNeasy Mini Kit for cells cultured in 6-well plates or the RNeasy Micro Kit for cells cultured in 12-well plates (both Qiagen). Following an initial wash with DPBS, cells were lysed directly in the well using RLT buffer, following the procedure as recommended by the manufacturer. Samples were passed eight times through a blunt 20-gauge needle (0.9 mm diameter, Fisher Scientific) and 1ml syringe (Fisher Scientific) for homogenisation. The RNA extraction was carried out following the manufacturer's instructions. Both kits use silica membranes to bind RNA, followed by successive ethanol washes. gDNA contamination was removed by incubation with DNAse I (DNAse kit, Qiagen) for 15 minutes at room temperature (RT). Total RNA was eluted in 30 µl (RNeasy Mini Kit) or 14 µl (RNeasy Micro Kit) and quantified using nanodrop spectrophotometry for subsequent cDNA synthesis. Remaining samples were stored at -80°C.

cDNA was synthesised (tetro cDNA synthesis, Bioline) using equal quantities of total RNA for each sample (ranging between 500 ng and 1 µg) and added to a master mix containing the following components: 1 µl oligo (dT)18 primer, 1 µl random hexamer primer, 1 µl 10 mM deoxynucleotides (dNTP) mix, 4 µl 5X reaction buffer, 1 µl RiboSafe RNAse Inhibitor and 1 µl Tetro Reverse Transcriptase (200 U/µL), reaching a final volume of 20 µl per reaction.

The reaction was incubated in a thermocycler using the following conditions:

1. 45°C for 1 hour
2. 85°C for 5 minutes

cDNA was stored either short term at 4°C or long term at -20°C, before being used for Reverse Transcription Polymerase Chain Reaction (RT-PCR) and/or quantitative PCR (qPCR).

2.1.3 Polymerase Chain Reaction (PCR) and Reverse Transcription PCR (RT-PCR)

Primers for gDNA/cDNA analysis were designed using NCBI Primer-BLAST (ncbi.nlm.nih.gov/tools/primer-blast). Target gene sequences were either inputted using their RefSeq ID or obtained through the Ensembl Gene Browser (ensemble.org). For the purpose of avoiding amplification of any residual gDNA contamination, exon-spanning primers were designed for cDNA amplification by RT-PCR. Plasmid DNA amplification for the pluripotency assay was carried out using primers designed to target episomal vector sequences, pCXLE-hUL (Addgene #27080), pCXLE-hSK (Addgene #27078) pCXLE-hOCT3/4-shp53-F (Addgene #27077). A full list of the primer sequences is specified in Table 2.1.

gDNA/cDNA amplification was conducted using standard PCR methods. A reagent master mix was prepared using 2x GoTaq Green master mix (Promega), 0.2 µM forward and reverse primers and double distilled water (ddH2O). 50 ng of gDNA or cDNA was loaded per 25 µl reaction before incubation in a thermocycler using the conditions specified below, with slight adaptations made to the number of cycles and extension and/or annealing temperature in the optimisation of conditions for specific primer pairs:

1. Denaturation step:
    a. 2 min at 95°C
2. Annealing + Extension step (repeated 30 times):
    a. 30 sec at 95°C
    b. 30 sec at 60°C
    c. 30 sec at 72°C
3. Final Extension step
    a. 5 min at 72°C

PCR products were run on a 2% (w/v) agarose (Bioline) gel containing 0.005% (v/v) Safeview nucleic acid stain (NBS Biologicals) and visualised using a BioRad ChemiDoc XRS+ (BioRad) and ImageLab software (BioRad).

2.1.4 PCR product purification

PCR products were purified using MultiScreen® PCR µ96 Filter Plate (Millipore). Briefly, the PCR reaction mix was diluted using ddH2O to a volume of 100 µl and pipetted into a

well of the filter plate. The plate was attached to a vacuum suction pump, where the excess liquid was filtered out and the DNA was bound to the membrane. Following a wash with 50 µl ddH2O, the plate was removed from the suction vacuum and the DNA was eluted in 25 µl of ddH2O by gentle agitation using a vortex for 10 minutes at RT.

Table 2.1 Primers used for PCR and RT-PCR reactions in the study. CDS = coding sequence, E = exon.

Gene target	Forward sequence	Reverse sequence	TA (ºC)
OCT3/4 CDS	CCCCAGGGCCCCATTTTGGTACC	ACCTCAGTTTGAATGCATGGGAGAGC	60
OCT3/4 plasmid	CATTCAAACTGAGGTAAGGG	TAGCGTAAAAGGAGCAACATA	60
SOX2 CDS	TTCACATGTCCCAGCACTACCAGA	TCACATGTGTGAGAGGGGCAGTGTGC	60
SOX2 plasmid	TTCACATGTCCCAGCACTACCAGA	TTTGTTTGACAGGAGCGACAAT	60
L-myc CDS	GCGAACCCAAGACCCAGGCCTGCTCC	CAGGGGGTCTGCTCGCACCGTGATG	60
L-myc plasmid	GGCTGAGAAGAGGATGGCTAC	TTTGTTTGACAGGAGCGACAAT	60
Lin28 CDS	AGCCATATGGTAGCCTCATGTCCGC	TCAATTCTGTGCCTCCGGGAGCAGGTTAGG	60
Lin28 plasmid	AGCCATATGGTAGCCTCATGTCCGC	TAGCGTAAAAGGAGCAACATA	60
TGFBI E4 gDNA	GTCAGAGAAGGGAGGGTGTG	AGCTTAACCCCAGAAACCA	60
TGFBI E4 cDNA	ATCAGCTACGAGTGCTGTCC	TGCCGTGTTTCAGCTCATCA	60

2.2 Sanger sequencing

DNA concentration was quantified by spectrophotometry using a Nanodrop 2000 (Thermo Fisher) and samples were sent to Source Biosciences (Cambridge), where Sanger sequencing was conducted using forward and reverse primers. PCR products were sequenced following a BigDye terminator sequencing protocol and analysed using an ABI PRISM 3100 Genetic Analyser (Applied Biosystems). Sequencing results were analysed using benchling (benchling.com).

2.3 Immunocytochemistry

Cell samples were washed with PBS and fixed in 4% (v/v) paraformaldehyde (PFA, Thermo Fisher) for 10 mins at RT. Samples were then permeabilised using 0.1% Triton-X100 (v/v; Sigma) for 15 minutes before being blocked using a solution containing 0.3% (w/v) bovine serum albumin (BSA, Sigma), 10% (v/v) normal donkey serum (NDS, Sigma) for 1 hour at room temperature (RT). Primary antibodies (Table 2.2) were diluted at the appropriate concentration in the blocking solution and incubated for 1 hour at RT. The primary antibody solutions were then aspirated and samples were subsequently washed 3x with PBS. Samples were then incubated with secondary antibodies that reacted against the primary antibody species (Table 2.3) for 1 hour at RT, before being washed 3x with PBS. Nuclei counterstaining was subsequently carried out using 4',6-diamidino-2-phenylindole dilactate (DAPI, Sigma, 1:5000) and slides were mounted using Dako fluorescent mounting medium (Dako).

Table 2.2 Primary antibodies used in immunocytochemistry experiments.

Antigen	Host	Clone	Isotype	Supplier	Catalogue number	Dilution
K3	Mouse	AE5	IgG	Abcam	AB77869	1:200
P63α	Rabbit	Polyclonal	IgG	NEB	4892	1:800
K12	Rabbit	EPR17882	IgG	Abcam	AB185627	1:200
K14	Rabbit	EPR17350	IgG	Abcam	AB181595	1:200
E-Cadherin	Rat	DECMA-1	IgG1	Abcam	AB11512	1:500
Cx43	Rabbit	Polyclonal	IgG	Abcam	AB11370	1:400
PAX6	Sheep	Polyclonal	IgG	Biotechne	AF8150	1:200
K5	Mouse	XM26	IgG1	Invitrogen	MA5-12596	1:400
TGFBI	Goat	Polyclonal	IgG	Abcam	AB99562	1:200
Nanog	Mouse	23D23C6	IgG	Invitrogen	MA1-017	1:150
Oct4	Rabbit	Polyclonal	IgG	Abcam	Ab19857	1:1000
SSEA4	Mouse	MC813	IgG3	Cell Signalling Technologies	4755	1:300
TRA-1-81	Mouse	cl.2A6	IgG	NEB	4745	1:1000

Table 2.3 Secondary antibodies used in immunocytochemistry experiments.

Antigen	Host	Fluorophore	Supplier	Catalogue number	Dilution
Rat IgG	Donkey	Alexa Fluor 488	Invitrogen	A21208	1:1000
Mouse IgG	Donkey	Alexa Fluor 488	Invitrogen	A21202	1:1000
Rabbit IgG	Donkey	Alexa Fluor 488	Invitrogen	A21206	1:1000
Mouse IgG	Donkey	Alexa Fluor 555	Invitrogen	A31570	1:1000
Rabbit IgG	Donkey	Alexa Fluor 555	Invitrogen	A31572	1:1000
Goat IgG	Donkey	Alex Fluor 488	Invitrogen	A11055	1:1000
Sheep IgG	Donkey	Alexa Fluor 488	Invitrogen	A11015	1:1000

2.4 Imaging and analysis

Confocal images were obtained using the Carl Zeiss LSM 700 laser-scanning confocal microscope (Zeiss, Germany). Proteins were visualised using a 546 nm excitation HeNe laser, a 488 nm argon ion laser and a 405 nm excitation diode laser. Different magnifications were utilised to obtain images of wider fields and to visualise cell populations, or to obtain a closer view of subcellular protein localisation. Fluorescence intensities were optimised to reduce photo bleaching and avoid saturation, and images were captured as maximum intensity projections using Z-stacks. Images were exported using the Zen 2009 and processed using Fiji (imagej.net/Fiji).

2.5 Protein extraction and quantification

For the extraction of total protein, cells were washed using cold PBS and lysed in cold radioimmunoprecipitation buffer (RIPA; see Appendix A for formulation) containing 2% (v/v) protease inhibitor cocktail (Sigma) and 1% (v/v) Phosphatase inhibitor cocktail (Sigma). Cell lysates were centrifuged at 13,000 g for 10 mins at 4°C for the removal of cellular and DNA debris. For the collection of secreted TGFBIp, cells were cultured in serum free media prior to collection and then centrifuged at 13,000 g for 10 mins at 4°C for removal of cellular debris. Samples were collected and stored at -80 ºC before being quantified.

Protein quantification was conducted using the Pierce Bicinchoninic acid (BCA) Protein Assay (Thermo Fisher) according to the manufacturer's instructions. Diluted cell lysates and supernatants were aliquoted into 96 well flat bottom plates. Known dilutions (25-2000 µg/ml) of bovine serum albumin (BSA) protein (Sigma), were also loaded into different wells of the plate for the generation of a standard curve. Both the samples of interest and the known dilutions were assayed in duplicate. 200 µl BCA Working Reagent was added to all samples and known dilutions. Following loading of the plate, the plate was incubated for 30 mins at 37°C, and a change in colour depending on the protein

concentration of the samples was observed. Quantification of absorbance at 562 nm was carried out using a spectrophotometer (Safire, Tecan) and the final sample concentrations were calculated through extrapolation of the BSA standard curve to the linear regression generated.

2.6 Western blotting

Following the extraction and quantification of samples, equal concentrations of each sample were mixed with sample loading buffer containing 150 mM Tris-HCl pH 7, 25% glycerol, 12% SDS, 0.05% bromophenol blue and 6% b-mercaptoethanol; boiled at 98°C for 3 minutes, and subsequently loaded into 8% acrylamide gels (see formulation in Appendix A), along with CozyHi ™ Prestained Protein Ladder (HighQu), and run at 100 volts for around one hour, or until the samples ran close to the bottom of the gel. Proteins were transferred from the gel onto a nitrocellulose membrane by wet transfer, at 100 volts for 90 minutes in cold transfer buffer (see formulation in Appendix A). Successful protein transfer was confirmed using Ponceau staining, followed by incubation of the membrane with 5% (w/v) milk (Marvel) diluted in PBS-T (PBS containing 0.1% TWEEN-20; Sigma) overnight at 4°C to block non-specific protein interactions. Incubation of primary antibodies (Table 2.4) diluted in the milk blocking solution was carried out for one hour at RT. Following 3x 10 mins PBS-T washes, membranes were incubated with HRP-conjugated secondary antibodies (Table 2.4) diluted to a concentration of 1:30,000 in milk/PBS-T for 1 hour at RT. Membranes were washed 3x in PBS-T for 10 mins each wash before detection of the target proteins using Luminata Forte (Millipore) and imaging of the blot using ImageLab on a BioRad ChemiDoc XRS+.

Blot image analysis and band densitometry were carried out using the Fiji software (imagej.net/Fiji) and Microsoft Excel, and results were plotted using the RStudio package ggplot2 v3.4.1.

Table 2.4 List of antibodies used for western blot experiments.

Antigen	Host	Clone	Isotype	Supplier	Catalogue number	Dilution
TGFBI	Rabbit	Polyclonal	IgG	Proteintech	10188-1-AP	1:1000
GAPDH	Mouse	1E6D9	IgG2b	Proteintech	60004-1-Ig	1:10,000
Rabbit-HRP	Goat	Polyclonal	IgG	Thermo Fisher	31460	1:30,000
Mouse-HRP	Goat	Polyclonal	IgG	Thermo Fisher	31430	1:30,000

2.7 Quantitative analysis of gene expression by qPCR

qPCR was used to determine relative levels of gene expression, by measuring the fluorescence emitted by DNA bound to the intercalating dye SYBR green.

2.7.1 qPCR reactions

20 µl reactions of each sample consisted of 10 µl of 2X LabTAQ Hi-rox Green master mix (Labtech), 0.8 µl of 10 µM forward and reverse primers and 3.4 µl ddH2O. Equal amounts of cDNA were assayed for samples that would be compared to each other. The optimal cDNA dilution was determined using the information obtained through the standard curve dynamic range (Section 2.7.3) and the ones that reached ct values between 22-30 were preferred. Reactions were assayed in triplicate and included a negative control set of reactions where ddH2O was added in place of cDNA. Reactions were loaded into MicroAmp™ Optical 96-Well Reaction Plates (Thermo Fisher), briefly mixed by vortex, centrifuged and inserted into a Quantstudio 6 Flex realtime PCR system (Thermo Fisher), where it underwent the following cycling run:

1. Denaturation step:
    a. 2 min at 95°C
2. Annealing and extension step (40 cycles of repetition):
    a. 15 sec at 95°C
    b. 20 sec at 60°C
3. Dissociation stage, where fluorescence decreases are detected upon reaching the melting temperature, and melting curves are generated.

2.7.2 Primer design

Forward and reverse primers were designed using the following parameters using NCBI Primer-BLAST (ncbi.nlm.nih.gov/tools/primer-blast):

- 18-24 nucleotides
- 50% minimum GC content
- Amplicon lengths between 50-150 bp
- Exon-spanning
- Compatible melting temperatures (within 5°C)
- No stable homo- and hetero-dimers predicted at the melting temperature
- Lower E-value for genomic sequences at the gene target locus, determined using the BLAST tool (blast.ncbi.nlm.nih.gov).

2-7 primer pairs per gene were designed using the Primer-Blast tool and purchased from SigmaAldrich for the purpose of identifying the pair with the optimal performance efficiency. cDNA from fibroblasts and differentiated CEpi samples was obtained as described in Section 2.1.2 and used to test primers using a standard RT-PCR reaction (see section 2.1.3). Specific PCR product amplification was assessed by resolving the product on a 2% (w/v) agarose gel and visualisation by trans-illumination using a Bio-Rad Chemidoc MP imaging system.

2.7.3 Absolute quantification and determination of amplification efficiency for primer selection

In order to assess primer pair efficiency and for comparison to reference gene primer pairs, a standard curve was determined by preparing serial dilutions (1:10, 1:50, 1:250, 1:1250, 1:1650) of cDNA for the qPCR reactions, using the conditions outlined in Section 2.7.1. In order to generate the standard curve, the number of cycles required to cross the amplification threshold (C_T) was plotted against the log of the cDNA input. The standard curve analysis generates data on the dynamic range of the cDNA input template and the target template amplification efficiency. Primer pair amplification efficiency was calculated by the standard curve slope (efficiency $=10^{1/\text{slope})}$-1) which determines whether they are suitable for a comparative C_T analysis. Primers generating very similar amplification efficiencies (less than 5% difference) were employed to calculate target gene expression. All qPCR reactions were carried out in triplicate to confirm assay accuracy and only triplicate average C_T values with a minimal standard deviation (SD) were considered valid.

2.7.4 Validation of target and reference gene amplification efficiencies for the comparative C_T analysis ($\Delta\Delta C_T$)

Following standard curved generation and calculation of primer pair efficiency, the ΔC_T for each sample triplicate C_T average was calculated as follows ΔC_T = (C_T target – C_T reference). Validation of the experiment was carried out by ΔC_T values plotting against the log value of the cDNA input and the slope of the plot was verified to be <0.1. Primer pair efficiencies meeting the criteria were selected and those used in the study are listed in Table 2.5.

Table 2.5 Primers used for qPCR experiments reported in the study.

Gene target	Forward sequence	Reverse sequence
TGFBI exon 9	GTCTGATGTGTCCACAGCCA	GGAGGGGTTCCATCTTTGAA
ΔNP63	AGTGAGCCACAGTACACGAA	TAGTCGGTGTTGGAGGGGAT
KRT3	TGGAGATCGACCCCCAGATT	AGGAACCGCACCTTGTCAAT
KRT14	ATGGCAGAGAAGAACCGCAA	CGGTTCAGCTCCTCTGTCTT
ABCG2	AAACCTGGTCTCAACGCCAT	CTAATAACGAAGATTTGCCTCCACC
PAX6	TCAGCTCGGTGGTGTCTTTG	GTCTCGGATTTCCCAAGCAA
GAPDH	CCCCACCACACTGAATCTCC	GGTACTTTATTGATGGTACATGACAAG
ACTIN	CCAACCGCGAGAAGATGA	CCAGAGGCGTACAGGGATAG

2.7.5 qPCR analysis by $\Delta\Delta C_T$ relative quantification

qPCR data were analysed using the $2^{-\Delta\Delta ct}$ method (Schmittgen & Livak, 2001), whereby target gene expression was normalised against reference gene expression, which were ACTIN and GAPDH combined in this instance:

$$\Delta CT = CT_{target} - CT_{reference}$$

Next, normalisation of the dependent sample against the independent sample which provides an internal control for the experiment:

$$\Delta\Delta CT = \Delta CT_{dependent\ sample} - \Delta CT_{independent\ sample}$$

Finally, gene expression values were calculated as the relative quantification (RQ) or fold difference of the target gene of interest respective to internal control, calculated as follows:

$$RQ = 2^{-\Delta\Delta CT}$$

2.8 Cell culture and iPSC reprogramming

2.8.1 Patient samples

Patient skin biopsies were obtained by Professor Stephen Tuft following informed consent of Moorfields Eye Hospital patients (ethics permission number: 13/LO/1084, Moorfields Eye Hospital Research Ethics) who had been previously genetically screened for *TGFBI* mutations. Genotype/phenotype details are provided in Table 2.6.

Table 2.6 Patients with *TGFBI* mutations recruited to this study, whose skin biopsies were used to generate fibroblast and iPSC lines. LCDI = Lattice Corneal Dystrophy Type I, GDCII = Granular Corneal Dystrophy Type II. F=Female, M=Male.

Patient ID	Age	Gender	cDNA variant	Protein variant	Diagnosis
Patient 1	48	M	c.370C>T	p.R124C	LCDI
Patient 2	54	M	c.370C>T	p.R124C	LCDI
Patient 3	34	M	c.371G>A	p.R124H	GCDII
Patient 4	66	F	c.371G>A	p.R124H	GCDII

2.8.2 Primary fibroblast cell lines

Skin biopsies were used to establish fibroblast cell lines by firstly, removing the epidermal layer of the biopsy, the remaining tissue was then placed into a culture dish. A coverslip was used to secure the samples and the space between the dish and the coverslip was filled with culture media to aid in biopsy attachment. Fibroblast cultures were maintained at 37°C and 5% CO2 in fibroblast growth media consisting of DMEM/F12+Glutamax (Gibco), 10% fetal bovine serum (FBS, Lonza), 1% v/v non-essential amino acids (NEAA, Gibco), 100 µg/ml penicillin and 100 U/ml streptomycin (Pen-Strep, Lonza). The cultures were passaged using Trypsin-EDTA (Gibco) once they reached confluency.

2.8.3 Generation of patient-derived induced pluripotent stem cell (iPSC) lines

Fibroblasts with a passage number lower than 15 were cultured in a T175 flask (Corning) until they reached approximately 90% confluency. The cells were then electroporated with four integration-free episomal vectors: pCXLE-hOCT3/4-shp53-F (Addgene plasmid #27077), pCXLEhSK containing SOX2 and KLF4 (Addgene plasmid #27078), pCXLE-hUL containing L-MYC and LIN28 (Addgene Plasmid #27080), and miRNA 302/367 plasmid (Gift from Dr J. A. Thomson, Regenerative Biology, Morgridge Institute for Research, Madison, Wisconsin, USA; Howden et al., 2015).

To carry out the procedure, the fibroblasts were trypsinised, centrifuged at 200 g for 5 min, and washed with Dulbecco's Phosphate-Buffered Saline (DPBS, Gibco). Subsequently, 1×10^6 cells were counted and resuspended in 100 µl Nucleofector solution from the Cell Line Nucleofector Kit R (Lonza). A master mix containing 1 µg of each one of the episomal vectors was added to the cell suspension, followed by electroporation using an Amaxa Nucleofector I device (Lonza) with the setting U-023. The cells were then replated in a 0.01% (v/v) gelatin-coated 10 cm^2 tissue culture dish in fibroblast media.

The media was changed the next day to fresh fibroblast media containing 0.5 mM sodium butyrate (SB, Sigma), and changed daily for a week. TrypLE was used to dissociate the cells, which were then replated in a Geltrex-coated dish at a density of 200,000 cells/cm^2 and maintained in fibroblast growth media for 24 hours. They were subsequently maintained in Essential 8 Flex media (E8F, Gibco) supplemented with 0.5 mM SB for the following 7 days.

From day 13 of reprogramming onwards, the cells were cultured in E8F alone until iPSC colonies appeared. Colonies were identified by their characteristic morphology, consisting of round colonies of densely packed cells, which were manually dissected and transferred to individual Geltrex-coated wells for further clonal expansion. At least six clonal iPSC lines were expanded for each line, and were considered suitable for differentiation based on their expression of stem cell markers (Section 3.2.3.1, Figure 3.4). Each clonal iPSC line selected for differentiation was cultured in E8F and split onto Geltrex-coated plates every 3-4 days following dissociation using enzyme-free cell dissociation buffer (Gibco).

2.8.4 Confirmation of fibroblast and iPSC line genotypes

Cell samples were subjected to genomic DNA extraction using the Wizard® SV Genomic DNA purification system (Promega). Specific primers targeting *TGFBI* exon 4 (Table 2.1) were used to amplify the region of interest by PCR using a 2X GoTaq green master mix (Promega). The PCR product was then purified using MultiScreen® PCR µ96 Filter Plates (Millipore) and sent for Sanger sequencing as detailed in Section 2.2.

2.8.5 Differentiation of corneal epithelial-like cells from patient-derived iPSC

For the generation of *in vitro* models for the study of TGFBI CDs, mutant and control iPSC lines (Chapter 3, Table 3.2) were differentiated towards a corneal epithelial-like (CEpi) cell lineage. An adapted version of the protocol published by Kamarudin et al. (2018) was used for the CEpi differentiation.

Upon reaching 70% confluency, iPSCs were detached using enzyme-free buffer (Gibco) and plated at a 1:2 dilution in a T25 flask coated with Geltrex (Gibco) – this step was considered differentiation day 0. They were cultured in E8F (Thermo Fisher) for 2 days before inducing embryoid body (EB) formation by using 2mg/mL dispase I (Thermo Fisher) to detach cell colonies without fully dissociating them. The cells were then resuspended in E8F supplemented with 10mM Blebbistatin (Sigma) and plated into ultra-low attachment culture plates (Corning). Over the next two days, a gradual media change to epithelial induction media (IM) containing DMEM/F12+Glutamax (Gibco), 1% N2, 1%

B27, 1% NEAA, 1% Pen-Strep, 25ng/mL bone morphogenetic protein 4 (BMP4, Peprotech) and 50ng/mL epidermal growth factor (EGF, Life Technologies) was carried out, with a 1:1 (v/v) E8F:IM on the first day and IM only on the second day. The EBs were maintained in IM for the following 5 days with media changes every two days. On differentiation day 9, the EBs were plated on adherent plates coated with 5µg/cm^2 collagen IV (Sigma) and 3.33 µg/mL laminin-521 (Thermo Fisher) and cultured in Cnt-30 (CellNtec), a commercial media that promotes corneal epithelial differentiation with an undisclosed formulation, supplemented with 10% FBS. The media was changed 3 times a week, and cells were kept until approximately day 30, with samples collected at days 16, 21, 25, and 30 for analysis.

2.9 Antisense oligonucleotides

2.9.1 ASO design

ASOs were designed complimentary to exon 4 of *TGFBI* comprising and surrounding the region of the R124C and R124H mutations.

2.9.2 Prediction of RNA secondary structures

A *TGFBI* reference sequence was obtained from Ensembl (ENST00000442011.7) and cross-checked against patient gDNA Sanger sequencing data to ensure sequence homology and lack of polymorphisms. The region comprising part of intron 3-4 through to intron 4-5 for each sequence of interest (WT, R124C and R124H) was converted to RNA for the prediction of *TGFBI* pre-mRNA secondary structure using the mfold web server (Zuker, 2003). The same process was carried out using only the exon 4 sequence without the intronic regions in order to predict the protein-coding mRNA folding of the region.

An important determinant of ASO efficacy is the accessibility of the target RNA. The mfold software predicts the accessibility of the target RNA by computing the likelihood of RNA base pairing and the resultant RNA secondary structure. Mfold analyses the input sequence and computes a list of predicted folded structures ranked by their free energy, with the reaction having the lowest free energy used as the reference structure.

The software outputs multiple files containing information on the folding propensities of the input sequence. The ‘ct file’ contains information on the nucleotides in the predicted RNA secondary structure. The first row of the ct file contains the total number of nucleotides in the structure, the energy value of the fold and the file name. Six columns are included in the file with the following fields from left to right:

1. Nucleotide number within the input sequence.

2. The type of nucleotide (A, G, U or C).
3. Nucleotide number within the input sequence starting from the 5'neighbour nucleotide (starts from zero).
4. Nucleotide number within the input sequence starting from the 3'neighbour nucleotide (starts from two).
5. The number of the nucleotide that the respective nucleotide of the row in question is paired with. If the value in this field is 0, the nucleotide contained column 1 for this row is unpaired.
6. Repeat of column 1.

Nucleotides with zero values contained in column five are favoured to be part of the target sequences, as they would be unpaired and more likely to be accessible for ASO binding. An extract from an example ct file is shown below (Table 2.7).

Table 2.7 An example of a ct file generated for the *TGFBI* mRNA sequence analysis. Numbers in the title column have been added to correspond to the description above.

1	2	3	4	5	6
243	G	242	244	270	243
244	C	243	245	0	244
245	U	244	246	0	245
246	A	245	247	267	246
247	C	246	248	266	247
248	C	247	249	265	248

Mfold also provides ss-count (single stranded-count) data for the input sequence, which indicates the likelihood of a nucleotide to be unpaired in multiple potential secondary structure predictions. Thus, bases with a high ss-count value would be more favourable than those with an ss-count value of zero, as a value of zero would suggest that the nucleotide is paired to another and inaccessible to ASO binding in all computed scenarios. Ss-counts of WT and mutant *TGFBI* pre-mRNA and protein-coding mRNA sequences are shown in Chapter 5 (Figure 6.7).

2.9.3 ASO sequence and structure selection

A previous study that investigated different gapmer ASOs in their activation of RNase H-mediated pre-mRNA and mRNA degradation found that ASOs that were 22 nucleotides in length, with either a 12, 10 or 8 nucleotide central DNA phosphorothioate (PS) backbone sequence flanked by 2'-OMe RNA nucleotides were more effective in comparison to ASOs of shorter lengths (Marrosu et al., 2017). Furthermore, locked nucleic acid (LNA) oligonucleotide substitutions complimentary to a particular single nucleotide polymorphism (SNP), have been shown to enhance allele-specificity of target

sequence binding (Naessens et al., 2019). Based on this research, the ASOs in the current study were designed to be 22 nucleotides in length, with either a 12, 10 or 8 nucleotide central DNA PS backbone sequence flanked by 2'-OMe RNA nucleotides, with an LNA base complimentary to the point mutation contained within the central DNA portion of the sequence. As the LNA base had to fall within a specific portion of the sequence, the final chemical structure of the ASOs was considered in the ASO sequence selections for each respective mutation. Other parameters of the ASO design are outlined below:

- GC content between 40-60%
- Target binding capacity. The free energy of the selected ASOs was calculated for each ASO alone using the AllSub platform and for each ASO as an ASO-ASO complex using the bifold platform (http://rna.urmc.rochester.edu/RNAstructureWeb/). The ideal free energy values are >-4 and >-15 for each of these calculations, respectively.
- Potential off target screening was conducted by aligning ASO sequences to the human genome using BLAT (Kent, 2002) and BLAST (Z. Zhang et al., 2000).

2.9.4 Chemical modifications

ASOs were chemically modified using a gapmer design where the central portion of the ASOs contained DNA with phosphorothioate (PS) backbone modifications and the flanking portions contained 2'-OMethyl modified RNA bases. The base of the ASO targeting the point mutation was modified with a locked nucleic acid. A control ASO was designed by scrambling of a 20 bp region containing the c.370C>T (p.R124C) *TGFBI* mutation. All ASOs were modified with a 5' conjugated 6-FAM fluorophore in order to monitor transfection efficiency. ASOs were synthesised by Eurogentech (Belgium). ASO sequences and modifications are shown in Table 2.8.

Table 2.8 Gapmer ASOs used for *in vitro* assays. Modifications: * = PS link, m = 2'-OMethyl RNA, + = locked nucleic acid.

ASO name	ASO target	ASO sequence and chemistry
C1	c.370C>T	5-'mUmCmCmGmUmGmC+AG*T*C*C*G*T*G*mUmAmCmAmGmCmU-3'
C2	c.370C>T	5'-mCmGmUmGmC+AG*T*C*C*G*T*G*T*A*C*A*mGmCmUmGmA-3'
H1	c.371G>A	5'-mAmGmCmUmUmCmUC*C*G*T*G*+TG*G*mUmCmCmGmUmGmU-3'
H2	c.371G>A	5'-mUmCmumCmCmGT*G*+TG*G*T*C*C*G*T*mGmUmAmCmAmG-3'
SCR	N/A	5'-mGmCmGmCmCT*C*G*T*A*G*G*A*C*C*mUmCmUmUmA-3'

2.9.5 *In vitro* ASO treatments

To evaluate the decrease in mutant TGFBI expression, ASOs were transfected into primary patient fibroblasts and patient iPSC-derived differentiated CEpi cells. Mutant fibroblast lines were plated at a density of 7.5 x 10^4 cells/cm^2, 24 hours before transfection. The corresponding ASO was transfected into the cells using a polyethilamine-based transfection reagent (Transporter5, Polysciences). The cells were incubated in fresh, serum-free, and antibiotic-free media for an hour before transfection. Therapeutic and control (SCR) ASOs, at 1µg were dissolved in 150 mM NaCl and mixed with Transporter5 at a 1:4 oligo:PEI ratio. The ASO and transfection reagent were gently mixed by pipetting before incubation at room temperature for 20 minutes to form ASO-DNA complexes before being added to the cells. RNA analysis was conducted 48 hours after the incubation period.

The liposome-based reagent Lipofectamin RNAiMax (Thermo Fisher) was used to transfect differentiated mutant CEpi cells. Cells were replated between day 21-25 and seeded at a density of 5-7.5 x 10^4 cells/cm^2 for transfection. To ensure accurate seeding, the cells were detached with TrypLE express (Thermo Fisher) and passed through a 70 µm Falcon cell strainer (Thermo Fisher) to separate clumps of cells. Before transfection, fresh, serum-free Cnt-30 media was added to the cells. To achieve a 300 nM ASO dose, OptiMem (Gibco) was used to dilute 3 µl of the reagent and the appropriate amount of ASO. The ASO and transfection reagent complexes were allowed to form for 5-10 minutes before being added to the cells in a drop-like manner. RNA extractions were carried out 48 hours following transfection, whereas protein extractions were carried out 72 hours post-transfection using lysate and/or supernatant samples.

2.10 Next generation sequencing and analysis

2.10.1 Targeted Next Generation Sequencing (NGS)

Total RNA was extracted from non-treated and ASO treated cells and synthesised into cDNA (Section 2.1.2). Dilutions containing a minimum concentration of 1ng of cDNA were prepared for each sample. Primer pairs that targeted either the gDNA or cDNA of *TGFBI* and flanked the region of the mutant nucleotide were designed. The primers included two overhang adaptor sequences, known as Illumina nextera transpose overhangs, at the 5' ends (Table 2.9), which are two universal sequences that are compatible with Illumina kits. Other requirements for the design of primers for the NGS include:

- A melting temperature of 60-65°C (not including the overhang sequences).

- Production of an amplicon between 100-400 bp (not including the tails)

Table 2.9 Primers used to generate amplicons for Illumina library preparation. Primers for targeted NGS were composed of the gene specific sequences (black), designed to amplify the region containing the mutated region, and the forward (red) and reverse (blue) illumina nextera overhang transposase sequences.

Primer direction	Target	5' – Sequence – 3'
Forward	gDNA	TCGTCGGCAGCGTCAGATGTGTATAAGAGACAGAGAGGCCATCCCTCCTTCTG
Reverse	gDNA	GTCTCGTGGGCTCGGAGATGTGTATAAGAGACAGTCATCTCACAGCTGGCAAGG
Forward	cDNA	TCGTCGGCAGCGTCAGATGTGTATAAGAGACAGGGCTGTCCAGCAGCCCTAC
Reverse	cDNA	GTCTCGTGGGCTCGGAGATGTGTATAAGAGACAGTTGCTGACCAGGGAGTCCA

The cDNA dilutions and primers were sent to the UCL genomics facility for sequencing. The cDNA was sequenced using the MiSeq reagent kit Nano (Illumina). A summary of the procedure is detailed below.

For the generation of a DNA library, the primers described above (Table 2.9) were used to generate a 200 bp long amplicon (not including tails), using KAPA HiFi HotStart ReadyMix (KAPA Biosciences). During this step, the nextera transposase sequences were incorporated into the amplified PCR product. The PCR product was then purified using AMPure XP beads, which work to remove the respective amplicons from the primers and other PCR reaction components. The AMPure XP beads were added to the PCR product and mixed. The mixture was then incubated for 5 mins at RT to allow for DNA binding. The DNA bound beads were then separated using a magnetic stand. Next, beads were washed twice with ethanol by using the magnetic stand to separate and remove the ethanol solution from the beads after each wash. Following the wash steps, the beads were left to air-dry and the DNA was eluted from the beads using 50 µl of 10 mM Tris pH 8 and the magnetic stand. For the removal of primer dimers, a short 2 min incubation at RT was followed by an additional clean-up step, where 20% 2.5M NaCl was added for rebinding of the DNA to the beads. The procedure outlined above was then repeated starting from the ethanol wash steps.

A second amplification reaction was carried out using the purified PCR product, KAPA HiFi HotStart ReadyMix and the Nextera XT Index 1 (N7XX) and 2 (S5XX) primers from the Nextera XT Index kit (Illumina). This second amplification product then underwent the same clean-up procedure as described above.

Upon generation of the cDNA libraries, the respective PCR products were quantified and pooled in order to obtain a minimum of 5000 reads. The libraries were then denatured with NaOH, rehybridized and subsequently heat denatured before proceeding with the sequencing. A PhiX Control v3 Library was then prepared and combined with the amplicon library. The PhiX control is a library derived from the small, well-characterised PhiX genome, which works to provide quality control for sequencing applications, and is especially necessary for low-diversity libraries such as the ones generated through targeted NGS, where only one specific DNA fragment is analysed. Samples were sequenced using a MiSeq sequencer (Illumina).

2.10.2 Quantification of WT/mutant allele expression

Allele expression was quantified using a Python v3.11.1 script (Appendix D) that counts the number of reads containing the WT base or mutant point mutation. The allele count quantifications were then divided by the total number of read counts for the particular samples to obtain the percentage of the WT and mutant base for each condition (gDNA, NT, SCR, ASO1 and ASO2).

2.10.3 Bulk RNAseq library preparation and sequencing

Total RNA was extracted as described in Section 2.1.2. Stranded RNAseq libraries were prepared by Genewiz, Azenta Life Sciences using the NEBNext Ultra Directional RNA Library Prep Kit for Illumina (New England BioLabs) following the manufacturers protocol. Indices were included to multiplex multiple samples. Briefly, mRNA was isolated from total RNA by utilizing poly-T oligo-attached magnetic beads. Following fragmentation, the first cDNA strand was generated using random hexamer primers, and subsequently, the second cDNA strand was synthesized. To create a strand-specific library, the synthesized cDNA underwent end repair, A-tailing, adapter ligation, size selection, and USER enzyme digestion. The library's insert size was verified and quantified using quantitative qPCR on an Agilent 2100 instrument. Finally, the libraries were subjected to paired-end sequencing with a 300bp insert size on an Illumina NovaSeq 6000 S4 flowcell.

2.10.4 Bulk RNA sequencing (RNAseq) pre-processing and analysis

Raw sequencing data was subject to quality control using FastQC v0.11.9 and MultiQC v1.14 (Appendix C). The transcript-level expression data was aligned to the reference transcriptome and genome sequences using Salmon v1.9.0 with GENCODE v42 hg38 reference sequences.

The tximport package v1.24.0 was used to import the data into RStudio (R v4.2.1) for differential gene expression analysis using the DESeq2 v1.36.0 package (Love et al.,

2014). The data was normalised using the DESeq2 normalisation method, which accounts for differences in library size and gene length. Differentiation batch effects were corrected for by including the batch variable as a covariate in the experimental design. Variance stabilising transformed data was subject to principal components analysis (PCA). A generalised linear model was fitted to the normalised counts using the negative binominal distribution. The differential gene expression analysis was carried out using the DESeq2 function with apeglm v1.18.0 shrinkage (Zhu et al., 2019), which allows for a more accurate estimation of fold changes and variances. Genes with an FDR-adjusted p value cut off of 0.1 were considered significant. The RStudio packages EnhancedVolcano v1.14.0 and Pheatmap v1.0.12 were used to generate the differential gene expression volcano plots and heatmaps respectively. Normalised counts of genes of interest were saved as a data frame using the plotCounts function of Deseq2 and plotted using ggplot2 v3.4.1. An over-representation analysis was carried out using the clusterProfiler package v4.4.4 for identification of biological processes, cellular components and molecular functions enriched in the significantly differentially expressed gene-set.

2.10.5 scRNAseq bioinformatics analysis

Publicly available scRNAseq data published by Català et al. (2021) was utilised to investigate gene expression patterns of four human donor corneas. The raw scRNAseq data, which was generated using the 10 × Genomics platform and processed with the Cell Ranger software, was downloaded from the Gene Expression Omnibus (GEO: ncbi.nlm.nih.gov/geo) repository and pre-processed using the Seurat package v4.3.0 in RStudio. In order to ensure high-quality data, cells with less than 1000 unique molecular identifiers (UMIs) per cell and those with a mitochondrial gene content exceeding 20% were filtered out. This resulted in a total of 10,580 cells that were retained for downstream analysis. The SCTransform function in Seurat was used to normalise the data and correct for technical variability and patient-specific effects.

Next the normalised data from the four donor corneas was integrated, which involved identifying the best anchors between the datasets using the findIntegrationAnchors function and then performing canonical correlation analysis (CCA) to align the datasets based on their shared variation.

PCA was used to reduce the dimensionality of the data and identify the most significant sources of variation among the cells. The cells were clustered using the graph-based clustering approach implemented in Seurat, which involves constructing a k-nearest neighbour graph and partitioning it into communities using the Louvain algorithm. The

resulting cell clusters were embedded in a uniform manifold approximation and projection (UMAP), a dimensionality reduction technique that preserves the global structure of the data. The FeaturePlot function of Seurat was used for the visualisation of gene expression for each individual dell in a given cluster.

2.11 Data visualisation and statistical analyses

All graphs presented in the thesis were generated using the RStudio package ggplot2 v3.4.1, unless specified otherwise in the respective material and methods or results section. ANOVA statistical analyses were carried out using the base R aov function and post-hoc analyses were carried out using the RStudio package rstatix v0.7.2.

Chapter 3: TGFBI corneal dystrophy patient cohort and generation of patient-derived iPSC lines.

3.1 Introduction

Animal models have been used to address many biological questions and have provided invaluable information to the field of biomedical science. Yet, in many cases, the commonly used murine models are not able to appropriately recapitulate human disease due to interspecies differences. Differences between mouse and human corneas are clear, with the *Krt3* gene being absent from the mouse genome (Ho et al., 2022), and mouse corneas displaying over 10-fold less TGFBIp expression relative to human corneas (Poulsen et al., 2018a). *In vitro* models represent an alternative and complimentary system to animal models for the investigation of molecular mechanisms of human disease and the development and testing of novel therapeutics. Patient-derived somatic cells that have been reprogrammed into iPSCs are capable of differentiating into previously unattainable disease-relevant cells which retain the genetic signature of the patient. Thus, patient-derived iPSCs can provide an unlimited source of disease-specific cells, enabling the experimental testing of potential therapeutics in a relevant disease model.

This chapter describes the medical histories of the individuals who agreed to participate in this study while providing confirmation of their pathogenic mutations at the p.R124 hotspot; and the generation of the control and patient-derived iPSC lines that were used throughout this study.

3.1.1 Genetic diagnosis and prevalence of TGFBI corneal dystrophies

A tight genotype-phenotype correlation between pathogenic mutations in *TGFBI* and the resulting phenotypic expression of autosomal dominant corneal dystrophies affecting the epithelial and stromal layers has been described through reports of genetic studies in the field (see Chapter 1, Section 1.4.1). To date, 78 pathogenic variants in *TGFBI* have been identified (Table 9.1, Appendix B) and linked to specific corneal phenotypes, with the likely possibility of rare novel mutations being reported in different populations in the future. The IC3D Classification of Corneal Dystrophies, written by experts in the field, defines the group of conditions known as corneal dystrophies, while incorporating clinical, histopathologic, and genetic information to enable a comprehensively accurate classification of TGFBI corneal dystrophies (Møller & Weiss, 2011; Weiss et al., 2008, 2015) (see Chapter 1, Section 1.4). As it is recognised that TGFBI corneal dystrophies affect multiple layers of the cornea (see Chapter 1, Section 1.4.1), the IC3D classifies

them as epithelial-stromal TGFBI corneal dystrophies, and subclassifies them based on clinical presentation and anatomic pathology.

The different phenotypes contained within the group of epithelial-stromal TGFBI corneal dystrophies can present with similar yet subtly different pathological features, perhaps due to lack of disease progression or discrepancies not possible to observe via slit lamp examination. In these cases, genetic screening provides a powerful method of accurate TGFBI CD diagnosis due to the well documented genotype-phenotype correlation (Dighiero et al., 2001; Evans et al., 2016; Paliwal et al., 2010; Zenteno et al., 2009). Past reports demonstrate that TGFBI CDs have been reported worldwide, with the highest prevalence reported in Europe, East Asia and North America (Chao-Shern et al., 2019).

Some studies have estimated the prevalence of the p.R124H mutation in their cohorts. In a study of 2068 Chinese refractive surgery candidates, four had corneal opacities in both eyes with a fifth individual harbouring the mutation despite no observation of a phenotype at the time, indicating a prevalence of 0.24% for the GCDII causing mutation p.R124H in this population (Y. Song et al., 2017). A Korean study of 2060 DNA samples obtained from a public umbilical cord blood bank determined that six of these samples (0.29%) were heterozygous for the p.R124H mutation (J. E. Park et al., 2021).

An American study estimated the prevalence of corneal dystrophies through analysis of a database comprising the ophthalmic medical claims of 6,626,976 individuals (Musch et al., 2011). The corneal dystrophies were categorised based on a general diagnosis and no genetic screening was carried out. A diagnosis of anterior corneal dystrophy was recorded in 15.6% of enrolees, while a diagnosis of lattice or granular corneal dystrophy was recorded in less than 1%.

Some reports have evaluated the distribution of TGFBI CDs in their local cohorts. An investigation into an Indian cohort of 37 patients with either LCD or GCD reported p.R124C and p.R555W to be the most common causative mutations (Chakravarthi et al., 2005). In a Chinese cohort of 355 patients with TGFBI CDs, p.R555W (GCDI) and p.R124H (GCDII) were the most common and p.R124C (LCDI) the second most common disease-causing variants (J. Yang et al., 2010). In an Iranian cohort of 24 TGFBI CD patients, the p.R124C (LCDI), p.R124H (GCDII) and p.R555W (GCDI) mutations were found to be the most common disease-causing variants (Jozaei et al., 2022).

A study conducted at Moorfields Eye Hospital on a multi-ethnic cohort of 68 patients demonstrated that p.R555Q (TBCD), p.R124C (LCDI) and p.R555W (GCDI) were the most common disease-causing variants (Evans et al., 2016). This work has since been continued in the Hardcastle Laboratory (unpublished data) to include 120 patients that

were clinically diagnosed as having an epithelial-stromal CD. Following genetic screening of all the patients included in the study, 110 individuals from this cohort were found to have pathogenic mutations in *TGFBI*. Many of these patients received a more accurate diagnosis following genetic screening (Figure 3.1), for example, around a quarter of the cohort was initially diagnosed with general GCD before genotyping, which allowed for a more precise subclassification and diagnosis. From this updated data, the p.R124C (LCDI) and p.R555Q (TBCD) variants were confirmed to be the most common.

A meta-analysis conducted on 257 published studies, reporting on a total of 4218 TGFBI CD patients demonstrated that around 50% of disease-causing variants were accounted for by the p.R124H (GCDII) mutation, and around 13% and 11% being made up of p.R124C (LCDI) and p.R555W (GCDI) mutations, respectively (Jozaei et al., 2022). The same study also showed that across the 4218 reported cases, 95% were heterozygous for the mutation, with a minority being homozygous (Jozaei et al., 2022).

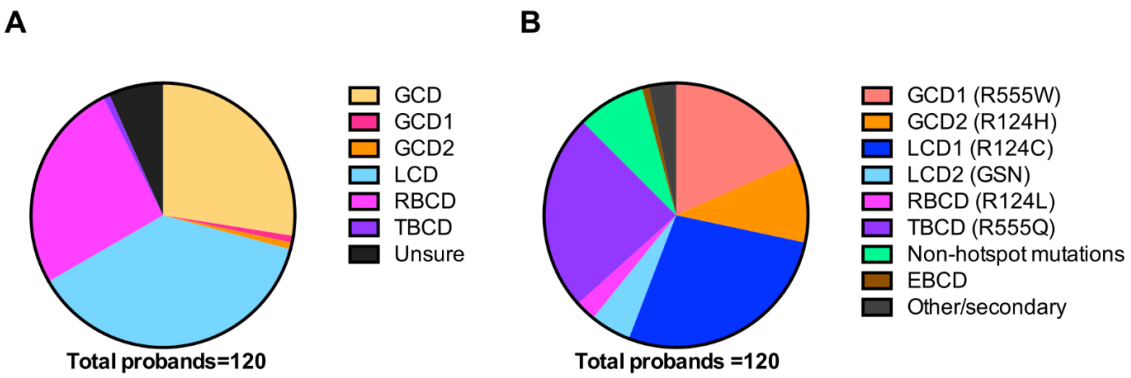

Figure 3.1 Epithelial-stromal CD diagnosis of the MEH patient cohort before and after genetic screening for TGFBI mutations. Reported MEH diagnoses of 120 unrelated cases of suspected epithelial-stromal CD before **(A)** and after **(B)** genetic screening to assess the prevalence of the different CDs in the cohort. GCD = granular corneal dystrophy; LCD= Lattice corneal dystrophy; RBCD= Reiss-Buckler corneal dystrophy; TBCD= Thiel-Behnke corneal dystrophy; EBCD=Epithelial Basement Membrane Corneal Dystrophy. Non-hotspot mutations include mutations in all other regions of TGFBI, and excludes codons R124 and R555. (Unpublished data).

3.1.2 Induced pluripotent stem cells (iPSCs)

In 2006, a major advancement was made in the field of biomedical research when it was reported that pluripotent cells resembling embryonic stem cells (ESCs) could be generated from mouse somatic cells through the retroviral-mediated transduction of a set of four transcription factors (K. Takahashi & Yamanaka, 2006). These genetically manipulated cells were termed induced pluripotent stem cells and the factors – *Oct4, Sox2, Klf4* and *c-Myc* – were named the Yamanaka factors. The following year, the same group reported that these factors were able to induce pluripotency via retroviral transduction in human somatic cells (K. Takahashi et al., 2007). Simultaneously, a

different group also reported the induction of pluripotency in human somatic cells via lentiviral transduction of a similar combination of factors – *OCT4, SOX2, NANOG*, and *LIN28* (J. Yu et al., 2007).

Since its discovery, iPSC technology has vastly expanded and other reprogramming methods and alternative combinations of transfection factors capable of inducing pluripotency have been identified. Concerns about the use of integrating viral vectors such as retroviral or lentiviral methods led to the development of non-integrating methods for pluripotency induction, such as episomal vectors, synthetic mRNA and sendai virus (Review: Shi et al., 2017). Additionally, research showed that the core reprogramming cocktail was comprised of Oct4, Sox2 and Klf4, and that this set of factors could be enhanced by the addition of other factors or microRNAs that work to enhance the efficiency of iPSC generation (Lüningschrör et al., 2013; Nakagawa et al., 2008; Wernig et al., 2008).

The forced expression of the relatively small set of defined transcription factors is thought to form a mutually regulated, hierarchal network of pluripotency in the induced cells starting from the beginning of the pluripotency pathway (Review: Adachi & Schöler, 2012). In this way, the transient expression of these master regulators of pluripotency that lie at top of the regulatory hierarchy can organise a stable network state of stem cellness. A transcription factor interaction analysis has indicated that lineage identity is indeed largely defined by co-expression of a small set of lineage-restricted transcription factors in conjunction with certain ubiquitously expressed transcription factors that physically interact with each other (Ravasi et al., 2010). Much research into the functions of the core and enhancer pluripotency factors have demonstrated how their roles vary (Review: Schmidt & Plath, 2012).

Various cell types of different development origins and species can be reprogrammed into iPSCs. The molecular process of pluripotency induction differs with different cell types. The first step, applicable to all cell types that have undergone reprogramming, is the concomitant increase in proliferation of a small proportion of cells and a decrease in cell size (Z. D. Smith et al., 2010). The next step involves the suppression of somatic cell pathways and the acquisition of certain properties of pluripotent cells, such as colony formation (Stadtfeld et al., 2008). In the case of fibroblast reprogramming specifically, the downregulation of mesenchymal regulators occurs simultaneously with the upregulation of epithelial genes, leading to mesenchymal-epithelial transition (R. Li et al., 2010; Samavarchi-Tehrani et al., 2010). In the final stages of pluripotency induction, the

cells begin expressing core pluripotency genes, thus establishing the endogenous pluripotency network (Mikkelsen et al., 2008).

The discovery of iPSC technology and its many applications has triggered enormous progress in the fields of stem cell biology, regenerative medicine, disease modelling and drug discovery. iPSCs allow for the generation of patient-specific or genetically engineered cells that have the capacity to differentiate into any somatic cell type thus, the translational applications of iPSCs in cellular therapy are compelling. Several early-phase clinical trials have demonstrated the feasibility of iPSC-based therapies in treating conditions such as macular degeneration (Mandai et al., 2017; Sugita et al., 2020) and Parkinson's disease (J. Takahashi, 2020). Nonetheless, challenges persist, including the necessity for rigorous characterisation of iPSC-derived cells, standardisation of manufacturing protocols, and addressing genomic instability and tumorgenicity which pose a barrier to widespread clinical implementation (Ortuño-Costela et al., 2019; Yamanaka, 2020). In the field of human genetic disease modelling, iPSCs provide a convenient system, as they retain the genetic signature of the patient while also being relatively easy to generate. Due to these rapid advances, iPSCs are now a commonly used research tool for disease modelling and drug screening.

3.1.2.1 iPSCs in disease modelling

The major advantages of iPSC technology are that it enables the generation of patient-specific pluripotent stem cells that have the capacity of self-renewal and the potential to give rise to any somatic cell types of the body. In comparison to their other pluripotent counterparts, ESCs, which are generated from fertilised pre-implantation embryos, they do not carry the same ethical issues.

The obtainment of iPSCs from patients harbouring a disease-causing mutation allows for research into specific genetic diseases and the development of therapeutic drugs, while overcoming limitations of animal models and primary cell cultures. Patient-specific iPSCs represent an unlimited source of easily accessible, disease-relevant cells that would otherwise be unattainable. However, effective differentiation of iPSCs to cell states which recapitulate disease conditions is still a scientific challenge, although remarkable advances have been made in the field.

The modelling of a disease in a cell autonomous fashion by generation of a single disease-relevant cell type has contributed to the understanding of molecular mechanisms underlying genetic disease. However, human disease usually occurs within a complex multicellular milieu wherein interactions occur between cells, extracellular matrices and other molecular systems. Thus, more complex iPSC-based differentiation

systems in the way of 3D organoids have been developed for tissues such as the cornea (Foster et al., 2017), brain (C. T. Lee et al., 2017), kidneys (Przepiorski et al., 2022) and retina (Afanasyeva et al., 2021). Co-cultures of two or more different cell types have also been generated using iPSCs to investigate cell-cell interactions in disease, for example, interactions between neurons and microglia (J. Park et al., 2018; Vahsen et al., 2022)

A wealth of research utilising iPSCs in disease modelling has demonstrated different disease phenotypes at the cellular level, including the impaired differentiation of motor neurons in iPSCs from spinal muscular atrophy patients (Ebert et al., 2009), the development of drusen in retinal pigment epithelium generated from macular dystrophy patients (Galloway et al., 2017) and prolonged action potential in cardiomyocytes derived from patients with familial long-QT syndrome (Moretti et al., 2010). iPSCs have also been used to model diseases of the cornea such as, aniridia (Ilmarinen et al., 2023), keratoconus (Joseph et al., 2016) and congenital hereditary endothelial dystrophy (Brejchova et al., 2019). Furthermore, recent advances in the gene editing technology such as CRISPR/Cas9 have enabled the generation of isogenic control lines for genetic disease modelling, allowing for genetically controlled comparisons between mutant vs WT *in vitro* cell models (Review: Bassett, 2017).

By establishing iPSC-derived models from patients with genetic disorders, drug screening can be carried out with the aim of modulating a specific molecular target. Investigations into the treatment of ocular-related disease using iPSC disease models have overcome the limitations associated with inaccessible ocular tissue while identifying potential strategies for therapeutic intervention for diseases such as, Leber congenital amaurosis (Parfitt et al., 2016), retinitis pigmentosa (Dulla et al., 2021) and age-related macular degeneration (Ebeling et al., 2022).

The cornea is the only tissue affected by disease-causing mutations in *TGFBI*. Mouse models of these conditions are not equivalent to human phenotypes (see Chapter 1, Section 1.5.3) and diseased primary tissue is difficult to obtain, thus, it is desirable to generate patient-derived cornea specific cells to enable the use of a relevant disease model. iPSC-derived corneal epithelial cells represent a potential new model system for reproducibly creating models of epithelial-stromal TGFBI corneal dystrophies, and the screening of potential therapeutics.

3.1.3 Chapter aims

In this chapter, the main research aim was to establish control and TGFBI corneal dystrophy patient-derived iPSC lines to enable the development of new disease models

and consequently to explore mechanisms of disease and to test potential therapeutic approaches.

3.2 Results

3.2.1 Patient selection for the establishment of *in vitro* cell models of epithelial-stromal TGFBI corneal dystrophies

To establish *in vitro* cell models of epithelial-stromal TGFBI corneal dystrophies (TGFBI-CD), individuals from the Moorfields patient cohort harbouring either c.370C>T (p.R124C) or c.371G>A (p.R124H) hotspot mutations in *TGFBI* were selected due to their prevalence in the general population. Patients were selected subject to confirmatory genetic analysis which was conducted by amplification of *TGFBI* exon 4 using gDNA-targeting primers (Chapter 2, Section 2.2.12) and willingness to participate in the study. Following the informed consent of participants, skin biopsies were obtained from 4 patients in total – 2 patients harbouring c.370C>T (p.R124C) mutations (referred to as patients 1 and 2) and 2 patients harbouring c.371G>A (p.R124H) mutations (referred to as patients 3 and 4) in *TGFBI* (Table 3.1).

Table 3.1 TGFBI corneal dystrophy patients who donated skin biopsies to this study.

Patient	Age at time of biopsy	Ethnic background	Mutation cDNA/protein	Condition	Deposit location	Deposit type
#1	48	Black/African	c.370C>T p.R124C	LCDI	Epithelium/stroma	Amyloid
#2	54	Turkish	c.370C>T p.R124C	LCDI	Epithelium/stroma	Amyloid
#3	34	White	c.371G>A p.R124H	GCDII	Anterior stroma	Amorphous
#4	66	White	c.371G>A p.R124H	GCDII	Anterior stroma	Amorphous

Patient #1 is a 52-year-old male who presented with reduced vision and painful corneal erosions. He received a clinical diagnosis of LCDI and this was confirmed to be due to a heterozygous c.370C>T (p.R124C) mutation in *TGFBI* (Figure 3.3A and 3.2A). He has a positive family history, with his mother and two out of four other siblings also affected (Figure 3.3B). For the treatment of his corneal dystrophy, he received a right penetrating keratoplasty (PK) in 2010 aged 39. He developed cataracts, likely secondary to the graft surgery and the use of topical corticosteroids and underwent a cataracts extraction in 2013. He received a subsequent phototherapeutic keratectomy (PTK) to the right graft in 2015 to reduce refractive error and a left anterior lamellar keratoplasty was received in 2017 for the treatment of his corneal dystrophy.

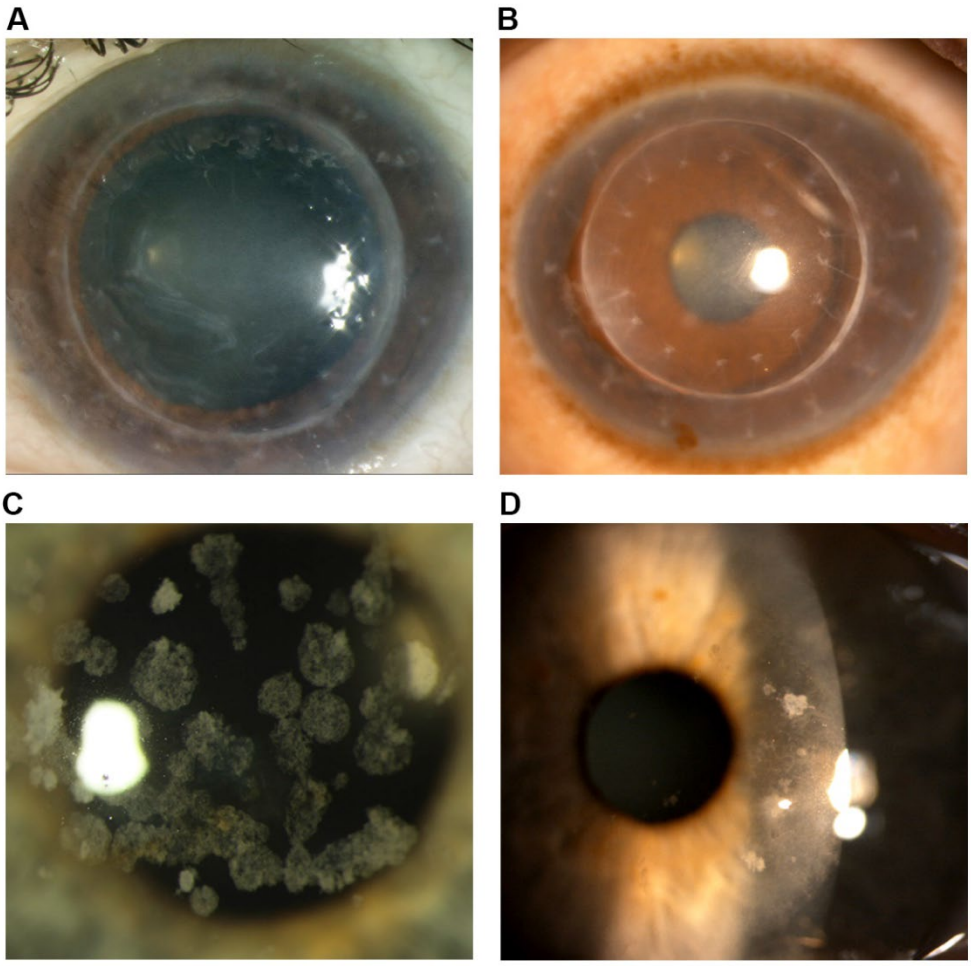

Figure 3.2 Clinical images of TGFBI CD patients recruited to this study. Slit-lamp examination images show phenotypic features of LCDI and GCDII. A) Image of patient 1 (LCDI, p.R124C) sometime following PK treatment. Recurrence of corneal opacities around the site of the graft sutures are observed as well as central corneal haze. **B)** Image of patient 2 (LCDI, p.R124C) sometime following PK treatment. Recurrence of numerous prominent corneal stromal opacities can be observed peripheral to the graft, with cloudiness of the central cornea also apparent. **C)** Image of patient 3 (GCDII, p.R124H) showing superficial circular stromal opacities of the cornea with no surgical intervention having been performed. **D)** Image of patient 4 (GCDII, p.R124H) showing some scattered anterior stromal opacities which have caused elevation of the corneal epithelial surface. Relatively few opacities are observed due to previous PTK treatment. All images were obtained by Mr S. Tuft.

Patient #2 is a 58-year-old male who presented with reduced vision and painful corneal erosions who received a diagnosis of LCDI (Figure 3.2B), confirmed by identification of a heterozygous c.370C>T (p.R124C) mutation in *TGFBI* (Figure 3.3A). No family history information could be obtained for this patient. This individual received a bilateral PK to the left eye in 1998 and to the right eye in 1999 prior to his referral to Moorfields Eye Hospital. He reported persistent issues with poor vision due to astigmatism and continued pain from recurrent epithelial erosions which required PTK treatment. Due to the severity of his corneal dystrophy, a second bilateral PK was received on his right and left eyes in 2017 and 2016, respectively. He experienced symptom reoccurrence in his

left eye and eventually suffered graft rejection. Doctors diagnosed him with irreversible graft failure and a new PK surgery was indicated for him. Other ocular conditions include glaucoma due to chronic topical corticosteroid use and uveitis due to his diagnosis of ankylosing spondylitis.

Patient #3 is a 36-year-old male with a history of corneal opacity first noted by his optometrist, receiving a GCDII diagnosis in 2010 (Figure 3.2C) confirmed to be due to a heterozygous c.371G>A (p.R124H) mutation in *TGFBI* (Figure 3.3A). A family history of the condition has not been reported for this patient. Most of his opacities are observed in the superficial cornea and off the visual axis causing a mild visual impairment. This individual has not undergone surgery to date.

Patient #4 is a 68-year-old female who received a diagnosis of GCDII (Figure 3.2D), confirmed by identification of a heterozygous c.371G>A (p.R124H) mutation in *TGFBI* (Figure 3.3A). This patient has a positive family history, with a sibling also affected by the condition (Figure 3.3C). A bilateral PTK was received for removal of superficial corneal opacities. This individual has not undergone corneal transplantation. Other ocular issues include age-related cataracts which were treated by surgery in 2018.

3.2.2 Establishment of patient-derived primary fibroblast cell lines and confirmation of pathogenic mutation

Skin biopsy procedures were carried out at Moorfields Eye Hospital (MEH) and delivered to the lab for processing. Fibroblast lines were cultured and were sufficiently expanded after approximately 3 weeks (as described in Chapter 2, Section 2.1.10). All patient lines were confirmed to harbour the expected heterozygous missense mutations in exon 4 of *TGFBI* by Sanger sequencing (Figure 3.3A)

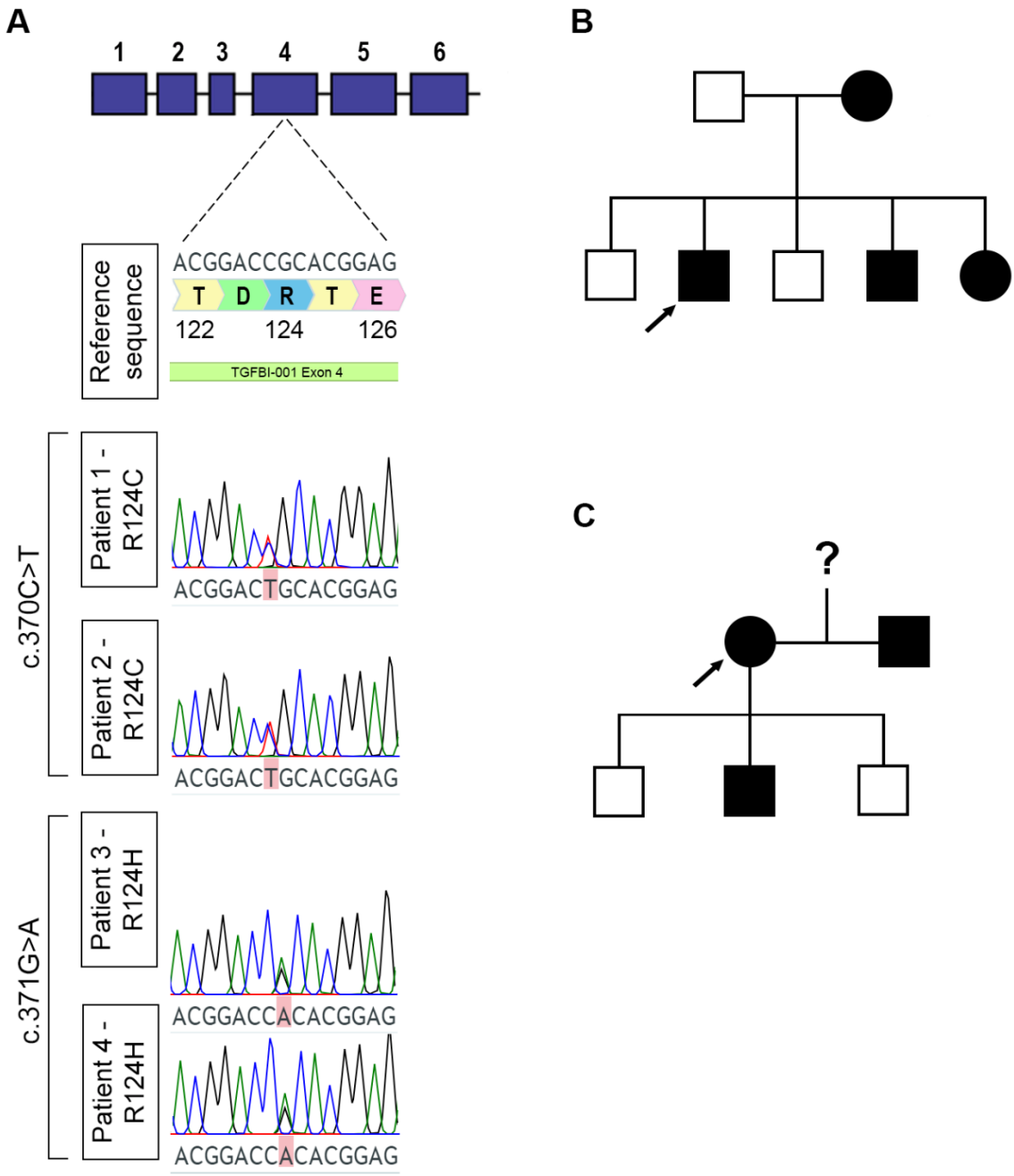

Figure 3.3 Primary patient fibroblast lines harbouring heterozygous TGFBI mutations. A) Sanger sequencing confirmed the heterozygous hotspot mutations c.370C>T (p.R124C) and c.371G>A (p.R124H). **B)** A pedigree representing the positive family history of patient #1. **C)** A pedigree representing the positive family history of patient #4.

3.2.3 iPSC lines

To obtain an *in vitro* TGFBI corneal dystrophy model that is physiologically relevant to the disease, iPSCs were generated from the 4 patient lines harbouring p.R124C or p.R124H mutations and 2 WT control fibroblast lines to enable differentiation towards a corneal epithelial cell lineage. Additionally, an isogenic CRISPR/Cas9 *TGFBI* knockout iPSC line (CKO) was previously generated in our lab from a control fibroblast line

(unpublished data, Beatriz Sanchez-Pintado). This line was also used in this study to explore the role of *TGFBI* in the *in vitro* model.

3.2.3.1 Patient-derived R124 mutant and control iPSC lines express pluripotency markers

Fibroblast lines from patients harbouring p.R124C (n=2) and p.R124H (n=2) mutations and 2 commercially available control fibroblast lines HDFs (control human dermal fibroblasts of neonatal origin, Sigma) and BJ (CRL-2522, ATCC) were reprogrammed to iPSCs (Table 3.2). The lines were nucleofected with non-integrating episomal vectors expressing pluripotency factors. iPSC clonal lines were then isolated and expanded in culture using a standard iPSC media. All iPSCs used in the study were analysed for the expression of pluripotency markers prior to implementation of the differentiation protocol.

Table 3.2 Patient and control iPSC lines.

iPSC line	Genotype	Protein change	Diagnosis
Patient 1	c.370C>T	p.R124C	LCDI
Patient 2	c.370C>T	p.R124C	LCDI
Patient 3	c.371G>A	p.R124H	GCDII
Patient 4	c.371G>A	p.R124H	GCDII
Control 1 (BJ)	WT	WT	Unaffected
Control 2 (HDF)	WT	WT	Unaffected
CKO	TGFBI KO	TGFBI KO	N/A

RNA from all iPSC lines was extracted and synthesised to cDNA (Chapter 2, Section 2.1.2). Endogenous expression of the pluripotency markers *OCT4, LIN28, SOX2* and *L-MYC* were detected by RT-PCR between passages 8-15 (Figure 3.4A), indicating that all iPSC lines had acquired self-renewal properties enabling their directed differentiation towards the target cell type. Expression of the episomal reprogramming vectors was also investigated in all the iPSC lines with no expression detected (Figure 3.4A). This confirms the transient expression of the vectors used for iPSC reprogramming and that the proliferation potential of the lines was maintained by induction of endogenous pluripotency gene marker expression.

Positive immunostaining of pluripotency markers further confirmed the pluripotent stem cell state of the iPSC lines (Fugure 3.4B-E). Nuclear expression of OCT4 and NANOG, along with the cell surface markers SSEA-4 and TRA-1-8 was observed in iPSC colonies.

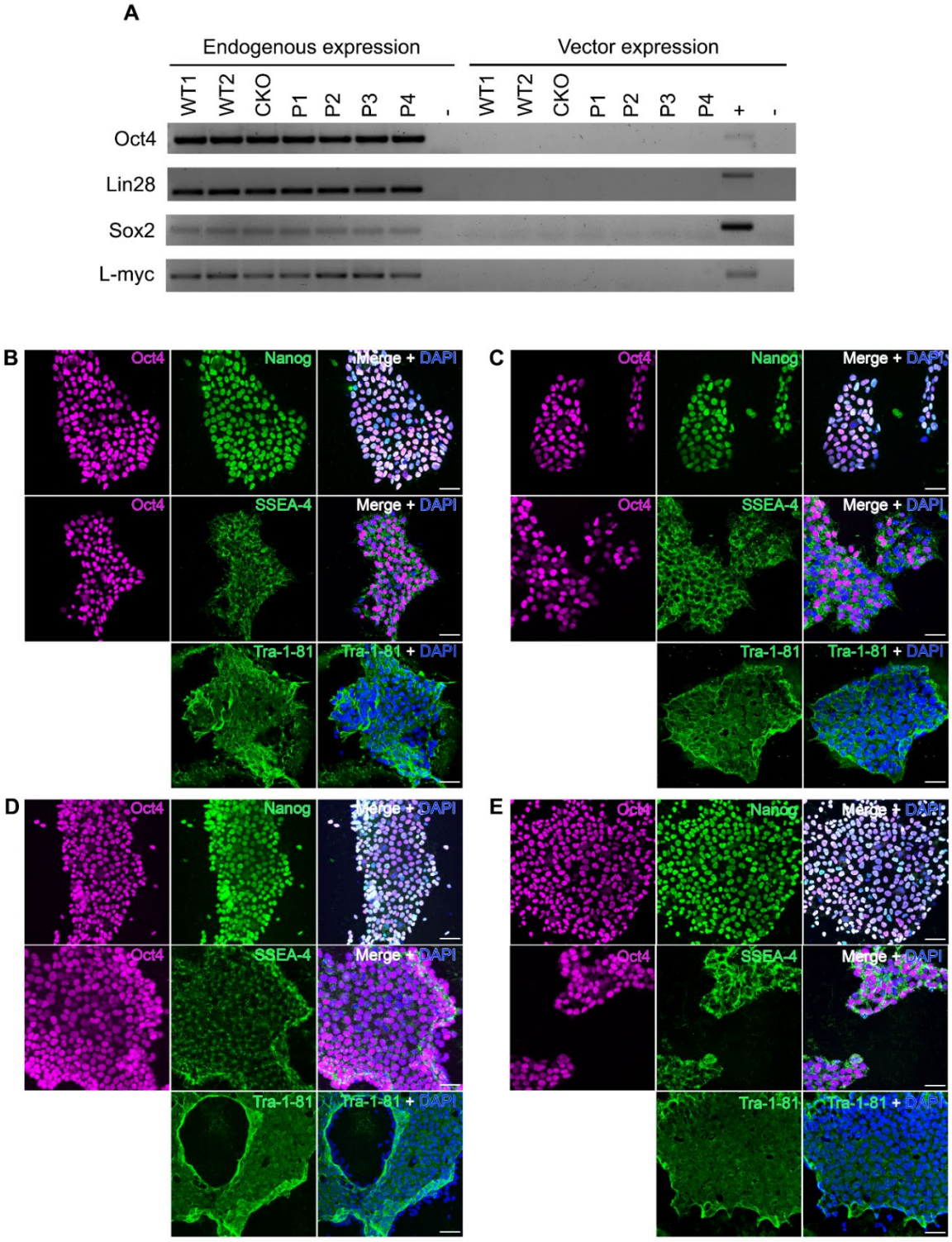

Figure 3.4 iPSC characterisation. A) Amplification of the pluripotency genes *OCT4, LIN28, SOX2 and L-MYC* by RT-PCR demonstrated endogenous expression across all iPSC lines at passages used for differentiations (passages 8-15), while no episomal reprogramming vector expression was detected. + = episomal vector; - = H2O only control. Examples of stem cell colonies carrying p.R124C **(B)** and p.R124H **(C)** mutations; a WT control line **(D)** and the CKO line **(E)** expressing the pluripotency markers OCT4, (magenta), NANOG (green), SSEA-4 (green) and TRA-1-81 (green). Nuclei were stained with DAPI (blue). Scale bar = 100μM.

3.2.4 *TGFBI*/TGFBIp expression in iPSC and fibroblast lines

TGFBI expression was investigated in fibroblast and iPSC lines. The iPSCs were found to express very low transcript levels of *TGFBI* compared to fibroblasts (Figure 3.5A). Since the fibroblasts express high levels of *TGFBI*, Western blotting of the cell lysates and supernatant was performed to assess any similarities and differences in TGFBIp expression. No differences in TGFBIp expression between control and mutant lines was detected (Figure 3.5B-C). Interestingly, a prominent double band staining pattern indicating 2 species of TGFBIp is present is apparent in the supernatant Western blot for all samples, which is not detected in the cell lysate protein blots. The lower molecular weight species (68kDa) appears to be absent in lysates, and may represent a specific secreted form of TGFBIp. The potential relevance of the two forms of secreted TGFBIp will be discussed later on in the thesis (Chapter 6, Section 6.3.1).

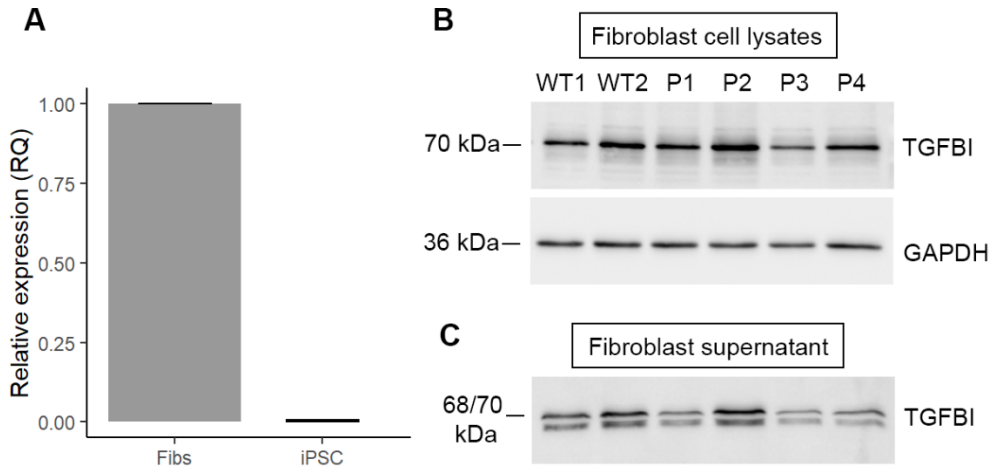

Figure 3.5 *TGFBI* expression in fibroblast and iPSC lines and TGFBIp expression in fibroblast cell lysates and supernatant. A) Relative *TGFBI* expression in fibroblast and iPSC lines, measured by qPCR. *GAPDH* and *ACTIN* were used as reference genes for normalisation. N=6. Bars represent mean ± SEM. **B)** TGFBIp expression in WT and mutant fibroblast cell lysates. GAPDH was used as a reference protein. **C)** TGFBIp expression in WT and mutant cell supernatants show an additional lower molecular weight species (68kDa) compared to cell lysates.

3.3 Discussion

Almost 80 pathogenic *TGFBI* mutations have been described to date (Table 9.1, Appendix B), and the most common mutations are missense variants occurring at the p.R124 or p.R555 hotspots of the protein. A consistent genotype-phenotype correlation between most *TGFBI* mutations and clinical CD phenotypes has been established (Evans et al., 2016; Paliwal et al., 2010). Initial diagnosis of TGFBI CD is made in the clinic via slit lamp microscopy through observation of the pattern and location of corneal opacities. The diagnostic process can be facilitated by genetic screening – a simple yet powerful tool that allows for an accurate subclassification of epithelial-stromal TGFBI CDs.

Some TGFBI CD phenotypes are not distinguishable until the disease sufficiently progresses. As described in the IC3D classification of corneal dystrophies, for almost 100 years, the phenotype that we now refer to as GCDII (caused by the p.R124H mutation) was considered to be a mild variant of GCDI until distinctions were made through observations of subtly different clinical phenotypes (Weiss et al., 2015). Then in 1988, Folberg et al. reported the histopathological observations of both Congo-red positive amyloid deposits and morphologically-typical granular deposits in the anterior stromas of a family presenting with this phenotype (Folberg et al., 1988). This mixed phenotype, now known as GCDII, was defined as an ‘atypical GCD’ due to its presentation of both granular and lattice-like deposits in the anterior corneal stroma. It is now recognised that GCDII is almost exclusively caused by the p.R124H mutation, whereas GCDI, which presents with only granular deposits, is caused by the p.R555W and p.R124S mutations (Bouyacoub et al., 2019; Munier et al., 1997, 2002; Weiss et al., 2015).

In the early stages of GCDII progression, typical granular deposits are usually observed prior to the development of lattice deposition, yet it is also possible that some GCDII patients only manifest the granular deposits without development of lattice deposits (Cao et al., 2009; K. E. Han et al., 2012; Rosenwasser et al., 1993). Furthermore, GCDII is generally a less severe phenotype than GCI. In such cases, genetic screening is particularly useful in the accurate identification of the phenotype and in predicting disease progression.

It is not always possible to obtain detailed medical and family histories of patients. Some patients included in the Moorfields TGFBI CD cohort, were referred following significant disease progression or even sometime following corneal transplantation. This makes it difficult to draw conclusions or correlations on disease progression or severity.

The patients recruited to the current study demonstrate a genotype-phenotype distinction between LCDI and GCDII cases. Around a quarter of the Moorfields cohort were clinically diagnosed with general GCD before receiving an accurate genetic diagnosis through genetic screening (Figure 3.1). Both of the patients with GCDII recruited to this study were initially diagnosed with general GCD before testing positive for the c.371G>A (p.R124H) variant resulting in a refined diagnosis of GCDII. As is shown by the clinical images of the GCDII phenotypes in figures (Figure 3.2), lattice-like deposits are not observed. This could either be due to masking of the lattice deposits by the granular deposits, lack of disease progression or an example of phenotypic variation perhaps resulting from variable expressivity of the gene.

It may be the case that some well-defined forms of CD present atypically upon clinical examination, perhaps leading to the assumption that a new CD has been discovered. In these cases, genetic screening is an essential tool in defining whether the presented case is indeed a novel CD that has not yet been reported, or whether it is an already defined CD that presents with atypical symptoms due to varying degrees of penetrance or variable expressivity of the pathogenic allele.

Patients with the same disease can display atypical patterns of protein deposition or variations in disease severity. This may be due to other genomic variants that could influence molecular pathways, transcription factor binding or cellular homeostasis. Thus, investigations into the full *TGFBI* cDNA sequence could have been carried out in order to identify whether the patients recruited to this study harbour other SNPs that may affect disease severity and progression, as carried out in Evans et al. (2016). However, it is likely that any polymorphisms affecting the penetrance or expressivity of the pathogenic allele would be contained within the promotor region of *TGFBI* causing altered transcription factor binding, resulting in variations in expressivity. This is an interesting research question that is discussed in more detail in Chapter 6, Section 6.3.3.

Over the years, the administration of LASIK (laser-assisted in situ keratomileusis) treatment for myopia and astigmatism correction has become more common. As GCDII can have a delayed presentation in patients with a heterozygous R124H mutation (Chao-Shern et al., 2018), a phenotype is not always observable in the first few decades of life. LASIK is contraindicated in GCDII and many reports have demonstrated exacerbation of corneal opacities post-LASIK treatment in patients with the R124H mutation (Banning et al., 2006; Chao-Shern et al., 2018; Chiu et al., 2007; Jiang & Zhang, 2021; T. I. Kim, Kim, et al., 2008; Poulsen et al., 2016; Roh, Grossniklaus, et al., 2006b, 2006a; Woreta et al., 2015; Xiu et al., 2002; Zeng et al., 2017). Due to the delayed phenotype of GCDII,

pre-LASIK genetic screening should be carried out, to rule out the possibility of disease exacerbation post-operation.

A therapeutic that targets the underlying genetic cause of disease is likely to be the most effective method of treatment for TGFBI CDs. Therefore, screening families with known TGFBI CD cases would be essential to allow for the strategic therapeutic intervention in the prevention of disease symptoms and would enable patients to be recruited to clinical trials when available.

TGFBI is a highly polymorphic gene with over 1000 variants reported in gnomAD (gnomad.broadinstitute.org: gnomAD v3.1.2), with 133 of these being synonymous variants and 290 being missense. Most pathogenic variants of *TGFBI* are found in the fourth FAS1 domain of TGFBIp (Table 9.1, Appendix B). More widespread genetic screening of CDs across different populations for the elucidation of accurate prevalence estimates would perhaps encourage more research into the disease-causing mechanisms of missense mutations of *TGFBI* and why specific mutations result in disease.

Genetic screening is clearly a powerful tool that should be utilised for the subclassification of disease and to inform the management of patients. A genetic diagnosis can help the clinician and the patient by enabling predictions of disease progression. Additionally, genetic screening can also be utilised for obtaining population prevalence estimates which is lacking for CDs.

Previously reported important studies elucidating pathophysiological features of *TGFBI*/TGFBIp in CDs have consisted of biophysical studies carried out on purified TGFBIp or laser capture microdissected corneal deposits from control and TGFBI CD patient corneas (Courtney et al., 2015; Karring et al., 2012; Runager et al., 2009, 2011; Venkatraman, Duong-Thi, et al., 2020; Venkatraman et al., 2017, 2019); molecular analyses of isolated control and TGFBI CD patient primary corneal stromal cells (S. il Choi et al., 2012; T. I. Kim et al., 2011) and histopathological analyses of patient and control corneal sections (Courtney et al., 2015; Dighiero et al., 2001; Patel et al., 2010; Qiu et al., 2016). While these studies have provided invaluable insights into TGFBI CD pathophysiology, the limitations and shortcomings of these methods must be considered in order to address gaps in our knowledge and understanding. Biophysical analyses of purified TGFBIp and TGFBIp protein deposits have provided insights into the structure, processing and protein-protein interactions of WT and mutant TGFBIp (see Chapter 1, Section 1.5; Chapter 6, Section 6.1.1.1.2). However, this approach is limited to examination of cellular and extracellular microenvironments and their effects on protein

function. Primary tissue samples allow for disease-relevant comparisons between control and affected tissue. Yet, the lack of availability of primary tissue samples and the limited growth potential of primary cells makes primary cell culture an inconvenient method for disease modelling and drug screening. Histopathological analyses of control and disease tissue provide excellent visualisations of disease phenotypes at the tissue level and such data has proved invaluable in disease diagnosis. However, such images usually demonstrate the end stage of disease and do not facilitate the development and screening of potential therapeutics.

For these reasons, an appropriate TGFBI CD disease model is needed that can be utilised for investigations into the physiopathology of TGFBI CDs and the screening of potential therapeutics. Although there are treatment options available for TGFBI CDs, the therapeutic effect is usually temporary as they do not target the underlying genetic cause of disease. Recurrence of symptoms following currently available treatments occurs, causing the need for repeat treatments. Patients 1 and 2 recruited to the current study are both cases where patients required repeated treatments on the same eye(s). These cases demonstrate the need for a therapeutic that targets the underlying genetic cause of disease, which along with genetic screening would allow for prevention of disease symptoms.

The ground-breaking technical advance of iPSCs in 2006 and 2007 has enabled their convenient generation in labs worldwide, serving as physiologically relevant, patient-derived *in vitro* disease models. Pluripotent stem cells capable of differentiating into any somatic cell type compliment other methods of research in the field by offering appropriate models for investigations into disease mechanisms and the screening of potential therapeutics in a cellular context.

In the current study, patient fibroblasts were reprogrammed into iPSCs by forced expression of the Yamanaka factors *OCT3/4, SOX2, KLF4* (K. Takahashi et al., 2007), with *C-MYC* substituted by *L-MYC,* as the latter has been shown to be more efficient and has less transformation activity (Nakagawa et al., 2010). *LIN28* and miRNA 302/367 were also included in the reprogramming cocktail for this study, as they have been reported to increase the efficiency of integration-free reprogramming (Okita et al., 2011; Ying et al., 2018). iPSC line characterisation demonstrated positive expression of the cell surface markers SSEA4 and TRA-1-60 – defined as ESC markers (Draper et al., 2002; Fong et al., 2009). Nuclear expression of self-renewal regulators, NANOG and OCT4 (Amini et al., 2014; Swain et al., 2020), was also observed in the iPSC lines. The expression of NANOG, SSEA4 and TRA-1-60 in the lines clearly demonstrates the

endogenous expression of pluripotency markers, as these factors were not used in the reprogramming cocktail. Thus, the forced expression of the transcription factors used in this study (*OCT3/4, SOX2, KLF4, L-MYC* and *LIN28*) resulted in the organisation of a stable network state of stem cellness. Furthermore, the endogenous expression *of OCT4, LIN28, SOX2* and *L-MYC* was demonstrated by RT-PCR amplification of the genes. Expression of the episomal vectors used for reprogramming however, was not detected at iPSC passage numbers typically used for differentiation (Figure 3.4). This is important to note as past research has shown that absence of silencing of the ectopic reprogramming factors predispose iPSCs to genomic instability (Ramos-Mejia et al., 2010). Collectively, the results presented confirm that the iPSC lines generated for the current study endogenously express key pluripotency markers. However, in order to properly confirm their pluripotent potential and suitability for cell differentiation iPSC lines should be assayed for their capacity to differentiate into all three germ layers by teratoma assay, trilineage differentiation assay or the TaqMan(®) hPSC Scorecard™ Panel.

Furthermore, quality control methods assessing the genomic stability of the lines were not employed in the current study. Genomic stability is required for the reproducibility of experimental data and would be essential for clinical use of iPSCs (H. T. Nguyen et al., 2014; Volpato et al., 2018). Additionally, incomplete DNA replication reprogramming has been demonstrated in iPSCs with low differentiation potential, indicating that genomic stability can impair iPSC differentiation (Paniza et al., 2020). As the genomic stability of iPSC lines used in this study was not assessed, the differentiation capacity of the lines was not confirmed. Genomic abnormalities may occur through the reprogramming process or by passaging induced mutations, resulting in the accumulation of genomic and tumorigenic abnormalities.

Some genomic regions are more prone to instability than others. Chromosome number abnormalities, known as aneuploidy, have been reported in both iPSC and ESC lines. These abnormalities can induce complex dysregulation of cell function (Upender et al., 2004). Trisomy of chromosome 12 and 20q are recurrent abnormalities in iPSC and ESC lines, the former being the most predominant, and trisomy 8 has been found to occur more commonly in iPSCs relative to ESCs (Mayshar et al., 2010; Taapken et al., 2011). A large scale study of 552 cultures from 219 human iPSC lines showed that 12.50% had abnormal karyotypes (Taapken et al., 2011). The same study demonstrated that the frequency and different forms of karyotypic abnormalities are not affected by reprogramming methods or growing substrates. Furthermore, it was demonstrated that rates of aneuploidy increase with increasing passage numbers, but that abnormal karyotypes can and do occur at low passage and normal karyotypes can also occur at

high passage numbers (Taapken et al., 2011). This suggests that regardless of the reprogramming method used or the passage number, routine investigation of karyotypic abnormalities should be conducted on iPSC lines used in scientific research.

Copy number variations (CNVs) can also occur due to genomic instability of iPSC lines. A large-scale study compared 506 iPSC lines to donor DNA and found that 149 of these lines showed CNV differences, amounting to 258 newly acquired CNVs (Kanchan et al., 2020). The genes mapping to regions of acquired CNVs demonstrated an enrichment in signalling cascades and cancer related processes, with particular regions of instability mapping to chromosome 1, 2, 3, 16 and 20. High resolution techniques such as array comparative genomic hybridisation can detect unbalanced genomic changes including CNVs.

For the routine use of iPSC lines in basic research applications, extensive high-resolution analyses are perhaps unnecessary and come with technical and financial prohibitions. Standard pluripotency assays and karyotyping should be sufficient, although the potential impact of genomic abnormalities on results should be considered. As genomic instability was not investigated in the current study, any observations that may pertain to disease phenotype cannot be confirmed without further examination of the quality of iPSC lines.

Independent control and patient-derived iPSC lines were generated for this study. However, advances in gene editing technology have recently enabled the generation of isogenic controls that can provide optimal disease modelling in genetically controlled conditions, as reported in various studies (Pires et al., 2016; Xu et al., 2017; Y. Zhang et al., 2017). This method can minimise genetic variability in genotype-phenotype investigations allowing for robust findings. Although isogenic controls are ideal in disease modelling, they were not employed in the current study. A CRISPR/Cas9 homozygous KO however, was used in the current study as a tool to measure TGFBI antibody specificity and any effect of the absence of TGFBIp on corneal epithelial cell differentiation. Heterozygous and homozygous TGFBI KO lines can facilitate investigations into TGFBIp function and downstream signalling. Due to the minimal expression of *TGFBI* transcript in iPSCs (Figure 3.5), TGFBIp expression in the CKO and other iPSC lines was not investigated.

Studies have demonstrated that TGFβ is a negative regulator of iPSC reprogramming and that inhibition of TGFβ signalling can facilitate the molecular reprogramming process by promoting mesenchymal to epithelial transition (Ichida et al., 2009; W. Li et al., 2016; Maherali & Hochedlinger, 2009). Thus, the TGFβ downstream signalling pathway target

genes are likely to be downregulated in iPSC cultures (J. Ge et al., 2015). Similarly, siRNA knockdown of *Tgfbi* increased reprogramming efficiency of mice embryonic fibroblasts, demonstrating that TGFBIp, along with other ECM proteins, are barriers to the reprogramming process (Z. Li et al., 2014). Therefore, the literature supports the lack of *TGFBI*/TGFBIp expression in iPSCs, indicating that different cell samples should be used for the analysis of this transcript/protein.

To summarise, this chapter describes the establishment of patient-derived iPSC lines for the study of two of the most common epithelial-stromal TGFBI corneal dystrophies, based on genetic prevalence of the MEH CD patient cohort and reports in the literature. Clinical details and genetic screening data for biopsied patients was collated as a basis for the understanding and interpretation of the *in vitro* disease model investigations. iPSC lines derived from two patients harbouring c.370C>T (p.R124C) and two patients harbouring c.371G>A (p.R124H) mutations in *TGFBI* were generated. The patient-derived iPSCs were cultured alongside two WT and a homozygous *TGFBI* KO line(s). The iPSC lines were confirmed to express key self-renewal genes via RT-PCR and ICC. However, a key limitation of this study was that the iPSC lines were not confirmed to have the capacity to differentiate into each of the three germ layers and their genomic stability was not assessed. Therefore, full conclusions on the suitability of the iPSC lines for differentiation into corneal epithelial-like cells cannot be made. Nonetheless, the TGFBI CD patient-derived iPSC lines established in this study allow for differentiation of corneal epithelial-like cells providing an appropriate *in vitro* disease model of CDs and the development and screening of potential therapeutics, thus, addressing gaps in the field poised by the lack of appropriate animal or other *in vitro* model systems.

Chapter 4: *In vitro* corneal epithelial cell model of TGFBI corneal dystrophies

4.1 Introduction

iPSC technology has enabled the generation of genetically specific and physiologically relevant cellular disease models. *TGFBI* corneal dystrophy phenotypes, like many human disease phenotypes, are not fully recapitulated in animals such as mice, which are the most commonly used animal models. Furthermore, culturing patient-derived disease tissue-specific samples is not always possible or convenient and usually only allows for the study of the end-stage of disease. Thus, iPSC-derived models have emerged as an important new system for the study of disease pathophysiology and the development and screening of potential therapies.

4.1.1 TGFBI expression in the cornea

TGFBI is widely expressed throughout tissues of the body (Ivanov et al., 2008; Skonier et al., 1992), with a particular abundance of TGFBIp demonstrated in the cornea (Dyrlund et al., 2012; Escribano et al., 1994). The concentration of wildtype TGFBIp in the healthy cornea has been estimated at approximately 26 μM (1.7 mg/ml) (N. S. Nielsen et al., 2020). TGFBIp expression in the human cornea increases by around 30% between the ages of 6 and 14 (Karring et al., 2010). In mice, *in situ* hybridisation demonstrated that *Tgfbi* mRNA was restricted to the corneal epithelium (Poulsen et al., 2018a). In humans, TGFBIp is expressed in all the layers of the human cornea and is the first and second most abundant protein in the corneal endothelium and stroma, respectively (Dyrlund et al., 2012). At the transcript level, *TGFBI* is most highly expressed in the corneal epithelium, relative to the other corneal compartments, and displays the highest expression level in the basal central corneal epithelium (Ligocki et al., 2021). Due to the particularly high expression of *TGFBI* in the basal central corneal epithelium and the presence of TGFBIp+ sub-epithelial corneal deposits in *TGFBI* corneal dystrophies, along with the corneal stroma being relatively acellular and TGFBIp being a secreted protein, it is thought that a substantial portion of TGFBIp expressed in the stroma is due to secretion of this protein by the corneal epithelium (Figure 4.1).

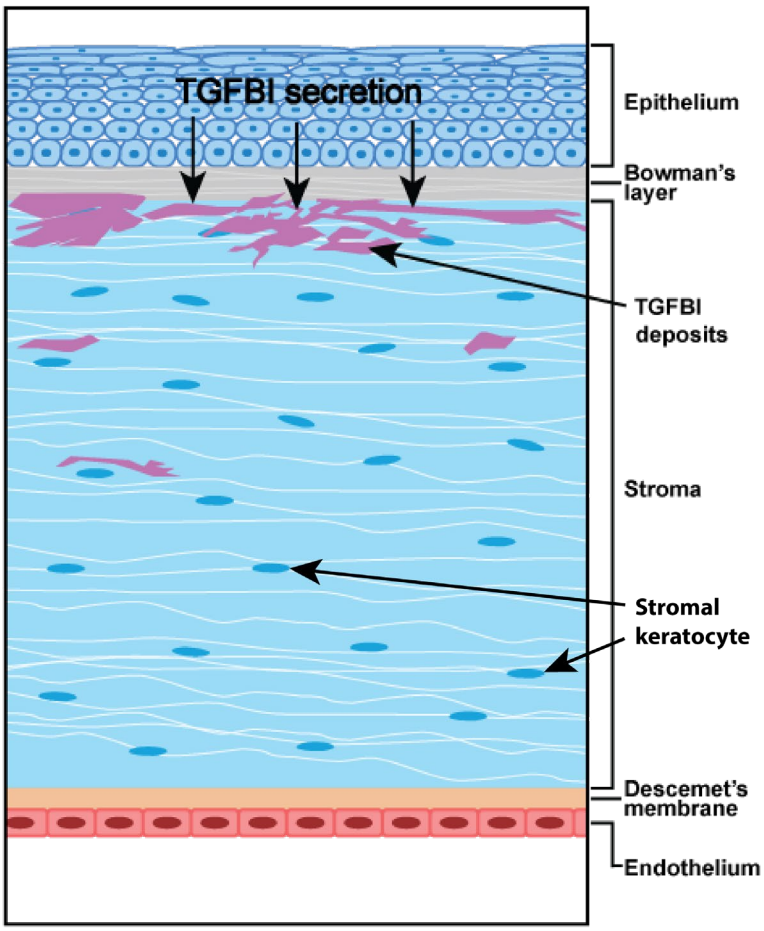

Figure 4.1 Illustration of the layers of the cornea and TGFBIp localisation in mutant conditions. The cornea is composed of three main layers: the outermost corneal epithelium, the middle stroma, and the innermost endothelium. In normal conditions, TGFBIp (Transforming Growth Factor Beta-Induced Protein) is thought to be secreted by the corneal epithelium and stromal keratocytes. TGFBIp is diffused throughout the stroma, where it plays a role in cell-collagen interactions. In the presence of TGFBIp mutations, however, the protein aggregates in the subepithelial layer and superficial stroma, leading to opacities and impaired vision.

4.1.2 Cells of the limbal and central corneal epithelium

The cornea is a heterogenous tissue, with the epithelium being the most heterogenous layer, containing more cell subpopulations than the stroma and endothelium (Català et al., 2021; J. Collin et al., 2021; Ligocki et al., 2021). The main cellular compartments of the corneal epithelium are the limbus and the central corneal epithelium (Figure 4.2). The limbus, located at the periphery of the cornea separating it from the conjunctiva, is comprised of limbal stem cells (LSCs), limbal epithelial progenitor cells (LPCs) and transit amplifying cells (TACs) in the basal layers (D. Q. Li et al., 2021) (Figure 4.2). Post-mitotic cells at various early stages of differentiation and terminally differentiated cells at more mature stages of differentiation, reside in the suprabasal and superficial layers of the limbus (Català et al., 2021; D. Q. Li et al., 2021).

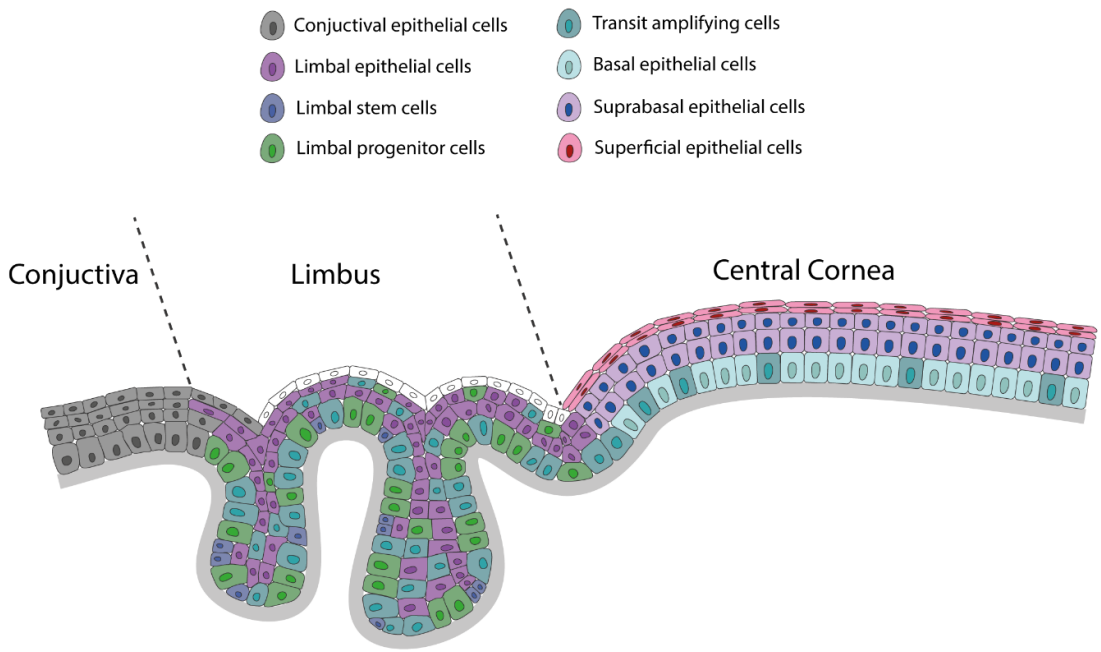

Figure 4.2 Cellular subpopulations of the limbus and corneal epithelium identified by single cell RNA sequencing (scRNAseq) reports. Limbal stem cells, limbal progenitor cells, transit amplifying cells and early differentiated limbal epithelial cells are located in the limbus. The central cornea is mainly comprised of basal, suprabasal and superficial corneal epithelial cells, however, some transit amplifying cells or cells with migratory and mitotic properties are also likely to be present.

Cells of the basal limbus account for ~15% of limbal cells and are significantly smaller than other cells of the limbus at around 10-20μm (Figure 4.3) (D. Q. Li et al., 2021). LSCs are slow-cycling, quiescent cells with high proliferation potential (Gonzalez et al., 2018; Lužnik et al., 2016). Due to the small numbers of LSCs, estimated at around ~320 cells per human corneal limbus, these cells have remained elusive and difficult to characterise (D. Q. Li et al., 2021). Li et al. (2021), was able to focus on defining the LSC population by sequencing a high number (16,360) of cells specifically isolated from the adult corneal basal limbus, yet only identified 69 (0.4%) cells as LSCs.

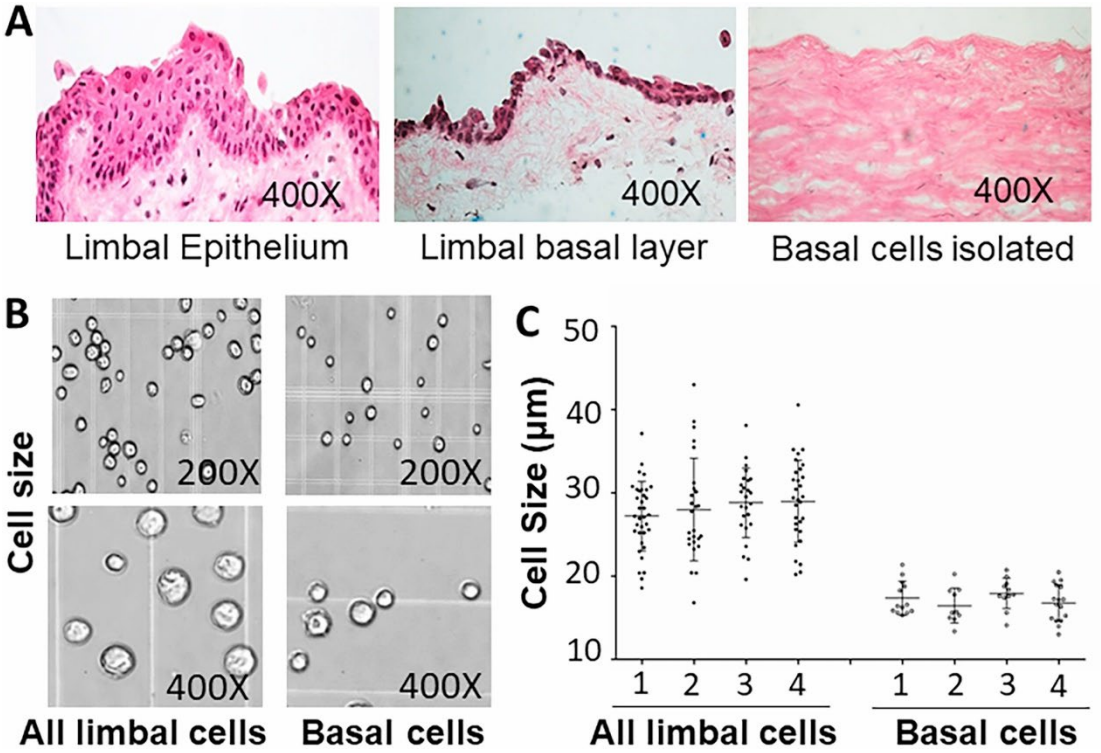

Figure 4.3 Size of isolated limbal basal cells from donor cornea. A) Imaging of sectioned corneal limbal tissue demonstrates the palisades of Vogt that contain 5-7 layers of limbal epithelial cells. 1-2 layers of limbal basal cells are observed following removal of the superficial layers. Limbal basal cells were isolated through dissociation from the underlying limbal stroma. **B-C)** Isolated limbal basal cells measured 10-20 µm in diameter and were significantly smaller than all other cells of the basal limbus ($P<0.01$, $n=4$). Figure from Li et al. (2021).

LSCs, like other adult stem cells, can divide asymmetrically or symmetrically. Asymmetric division generates one stem cell and one daughter cell committed to a progenitor cell or a TAC which would eventually differentiate into mature cells. Whereas symmetric division can create two identical stem cells or two daughter cells. TACs are able to rapidly proliferate to generate many differentiated cells during both development and regeneration and are defined as an intermediate subpopulation of cells between the adult stem cell and differentiated cell state (J. M. Li et al., 2021; Rangel-Huerta & Maldonado, 2017). scRNAseq studies have characterised TACs of the limbus and confirmed their high expression of major proliferation and cell-cycle dependent genes such as *TOP2A*, *MKI67*, *FOXM1*, and *PLK1*, and low expression of differentiation markers (Català et al., 2021; J. M. Li et al., 2021).

Precisely defining and distinguishing between the molecular signatures of LSCs, LPCs and TACs is a challenging task. Dou et al. (2021) provided an insightful study which grouped LSCs and LPCs together, although, a hierarchy of four LSC/LPC subtypes was precisely defined based on their molecular profile, with two subclusters exhibiting a higher stem state, and the two others exhibiting a higher state of differentiation, potentially corresponding to LSC and LPC subtypes respectively. Interestingly, upon

investigation of cellular and molecular alterations during physiological aging, it appeared that LSCs/LPCs maintained an age-independent state (Dou et al., 2021). No differences in proportions of LSCs/LPCs or stemness-potential across donor corneas of 13y, 54y, 64y or 95y old individuals were observed (Dou et al., 2021).

The central corneal epithelium is more clearly defined than the limbus, with reports investigating this corneal compartment agreeing that the main cell subtypes can be defined based on where in the tissue they reside, either the basal, suprabasal or superficial central corneal epithelium (Figure 4.3) (Català et al., 2021; J. Collin et al., 2021; Ligocki et al., 2021). Analyses of limbal and corneal epithelial cell subpopulation markers has revealed both exclusively expressed and overlapping marker genes expressed among the subsets of cell clusters (Català et al., 2021; J. Collin et al., 2021; Dou et al., 2021; D. Q. Li et al., 2021; Ligocki et al., 2021). This is consistent with the different forms of progenitor and differentiated epithelial cells possessing different functions, yet also maintaining a continuous epithelial structure from the basal to superficial layer of the limbal, peripheral and central cornea.

4.1.3 Markers of limbal and central corneal epithelial cells

The recently published scRNAseq studies on corneal tissue have provided invaluable information on key markers of the various cellular subpopulations of the human corneal epithelium. The data obtained from these studies, in conjunction with immunostaining and proteomic analyses of the cornea, allow for the comparison of expression profiles between corneal epithelial-like cells (CEpi) described in this chapter and the native corneal epithelium therefore enabling the validation of an *in vitro* iPSC-CEpi model appropriate for the study of epithelial-stromal corneal dystrophies and the screening of potential therapeutics.

4.1.3.1 Keratins

Keratins are intermediate filament proteins which play a structural role in the mechanical stability and integrity of individual epithelial cells and epithelial tissue via the formation of cell-cell contacts (Moll et al., 2008). In the corneal epithelium, keratins are the most abundantly expressed proteins, with a proteomic study demonstrating that K12, K5, K3, K15, K4, K8, K19 and K14 are amongst the top 30 proteins expressed in the human tissue (Dyrlund et al., 2012). scRNAseq has provided insight into the keratin expression profile of the different subpopulations in the limbal and central corneal epithelium, with *KRT15* and *KRT14* being highly expressed by basal cells of the limbus; *KRT5*, *KRT3* and *KRT12* being generally expressed the suprabasal and superficial cells of the limbus

and most cells of the central corneal epithelium; and *KRT24* being expressed by the superficial cells of the central epithelium (Català et al., 2021; J. Collin et al., 2021).

Intermediate filament proteins have been classified into six groups (types I to IV) based on similarities between amino acid sequence. Keratins make up the type I (acidic) and II (neutral/basic) classes of intermediate filament proteins. Type I and type II keratins form obligate pairs which copolymerise to form filaments. Conventionally, it is expected that there should be equimolar amounts of the respective paired keratins expressed in any given epithelial cell, with the stability of a keratin in cell culture being dependent on the expression of its partner keratin (Kulesh et al., 1989; Kulesh & Oshima, 1988; X. Lu & Lane, 1990). However, previous reports have shown that this pattern of keratin pairing is not always followed faithfully, with one keratin perhaps more dominantly expressed than its expected obligate partner (Bloor et al., 2000; Guldiken et al., 2015). In the case of differing expression levels within pairs, it is apparent that another compatible keratin may compensate by acting as an alternative co-expression partner (Bloor et al., 2000; Fischer et al., 2014; Lloyd et al., 1995; H. Lu et al., 2006). Of note, keratins are regulated independently of each other, primarily through transcriptional regulation by transcription factor binding to their gene promoter regions (Review: Blumenberg, 2013).

The keratin expression profile of the cell is tissue specific and differentiation dependent and can therefore be used to identify the state of epithelial differentiation. In stratified epithelia, the respective type II and type I paired keratins **K5** and **K14**, are expressed in the basal proliferative layer, indicating a possible role for these partners in the maintenance of cell proliferation potential (Alam et al., 2011; Moll et al., 1982). As K5/K14+ cells gradually migrate upwards, differentiating along the way, expression of this keratin pair is usually reduced, and expression of a different and more characteristically mature keratin pair is induced depending on tissue type (Fuchs & Green, 1980).

Transcriptomic data on the expression of *KRT5* and *KRT14* demonstrates their expression in the limbus and basal layer of the central corneal epithelium (Català et al., 2021; J. Collin et al., 2021). This is further corroborated by immunofluorescent staining on corneo-scleral discs showing strong reactivity of K5 and K14 in both the limbal and central layers of the corneal epithelium, with K14 being localised more specifically to the basal layers (Figure 4.4) (Merjava et al., 2011).

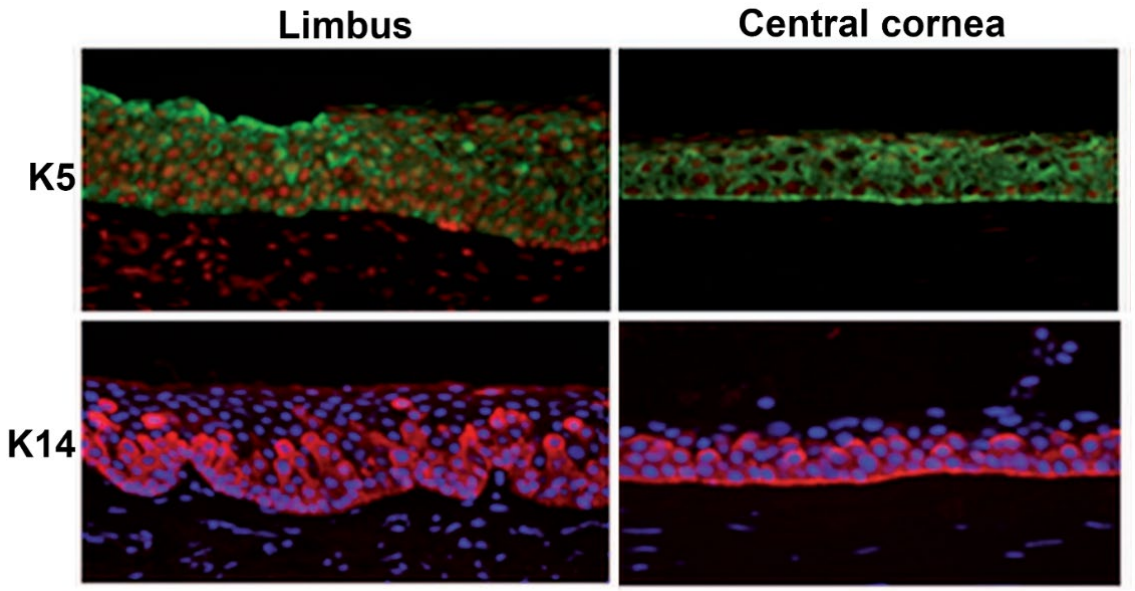

Figure 4.4 Keratin 5 (K5) and keratin 14 (K14) expression in the human limbal and central corneal epithelium. K5 staining is observed throughout the layers of the limbus and central cornea, whereas K14 staining shows specific positivity at the basal layers of both corneal compartments. Images from Merjava et al. (2011).

Dominant negative mutations of *KRT5* or *KRT14* cause the hereditary blistering skin disease emidemolysis bullosa simplex (Lane & McLean, 2004). In K14 null mice, severe blistering in the skin and oral mucosa is observed, with the death of most mice occurring within days 3-5 following birth (Lloyd et al., 1995). K5 null mice display a similar yet more severe phenotype to K14 knockouts, with death occurring shortly after birth (Peters et al., 2001). K5 null mice do stably express K14, as well as other type I keratins, with only a minor reduction in expression observed, contradicting previous data showing that the stability of keratin expression is dependent on expression of its partnered keratin. These data indicate that in the absence of their natural partner, keratins can form novel heteromeric complexes, provided that an alternative compatible keratin is expressed within the tissue (Lloyd et al., 1995; H. Lu et al., 2006; Peters et al., 2001; Troy & Turksen, 1999).

The expression of the paired **K3** and **K12** keratins are specific to the corneal epithelium. Mutations in these keratins affect the cornea specifically, causing Meesmann's corneal dystrophy, which presents with intraepithelial microcysts in the corneal epithelium (Irvine et al., 1997). scRNAseq has demonstrated *KRT3*/*KRT12* transcript expression throughout the layers of the central corneal epithelium (Català et al., 2021; Collin et al., 2021). Through immunofluorescent K3 and K12 staining of corneas, strong expression is observed in all layers of the central corneal epithelium, as well as some positive reactivity in the suprabasal and superficial cells of the limbus (Figure 4.5) (J. Collin et al., 2021; Merjava et al., 2011; Ouyang et al., 2014a).

The *KRT12* gene is highly conserved in its expression in the corneal epithelium in all species that have undergone examination, while the *KRT3* gene shows interspecies differences (Chaloin-Dufau et al., 1993). In mice, *KRT3* is a pseudogene and corneal epithelial differentiation is marked by the expression of K5/K12. K12 null mice are viable and show a cornea-specific phenotype of fragile corneal epithelia and corneal erosions, no defects in skin and hair were noted by gross examination (Kao et al., 1996).

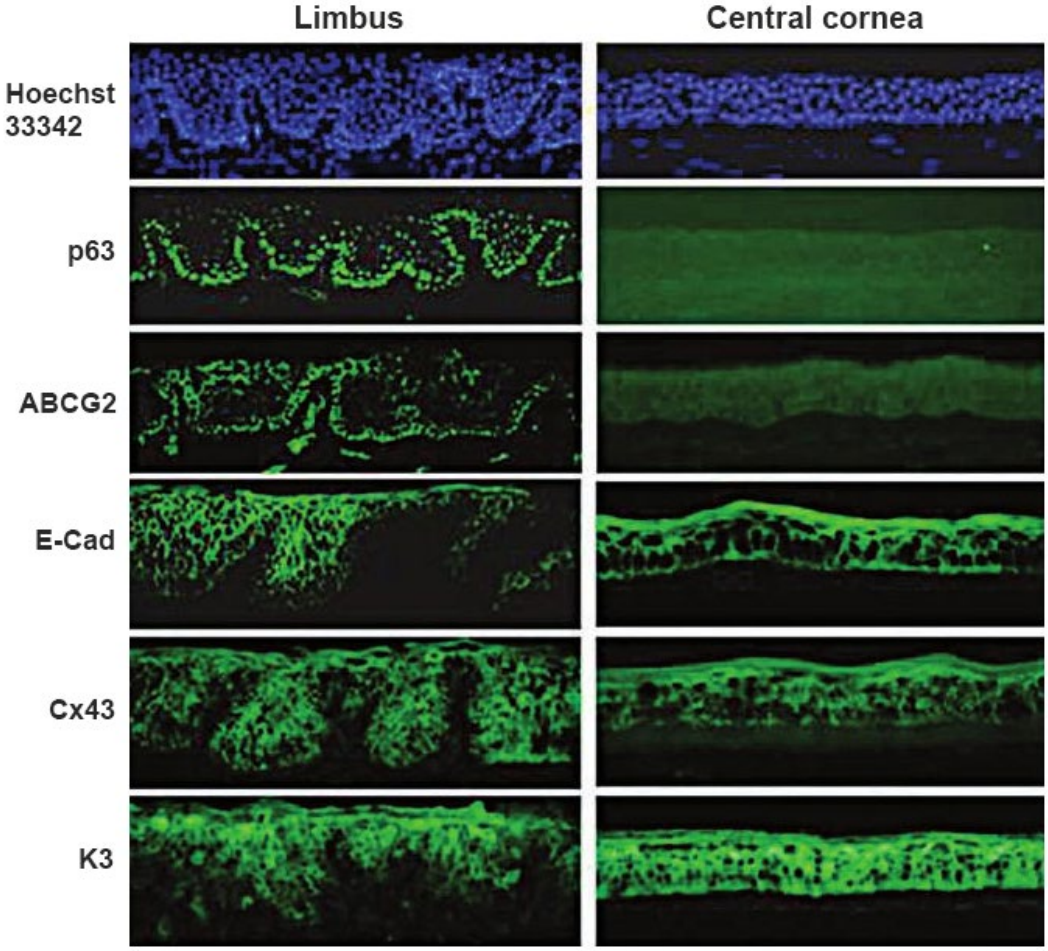

Figure 4.5 Immunostaining of corneal epithelial LSC/LPC markers p63 and ABCG2, cell-cell junction markers E-Cadherin (E-Cad) and Connexin 43 (Cx43) and specific marker Keratin 3 (K3) in human limbal and central corneal epithelium sections. Hoechst 33342 was used as a counterstain. Images are from Z. Chen et al. (2004).

4.1.3.2 PAX6

The paired box protein PAX6 is a highly conserved transcription factor that is essential for the formation of the surface ectoderm and controls many downstream genes involved in eye morphogenesis and corneal maintenance (Kitazawa et al., 2017; Polisetti et al., 2023; Sunny et al., 2022; Takamiya et al., 2020). PAX6 expression determines the fate of LSC/LPCs and regulates corneal epithelial cell identity (G. Li et al., 2015; Sunny et al., 2022). PAX6 is expressed throughout the limbal and central corneal epithelium, while no expression is detected in the stroma (Figure 4.6) (Ouyang et al., 2014b; Polisetti et al.,

2023). *PAX6* knockdown in cultured human LPCs and corneal epithelial cells activates the expression of skin epidermis-specific genes, consistent of induction towards an epidermal cell fate (Kitazawa et al., 2017; G. Li et al., 2015; W. Li et al., 2008; Ouyang et al., 2014). Therefore, PAX6 expression appears to be a critical determinator of corneal epithelial cell fate and is a key differentiator between the corneal epithelium and the skin epidermis.

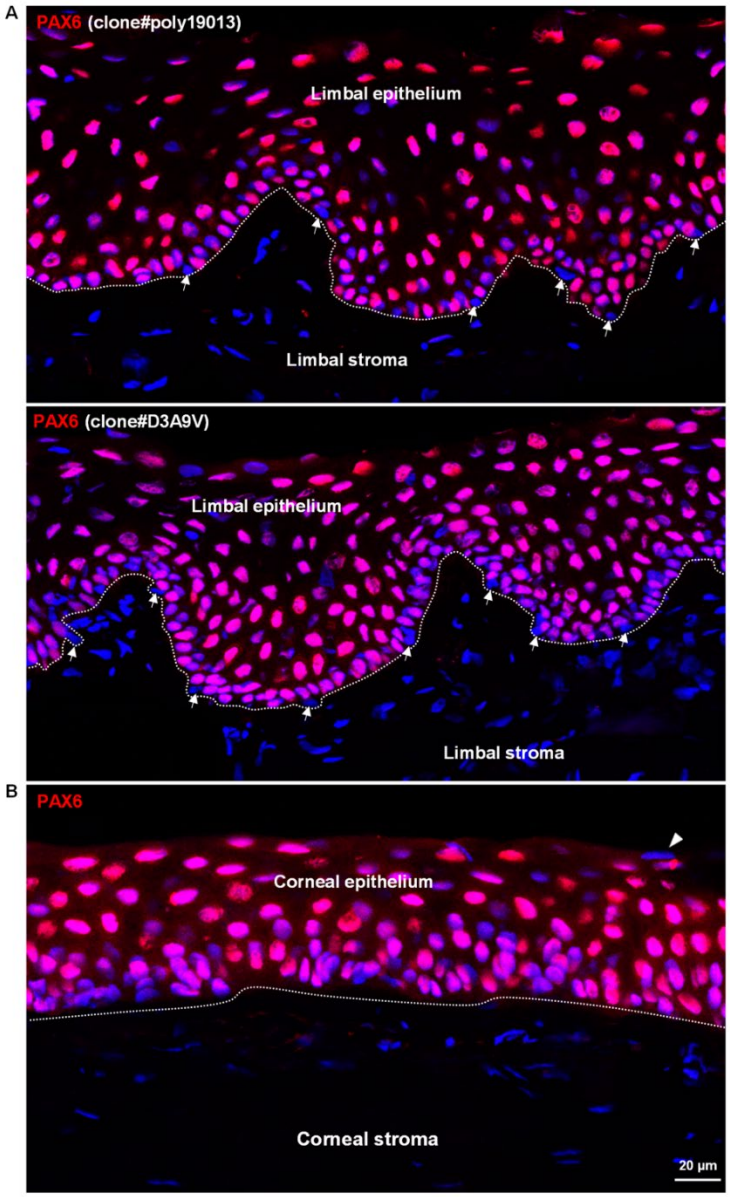

Figure 4.6 PAX6 expression in the limbal and central corneal epithelium. A) Immunostaining of human corneoscleral tissue sections using two distinct clones of PAX6 antibodies shows the nuclear expression of PAX6 (red) throughout the limbal epithelium. PAX6-negative cells (arrows) observed in the basal layer of the limbal epithelium correspond to vimentin+ limbal niche cells that likely originate from the neural crest. **B)** immunostaining of corneal tissue demonstrated PAX6 expression (red) throughout the corneal epithelium, with the exception of very few superficial cells (arrowhead) where loss of PAX6 expression is associated with cell shedding. PAX6 expression is not observed in the stroma. Dashed line represents the basement membrane. Nuclear counter staining with DAPI (blue). Figure from Polisetti et al., 2023.

4.1.3.3 Cell-cell junction markers

Four types of cell-cell junctions are found within the corneal epithelium: desmosomes, gap junctions, adherens junctions and tight junctions. Cell-cell junction marker expression in the corneal epithelium differs depending on the cellular subpopulation.

Gap junctions are intracellular connections that allow direct communication and exchange of small molecules, ions and electrical signals between adjacent cells. The connections are composed of proteins called connexins, which form hexameric complexes called connexons. **Connexin 26** (Cx26, encoded by *GJB2*) and **Connexin 30** (Cx30, encoded by *GJB6*) expression is limited to the basal layer of the central epithelium (Català et al., 2021; J. Collin et al., 2021; Shurman et al., 2005). **Connexin 43** (Cx43, encoded by *GJA1*) is the most abundantly expressed gap junction protein in the human corneal epithelium, and has been detected at the transcript and protein level throughout all layers of the limbus and central corneal epithelium, with the exception of the most superficial and individual basal cells of the limbus (Figure 4.5) (Català et al., 2021; Z. Chen et al., 2004; Dou et al., 2021; Shurman et al., 2005).

Adherens junctions are located throughout the layers of the corneal epithelium and function to stabilise cell-cell adhesion (Hartsock & Nelson, 2008). The main component of adherens junction structure is **E-Cadherin**, a transmembrane glycoprotein which consists of an extracellular domain that forms adhesions between epithelial cells, and a cytoplasmic domain that is connected by the actin cytoskeleton (Yuksel et al., 2021). E-cadherin is expressed throughout the corneal epithelium, with the exception of the basal layer of the limbus (Figure 4.5) (Z. Chen et al., 2004; Dou et al., 2021).

4.1.3.4 Limbal stem and progenitor cell markers

ABCG2 is a member of the ATP-binding cassette (ABC) family of cell surface transport proteins, and its expression is a conserved feature of stem cells of a variety of tissue types (Scharenberg et al., 2002; S. Zhou et al., 2001). Transcript and protein expression of ABCG2 in the cornea is defined as an exclusive marker of cells residing in the basal layer of the limbus (Figure 4.5) and it has since been used as an identifier of LSCs (de Paiva et al., 2005). The population of ABCG2+ LSCs is indeed rare, with some of the recently published scRNAseq on the whole cornea having not identified a substantial ABCG2+ population of cells, likely due to insufficient sequencing depth (Català et al., 2021; J. Collin et al., 2021; Ligocki et al., 2021). However, scRNAseq of the basal layer of the limbus did identify a population of cells that highly expressed putative stem cell markers including, *ABCG2*, *ABCB5*, *ITGA9*, *LEF1* and *POSTN*, and the newly identified LSC markers, *TSPAN7* and *SOX17*, the majority of which were in a quiescent, slow

cycling cell state (D. Q. Li et al., 2021). Interestingly, the same markers were moderately expressed by a subpopulation of cells identified as TACs that were in cell proliferation cycle states, which also showed high expression of proliferation markers such as *CCNB1*, *BIRC5*, *TOP2A* and *MKI67* (J. M. Li et al., 2021).

P63 is a protein of the p53 protein family, encoded by the *P63* gene expressed as at least six isoforms. Three of these isoforms are generated by an upstream promoter giving rise to the transactivating classes of p63 (Ap63α, Tap63β, Tap63γ). The remaining three isoforms are generated by an intronic promoter giving rise to the ΔN classes of p63 which lack the transactivating domain (ΔNp63α, ΔNp63β, and ΔNp63γ) (Review: Murray-Zmijewski et al., 2006). In the normal corneal limbus, ΔNp63α is exclusively expressed, whereas expression of the ΔNp63β, and ΔNp63γ isoforms is activated upon wounding (di Iorio et al., 2005; Pellegrini et al., 2001). Immunostaining and scRNAseq on the cornea has confirmed the enrichment of *P63* in the human corneal limbus, particularly in the basal layer (Figure 4.5) (Català et al., 2021; Collin et al., 2021; Dou et al., 2021).

Mice lacking p63 present with a fundamental defect in epithelial differentiation and fail to develop stratified epithelia (Mills et al., 1999; A. Yang et al., 1999). The surface epithelium of these mice consists of a single layer that lacked K5 and K14 expression (Mills et al., 1999; A. Yang et al., 1999). Based on these findings, it seems that p63 is a transcriptional regulator of *KRT5* and *KRT14* in mice. In human epithelial tissue, it was found that all stratified epithelia investigated displayed intense immunoreactivity of p63 in the basal layer, with a gradual diminution of staining in the more superior, terminally differentiated cell layers (di Como et al., 2002). Therefore, p63 maintains the balance between cell proliferation and the initiation of epithelial stratification (Koster et al., 2004).

Additionally, scRNAseq has newly identified ***GPHA2*** (glycoprotein hormone subunit alpha 2) as a marker of human LPCs (J. Collin et al., 2021). RNA interference of *GPHA2* resulted in the decrease of the LPC marker *KRT15* and an increase in the differentiation markers *KRT3* and *KRT12*, along with a reduction in colony forming efficiency (J. Collin et al., 2021). Taken together, it appears that GPHA2 expression positively controls the progenitor state of human LPCs (J. Collin et al., 2021). Subsequent scRNAseq studies have utilised the identification of *GPHA2*+ cells in the characterisation of their datasets (Ligocki et al., 2021; Maiti et al., 2022).

4.1.4 Corneal epithelial cell signalling

The embryonic development and maintenance of the corneal epithelium requires complex signalling pathways that involve a range of molecules and factors. The understanding of which factors influence and regulate cell fate determination is important

for the directed differentiation of human pluripotent stem cells (hPSCs) towards a corneal epithelial cell fate. Key signalling pathways reportedly involved in the development and maintenance of the corneal epithelium are outlined below:

Suppression of canonical Wnt signalling is necessary for the induction of lens placode formation in the head ectoderm (Kreslova et al., 2007; A. N. Smith et al., 2005), consistent with no canonical Wnt reporter activity in presumptive mouse corneal epithelial cells that co-expressed the epithelia marker keratin 8 (Y. Wang et al., 2018). This data suggests that inhibition of Wnt signalling is necessary for the induction of corneal epithelium formation. However, the role of Wnt signalling in the maintenance of the stratified corneal epithelium is unclear. Many Wnt ligands, receptors and inhibitors are differentially expressed between the corneal epithelium and limbus (Z. Ding et al., 2008; Nakatsu et al., 2011, 2013). The administration of a Wnt mimic to cultured limbal explants has been shown to maintain LSCs *in vitro* (González, Oh, et al., 2019). Additionally, inhibition of canonical Wnt signalling increases the percentage of K12+ cells and decreases the colony-forming efficiency of LSCs cultured of human limbal niche cells (B. Han et al., 2014), indicating that Wnt signalling is necessary for maintenance of the limbal stem cell state. However, deletion of the gene encoding the Wnt inhibitor, *Dkk2*, in mice results in the transdifferentiation of the corneal epithelium into an opaque epidermal-like tissue (Mukhopadhyay et al., 2006). Canonical Wnt signalling has also been detected in the wing and squamous layers of the mouse corneal epithelium (Y. Wang et al., 2018). Nonetheless, the balance of the Wnt signalling pathway in the differentiation and maintenance of the corneal epithelium is complex and at this moment, not fully defined.

Inhibition of the TGFβ signalling pathway is necessary for specification of the ocular surface ectoderm (Dupont et al., 2005). TGFβ signalling is induced upon the binding of a TGFβ superfamily ligand such as, BMPs, Activin, Nodal and TGFβs to a TGFβ type II receptor which phosphorylate and activate type I receptors. Early studies on human and rat corneas demonstrated that TGFβ receptors are more highly expressed in the basal layers of the limbus relative to the suprabasal and superficial limbus (Joyce & Zieske, 1997; Zieske et al., 2001). Immunostaining of TGFβ1 (Pasquale et al., 1993), TGFβ2 (K. Nishida et al., 1994; Pasquale et al., 1993), TGFβ receptor I and TGFβ receptor II (Joyce & Zieske, 1997) has been reported in the human limbus. However, genetic ablation of individual TGFβ genes in the corneas of mice demonstrated that *Tgfb2* inactivation, but not *Tgfb1* or *Tgfb3* inactivation, results in the abnormal fusion of the corneal epithelium to the lens (Saika et al., 2001). Furthermore, the TGFβ ligand, BMP4, is upregulated in the human limbus compared to the rest of the cornea (Nakatsu et al., 2013). The TGFβ

signalling pathway is involved in the development and maintenance of the cornea, although not fully defined.

The **Notch signalling pathway** is a highly conserved pathway that plays an essential role in the development and maintenance of many tissues, including the corneal epithelium. Notch ligands and receptors have been shown to be widely distributed across the layers of the corneal epithelium and limbus (Djalilian et al., 2008; Kulkarni et al., 2010; A. Ma et al., 2007; Thomas et al., 2007). Knockout of the Notch signalling target gene, *HES1*, in mice disrupted corneal development due to abnormal junction formation, LSC differentiation and cell proliferation (T. Nakamura et al., 2008). Inhibition of Notch signalling in human LSCs *in vitro* led to an increase in cell proliferation and a decrease in the percentage of differentiated K12+ cells (González, Uhm, et al., 2019). Activation of Notch signalling in cultured human LSCs resulted in the downregulation of p63α, loss of asymmetric division and reduced stratification (González et al., 2020). Additionally, the Notch signalling pathway is reportedly upregulated during corneal epithelial wound healing in mice (H. Lu et al., 2012). Overall, Notch signalling appears to be important for the positive regulation of corneal epithelial cell differentiation and its inhibition is necessary for maintenance of the progenitor cell population.

4.1.5 The generation of an *in vitro* CEpi model

For the study of diseases attributed to the corneal epithelium and to test potential therapeutics for these conditions, the development of an appropriate CEpi cell model is essential. As patient-derived limbal stem cell biopsies are not usually easily obtainable and only provide limited expansion potential, an effective protocol for the generation of patient-derived iPSC-CEpi models could be implemented for the study of relevant diseases and testing of potential therapeutics.

4.1.5.1 Pluripotent stem cell-derived corneal epithelial cell differentiation

Based on knowledge of the components of the LSC niche and the trajectory of corneal epithelial cell differentiation, protocols attempting to recapitulate this process *in vitro* have been developed. The generation of progenitor and mature corneal epithelial cells from hPSCs not only allows for the modelling of diseases affecting this tissue but is also a promising option for the treatment of bilateral limbal stem cell deficiency (LSCD) (Reviews: Chakrabarty et al., 2018; Ghareeb et al., 2020).

The first protocol published on the differentiation of human CEpi cells used a method of culturing ESCs with limbal fibroblast conditioned media and plating the cells on to collagen IV coated plates, in an attempt to recapitulate characteristics of the limbal stem cell niche (Ahmad et al., 2007).

Hayashi et al. (2012) described a method of CEpi generation from iPSCs using a stromal cell-derived inducing activity method, which utilised feeder PA6 cells to promote an ectodermal cell lineage, which is a derivative of a protocol originally described for the generation of dopaminergic neurons (Kawasaki et al., 2000). Using this method, the authors compared the CEpi differentiation potential between iPSCs derived from either HDFs or human adult corneal limbal epithelial cells (HLECs) following a prolonged period of differentiation culture (12 weeks) (Hayashi et al., 2012). Using this protocol, iPSCs derived from HLECs displayed a higher CEpi differentiation potential, expressing the relevant markers K12 and K3 earlier and at a higher level respective to the HDF-derived iPSCs. This effect was attributed to the retainment of epigenomic signatures of iPSCs following reprogramming (Hayashi et al., 2012). A few years later, the same group established a new feeder-free CEpi differentiation protocol based on the formation of a 2D 'SEAM' (self-formed ectodermal autonomous multizone) composed of four concentric zones that have the potential to give rise to different ocular lineages (Hayashi et al., 2017). The corneal epithelial progenitors contained within this heterogenous culture were isolated by fluorescence activated cell sorting (FACS) based on their positive expression of ITGB4 and SSEA-4, and negative expression of TRA-1-60 or CD200 (Hayashi et al., 2018). The corneal epithelial cell sheets generated from this work were transplanted in a non-human primate model of LSCD and a uniformly stratified corneal epithelium was observed six months post-transplantation (Yoshinaga et al., 2022).

Other protocols have utilised small molecules to direct the differentiation of hPSCs towards a CEpi lineage. One focused on the induction of epithelial differentiation by modulation of β-catenin localisation upon treatment of hPSCs with the Src family kinase inhibitor SU6656 or retinoic acid (RA) (Lian et al., 2013). A strong upregulation of the epithelia keratin markers K18/K8 and repression of the pluripotency marker Oct4 was observed following SU6656 treatment (Lian et al., 2013).

Another protocol induced CEpi differentiation of iPSCs by attempting to replicate signalling cues during ocular surface ectoderm development through TGF-β inhibitor SB-505124 and Wnt inhibitor IWP-2 administration in combination with basic fibroblast growth factor (bFGF) in serum and feeder-free conditions. By day 44 of this protocol, pluripotency markers were downregulated and the corneal epithelial markers *PAX6*, *P63*, *KRT15*, *KRT3* and *KRT12* were upregulated (Mikhailova et al., 2014). However, due to issues with excessive cell death and spontaneous neuronal differentiation as a result of this method, the authors built on the protocol through specific modifications. Embryoid bodies were formed from iPSCs and underwent an initial one-day ectodermal induction with SB-505124 and bFGF, followed by a two-day mesodermal induction with bone

morphogenetic protein 4 (BMP4). Cells were then plated onto Laminin-521 and collagen IV coated plates and cultured in the commercial Cnt-30 corneal epithelial medium. By day 22, cells expressed the corneal epithelial progenitor markers P63, K14 and K15, yet no expression of the corneal epithelial-specific markers K12 and K3 were observed at this point (Hongisto et al., 2017).

Kamarudin et al. (2018) also observed the positive effect of the role of BMP4 in the induction of CEpi cells from iPSCs following the assessment of supplementation of different growth factors and morphogens to the induction media. They concluded that a combination of BMP4, RA, and epidermal growth factor (EGF) resulted in the most successful induction of corneal epithelial cells as evidenced by this condition showing highest expression levels of *P63* and *KRT12* at day 20 respective to other culture conditions (Kamarudin et al., 2018).

4.1.6 Chapter aims

The main aim of this research chapter was to characterise and validate the iPSC-derived corneal epithelial cell *in vitro* model used in this study by:

- Justification of the development of a corneal epithelial cell-like model to study TGFBI corneal dystrophies.
- Assessment of the gene and protein expression profile of the differentiated samples over the course of the differentiation protocol.
- Assessment of differentiation to a corneal epithelial-like (CEpi) lineage as a model system.
- Defining the optimal experimental timepoint for ASO treatment.

4.2 Results

4.2.1 *TGFBI* expression in the human cornea

In light of the wealth of recently published scRNAseq data on the human cornea, markers of the human cornea have become well defined. As TGFBI CDs are known to involve multiple layers of the cornea, namely the corneal epithelium and the stroma, the *in vitro* modelling of these conditions is not straight forward. It has previously been reported that *TGFBI* mRNA is more highly expressed in the corneal epithelium relative to the stroma (Escribano et al., 1994), leading to the hypothesis that TGFBIp is secreted from the cell-dense epithelium, into the acellular Bowman's layer and relatively acellular stroma, where the majority of TGFBIp+ corneal deposits aggregate.

In order to address this hypothesis, publicly available scRNAseq data on four human donor corneas published by Català et al. (2021) was obtained via the Gene Expression Omnibus database. Following the filtering of low-quality cells, the transcriptome profiles of 10,580 cells were subject to a preliminary single-cell Seurat analysis (Hao et al., 2021) in RStudio (Chapter 2, Section 2.10.5) to examine the expression of *TGFBI* in relation to the defined limbal and central corneal epithelium markers *GJA1*, *KRT12*, *KRT3*, *PAX6* and *TP63* (Figure 4.7). The sequenced cells were embedded in a uniform manifold approximation and projection, and clustering revealed 12 cell clusters. UMAP plots indicate that *TGFBI* and *GJA1* are more widely expressed throughout the corneal compartments respective to *KRT12*, *KRT3*, *PAX6* and *TP63*. *TP63* expression appears to be less widely distributed than all the other markers, consistent with its specification as an LSC/LPC marker. The clusters 6-10 demonstrate the highest levels of *TGFBI* expression and this corresponds to the clusters demonstrating the highest expression levels of the corneal epithelial markers *GJA1*, *KRT12* and *KRT3* and *PAX6*. This indicates that *TGFBI* mRNA is most highly expressed in the corneal epithelium, supporting the hypothesis that mutant TGFBIp is secreted from the corneal epithelium, leading or contributing to the aggregation of TGFBIp+ deposits in the subepithelial layers. Nonetheless, the sparse keratocytes of the stroma also express *TGFBI* and secrete TGFBIp into the ECM, although perhaps to a lesser extent. These findings provide a basis for the *in vitro* modelling of TGFBI CDs through the generation of patient-derived iPSC-CEpi cells, as the corneal epithelium appears to be the major source of CD deposits and any ASO treatments would need to effectively target the *TGFBI* produced by the cells of this tissue.

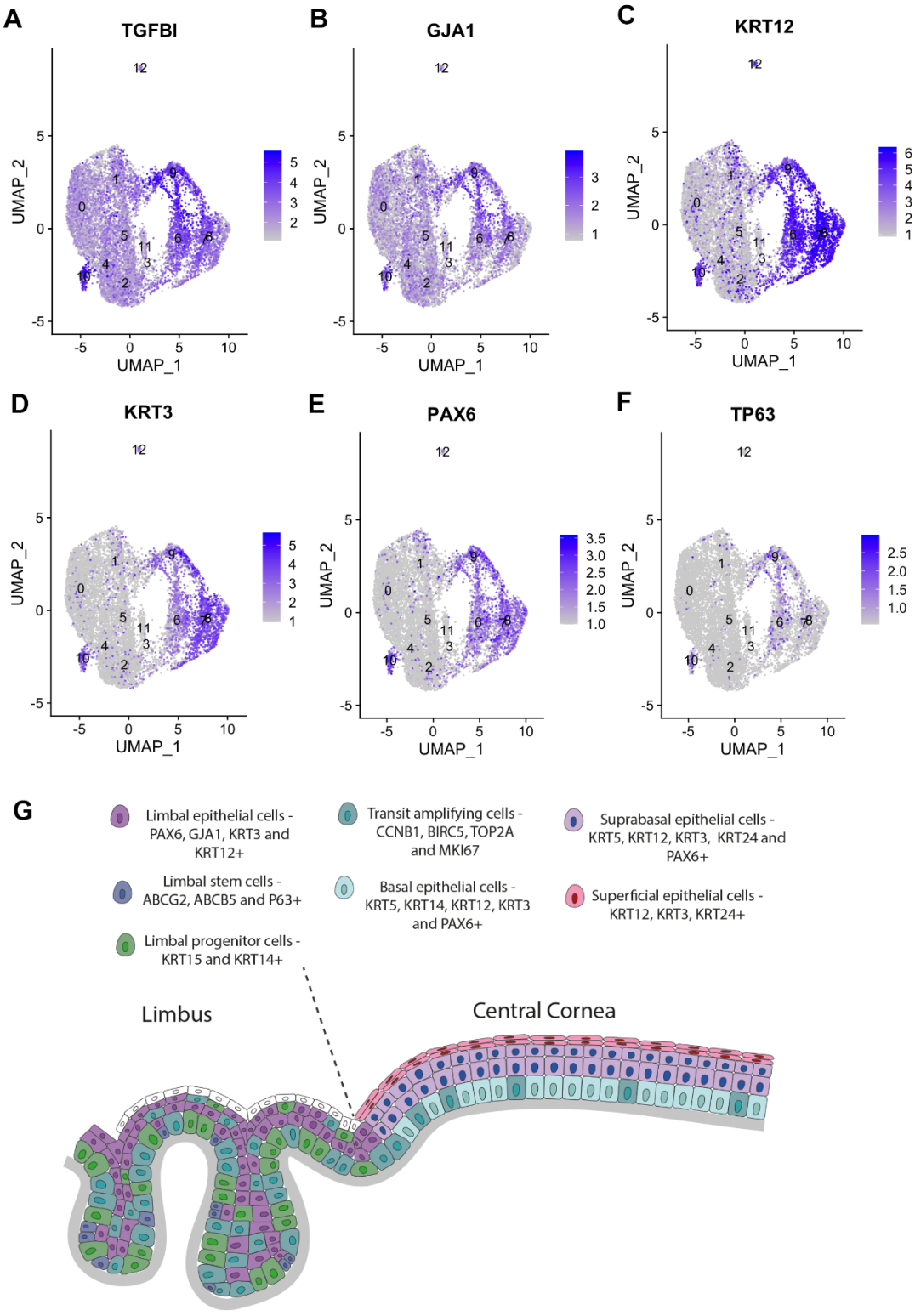

Figure 4.7 UMAP plot of *TGFBI* and corneal epithelial marker expression in the human cornea assessed by scRNAseq analysis. Publicly available raw scRNAseq data on human corneal tissue including the epithelial, stromal and endothelial layers of the central cornea was obtained from Català et al., (2021). A preliminary analysis using the Seurat package in RStudio was conducted on the dataset in order to assess the distribution of **A)** *TGFBI* expression in the cornea. The highest density of *TGFBI* expression is observed within clusters 6-10 and corresponds to the highest density of **B)** *GJA1* expression, a known corneal epithelium marker. The two specific corneal epithelium markers **C)** *KRT12* and **D)** *KRT3* also display their highest

expression densities within these clusters. **E)** *PAX6* and **F)** *TP63*, two transcription factors involved in corneal epithelial fate determination are also most highly expressed in these clusters, with *TP63* showing a more restricted distribution consistent with its specification as a limbal stem/progenitor cell marker. Overall, the scRNAseq data indicate that *TGFBI* is most highly expressed within the corneal epithelium, relative to the stroma and endothelium. **G.** Cellular subpopulations of the limbus and corneal epithelium and their highly expressed genes as identified by single cell RNA sequencing (scRNAseq) reports.

4.2.2 Corneal epithelial differentiation protocol

Based on unpublished data obtained in our lab (Beatriz Sanchez-Pintado), a CEpi differentiation protocol (Figure 4.8) adapted from Kamarudin et al. (2018) was implemented in order to differentiate patient and control iPSCs to CEpi cells. Kamarudin et al. (2018) reported that induction media supplemented with BMP4 (25 µl/ml), All trans retinoic acid (10 mM) and EGF (0.5 mg/ml) led to the stepwise generation of corneal epithelial cells in 20 days. This induction phase was carried out using adherent iPSC cultures which were split and plated on day 9 to Collagen IV coated plates. The four main modifications made to this protocol were as follows:

- The induction media was supplemented with 50 ng/ml EGF and 25 ng/ml BMP4.
- The induction phase of the differentiation was carried out in suspension for one week – during the first two days, a slower transition from the stem cell media to the induction media was carried out (as described in methods chapter).
- On day 9, cells were plated onto Laminin-521 and collagen IV coated plates.
- The differentiations were assessed during a longer period, until day 30.

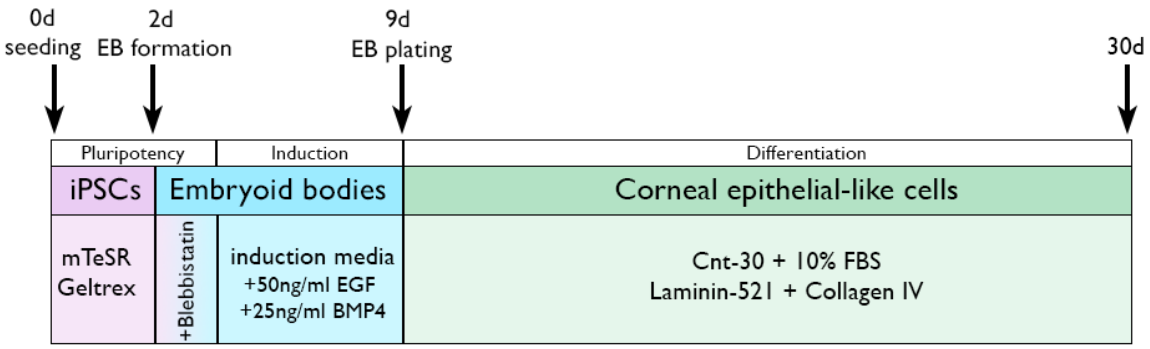

Figure 4.8 Protocol used for the differentiation of iPSC into CEpi cells. iPSCs were split onto geltrex coated plates and allowed to expand for 2 days while being cultured in mTeSR media. On day 2, iPSC colonies were formed into embryoid bodies, and the mTeSR media was progressively changed into induction media containing 50 ng/ml EGF and 25 ng/ml BMP4 over 3 days to allow the cells to adjust. After the 7-day induction period, the embryoid bodies were plated onto Laminin-521 and collagen IV coated plates and cultured in Cnt-30 differentiation media supplemented with 10% FBS.

4.2.3 Characterisation of iPSC-derived corneal epithelial-like cells

Control and mutant cells lines were differentiated following modifications to the Kamarudin et al. (2018) protocol outlined in Figure 4.8 (Chapter 2, Section 2.8.5). Progress throughout the differentiation was recorded at key time points by bright field microscopy which demonstrates that cells obtained a typical epithelial morphology with differentiation (Figure 4.9). During the induction period, the embryoid bodies grew and expanded. Following plating of the embryoid bodies on to coated plates, the majority attached and the day after, small cells with an epithelial-like morphology had emerged (Figure 4.9, day 10). The cells expanded rapidly and on day 16 of the differentiation, cells with a typical epithelial polygonal morphology with pronounced cell-cell junctions were observed (Figure 4.9, day 16). As the cells expanded and the differentiation progressed, epithelial cells of different sizes and morphologies were observed. Some cells were more elongated with a 'squamous' morphology and others were more cuboidal in shape. By day 21 cells had become more confluent and multilayering of cells was observed.

However, different cell types with different morphologies were observed particularly as the cells proliferated further from the embryoid bodies indicating the differentiation protocol did not result in a monoculture. Around the embryoid bodies, cells with a typical compact epithelial morphology forming a cobblestone pattern with prominent cell-cell junctions were observed and accounted for the largest proportion of differentiated cells. Another cell type also had prominent cell-cell junctions but a much larger cell-to-nucleus ratio (Figure 4.10B). Cells with stromal like morphologies were also observed, with some displaying a typical elongated fibroblast shape and others with large, flattened morphologies (Figure 4.10C). Rarely, neuronal cell types with processes were observed (Figure 4.10D). As the culture continued to mature, the different cell types continued to expand. Variation in the proportions of the different cell populations between culture plate wells was also noted.

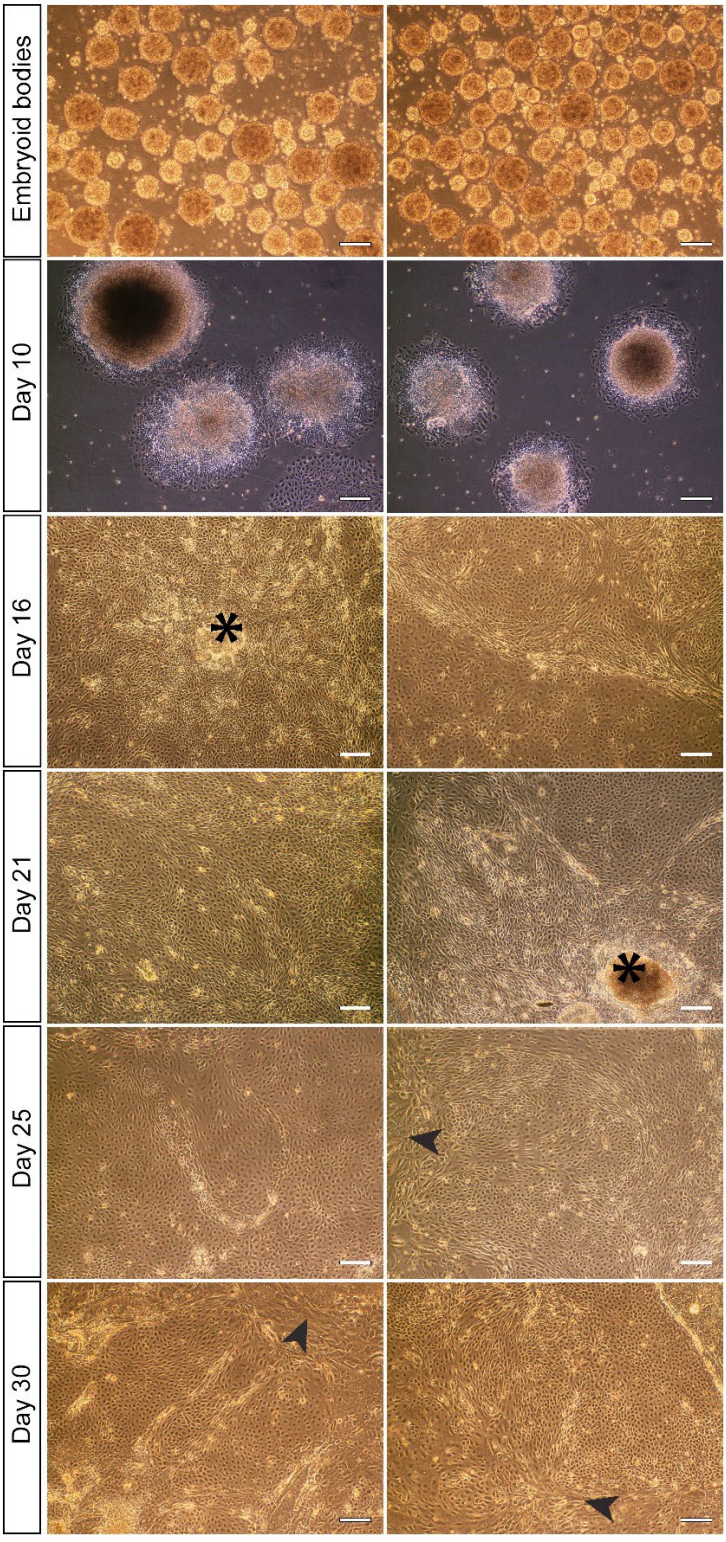

Figure 4.9 CEpi differentiation and morphology. Bright field images show the morphology of the cells during different stages of the differentiation. iPSC colonies were formed into embryoid bodies (EBs) and were cultured in suspension for 7 days. Following plating onto coated plates, polygonal cells of different sizes and morphologies emerged from the EBs (asterisks) and continued to proliferate throughout the differentiation. Multilayering of epithelial-like cells was apparent. Additionally, other cell morphologies are observed (arrowhead) which also continued to expand. Scale bar = 100 μM.

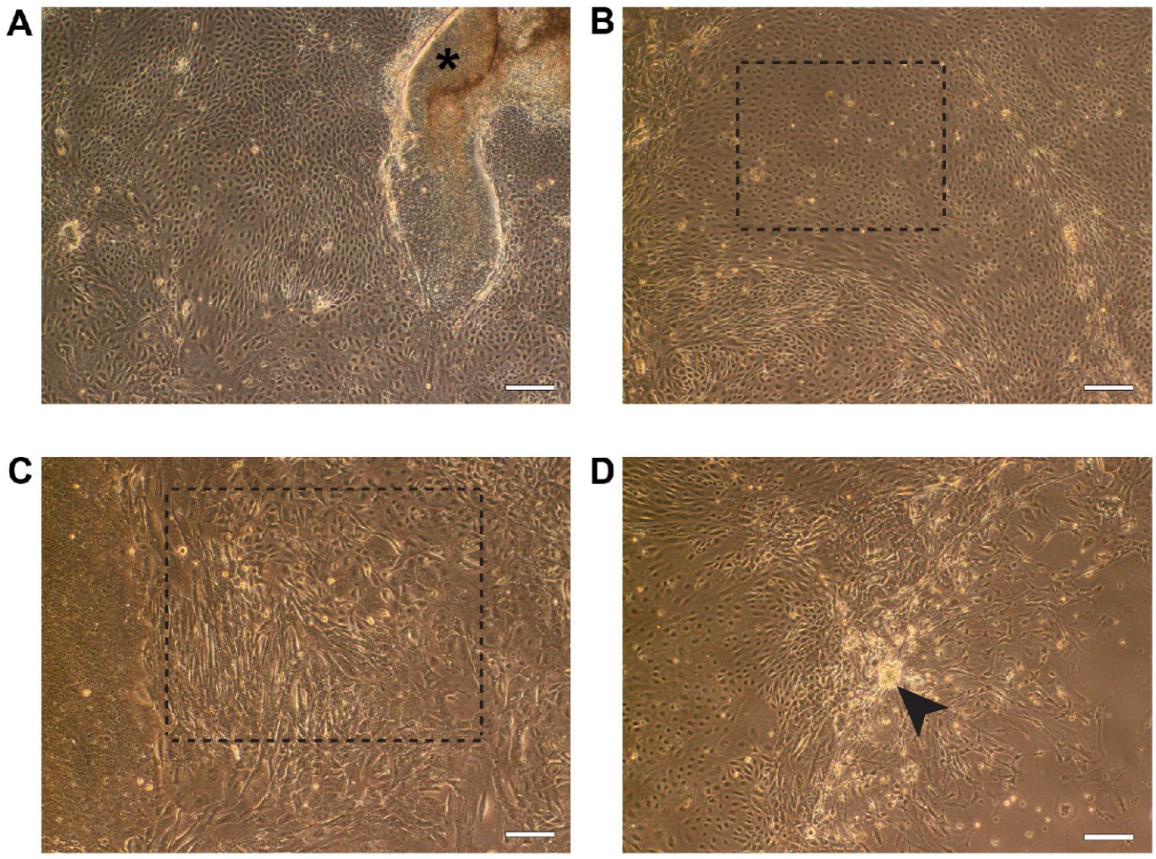

Figure 4.10 CEpi cell culture heterogeneity at day 25 of differentiation. A) Cells with a typical polygonal morphology that displayed prominent cell junctions and formed a cobblestone pattern proliferated from the embryoid bodies (asterisk). **B)** Patches of cells that also formed visible cell junctions but had a larger cell-nucleus ratio were observed (highlighted with dotted outline). **C)** Stromal cells with a typical elongated fibroblast shape along with cells that displayed a wider, flatter phenotype were found towards the periphery of the cultures (highlighted with dotted outline). **D)** Rarely, neuronal-type cells with processes formed (arrowhead). Scale bar = 100 µM.

4.2.4 Characterisation of corneal epithelial marker gene expression during differentiation

Gene expression analysis of relevant corneal epithelial markers was carried out by qPCR (Chapter 2, Section 2.7) to assess whether CEpi cells shared a comparable molecular profile to the native tissue. RNA samples were extracted (Chapter 2, Section 2.1.2) at various key time points (day 16, day 21, day 25 and day 30) of the differentiation to determine the optimal experimental window for downstream studies.

The corneal epithelial-specific markers *KRT3* and *KRT12* were assessed by RT-PCR and while *KRT3* expression was detected, no specific *KRT12* transcript was amplified (data not shown), therefore, only *KRT3* expression was assessed by qPCR.

Expression of genes encoding transcription factors crucial for ocular development and corneal epithelial cell maintenance (*PAX6*), markers of limbal stem cell and corneal epithelial progenitors (*ABCG2* and *ΔNTP63*) and corneal epithelial keratins (*KRT14* and

KRT3) was assessed to characterise different stages of differentiation. In the original published protocol, the terminal timepoint was day 20. For the current study, the experimental window was extended to day 30 to assess prolonged cell culture. All seven independent cell lines included in this study (two WT, two p.R124C, two p.R124H and one *TGFBI* KO line) were assessed over 1-2 independent differentiations for marker expression (N=7-11).

Expression of the limbal stem cell marker *ABCG2* peaked at day 16 and continued to decrease during the three later timepoints relative to iPSC (Figure 4.11A). This is indicative of a surge of limbal epithelial-like cell proliferation between the naïve pluripotent state and day 16, which gradually decreases as the more mature cells expand. Expression of the limbal stem cell and corneal epithelial progenitor marker *ΔNTP63* increased with respect to iPSC and was maintained at the same level on average throughout the differentiation timepoints (Figure 4.11B), indicating that *ΔNTP63*+ cells stably proliferated throughout the protocol. Expression of the corneal epithelial progenitor and basal corneal epithelium keratin *KRT14* increased from iPSC to day 16 but then remained at similar expression levels until day 21, before increasing on days 25 and 30 (Figure 4.11C). *PAX6* expression continued to increase incrementally throughout the differentiation (Figure 4.11D). Whereas *KRT3* expression peaked at day 25 but was decreased on average on day 30 (Figure 4.11E). This observation may indicate that after day 25, the proportion of non-CEpi cells in the culture expand and start outnumbering the *KRT3*-expressing CEpi cells. *TGFBI* expression levels over the differentiation timepoints were also assessed (N=6) (Figure 4.11F). A significant increase of *TGFBI* expression was observed at day 25 of the differentiation respective to iPSCs and continued to increase until day 30.

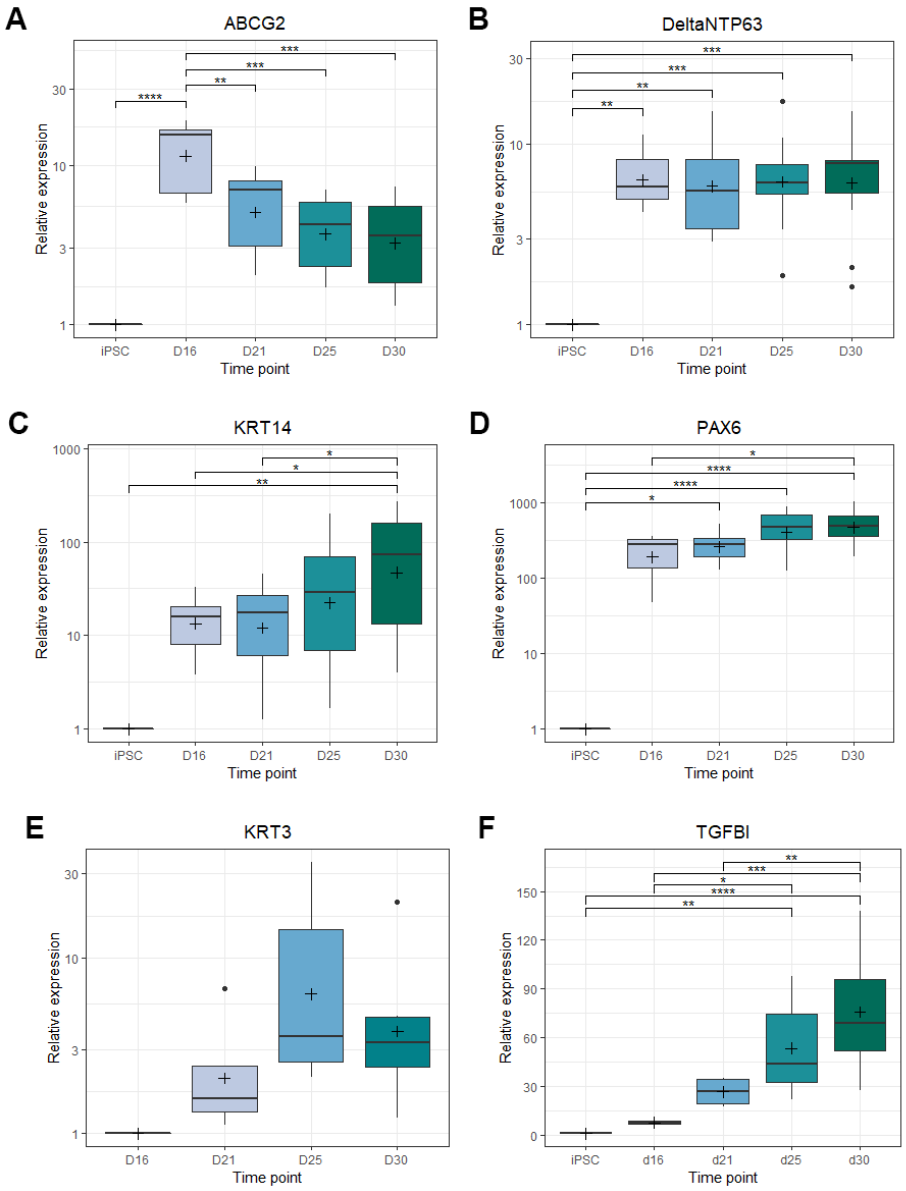

Figure 4.11 Gene expression of iPSC and CEpi samples. qPCR was used to assess the expression of **A)** *ABCG2*, **B)** *ΔNTP63*, **C)** *KRT14*, **D)** *PAX6*, **E)** *KRT3*, **F)** *TGFBI* throughout the differentiation process, days (D) 0 = iPSC to d30. Gene expression was normalised to *ACTIN* and *GAPDH* expression, and relative quantification values were calculated relative to iPSC or D16 expression (*KRT3* was not detected in iPSC). The mean is represented by the + symbol, whereas the median is represented by the horizontal line. A-E: N=7-11 iPSC lines and independent differentiations of the different lines (2xWT, 2xR124C, 2xR124H, 1x*TGFBI* KO); F: N=6 independent differentiations of different lines (2xWT, 2xR124C, 2xR124H). Statistical analysis was performed using a one-way ANOVA and a post-hoc Tukey's HSD test. * P<0.05, ** P< 0.01, *** P<0.001, **** P<0.0001.

4.2.5 Characterisation of CEpi marker protein expression

The protein expression of CEpi markers were investigated by immunocytochemistry (ICC) of the differentiations (Chapter 2, Section 2.3). Different markers were compared across cell lines at days 21 and 25 to observe whether staining patterns were comparable across samples and key differentiation points.

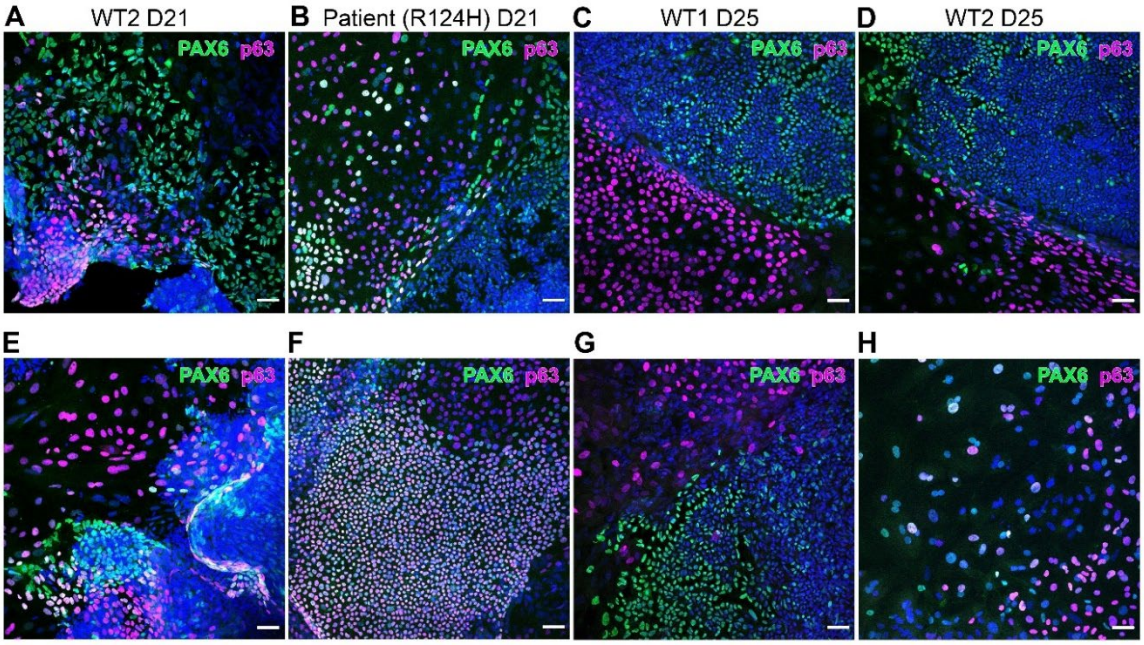

Figure 4.12 Characterisation of CEpi cultures: PAX6 and p63 protein expression at day 21 and day 25. ICC analysis of the WT2 and a patient line at day 21 **(A, B, E, F)** and the WT1 and WT2 line at day 25 **(C, D, G, H)**. Separate populations of PAX6+ and p63+ cells are observed, with some co-localisation of the two transcription factors. Scale bars = 50 μM.

Expression of the transcription factors p63, a protein expressed by limbal stem/progenitor cells and PAX6, expressed by cells of the corneal limbus and epithelium, was investigated in the CEpi samples at day 21 for the WT2 and R124H patient (patient 4) lines and at day 25 for the WT1 and WT2 lines. To note, the p63 antibody detects both the TA and ΔN isoforms of the protein, however only the ΔNp63 isoform is expressed in the human cornea.

Typical nuclear expression was observed for both of the transcription factors across the samples (Figure 4.12A-H). At day 21, patches of cells expressing p63 or PAX6 were observed emerging from densely DAPI-stained cell clusters, with some cells co-expressing the markers (Figure 4.12A, B, E). Cells with different sized nuclei are observed and different cell subpopulations in close proximity to each other and heterogeneity of the cultures is apparent in all stained samples. Multi-cell layering is also apparent, with PAX6 and p63+ cells overlapping with DAPI-stained nuclei (Figure 4.12A, B and E). Many of the cells that only show PAX6+ expression at day 21 appear to show

elongated/aberrantly shaped nuclei or two nuclei very close together (Figure 4.12A and B), which are indicative of cells undergoing mitosis. In Figure 4.12F a dense sheet of tightly packed cells co-expressing both p63 and PAX6 is observed, these cells are smaller in size than cells expressing either only p63 or PAX6, indicating they may represent a population of LPCs.

P63 is a marker of cells residing in the corneal limbus, thus, p63+ cells potentially represent a population of less differentiated cells. Whereas PAX6 is expressed throughout the limbal and central cornea and its expression could be representative of a general CEpi cell type. Thus, some co-expression of p63 and PAX6 is expected, although, PAX6+/p63- cells would also be expected, as demonstrated by figure (Figure 4.7 E-F) which shows the more general expression pattern of *PAX6* in the human cornea.

Different patterns of staining are noted, with some images displaying PAX6 expression at the outer rim of colonies of smaller cells with smaller nuclei potentially indicating proliferative cell colonies (Figure 4.12C, D and G). Differentiation generally occurs at the outer colony edge of pluripotent cell colonies, thus their positive expression of PAX6 indicates that these cells have committed to a neuroectoderm or surface ectoderm cell fate. The p63+ cells adjacent to the PAX6+ outer rim cell colonies have bigger nuclei and are potentially representative of more differentiated epithelial cells. At day 25, the cultures show that the majority of cells do not co-express PAX6 and p63 with a clear segregation between PAX6+ and p63+ cells observed (Figure 4.12C, D and G). This indicates that by this timepoint, the putative population of limbal stem/progenitor cells co-expressing PAX6 and p63 has diminished.

Immunocytochemistry staining was also used to visualise the distribution of the keratin proteins K5 and K14 in the CEpi cells at day 21 (R124H patient and WT2 lines) and day 25 (WT2) (Figure 4.13). It should be noted that the day 25 WT1 differentiation presented in the other immunostaining figures was stained for K5 and K14 and although this sample demonstrated positive staining of the other markers tested (Figure 4.12C, G; Figure 4.14C, G), K5 and K14 positive staining was not observed in this particular sample (data not shown).

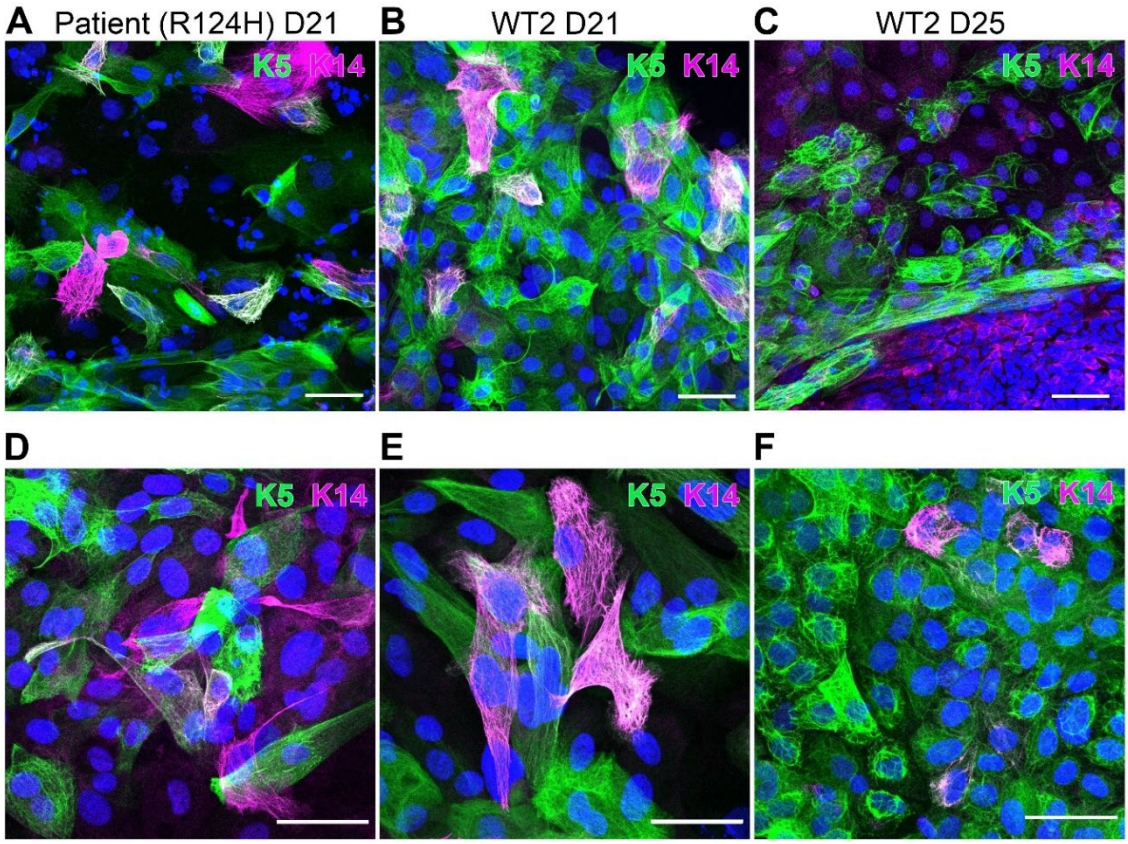

Figure 4.13 Characterisation of CEpi cultures: K5 and K14 protein expression at day 21 and day 25. ICC analysis of a patient line and the WT2 line at day 21 **(A, B, D, E)** and the WT2 line at day 25 **(C, F)**. K5 and K14 are obligate keratin pairs that are known to form heterodimers. Sheets of K5+ cells are observed, with some cells demonstrating K14+ expression and some cells demonstrating co-localisation of the two keratins. Both the keratins display a filamentous staining pattern, with K5 expression being noticeably more dominant than K14 expression. Scale bars = 50 μM.

K5 and K14 are defined as obligate heterodimers critical for the proper assembly of intermediate filaments in stratified epithelial tissue. Cells with an epithelial morphology show expression of K5 and K14. Both proteins display an elaborate filament network crossing through the cell cytoplasm, extending through the nucleus or the nuclear envelope, to the plasma membrane or to the cytoplasm of a neighbouring cell, linking them together. Cells of different morphologies and sizes show positive staining for both of these proteins, yet K5 shows a wider staining distribution than K14. This is also the case in the corneal limbus and epithelium, with K14 expression localised to the basal tissue layers and K5 being more generally expressed throughout. In some cells, K5 and K14 show co-localisation, consistent with their formation of obligate heterodimers. However, co-localisation of the two proteins is not as extensive as would be expected in fully mature CEpi cells. Nonetheless, the staining shows structured intermediate filaments forming cytoskeletal networks, indicating that in areas where positive staining of either K5 or K14 is observed but not the other, the respective keratin protein is forming

a pair with an alternate keratin. More K5 and K14 positive staining is observed in cell dense areas where tightly packed cells with smaller nuclei have formed epithelial sheets (Figure 4.13B and F). The day 21 and day 25 samples of the WT2 line demonstrate similar staining patterns with large patches of K5+ cell sheets with a lower distribution of K14+ cells, indicating that there is not an observable difference in K5 and K14 staining between these two timepoints in the same cell line (Figure 4.13B, C, E, F).

The expression of K3, a keratin exclusive to the cornea, expressed throughout the corneal epithelium and the suprabasal and superficial layers of the limbus, was investigated in conjunction with the cell-cell junction markers connexin 43 (Cx43) at day 21 (R124H patient and WT2) (Figure 4.14A, B, E, F) and E-cadherin at day 25 (WT1 and WT2) (Figure 4.14C, D, G, H). Confocal imaging revealed that K3 and Cx43 were both expressed in the CEpi cells at day 21. K3 staining was primarily localized to the cell membrane and cytoplasm, while Cx43 staining was detected at cell junctions, vesicles and the nucleoplasm.

Co-staining of K3 and Cx43 (Figure 4.14A, B) demonstrates expression in the same cells, but each showing a distinct staining pattern. In some cells, K3 staining was more intense than Cx43 staining, while in others, the opposite was observed. Specifically, cells that showed the highest density of K3+ staining (Figure 4.14A) showed Cx43+ staining localised to vesicles. Additionally, in some areas of the culture, K3 and Cx43 staining appeared to overlap, suggesting possible interaction between the two proteins. In order to more thoroughly examine the cellular heterogeneity of cells co-expressing K3 and Cx43, images taken of the day 21 WT2 sample are presented in Figure 4.15. At a lower magnification, the wider distribution of different cell populations expressing K3 is observed (Figure 4.15A). Different sizes of cells arranged in differing densities and showing different K3 and Cx43 staining patterns are observed (Figure 4.15B-D). Overall, K3+ cells do appear to express Cx43, which is also the case in the native cornea.

Co-staining of K3 and E-cadherin demonstrates two populations of K3+ cells, that are either positive or negative for E-cadherin (Figure 4.14C, D). Positive E-cadherin staining shows a typical expression pattern at the periphery of the cells, corresponding to the adherens junctions. K3+ cells that are also positive for E-cadherin are larger and have larger nuclei, whereas K3+ cells that are negative for E-cadherin are much more densely packed, with smaller nuclei. Figure 4.14D clearly demonstrates the distinction between these two subpopulations of K3+ cells and their close proximity could indicate the proliferation of the smaller K3+/E-cadherin- cells into the larger E-cadherin+ cells that have a more diffuse K3 staining pattern. This would suggest that the smaller K3+/E-

cadherin- cells are more naïve and mitotically active that the larger E-cadherin+ cells that show cell-cell adhesion.

K3+ staining demonstrated a different pattern to the typical filamentous pattern observed with K5 and K14 staining (Figure 4.13). More than one type of K3 staining pattern was observed, with a denser network of K3+ filaments in some smaller cells (Figure 4.14A, F), some larger cells demonstrating a filamentous pattern (Figure 4.14B, E, G) and some cells showing a more diffuse and less distinct pattern of staining (Figure 4.14C, D, H). In Figure 4.14F, a patch of multi-layered cells is observed with K3 positivity outlining the cell shape. Overall, due to the cellular heterogeneity, it is difficult to compare any differences between the cells at day 21 and day 25, although a range of cell types with similar staining patterns are observed at both timepoints.

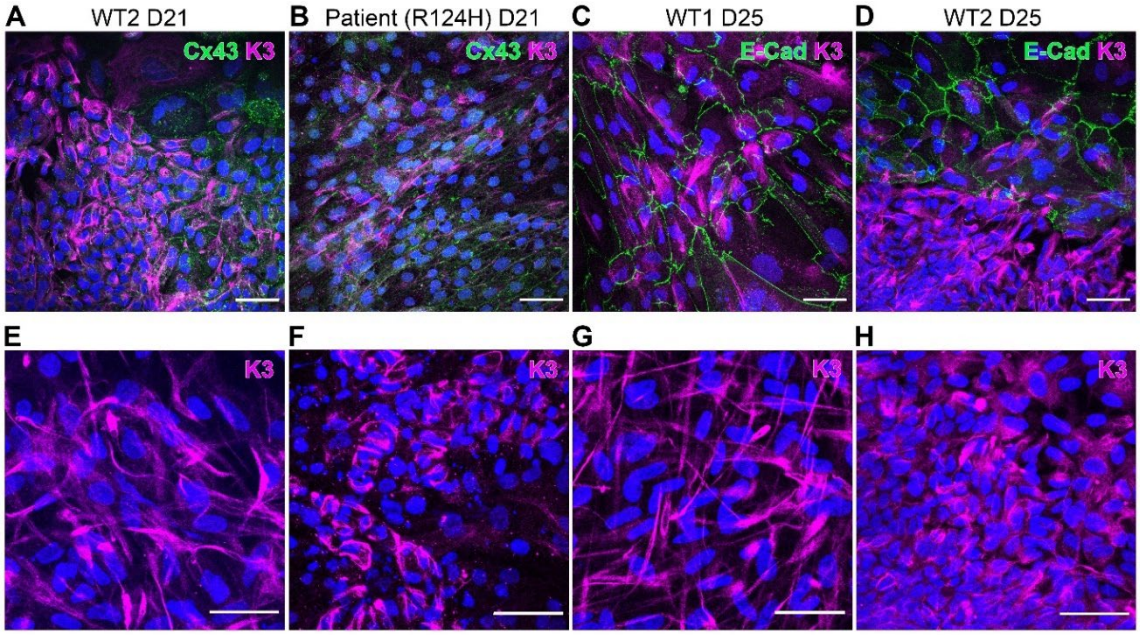

Figure 4.14 Characterisation of CEpi cultures: Cx43 and K3 expression at day 21 and E-cadherin (E-Cad) and K3 expression at day 25. ICC analysis of a patient line and the WT2 line at day 21 **(A, B, D, E) and** the WT1 and WT2 line at day 25 **(C, D, G, H)**. K3 staining demonstrates different subpopulations of cells showing different K3+ staining patterns. K3+ cells co-express Cx43 (A, B), whereas co-staining of K3 and E-Cad demonstrates a population of cells that are positive for both K3 and E-Cad (C, D) and another population of densely packed K3+ cells that are E-Cad- (D). Scale bars = 50 μM.

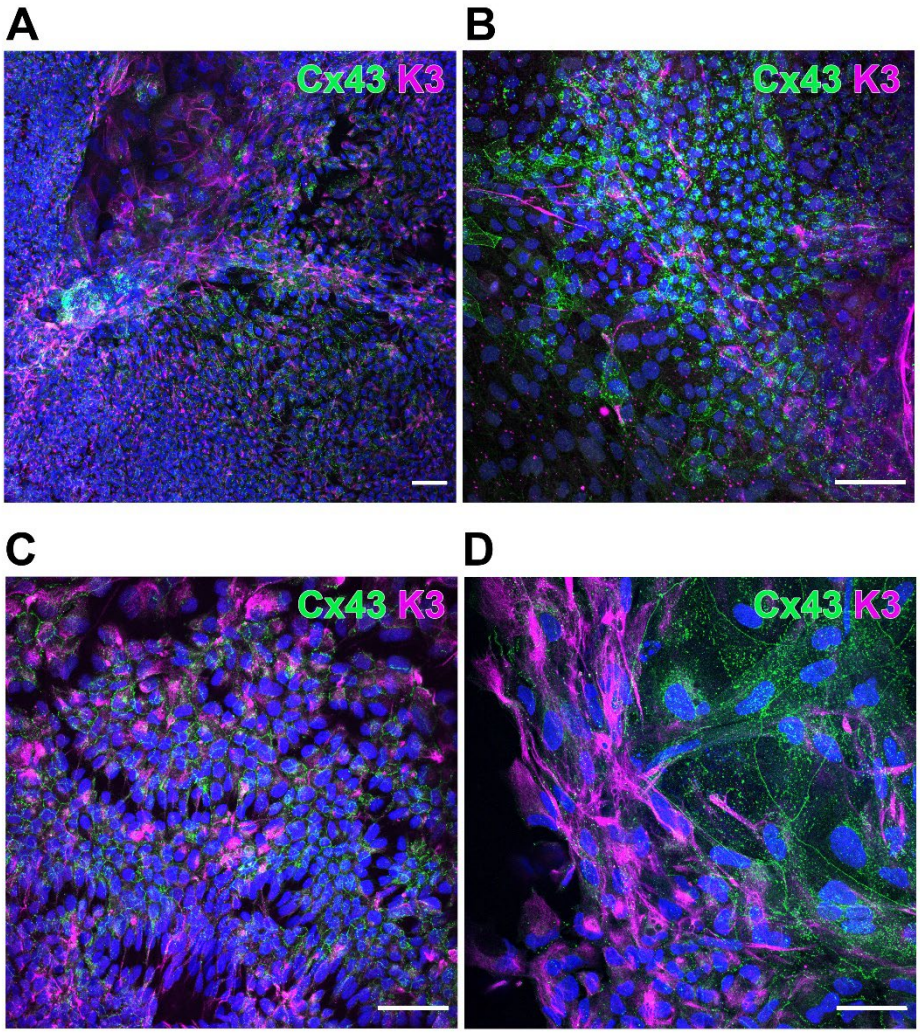

Figure 4.15 Heterogeneity of CEpi cultures demonstrated by Cx43 and K3 staining of the WT2 line at day 21. Imaging at a lower magnification **(A)** shows a heterogenous population of cells of different sizes and cellular densities. K3+ and Cx43+ cells show different staining patterns **(B-D)**. Scale bars = 50 μM.

Corneal epithelial protein marker expression was also assessed in the *TGFBI* KO line on day 25, in order to understand whether the lack of TGFBIp expression would affect the cell's ability to form cell-cell junctions or keratin filaments. Co-staining of E-cadherin and K14 shows cells that express a complex K14 filamentous network, adhered together by E-cadherin+ cell-cell junctions (Figure 4.16A, D). Similarly, Cx43 and K5 co-staining shows sheets of cells positive for both of these markers. K5+ staining shows strong expression in the cytoplasm and Cx43 shows diffuse staining throughout the cell, with puncta in some areas and others areas showing the strongest staining intensity at cell-cell junctions, consistent with the presence of Cx43 localised intracellularly and to gap junctions. The images presented in Figure 4.16A and B demonstrate different shapes and sizes of cells with an epithelial morphology. The E-Cad/K14 and Cx43/K5 staining shows that despite the lack of TGFBIp in these cells, the cellular integrity of the epithelial-

like cells remains. Co-staining of p63 and K3 demonstrates that the *TGFBI* KO cells can form p63+ epithelial sheets (Figure 4.16C). Higher density of K3+ staining is apparent in areas of p63- cells (Figure 4.16F). This corroborates the scRNAseq data shown in Figure 4.7D and F, *P63* and *KRT3* expression is not expected to be mutually exclusive, although cellular populations expressing either one or the other are expected. Altogether, immunostaining of the *TGFBI* KO line indicates that the absence of TGFBIp does not cause abnormalities in CEpi protein marker expression. This supports the bulk RNAseq data presented in Chapter 5, where no CEpi markers used to characterise the model in the current chapter were significantly differentially expressed in the *TGFBI* KO vs WT comparison.

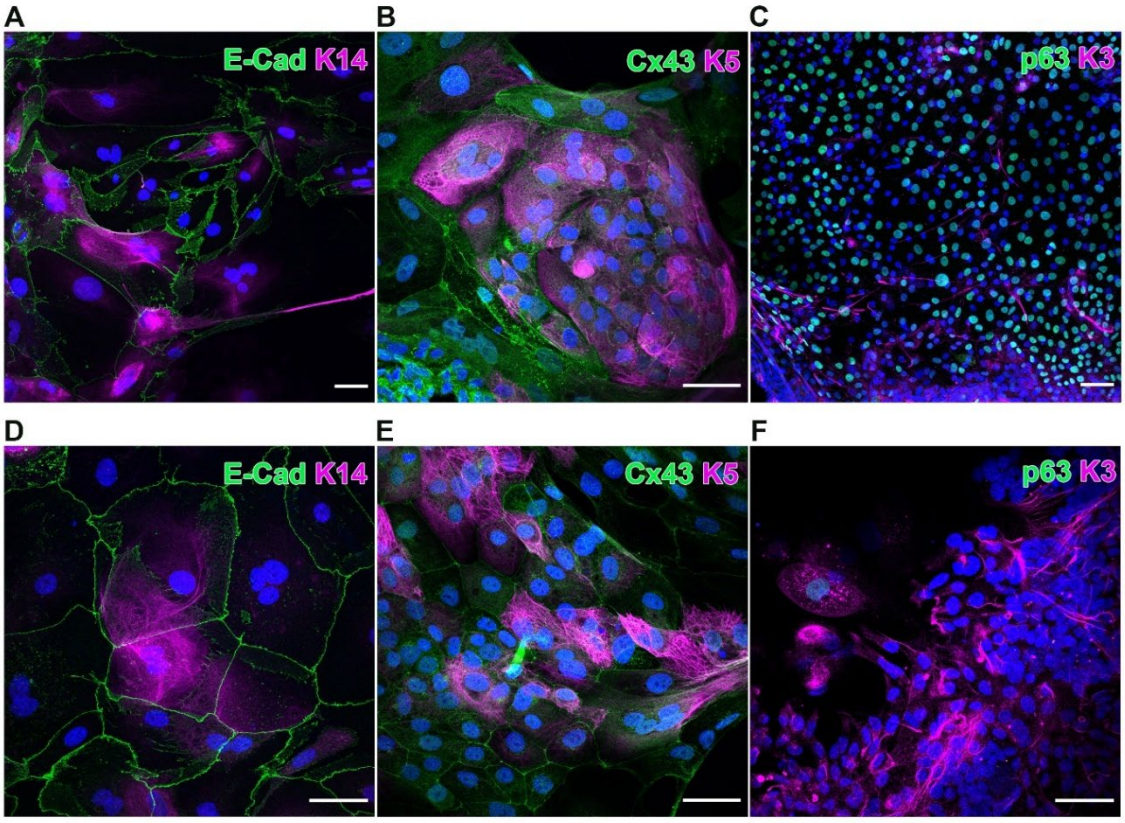

Figure 4.16 Characterisation of the CEpi TGFBI KO line: E-Cad, K14, Cx43, K5, p63 and K3 protein expression at day 25. Co-staining of E-Cad/K14 **(A, D)** and Cx43/K5 **(B, E)** demonstrates that the in the absence of TGFBIp expression, CEpi cells are still able to form cell-cell junctions and intermediate filaments. Co-staining of p63 and K3 **(C, F)** shows that TGFBI KO CEpi cells generate p63+ cell sheets that are mostly negative for K3, and areas where denser K3 staining is observed are negative for p63. Scale bars = 50 μM.

Several anti-TGFBIp antibodies were tested for specific staining of TGFBIp in CEpi cells by immunocytochemistry, however, upon comparison of the staining to the negative control line (*TGFBI* KO line) it was apparent that the antibodies tested were not specific. Nevertheless, one antibody tested for TGFBIp specific subcellular staining in the WT1

line at day 30 did show specific staining, as the same staining pattern was not observed in day 30 *TGFBI* KO CEpi cells (Figure 4.17). TGFBIp+ staining was observed surrounding the nuclear envelope, where the endoplasmic reticulum (ER) is located and diffuse staining appears to extend to the location of the Golgi apparatus (GA), although co-staining of markers known to localise to both the ER and GA organelles is necessary to fully confirm this. Intracellular TGFBIp is known to be processed through the ER and GA before it is secreted, consistent with the TGFBIp+ staining presented here.

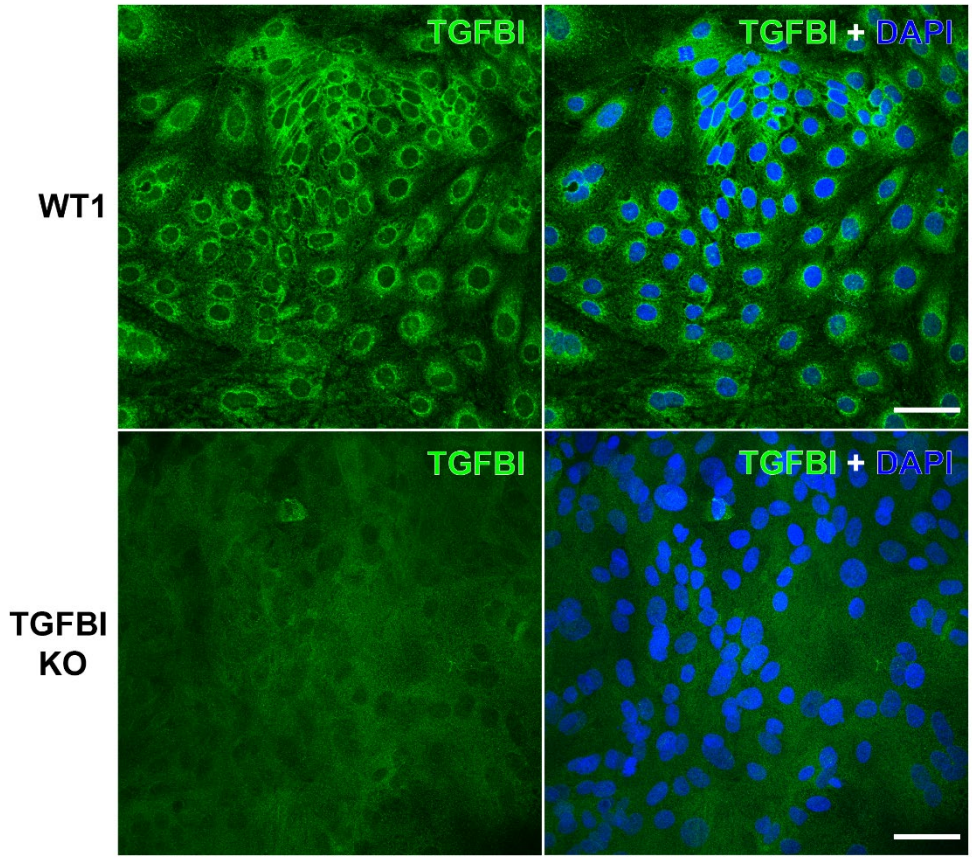

Figure 4.17 TGFBIp staining in the WT1 and TGFBI KO CEpi line at day 30. Staining of TGFBIp in the WT1 line demonstrates expression consistent with the endoplasmic reticulum and Golgi apparatus. The TGFBI KO line was used as a negative control in order to confirm the specificity of the antibody. Scale bars = 50 μM.

4.3 Discussion

The ECM protein TGFBIp is the second most abundant protein expressed in the human corneal stroma (Dyrlund et al., 2012). Both corneal epithelial and stromal cells produce TGFBIp (Akiya et al., 1999; Escribano et al., 1994; Korvatska et al., 1999; Lisch & Seitz, 2014; Menasche et al., 1992; Wittebol-Post et al., 2010). The stroma is not completely acellular, but it is mostly an ECM structure, with only around 3-5% of its volume comprised of stromal cells (Beuerman & Pedroza, 1996; Dua et al., 2013). TGFBIp+ deposit location in the cornea varies depending on the specific phenotype, they are mostly located in the basal epithelium and superficial stroma in GCDI, the Bowman's layer in RBCD and TBCD, and the superficial and deep stroma in GCDII and LCDI (K. E. Han et al., 2016). Based on the scRNAseq analysis on publicly available data on the human cornea presented in the current study, it appears that *TGFBI* mRNA is more highly expressed in the corneal epithelium relative to other layers of the cornea, this is consistent with a previous scRNAseq report that also found *TGFBI* transcript to be most highly expressed by cells of the corneal epithelium (Ligocki et al., 2021). Taking these factors into consideration, it is likely that both the corneal epithelium and stroma are contribute to abnormal TGFBIp aggregate formation, but that the majority of the mutant protein is secreted by the epithelium.

With the wealth of recently published scRNAseq data on the cornea, a focus on genes implicated in corneal disease, such as *TGFBI*, would be highly informative to assess spatial expression. This would provide information on the specific corneal compartments involved in disease pathogenesis and elucidate which cells should be targeted therapeutically. Given the implication that the corneal epithelium expresses more *TGFBI* mRNA than the stromal keratocytes, any potential therapeutics that exert a mechanism of *TGFBI* transcript reduction should be tested and validated in corneal epithelial cells. This is also supported by reports showing that following PK, LCDI and GCD patients develop diffuse superficial opacities in the epithelium and subepithelium that are much more prominent than deposits in the stroma (Frising et al., 2006; Johnson et al., 1981; Lisch & Seitz, 2014; Lyons et al., 1994). Due to the limited availability of corneal donor tissue, a patient-derived *in vitro* iPSC-corneal epithelial model offers an alternative unlimited source of disease-relevant cells that facilitate the screening of potential therapeutics and to enable replicate experimentation.

For this purpose, multiple published CEpi differentiation protocols were tested in the Hardcastle laboratory (unpublished data) before implementation of an optimised version of the protocol published by Kamarudin et al. (2018). The report describing this protocol

highlighted the effect of BMP4 as an important induction agent of pluripotent stem cell differentiation towards a non-neural ectodermal lineage (Kamarudin et al., 2018). This is supported by previous research that demonstrates that pluripotent cultures treated with media containing BMP4 were directed to an epithelial lineage through *P63* induction (Metallo et al., 2008). Additionally, BMP4 treatment of pluripotent stem cells leads to apoptosis of neural precursor cells and the induction of ΔNp63+ epithelial differentiation through the binary neuroectodermal choice (neural vs surface ectoderm) (Aberdam et al., 2007; Gambaro et al., 2006).

Some alterations were made to optimise the published differentiation protocol. One such difference was the exclusion of RA following the induction period. RA promotes neural lineage entry of pluripotent stem cells (J. Lu et al., 2009; Y. Okada et al., 2004; S. Yu et al., 2012). Through the comparison of the CEpi differentiation period with or without RA, the proportion of polygonal epithelial-like cells was increased when media was not supplemented with RA (unpublished data). The authors of the original protocol concluded that media supplemented with both BMP4 and RA resulted in the successful generation of corneal epithelial progenitors (Kamarudin et al., 2018) and a previous study has shown that RA and BMP4 synergise to promote non-neural ectodermal differentiation of pluripotent stem cells (Metallo et al., 2008). Nonetheless, during the induction period of the protocol implemented in this thesis, the media was supplemented with B27 containing vitamin A (Chapter 2, Section 2.8.5), thus, it was not completely absent from the protocol and its presence at a minimal concentration is likely to have promoted RA-induced differentiation.

The resulting cultures were initially characterised for expression of corneal epithelial-related genes by qPCR over the differentiation timepoints. Expression of the LSC marker *ABCG2* peaked at day 16, indicating that around this stage, the highest number of LSC-like cells are present. Expression of the LSC and LPC marker *DeltaNp63* remained similar over all the timepoints. Average expression of *KRT14* and *PAX6* remained similar during days 16 to 21, but then increased during day 25 to 30. However, *KRT3* peaked at day 25, and was reduced by day 30, indicating that this timepoint contains the highest density of CEpi cells, but this does not indicate the proportion of the desired cell type to any non-specific cells present. Based on the results of the CEpi characterisation by qPCR analysis, the optimal experimental timepoint for ASO treatment was defined at around day 25, as cells expressed high transcript levels of corneal epithelial markers and *TGFBI* during this timepoint.

Attempting to elucidate at which point the cells are most corneal epithelial-like in a mixed population is a difficult task, especially when relying on measurements of transcript expression of the whole well. A more effective method would be to quantitatively assess the protein expression of the different cell types by flow cytometry, while also considering the size and complexity of the cells. The transcriptome profile of corneal epithelial cell subpopulations has never been more well-defined thanks to the recent scRNAseq publications on the cornea. This information would assist the characterisation of iPSC-derived CEpi cells by flow cytometry, and facilitate the isolation of the target cell types by FACS at an early timepoint in the differentiation.

The inherent nature of pluripotent stem cells is their ability to differentiate into cell lineages of the three germ layers. Thus, a certain degree of cellular heterogeneity is to be expected with some protocols of directed differentiation. iPSCs are affected in their differentiation potential by their original cell type, as the cells retain their original cell memory and have the propensity to differentiate into their original cell type (Bock et al., 2011; Q. Hu et al., 2010; K. Kim et al., 2010). One group compared the differentiation efficiency of iPSCs reprogrammed from either corneal limbal cells or fibroblasts and determined that the iPSCs derived from corneal limbal cells expressed the relevant markers such as *KRT12* and *KRT3* earlier and at a higher level in comparison to the fibroblast-derived iPSCs (Hayashi et al., 2012). This indicates that the epigenomic status of iPSCs affects their propensity to differentiate. All the iPSC lines used in the current study were reprogrammed from fibroblasts, and a proportion of fibroblast-like cells was noted in the differentiated cultures, potentially indicating that the lines had a propensity to differentiate back into their original cell type. However, in order to confirm the cell types of the non-target cell populations produced from the differentiations, immunostaining should be carried out in investigation of markers not expressed by corneal cell types.

Indeed, the protocol implemented by the current study resulted in a mixed population of cells. FACS utilising limbal stem and progenitor cell surface markers such as ABCG2, ABCB5 and GPHA2 could be employed at an early timepoint in the differentiation to purify the target cell type, allowing the maturation of a homogenous corneal epithelial cell population. A previous report showed the successful isolation of iPSC-derived corneal epithelial lineage cells by FACS using the markers SSEA-4, ITGB4 and TRA160 (Hayashi et al., 2018). However, this protocol extended over a much longer period of time than the one used in the current study, as FACS was carried out between weeks 10-15 of the protocol.

The heterogeneity of the cultures differentiated for the current study was demonstrated by immunostaining. Multiple cell morphologies were apparent through K3+ staining of CEpi cultures. One cell population appeared to consist of small compact cells that exhibited a less defined and more diffuse K3 staining pattern, while showing negative expression of E-Cadherin (Figure 4.14D; Figure 4.15D). Adjacent to these cells were cells with a larger morphology that were positive for E-cadherin staining. As the larger E-cadherin+ cells were directly adjacent to the smaller E-cadherin- cells, it may be the case that the smaller cells proliferated into the larger cells, indicating that this smaller cell population represents a more naïve CEpi-like cell that has migratory properties.

When the different morphologies of K3+ cells were compared in the same cell line at the same magnification (Figure 4.15B-D), it appeared that the larger K3+ cells expressed more of the protein than the smaller K3+ cells. Cultured limbal explants produce primary limbal epithelial cells that are heterogeneous ranging from small progenitors to larger differentiated cells (De Paiva et al., 2006; J. M. Li et al., 2021). Similarly, the percentage of K3+ cells was significantly higher in the larger cell population produced from cultured limbal explants in comparison to three other smaller cell populations (De Paiva et al., 2006). These findings are reinforced by scRNAseq studies on the cornea, which demonstrate that the human corneal limbus and epithelium is heterogenous, consisting of around 5-8 different subpopulations (Català et al., 2021; J. Collin et al., 2021; Dou et al., 2021; Ligocki et al., 2021). Thus, a heterogenous population of cells is to be expected when differentiating pluripotent stem cells towards a corneal epithelial lineage, as recapitulation of the native tissue would ensue different subpopulations of CEpi cells, with different sizes, expression profiles and growth potential.

An imbalance in keratin partner expression was observed between the K5 and K14 pairs at the protein level through immunostaining (Figure 4.13), and the *KRT3* and *KRT12* pairs at the transcript level, as the latter was not detected by PCR amplification, whereas the former was detected by qPCR and immunostaining (Figure 4.11E; Figure 4.14). Early studies established the general principle that obligate keratin pairs, made up of a type I and a type II keratin, are expected to be expressed at a 1:1 molar ratio (Giudice & Fuchs, 1987; K. H. Kim et al., 1984). However, at the mRNA level this is not always the case. A recent study investigated keratin mRNA expression levels in the human and mouse epidermis through analysis of publicly available scRNAseq data and concluded that some populations of individual cells show an imbalance between type I and type II keratin transcripts (Cohen et al., 2022). In mice, knockout models have shown that in the absence of one obligate keratin partner, another keratin of the same type (either I or II) can act as a replacement, exemplified by the induction of K19 in K18-null mice (Magin

et al., 1998), K8 induction in the embryonic epidermis of K5-null mice (H. Lu et al., 2005) and, K4 induction in the cornea of K5-null mice (H. Lu et al., 2006). Therefore, in the absence of the defined obligate keratin partner, an alternative keratin can act as a substitute, allowing for the formation of functional keratin heterodimers that assemble intermediate filaments. On the other hand, some evidence suggests that excess of one type of keratin is inherently unstable and rapidly degraded (Giudice & Fuchs, 1987; Kulesh & Oshima, 1988).

Through the preliminary analysis of publicly available scRNAseq data on the human cornea (Figure 4.7C, E), it appears that *KRT12* transcript levels are higher than that of its partner *KRT3*. This does appear to translate to the protein level, as a separate study investigating the proteome of the human cornea identified K12 as the most abundantly expressed protein in the corneal epithelium, whereas its obligate partner K3, was the fourth most abundant protein in the same samples (Dyrlund et al., 2012). The typical keratins expressed predominately in the basal layer of stratified epithelial cells are K5 and K14. *KRT5* is more highly expressed in multiple tissues relative to *KRT14* (Ho et al., 2022). In the current study, K5 was observed to be more widely expressed in CEpi cells in comparison to K14, as observed through immunocytochemistry (Figure 4.13). In cells that were K5+ but K14-, elaborate tonofilament-like networks were observed through K5 staining, indicating the stable expression of K5 and potentially, its pairing with an alternative keratin. K3 staining patterns were however variable, with some populations of cells appearing to express denser K3+ filaments than other populations (Figure 4.14; Figure 4.15). In the cell populations demonstrating denser K3 staining and in the absence of K12 expression, it may be the case that K3 is stably expressed through the pairing with an alternative type I keratin. Cells that showed sparser K3 staining could be representative of unstable K3 expression. Nonetheless, an extensive investigation into keratin expression of the CEpi cells at the transcript and protein level would be highly informative in understanding the paired keratin expression profile of these cells.

PAX6 and p63 are two important transcription factors in corneal epithelial cell fate determination. In the human cornea ΔNp63 is a marker of corneal development and limbal stem/progenitor cell proliferation (Bhattacharya et al., 2019; X. wei Ding et al., 2010; Nowell & Radtke, 2017). *TP63* transcript expression has been utilised as a marker of corneal epithelial stemness and cells expressing the ΔNp63 protein form reside specifically within the basal layer of the corneal limbus (Z. Chen et al., 2004; Dou et al., 2021). The ΔNp63α isoform is recognised as a marker of basal cells of the limbus, yet the β and the γ isoforms are also expressed in other limbal cells and play roles in limbal cell migration, wound healing of the cornea, and differentiation (Di Iorio et al., 2012).

Nonetheless, the antibody used in the current study to detect *TP63* protein products detects the TA and ΔN isoforms of the protein (Figure 4.12), thus, discernment of specific *TP63* isoform expression is not possible in this study.

ΔNp63 is not a specific marker of the corneal epithelium, rather, its expression is representative of stratified epithelial tissue, including the skin epidermis (Candi et al., 2007; Medawar et al., 2008; Shalom-Feuerstein et al., 2011). Co-expression of ΔNp63 and PAX6 are necessary for corneal epithelial cell specificity, and loss of PAX6 induces a skin-epidermis phenotype (G. Li et al., 2015; W. Li et al., 2008; Ouyang et al., 2014). As demonstrated by the preliminary scRNseq analysis, a small population of *TP63*+ cells were detected, and this population also appeared to express other corneal epithelial specific markers, including PAX6. Co-expression of p63 and PAX6 is expected in LSC/LPCs, however, PAX6 is also expressed in more mature corneal epithelial cells and is more generally expressed in the corneal epithelium respective to p63, thus, PAX6+/p63- cells are also expected.

Staining of PAX6 and p63 at day 21 of the differentiation protocol demonstrated both co-expressing and separate populations of PAX6+ and p63+ cells emerging from dense cell clusters which were likely embryoid bodies. The patient 4 (R124H) cell line was the only line that had large patches of cells with relatively small nuclei that co-expressed both PAX6 and p63 (Figure 4.12B, F), these cells are likely representative of smaller limbal stem/limbal progenitor cells. At day 25, the WT2 line showed patches of cells with larger nuclei that co-expressed both the markers, however, the expression of PAX6 and p63 was completely segregated in the WT1 line at this timepoint. This potentially indicates that this cell line was less responsive to the differentiation protocol. Nevertheless, K3 expression was detected in this same line (Figure 4.14C, G) thus, the lack of PAX6 and p63 co-expression may be due to the later timepoint in the differentiation. However, day 25 WT1 samples were negative for K5 and K14, providing further indication that this line is less responsive to the differentiation protocol or a specific issue with the well that was used for ICC. If it is the case that the WT1 line was less responsive to the differentiation protocol, this could skew data on the characterisation of the cells and any comparisons made between WT and patient-derived cells. Kamarudin et al. (2018) demonstrated that a particular iPSC line was less responsive to the CEpi differentiation, and this was attributed to lower level of endogenous BMP activity when compared with responsive lines. The authors rectified the issue of the non-responsive iPSC line through media supplementation of the TGFβ inhibitor SB431542, which led to increased *ΔNp63* expression.

During the course of the current study, numerous anti-TGFBIp antibodies were tested for specific subcellular staining through immunocytochemistry utilising the confirmed *TGFBI* KO line as a negative control. Most of the antibodies tested showed non-specific staining as the same staining patterns were also observed in the *TGFBI* KO line (data not shown), highlighting caution when interpreting publications using these antibodies and their interpretation of the data. A specific anti-TGFBIp antibody was identified for immunocytochemistry applications, as demonstrated in Figure 4.17, which shows localisation of TGFBIp in the ER and GA of the WT1 line, along with negative staining in the *TGFBI* KO line. As a secreted protein that contains an NH_2-terminal signal sequence, intracellular TGFBIp is expected to undergo folding within the ER before being subsequently transported to the GA prior to secretion (B. Y. Kim et al., 2009). Therefore, the immunocytochemistry analysis of TGFBIp in the WT1 CEpi line at day 30 is consistent with the expected folding and processing of TGFBIp.

Nonetheless, due to the identification of this antibody later in the study, co-localisation and mutant vs WT experiments using the TGFBIp antibody were not conducted due to time constraints. Previous research has shown mislocalisation of mutant R124H-TGFBIp to the lysosome via Lamp2 co-staining in corneal stromal cells cultured from GCDII patients (B. Y. Kim et al., 2009). The same study demonstrated that periostin staining was also altered in GCDII patient corneal stromal cells in comparison to WT (B. Y. Kim et al., 2009). Further characterisation of mutant vs WT TGFBIp localisation in CEpi cells would be informative in understanding the pathogenesis of TGFBI CDs, and may help to elucidate impaired protein interactions of mutant TGFBIp. These results also reiterate the fundamental necessity of utilising negative controls when assessing subcellular protein expression through immunostaining in the discernment of specific staining versus non-specific signals and false positive results.

The data presented in this chapter demonstrates the characterisation of iPSC-derived cells that have been successfully differentiated towards a CEpi-lineage. Nonetheless, the lack of expression of the key corneal epithelial marker *KRT12* and the heterogeneity of the cultures indicates that the differentiation protocol still has room for optimisation. The current differentiation protocol utilised BMP4 in order to promote differentiation towards a non-neural ectoderm cell lineage (I. et al., 2011; Kamarudin et al., 2018; Metallo et al., 2008). Other small molecules or factors that can modulate signalling pathways that regulate the differentiation of pluripotent cells into corneal epithelial-like cells could also be screened in optimisation of the protocol.

Specific embryonic development signalling pathways have not been fully elucidated, although it is recognised that inhibition of the TGFβ/Nodal and Wnt/β-catenin signalling pathway is essential for head/ocular surface ectoderm development (Arkell & Tam, 2012; Dupont et al., 2005; Fuhrmann, 2008; Gage et al., 2008). Some protocols developed for corneal epithelial differentiation have utilised TGFβ inhibitors during the induction phase of differentiation with positive results (Kamarudin et al., 2018; Mikhailova et al., 2014). In particular, Kamarudin et al. (2018) reported that the TGFβ inhibitor SB431542 was more effective in enhancing iPSC differentiation to corneal epithelial cells compared to SB505124, another TGFβ inhibitor. Another protocol reported the beneficial use of the Wnt inhibitor IWP-2 in corneal epithelial differentiation (Mikhailova et al., 2014). However, the same group published a later study describing excessive cell death as part of the protocol that decreased following elimination of the Wnt inhibitor, indicating that it is not a suitable small molecule in application (Hongisto et al., 2017).

Nonetheless, the inhibition of the Wnt signalling pathway is important in the determination of a corneal epithelial-specific cell fate (Dhouailly et al., 2014; Y. Kobayashi et al., 2020; Mukhopadhyay et al., 2006). Expression of the Dickkopf 2 (*Dkk2*) protein, which functions as a Wnt signalling inhibitor, is essential in ocular surface fate determination, as evidenced by *Dkk2* KO mice that presented with opaque corneas that grew hair while lacking expression of PAX6 and K12 (Mukhopadhyay et al., 2006). Evidently, the corneas of *Dkk2*-null mice resembled stratified epidermal tissue, demonstrating the importance of Dkk2 expression in corneal epithelial cell fate determination (Mukhopadhyay et al., 2006). Therefore, a potential avenue of increased differentiation efficacy towards more mature CEpi could be the addition of recombinant Dkk2 protein into the CEpi induction media, in attempts to specify a corneal epithelial progenitor cell lineage that co-express ΔNp63 and PAX6. Research that aims to further define the signalling milieu of the developing corneal epithelium would facilitate the *in vitro* generation of this cell lineage.

Like the epidermis, the corneal epithelium is avascular, providing an advantage for its *in vitro* generation from pluripotent stem cells. Similarly, both the epidermis and the corneal epithelium are stratified epithelial tissues, composed of several layers of tightly packed cells. Air-lifting is a method of inducing stratification that was originally applied to epidermal epithelial cells, through exposure to an air interface on one side and contact with the culture media on the other (Rosdy & Clauss, 1990). This method has also been applied to limbal stem cells and has proven effective in inducing the stratification of differentiated corneal epithelial cells (L. Chen et al., 2017; González, Uhm, et al., 2019). One study used limbal stem cells isolated from rabbit corneas and reported that corneal

epithelium thickness increased the longer they were cultured through this technique (L. Chen et al., 2017). Furthermore, cells cultured using the air-lift method demonstrated a time-dependent increase in the size of surface epithelial cells with a squamous-like morphology and an increase in transepithelial electric resistance, indicating the formation of functional corneal epithelium tissue *in vitro* (L. Chen et al., 2017). This method has also been applied to iPSC-derived CEpi cells with success (Mikhailova et al., 2014).

An alternative method of generating CEpi cells *in vitro* is to generate corneal organoids. Numerous corneal organoid differentiation protocols have been published (Foster et al., 2017; Isla-Magrané et al., 2021; Shiju et al., 2020; Susaimanickam et al., 2017). A comparison of the single cell transcriptome profile of iPSC-derived corneal organoids to the human cornea identified differences in terms of cellular proportions, however, cell clusters that resembled and expressed key markers of the corneal epithelium, stroma and endothelium were observed (Maiti et al., 2022). The generation of corneal organoids from TGFBI CD patient-derived iPSCs may be beneficial for the study of disease pathogenesis as these conditions involve more than one layer and cell type of the cornea. However, the 3D structure of organoids may not be amenable to attempting transfections. Therefore, for preliminary screening of ASO efficacy, 2D cultures provides a more reliable method for transfection efficiency.

To summarise, this chapter utilises publicly available scRNAseq data, along with qPCR and immunostaining analyses over key differentiation timepoints for the validation and characterisation of an *in vitro* iPSC-derived CEpi model. The cell model generated demonstrated expression of relevant corneal epithelial cell markers at the transcript and protein level, along with an epithelial cell morphology. However, the protocol could still benefit from optimisation. The analysis of other cell types in the cultures, such as those expressing specific epidermal markers would allow for a measure of differentiation efficacy and also aid the isolation of the desired cell population, through elimination of cells expressing inappropriate cell surface markers. There is much to still be discovered on the precise differentiation pathways of the human corneal epithelium. As similarities in expression profile between the corneal epithelium and the skin epidermis are noted, scRNAseq comparing both of these tissue types could be informative in understanding the key differences between them.

Chapter 5: Transcriptome analysis of mutant vs WT day 21 CEpi samples

5.1 Introduction

A striking TGFBI CD genotype-phenotype correlation has been observed, yet the molecular mechanisms underlying these conditions are not clear. Even if different TGFBIp mutations result in the same phenotype, different pathological mechanisms of mutant TGFBIp seem to underlie deposit formation (N. S. Nielsen et al., 2020). For example, the p.R124C mutation in TGFBIp causing LCDI appears to result in TGFBIp amyloid fibril formation by a different mechanism than LCDI-causing variants in the fourth FAS1 domain of TGFBIp (Courtney et al., 2015; Runager et al., 2011; Schmitt-Bernard et al., 2000; Venkatraman et al., 2019). Most investigations into LCDI have focused on pathogenic variants in the fourth FAS1 domain of the protein, thus, not much is known about the pathogenesis underlying p.R124C LCDI. On the other hand, the p.R124H TGFBIp mutation likely accounts for the majority of GCDII cases and has received attention in the field due to its prevalence.

TGFBI is highly expressed in the human cornea, and although it is also widely expressed in other tissues, it is not understood why pathology is restricted to a specific tissue. The mechanism of how different protein variants cause different phenotypic manifestations is also not fully understood. Current knowledge on these will be discussed in detail in Chapter 6, however, the transcriptional landscape of TGFBI CDs has thus far, not been thoroughly investigated.

RNA sequencing (RNAseq) is a powerful high-throughput technique that allows for the quantification and characterisation of transcriptomes. In recent years, RNAseq has become the standard method of measuring gene expression in a wide range of biological systems. In comparison to the older and more limited cDNA microarray techniques, RNAseq allows for the simultaneous analysis of the whole transcriptomic profiling of a sample. The present study utilises bulk RNAseq to explore the transcriptional landscape of mutant vs WT CEpi day 21 samples. By understanding the complex interplay of gene expression in this new model system, we hope to gain insight into the pathological process underlying TGFBI CDs. In particular, identification of biomarkers differentially expressed between the mutant cells and WT cells may provide the basis for functional analyses and readout of disease prevention following therapeutic ASO treatment. Additionally, establishing the causative relationships between different genetic variants in TGFBIp and gene expression patterns could illuminate disease aetiology (Schadt et al., 2005).

The model used in the current study was developed primarily to assess *TGFBI*-downregulation following ASO treatment in CEpi cells, as corneal epithelial cells produce a large proportion of TGFBIp in the human cornea (Chapter 4, Section 4.1.1). However, TGFBI aggregates primarily manifest in the corneal sub-epithelium and stroma of TGFBI CD patients, and up till now, investigations into the pathology of TGFBI CDs have largely focused on proteomics analyses of corneal stroma deposits (Chapter 6, Section 6.1.1). It is not known whether the transcriptomic profile of the corneal epithelium is altered in TGFBI CD respective to healthy tissue and this question has not previously been explored. Thus, RNAseq was carried out on the CEpi samples in order to explore whether any disease-relevant differences could be observed between WT and mutant cells using this particular *in vitro* model.

5.2 Results

Preliminary data obtained by Beatriz Sanchez-Pintado (unpublished data) using the same differentiation protocol as the current study, indicated that the key corneal epithelial marker *KRT3* was most highly expressed at the transcript level at day 21. Due to this finding, day 21 CEpi samples were selected for bulk RNAseq analysis, despite the data presented in the current study indicating that *KRT3* levels were highest at day 25 (Chapter 4, Section 4.2.4, Figure 4.11). Total RNA from a total of two samples per cell line (Table 5.1) was extracted (Chapter 2, Section 2.1.2), with each sample obtained from two independent differentiations. Samples were sequenced using the Illumina NovaSeq platform (Chapter 2, Section 2.10.3) and FASTQ files were aligned to the reference transcriptome and genome sequences using Salmon (Chapter 2, Section 2.10.4). The aligned counts were imported into RStudio for normalisation and differential gene expression analysis using DESeq2 (Chapter 2, Section 2.10.4). Depending on the differentiation they originated from, the two biological replicates per cell line were assigned to either differentiation batch A or B. Altogether, the two WT lines, two p.R124C, two p.R124H and one *TGFBI* KO line was included in the RNAseq analysis (Table 5.1). Differences in transcriptome profile were then investigated for three comparisons:

1. p.R124C vs WT
2. p.R124H vs WT
3. *TGFBI* KO vs WT

Preliminary analyses of differential gene expression between the groups of interest led to the conclusion that a relaxed false discovery rate (FDR)-adjusted pvalue cut off of 0.1 should be used for all comparisons. This was due to the relatively low numbers of significantly differentially expressed genes (DEGs) identified when the analysis was carried out using the conventional pvalue cut off of 0.05. Furthermore, in order to facilitate the detection of consistently robust yet smaller changes in the transcriptomic profiles of group comparisons, no log2 fold change (LFC) cut off was used in the identification of significant DEGs.

Table 5.1 Day 21 CEpi cell lines included in the bulk RNAseq analysis.

Cell line	Genotype	Condition	Sex	n of biological replicates
WT1	WT	Unaffected	Male	2
WT2	WT	Unaffected	Male	2
Patient 1 (P1)	p.R124C	LCDI	Male	2
Patient 2 (P2)	p.R124C	LCDI	Male	2
Patient 3 (P3)	p.R124H	GCDII	Male	2
Patient 4 (P4)	p.R124H	GCDII	Female	2
CKO	TGFBI CRISPR KO	N/A	Male	2

5.2.1 Analysis of p.R124C vs WT

5.2.1.1 Hierarchical clustering analysis

Sample-to-sample distances were plotted by scree plot, principal component analysis (PCA) and hierarchal clustering analysis heatmap (Chapter 2, Section 2.10.4) to determine similarities of global expression profile across p.R124C and WT day 21 CEpi samples (Figure 5.1). As the RNA samples included in the experiment were extracted from two independent differentiations, batch effects were corrected for, prior to the PCA, by including it as a factor in the DESeq2 experimental design (Chapter 2, Section 2.10.3).

Despite the batch correction, the differentiation batch effects seem to be partially directing principal component (PC) 1 (Figure 5.1A), yet no clearly observable clustering pattern is apparent for this PC, although sample P1.1 (patient 1, differentiation batch 1) appears to be an outlier in this case. However, on the y-axis, which represents PC2, individual differences of the respective sample, regardless of differentiation batch, along with the genotype of the sample (either WT or p.R124C) accounts for the greatest source of variation. This is also observable in the plot comparing PC2 and PC3 (Figure 5.1B), where the respective replicates for each sample are aligned along the x-axis, representing PC2. Sample P1.1 does not appear to be an outlier in PC2, therefore this sample was not defined as an outlier and was included in the downstream analysis

The greatest spread in PC2 global expression pattern within sample replicate groups occurs in the WT2 group. Furthermore, the respective P1 and P2 sample replicates appear to cluster together, whereas the WT1 and WT2 samples exhibit a greater global spread in their expression pattern, indicating that the p.R124C patient samples are more similar to each other than the WT samples which seem less homogenous in their expression. The global spread observed between the two different WT lines could be due to discrepancies in differentiation efficiency – as previously mentioned (Chapter 4, Section 4.2.5), the key markers of stratified epithelia, K5 and K14, were not detected in

the WT1 CEpi cells by ICC, indicating that this line may be less responsive to the differentiation protocol respective to the WT2 line, which did sufficiently express these markers. Nonetheless, as the WT1 and WT2 lines are both derived from different fibroblast cell lines, it is expected that there would be biological variation between them.

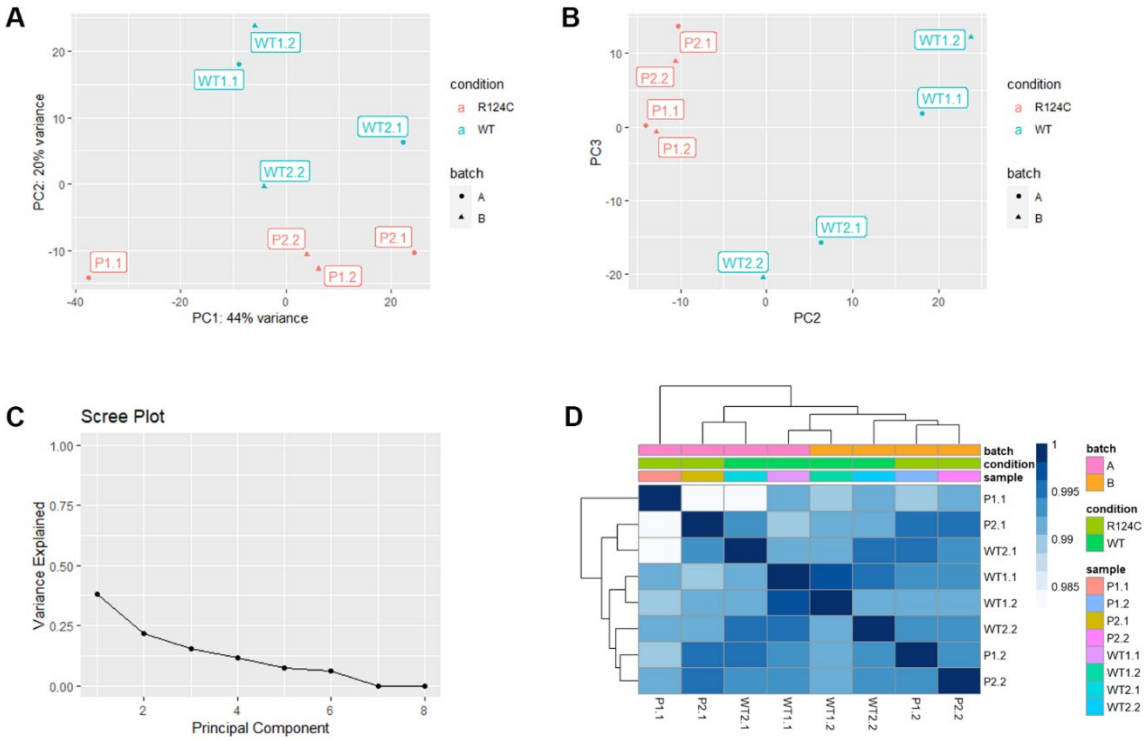

Figure 5.1 Principal component (PC) and hierarchal clustering analysis of p.R124C and WT control day 21 CEpi samples. Plots comparing PC1 and PC2 **(A)** and PC2 and PC3 **(B)** showing a two-dimensional map of the batch-corrected variance between samples, performed using DESeq2 variance stabilised transformed (vst)-normalised bulk RNA-seq data. In the key, batch A and B corresponds to the .1 and .2 sample labels respectively, and refers to the two independent differentiations (biological replicates). **C)** Scree plot illustrating the total number of defined PCs and the percentage of variance explained by each. **D)** Hierarchal clustering analysis heatmap performed using DESeq2 vst-normalised bulk RNA-seq data, displaying the correlation of gene expression for all pairwise sample combinations.

5.2.1.2 Differential gene expression analysis of p.R124C vs WT CEpi samples

Patient 1 and patient 2 (p.R124C) day 21 CEpi biological replicates were compared with WT1 and WT2 day 21 CEpi replicates to obtain significantly differentially expressed genes (DEGs) using DESeq2 (Love et al., 2014). Out of 61,059 mapped genes, 318 DEGs (0.52%) were identified at an FDR corrected p-value (padj) cut off of <0.1. The overall DEG results were visualised by volcano plot (Figure 5.2A) and normalised gene count Z-scores of the 20 most significant DEGs were visualised by heatmap (Figure 5.2B).

The DEG reaching the smallest padj value (1.25E-33) and biggest log_2 fold change (-15.24) was cystathionine beta-synthase-like (*CBSL* - ENSG00000274276) – a gene annotated as an artifactual duplication that is located within the artifactual human chromosome 21 region in the Ensembl genome browser (release 109), the real copy of which is the gene *CBS* (ENSG00000160200). *CBS* codes for the enzyme cystathionine beta-synthase which catalyses the first step of the trans-sulfuration pathway. It is abundantly expressed in the anterior segments of the eye, particularly the corneal epithelium (Persa et al., 2006), and its deficiency has been implicated in numerous disorders of the eye (Kruger, 2017). However, upon plotting of the normalised counts for *CBSL* and *CBS*, it is clear there is no reduction in expression of the protein coding form of the *CBS* transcript in p.R124C samples compared to WT and it is not a DEG (Figure 5.3). Thus, the dramatic downregulation of *CBSL* in p.R124C patient samples compared to WT is considered an artifact of RNA sequencing data alignment due to errors in the assembly and sequencing of the reference genome.

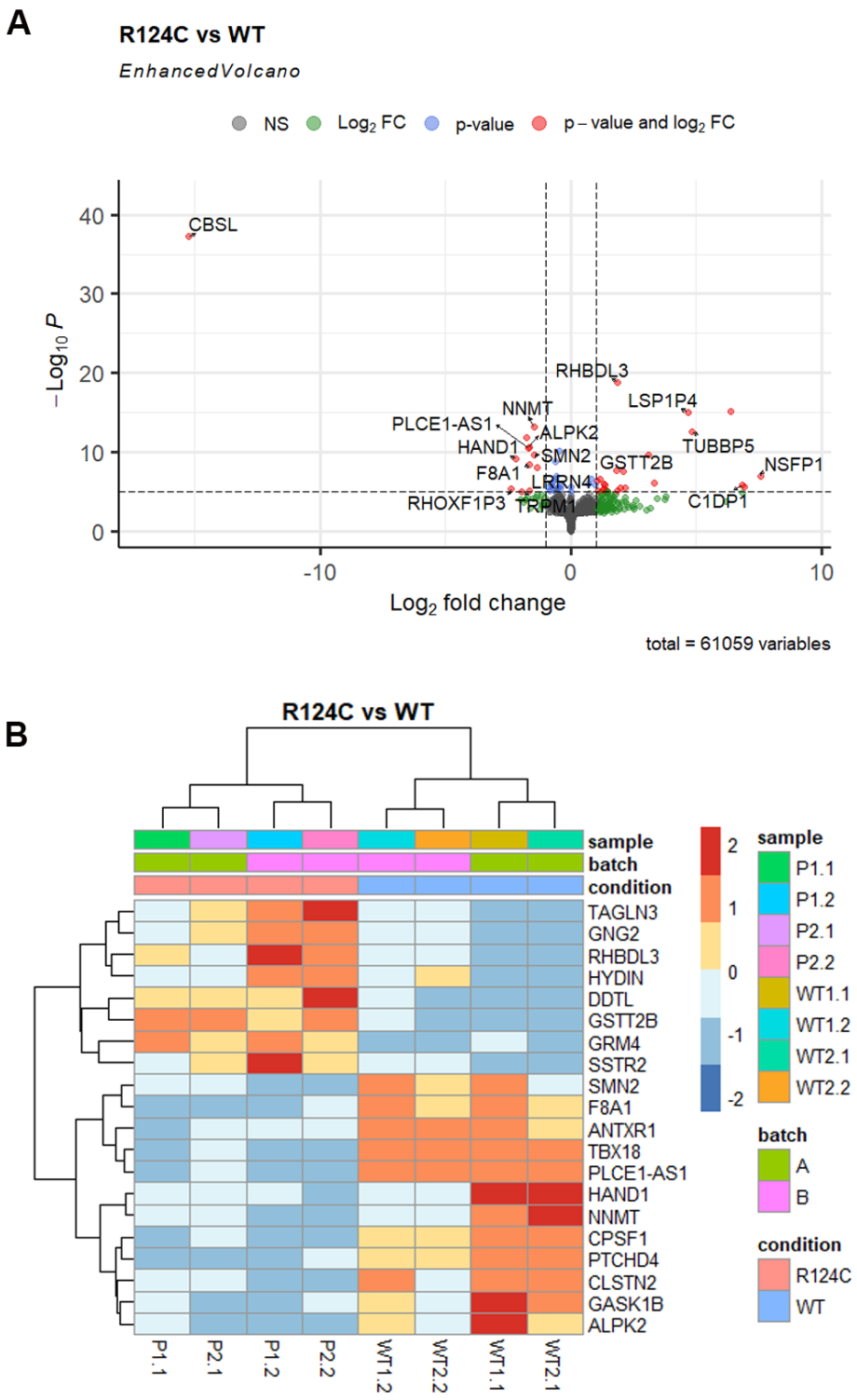

Figure 5.2 Differential gene expression analysis of p.R124C and WT day 21 CEpi samples. The DESeq2 RStudio package (Love et al., 2014) was used to identify differentially expressed genes between p.R124C and WT CEpi samples. **A)** Enhanced volcano plot showing significantly differentially expressed genes. Each gene is represented by a dot, the colour of the dot indicates its p-value and log2 fold change. The -log10 (p-value) is shown on the y-axis vs the log2 fold change on the x-axis. **B)** Normalised gene count Z-scores of the top 20 differentially expressed genes are plotted by heatmap. Red and blue colours indicate the relative over-or under-expression of genes, respectively. Batch refers to the CEpi differentiation batch, with batch A corresponding to samples labelled with .1 and batch B corresponding to samples labelled with .2.

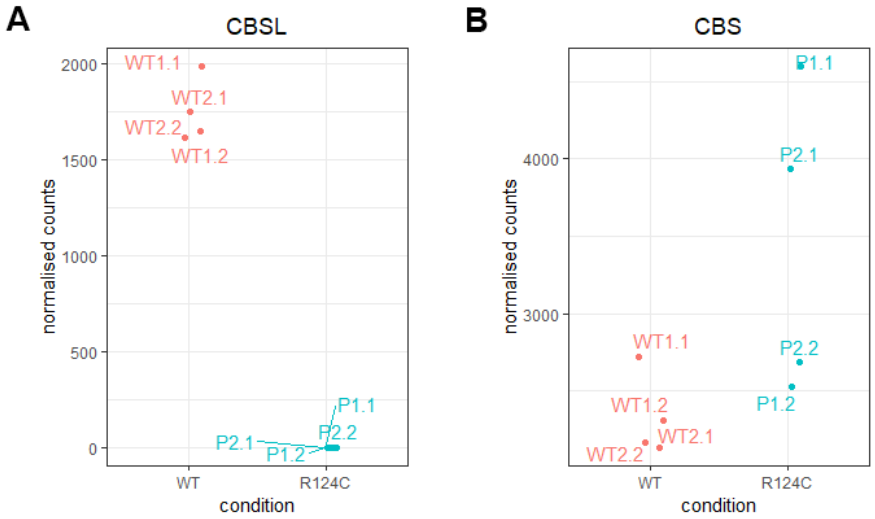

Figure 5.3 Normalised count values of cystathionine beta-synthase-like (CBSL) and cystathionine beta-synthase (CBS) in WT and p.R124C CEpi samples. A) The artificial duplication gene CBSL was found to be significantly downregulated in p.R124C CEpi samples (LFC -15.237, padj 1.25E-33). **B)** The protein coding gene CBS was not significantly differentially expressed between p.R124C and WT samples (LFC 0.372, padj 0.117) indicating that the apparent downregulation of CBSL is an artifact due to errors in the assembly and sequencing of the reference genome.

TGFBIp is an ECM protein that reportedly undergoes abnormal proteolysis in the pathogenesis of LCDI (Y. P. Han et al., 2011; Takács et al., 1998). The serine protease HtrA1 has been implicated in proteolytic processing of LCDI mutant TGFBIp species and has been identified as a constituent of p.R124C TGFBIp+ corneal deposits in the stroma (Courtney et al., 2015). However, *HTRA1* was not found to be significantly differentially expressed between p.R124C and WT samples in the current dataset. Nevertheless, numerous other proteases, particularly those of the metalloproteinase class, were found to be DEGs (Table 5.2; Figure 5.4). This was reflected by the gene ontology (GO) molecular function (MF) over-representation analysis carried out using the clusterProfiler package in RStudio (Chapter 2, Section 2.10.3) on all identified significant (padj value <0.1) DEGs, with metallopeptidase activity (GO:0008237) being significantly overrepresented (<0.05) along with collagen binding (GO:0005518) (Figure 5.4).

Apart from DEGs coding for proteases, other DEGs of interest were identified and assessed for relevance (Figure 5.5). *TGFβ1*, which codes for TGFβ ligand 1 and is responsible for the induction of *TGFBI* expression, was found to be downregulated in p.R124C samples compared to WT (LFC -0.420, padj 0.085). TGFβ signalling results in the activation of different SMADs depending on the context. Correlating with the downregulation of *TGFβ1, SMAD1* (LFC -0.320, padj 0.0358) and *SMAD3* (LFC -0.253, padj 0.097) were also downregulated. Interestingly, the gene encoding TGFβ receptor *ITGAV* was also significantly downregulated in the p.R124C samples relative to the WT

(LFC 0.433, padj 0.001). Additionally, *LUM* encoding for the ECM protein Lumican which is a major constituent of the corneal ECM and is also involved in the TGFβ pathway (Saika et al., 2001), was significantly downregulated (LFC -0.721, padj 0.049).

Another GO over-representation analysis using the biological process (BP) ontology subclass (Chapter 2, Section 2.10.3) was carried out on all identified significant (padj value <0.1) DEGs (Figure 5.6). Over-represented BPs included cell junction assembly (GO:0034329), regulation of TGFβ production (GO:0071634), microtubule bundle formation (GO:0001578), protein localisation to the extracellular region (GO:0071692), SMAD protein complex assembly (GO:0007183) and camera-type eye development (GO:0001654), indicating that the DEGs were strongly associated with these BPs.

Furthermore, various GO terms relating to development were identified as over-represented, these included regulation of developmental growth (GO:0048638), positive regulation of cellular component biogenesis (GO:0044089) and regulation of cell development (GO:0060284). The over-representation of these processes within the current dataset is likely to reflect variance in the differentiation process, which may be contributing to the spread of the samples in PC1 (Figure 5.1A).

The net plot presented in Figure 5.6 allows for the identification of DEGs that are associated with the over-represented BP GO terms.

Table 5.2 p.R124C vs WT differently expressed genes coding for proteases.

symbol	Ensembl ID	log2Fold Change	padj value	protease class
CAPN5	ENSG00000149260	0.297	0.048	cysteine protease
TPP1	ENSG00000166340	-0.337	0.043	serine protease
TMPRSS4	ENSG00000137648	1.103	0.096	serine protease
RHBDL3	ENSG00000141314	1.861	1.43E-15	serine protease
CPQ	ENSG00000104324	-0.532	0.025	metalloprotease
NAALAD2	ENSG00000077616	-0.645	0.027	metalloprotease
ADAMTS12	ENSG00000151388	-0.395	0.049	metalloprotease
PHEX	ENSG00000102174	-1.822	0.021	metalloprotease
TRHDE	ENSG00000072657	1.263	0.005	metalloprotease
MMEL1	ENSG00000142606	1.416	0.053	metalloprotease
ADAMTS18	ENSG00000140873	-0.590	0.066	metalloprotease
ADAM11	ENSG00000073670	0.479	0.057	metalloprotease
AMZ1	ENSG00000174945	1.126	0.070	metalloprotease
PAPPA2	ENSG00000116183	-1.015	0.042	metalloprotease

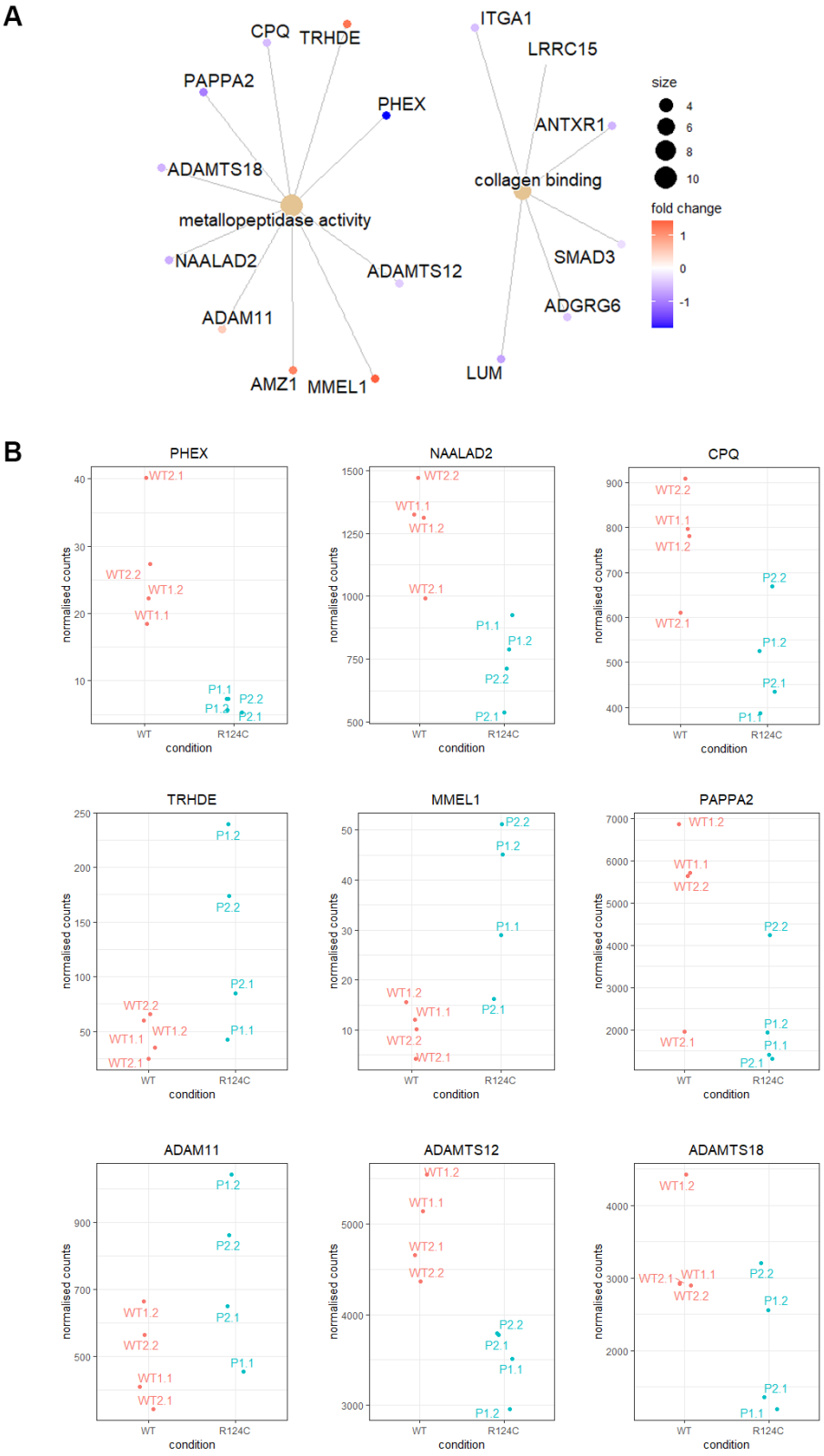

Figure 5.4 Molecular function gene ontology (GO) over-representation analysis of p.R124C and WT CEpi samples. A) Category netplot showing the relationship between genes and associated overrepresented molecular function GO terms. The size of the GO term represents the number of genes associated with that term. The colour of the gene indicates its log2 fold change in the p.R124C group relative to WT. **B)** Dotplots showing normalised count values of significantly differentially expressed (P < 0.1) metalloproteinase-related genes.

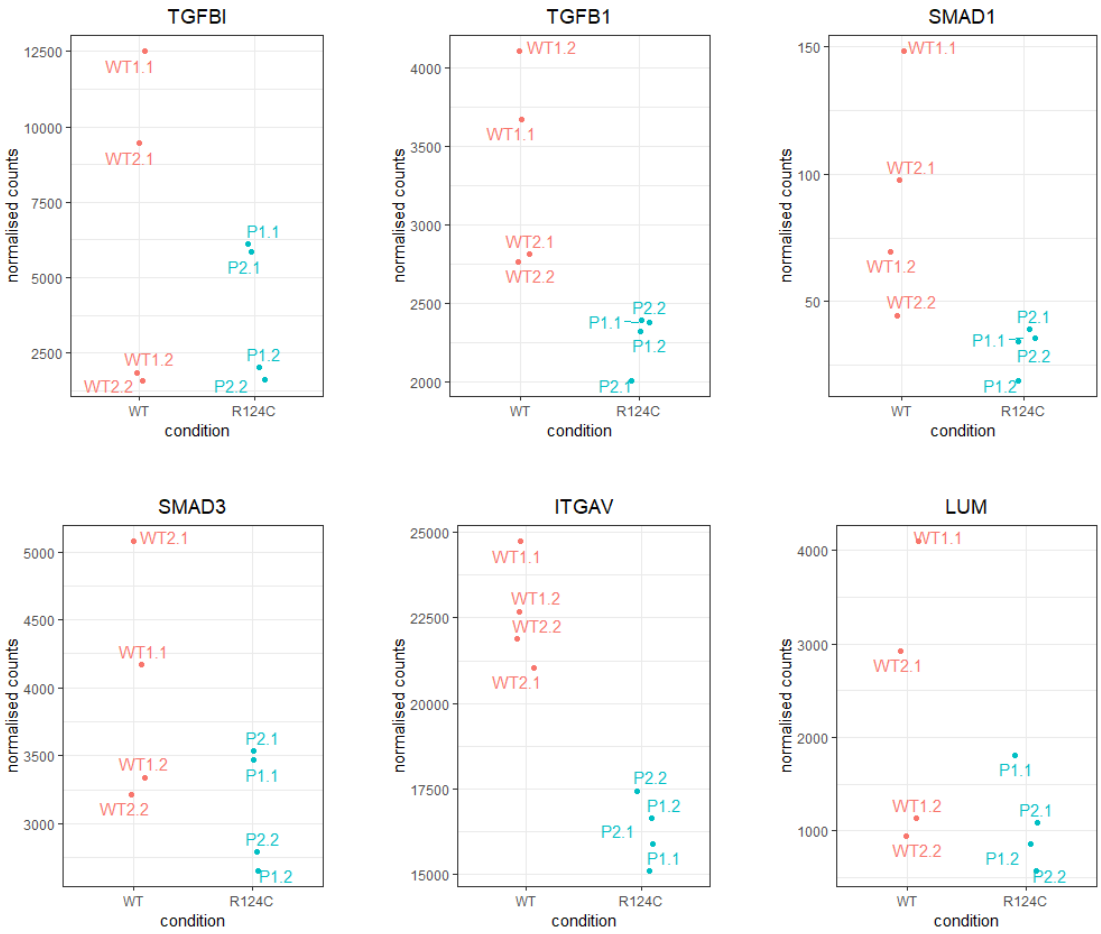

Figure 5.5 Normalised count values of TGFBI and significantly differentially expressed genes that are involved in the TGFβ signalling pathway. TGFBI was not significantly differentially expressed between p.R124C and WT samples (LFC -0.015, padj 0.676), yet various other genes involved in the TGFβ signalling pathway were significantly differentially expressed (padj <0.1).

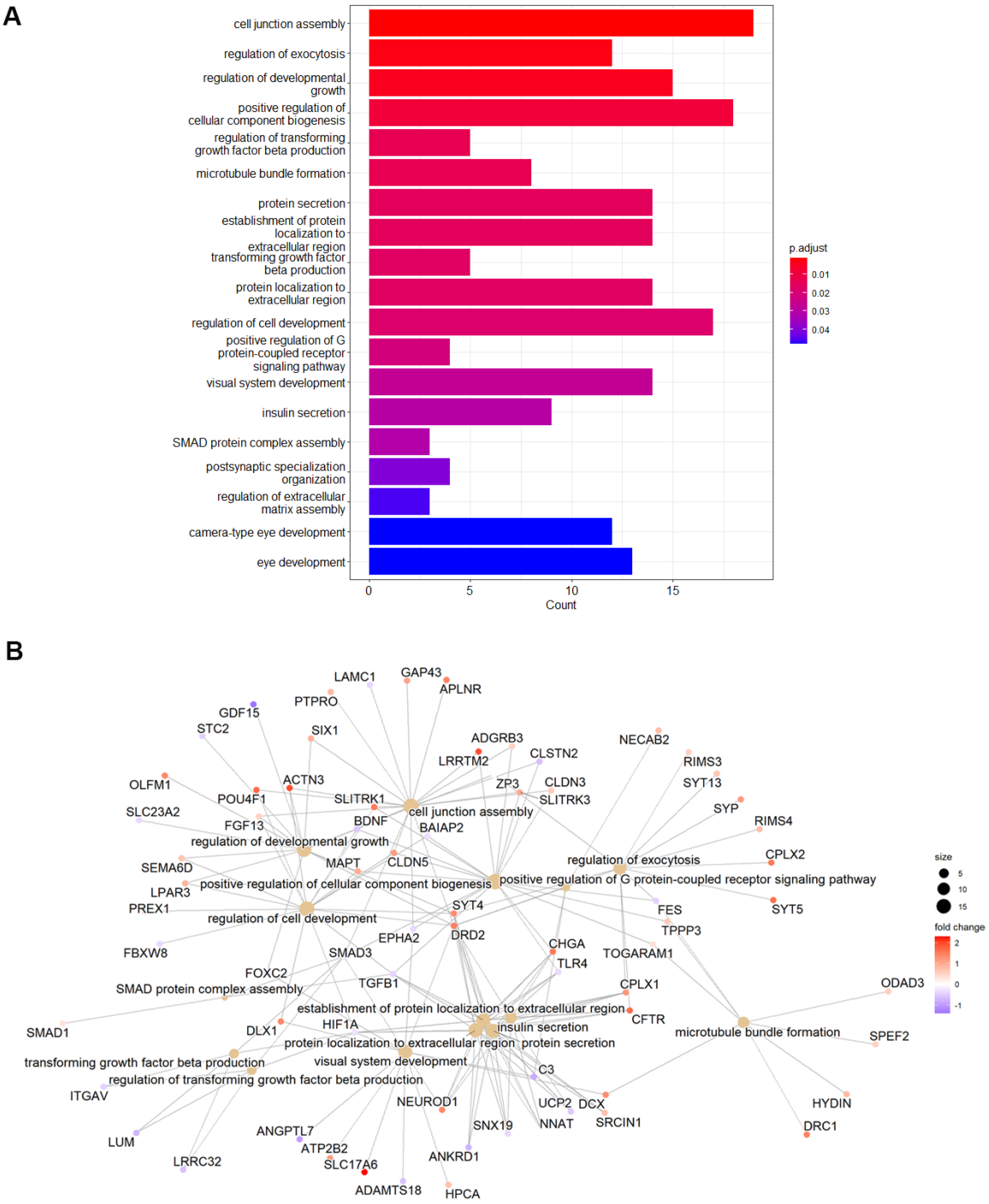

Figure 5.6 Biological process gene ontology (GO) over-representation analysis of p.R124C vs WT samples. The ClusterProfiler RStudio package was used to identify over-represented biological process GO terms based on significantly differentially expressed genes (padj <0.1) between p.R124C and WT CEpi samples. The results of the analysis are presented as a barchart **(A)** where the colour of the bar represents the padj value of the term, and the length of the bar represents the number of genes associated with that GO term; and as a category netplot **(B)** showing the relationship between genes and associated overrepresented biological process GO terms. The size of the GO term represents the number of genes associated with that term. The colour of the gene indicates its log2 fold change in the p.R124C group relative to WT.

5.2.2 Analysis of p.R124H vs WT

5.2.2.1 Hierarchical clustering analysis

Sample-to-sample distances were plotted by scree plot, PCA and hierarchal clustering analysis heatmap to determine similarities of global expression profile across p.R124H and WT day 21 CEpi sequenced samples (Figure 5.7). As the RNA samples included in the experiment were extracted from two independent differentiations, batch effects were corrected for, prior to the PCA, by including it as a factor in the DESeq2 experimental design.

Clear clustering of samples by individual genotype is observed by PC1 and PC2 for all samples apart from sample P4 which demonstrates relatively low variability along PC1 but the greatest global spread in expression pattern in PC2 as well as PC3 (Figure 5.7A-B). Patient 4 was the only female sample included in this study and a clear sex effect is observed between the CEpi samples, with the two P4 samples clustering away from the other male samples. Furthermore, in PC2, P3 samples are more similar to the WT1 and WT2 samples than they are to each other. A substantial global spread is observed for the WT2 duplicates along PC3 (Figure 5.7B). Taking all this into consideration, it appears that PC1 corresponds to the variability of interest for the p.R124H vs WT comparison. Although, the sex difference is expected to have an effect, the female samples were not excluded, due to the small sample size included in this study.

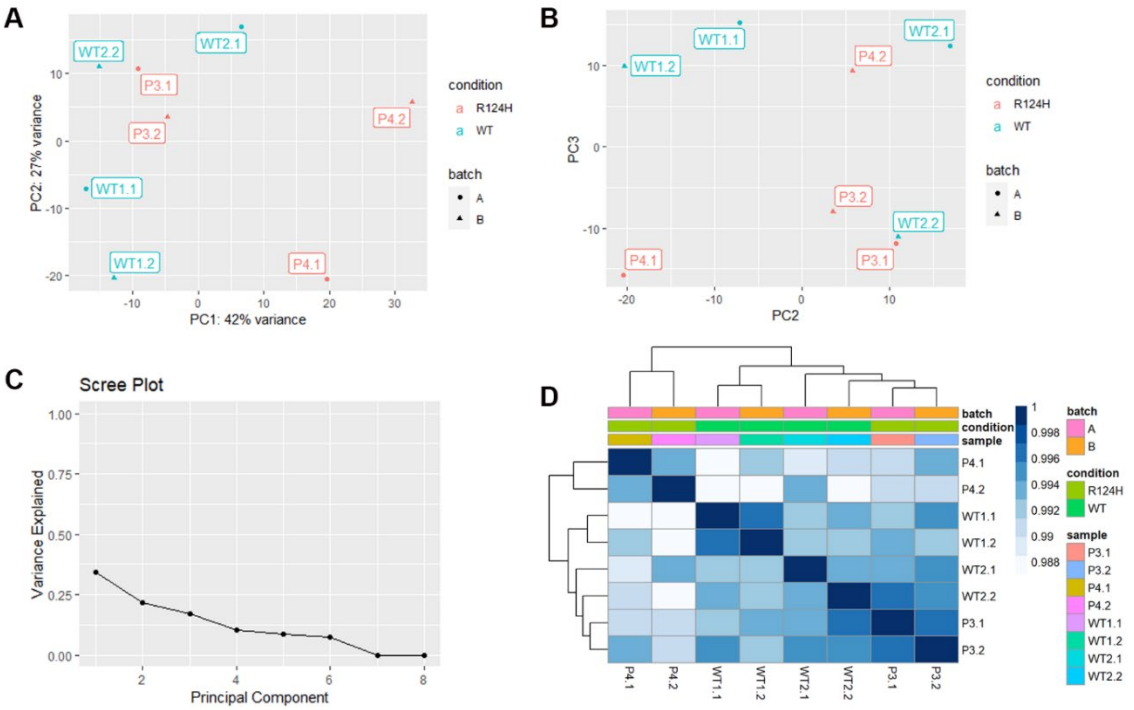

Figure 5.7 Principal component (PC) and hierarchal clustering analysis of p.R124H and WT control day 21 CEpi samples. Plots comparing PC1 and PC2 **(A)** and PC2 and PC3 **(B)** showing a two-dimensional map of the variance between samples, performed using DESeq2 vst-normalised bulk RNA-seq data. In the key, batch A and B corresponds to the .1 and .2 sample labels respectively, and refers to the two independent differentiations carried out in obtainment of the samples. C) Scree plot illustrating the total number of defined PCs and the percentage of variance explained by each. **D)** Hierarchal clustering analysis heatmap performed using DESeq2 vst-normalised bulk RNA-seq data, displaying the correlation of gene expression for all pairwise sample combinations.

5.2.2.2 Differential gene expression analysis of p.R124H vs WT CEpi samples

Patient 3 and patient 4 (p.R124H) day 21 CEpi biological duplicates were compared with WT1 and WT2 day 21 CEpi duplicates to obtain significantly DEGs using DESeq2 (Love et al., 2014). Out of 61,059 mapped genes, 150 DEGs (0.25%) were identified at an FDR corrected p-value (padj) cut off of <0.1. The overall DEG results were visualised by volcano plot (Figure 5.8A) and normalised gene count Z-scores of the 20 most significant DEGs were visualised by heatmap (Figure 5.8B).

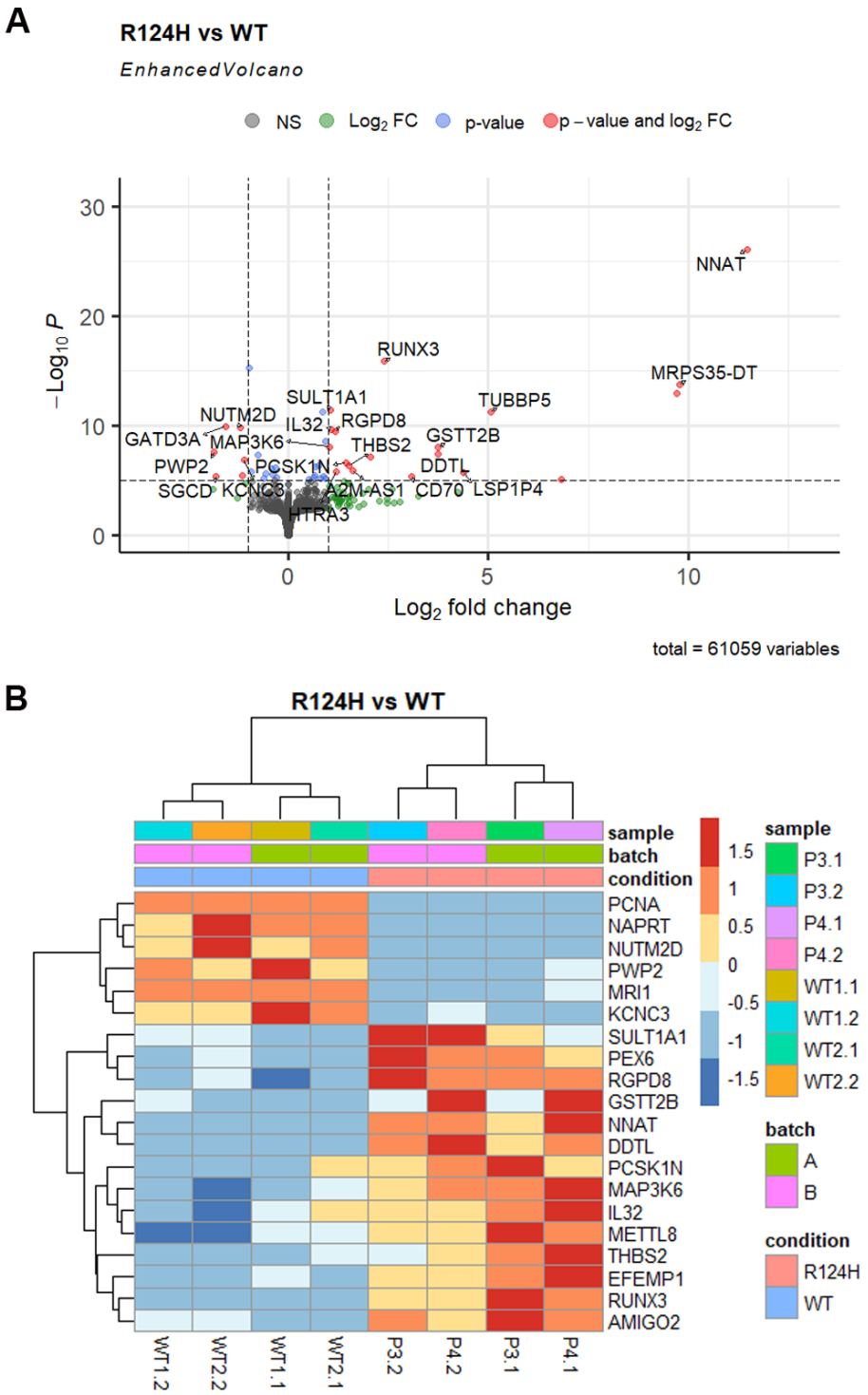

Figure 5.8 Differential gene expression analysis of p.R124H and WT day 21 CEpi samples. The DESeq2 RStudio package (Love et al., 2014) was used to identify differentially expressed genes between p.R124H and WT CEpi samples. **A)** Enhanced volcano plot showing significantly differentially expressed genes. Each gene is represented by a dot, the colour of the dot indicates its p-value and log2 fold change. The -log10 (p-value) is shown on the y-axis vs the log2 fold change on the x-axis. **B)** Normalised gene count Z-scores of the top 20 differentially expressed genes are plotted by heatmap. Red and blue colours indicate the relative over-or under-expression of genes, respectively. Batch refers to the CEpi differentiation batch, with batch A corresponding to samples labelled with .1 and batch B corresponding to samples labelled with .2.

Abnormal proteolysis of TGFBIp is involved in CD pathogenesis (see Chapter 6, Section 6.1.1.1.1). In the case of GCDII corneas, p.R124H TGFBIp appears to display similar levels of stabilty and proteolytic resistance to WT TGFBIp (Runager et al., 2011). Although, the mixed amorphous and amyloid deposit phentoype of GCDII indicates that multiple pathological mechanisms results from the p.R124H mutation in TGFBIp. Abberant proteolysis may form the less commonly observed, deeper amyloid deposits. A total of five proteases were identified as significant DEGs (<0.1), along with two protease inhibitors (Figure 5.9). For this comparison, a clear pattern of protease transcript upregulation was observed. Of particular interest is the differential expression of the matrix metalloproteinases *MMP2*, encoding matrix metalloproteinase 2 (LFC 0.629, padj 0.094), *MMP23B*, encoding matrix metalloproteinase 23 (LFC 0.584, padj 0.020) and the serine protease *HTRA3*, encoding high temperature requirement A protease 3 (LFC 1.193, padj 0.001). The two significantly differentially expressed transcripts coding for the protease inhibitors *SERPINA1*, encoding alpha-1 antitrypsin (LFC 1.999, padj 0.020) and *SERPINB7* encoding Serpin Family B Member 7 (LFC 1.226, padj 0.014) were also upregulated. However, upon closer inspection of the individual normalised gene count values for each protease inhibitor, it is apparent that *SERPINA1* is dramatically upregulated in sample P4.1 only, whereas *SERPINB7* is more consistantly upregulated across the p.R124H patient samples in comparison to the WT samples of the same differentiation batch (Figure 5.9). This highlights the importance of insepcting the normalised cell counts for each sample before making conclusions on DEGs, as differential expression value averages can be dramatically influenced by one single sample in a small sample size, such as the one included in the current study.

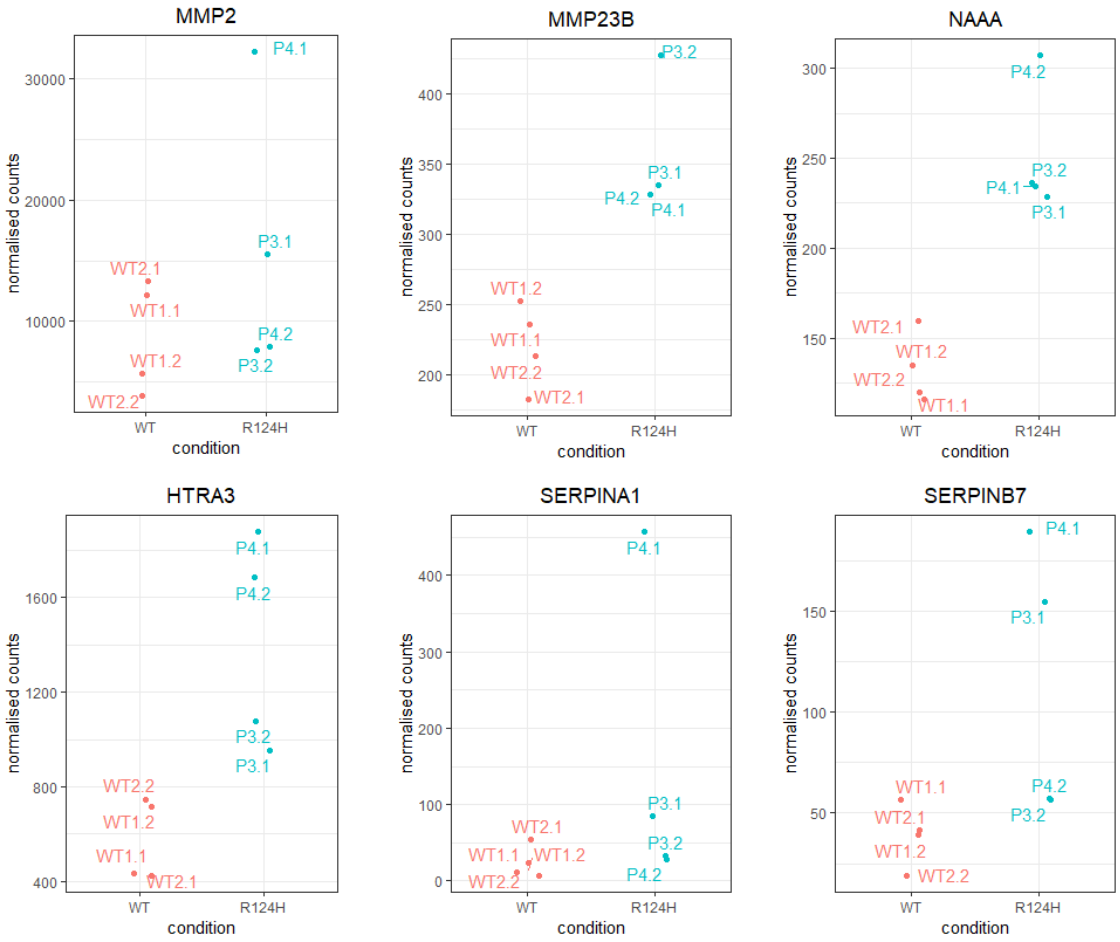

Figure 5.9 Dysregulation of genes encoding proteases and protease inhibitors. Normalised count values of protease and protease inhibitor coding genes that were found to be significantly differentially expressed (padj <0.1) between p.R124H and WT CEpi day 21 samples are presented by dotplot.

A GO over-representation analysis using the CC ontology subclass was carried out on all identified significant (padj value <0.1) DEGs (Figure 5.10). Only two CC GO terms were found to be over-represented fo the p.R124H vs WT comparison (Figure 5.10). These over-represented CCs corresponded to the collagen-containing extracellular matrix (GO:0062023) and the endoplasmic reticulum lumen (GO:0005788).

DEGs of interest, including some of those highlighted by the GO over-representation analysis, were identified and plotted to enable observation of normalised gene count values for each sample included in this comparison (Figure 5.11). *TGFBI* was not significantly differentially expressed, although all the other genes presented in Figure 5.11 were DEGs. The *TGFBI* paralog *POSTN* coding for the ECM protein Periostin was found to be a signficant DEG, and was upregulated in the p.R124H sample group compared to WT (LFC 1.519, padj 0.006). Variation in *POSTN* upregulation was observed between differentiation batches, with p.R124H samples from differentiation batch one (P3.1 and P4.1) demostrating a clear upregulation of *POSTN* that was not

replicated by the p.R124H differentiation batch two samples (P3.2 and P4.2) (Figure 5.11).

As highlighted by the GO over-representation analysis, other genes coding for ECM proteins were also differentially expressed. *EFEMP1* encodes the ECM protein EGF containing fibulin extracellular matrix protein 1 (Fibulin-3), p.R345W mutations in this gene cause Doyne honeycomb retinal dystrophy which presents with the accumulation of drusen beneath the retinal pigment epithelial monolayer (Stone et al., 1999). *EFEMP1* was significantly upregulated in p.R124H samples compared to WT (LFC 0.486, padj 1.57E-08) (Figure 5.11). *COL5A1* codes for the ECM protein Collagen Type V Alpha 1 Chain which has been linked to central corneal thickness and suceptability to kerataconus (Li et al., 2013; Vitart et al., 2010). *COL5A1* was also found to be significantly upregulated in the p.R124H group compared to the WT group (LFC 0.435, padj 0.023) (Figure 5.11).

S100A4 codes for the calcium binding protein S100-A4. Interstingly, this protein has previously been reported to be a constituent of p.R124C LCDI Bowman's layer deposits (Courtney et al., 2015). In the current dataset *S100A4* was significantly upregulated in p.R124H samples respective to WT (LFC 0.901, padj 0.027) (Figure 5.11).

ERP27 codes for the ERp27 chaperone protein of the protein-disulfide isomerase (PDI) family. This protein is found to be upregulated during ER stress (Kober et al., 2013) and in the current study, the *ERP27* transcript was found to be signifcantly upregulated in p.R124H CEpi samples compared to WT (LFC 1.482, padj 0.060) (Figure 5.11).

A significant upregulation of the oxidative stress defense gene *ALDH18A1* was noted (LFC 0.217, padj 0.029) (Figure 5.11). *ALDH18A1* encodes the delta-1-pyrroline-5-carboxylate synthase (P5CS) enzyme, which is a key enzyme involved in the biosynthesis of proline, an important amino acid involved in various cellular processes, including oxidative stress defence (Krishnan et al., 2008). Furthermore, *SELENOM* encoding Selenoprotein M (SELENOM), an ER-localised protein that is also involved in oxidative stress defence (Pitts & Hoffmann, 2018; Varlamova et al., 2022), was also found to be upregulated in p.R124H samples respective to WT (LFC 0.646, padj 0.003) (Figure 5.11).

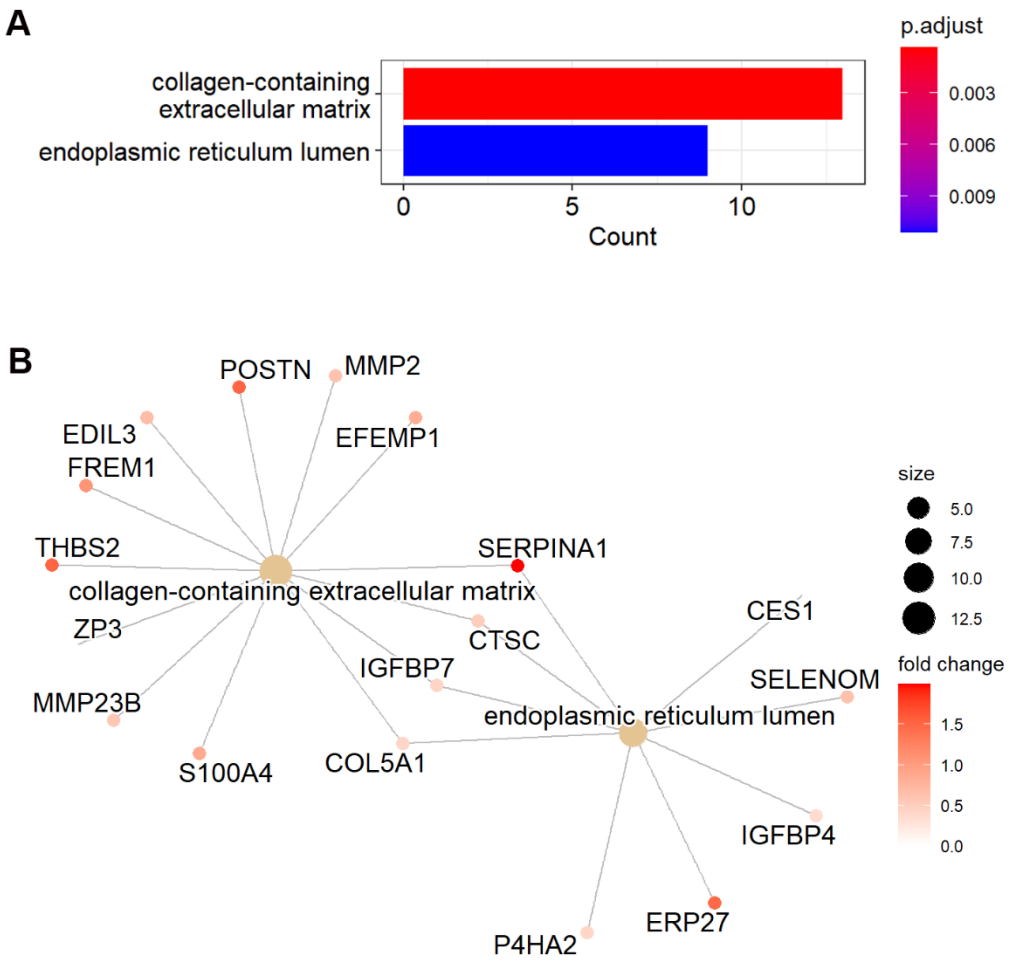

Figure 5.10 Cellular compartment gene ontology (GO) over-representation analysis of p.R124H vs WT samples. The ClusterProfiler RStudio package was used to identify over-represented cellular compartment GO terms based on significantly differentially expressed genes (padj <0.1) between p.R124H and WT CEpi samples. The results of the analysis are presented as a barchart **(A)** where the colour of the bar represents the padj value of the term, and the length of the bar represents the number of genes associated with that GO term; and as a category netplot **(B)** showing the relationship between genes and associated overrepresented cellular compartment GO terms. The size of the GO term represents the number of genes associated with that term. The colour of the gene indicates its log2 fold change in the p.R124C group relative to WT.

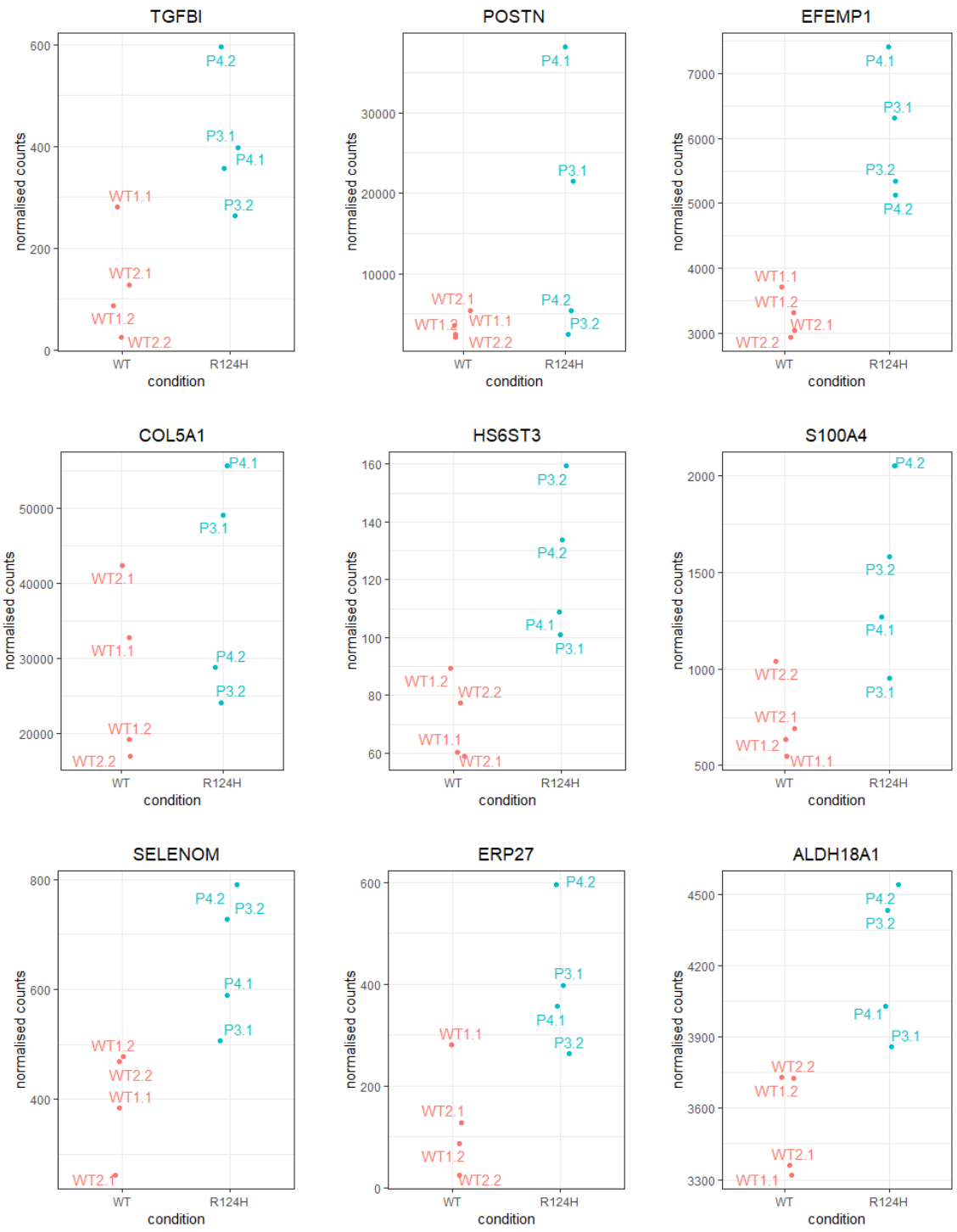

Figure 5.11 Normalised count values of genes of interest. Normalised count values of genes of interest found to be significantly differentially expressed (padj <0.1) between p.R124H and WT CEpi day 21 samples are presented by dotplot. All genes presented are significantly differentially expressed apart from *TGFBI*.

5.2.3 Analysis of *TGFBI* knockout (CKO) vs WT

5.2.3.1 Hierarchical clustering analysis

Sample-to-sample distances were plotted by scree plot, PCA and hierarchal clustering analysis heatmap to determine similarities of global expression profile across *TGFBI* KO (CKO) and WT1 day 21 CEpi sequenced samples (Figure 5.12). As the RNA samples included in the experiment were extracted from two independent differentiations, batch effects were corrected for prior to the PCA by including it as a factor in the DESeq2 experimental design.

The respective sample duplicates cluster together on PC1 (Figure 5.12A) indicating that PC1, which accounts for the strongest point of variation is the variation of interest for this comparison. Although the *TGFBI* KO sample and WT1 sample are isogenic controls, they are spread out from each other on PC1, indicating that these two cell lines were not very similar to each other at day 21 of the CEpi differentiation, which may be due to the lack of *TGFBI* expression in the CKO line. The clustering pattern of PC2 is not clear, as it appears to indicate that CKO.2 is more similar to WT1.1 and that CKO.1 is more similar to WT1.2, even though the .1 and .2 samples are derived from independent differentiations. Nonetheless, the variance displayed by PC2 does not appear to be of interest for this comparison. Observation of PC3, suggests that sample CKO.2 is an outlier of this PC, as the other three samples included in this comparison are clustered closely together (Figure 5.12B).

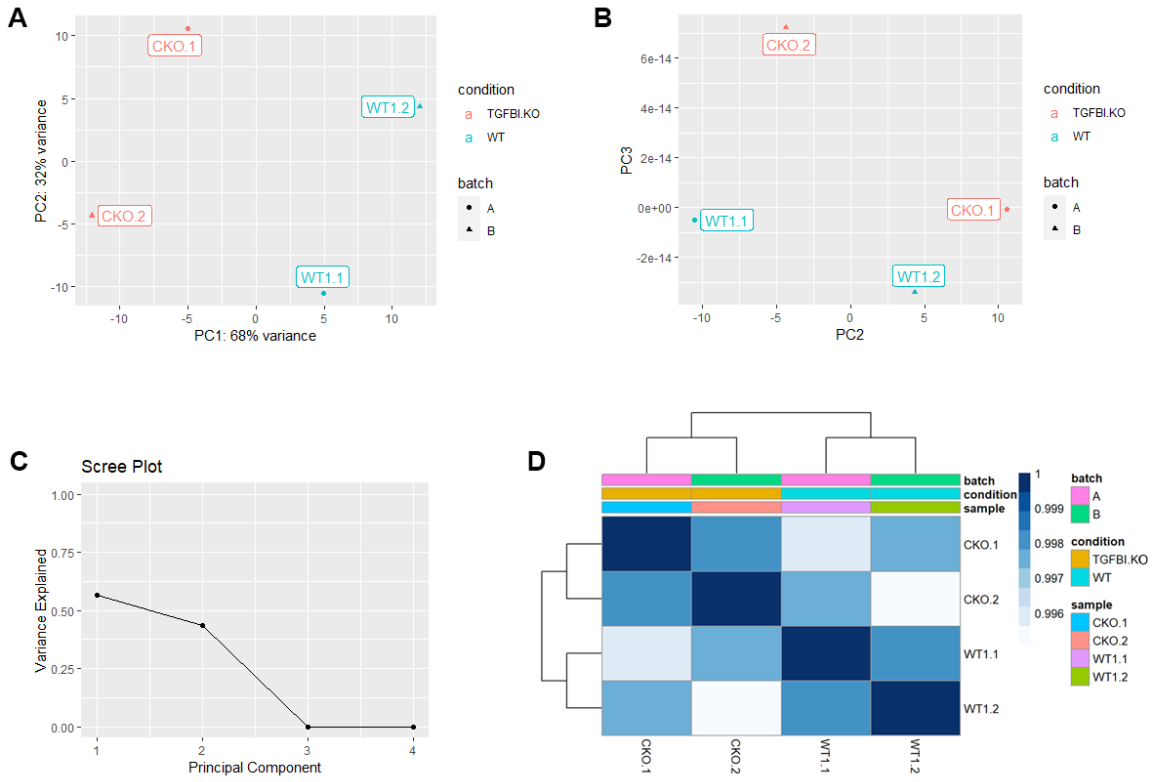

Figure 5.12 Principal component (PC) and hierarchal clustering analysis of TGFBI KO (CKO) and WT1 control day 21 CEpi samples. Plots comparing PC1 and PC2 **(A)** and PC2 and PC3 **(B)** showing a two-dimensional map of the variance between samples, performed using DESeq2 vst-normalised bulk RNA-seq data. **C)** Scree plot illustrating the total number of defined PCs and the percentage of variance explained by each. **D)** Hierarchal clustering analysis heatmap performed using DESeq2 vst-normalised bulk RNA-seq data, displaying the correlation of gene expression for all pairwise sample combinations.

5.2.3.2 Differential gene expression analysis of *TGFBI KO* vs WT CEpi samples

The CKO iPSC line was generated by CRISPR KO of *TGFBI* in the WT1 line providing an isogenic control. CKO day 21 CEpi biological replicates were compared with WT1 day 21 CEpi replicates to obtain significantly differentially expressed genes (DEGs) using DESeq2 (Love et al., 2014). Out of 61,059 mapped genes, 145 DEGs (0.24%) were identified at an FDR corrected p-value (padj) cut off of <0.1. The overall DEG results were visualised by volcano plot (Figure 5.13A) and normalised gene count Z-scores of the 34 most significant DEGs were visualised by heatmap (Figure 5.13B).

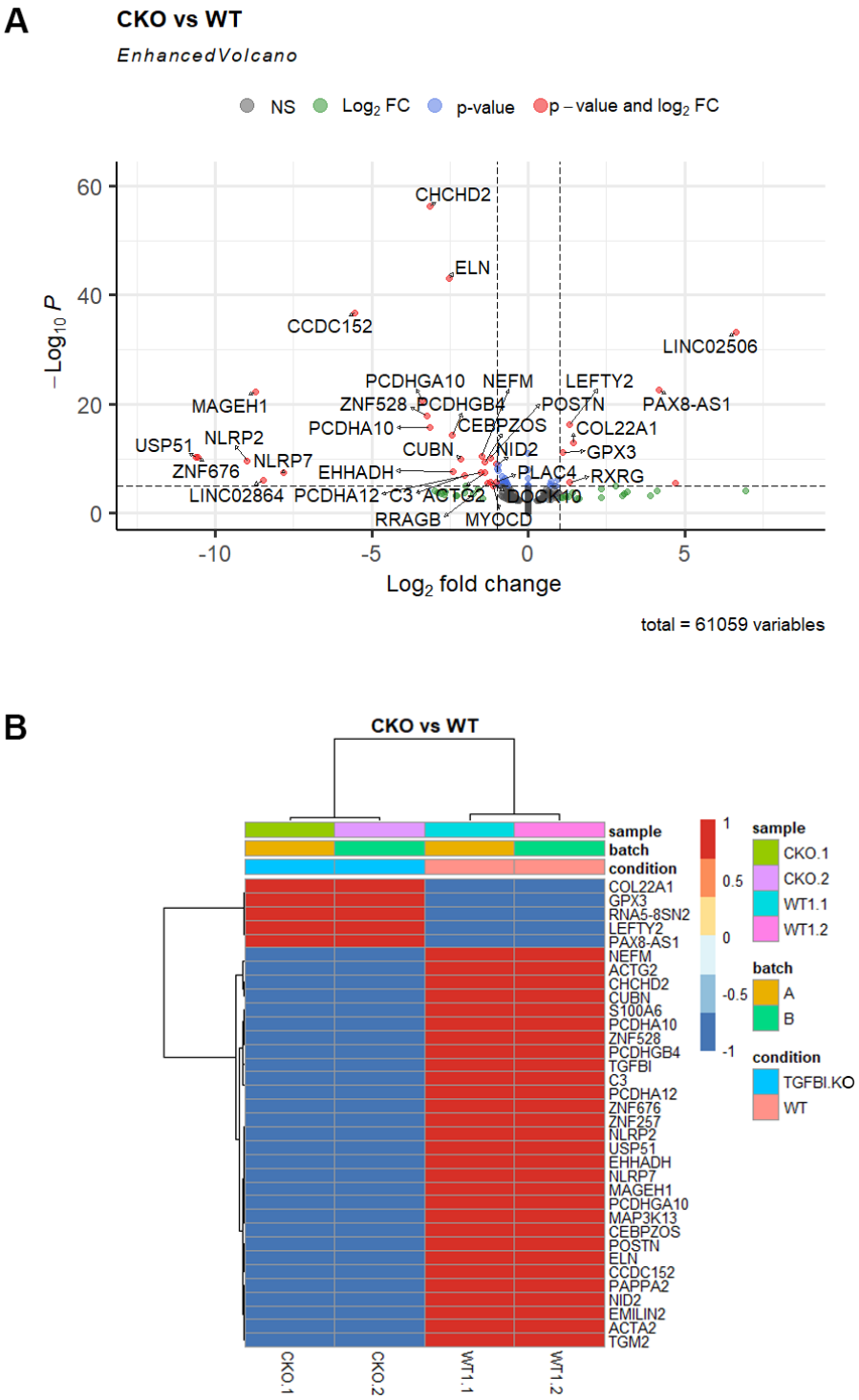

Figure 5.13 Differential gene expression analysis of *TGFBI* knockout and WT1 day 21 CEpi samples. The DESeq2 RStudio package (Love et al., 2014) was used to identify differentially expressed genes between *TGFBI* knockout and WT1 CEpi samples. **A)** Enhanced volcano plot showing significantly differentially expressed genes. Each gene is represented by a dot, the colour of the dot indicates its p-value and log2 fold change. The -log10 (p-value) is shown on the y-axis vs the log2 fold change on the x-axis. **B)** Normalised gene count Z-scores of the top 34 differentially expressed genes are plotted by heatmap. Red and blue colours indicate the relative over-or under-expression of genes, respectively. Batch refers to the CEpi differentiation batch, with batch A corresponding to samples labelled with .1 and batch B corresponding to samples labelled with .2.

As expected, *TGFBI* was significantly downregulated in the CKO day 21 CEpi duplicates respective to the WT samples (LFC -3.74E-06, padj 0.0002) (Figure 5.16). The *TGFBI* paralog *POSTN,* encoding the ECM protein Periostin, was also found to be significantly downregulated in the CKO samples respective to the WT samples (LFC -1.217, padj 8.42E-08) (Figure 5.16), indicating that *POSTN* does not compensate for lack of *TGFBI* expression, rather, the lack of *TGFBI* results in a decrease of *POSTN* expression in this model system.

A GO over-representation analysis was carried out using the CC ontology on all identified significant (padj value <0.1) DEGs (Figure 5.14). Six over-represented CCs were identified, three pertaining to the ECM, namely, the collagen-containing ECM (GO:0062023), collagen trimer (GO:0005581) and basement membrane (GO:0005604). The other three were related to the cytoskeleton, specifically, the actin filament bundle (GO:0032432), myosin filament (GO:0032982) and dynactin complex (GO:0005869), indicating that *TGFBI* KO results in dysregulation of these compartments in CEpi cells at day 21. The net plot presented in figure allows for the identification of DEGs that are associated with the over-represented CC GO terms.

A GO over-representation analysis was then carried out using the BP ontology subclass on all identified significant (padj value <0.1) DEGs (Figure 5.15). BP GO terms related to ECM organisation (GO:0030198, GO:0043062, GO:0045229), muscle development (GO:0007517, GO:0033002), heart development (GO:1905207, GO:1905314) and cell-cell adhesion (GO:0098742) were over-represented in the *TGFBI* KO samples compared to control indicating that *TGFBI* expression is involved in these biological processes.

From the netplot (Figure 5.15B), which shows the association of differentially regulated genes to the top eight GO BP terms, it appears that differential expression of *TGFB2* is linked to each of the over-represented terms. TGFβ proteins are known to induce *TGFBI* expression (Skonier et al., 1992). *TGFB2* was significantly downregulated in the *TGFBI* KO CEpi line (LFC -0.497, padj 0.046), indicating that *TGFBI* may regulate *TGFB2* expression through a feedback loop mechanism and that the functions of TGFBIp may rely on this signalling pathway.

The netplot also demonstrates that seven genes belonging to the clustered protocadherins family, which are clustered together in a single genomic locus are differentially expressed, and that these genes are associated with the cell-cell via adhesion plasma-membrane adhesion molecules GO term (Figure 5.15B). Protocadherins are the largest subgroup of the mammalian cadherin family. Their roles in neuronal cell types have been extensively studied, however, they are also expressed

in ESCs and adult tissues (M. D. West et al., n.d.). Interestingly, the human genomic locus of the clustered protocadherins is around 4-5 megabases downstream of the *TGFBI* gene on chromosome 5q31.

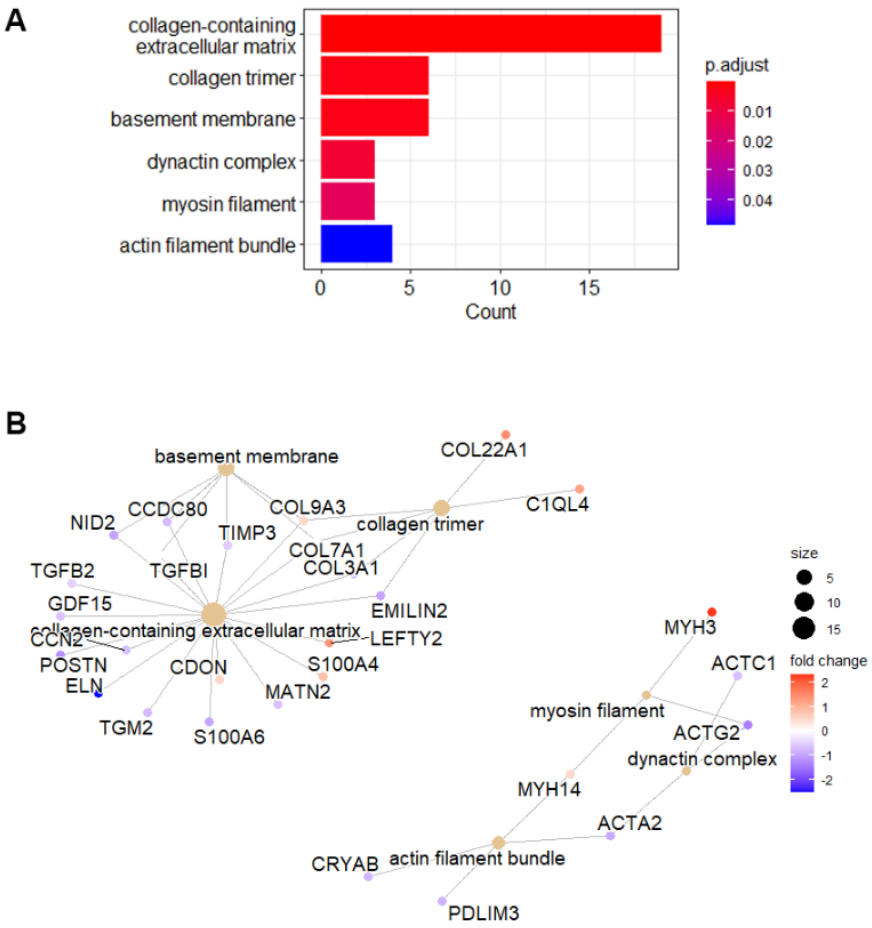

Figure 5.14 Cellular component gene ontology (GO) over-representation analysis on *TGFBI* KO vs WT1 samples. The ClusterProfiler RStudio package was used to identify over-represented cellular component GO terms based on significantly differentially expressed genes (padj <0.1) between *TGFBI* KO and WT1 CEpi samples. The results of the analysis are presented as a barchart **(A)** where the colour of the bar represents the padj value of the term, and the length of the bar represents the number of genes associated with that GO term; and as a category netplot **(B)** showing the relationship between genes and associated overrepresented cellular compartment GO terms. The size of the GO term represents the number of genes associated with that term. The colour of the gene indicates its log2 fold change in the *TGFBI* KO group relative to WT1.

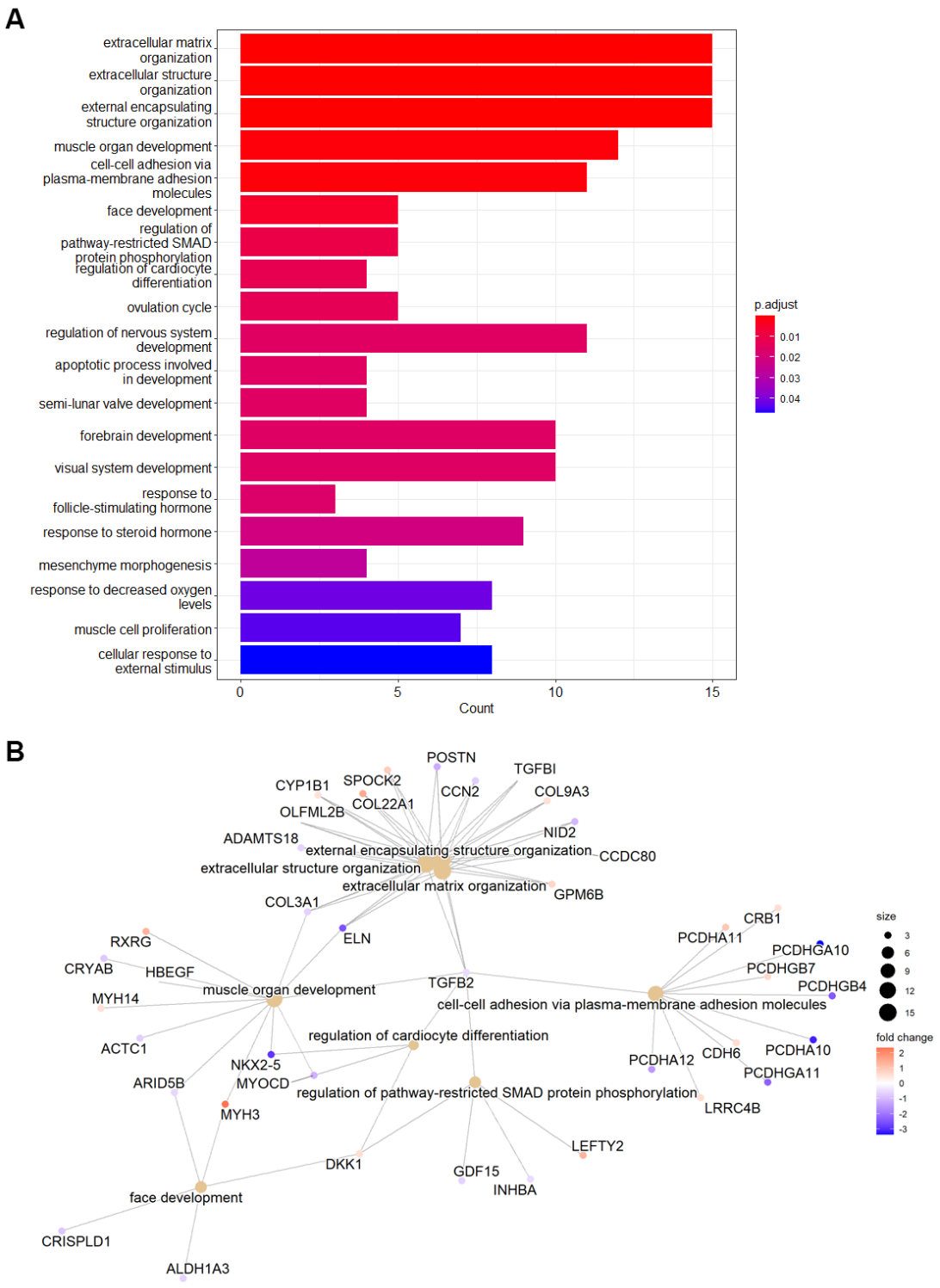

Figure 5.15 Biological process gene ontology (GO) over-representation analysis on TGFBI KO vs WT1 samples. The ClusterProfiler RStudio package was used to identify over-represented biological process GO terms based on significantly differentially expressed genes (padj <0.1) between TGFBI KO and WT1 CEpi samples. The results of the analysis are presented as a barchart **(A)** where the colour of the bar represents the padj value of the term, and the length of the bar represents the number of genes associated with that GO term; and as a category netplot **(B)** showing the relationship between genes and associated overrepresented biological process GO terms. The size of the GO term represents the number of genes associated with that term. The colour of the gene indicates its log2 fold change in the TGFBI KO group relative to WT1.

DEGs involved in the ECM that were highlighted by the GO over-representation analyses were plotted to enable the observation of batch-corrected normalised gene count values for the *TGFBI* KO line and its isogenic control (Figure 5.16).

The two collagen coding genes reaching the lowest padj value were *COL3A1* (LFC -0.644, padj 0.002), encoding a fibrillar collagen expressed in connective tissues such as the vascular system and *COL22A1* (LFC 1.453, padj 1.91E-10) a TGFβ-inducable collegen that is concentrated at tissue junctions in the muscle, tendons, heart, articular cartilage and skin (M. Koch et al., 2004; T. Watanabe et al., 2019).

Another significantly downregulated ECM gene was *MATN2* (LFC -0.685, padj 0.032) (Figure 5.16), encoding Matrilin-2, an ECM protein involved in muscle formation that is also expressed in the cornea (Korpos et al., 2015; Szalai et al., 2012). Furthermore, two genes coding for S100A calcium-binding proteins were dysregulated in the *TGFBI* KO samples (Figure 5.16). *S100A4* was singifcantly upregulated (LFC 0.833, padj 0.014). Interestingly, the S100A4 protein interacts with actin and is one of the highest expressed proteins in the corneal epithelium (Boye & Mælandsmo, 2010; Dyrlund et al., 2012; Y. Watanabe et al., 1993). *S100A6* was signifcantly downregulated in the *TGFBI* KO samples (LFC -0.966, padj 9.79E-06). The S100A6 protein also interacts with actin and is expresssed throughout the cornea (Y. Chen et al., 2013; Jurewicz et al., 2020; J. Li et al., 2011).

A subset of DEGs known to be markers of heart and muscle tissue, some also within the category of ECM genes, were also plotted (Figure 5.17). Three different genes coding for actin protein isoforms were signifcantly downregulated in the *TGFBI* KO samples, namely, *ACTA2*, encoding alpha-smooth muscle actin (α-SMA) (LFC -0.947, padj 1.03E-06), *ACTC1*, encoding alpha-cardiac muscle actin (LFC -0.696, padj 0.001) and *ACTG2*, encoding gamma-enteric smooth muscle actin (LFC -1.387, padj 2.52E-05). These three genes are expressed by different tissues, although they all share a common function in the regulation of muscle contraction.

Genes involved in ECM elastic fibril formation of elastic tissues such as heart and muscle tissue were significantly downregulated in the *TGFBI* KO samples (Figure 5.17), specifically, *ELN*, encoding the elastin protein (LFC -2.532, padj 8.74E-40) and *EMILIN2*¸ encoding the elastin microfibril interfacer 2 (Emilin2) (LFC -0.984, padj 5.86E-06). Indicating TGFBIp may be involved in elastic fibril formation.

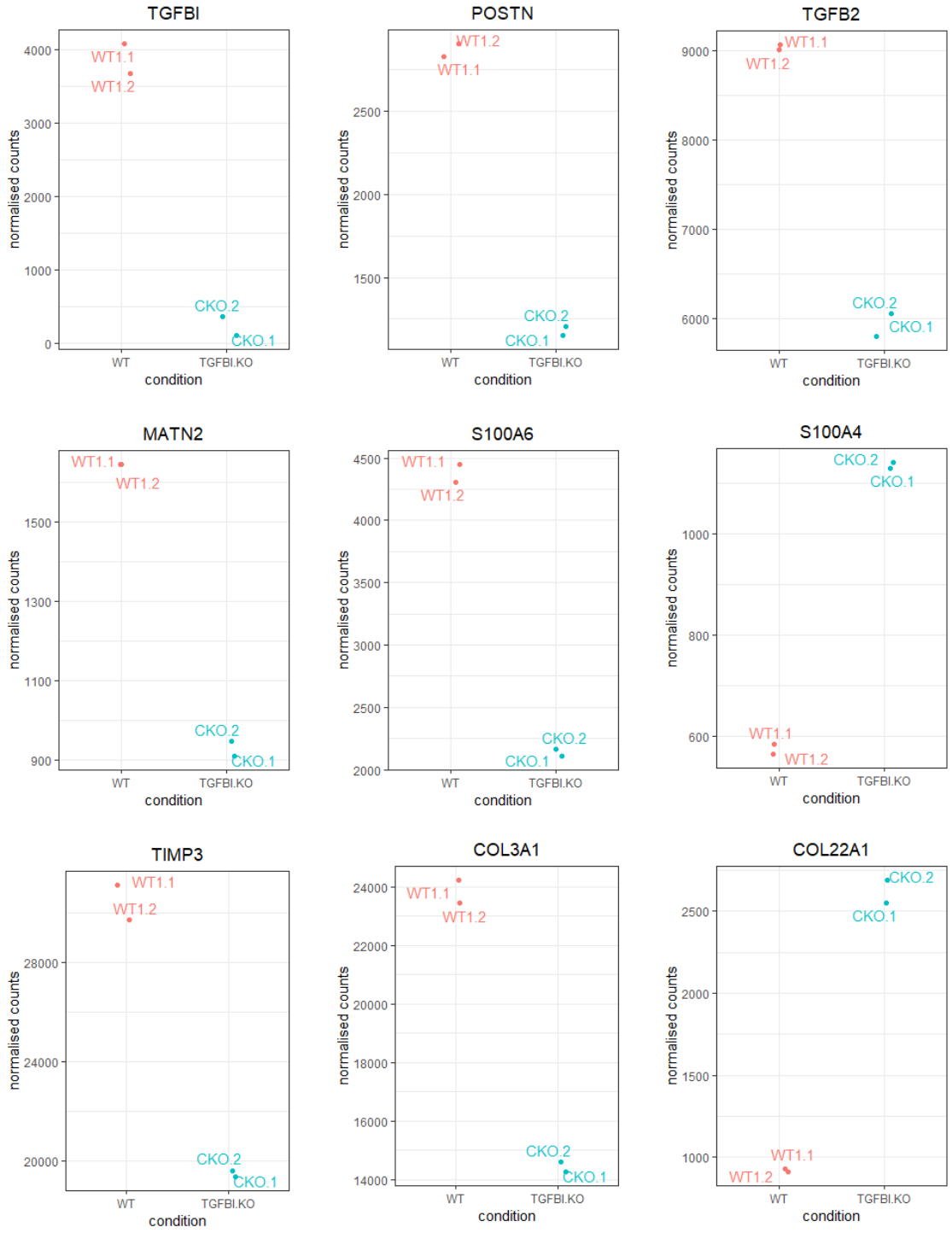

Figure 5.16 Significantly differentially expressed ECM genes between the *TGFBI* knockout and WT1 line. The normalised count values for significantly differentially expressed (padj <0.05) genes of interest are visualised by dotplot.

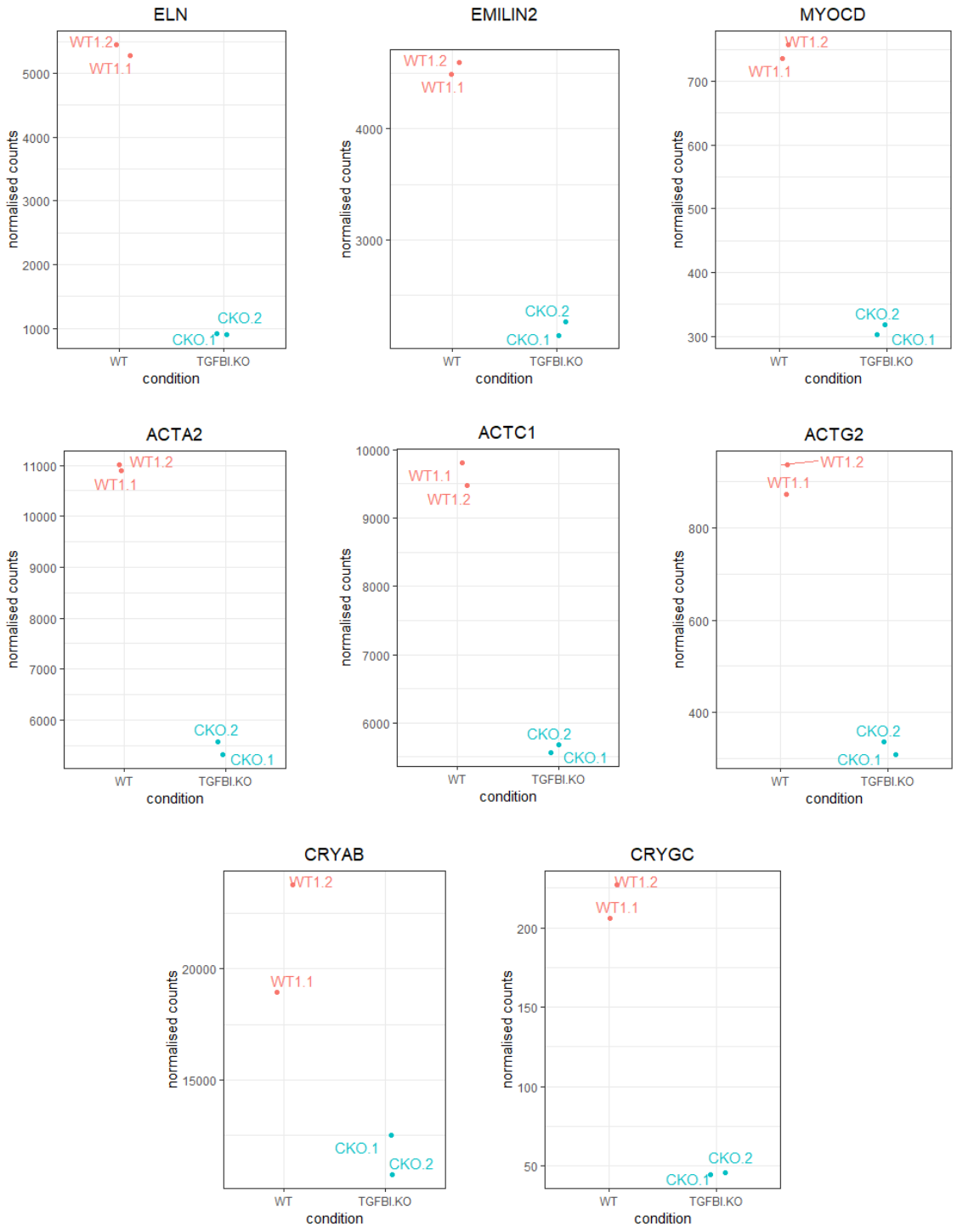

Figure 5.17 Significantly differentially expressed heart and muscle-related genes between the *TGFBI* knockout and WT1 line. The normalised count values for significantly differentially expressed (padj <0.05) genes of interest are visualised by dotplot.

5.3 Discussion

Transcriptomic analysis of TGFBI CD corneal epithelial and stromal tissue would allow for the elucidation of the pathophysiological processes underlying these conditions. This work would be invaluable to the study of TGFBI CD, however, availability of TGFBI CD tissue is extremely limited and insights would only relate to the end-stage of disease. The current CEpi model generated from patient-derived iPSC lines allows for investigations into the transcriptomic profile of patient-derived CEpi samples, circumventing the aforementioned issue of tissue availability and also allowing for investigations into disease onset and pathogenesis. Through the partial reproduction of the corneal epithelium *in vitro*, molecular biomarkers of disease can be investigated and identified, including for validation of the ASO treatment efficacy in inhibiting disease progression.

Nonetheless, iPSC-derived models of disease are known to pose issues of experimental reproducibility due to variation in the derived differentiated cells, which can confound their expression profile (Volpato et al., 2018). iPSC culture and differentiation are multistep procedures, and small variations during each step can accumulate leading to significantly different outcomes (Popp et al., 2018). The substantial impact on the resulting expression profiles of the differentiated cells can confound identification of any biological variations of interest (Ghaffari et al., 2018).

The data presented in this chapter is an example of the limitations posed by iPSC models, as variation between the two differentiations carried out to obtain biological replicates of each of the CEpi samples used for RNAseq is observed. Several groups have reported that non-genetic variation in routine cell culture such as passage number and culture media factors contribute to differentiation variability (Fossati et al., 2016; B. Y. Hu et al., 2010; Schwartzentruber et al., 2018; Volpato et al., 2018). Specifically, higher passage numbers of iPSCs affect the differentiation potential of the cells (Cantor et al., 2022). Furthermore, FBS is a common media supplement the constituents of which vary from batch to batch, accordingly its effects on the reproducibility of cell experiments are recognised (S. Liu et al., 2023; van der Valk, 2022). However, the strongest source of variation between experimental conditions is of course, genetic background (Burrows et al., 2016; Kilpinen et al., 2017; Kyttälä et al., 2016). Thus, the use of isogenic controls to control for genetic variation in cell experiments has recently surged.

Despite the limitations of the current study, differential gene expression that was not consistent between different differentiations of the current study should not be completely ruled out. As variation between sample replicates is most likely to do with reproducibility

of the differentiation process and does not rule out the possibility that aberrant expression of a certain genes is not involved in the disease process. Moving forward, various strategies to reduce variation could be implemented. One such strategy would be to purify the iPSC-derived cell types during the differentiation protocol. As previously discussed in Chapter 4 (Section 4.2.3), the differentiation protocol used resulted in a heterogeneous cell culture, therefore, FACS would be useful in purification of the target cell type. Additionally, the use of isogenic controls would certainly reduce the variability and result in more robust differences in expression, as evidenced in the *TGFBI* KO vs isogonic control analysis in this study, compared to the comparisons with different patient lines.

The variation posed by the use of iPSC models undermines the generalisation of differential expression results obtained through RNAseq analysis, and this is true of experiments using both small and large sample sizes (Cui et al., 2021). Nonetheless, the consensus is that relatively large sample sizes are preferable over smaller ones. Schurch et al. (2016) recommended that RNAseq experiments should be designed to include at least six biological replicates per condition, with an ideal experimental set up consisting of at least 12 replicates. Although some reports suggest that the minimum number of biological replicates is three or four (Conesa et al., 2016; Lamarre et al., 2018). Multiple studies have indicated that a sufficient number of biological replicates is more powerful than sequencing depth (Ching et al., 2014; Lamarre et al., 2018; Y. Liu et al., 2014). Additionally, a study found that in the case of <12 replicates per condition, DESeq2 is the best performing differential expression tool out of 11 tested (Schurch et al., 2016). Overall, DEG results should be interpreted cautiously, unless reliably validated.

5.3.1 p.R124C vs WT

The PCA comparing p.R124C vs WT day 21 CEpi samples indicated that the greatest source of variation, principal component 1, was partially accounted for by batch effects or differentiation efficacy and was not the variation of interest for this study (Figure 5.1A). Therefore, it was expected that some identified DEGs were not relevant to mutant *TGFBI* expression. Identification of the top DEGs for this comparison did not reveal many differentially expressed genes of relevance to the corneal epithelium or mutant *TGFBI* expression.

One top DEG was *NNMT*, encoding the metabolic enzyme nicotinamide N-methyltransferase (NNMT). *NNMT* is reported to be highly upregulated in naïve hESCs and knockdown experiments have identified the enzyme as a regulator of the metabolic switch in naïve-to-primed transition (Sperber et al., 2015). This indicates that the

significant downregulation of *NNMT* expression in the p.R124C samples compared to WT may be due to differentiation efficacy and is likely not relevant to CD pathogenesis. Nonetheless, *NNMT* expression has been identified as a marker of both corneal stromal cells and ABCB5+/ABCG2+ quiescent limbal stem cells, respectively, by two separate scRNAseq studies (Català et al., 2021; D. Q. Li et al., 2021).

Six out of the 10 top DEGs did not correspond to protein coding genes, rather, they coded for artificial duplication genes, pseudogenes or lncRNAs. Artificial gene duplications are errors or artifacts that arise during the process of sequencing and assembling a genome. Pseudogenes are a segment of DNA that resembles a functional gene but is not protein-coding, they are abundant in genomes and were once treated as 'junk DNA'. Recent research has shown that some pseudogenes have important functions as parent gene regulators (Tutar, 2012). Some pseudogenes are relevant to human disease as they have been found to accumulate and harbour pathogenic variations over time (Bischof et al., 2006; Sen, 2013). One pseudogene that was found to be significantly upregulated in the p.R124C samples compared to control was the ribosomal protein L29 (RPL29) pseudogene (ENSG00000230202). Ribosomal protein pseudogenes account for the largest class of pseudogenes within the human genome, and they appear to be expressed in a tissue-specific manner (Tonner et al., 2012). Although further work is required to assess the biological relevance of such expressions.

Similarly, lncRNAs were also once treated as 'junk' DNA but they are now known to play important roles in many cellular processes such functioning as enhancer RNAs or by acting as scaffolds for protein complexes (Blythe et al., 2016; L. Koch, 2017; J. Luo et al., 2021). Biological functions are known only for a small set of lncRNAs (L. Koch, 2017), thus, defining the function of lncRNAs identified as DEGs is still a challenge.

5.3.1.1 TGFb signalling pathway and integrins

The GO over-representation analysis highlighted some biological processes that appeared to be dysregulated in p.R124C samples compared to WT. One pathway that was downregulated in the p.R124C group compared to WT was the TGFβ signalling pathway, which included the downregulation of *TGFB1*, *ITGAV, SMAD1, SMAD3* and *LUM*. Interestingly, downregulation of the TGFβ signalling pathway has also been implicated in keratoconus pathogenesis by multiple reports (Chaerkady et al., 2013; Collin et al., 2021; Kabza et al., 2017).

On average, *TGFBI* transcript expression was lower in the p.R124C group compared to controls, however, this was not a consistent finding across all samples and *TGFBI* was not significantly differentially expressed in this group comparison. However, *TGFβ1*

expression, the protein product of which is known to induce TGFBIp expression (Skonier et al., 1992), was significantly downregulated in the p.R124C group in comparison to WT. TGFβ1 exerts positive and negative regulatory effects on TGFBIp expression (S. Il Choi et al., 2016), thus, lower *TGFβ1* expression does not always translate to lower *TGFBI* expression. TGFBIp is synthesised in the corneal epithelium and corneal stroma and has been suggested to play a role in corneal epithelial integrity (Hirano et al., 1996; Rawe et al., 1997). It is possible that abnormal TGFBIp proteins could impair the integrity of the corneal epithelium by altering protein/receptor interactions. TGFBIp influences cell adhesion and migration through interactions with various integrins, including the αV integrins αvβ3, and αvβ5 (Costanza et al., 2019a; H. Ge et al., 2013; J. E. Kim et al., 2000; J. E. Kim, Park, et al., 2002; M. Liu et al., 2021). The *ITGAV* gene encodes the αV integrin subunit of the heterodimeric αVβ integrin receptors.

A previous study demonstrated the colocalization of TGFBIp and ITGAV in glioma stem cells and verified the interaction between TGFBIp and ITGAV by co-immunoprecipitation, concluding that TGFBIp is a ligand of integrin αvβ5 which is formed by the ITGAV and ITGB5 integrin subunits (Peng et al., 2022). Another study demonstrated that TGFBIp binds to the integrin αv subunit, with a higher binding affinity to its heterodimer form αvβ5, in a pancreatic cell line (Costanza et al., 2019b). All FAS1 domains and the RGD motif of TGFBIp have been found to interact with certain αV integrins, with all of these TGFBIp domains working cooperatively to bind to αV integrins (Son et al., 2013). Additionally, glioma stem cells expressing high levels of *TGFBI* expressed significantly higher levels of *ITGAV* in comparison to cells expressing low levels of *TGFBI*, demonstrating the positive regulation of *TGFBI* expression on *ITGAV* (Peng et al., 2022).

Various TGFBIp motifs are able to interact with different integrins in different cellular contexts, with different motifs used for integrin binding in corneal epithelial cells and corneal stromal cells (J. E. Kim et al., 2000; J. E. Kim, Park, et al., 2002). A previous study reported that p.R124C, p.R124H, p.R124L, p.R555Q and p.R555W TGFBIp mutants generated by transient transfection were able to mediate cell adhesion as efficiently as the WT form in a human immortalised corneal epithelial cell line, indicating that mutant TGFBIp does not result in impaired interactions with integrins (J. E. Kim, Park, et al., 2002). Although as mentioned, protein interactions are context specific and ultimately, this finding does not translate to the appropriate biological context as it is not reflective of the native cornea.

Although previous reports have not noted any structural consequences of the most common TGFBIp mutations, impaired interactions of mutant TGFBIp to binding partners

has previously been demonstrated. Specifically, impaired p.R124H mutant TGFBIp binding to its ECM protein paralog Periostin has previously been shown (B. Y. Kim et al., 2009).

In general, when mutations occur at the surface of a protein, they affect specific protein binding capabilities. Whereas, mutations occurring within the core of a protein domain can impair folding or secretion, resulting in altered structure and stability and thus, insoluble protein aggregates (Kannabiran & Klintworth, 2006; Runager et al., 2011). In the case of multidomain proteins, such as TGFBIp, mutations of the surface of a domain can alter protein stability if they are in contact with domain interfaces (García-Castellanos et al., 2017). Additionally, mutations can alter protein degradation pathways through targeting of specific cleavage sites, contributing to the altered proteolysis and aggregation (K. E. Han et al., 2016). Mapping of the p.R124 mutation hotspot reveals its location at a surface-located helix of the protein indicating its involvement in protein-protein interactions and domain stability (García-Castellanos et al., 2017) (Figure 5.18).

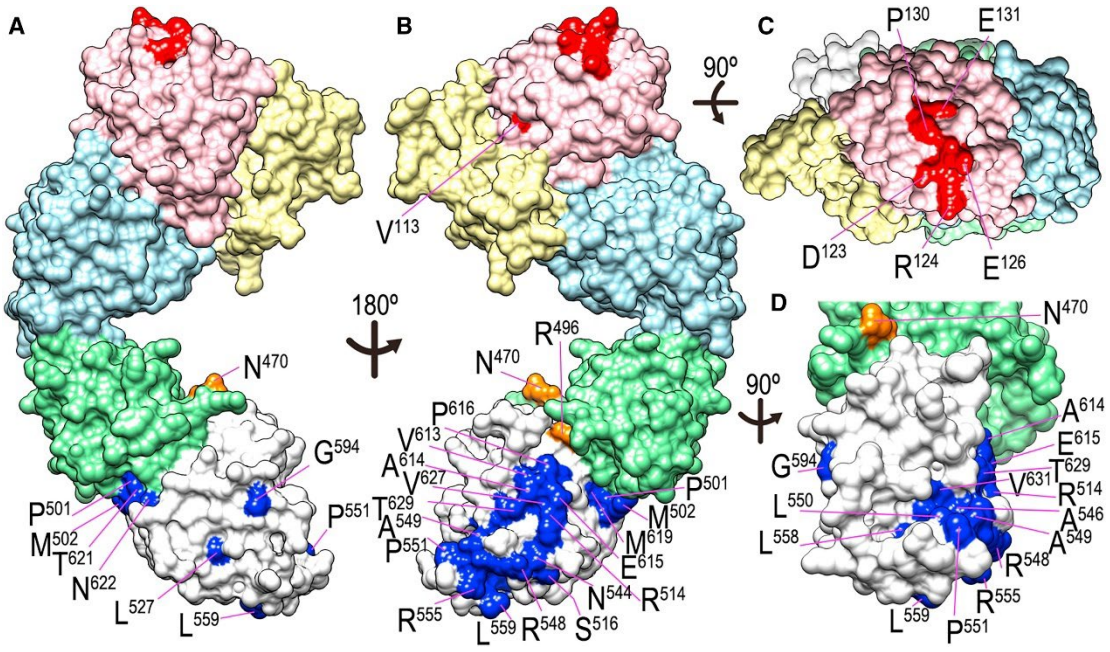

Figure 5.18 3D structure of TGFBIp showing positions of residues implicated in corneal dystrophies. A) Surface representation of TGFBIp. Pathogenic residues are mapped on to the FAS1-1 domain in red, the FAS1-3 domain in orange and the FAS1-4 domain in dark blue. **B)** Back view of A). **C)** Top view of B). **D)** Close up of B) centred on FAS1-4 and rotated vertically by 90°. (From García-Castellanos et al., 2017)

In the current study, p.R124C CEpi cells were found to express significantly less *ITGAV* transcript than WT CEpi cells, with a clear observation of decreased *ITGAV* expression across all the p.R124C samples respective to WT (Figure 5.5). *TGFBI* was not

significantly differentially expressed between the p.R124C and WT groups. Both of these observations together could potentially indicate that p.R124C mutant TGFBIp impairs the interaction between *TGFBI* and *ITGAV* products, resulting in reduced *ITGAV* expression. Whether this has an effect on the pathogenesis of p.R124C LCDI is not clear. Nonetheless, the clear link between TGFBIp and ITGAV as reported by previous studies presents the decreased expression of *ITGAV* in p.R124C samples as an intriguing finding.

Fibrillin-1 is another ECM αV integrin-binding protein, encoded by the *FBN1* gene. A subset of missense mutations within the RGD-binding domain of Fibrillin-1 are thought to result impaired αV integrin binding leading to an autosomal dominant form of scleroderma (Del Cid et al., 2019). As TGFBIp utilises multiple domains for αV integrin binding, and a correlation between *TGFBI* and *ITGAV* expression has been previously shown, it may be the case that the p.R124C mutation in TGFBIp results in impaired αV integrin binding, resulting in a decrease of *ITGAV* expression. The integrin binding domains of TGFBIp act in a tissue-specific fashion, therefore, the p.R124C mutation may impair TGFBIp binding to αV integrin subunits in CEpi cells and/or the cornea specifically.

Impaired binding of TGFBIp to αV integrins could have effects on the expression and transcriptional regulation on *ITGAV* though a feedback loop mechanism, leading to various altered molecular mechanisms. αV integrins also function to activate TGFβ cytokines by binding to their latent form (Mamuya & Duncan, 2012). In this way, impaired TGFBIp-integrin αV binding may indirectly regulate TGFβ1, resulting in the decrease of *TGFB1* expression. The specific binding motifs and partners of TGFBIp in WT and dystrophic corneas should be further investigated to understand whether it plays a role in CD pathogenesis.

5.3.1.2 Metalloproteinases and HTRA1

Metalloproteinase activity was identified as an over-represented MF GO term in the p.R124C vs WT comparison. This is a particularly interesting finding as LCDI causing mutations in TGFBIp cause aberrant proteolysis of the protein resulting in the accumulation of amyloid deposits in the cornea (see Chapter 6, Section 6.1.1.1.1). The protein constituents of p.R124C TGFBIp deposits of LCDI corneas have previously been reported, with the serine protease HtrA1 found to be specifically within amyloid deposits of the stroma and not present within TGFBIp+ granular corneal deposits (Courtney et al., 2015). The presence of HtrA1 within LCDI deposits indicates that HtrA1 either cleaves p.R124C mutant TGFBIp releasing the mutated amyloidogenic seed or, attempts to

cleave the already misfolded TGFBIp amyloid fibrils resulting in co-aggregation of the proteins.

Differential expression of *HTRA1* was not observed in the current comparison. However, a patten of differential metalloproteinase activity was observed, with 10 metalloproteinase transcripts being differentially expressed (6 downregulated, 4 upregulated) in the p.R124C group compared to control. Metalloproteinases refer to any type of protease that requires a metal ion, usually zinc, to function properly. One significantly upregulated metalloproteinase was *MMEL1,* encoding the membrane metallo-endopeptidase-like 1 protein, also known as neprilysin 2 (NEP2), which is a member of the neprilysin (NEP) family of zinc metalloproteinases. Members of the NEP family are known to have a role in amyloid-β peptide degradation (Hafez et al., 2021). Specifically, NEP2 deficient mice showed significant elevations of total amyloid-β species in the brain, demonstrating the role of NEP2 in amyloid metabolism (Hafez et al., 2021). Thus, *MMEL1* upregulation in p.R124C CEpi samples may be due to the presence of p.R124C-TGFBIp amyloid species and expression of this gene and protein should be investigated as a potential biomarker of disease.

Additionally, *PAPPA2* encoding the Pregnancy-associated plasma protein A2 (PAPP-A2), a metalloproteinase belonging to the insulin-like growth factor (IGF) signalling pathway, was found to be significantly downregulated in p.R124C samples compared to WT. PAPPA2 overexpression promotes amyloid-β peptide accumulation in Alzheimer's disease (Mihelčić et al., 2017). Thus, the concomitant increase of *MMEL1* and decrease of *PAPPA2* in the p.R124C samples may be reflective of amyloid-β proteolytic machinery.

Further work should be carried out to thoroughly investigate whether mutant TGFBIp results in altered protein interactions and signalling pathways and whether this contributes to protein aggregation in a cornea-specific context. As proteolysis is known to be involved in p.R124C LCDI pathogenesis, proteases that take p.R124C TGFBIp as a substrate in the cornea should be investigated.

5.3.2 p.R124H vs WT

For the p.R124H vs WT comparison, fewer genes were significantly differentially expressed than the p.R124C vs WT comparison. Only two CC GO ontologies were found to be significantly overexpressed through the GO overrepresentation analysis. Although this comparison was seemingly confounded by the sex differences, the two overrepresented CC GO ontologies, the extracellular matrix and the endoplasmic reticulum lumen, are relevant to the specific disease pathology. Similar to the p.R124C

vs WT comparison, a pattern of differential protease transcript expression was noticed in the p.R124H group compared to WT. Interestingly, differentially expressed genes did not overlap between the p.R124C and p.R124H group comparisons, reflecting the differential disease mechanisms underlying LCDI and GCDII, respectively.

5.3.2.1 Metalloproteinases and serine proteases

In comparison to LCDI, much more work has been done in identifying the pathological mechanisms underlying GCDII due to its prevalence in certain geographical regions. A previous report investigated the differential gene expression of stromal cells isolated from corneas of WT and p.R124H heterozygous and homozygous individuals by cDNA microarray (Choi et al., 2010). Similar to the current study, differential expression of ECM-associated genes was identified in the GCDII stromal cells compared to WT, including proteolytic enzymes such as MMPs, specifically, *MMP1* and *MMP2*. Another study found that overexpression of TGFBIp in human corneal epithelial cells resulted in an increase of MMP1 and MMP3 expression along with a decrease of the MMP inhibitor tissue inhibitor matrix metalloproteinase-1 (TIMP1) (Niu et al., 2012). These findings should be taken into account with the accumulation of full length and near-full length p.R124H TGFBIp observed in GCDII corneal deposits (Courtney et al., 2015; Korvatska et al., 2000), indicating that aberrant proteolysis of this form of TGFBIp may be partially responsible for its propensity to aggregate (discussed in detail in Chapter 6, Section 6.1.1.1).

Two MMPs were significantly upregulated in the p.R124H samples compared to WT, one of them being *MMP2*, which has previously been associated with *TGFBI* in other disease processes such as atrial fibrillation and cancer (Guan et al., 2022; Wen et al., 2011) and the other being *MMP23B*. Upon closer examination of the normalised counts for these two MMPs (Figure 5.9) differential expression of *MMP2* was variable and not completely consistent between p.R124H samples, whereas differential expression of *MMP23B* was consistent. Whether TGFBIp is a substrate of ECM proteolytic enzymes such as those in the MMP family is properly defined. Nonetheless, the research presented here and in previous publications suggests that proteases of the ECM may play a role in the pathogenesis of CD and further investigations are warranted.

In addition to differential MMP expression, the serine protease *HTRA3*, along with the serine protease inhibitors *SERPINB7* and *SERPINA1* were found to be significantly upregulated in the p.R124H samples compared to control (Figure 5.9). *HTRA3* encodes the high-temperature requirement A3 (HtrA3) protease which shares high structural similarity with HtrA1 as its closet paralog, both are broadly expressed although they are

reported to have different functions (Runyon et al., 2007; Y. Wang & Nie, 2021), however the function of HtrA3 is less well defined (Y. Wang & Nie, 2021). In mice embryos, HtrA3 and HtrA1 both carry out their function in the extracellular space and show similar expression patterns and substrate specificities, with both of these proteases exhibiting the same TGFβ signalling inhibitory effects during mouse development (Tocharus et al., 2004). Both HtrA1 and HtrA3 can degrade can degrade ECM proteins such as decorin and biglycan, indicating that they exert complimentary roles in ECM remodelling (Tocharus et al., 2004).

Both of the differentially expressed serine protease inhibitors encode members of the Serpin superfamily of proteins and family members function by irreversibly inhibiting their target protease by undergoing a large conformational change to disrupt the targets active site (Gettins, 2002; Huntington et al., 2000). Knowledge of the function of *SERPINB7* encoding Serpin B7, is limited, although it is known to be highly expressed in the skin epidermis (Wang et al., 209). *SERPINA1* encodes Alpha-1 antitrypsin, a protease inhibitor that inhibits various types of proteases and is the second most abundant circulating human serum protein (Ferrarotti et al., 2012). Another member of the Serpin superfamily, Serpin B12, has been identified as a constituent of LCDI stromal deposits (Courtney et al., 2015; Poulsen et al., 2014). Closer examination of the normalised counts for *SERPINA1* demonstrated that one sample was dramatically increasing the average expression value of the p.R124H group, whereas the upregulation of *SERPINB7* appeared to be consistent across the samples. Nonetheless, the described altered proteolytic processing of mutant TGFBIp (Chapter 6, Section 6.1.1.1) along with the previously described associations of proteases and protease inhibitors with mutant TGFBIp and the data presented in this chapter, provide support for further investigation into the relationship between both mutant and WT TGFBIp and proteolytic processes.

5.3.2.2 Extracellular matrix

In addition to differentially expressed ECM-related proteases and protease inhibitors, genes encoding ECM constituents were also dysregulated in the p.R124H vs WT comparison. Previous studies have reported the accumulation of full size and near-full size TGFBIp in GDCII corneal deposits (Courtney et al., 2015; Korvatska et al., 2000), indicating that p.R124H TGFBIp may be proteolytically resistant respective to WT. In this case, the aberrant proteolysis of p.R124H may affect its ECM binding function causing its accumulation (Chapter 6, Figure 6.1).

One particular gene of interest that was found to be upregulated in p.R124H samples is *POSTN*, encoding the secreted ECM protein and TGFBIp paralog Periostin. Periostin is

expressed in the corneal epithelium and stroma and has been found to interact with TGFBIp (B. Y. Kim et al., 2009). p.R124H mutant TGFBIp demonstrates impaired binding of Periostin in comparison to WT, p.R124C, p.R124L, p.R555W and p.R555Q TGFBIp, potentially indicating that impaired TGFBIp-Periostin interactions are involved in p.R124H-GCDII pathogenesis (B. Y. Kim et al., 2009). Furthermore, GCDII corneas immunostained with Periostin-specific antibodies demonstrated strong immunoreactivity within TGFBIp+ deposits (B. Y. Kim et al., 2009). The same study however, demonstrated that although Periostin accumulates in mutant TGFBIp corneal deposits and is more highly expressed in GCDII corneas respective to WT, no difference in *POSTN* expression at the transcript level was observed between WT and GCDII corneal tissues, indicating that the increase in protein levels in due to accumulation within extracellular deposits. Nevertheless, *POSTN* was significantly upregulated in p.R124H samples compared to WT, indicating that *POSTN* expression is dysregulated in p.R124H CEpi cells. Further work is required to fully define the role of Periostin in GCDII pathogenesis.

Another ECM constituent coding gene found to be differentially expressed was *EFEMP1*, encoding Fibulin-3, a secreted glycoprotein broadly expressed in epithelial and endothelial cells (Stone et al., 1999). A single p.R345W missense mutation in Fibulin-3 causes a rare autosomal dominant macular dystrophy, called Doyne honeycomb retinal dystrophy, characterised by the formation of drusen underneath the RPE monolayer (Stone et al., 1999). Similarl to TGFBIp and Periostin, Fibulin-3 is involved in the development of several cancers, having either a tumour suppressor or promotor role depending on the context (I. G. Kim et al., 2014; J. Li et al., 2018; Nandhu et al., 2017; H. Tian et al., 2015). The exact function of Fibulin-3 is not clear, yet studies suggest that accumulation of the protein may alter ECM homoeostasis through interactions with basement membrane proteins such as tissue inhibitor of metalloproteinase-3 (TIMP3), MMPs (Klenotic et al., 2004), various collagens (N. Kobayashi et al., 2007) and ECM regulatory proteins such as members of the TGFβ family (Hulleman et al., 2016). Interestingly, Fibulin-3 is the predominant fibulin form expressed in the mouse cornea. Fibulin-3 knockout mice do not display structural abnormalities of the retina or retinal pigment epithelium, rather, a significant reduction in corneal stroma thickness was observed, along with progressive corneal opacification and vascularisation (Daniel et al., 2020). Thus, these results indicate that *EFEMP1* expression is essential for corneal integrity. Whether TGFBIp interacts with Fibulin-3 has not been investigated, but both ECM proteins are highly expressed in the cornea. Taken along with the significant upregulation of *EFEMP1* in p.R124H samples in this study and the previously identified

impaired binding of TGFBIp to the other corneal ECM component Periostin, it is possible that aberrant *EFEMP1* expression plays a role in GCDII pathogenesis.

5.3.2.3 Other DEGs of interest

The endoplasmic reticulum lumen was the second over-represented MF GO term identified for the p.R124H vs WT comparison. One significantly upregulated gene associated with this GO term was *ERP27* encoding ERp27. ERp27 is able to selectively bind to unfolded proteins and is induced during oxidative strees and the unfolded protein response (UPR). TGFBIp is secreted into the ECM through the conventional ER/Golgi-dependent secretory pathway. Previous research has suggested that p.R124H mutant TGFBIp is linked to ER stress, with GCDII corneal stromal cells demonstrating increased susceptibility to cell death during ER stress in comparison to WT (S. il Choi et al., 2016; S. Il Choi et al., 2017).

Other genes involved in oxidative stress such as *ALDH18A1* and *SELENOM* were also upregulated the p.R124H samples compared to WT. Previous research has indicated that GCDII corneal stromal cells express higher levels of reactive oxygen species and antioxidant enzymes than WT cells, indicating that they are in an oxidative stress state (S. il Choi et al., 2009). GCDII stromal cells were also more susceptible to oxidative damage in comparison to WT cells (S. il Choi et al., 2009) (discussed in Chapter 6, Section 6.1.1.2.1). Thus, the upregulation of various genes involved in oxidative stress in the p.R124H samples relative to control supports past research on the involvement of oxidative stress in GCDII pathogenesis.

5.3.3 *TGFBI* KO vs WT

A prominent limitation of this comparison is the very small sample size. Nonetheless, the *TGFBI* KO line was generated from the WT1 line, providing an isogenic comparison. Even though the data presented for this comparison can only be considered as preliminary, the findings were intriguing and they encourage further confirmation and investigations.

5.3.3.1 Periostin

It has previously been hypothesised that knockdown of TGFBIp would lead to an increase in the expression of its paralog Periostin (Poulsen et al., 2018). Hypotheses such as these are usually investigated via knockout mouse models, however, there are key differences in the expression of TGFBIp and Periostin between human and mouse corneas. Therefore, corneal observations of TGFBIp knockout mouse models cannot simply be extrapolated to humans. One such difference is that *POSTN* mRNA is not expressed in WT mouse corneas (Poulsen et al., 2018), whereas Periostin is expressed

in the human corneal epithelium and stroma (B. Y. Kim et al., 2009). It is also clear that TGFBIp is much more predominately expressed in the human cornea relative to the mouse cornea, specifically, human corneal TGFBIp levels exceed mice by over 10-fold (Poulsen et al., 2018). Furthermore, mouse models of TGFBI CD do not accurately recapitulate the human pathological features (discussed in detail in Chapter 1, Section 1.5.3), with homozygosity of p.R124 CD-causative *TGFBI* mutations required for aggregate formation in these animal models (Kitamoto et al., 2020; Yamazoe et al., 2015).

Nonetheless, *Tgfbi* knockout mice demonstrated a non-significant (P = 0.3) upregulation of Periostin in the cornea in comparison to WT (Poulsen et al., 2018), providing preliminary evidence that Periostin does not necessarily exert a compensatory role in the absence of TGFBIp expression. It is also apparent that Periostin does not interact with the TGFBIp-binding partner collagen VI, demonstrating that despite the large degree of sequence similarity, Periostin and TGFBIp are not entirely able to substitute function (B. Y. Kim et al., 2009). Although, interactions and compensatory roles between TGFBIp and Periostin are likely tissue specific (Mosher et al., 2015; Schwanekamp et al., 2017). The data presented in this chapter, comparing the *TGFBI* knockout line to the WT CEpi line, expands on the relationship between *TGFBI* and *POSTN*, by confirming that Periostin is not likely to produce a compensatory effect in the absence of TGFBIp expression in CEpi cells, rather, the lack of *TGFBI* mRNA leads to a significant reduction of *POSTN* mRNA expression.

One possible mechanism underlying this decrease may be that the two paralogs are part of a regulatory feedback loop, where the expression of *TGFBI* regulates the expression of *POSTN.* This could manifest due to the lack of TGFBIp-Periostin binding, resulting in a negative effect on *POSTN* expression. Additionally, both TGFBIp and Periostin are regulated by TGFβ signalling (Mosher et al., 2015), therefore, knockout of *TGFBI* could disrupt this signalling pathway, producing a decrease in *POSTN* expression. This possibility is supported by the significant decrease of *TGFB2* expression for this experimental comparison.

As previously mentioned, TGFBIp-protein binding is dependent on cellular context, thus TGFBIp-Periostin binding may follow a specific pattern in corneal tissues. Whether *TGFBI* knockout in the cornea and other tissues results in decreased *POSTN* expression is likely to be tissue dependent. One report demonstrated an increase of TGFBIp expression in the heart tissue of *POSTN*-null mice, yet Periostin expression levels were not changed in the heart tissue of *TGFBI*-null mice compared to WT (Schwanekamp et

al., 2017). Other reports have investigated the knockout of *TGFBI* or *POSTN* separately, and have confirmed that TGFBIp and Periostin do carry out different functions, although systematic observations have not been reported, with reports usually focusing on a specific tissue type (Mosher et al., 2015). Additionally, observations are usually directed to one protein and not the other (Mosher et al., 2015).

The p.R124H mutation in TGFBIp is reported to impair binding of the protein to Periostin in corneal stromal cells (B. Y. Kim et al., 2009). This mutation may alter TGFBIp-Periostin binding in a cornea-specific manner, contributing to GCDII pathogenesis such that knockout of *TGFBI* may lead to a decrease of *POSTN* expression in CEpi cells specifically. Further investigations, such as comparisons of Periostin immunostaining in the *TGFBI* KO line and WT line would be informative in addressing this possibility.

5.3.3.2 Extracellular matrix

The GO over-representation analysis using both the cellular component and biological function ontology subsets highlighted the extracellular matrix as a dysregulated feature of the *TGFBI* KO CEpi samples. TGFBIp is an ECM constituent of many tissue types although there is still much to be discovered about its function. *Tgfbi* KO mouse models did not show a corneal phenotype which is likely due to biological robustness or to interspecies differences (Barbaric et al., 2007; Poulsen et al., 2018a). Investigations into the transcriptome of *TGFBI* KO iPSC-CEpi cells potentially offers a more relevant approach for the study TGFBIp function in human cells.

One dysregulated ECM constituent gene that was significantly downregulated in the *TGFBI* KO line was *MATN2*, encoding matrilin-2, which functions as an adaptor molecule connecting other ECM proteins to form filamentous networks (S. Zhang et al., 2014). One study reported that mice lacking this protein develop without any obvious abnormalities (Mátés et al., 2004). Although another study reported that *Matn2*-null mice exhibit delayed muscle regeneration and that *Matn2* is involved in integrin and focal adhesion kinase signalling pathways (Deák et al., 2014). Interestingly, a strong increase of matrilin-2 expression in the corneal epithelium of LCDI and GCDI corneas has been reported, indicating that this protein is involved in the pathogenesis of different CD phenotypes (Szalai et al., 2012). The downregulation of *MATN2* in the current study along with its implication in CD pathogenesis warrants further work to investigate the interaction between TGFBIp and matrilin-2 in the cornea.

ECM components not expected to play a prominent role in the cornea were also dysregulated, potentially also providing information on TGFBIp function in other tissues. *ELN* the gene coding for the elastin protein, was the second most significantly

dysregulated gene in the *TGFBI* KO line. *ELN* expression is enriched in connective tissue, cardiac tissue, the lungs and the skin. *ELN* was significantly downregulated along with *EMILIN2*, which encodes the elastin microfibril interfacer 2. Emilin2 interacts with elastin and fibrillin proteins to form a stable complex that promotes the assembly and organization of elastic fibres. Elastic fibres are a core component of the ECM of various tissues. Elastin is not typically expressed in the central anterior cornea, however, elastin microfibril bundles are present within the corneal limbus and the posterior central stroma, with an especially high concentration located immediately anterior to Descemet's membrane (Lewis et al., 2016; White et al., 2017). An association between TGFBIp expression and elastin fibres has previously been made. In mice, genetic ablation of *Tgfbi* resulted in morphologically abnormal lungs that lacked proper elastin expression and displayed diminished elastic recoil, indicating that *Tgfbi* expression is required for normal elastic lung properties (Ahlfeld et al., 2016). Moreover, TGFBIp is colocalised with elastin microfibrils in bovine tissues (Gibson et al., 1997). These reports along with the data presented here indicates that TGFBIp expression is important in the formation of elastic fibres, however, genes coding for the other protein components that makes up these fibres, such as fibrillin, were not found to be significantly dysregulated in this dataset. This is likely due to the small sample size included in this study, or it may indicate a specific relationship between elastin and TGFBIp that does not involve fibrillin.

The results of the BP and CC GO over-representation analysis indicated that key genes involved in muscle formation were dysregulated in the *TGFBI* KO line. One such gene was *ACTA2* which codes for α-SMA. *ACTA2* was found to be downregulated in *TGFBI* KO samples. *Tgfbi* null mice have demonstrated α-SMA mislocalisation in the lungs, demonstrating a link between TGFBIp expression and α-SMA. Furthermore, studies in zebrafish and Xenopus have indicated a role for *Tgfbi* in myofibril bundling and muscle growth (H. R. Kim & Ingham, 2009; F. Wang et al., 2013).

Upon further investigation of the dysregulated genes specific to muscle tissue, a few are related to cardiac tissue, such as, *ACTC1, MYOCD* and *CRYAB*, all of which were downregulated in the *TGFBI* KO line. Reports on the function of TGFBIp in the heart are relatively limited, although the role of Periostin in the heart has been subject to much research (Y. Choi et al., 2020; Dixon et al., 2019; Schwanekamp et al., 2017; Shimazaki et al., 2008; Snider et al., 2009; Zhao et al., 2014). Nonetheless, two studies have demonstrated that *Tgfbi* is induced upon heart injury or failure in mice (J. H. Lee et al., 2011; Schwanekamp et al., 2017). The results presented here suggest that *TGFBI* is important in the proper expression of key muscle and heart-related genes.

5.3.3.3 TGFBI signalling

As previously discussed, TGFBIp binds to various types of integrins, and in doing so, is able to activate the focal adhesion kinase (FAK) signalling pathway (Costanza et al., 2019)(Costanza et al., 2019). Focal adhesions are multiprotein structures that assemble mechanical links between the intracellular actin filament bundles and the ECM via integrin receptors (C. Wu, 2007)(C. Wu, 2007). The FAK pathway regulates actin dynamics and organisation through various mechanisms (Carragher & Frame, 2004).As three actin isoforms were significantly downregulated in the *TGFBI* KO line compared to its isogenic control, it may be the case that *TGFBI* expression regulates actin expression through the FAK pathway. Although, it is not clear how *TGFBI* expression would elicit this effect, as the FAK pathway was not highlighted by the over-representation analysis and no FAK proteins were found to be DEGs. This is perhaps due to the very small sample number for this comparison which does not facilitate the identification of small changes in differential transcript expression.

Based on past reports, it is clear that TGFBIp exerts a pleiotropic function, using different domains to interact with different proteins in different cellular contexts. Through the analysis of this dataset, it seems that *TGFBI* expression can regulate the expression of *TGFB* family members and that this ability may be a mechanism of TGFBIp function. In order to elucidate the roles of different TGFBIp isoforms in the cornea and identify the signalling pathways underlying disease, WT and TGFBI CD corneal tissue should undergo transcriptomic analysis. ScRNAseq of control and dystrophic corneas would allow for discernment of the different disease mechanisms within the two relevant tissue types, the corneal epithelium and the stroma. Furthermore, the current transcriptomic study could be greatly improved through the use of isogenic controls and increased biological replicates.

Although multiple factors indicate that *TGFBI* knockdown would not be detrimental (discussed in Chapter 6, Section 6.3.2), TGFBIp is an important protein involved in cell signalling processes. Preservation of WT *TGFBI* allele expression would be essential for an effective ASO treatment to mitigate any unintended side effects. Thus, the results presented here further reinforce the importance of allele-specific ASOs, such as the ones designed in the current study, in the effective treatment of heterozygous TGFBI CDs.

5.3.4 Chapter conclusion

This chapter highlights the confounding variable of biological variation in RNAseq experiments. Although biological variation is expected between samples, the generation of isogenic controls from *TGFBI* mutant iPSC lines would allow for a more powerful

experimental design that could help elucidate any differences between WT and mutant *TGFBI* CEpi cells. This was highlighted through the WT and *TGFBI* KO transcriptomic analysis (Section 5.2.3) which did utilise isogenic control cell lines. Overall, this chapter highlights the importance of isogenic controls and provides a basis for the optimisation of future experiments.

Despite the lack of isogenic controls, key questions on TGFBIp-protein interactions were raised. The R124 mutations are predicted to potentially affect TGFBIp binding to other proteins due to their localisation at a surface-located helix of the protein (Figure 5.18). Further, past research has demonstrated disrupted p.R124H TGFBIp-Periostin binding (Section 5.3.3.1). Taking these points into account, future experiments exploring protein binding differences of R124-mutant TGFBIp respective to WT would contribute to the understanding of TGFBI CD pathogenesis. Futhermore, the *TGFBI* KO vs WT analysis highlighted key proteins that TGFBIp may bind to and key pathways that TGFBIp may play a role in, while also highlighting the lack of knowledge on TGFBIp-protein interactions. Further replication of the *TGFBI* KO vs WT transcriptomic analysis would allow for a more robust conclusion to be made on the possible protein interactions of TGFBIp and would also provide a basis for further experiments assessing the function of TGFBIp.

Chapter 6: Antisense oligonucleotide treatment of TGFBI corneal dystrophies

6.1 Introduction

TGFBIp is an extracellular matrix protein that is widely expressed in human tissues, although its role has not yet been fully defined. Pathogenic CD causing mutations in *TGFBI* specifically affect the cornea and do not result in other systemic phenotypes (el Kochairi et al., 2006), indicating that cornea-specific factors, such as the absence of blood vessels, may contribute to abnormal TGFBIp deposition (K. E. Han et al., 2016). The pathogenesis of the different phenotypes of TGFBI CD are not yet fully characterised and currently available treatment strategies do not target the underlying genetic cause of disease and thus, do not prevent recurrence of symptoms. The development of novel therapeutics that target the genetic cause of disease can be used alongside genetic screening to prevent the onset of disease symptoms or, be administered in conjunction with the currently available treatments of CD to prevent disease recurrence.

6.1.1 TGFBI CD pathophysiology

An understanding of what is currently known on the pathogenesis of TGFBI CD is insightful for the development of potential therapeutics of the disease and potential readouts of efficacy. As certain pathogenic mutations in *TGFBI* likely lead to different mechanisms of pathology, the disease mechanisms of the two mutations of interest for this study (p.R124C and p.R124H) are considered in detail. Past research has provided some elucidation of how these different phenotypes arise, although specific mechanisms have not yet been defined and further research is required.

6.1.1.1 Proposed disease mechanisms

Differences in cornea-specific protein aggregation occur depending on the missense mutation and where/how it affects TGFBIp. Although we know that these mutations affect TGFBIp through different underlying mechanisms, no consensus on the pathogenesis of TGFBI CDs has been established.

6.1.1.1.1 Abnormal TGFBIp degradation

The disruption of protein degradation pathways plays a crucial role in the development of numerous human diseases (Fändrich et al., 2001; Hanna et al., 2019; Munishkina et al., 2004). In the WT cornea, TGFBIp undergoes proteolytic processing into a C-terminal truncated fragment (see Chapter 1, Section 1.51). The proteolysis and turnover of

TGFBIp is reportedly altered in a mutation-specific manner in the pathogenesis of TGFBI CD.

Western blot and proteomics methods have been employed to define the TGFBIp fragment composition of corneal deposits caused by various pathogenic TGFBIp mutations located in the FAS1-1 region. However, it should be noted that characterisation of the molecular composition of the aggregation is potentially confounded due to harsh extraction methods, such as high salt concentration, denaturant or proteases (Tennent, 1999). Other reports have used recombinant or synthesised TGFBIp to investigate the generation of abnormal proteolytic fragments of the mutant protein.

Takács et al. 1998 found that abnormal truncated 42-kDa and 30-kDa proteolytic TGFBIp fragments were present in deposits of LCDI corneas. Sequencing of the amino terminal region demonstrated that the 42-kDa fragment was a C-terminus truncated form of TGFBIp which was not present in WT corneas, indicating that this fragment is involved in LCDI pathogenesis. No genetic screening was carried out to identify the LCDI causative mutation in this study, thus, no association between a specific *TGFBI* mutation and the TGFBIp fragments observed could be concluded.

Korvatska et al. (2000) demonstrated that amyloid deposits of R124C and the granular deposits of R124H and R124L corneas are associated with abnormal turnover and processing of mutant TGFBIp. In R124C corneas, no significant difference between the amount of the full length 68-kDa TGFBIp in comparison to WT was found, however, an excessive accumulation of 44-kDa N-terminal TGFBIp fragments was reported, with the total concentration of TGFBIp and its fragments being 3-fold greater than a WT cornea. Based on these findings, the authors concluded that these fragments are perhaps amyloidogenic, indicating that the R124C mutation causes the FAS1-1 domain of TGFBIp to become amyloidogenic. R124H GCDII corneas displayed twice the amount of the full length 68-kDa TGFBIp in comparison to WT, and the main TGFBIp species present was a 66-kDa fragment which was not observed in WT corneas. R124L Reis-Bücklers corneas showed ~2.5-fold excess of 68-kDa TGFBIp in comparison to WT corneas. Altogether, the authors demonstrated that pathogenic mutations in the FAS1-1 domain of TGFBIp results in different abnormal proteolytic processing pathways specific to each mutation, as well as slower turnover of TGFBIp.

Another group also reported unique fragments in the cell lysates of recombinant TGFBIp expressed by transfected HEK293 cells (Y. P. Han et al., 2011, 2012). Immunoblotting using different antibodies detected 43-kDa protein fragments of p.R124C and p.L527R;

and 47-kDa protein fragments of p.L518P in cell lysates (Y. P. Han et al., 2011). These fragments were not detected in the WT or p.R124H cell lysates indicating that they may be amyloidogenic TGFBIp fragments. Using similar methods, the same authors detected 35-kDa fragments in p.R124H and p.R555W cell lysates that were not present in WT or p.R124C (Y. P. Han et al., 2012). The authors concluded that these fragments may be responsible for the formation of granular deposits in GCDI and GCDII. These studies provide additional support for the role of abnormal proteolysis of mutant TGFBIp in the pathogenesis of this group of CDs.

Despite different *TGFBI* mutations resulting in similar clinical phenotypes, the molecular basis of the clinical presentation can differ. This is the case for the different LCD-causative mutations of *TGFBI*. Although most amyloidogenic mutations in *TGFBI* are located in the fourth FAS1 domain, the p.R124C mutation, arguably the most common LCDI-causing mutation, is located in the first FAS1 domain. A 22-amino acid peptide spanning p.R124C is capable of forming amyloid fibrils *in vitro*, whereas the native peptide shows little potential to do the same (Schmitt-Bernard et al., 2000). Blocking the Cys-Cys disulfide bonding of this synthetic p.R124C peptide resulted in a 50% decrease of amyloid fibril formation, indicating that its increased propensity to form amyloid fibrils is at least partially due to disulfide bonding, which act to stabilise aggregation of the peptide (Schmitt-Bernard et al., 2002).

Furthermore, it was shown that when cell free media containing different TGFBIp variants (WT, p.R124C, p.R124H, p.R124L, p.R124S and p.R555W) was incubated with amyloid-beta (Aβ) peptides, the media containing R124 mutant TGFBIp displayed Aβ aggregate formation, whereas the WT and R555 TGFBIp variants did not (Yam et al., 2012). This finding demonstrates the amyloidogenic properties of R124 mutant TGFBIp.

Stix et al. (2005) used SDS-PAGE to investigate amyloid deposits of corneas with the late onset lattice corneal dystrophy IIIA caused by the p.F540S mutation (Stix et al., 2005). In addition to detection of the 68-kDa form of TGFBIp, several low molecular weight fragments (6.5, 6.9, 14, 17, and 21-kDa) of the protein were detected.

The data indicate that abnormal proteolysis resulting in the accumulation of low molecular weight fragments of TGFBIp is a pathogenic feature of LCD. The mixed amyloid/non-amyloid deposit phenotype of GCDII caused by the p.R124H mutation is clear, indicating this form of TGFBIp has amyloidogenic potential. The disproportionate accumulation of full-length and close to full-length p.R124H TGFBIp products previously reported are likely constituents of the observed non-amyloid amorphous aggregates. The build-up of p.R124H TGFBIp is likely to result in supersaturation of the mutant protein in

the cornea, leading to protein aggregation. Supersaturation of proteins has previously been found to be a driving force of aggregation (Ciryam et al., 2013, 2015). Overall, current knowledge suggests that the common CD causative mutations in the 1st FAS1 domain of TGFBIp either result in this domain becoming amyloidogenic or in the case of the GCD phenotypes, potentially cause TGFBIp to become proteolytically resistant, resulting in protein aggregation (Figure 6.1).

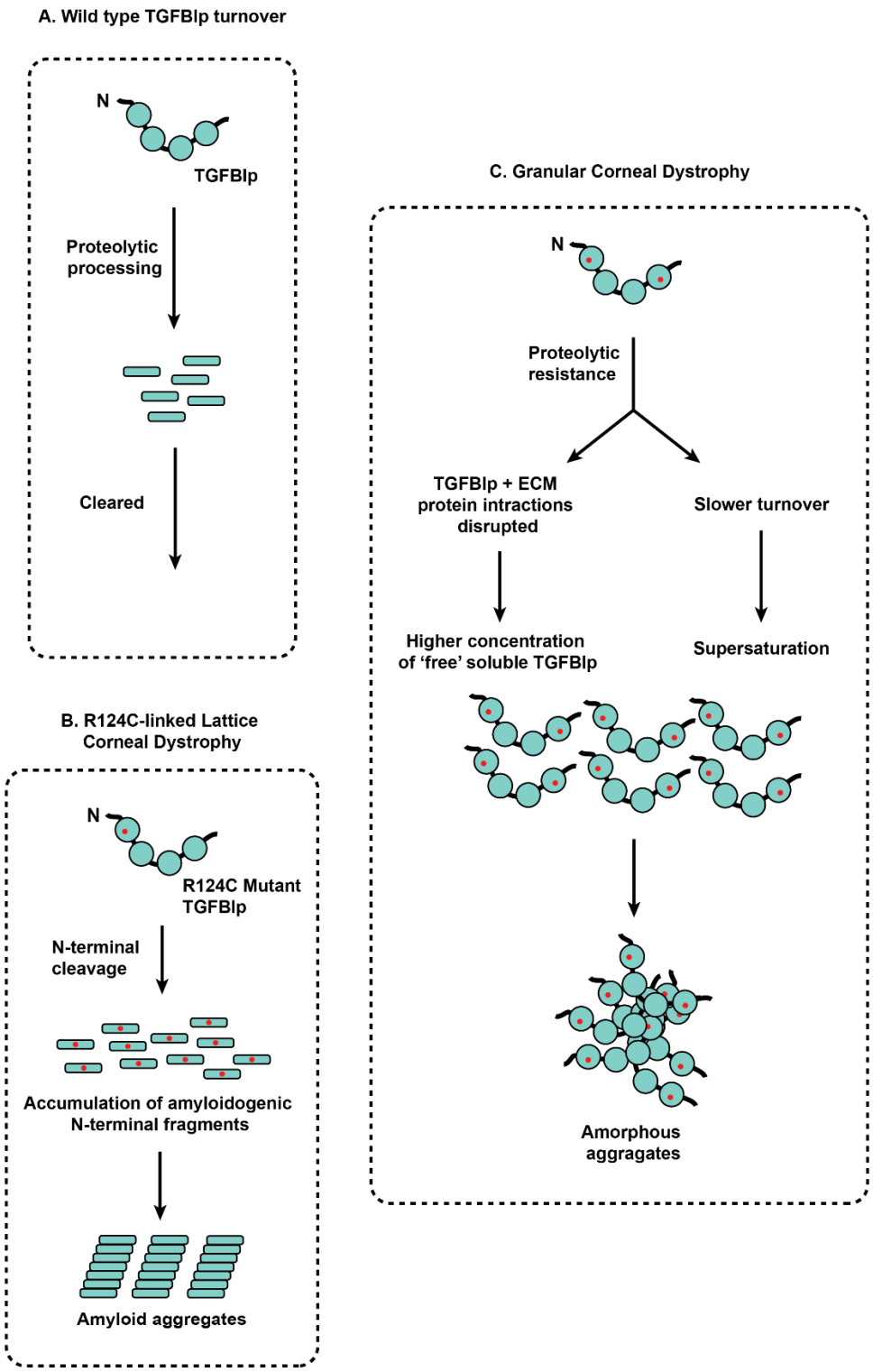

Figure 6.1 Possible aggregation pathways of TGFBI CDs. A) Wild type TGFBIp undergoes normal proteolytic processing in the cornea, leading to the successful clearance and efficient turnover of TGFBIp. **B)** Abnormal cleavage of p.R124C TGFBIp resulting in the accumulation of amyloidogenic N-terminal fragments appears to underlie LCDI pathogenesis (Korvatska et al., 2000). **C)** The accumulation of full size or near full size p.R124H or p.R555W TGFBIp in GCDII and GCDI corneas respectively, indicates the proteolytic resistance of these forms of TGFBIp (Courtney et al., 2015; Korvatska et al., 2000). This could lead to the slower turnover of TGFBIp and the disruption of TGFBIp-ECM interactions (Chapter 5, Section 5.3.2.2), leading to the development of amorphous aggregates. Pathogenic mutations are depicted in red.

6.1.1.1.2 Proteomic profile of corneal deposits

The formation of insoluble protein aggregates is a well-recognised feature of many diseases (Basso et al., 2009; Kepchia et al., 2020; J. Song, 2013). The two main protein aggregation pathways lead to either the formation of highly ordered β-amyloid sheet structures or irregular amorphous aggregates. In the case of TGFBIp, the protein has the potential to form both amyloid and/or amorphous aggregates, leading to different phenotypic outcomes. The proteomic profile of lattice and granular deposits have been characterised via isolation by laser capture microdissection and subsequent mass spectrometry analysis.

Deposits isolated from p.R124H GCDII corneas demonstrated the accumulation of intact or near intact TGFBIp, as well as serum amyloid P-component, clusterin, type III collagen, keratin 3, and histone H3-like protein (Karring et al., 2012). Type III collagen appears to play a role in wound healing (Volk et al., 2011), thus its presence within GCDII aggregates may indicate an attempt to promote healing of the damaged tissue. Intact TGFBIp aggregation was also observed in p.R555W GCDI corneal deposits suggesting it is proteolytically resistant (Courtney et al., 2015). Only three unique proteins were found within GCDI aggregates that are absent from healthy control corneas, namely hemoglobin subunit beta, actin cytoplasmic 1 and desmoplakin (Courtney et al., 2015). These findings suggest that despite the GCD mutations being in different FAS domains (R124H mutation in the FAS1-1 domain and the R555W mutation in the FAS1-4 domain), both lead to proteolytically resistant TGFBIp within aggregates (Figure 6.1).

LCDI deposits of p.R124C from both the stroma and Bowman's layer were characterised by mass spectrometry (Courtney et al., 2015). When compared to control corneal tissue, an additional 18 and 24 proteins were present in stromal and Bowman's layer deposits, respectively. The proteomic composition of the two deposit types were comparable, although some differences, such as the presence of HTRA1 in stromal but not the Bowman's layer deposits, were observed. The most abundant form of TGFBIp observed in both deposit types were semitryptic peptides of the polypeptide region L128-R172.. Interestingly, the L128-R172 polypeptide region partially overlaps with the amyloidogenic peptide reported by Schmitt-Bernard et al. (2000). Proteomics analyses have not reported this specific polypeptide region as a prominant TGFBIp species in LCDI corneas caused by FAS1-4 pathogenic mutations (Karring et al., 2012, 2013; Poulsen et al., 2014). Specifically, the C-terminal TGFBIp fragment encompassing residues Y571-R588 of the fourth FAS1 domain was found to accumulate in FAS1-4 mutated LCDI corneas

(Karring et al., 2013). In summary, the pathogenesis of LCDI appears to differ depending on whether the amyloidogenic mutation is within the 1st or 4th FAS1 domain of TGFBIp.

6.1.1.2 Mechanisms of pathology in p.R124H GCDII

In South Korea the p.R124H GCDII has been shown to be the most prevalent cause of disease (Chapter 3, Section 3.1.1) (K. E. Han et al., 2016).As corneal keratocytes have an important role in maintaining the transparency and ECM environment of the stroma, the differences between control and GCDII p.R124H homozygote corneal keratocytes have been explored.

6.1.1.2.1 GCDII corneal fibroblast morphology and mitochondrial dysfunction

Morphological differences between keratocytes extracted from WT and GCDII corneas have been observed, with the latter being larger and showing intracellular deposits (K. E. Han et al., 2016). Transmission electron microscopy revealed more elongated or fragmented swollen mitochondria in GCDII corneal keratocytes when compared to WT (S. il Choi et al., 2015; T. I. Kim, Choi, et al., 2008). Corneal keratocytes from p.R124H homozygotes were found to be adversely affected with increasing passage numbers, with disorganisation and decreased numbers of mitochondria observed in late passage, and limited survival after only 8 passages, in comparison to WT corneal keratocytes that could be passaged over 24 times. By immunostaining of markers of mitochondrial function, a rapid decrease in the mitochondrial function and mitochondrial membrane potential is observed in GCDII corneal keratocytes of increasing passage numbers, while remaining constant in WT cells (T. I. Kim et al., 2011).

The cornea is directly exposed to the atmosphere and absorbs the majority of ultraviolet (UV) light reaching the eye (Wenk et al., 2001). UV exposure generates reactive oxygen species that can lead to oxidative stress, which can cause a decline in mitochondrial function and subsequently, apoptosis. In line with the differences in mitochondrial morphology and function observed between GCDII and WT corneal keratocytes, diseased corneal keratocytes are more susceptible to oxidative damage and thus, more likely to become dysfunctional due to environmental stress (Choi et al., 2009). These findings are also consistent with the increased sensitivity to environmental stressors such as LASIK surgery which results in exacerbation of GCDII (Chapter 3, Section 3.3). These data suggest that the p.R124H mutation affects the mitochondrial structure and function of corneal keratocytes, causing a decline in corneal fibroblast cell function and viability.

6.1.1.2.2 Defective autophagy in GCDII

TGFBIp is degraded by autophagy (S.-I. et al., 2012). Mutant p.R124H TGFBIp is found to extensively co-localise with the autophagosome marker microtubule-associated protein 1 light chain 3β (LC3) and is enriched in cytosolic vesicles in primary cultured GCDII corneal keratocytes (S.-I. et al., 2012). Further investigation demonstrated that LC3 levels and the number of endogenous LC3 puncta were significantly increased in GCDII corneal keratocytes in comparison to controls. Co-localisation of the lysosomal enzyme cathepsin D and TGFBIp was also observed in GCDII corneal keratocytes (S.-I. et al., 2012). Furthermore, the accumulation of p.R124H-TGFBIp as observed by qPCR and western blotting of GCDII corneal fibroblast samples, indicates that this form of TGFBIp is insufficiently degraded in this cell type (S. il Choi et al., 2014).

When protein synthesis was inhibited, TGFBIp was almost absent in WT corneal keratocytes after 40 minutes, whereas TGFBIp remained in p.R124H cells after 60 minutes, suggesting that intracellular accumulation of TGFBIp is either due to defective degradation or delayed secretion (S. il Choi et al., 2014). These data suggest that autophagy is induced in GCDII corneal keratocytes but is not sufficient to clear mutant TGFBIp, resulting in the pathological accumulation within autophagosomes (S. il Choi et al., 2014). The autophagy system functions to degrade both proteins and intracellular organelles such as mitochondria, and in particular, damaged mitochondria (Kiššová et al., 2004; Takeshige et al., 1992). Autophagy has been shown to become defective under oxidative stress, which could lead to mitochondrial accumulation (Luo et al., 2013). Thus, the GCDII corneal fibroblast dysfunction of both mitochondria and autophagy are potentially either indirectly or directly related.

6.1.1.3 Corneal specificity and location of deposits

CD mutations in *TGFBI* specifically affect the cornea, with no symptoms presenting in other tissues (el Kochairi et al., 2006). This is perhaps due to the particularly high concentration of TGFBIp in the cornea (Dyrlund et al., 2012) in combination with other cornea-specific factors.

TGFBIp undergoes differential proteolytic processing in different tissues, as evidenced by immunoblotting of TGFBIp derived from the cornea, skin, plasma and platelets (Nielsen et al., 2020). Interestingly, cultured corneal keratocytes harbouring the p.R124C mutation do not spontaneously produce amyloid, likely due to the lack of their native microenvironment (Korvatska et al., 2000).

Non-protein macromolecules called glycosaminoglycans (GAGs) have been observed to have an effect on protein fibrillation, including heparin. Heparin is a highly sulfated GAG that can induce fibrillation of several proteins, including amyloid β, p25α and gelsolin (Ariga et al., 2010; S. B. Nielsen et al., 2012; Suk et al., 2006). Heparin sulfate has been found in amyloid β plaques and is thought to have a role in the pathogenesis of protein aggregation (Ancsin, 2003; Snow et al., 1988). Heparin has been observed to promote fibrillation of destabilised LCD mutants, whereas it does not seem to affect the aggregation propensity of WT or GCD-mutant TGFBIp (Andreasen et al., 2012; Stenvang et al., 2018). The speed of oligomerisation and fibrillation of destabilised TGFBIp increases with the extent of GAG sulfation (Malmos et al., 2017). Interestingly, the proportion sulfated heparin increases dramatically with age in the cornea (Pacella et al., 2015). Along with the age-correlated increase in concentration of TGFBIp in the cornea, the increase of sulfated GAGs could drive aggregation in LCD, and these factors together may contribute to the cornea-specific amyloidosis in LCD.

Another important feature to note is that the central cornea is uniquely avascular, whereas blood vessels are present within the conjunctiva and corneal limbus. A lucid interval between the limbus and deposits is usually apparent in TGFBI CD (K. E. Han et al., 2016; J. H. Lee et al., 2006). Furthermore, deposits do not appear following injury to the perilimbal region, such as cataract incisions, however, injury to the central cornea usually leads to dense exacerbation of deposits (Feizi et al., 2007; T. I. Kim, Choi, et al., 2008; J. H. Lee et al., 2006; Roh, Chung, et al., 2006; Xiu et al., 2002). These observations suggest that blood vessels play a role in preventing the formation or accumulation of deposits.

During normal corneal homeostasis, the majority of TGFBIp is produced by the corneal epithelium (Chapter 4, Section 4.1.1; Section 4.2.1). However, stromal keratocytes are also capable of producing TGFBIp, as evidenced by the presence of TGFBIp surrounding both the epithelial and stromal cells during wound healing (Takács et al., 1999). It is clear that both the epithelium and stroma contribute to opacification of the cornea in the development of TGFBI CD. However, post-transplantation evaluation of patient corneas demonstrates the particularly predominant role of the epithelium in disease recurrence and progression, likely due to its rapid turnover and high TGFBIp expression levels.

In LCDI, diffuse opacities present within the epithelium and subepithelium, whereas lattice lines run throughout the stroma. Shortly following PK, the donor epithelium is replaced by the host epithelium which continues to produce abnormal TGFBIp protein, whereas donor stromal keratocytes persist long enough to prevent abnormal TGFBIp

build up in the stroma. This has been observed following PK of LCDI patients, as diffuse superficial opacities develop in the epithelium and subepithelium but not in the stroma (Lisch & Seitz, 2014; Snead & Mathews, 2002). Thus, the lack of stromal lattice lines following PK provides an indirect indication that stromal keratocytes are responsible for the presentation of this symptom.

In the case of GCD, the recurrence of corneal deposition is more prominent near the epithelial layer following PK, thus indicating that the epithelium is responsible for the build-up of abnormal TGFBIp (Frising et al., 2006; Johnson et al., 1981; Lyons et al., 1994).

In summary, the unique combination of cornea-specific factors, such as high expression levels of TGFBIp, TGFBIp processing, the lack of blood vessels, high turnover of the corneal epithelium and the presence of macromolecules such as GAGs, contribute to the cornea-specific phenotype of TGFBI CDs.

6.1.2 Currently available TGFBI CD treatments

Currently available treatments for TGFBI CD are reliant on the physical removal of corneal deposits by either laser ablation or corneal transplantation. PTK allows for the laser ablation of shallow corneal deposits. For deposits located deeper into the epithelium or stroma, either PK or deep anterior lamellar keratoplasty (DALK) can be administered depending on diagnosis and severity, with the latter being a less difficult process. However, injury to the cornea can exacerbate protein deposition (Banning et al., 2006; Kwak et al., 2021; W. B. Lee et al., 2007), as demonstrated by the patient images presented in Chapter 3 (Figure 3.2A-B) which show prominent protein deposition around the site of graft sutures. Additionally, secondary complications of surgery can occur such as cataracts or glaucoma due to post-operative topical corticosteroid used to improve graft survival, as was the case for patients 1 and 2 included in this study. Other complications relating to graft failure are also a risk. Furthermore, the treatments do not prevent recurrence of the symptoms, thus repeated treatments may be necessary, as was also the case for patients 1 and 2 included in this study.

Reports of recurrence rates are impacted by many factors, such as the definition of recurrence and the length of follow up. The recurrence rate following PK for LCD patient is reported to be 50-60% at 48-135 months (Ellies et al., 2002). Following DALK, the recurrence rate has been reported to be approximately 35% for LCD and 22% for GCD following 12-96 months post-operation (Ünal et al., 2013). Recurrence rates do vary greatly between individuals and different corneal dystrophies.

The corneal epithelium seems to be largely responsible for the recurrence of corneal deposits, as evidenced by the location of deposits following surgery. Due to the proliferative nature of the corneal epithelial cells causing the continuous production of mutant TGFBIp, along with the exacerbation of symptoms due to corneal wounding, alternative treatments that target the underlying genetic cause of the disease rather than the symptoms, may be a more effective therapeutic approach. However, such treatments would either be administered as a preventative therapeutic before significant opacification and sight loss, or following PTK or corneal transplantation.

6.1.3 Alternative potential treatments

As currently available treatments for TGFBI CD can lead to disease exacerbation, and do not prevent recurrence of the symptoms or target the underlying molecular mechanism of pathogenesis, alternative treatments have been proposed and investigated.

6.1.3.1 Pharmacological compounds

Based on some of the findings previously discussed (Section 6.1.1.1) on the molecular mechanisms underlying TGFBI CD, pharmacological compounds have been proposed as potential alternative treatments. However, the underlying molecular mechanisms of TGFBI CD pathogenesis are not well defined, presenting a substantial challenge for the development and validation of pharmacological compounds in the effective treatment of these conditions.

It has been reported that lithium chloride-based treatments can work to inhibit TGFBIp expression and enhance autophagic degradation of TGFBIp in both patient-derived primary corneal keratocytes with the p.R124H mutation and primary corneal keratocytes overexpressing this variant of TGFBIp (S. il Choi, Kim, et al., 2011; Nie et al., 2018). Other compounds enhancing autophagy, such as melatonin and rapamycin, have also been investigated and proposed as potential therapeutics for the treatment p.R124H GCDII (S. il Choi, Dadakhujaev, et al., 2011; S. il Choi et al., 2012, 2013).

Chemical chaperones have been investigated as a potential therapeutic mechanism for the prevention of protein misfolding and promotion of intracellular protein trafficking (Kolter & Wendeler, 2003). Trimethylamine N-oxide (TMAO), a chemical osmolyte which facilitates chaperoning, demonstrated suppression of p.R124 mutant induced Aβ aggregation *in vitro* (Yam et al., 2012).

Moreover, fragment-based drug screening has been implemented as a drug discovery method to identify chemical modulators capable of binding to mutant TGFBIp to prevent

it from being processed into smaller amyloidogenic fragments and thus delaying protein aggregation (Venkatraman, Duong-Thi, et al., 2020).

6.1.3.2 Genome editing

CRISPR/Cas9 (clustered regularly interspaced short palindromic repeats/CRISPR associated protein 9) technology has shown promise in gene editing applications. Cas9 is a nuclease directed by small guide RNAs (gRNAs) through Watson-Crick base pairing to target DNA (Ran et al., 2013). Cas9 induces targeted DNA double-strand breaks (DSBs) at target genomic loci (Ran et al., 2013). Following Cas9 cleavage the target locus undergoes DNA damage repair by one of two different pathways: non-homologous end joining (NHEJ) or homology-directed repair (HDR). NHEJ re-attaches the broken ends through an error prone system that is inclined to introduce small deletions and/or insertions at the DNA break site known as indels, usually generating a premature stop codon and a frameshift. HDR is a process of homologous recombination, where a DNA template is used to give the necessary homology needed to precisely repair the DSB. HDR can be utilised alongside large quantities of a synthetic donor DNA template to generate a precise genetic modification.

TGFBI CDs have an autosomal dominant mode of inheritance and the desired outcome of any genetic therapy applied to these disorders would be to supress the expression of mutated allele, leaving the WT allele functioning as normal. Courtney et al, (2016) demonstrated that CRISPR/Cas9 can be used for allele-specific gene editing by utilising a single nucleotide polymorphism-derived protospacer adjacent motif (PAM) in the *Krt12* gene. In a mouse model of Meesmann's epithelial corneal dystrophy (MECD), caused by a heterozygous SNP in *Krt12* which results in a novel PAM, it was observed that the CRISPR/Cas9 and short-guide RNA expression plasmid construct injected into the corneal stroma resulted in NHEJ repair and consequently, allele-specific frame-shifting deletions (Courtney et al., 2016). This data indicates that the CRISPR/Cas9 targeting of SNPs that generate a novel PAM site is feasible.

CRISPR/Cas9 technology has also been explored as a potential therapy in the treatment of TGFBI CD. The successful CRISPR/Cas9 knockout of *TGFBI* has been reported in LSCs extracted from healthy human corneas, providing a basis for the autologous corneal transplantation of *TGFBI*-negative LSCs (E. K. Kim et al., 2019). Taketani et al. (2017) demonstrated the successful correction of the GDCII-causative c.371G>A (p.R124H) mutation in primary corneal keratocytes obtained from a GDCII patient by the *in vitro* delivery of a CRISPR plasmid expressing Cas9/guide RNA and a single-stranded oligodeoxynucleotide HDR donor template. Christie et al. (2017) identified the issues

with mutation-dependent CRISPR-Cas9 gene editing of *TGFBI* using an *in vitro* model, outlining that the gRNA designed to target the p.R124C mutation was allele-specific, although it cut with a low efficiency of 26%. The gRNAs designed to target the p.R124H, p.R124L, p.R555Q and p.R555W mutations worked at a higher efficiency, but also targeted the WT allele (Christie et al., 2017). The authors concluded that a mutant allele-specific CRISPR/Cas9 treatment strategy is not suitable in the targeting of autosomal dominant *TGFBI* mutations, as a near perfect off-target site exists in the form of the WT allele. This strategy would work if the missense mutation generated a PAM, however, the five most common mutations that account for the majority of associated CDs (p.R124C, p.R124H, p.R124L, p.R555Q and p.R555W) do not generate a PAM, with less than a third of TGFBI CD-causative mutations generating a novel PAM site (Christie et al., 2017). Thus, the same group developed an alternative mutation-independent approach for the allele-specific CRISPR/Cas9 targeting of *TGFBI*, by utilising SNPs that naturally occur in the mutant allele, regardless of where the pathogenic mutations are found. The applications of CRISPR-based treatment continue to evolve and are explored as a potential treatment option for TGFBI CDs (N. S. Nielsen et al., 2020).

6.1.3.3 Oligonucleotide therapeutics

Oligonucleotide therapeutics comprise short interfering RNAs (siRNAs) or antisense oligonucleotides (ASOs) which exert their effects at the post-transcriptional level. These therapeutics can act through various mechanisms and targets depending on their structure and chemistry.

6.1.3.3.1 Short interfering RNAs

siRNAs act by silencing gene expression via the RNA interference pathway that was discovered in 1993 (R. C. Lee et al., 1993). siRNA molecules are double stranded RNA sequences of 20-24 base pairs that are made up of a passenger strand (sense) and a guide strand (antisense). The guide strand, which is complimentary to the target RNA, becomes incorporated into a ribonucleoprotein called the RNA-induced silencing complex (RISC), where it interacts with the Argonaute protein which unwinds the siRNA. The guide strand of the siRNA is preserved by the Argonaute protein and the passenger strand undergoes degradation. The activated RISC recognises the complementary mRNA of the target sequence and induces mRNA degradation (review: Alshaer et al., 2021).

Previous research has identified a lead siRNA from a panel of 19 for the reduction of p.R124C *TGFBI* at the mRNA and protein level (Courtney et al., 2014), demonstrating proof-of-concept for *TGFBI* oligonucleotide-based knockdown.

6.1.3.4 Antisense oligonucleotides

ASOs are short, synthetic, single-stranded nucleotide polymers usually around 14-25 bases in length. They are able to bind to complementary mRNA and pre-mRNA sequences through Watson-Crick base pairing, potentially leading to the manipulation of gene expression through three main molecular pathways (Figure 6.2). The effect of the ASO is reliant on its chemical make-up and its target sequence (see Section 6.1.3.4.1: Chemical Modifications of ASOs). The RNase H mediated pathway occurs through binding of the ASO to the target RNA, forming an RNA:DNA heteroduplex. This induces cleavage of the target sequence by RNase H and prevents the translation of the mRNA into a protein. ASOs can also function through translational arrest, whereby ASOs targeting a start codon can interfere with ribosomal binding of mRNA, resulting in steric blocking of ribosomal machinery and prevention of protein synthesis. ASOs are also able to influence splicing events and these are termed ‘splice switching oligonucleotides’ (SSOs). SSOs complementary to target pre-mRNA could bind to exonic splicing silencers or intronic splicing silencers, consequently blocking splicing and resulting in exon inclusion. SSOs can also promote exon exclusion by binding to splice site sequences or splicing enhancer elements.

In contrast to DNA, mRNA is not protected by repair machinery, therefore, modulation of mutant mRNA translation is seemingly less difficult than modulation of transcription or alteration of the gene. One of the main obstacles to ASO therapy is effective delivery to the target tissue, particularly in neurological disorders as ASOs do not readily cross the blood brain barrier.

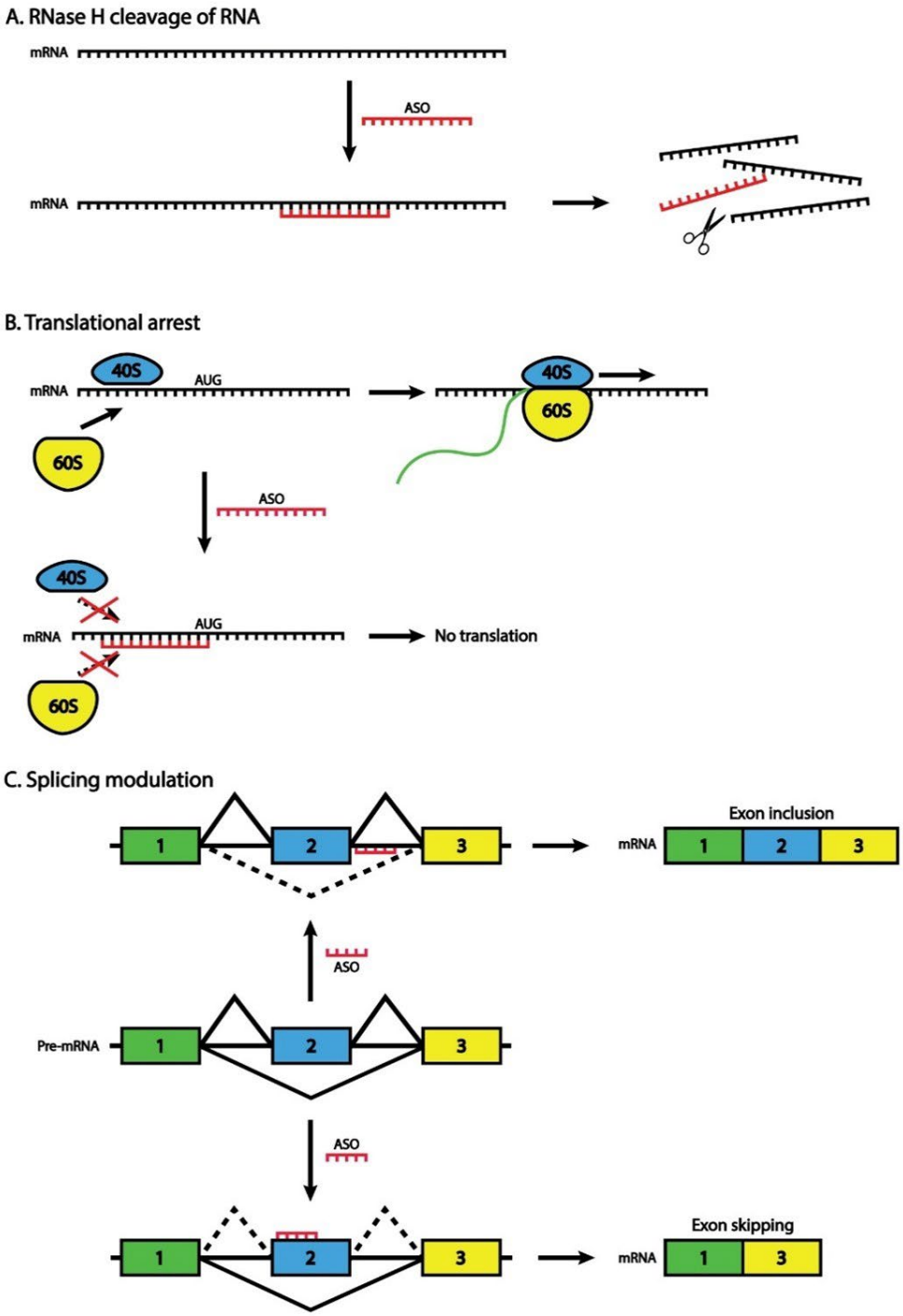

Figure 6.2 Different mechanisms of antisense oligonucleotide action.
A) RNase H mediated pathway: an RNA:DNA heteroduplex is formed upon binding of the ASO to target RNA, resulting in RNase H mediated RNA cleavage, preventing mRNA translation into a protein.
B) Translational arrest: ASOs targeting the AUG start codon could interfere with ribosomal binding of mRNA, resulting in steric blocking of ribosomal machinery and prevention of protein synthesis.
C) Splicing modulation: ASOs designed to influence splicing events are termed 'splice switching oligonucleotides' (SSOs). SSOs complementary to target pre-mRNA could bind to exonic splicing silencers or intronic splicing silencers, consequently, blocking splicing and resulting in exon inclusion. SSOs can also promote exon exclusion by binding to splice site sequences or splicing enhancer elements. Solid lines depict possible splicing events, whereas dotted lines depict splicing events that are not possible.

6.1.3.4.1 Chemical Modifications of ASOs

Initially, *in vivo* applications of ASOs displayed limited clinical potential due to the susceptibility of ASOs with unmodified backbones to be degraded by endonucleases and exonucleases (Eder et al., 1991). Since then, ASO technology has evolved through the application of various chemical modifications which alter the mechanism of action of the ASO, modifying its pharmacological effect (Figure 6.3). The majority of ASO modifications work by improving resistance to nucleases, increasing their half-life, or by enhancing the binding affinity of the target RNA. These modifications are mainly applied to the backbone and sugar moieties of the ASOs.

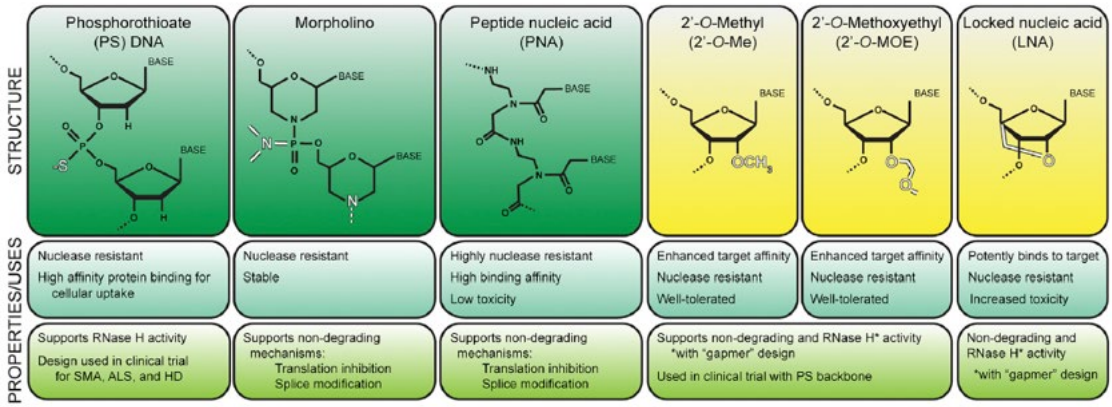

Figure 6.3 Antisense oligonucleotide chemical modifications, attributes and functions (Schoch & Miller, 2017). Chemical modifications to ASOs can alter their affect by improving resistance to nucleases or by enhancing their binding affinity. Phosphorothioate (PS) DNA, morpholino modifications and peptide nucleic acid (PNA) modifications enforce improved nuclease resistance for more potent ASO activity. PS modified ASOs have been utilised in preclinical and human clinical trials for diseases such as spinal muscular atrophy (SMA), amyotrophic lateral sclerosis (ALS) and Huntington's disease (HD). Ribose substitutions such as, 2′-O-methyl (2′-OMe), 2′-O-methoxyethyl (2′-MOE), and locked nucleic acids (LNAs), are used to increase ASO stability and enhance RNA target binding and increase resistance to nuclease degradation. 2' modifications support alternative mechanisms of action to nuclease degradation, such as splice site modification and translational arrest. However, ASOs designed using a gapmer strategy incorporate a middle RNase H activating domain and flanking 2' modifications which increases target affinity and confers additional nuclease resistance.

Unmodified DNA and RNA sequences are comprised of deoxyribose and ribose rings, respectively, that are linked to a base, adenine, guanine, cytosine or thymine/uracil, on the first carbon of the ribose ring, and to a phosphate group, which links it to the ribose ring of the sequential nucleotide. In order to enhance the effects of unmodified DNA sequences in the regulation of gene expression, 'first generation' ASO modifications were developed. These modifications conferred alterations of ASO backbone chemistry, which denotes alterations of the phosphate link between two nucleotides of the sequence.

One such first generation modification, likely the most commonly utilised ASO modification, is the **phosphorothioate (PS)** backbone where one of the non-bridging oxygen atoms is replaced with a sulfur that greatly improves resistance of the ASO to nucleases. This modification increases the half-life of ASOs in serum while activating the RNase H degradation pathway and downregulating the target RNA (T. A. Watanabe et al., 2006). Upon binding to complimentary RNA, ASOs with a PS backbone are capable of recruiting the RNase H enzyme to trigger cleavage and subsequent degradation of the bound RNA (Cerritelli & Crouch, 2009). PS-modified ASOs are also able to bind to proteins, such as plasma proteins, that facilitate their systemic distribution (Geary, 2009). Of the ASOs with solely first-generation modifications that reached clinical trial, only fomivirsen (Vitravene1) was approved for intraocular treatment of cytomegalovirus retinitis (Dias & Stein, 2002).

Second generation ASOs refer to those with modifications at the 2' position of the ribose sugar to increase hybridisation affinity to target RNA and protect the small molecule from nuclease degradation (Marrosu et al., 2017). **2'-O-methyl (2'-OMe)** RNA is a naturally occurring form of RNA where a methyl group is added to the 2' hydroxyl position of the ribose moiety (Dimitrova et al., 2019). Another RNA of this category is the **2'-O-methoxy-ethyl (2'-MOE)** modification. However, 2' ribose sugar modifications preclude RNase H cleavage of the target RNA, thus, many ASOs are designed as 'gapmers'.

Third generation ASOs consist a wide variety of molecules, such as locked nucleic acids (LNAs), morpholino oligomers and peptide nucleic acids (PNAs).

Morpholino oligomers have a high affinity for target RNA while being completely nuclease resistant. Morpholinos do not possess the natural phosphoribose backbone, rather they encompass a morpholine ring in place of their deoxyribose moiety, which are linked through phosphorodiamidate groups. These ASOs still undergo Watson-Crick base pairing but they do not act through degradation of their target RNA, instead through steric blocking, by binding to the target RNA and inhibiting molecules that interact with the RNA, they prevent translation and protein synthesis (Hudziak et al., 2000). Eteplirsen is a Food and Drug Administration (FDA) approved morpholino ASO that modulates splicing in order to treat Duchenne muscular dystrophy patients (Aartsma-Rus & Krieg, 2017).

Peptide nucleic acids, like morpholinos, also function via a steric block mechanism and do not possess the natural phosphoribose backbone. Instead, the backbone is replaced by a pseudopeptide polymer to which the bases are linked. This modification results in

the absence of negative charges and allows hybridisation to complimentary DNA or RNA in a highly sequence specific manner (Oberemok et al., 2018).

A **locked nucleic acid (LNA)** is a modified RNA nucleotide whose ribose sugar moiety is connected by a methylene bridge from its 4'-carbon to its 2'-oxygen. This bridge locks the base into a 3'-endo conformation, increasing binding affinity to target sequences. LNAs are able to form highly stable hybridisations with both DNA and RNA (M. A. Campbell & Wengel, 2011) and are capable of activating the RNase H pathway (Wahlestedt et al., 2000). LNA oligonucleotide modifications enhance scientific techniques such as allele-specific PCR discrimination in SNP genotyping (Latorra et al., 2003) and provide increased hybridisation efficiency of fluorescence *in situ* hybridisation probes (Kubota et al., 2006). The therapeutic applications of LNA based oligonucleotides are being explored (Petersen & Wengel, 2003) for conditions such as chronic lymphocytic leukaemia (Dürig et al., 2011) and hepatitis c (Gebert et al., 2014). This ASO modification can be utilised to target disease-causing heterozygous point mutations, enhancing binding specify of the ASO to the mutated allele.

ASOs can be designed to have different combinations of chemical modifications in order to obtain an optimal molecule. **Gapmer** ASOs are designed to confer nuclease resistance while being capable of activating RNase H. Gapmer ASOs consist of a central DNA region linked by a PS backbone which activate the RNase H degradation pathway, flanked by short sequences of 2'OMe RNA nucleotides at both ends to protect the small molecule from nuclease degradation. Gapmers are designed to work by recruiting the endonuclease RNase H1 to cleave the RNA strand of the DNA:RNA hybrid formed upon binding of the ASO to its RNA target, consequently reducing expression of the target gene (H. Wu et al., 1999). The central DNA region of gapmer ASOs should be complementary to the specific mutation being targeted (Figure 6.4). For autosomal dominant diseases, such as TGFBI corneal dystrophies, the aim of ASO therapy is to induce RNase H1-mediated cleavage of only the disease-causing allele, leaving the expression of the other allele unaffected.

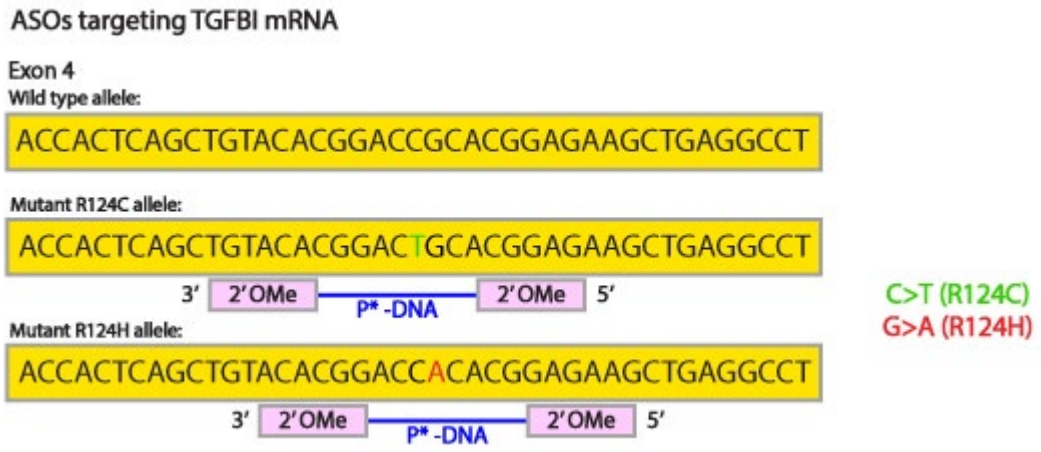

Figure 6.4 Gapmer ASOs targeting the mutant alleles of *TGFBI*. Exon 4 of TGFBI encompasses the mutational hotspot codon p.R124. The c.370C>T, p.R124C (green) and c.371G>A, p.R124H (red) are two different heterozygous missense mutations that cause phenotypically distinct epithelial corneal dystrophies. Gapmer ASOs can be designed to target the mutant allele of *TGFBI*, with a central RNase H activating DNA nucleotide sequence linked by PS bonds (P*-DNA), flanked by nuclease resistant 2'OMe RNA bases.

Numerous ASO and siRNA therapeutics have been extensively tested and FDA-approved for the treatment of various rare diseases. The first oligonucleotide-based therapeutic approved by the FDA in 1998 targets the cytomegalovirus mRNA responsible for cytomegalovirus-induced retinitis delivered by intravitreal injection (Jabs & Griffiths, 2002). In 2013, a 2'-OMe gapmer ASO called Mipomersen was FDA-approved for the targeting of the *APOB* transcript that codes for the apolipoprotein B-100 protein in the treatment of familial hypercholesterolemia (Duell & Jialal, 2016; Hovingh et al., 2013). Splice modulating ASOs have also been approved for the treatment of Duchenne muscular dystrophy (DMD) (Eteplirsen) and spinal muscular atrophy (Nusinersen). Eteplirsen is a morpholino ASO based drug approved which induces exon 51 skipping of dystrophin mRNA to restore the reading frame and recover partial function of the protein (Khorkova & Wahlestedt, 2017). Nusinersen is a 2-MOE modified ASO that corrects *SMN2* exon 7 splicing by blocking the intronic splicing silencer N1 in the treatment of spinal muscular atrophy (Chiriboga et al., 2016). Recently, numerous ASO drugs have received FDA approval for clinical administration. Two 2-MOE gapmer ASOs, Inotersen and Volanesorsen, have been approved in the treatment of nerve damage caused by hereditary transthyretin-mediated amyloidosis (Benson et al., 2018) and familial chylomicronemia syndrome (Warden & Duell, 2018), respectively. Furthermore, two additional morpholino ASOs, Golodirsen and Casimersen, have been approved for the treatment of cardiomyopathy in DMD (Q. Nguyen & Yokota, 2019).

6.1.3.4.2 Advances in experimental ASO Therapy

Research into the potential of ASOs as a genetic therapy for a wide range of hereditary disease is currently under way as experimental porof-of-concept and clinical trials.

Fuchs endothelial corneal dystrophy (FECD) can be caused by a CTG triplet repeat expansion (≥50 copies) in an intronic region of the gene *TCF4*. Transcripts containing the triplet repeat expansion accumulate as RNA foci in the corneal endothelium leading to endothelial cell death. Treatment with gapmer 2-'OMe ASOs targeting the repeat expansion has been observed to result in a significant reduction in the incidence of nuclear foci in primary corneal endothelial cells, demonstrating the therapeutic potential of ASO treatment in FECD (Zarouchlioti et al., 2018).

MALAT1 is a non-coding nuclear RNA that is highly expressed in corneal endothelial cells. 2-MOE gapmer ASOs targeting the *MALAT1* transcript have been tested in *ex vivo* human corneal endothelial cells and *in vivo* in mice and have demonstrated a successful reduction in transcript expression, providing proof of efficacy for the targeting of corneal proteins (Chau et al., 2020). This study also demonstrated that *in vivo* delivery of ASOs to the corneal tissue via intracameral and intravitreal injection is feasible and effective in gene expression regulation.

Leber congenital amaurosis (LCA) is a severe form of inherited retinal degeneration. Autosomal recessive intronic mutations in the gene *CEP290* are the most frequent cause of LCA. Gapmer ASOs have been successful in the modulation of pre-mRNA splice defects in *CEP290* patient-derived immortalized lymphoblastoid cells and 3D retinal organoids (R. W. Collin et al., 2012; Dulla et al., 2018; Parfitt et al., 2016). ASO treatment for *CEP290*-associated LCA10 has reached phase 2 clinical trial, with the preliminary results supporting an acceptable safety profile and improvements in visual acuity and light sensitivity (Russell et al., 2022).

The CAG triplet repeat expansion mutation in the *HTT* gene is responsible for the expression of the mutant huntingtin protein which leads to neurodegeneration in Huntington's disease (C. A. Ross & Tabrizi, 2011). Expression of the mutant huntingtin protein has been successfully reduced *in vitro* and in animal models by ASO treatment (Keiser et al., 2016). Results indicate that ASO treatment could substantially delay the onset of Huntington's disease symptoms in those carrying the mutation (Keiser et al., 2016). Clinical trials are currently underway investigating the use of ASOs in the treatment of Huntington's disease. Initial results demonstrate that treatment was not accompanied by any serious adverse events and a dose-dependent decrease in the mutant Huntingtin protein was observed (Tabrizi et al., 2019). The ASOs in trial are made

up of phosphodiester ribose nucleoside wings on either side of a central PS deoxyribose nucleoside sequence.

Collectively, these and other studies demonstrate that ASO therapy has great potential in the treatment of a wide range of genetic diseases.

6.1.4 Chapter aims

The aim of this chapter was to assess the therapeutic potential of ASOs in the treatment of autosomal dominant TGFBI CD. The *in vitro* model described in Chapter 4 was utilised to screen the ASOs designed as part of this study for their efficacy of reducing TGFBI expression at the transcript and protein level. These ASOs were designed with the aim of specifically reducing the expression of the mutant allele of *TGFBI* which would prevent the formation of dysfunctional TGFBIp aggregates in the cornea, preventing the development of corneal opacities and thus, visual impairment. The assessment of the molecular efficacy of the ASOs was divided into the following sub-aims:

1. Examination of *TGFBI* and TGFBIp expression in mutant and control CEpi differentiation cultures to provide a baseline understanding of TGFBI expression in these lines.
2. The design process of the ASOs, which involves selecting optimal ASO sequences and chemistries that target the mutant allele.
3. Evaluation of ASO efficacy of reducing TGFBI expression at the transcript and protein level in the differentiated CEpi cultures.
4. Investigation of the allele specificity of the ASOs.

6.2 Results

6.2.1 TGFBI/TGFBIp expression in control and mutant CEpi lines

WT, p.R124C and p.R124H iPSC lines were differentiated into CEpi cells (Chapter 4, Section 4.2). The homozygous CKO iPSC line was differentiated alongside the other lines to confirm the specificity of the TGFBIp antibody and primers used to amplify the *TGFBI* transcript.

Baseline day 30 expression levels of the *TGFBI* transcript and TGFBIp were assessed in the differentiated CEpi lines. Total RNA and protein samples from WT and mutant lines were extracted (Chapter 2, Section 2.1.1; Section 2.5) at day 30 in order to investigate possible differences in expression levels of *TGFBI*/TGFBIp across the cell lines (Figure 6.5). qPCR primers targeting exon 9 were used to assess differences in transcript expression between lines (Figure 6.5A). Lack of expression of *TGFBI* in the CKO CEpi line confirmed specificity of the primers used and demonstrated the successful KO of TGFBI.

Immunoblotting of TGFBIp expressed by CEpi cell lysates was replicated across two independent differentiations (Figure 6.5C). A double band representing the full length TGFBI protein (68/70 kDa) is observed across both the blots at different intensities for each cell line. Only the monomer forms of TGFBIp were detected in these blots, with no other higher or lower molecular weight forms observable in any sample. Absence of the double band in the CKO negative control sample confirms the specificity of the antibody. Densitometry data on the double bands for both blots was obtained using the Fiji software (imagej.net/Fiji). Although variance in band intensity is observed between the respective sample replicates, a similar level of intensity is replicated across both blots for each sample. A consistent pattern of expression level is comparable across the transcript and protein levels of TGFBI for each specific sample set.

Differences in *TGFBI*/TGFBIp expression levels are observed between cell lines. The variance in *TGFBI*/TGFBIp expression between samples does not appear to be correlated by the genotype of the sample, therefore, differences in expression appear to occur independent of the mutation. The similarity in expression levels across the transcript and protein forms of TGFBI for each differentiated cell line indicate that they are a result of differences in transcript expression level, rather than post-transcriptional modifications.

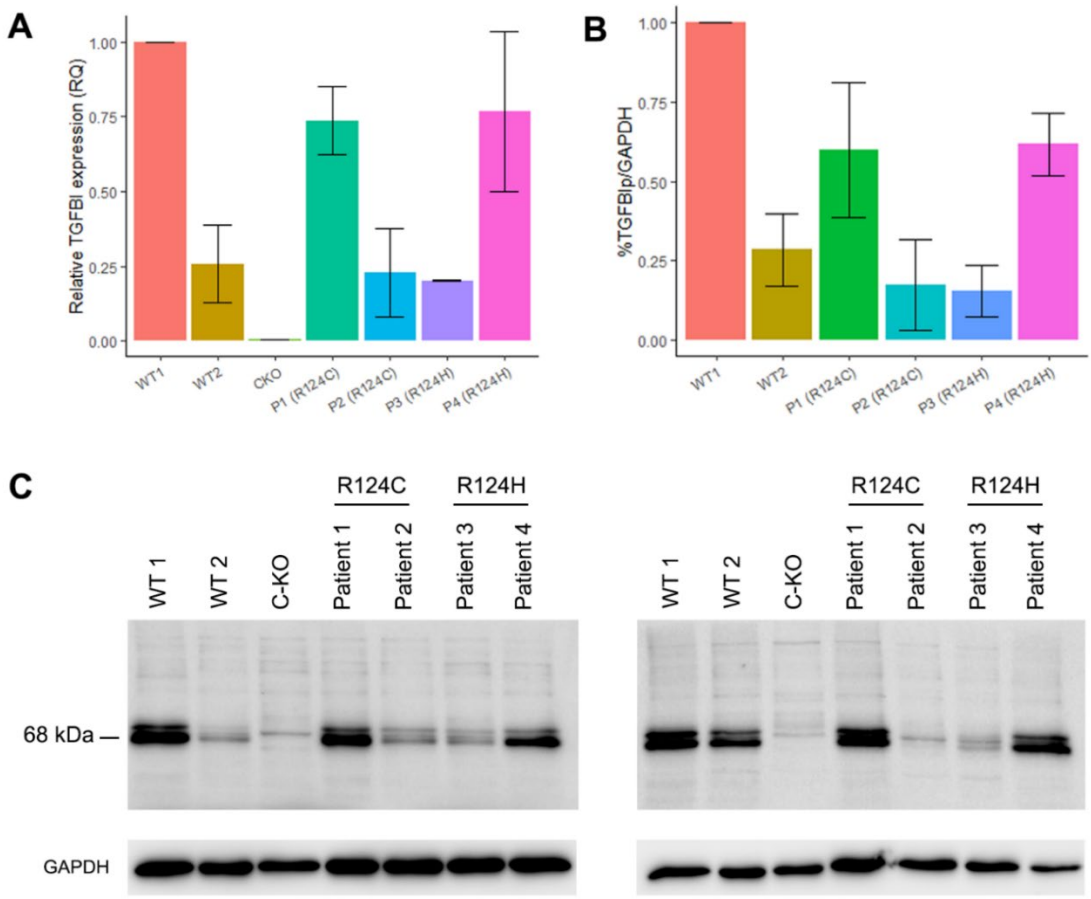

Figure 6.5 *TGFBI*/TGFBIp expression in control and mutant CEpi at day 30. Transcript (A) and protein (B, C) expression of control (WT1 and WT2), TGFBI knock-out (C-KO), p.R124C and p.R124H patient lines was assessed by qPCR and western blotting over two independent differentiations. **A)** *TGFBI* expression was normalised against *ACTIN* and *GAPDH* expression and values were calculated relative to WT1 average expression from a matched differentiation batch. Mean values ± SEM are represented in the graph. N=2 independent differentiations per cell line plotted in the graph. **B)** Quantification of monomer TGFBI (68/70 kDa) from the blots below. GAPDH expression was used for loaded protein normalisation. Percentages are expressed relative to WT1. Mean from the two immunoblots ± SEM are represented in the graph. **C)** TGFBI positive bands were detected at 68/70 kDa. WT=wild type. Patients 1 and 2 carry heterozygous p.R124C mutations. Patients 3 and 4 carry heterozygous p.R124H mutations.

6.2.2 *In silico* analysis of ASO and target transcript thermodynamic properties and secondary structure

An *in-silico* analysis was conducted to assess the thermodynamic properties and secondary structure folding conformations of the *TGFBI* pre-mRNA and coding mRNA regions. Based on the parameters described in Chapter 2, Section 2.9.3, candidate ASO sequences were selected for each mutation and then also assessed for thermodynamic stability and secondary structure formation as part of the design and validation process.

6.2.2.1 Target RNA secondary structure analysis

To assess whether the target sequence would be accessible to ASO binding, predicted *TGFBI* RNA secondary structures were generated using the mfold software and analysed, paying particular attention to the regions surrounding the mutation sites. As ASOs are able to target both transcript forms, the pre-mRNA and mRNA sequences of *TGFBI* containing the target regions were assessed. Predicted secondary structures were outputted by the software, ranked by their free energy.

An example of a pre-mRNA secondary structure is shown for the c.370C>T (p.R124C) *TGFBI* sequence (Figure 6.6). The secondary structures generated provide a visual of the predicted RNA sequence folding. Alongside the secondary structure confirmations, additional information to help guide the ASO design process is provided by the software in a range of formats (outlined in Chapter 2, Section 2.9.2).

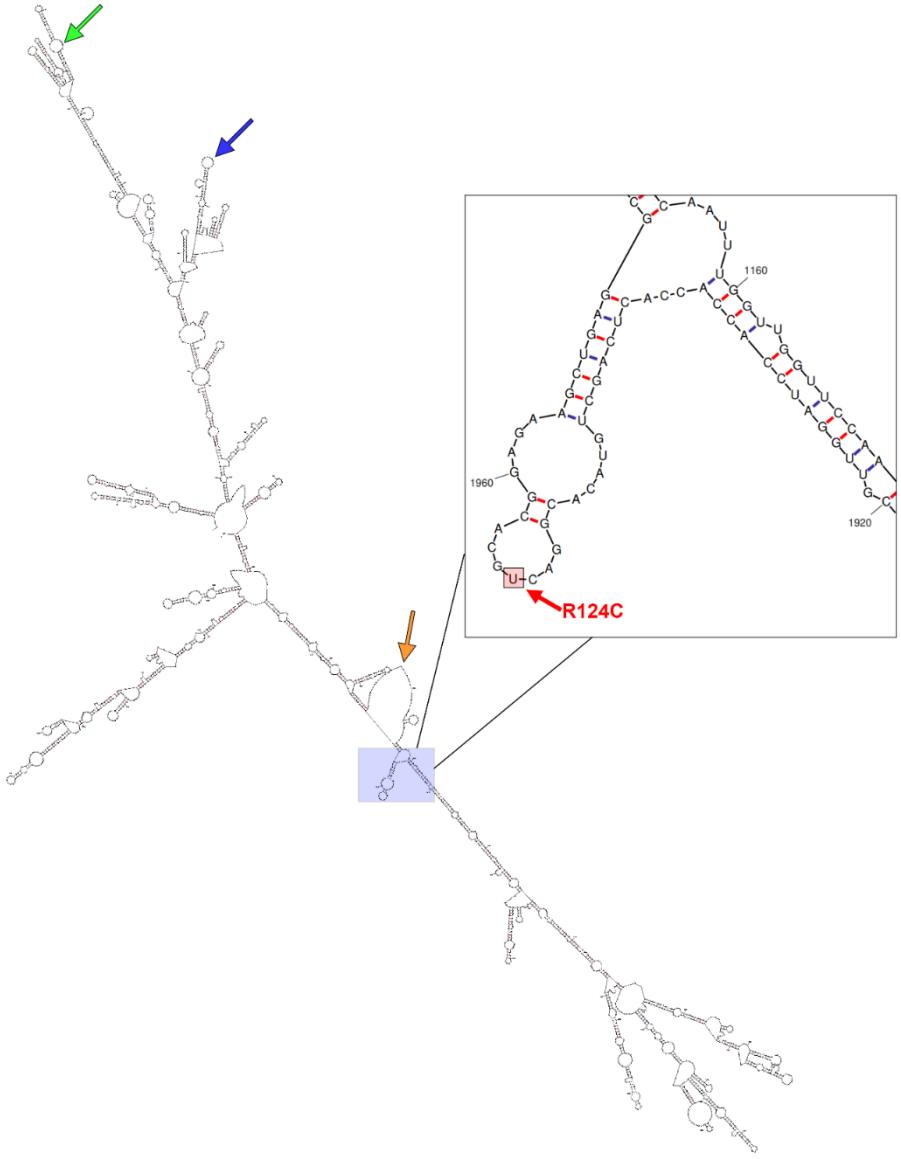

Figure 6.6 A predicted secondary structure of the *TGFBI* pre-mRNA sequence harbouring the c.370C>T (p.R124C) mutation. A fragment of the *TGFBI* pre-mRNA sequence covering the mutation site (p.R124C) and part of intron 3 to intron 4 was used as input into the mfold software which computes a series of likely secondary structures ranked by their free energy. An example of an output is shown, in which open conformations such as hairpin loops (blue arrow), internal loops (green arrow) and bulge loops (orange arrow) are observed. A close up of the region surrounding the c.370C>T (p.R124C) mutation is shown. In this particular folding conformation, the target base (U), along with bases up and downstream of the mutation are shown to be unpaired, indicating availablity for ASO binding.

As there are many potential secondary structures that could result from complementary RNA bases binding to each other, the ss-counts outputted by the mfold software are particularly useful for summarising the accessibility of target sequences as these values denote the average propensity of a target nucleotide to be unpaired (Chapter 2, Section 2.9.3). It is important to note that the software accepts a maximum of 2400 bases as an

input, and it is likely that *in vivo,* more RNA secondary structure conformations would be possible than predicted by the software. Ss-count data was gathered from the mfold analysis for pre-mRNA and mRNA of WT, c.370C>T (p.R124C) and c.371G>A (p.R124H) *TGFBI* sequences (Figure 6.7A), and demonstrates that a point mutation affects the secondary structure of the RNA, although all of the three different *TGFBI* sequences for the respective transcript form follow a similar pattern of open and closed conformations. Furthermore, between the different transcript forms (pre-mRNA and mRNA) inputted into the software, the patterns of base availability differed in some regions. GGGenome (GRCh38/hg38 (Dec, 2013)) was set to permit one mismatch (the mutant nucleotide) and returned only one perfectly matching sequence, with the genomic coordinates chr5:136046390-136046419, corresponding to *TGFBI*.

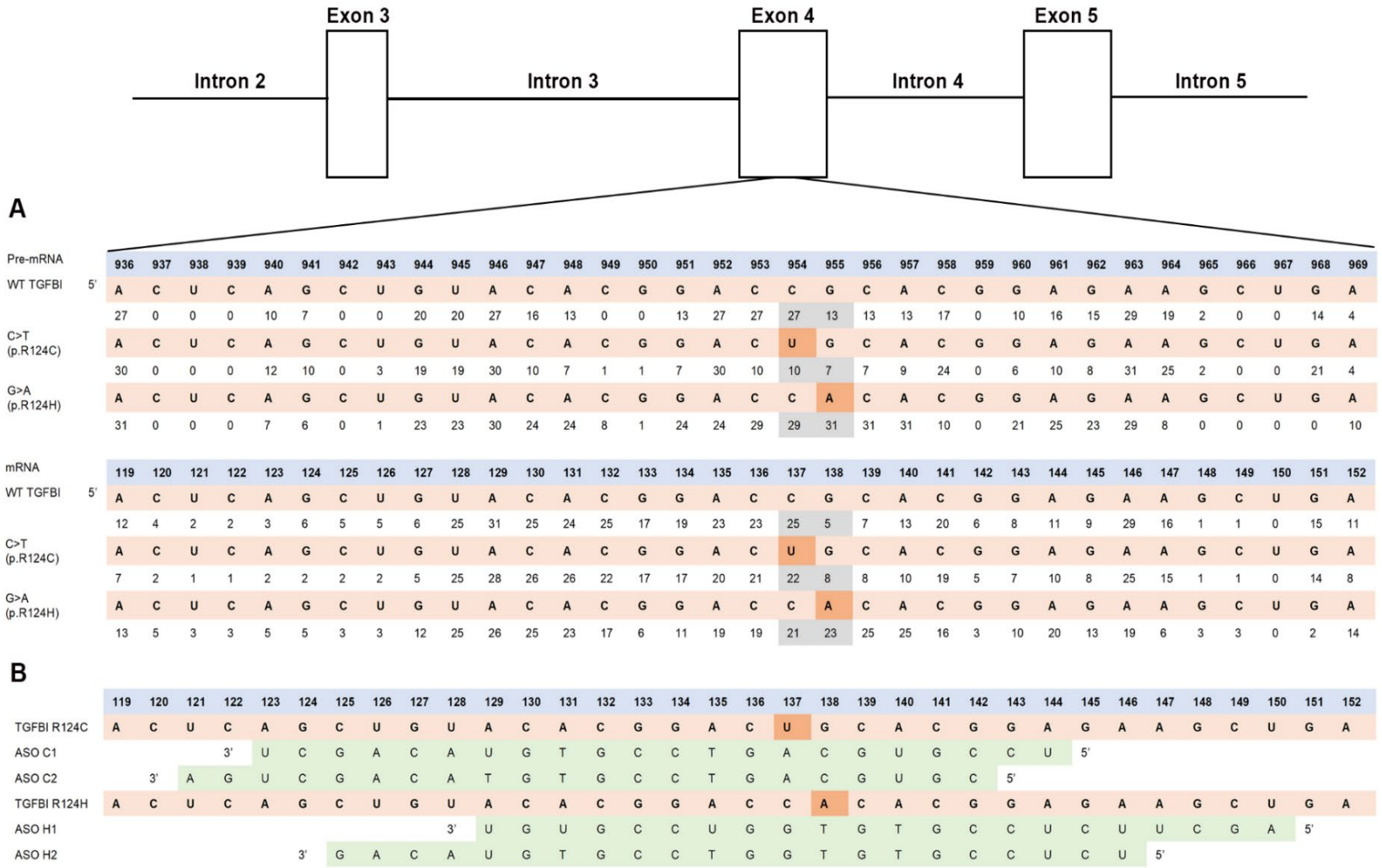

Figure 6.7 ss-count analysis for WT and mutant *TGFBI* nucleotides. A) Sequences comprising exon 4 of WT and mutant *TGFBI* pre-mRNA and coding mRNA were inputted into the mfold software which generates ss-counts that define the accessibility of target sequences by denoting the average propensity of a target nucleotide to be unpaired. A value of zero indicates the nucleotide is bound to another in all predicted conformations. The ss-counts for the WT and mutant *TGFBI* sequences were assessed. Mutation sites are highlighted in grey with the specific mutations for that sequence highlighted in orange. B) Candidate ASO sequences were selected and further assessed. The ASOs selected (highlighted in green) are shown aligned to their target RNA.

At the p.R124 codon, all three of the *TGFBI* sequences analysed (WT, R124C and R124H), displayed ss-counts that indicate that they would be accessible for ASO binding in both the pre-mRNA and coding mRNA transcript forms (Figure 6.7A). The p.R124H point mutation, respective to the other two *TGFBI* sequences analysed, appears to have the highest ss-count values (Figure 6.7A), indicating that this particular sequence may be the most accessible for ASO binding. Based on this analysis, the target regions for both mutations of interest demonstrate acceptable accessibility to ASO binding. Thus, the subsequent ASO sequence selection was afforded some flexibility and at least five candidate sequences for each mutant sequence were identified for further analysis before selecting the final two ASO sequences for each target mutation (Figure 6.7B; Table 6.1).

Table 6.1 Gapmer ASOs designed for this study. Two gapmer ASOs were designed for each mutation, along with the SCR ASO which is a scrambled version of ASO C1. RNA 2'-OMe modifications are represented by square brakets [ ]. The LNA bases are represented by curly brackets { }. PS backbone modifications are represented by an asterisk * following the base. Melting temperature ™ and free energy (dG – representing the quantity of energy needed to fully break a secondary DNA structure) values were obtained through the Oligo Analyzer online tool (https://www.idtdna.com/pages/tools/oligoanalyzer). Lowest dG values are represented in the table.

ID	Target mutation	Sequence	Length (nt)	% GC	Tm (°C)	dG Hairpin	dG Self-dimer (kcal/mol)	dG ASO-TGFBI (kcal/mol)
ASO C1	c.370C>T p.R124C	5'[UCCGUGC]{A}G*T*C*C*G*T*G*[UACAGCU]3'	22	59.1	62.1	-0.88	-7.55	-43.07
ASO C2	c.370C>T p.R124C	5'[CGUGC]{A}G*T*C*C*G*T*G*T*A*C*A*[GCUGA]3'	22	59.1	60.6	-0.93	-10.24	-41.96
ASO H1	c.371G>A p.R124H	5'[AGCUUCU]C*C*G*T*G*{T}G*G*[UCCGUGU]3'	22	59.1	57.5	-0.35	-6.34	-43.61
ASO H2	c.371G>A p.R124H	5'[UCUCCG]T*G*{T}G*G*T*C*C*G*T*[GUACAG]3'	22	59.1	58.3	-0.35	-7.55	-41.18
SCR	N/A	5'[GCGCC]T*C*G*T*A*G*G*A*C*C*[UCUUA]3'	20	60	53.1	-1.3	-9.89	-14.34

6.2.2.3 Thermodynamic properties of ASO-ASO and ASO-target mRNA interactions

Candidate sequences that contained the complimentary base towards the centre of the ASO were selected based on the parameters described in methods (Chapter 2, Section 2.9.3). The predicted free energy of inter-oligonucleotide pairing of candidate ASOs was calculated using the bifold RNAstructure software (http://rna.urmc.rochester.edu/RNAstructureWeb/). The two ASOs with the most favourable inter-oligonucleotide pairing free energies within the groups of candidate ASOs were picked for each mutation. All the lowest free energies of the ASO-ASO interactions for each of the four ASOs selected are >-15 kcal/mol as per the guideline set by Slijkerman et al. (2018) (Figure 6.8). ASO C2 shows the lowest free energy compared to the other three ASOs, indicating that this ASO would form the most thermodynamically stable inter-oligonucleotide pairs and thus, would be the least likely to effectively bind to the target sequence respective to the others.

The thermodynamic binding stability of the ASO to its target RNA was then analysed. First, the 161 bp sequence making up exon 4 of *TGFBI* for both of the mutations of interest (p.R124C and p.R124H) was input into the AllSub web server (RNAstructure, University of Rochester) in order to calculate the predicted free energy of the target RNA sequence. Then, the bifold web server (RNAstructure, University of Rochester) was used to predict the free energy of the ASOs bound to their target sequence (Figure 6.9; Figure 6.10). The free energy of the ASO bound to the target RNA should be lower, and thus, more thermodynamically stable than the free energy of the target RNA alone. As defined by Slijkerman et al. (2018), the calculated difference between these free energy values should be >21 kcal/mol. All the ASO sequences selected for this study meet this requirement. Both the p.R124C targeting ASOs display a similar predicted free energy value when bound to the target RNA. However, ASO H2 has a lower predicted free energy value when bound to the target RNA than ASO H1, indicating that the former ASO-target RNA interaction may be more thermodynamically stable than the latter. Furthermore, when comparing the p.R124C (Figure 6.9A) and p.R124H (Figure 6.10A) values, it appears that the p.R124C exon 4 sequence has a slightly lower free energy value than the p.R124H sequence, indicating that the former would be more thermodynamically stable than the latter. Both of the ASOs for each mutation also seem to cause differences in the folding of the surrounding *TGFBI* RNA, which form a slightly different secondary structure to each other when bound to the ASO.

The specificity of the ASO sequences was validated by alignment to the target sequences and the human genome using the online platforms BLAST (https://blast.ncbi.nlm.nih.gov) and GGGenome (http://gggenome.dbcls.jp).

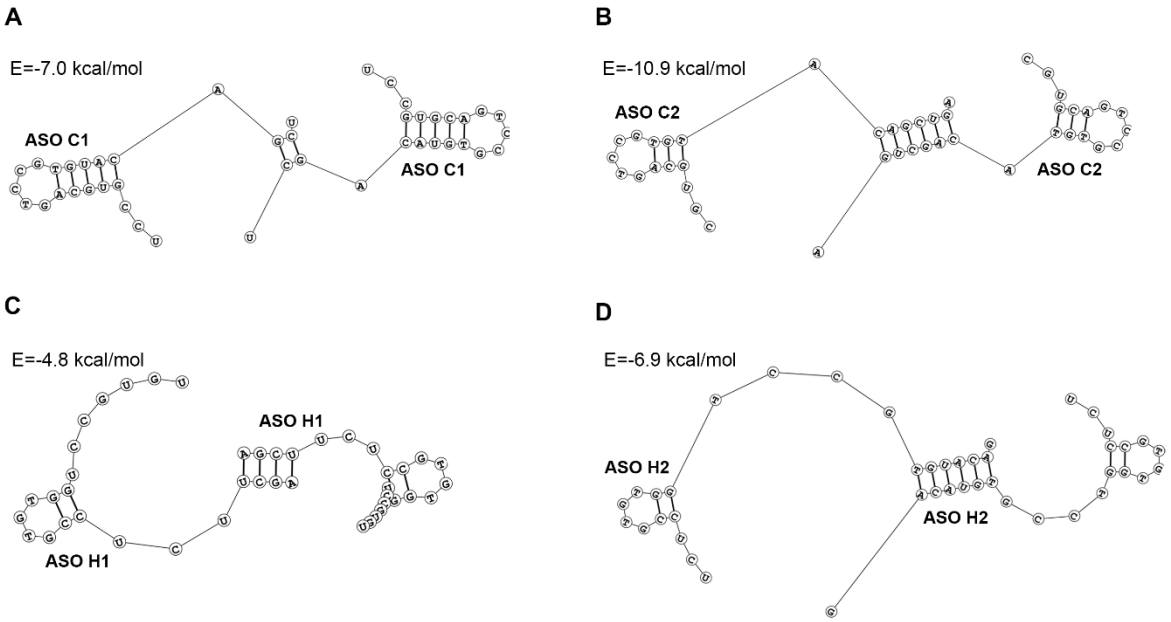

Figure 6.8 Predicted ASO-ASO interaction secondary sequences. The bifold platform (RNA Structure) was used for the prediction of inter-oligonucleotide secondary structures of ASO C1 **(A)**, ASO C2 **(B)**, ASO H1 **(C)** and ASO H2 **(D)**. Free energy values (E) denote the predicted thermodynamic stability of the inter-oligonucleotide pairings, with the more negative values indicating higher thermodynamic stability.

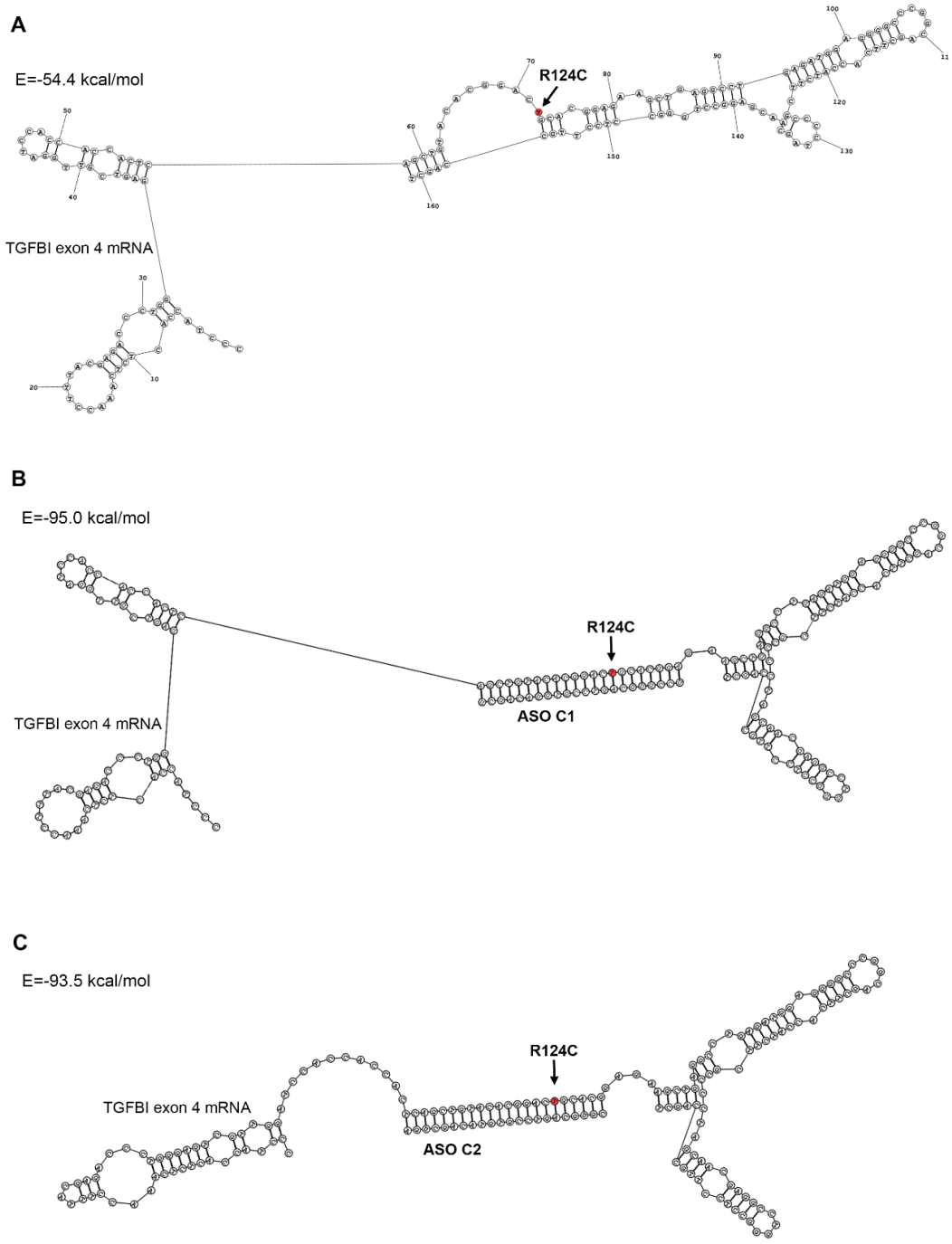

Figure 6.9 Predicted secondary structures of mutant p.R124C *TGFBI* exon 4 and ASO:RNA heteroduplexes. The target mRNA sequence was inputted into the bifold software (RNA Structure) for prediction of its secondary structure alone **(A)**, or in the presence of ASO C1 **(B)** or ASO C2 **(C)**. For the predicted binding affinity of the ASO to the target RNA to be more energetically favourable than the RNA binding to itself preventing access to the ASO, the calculated difference between these free energy values should be >21 kcal/mol in the negative direction. The p.R124C mutation is highlighted in red.

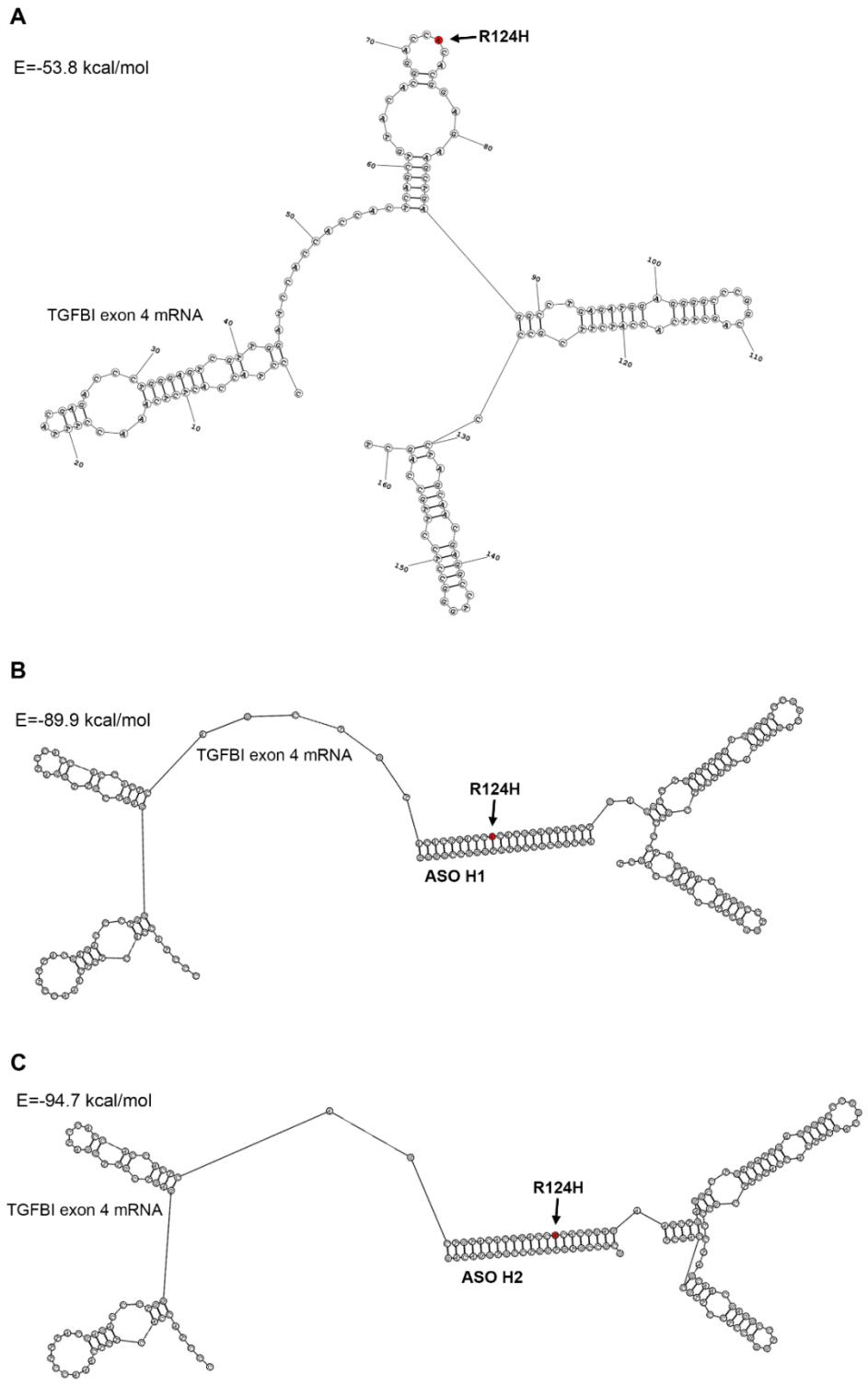

Figure 6.10 Predicted secondary structures of mutant p.R124H *TGFBI* exon 4 and ASO:RNA heteroduplexes. The target mRNA sequence was inputted into the bifold software (RNA Structure) for prediction of its secondary structure alone **(A)**, or in the presence of ASO H1 **(B)** or ASO H2 **(C)**. For the predicted binding affinity of the ASO to the target RNA to be more energetically favourable than the RNA binding to itself preventing access to the ASO, the calculated difference between these free energy values should be >21 kcal/mol in the negative direction. The p.R124H mutation is highlighted in red.

6.2.3 Gapmer ASO screening in patient-derived fibroblasts

The ASO sequences were selected with the intention of chemically modifying them into 'gapmer' structures, with an LNA base (a base 'locked' into an ideal Watson-Crick base pairing conformation) complimentary to the point mutation and a central DNA PS strand which is flanked by 2'-OMe RNA bases. ASO C1 and ASO H1 followed a 7-8-7 gapmer conformation, ASO C2 and ASO H2 followed a 5-12-5 and 6-10-6 gapmer conformation, resectively. A scrambled control ASO was designed based on the p.R124C target *TGFBI* sequence and also chemically modified with a gapmer design.

An initial screening of the ASOs was carried out in the patient-derived fibroblast lines, in order to assess the efficacy of the ASOs to enter the cells and bind to the *TGFBI* transcript, causing its degradation. The PEI-based reagent Transporter 5 (Polysciences) was used to transfect a 1 µg dose of the ASOs into the cells, as instructed by the reagent manufacturer (Chapter 2, Section 2.9.5). Following transfection, a high percentage of cell stress and death was observed in all of the transfected conditions for all cell lines, including the transfection only condition, indicating that treatment with the Transporter 5 reagent causes cellular toxicity. RNA was extracted from all experimental conditions following 48 h culture post transfection and subsequently transcribed into cDNA (Chapter 2, Section 2.1.1). qPCR analysis demonstrated a decrease in total *TGFBI* transcript expression in both the p.R124C and p.R124H *TGFBI*-targeting ASO conditions, relative to the no treatment (transfection only) and SCR ASO conditions (Figure 6.11). The transfection of the p.R124C ASOs led to a decrease in *TGFBI* transcript levels of around 50-80% (n=2) indicating that ASO C1 and ASO C2 were likely not discriminating between the mutant and WT *TGFBI* allele following transfection into the fibroblasts. However, it could also be an effect of cellular stress and cytotoxicity due to the transfection reagent, or due to the high dose of ASO transfected. Based on this preliminary screening in fibroblasts, a lower ASO dose was selected for the subsequent experiments in the CEpi cells. The variability observed in the ASO C2 condition (Figure 6.11A) is likely due to the high levels of cellular toxicity caused by the transfection reagent used. Additional attempts to replicate the ASO treatments in fibroblasts failed, as too many of the cells died, resulting in an inability to extract a sufficient quantity of RNA post-treatment. This could not be quantified as cell survival was very minimal, however, no differences were observed between transfected cell lines. Although the ASOs designed seem to be effective in targeting *TGFBI*, fibroblasts were not a convienent model for testing this therapeutic and a more reliable cellular model is required.

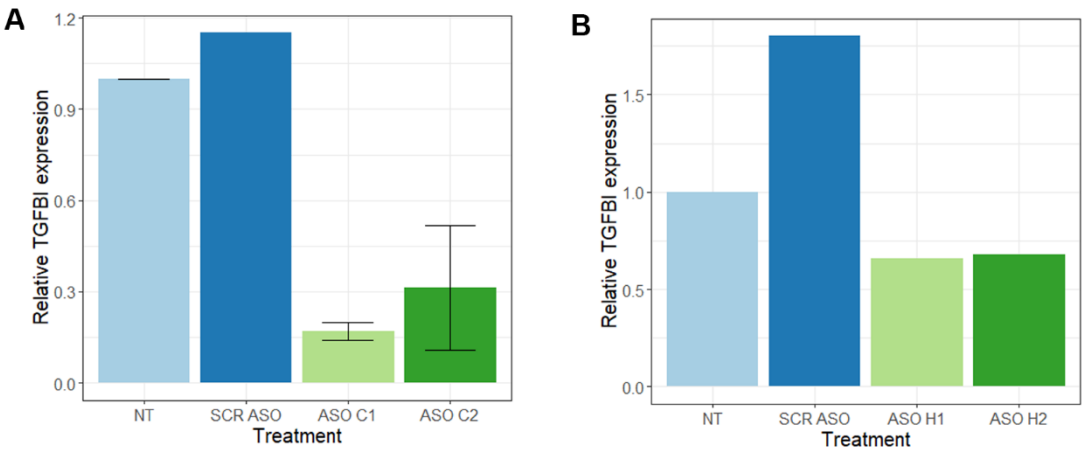

Figure 6.11 Gapmer ASO treatment of patient-derived fibroblasts. Transfection of primary patient-derived fibroblasts with the two ASOs designed for each mutation p.R124C **(A)** and p.R124H **(B)** showed a reduction in *TGFBI* transcript expression by qPCR. Gene expression was normalised to *ACTIN* and *GAPDH* expression, values were calculated relative to the no treatment (NT, transfection reagent only) condition. N=1-3 independent transfections per line. Bars represent mean ± SEM.

6.2.4 Gapmer ASOs reduce CEpi *TGFBI* and TGFBIp expression

Based on the results from the ASO transfections of the fibroblasts, a lower ASO dose of 300 nM was selected for the patient-derived CEpi transfections in order to reduce the potential of cell death asociated with a high dose in fibroblasts, yet provide enough ASO concentration for the high density of CEpi cells that were observed in culture. All four of the patient lines described in Chapter 3 (Section 3.2.3.1, Table 3.2) were used for the ASO transfections. The transfection reagent Lipofectamine RNAimax (ThermoFisher Scientific) was used to transfect the CEpi cultures, as this reagent has previously been shown to provide a high transfection efficiency for cultured corneal epithelial cells (Baran-Rachwalska et al., 2020). The ASOs used for CEpi transfection were conjugated at the 5' end to a 6-FAM fluorophore, thus, confirmation of ASO transfection was obtained by observation of 6-FAM fluorescence, which demonstrated a transfection efficiency of around 60-70% (Figure 6.12A). Samples were collected 48 hours post-transfection for transcript analysis (Chapter 2, Section 2.9.5). Total *TGFBI* transcript expression was initially assessed in untreated and treated p.R124C (Figure 6.12C) and p.R124H (Figure 6.12D) patient CEpi lines, and a WT line (Figure 6.12E).

The objective of the ASO development was to assess whether the gapmer ASOs designed to target the p.R124 mutations would result in a decrease of *TGFBI* transcript expression in an allele-specific manner. The ideal effect of ASO treatment in these heterozygous *TGFBI* mutant iPSC-derived models would reduce expression of the mutant allele as much as possible, whilst having no or little effect on WT lines. In this

study (see Section 6.2.5) allele skewing was observed in different cell lines from different individuals. Therefore the degree to which the mutant allele is expressed, relative to the WT allele, can differ.

Treatment of the patient-derived mutant *TGFBI* CEpi lines demonstrated a 20-40% reduction in total *TGFBI* transcript expression following administration of the therapeutic ASO relative to the control ASO and no treatment conditions, as assessed by qPCR (Figure 6.12C-D). A WT CEpi line was also treated with a 300 nM dose of all the ASOs (Figure 6.12E) in order to assess the affect of ASO treatment on WT *TGFBI* transcript expression. qPCR analysis of total *TGFBI* expression demonstrates that the ASO did not significantly affect WT *TGFBI* expression, indicating that the ASOs are able to discriminate between the mutant and WT alleles and reduce *TGFBI* expression in an allele-specific manner.

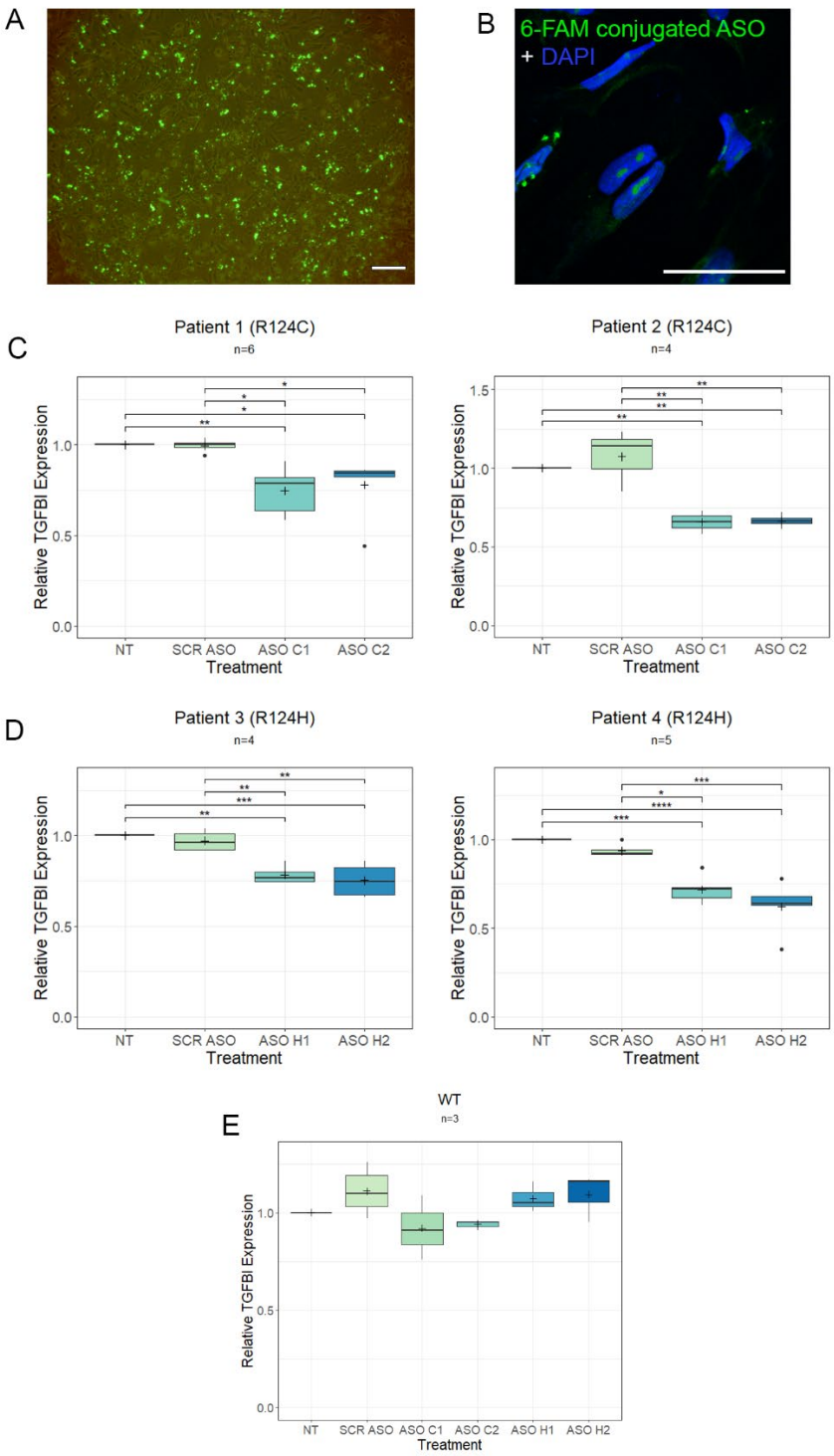

Figure 6.12 300nM ASO induced reduction of TGFBI transcript expression in patient-derived CEpi lines. A) Green fluorescence demonstrated successful 6-FAM conjugated ASO transfection of CEpi cells. Scale bar = 100 µm. **B)** The localisation of a transfected 6-FAM conjugated ASO was observed in the nuclei by confocal microscopy. Scale bar = 100 µm. **C-D)** RNA was collected 48 h post-transfection and total *TGFBI* transcript expression of p.R124C (C, patients 1 and 2), p.R124H (D, patients 3 and 4) and WT control CEpi **(E)** lines was quantified by qPCR. *TGFBI* expression was normalised to *ACTIN* and *GAPDH,* and relative quantification values were calculated relative to the no treatment (NT = transfection reagent only) samples. The mean is represented by the + symbol, whereas the median is represented by the horizontal line. N=3-6 independent treatments per CEpi line. Statistical analysis was performed using a one-way ANOVA and a post-hoc Tukey's HSD test. * P<0.05, ** P< 0.01, *** P<0.001.

Next, the effect of ASO transfection on TGFBIp expression was investigated by western blot. TGFBIp expression was assessed in CEpi cell lysates 72 h post-transfection with 300nM of the SCR, ASO 1 and ASO 2 for the respective mutation. Total protein was extracted from CEpi cell lysates and resolved by SDS-PAGE. TGFBIp expression was visualised by immunoblotting, along with GAPDH as a reference protein (Figure 6.13A).

Densitometry was used to quantify the TGFBIp specific bands, which were then normalised to GAPDH, revealing a 25-50% reduction of TGFBIp in samples collected 72 h post-treatment with the therapeutic ASOs (Figure 6.13B). The western blot data corresponds with the results obtained at the transcript level (Figure 6.12C-D). However, patient 2 did not express a sufficient amount of TGFBIp for western blot analysis, and is also consistent with the low levels of TGFBIp observed for this patient line in the day 30 TGFBIp characterisation blots (Figure 6.5C), thus, the results of ASO treatment could not be quantified for this patient sample.

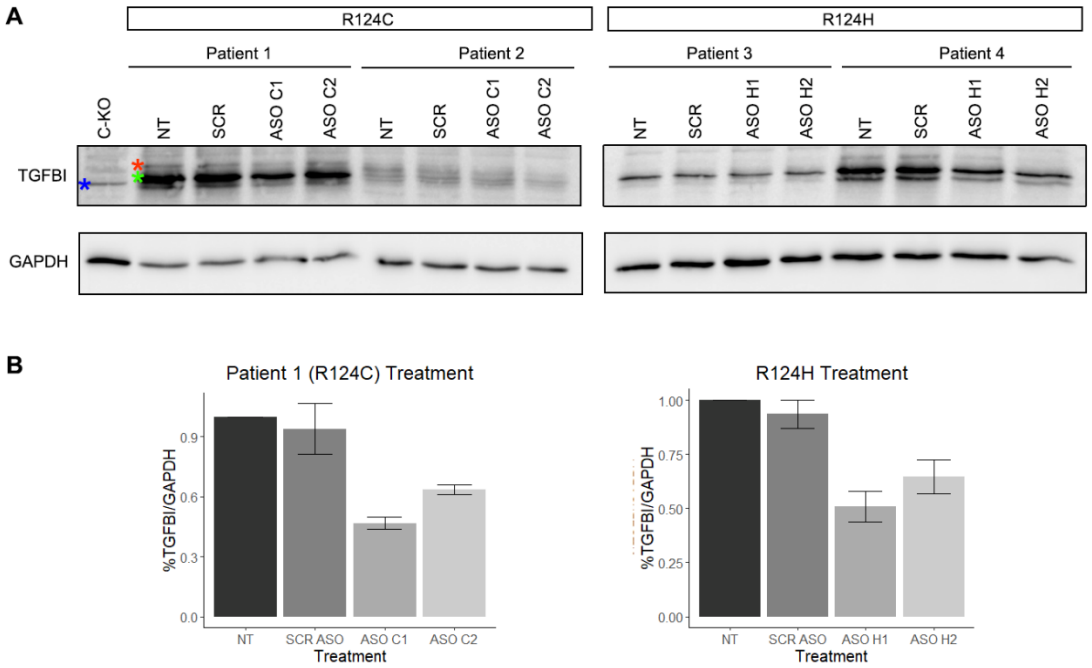

Figure 6.13 Reduction of TGFBIp in CEpi cell lysates 72 h post ASO treatment. A) Lysates from patient-derived CEpi in no treatment (NT, transfection reagent only); 300nM of SCR ASO; 300nM of ASO C1 and ASO C2 (patients 1-2) and 300nM of ASO H1 and ASO H2 (patient 3-4) conditions were collected and analysed by western blot, using antibodies against TGFBIp and GAPDH. A C-KO sample that was differentiated alongside and extracted at the same time point as the patient samples was included as a negative control for the TGFBIp antibody. The blue asterisk shows the non-specific band, identified by the C-KO sample. The red and green asterisks show the TGFBIp+ bands that were quantified. **B)** Quantification of the TGFBIp specific bands revealed a reduction of around 40-50% of total TGFBIp in the patient 1 therapeutic ASO treatments, and 25-50% of total TGFBIp for the patients harbouring a p.R124H mutation (combined data for patients 3 and 4) therapeutic ASO treatments. The patient 2 samples did not express a sufficient amount of TGFBIp to allow for quantification. Protein expression was normalised to the expression of GAPDH, and expressed relative to the expression of TGFBIp/GAPDH in the no treatment (NT) condition. Bars represent mean values ± SEM. N=2 and N=3 independent treatments for patient 1 (R124C) and R124H treatments, respectively.

As TGFBIp is a secreted protein, expression of secreted TGFBIp was also assessed by western blot, following the collection of media from non-treated and treated cells 72 h post-transfection, that underwent a media change 48 h post-transfection (Figure 6.14). Thus, the western blot analysis was carried out on media that had been conditioned during the last 24 h of the 72 h treatment.

Following media collection and protein quantification by BCA analysis, samples were standardised, loaded in equal amounts and resolved by SDS-PAGE, before being transferred onto a membrane and immunoblotted for TGFBIp. A high molecular weight non-specific band was observed in the knockout line, and two specific protein species representing TGFBIp was observed. No striking differences in TGFBIp intensity were observed between control and treated patient-derived CEpi samples. Furthermore, there

is currently no known loading control available for secreted proteins such as TGFBIp, so it was not possible to accurately quantify the positive TGFBIp bands. As was the case in the cell lysate blots for patient 2 samples (Figure 6.5C; Figure 6.13A), insufficient amounts of TGFBIp were detected and thus, could not be visualised.

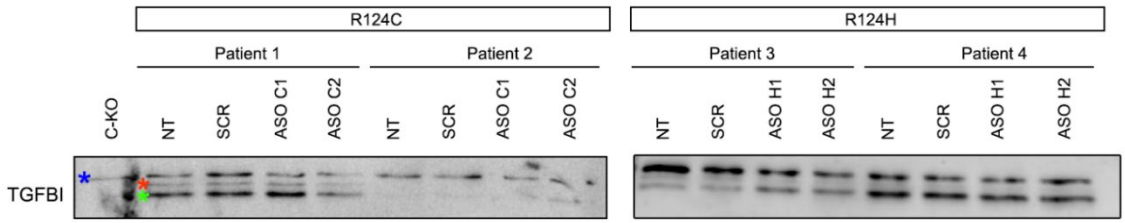

Figure 6.14 Secreted TGFBIp expression 72 h post ASO treatment. CEpi cells were treated with both ASOs designed for the respective mutation. Conditioned media was collected 72 h post-transfection, following a media change at 48 h (24 h conditioning), and analysed by western blot for TGFBIp expression. The 68/70 kDa TGFBIp positive double band is observed in the patient 1, 3 and 4 samples, along with a non-specific band, as demonstrated by the C-KO negative control sample, labelled with the blue asterisk. The red and green asterisks show the TGFBIp-specific bands. Patient 2 expression of secreted TGFBIp was not sufficient for visualisation.

6.2.5 Allele specificity of R124 *TGFBI*-targeting ASOs in CEpi cells

In order to assess whether the ASO-mediated reduction of *TGFBI* expression was allele specific, non-treated and treated cDNA samples underwent Sanger sequencing using primers that produced an amplicon covering the point mutations of interest: c.370C>T and c.371G>A, which result in the p.R124C and p.R124H amino acid changes, respectively.

Differences in Sanger sequencing trace peaks were visualised using Benchling to allow for the semi-quantitative assessment of mutant trace peaks between non-treated and treated samples (Figure 6.15). In the patient samples harbouring the p.R124C mutation (patient 1 and 2) that had been treated with ASOs C1 and C2, a complete reduction in the mutant allele trace peak is observed respective to the no treatment and SCR ASO treated samples. In the patient samples harbouring the p.R124H mutation (patient 3 and 4) that had been treated with ASOs H1 and H2, a reduction in the mutant trace peak is observed respective to the no treatment and SCR ASO treated samples, with the WT allele more dominantley expressed in comparison to the mutant allele following therapuetic ASO treatment. The data obtained by Sanger sequencing provided preliminary confirmation that the ASOs were reducing the expression of *TGFBI* in an allele-specific manner, with preferential targeting of the mutant allele.

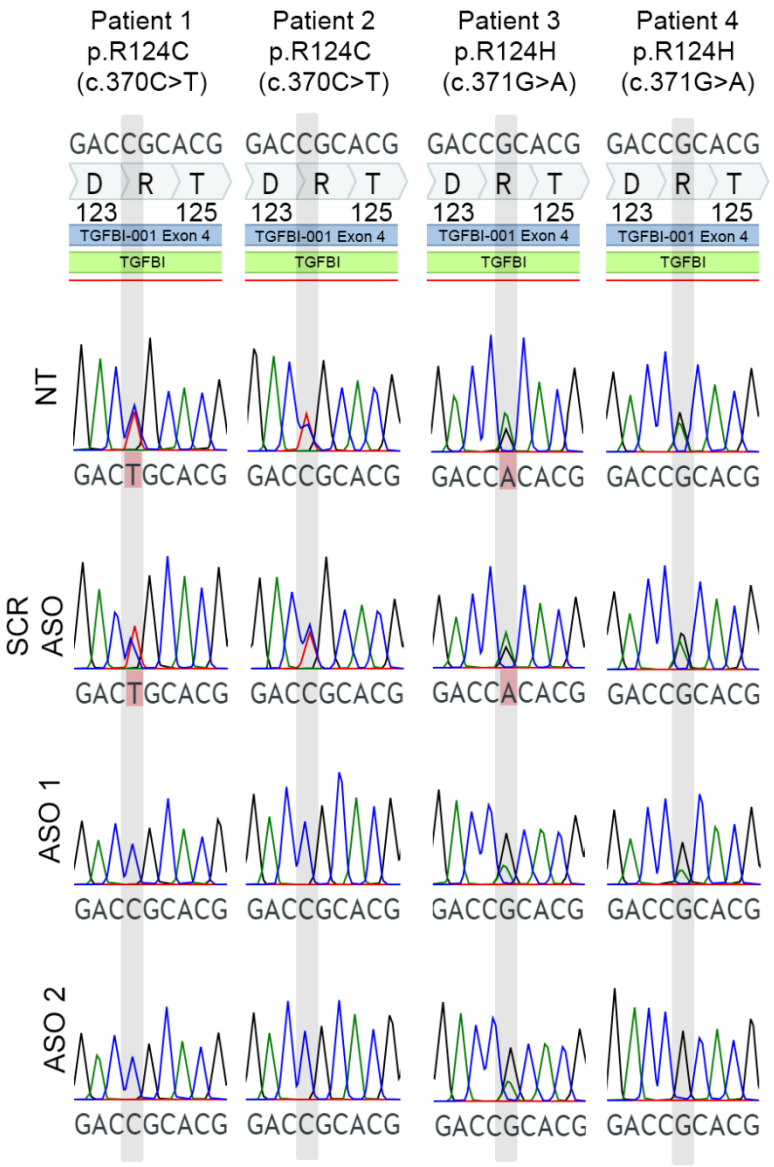

Figure 6.15 Reduction of the mutant *TGFBI* cDNA Sanger sequence trace peak following therapeutic ASO treatment. Sanger sequencing chromatograms of non-treated (NT) and treated cDNA amplified using primers producing an amplicon that encompasses the c.370C>T (p.R124C) and c.371G>A (p.R124H) regions of *TGFBI*. The two peaks representing the heterozygous mutation can be observed in the NT samples (shaded). A complete reduction of the mutant allele trace peak is observed in the patient 1 and 2 with both therapeutic ASO (C1 and C2) treatment conditions. The mutant allele trace peak shows a decrease in expression relative to the WT allele in the patient 3 and 4 with both therapeutic ASO (H1 and H2) treated samples. Peak colours = adenine = green, guanine = black, cytosine = blue and thymine = red.

With the preliminary semi-quantitative confirmation of allele-specificity of the ASO treatments (Figure 6.12E) from Sanger sequencing (Figure 6.15), a quantitative targeted next generation sequencing (NGS; Chapter 2, Section 2.10.1) approach was used to further investigate the allelic discrimination of the ASOs. Illumina MiSeq sequencing was carried out on gDNA sample duplicates and three independent treatments per patient line and subsequently quantified (see Chapter 2, Section 2.10.2). This quantitative investigation in the gDNA demonstrated a 50:50 split between the WT and mutant alleles

of *TGFBI,* as expected, confirming equal copy number. Upon investigation of cDNA data, differences between baseline levels of WT and mutant allele expression were observed in the non-treated and SCR ASO treated in 3 out of 4 patient samples, which also corroborated the trace peak visualisations obtained by Sanger sequencing. Patient 1 with the p.R124C mutation showed no differences in basal expression levels between WT and mutant alleles (Figure 6.16A). In contrast, patient 2 with the p.R124C mutation; and patient 4 with the p.R124H mutation, both displayed higher basal expression levels of the WT allele compared to the mutant allele, whereas patient 3, who harbours the p.R124H mutation, displayed a higher basal expression level of the mutant allele, compared to the WT allele.

The NGS approach enabled quantification of the observed allele skewing, patient 1 displays a 50:50 WT:mutant allelic expression (Figure 6.16A), patient 2 displays a 55:45 WT:mutant allelic expression (Figure 6.16B), patient 3 displays a 45:55 WT:mutant allelic expression (Figure 6.16C) and patient 4 displays a 60:40 WT:mutant allelic expression (Figure 6.16D). The difference in baseline levels of allelic expression need to be considered when investigating ASO treatment effects.

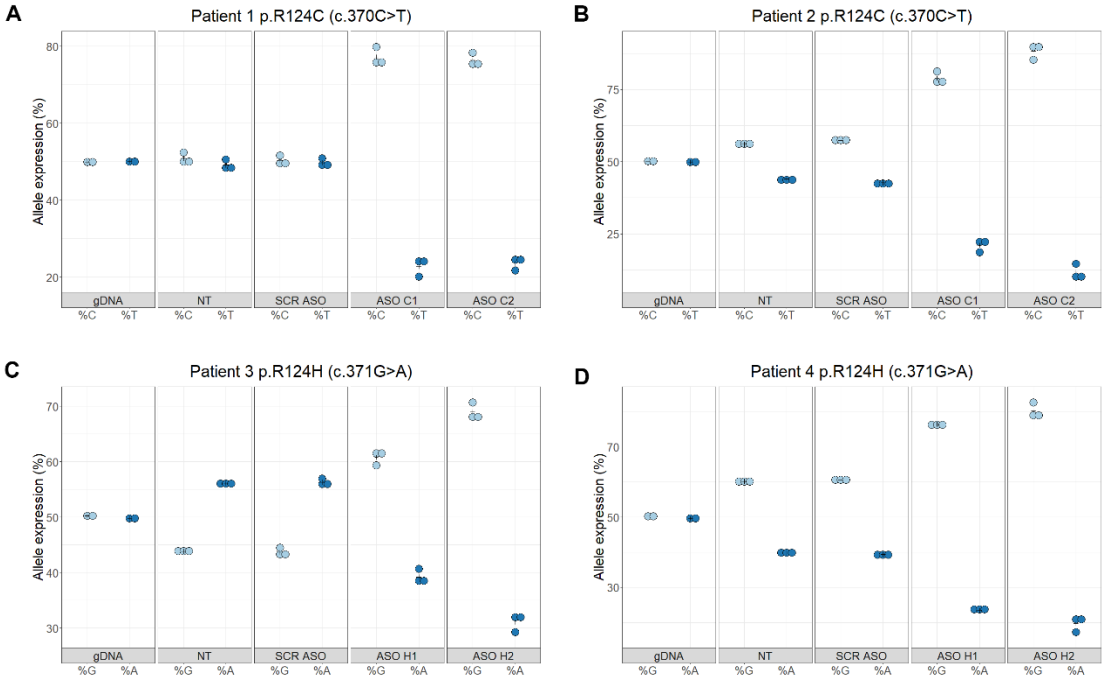

Figure 6.16 Targeted next generation sequencing of *TGFBI* exon 4 in non-treated and treated CEpi samples. The percentage of *TGFBI* allelic expression was assessed in patient-derived gDNA; and non-treated, SCR and therapeutic ASO treated CEpi cDNA samples. A 50:50 split of allelic expression is observed in all gDNA samples. Allele skewing at the cDNA level is observed in the no treatment (NT, transfection reagent only) and SCR treated patient 2 **(B)**, 3 **(C)** and 4 **(D)** samples. A clear reduction of the mutant transcript expression is observed (T in p.R124C patients 1 and 2, graphs A and B; and A in p.R124H patients 3 and 4, graphs C and D) following 300nM treatment of therapeutic ASOs for the respective mutation (ASO C1 and C1 – patients 1 and 2, ASO H1 and H2 – patient 3 and 4). N=3 independent treatments per patient line.

Most importantly, a clear reduction in the percentage of mutant allele expression was observed in all patient lines following therapeutic ASO treatment, irrespective of baseline levels of allelic expression. These data correlate with the semi-quantitative data obtained via Sanger sequencing (Figure 6.15). The percentage of WT allele expression ranged from 60% to 80% of the total transcript reads in the treated samples. Interestingly, for patient 2 CEpi that are more highly skewed towards expressing the mutant allele, ASO H2 was still effective at reducing the expression of the mutant transcript from 55% of reads to 30% of reads.

In order to further understand how the ASO treatments are affecting the expression of the WT and mutant alleles of *TGFBI* respective to total *TGFBI* transcript expression, the ASO treatment data obtained via qPCR was collated with the NGS data. First, the percentage of allelic expression was calculated compared to total levels of *TGFBI* transcript (Figure 6.12), and the data were then normalised to the no treatment control condition for the respective data group (WT or mutant allele) (Figure 6.17).

No significant differences between the control (no treatment and SCR ASO) and therapeutic ASO treatment conditions are observed for the expression of the WT allele in all data groups. However, significant reductions in *TGFBI* expression are observed following therapeutic ASO treatment in comparison to the control conditions (no treatment and SCR ASO), confirming allele specificity with little or no effect on the WT allele. Both ASOs targeting the p.R124C allele appear to be equally effective at targeting the mutant allele, however ASO H2 is significantly more effective at reducing the expression of the p.R124H allele compared to ASO H1.

These quantitative data show that the ASOs are specifically targeting and significantly decreasing the expression of the mutant allele of *TGFBI* in CEpi, with little to no effect on the WT allele. These results are further supported by the WT ASO treatments (Figure 6.12E) showing no effect on *TGFBI* transcript expression in CEpi that lack mutations that cause corneal dystrophies.

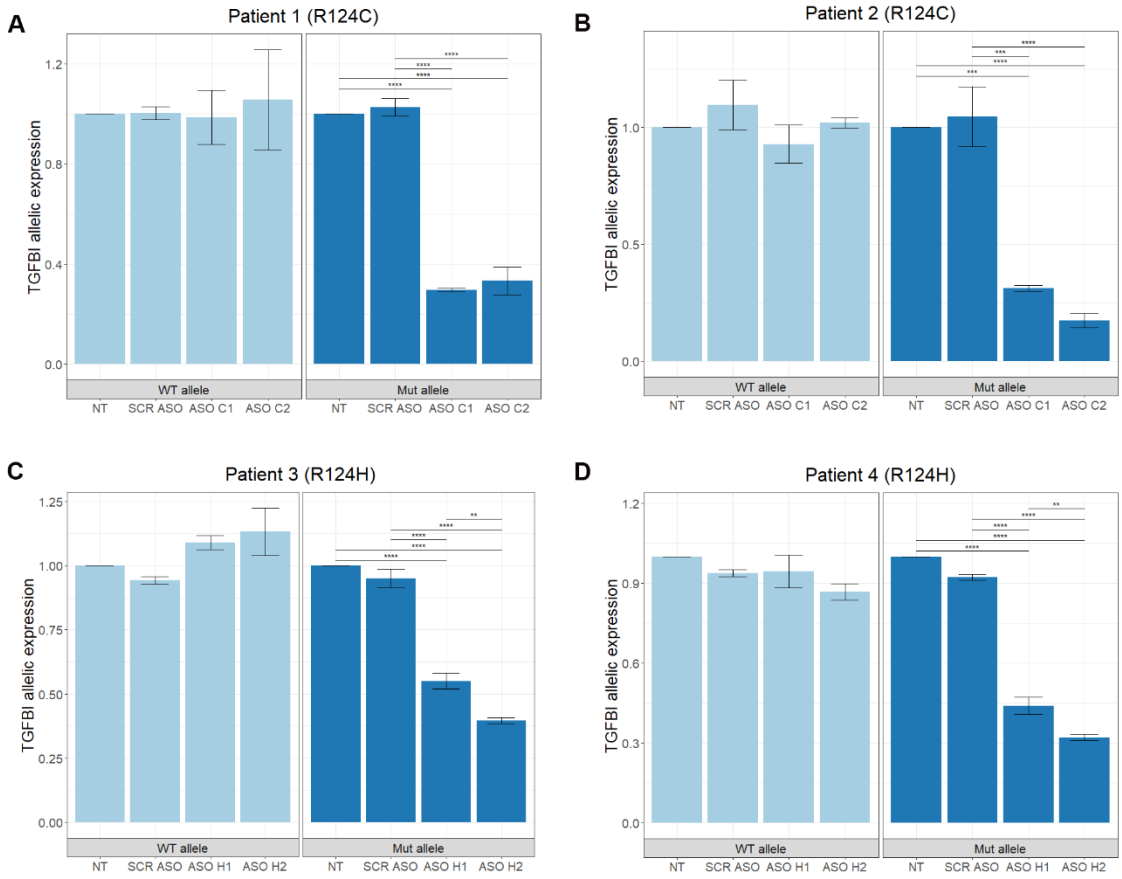

Figure 6.17 WT and mutant *TGFBI* transcript expression following ASO treatment in CEpi. To further demonstrate the allele-specificity of the therapeutic ASO treatments, the percentages of WT and mutant *TGFBI* expression in non-treated (NT, transfection reagent only) and treated samples quantified by targeted NGS were applied to the total levels of transcript expression quantified by qPCR. Mean ± SEM expression values are visualised by the graphs relative to the expression of each allele in the no treatment (NT, transfection reagent only) condition for each patient-derived CEpi line. Graphs **A)** and **B)** represent treatment of the p.R124C mutant lines with ASO C1 and ASO C2; graphs **C)** and **D)** represent treatment of the p.R124H mutant lines with ASO H1 and ASO H2. N=3 independent treatments per CEpi line. Statistical analysis was performed by ANOVA and Tukey's HSD test. ** P< 0.01, *** P<0.001, ****P<0.0001.

6.3 Discussion

The pathogenesis of TGFBI CD is unclear, with different mechanisms likely underlying each phenotype and even the same phenotypes when caused by different mutations. However, in the majority of cases, CD mutations in *TGFBI* present with TGFBIp+ deposits in the corneal epithelium and stroma. The majority of reports investigating the pathogenesis of these conditions imply that pathogenic mutations result in abnormal proteolytic processing of TGFBIp causing its aggregation. Furthermore, some studies have focused on the pathology underlying GCDII and have highlighted defective cellular processes, such as abnormal autophagy and mitochondrial function as having a potential role in disease progress (K. E. Han et al., 2016).

6.3.1 Proteolytic processing of TGFBIp in mutant and control lines

TGFBIp undergoes proteolytic processing, which involves the cleavage of its precursor into its active form (see Chapter 1, Section 1.5.1). The proteolytic processing of TGFBIp is important for its proper function in various cellular processes, such as cell adhesion, migration, and differentiation. Abnormal proteolytic processing of TGFBIp has been implicated in the pathogenesis of CD, so understanding its processing is important for understanding the molecular mechanisms underlying these diseases and for the development of new therapeutic strategies.

Abnormal TGFBIp products have previously been reported to accumulate in the corneas of p.R124C and p.R124H CD patients via distinct aggregation pathways that involve altered protein metabolism and turnover (Korvatska et al., 2000; Takács et al., 1998). Levels of *TGFBI*/TGFBIp were assessed in the CEpi control and mutant lines (Figure 6.5), however, no mutation-dependent effect on expression levels was observed. Nonetheless, TGFBIp expression of each cell line reflected expression levels at the transcript level, indicating that differences in protein expression between samples is driven by pathogenic-mutation independent-factors driving RNA transcription. As demonstrated, *TGFBI* expression increases rapidly during differentiation from iPSCs into CEpi cells (Figure 4.11), thus, variability in TGFBIp expression levels in samples between different differentiation batches may be due to variability in the maturation of CEpi cultures. In addition, no relationship was found between *TGFBI* variants and cellular expression in the current CEpi model, indicating that individuals may naturally express TGFBIp at different levels, independent of disease.

Abnormal proteolytic processing of TGFBIp resulting in the accumulation of unique protein fragments has been demonstrated in cells expressing recombinant p.R124

mutant TGFBIp (Y. P. Han et al., 2011, 2012) and p.R124 mutant corneal tissue (Korvatska et al., 2000; Takács et al., 1998). Furthermore, multimerization of TGFBIp has been demonstrated at increased concentrations through a small-angle X-ray scattering model (Basaiawmoit et al., 2011). The dimerization of TGFBIp has also been visualised by western blotting of cells expressing control and mutant recombinant TGFBIp (Y. P. Han et al., 2011, 2012). However, western blotting analysis of the control and mutant CEpi samples in the current study only detected the expected monomeric 68/70 kDa TGFBIp+ band, with no smaller fragments representative of proteolysis or larger products representative of multimerization, detected.

As the multimerization of TGFBIp is reportedly concentration-dependent (Basaiawmoit et al., 2011), it may be the case that TGFBIp did not reach sufficient levels of concentration before samples were extracted, compared to those in vitro studies overexpressing TGFBIp by transfection, resulting in no observations of higher molecular weight TGFBIp species in the western blots (Figure 6.5). It is unclear whether TGFBIp undergoes multimerization prior to or following secretion, however, as the media samples investigated in the current study were only conditioned for 24 (Figure 6.14), it may be the case that a sufficient concentration of TGFBIp to induce multimerization was not reached during this time. Furthermore, the antibody used may not sensitively detect multimerized forms of TGFBIp.

Disease onset of TGFBI CD usually occurs within the first or second decade of life, depending on the phenotype. Furthermore, CD mutations in *TGFBI* do not result in any signs of systemic abnormality, even in homozygous patients. These two considerations indicate that abnormal TGFBIp deposition is accelerated by age-related and tissue-specific factors. Thus, an especially unique environment is necessary for abnormal TGFBIp deposition to occur, which may have not been achieved with the current CEpi model. However, other TGFBIp antibodies targeting different epitopes could be explored for a more thorough investigation of WT vs mutant TGFBIp products.

A double band representing the two monomeric isoforms of TGFBIp is observed in both the cell lysate and supernatant sample blots of the CEpi models (Figure 6.5C; Figure 6.13; Figure 6.14). The double band staining pattern of TGFBIp has also been shown in previous studies in human immortalised corneal keratocytes (S. il Choi et al., 2020), human primary limbal epithelial stem cells (E. K. Kim et al., 2019) and in a cancer cell line (Tumbarello et al., 2016). The full-length 70 kDa form of TGFBIp undergoes cleavage, resulting in the removal of 26 C-terminal residues, leaving the RGD motif exposed to allow for physiological interactions such as integrin binding (Andersen et al.,

2004). These two forms of TGFBIp could account for the double band staining pattern observed in the blots presented in the current study. The more abundant species of TGFBIp expressed by all the CEpi samples analysed in this study, is the truncated form of the protein (lower band) (Figure 6.5C; Figure 6.13; Figure 6.14). This is supported by previous research that found that the C-terminal truncated form of TGFBIp is the most abundant form of the protein in the mammalian cornea (Andersen et al., 2004) and suggests the CEpi models described recapitulate at least some of the features identified *in vivo*.

6.3.2 Antisense oligonucleotide therapy as a targeted treatment for TGFBI CD

Currently available treatment options for TGFBI CDs are highly invasive, entail a substantial recovery period and can lead to lasting complications such as graft rejection. These treatments do not target the underlying genetic defect of the disease leading to disease recurrence within a few years post-operation. This is due to high expression of TGFBIp in the cornea and high turnover of the corneal epithelial cells, making laser ablation and PK ineffective in the long term. In addition, for CDs such as GCDII, currently available treatments are likely to exacerbate the severity of the recurrent disease (Awwad et al., 2008). Thus, the focus of this study was to develop an effective treatment that targets the underlying genetic cause of the disease, to enable prevention of disease and preserve vision.

Following the generation of an *in vitro* patient-derived CEpi model that expresses TGFBIp, an ASO-based therapeutic strategy was designed with the aim of reducing mutant *TGFBI* expression in an allele-specific manner. Antisense technology utilises a simple yet versatile method of gene expression regulation based on Watson-Crick base pairing, thus, ASOs are emerging as an attractive therapeutic strategy for a wide variety of conditions with a genetic basis.

Several factors are likely to influence the effects of ASO activity *in vitro*, including its chemical make-up (Marrosu et al., 2017), secondary structure/thermodynamic properties, delivery and bioavailability (as described in Section 6.1.3.4). An *in-silico* analysis was performed on the *TGFBI* mRNA sequence in evaluation of the predicted RNA secondary structure thermodynamic properties and to allow for ASO sequence selection (Section 6.2.2). Secondary RNA structures result in some bases being paired and some being free for ASO binding, thus influencing the hybridisation affinity and efficiency of ASOs (Eckardt et al., 1997; Fedor & Uhlenbeck, 1990; Herschlag & Cech, 1990; Vickers et al., 2000). Areas of unpaired bases are preferred for ASO targeting,

although, oligonucleotide potency can be enhanced via chemical modifications even in highly structured mRNA target regions (Vickers et al., 2000). If the aim of the ASO treatment is to target a specific mutation or target region rather than employing a general gene knockdown method, as it is in the current study, the target area is limited. The ss-count data outputted by the mfold software predicted that the RNA secondary structure of the target *TGFBI* sequence consists of bases with a propensity to be unpaired in multiple RNA folding conformations (Figure 6.7), indicating potential sites available for ASO binding. It is interesting to note that even though the mfold software predicted certain bases targeted by the ASO to be paired to another base in every folding conformation, the ASOs successfully bound and effectively reduced the expression of the target transcript, as shown by the qPCR and MiSeq data (Figure 6.12; Figure 6.16; Figure 6.17). Within the cell, the target RNA is likely to form alternative secondary structures that may not be captured by *in-silico* predictions as they do not take into account other biological influences such as RNA-binding proteins.

Binding affinity is an important factor for ASO:RNA hybridisation. For the efficient binding to a target sequence, the free energy of the ASO-target complex must be lower than that of the target sequence itself (Matveeva et al., 2003), which is the case for all *TGFBI* ASO:RNA complexes in this study (Figure 6.9; Figure 6.10). However, hybridisation free energies cannot be accurately predicted for complexes between chemically modified gapmer ASOs and the target RNA. Thus, the *in-silico* evaluation of the hybridisation capacities for ASO:RNA complexes may not be accurate and can be used for guidance purposes only.

As ASOs are generally short, they are unlikely to form stable secondary structures, although, most ASOs are able to form ASO-ASO complexes with other ASOs of the same sequence (Aartsma-Rus et al., 2009). Despite ASO C2 having the lowest free energy value for ASO-ASO binding out of the four ASOs designed (Figure 6.8), indicating that it would form the most stable internucleotide complexes, it was not less effective at decreasing *TGFBI* expression.

Thus, the results from the *in-silico* analysis were informative, but they do not accurately recapitulate the *in vitro* or *in vivo* process of RNA secondary structure formation. Online RNA-structure modelling tools can be used to facilitate ASO design by predicting thermodynamic stability *in-silico*, which does not necessarily reflect biological stability. A process of informed trial and error is still required in the design of effective ASOs.

Even when targeting a specific point mutation in a particular gene, there are many different factors one could combine in the design of the ASO, such as different lengths

and different combinations of chemical modifications. It would be ideal to test as many different ASOs as possible, however, this is not normally the approach in research labs due to time and financial constraints and is usually undertaken by biotechnology companies during pre-clinical development. For the current study, a length of 22 nucleotides was chosen for all ASOs, as previous research has found this sequence length favourable for RNase H recruitment (Marrosu et al., 2017) and the number of unintended complementary regions increases as the oligonucleotides become shorter (Yasuhara et al., 2022). In the case of allele-specific gene regulation, it is possible that as the length of the ASO increases, the ability of the ASO to discriminate between the mutant and WT alleles decreases. The ASOs designed for the current study were able to discriminate between the WT and mutant alleles (Figure 6.17) and demonstrated allele-specificity in targeting the mutant allele.

It has been observed that ASOs of 25-31 nucleotides in length are favourable for inducing exon skipping or exon inclusion at lower doses than shorter counterparts (Harding et al., 2007; H. Zhou et al., 2013). However, one report demonstrated that for RNase H recruitment LNA-modified ASOs of 12 and 13 nucleotides were more effective than longer counterparts (Straarup et al., 2010; H. Zhou et al., 2013). LNA modified ASOs increase the melting temperature by approximately 3.5°C per modification, resulting in increased ASO binding affinity and thus, potency (Simões-Wüst et al., 2004). Therefore, further optimisation of the ASOs used in the current study may explore the efficacy of shorter sequences.

The central PS backbone DNA region of gapmer ASOs is necessary for RNase H-mediated cleavage of the target RNA, whereas the flanking modified RNA residues protect the ASO from nuclease degradation (Monia et al., 1993). RNase H-mediated RNA degradation using gapmer ASOs with a central PS backbone and flanking 2'-O-modifications is a commonly used strategy for regulating gene expression, with increasing numbers of such ASOs progressing to clinical trial in the last decade for the treatment of various diseases (reviews: (Dhuri et al., 2020; Evers et al., 2015; Lundin et al., 2015; Moumné et al., 2022). RNase H is a ubiquitous enzyme found in the nucleus and to a lesser extent, the cytoplasm of all cells (ten Asbroek et al., 2002). Furthermore, unlike pre-mRNA which is exclusively located in the cell nucleus, coding mRNA molecules are transported through the nuclear envelope to the cytoplasm. Considering both of these factors, it may be possible for ASO:RNA heteroduplex formation to recruit RNase H not just in the nucleus, but also in the cytoplasm. As demonstrated in Figure 6.12B, the ASO was able to successfully reach the cell nucleus following transfection. The 6-FAM-conjugated ASO was also visible in the cytoplasm. A putative cytoplasmic

pathway of gapmer ASO gene regulation following both ASO transfection and gymnotic administration has been described, indicating that nuclear targeting is not the only mechanism of ASO gene silencing (Castanotto et al., 2015). This is supported by another study that demonstrated the increased efficacy of ASOs designed to target mRNA in comparison to those designed to target pre-mRNA, potentially due to the ability of RNase H to elicit its effects in both the nucleus and cytoplasm (Marrosu et al., 2017).

In order to induce mRNA degradation by RNase H, a central portion of at least 5 nucleotides with a PS backbone, with 7-10 being optimal, is usually incorporated into the gapmer ASO design (Frieden et al., 2003; Marrosu et al., 2017; Monia et al., 1993). The efficacy of differing lengths of PS DNA gaps in the central portion of the ASO were explored in the current study. ASOs for each mutation were designed with either a shorter central PS backbone region (ASO C1 and ASO H1 = 7 nucleotides) or a longer central PS backbone region (ASO C2 = 11 nucleotides, ASO H2 = 9 nucleotides). No significant differences in ASO-mediated effects of reducing the mutant *TGFBI* transcript were observed between ASO C1 and ASO C2 (Figure 6.12C). Therefore, in this case, the length of the central PS DNA portion did not seem to significantly affect the efficacy of the ASO. However, in ASO H2 treated samples the mutant transcript was expressed at significantly lower levels than ASO H1 treated samples, indicating that a longer PS backbone was more favourable in this case.

Efficient siRNA-mediated allele-specific knockdown of p.R124C *TGFBI* has previously been reported (Courtney et al., 2014). siRNA administration is a potent method of gene silencing *in vitro*, however, challenges such as the poor *in vivo* stability of the unmodified nucleotides, ineffective cellular uptake, potential off-target effects and immune stimulation have hindered is translation from the bench to the clinic (Frieden et al., 2003). Chemically modified ASOs, such as the ones designed in this study, offer an attractive alternative to siRNA-based therapies.

The reduced expression of *TGFBI* as assessed by qPCR, was supported by the 25-50% reduction in TGFBIp expression observed via western blotting analysis of CEpi cell lysate samples, demonstrating that the ASOs are effective in reducing TGFBI expression at the mRNA and protein level. However, TGFBIp is a secreted ECM protein and evaluating TGFBIp expression levels in the supernatant presented a challenge due to the lack of a secreted reference protein that can be used for quantification. This is a known issue in the evaluation of secreted protein expression (Zou et al., 2019). Alternative methods such as ELISA or a dual secreted luciferase assay may be able to sensitively detect and quantify ASO-medicated knockdown of secreted TGFBIp.

Based on the Sanger sequencing (Figure 6.15) MiSeq and qPCR results (Figure 6.17), WT ASO treatment (Figure 6.12E) the WT transcript was not affected by the ASOs and reduced expression of *TGFBI* was allele specific. This indicates that the potential of ASOs if used in a clinical setting to leave the WT allele of *TGFBI* functioning as normal, while preventing or substantially delaying the onset and severity of mutant TGFBIp accumulations in the cornea. However, unintended potential physiological effects of knocking down one *TGFBI* allele must be considered. Human genome data deposited in the gnomAD database displays the *TGFBI* gene as having a pLI score of zero, indicating that it has a high loss-of-function tolerability and that haploinsufficiency of *TGFBI* does not result in pathology (Fuller et al., 2019). Furthermore, *TGFBI*-null mice do not display corneal abnormalities, with the collagen scaffold comparable to WT mice, supporting *TGFBI* knockdown as a therapeutic prospect (Poulsen et al., 2018). Interestingly, the *TGFBI* CKO iPSC line was successfully differentiated into CEpi cells (Chapter 4, Section 4.2), indicating that *TGFBI* expression is not essential for corneal epithelial cell viability and function. This suggests that partial knockdown of the WT allele by an ASO targeting a *TGFBI* mutation would not result in pathological effects in the cornea. On the other hand, interspecies differences must be considered, *TGFBI* expression is around 10-fold higher in the human cornea respective to mice (Poulsen et al., 2018a). Thus, *TGFBI* expression likely has a more prominent role in the human cornea and we cannot simply extrapolate this finding to humans. Furthermore, TGFBIp has been shown to play a role in wound healing, suggesting that *TGFBI* expression is necessary for corneal homeostasis (Maeng et al., 2017). Although the role of TGFBIp is not fully defined in the human cornea, the ASOs offer a promising option for the treatment of TGFBI CDs due to their allele-specificity.

6.3.3 Allelic imbalance of *TGFBI* in patient derived cell lines.

Allelic imbalance refers to the unequal expression of two different alleles at a particular gene locus. Differential allelic expression is a common occurrence affecting the expression of 20% of human genes which likely partially accounts for inter-individual differences in gene expression and disease phenotypes (Serre et al., 2008). Allelic imbalance has been well documented in various systems, including human, mice and drosophila (C. D. Campbell et al., 2008; Cheung et al., 2005; Cowles et al., 2002; Gruber & Long, 2009; Morloy et al., 2004; Wittkopp et al., 2004; Yan et al., 2002). The targeted NGS data analysis (Figure 6.16) revealed the allelic imbalance of *TGFBI* in 3 out of 4 of the patients included in this study. Allele skewing occurred independent of the pathogenic mutation, as skewing was either not observed or, observed in favour of the WT or mutant allele. Since the specific pathogenic mutations were not responsible for

the differences in allelic balance it is likely that the balance of allele expression may be regulated by *cis*-regulatory polymorphisms in the promoter and enhancer regions of the *TGFBI* gene. These *cis*-regulatory polymorphisms can affect the initiation, rate and pattern of gene transcription, determining the amount of gene product (mRNA and protein) produced by a cell and likely having an effect on disease pathogenesis.

Allelic imbalance has been reported to affect the phenotype of Mendelian disease such as hypertrophic cardiomyopathy and Zellweger spectrum disorder (Falkenberg et al., 2017; Glazier et al., 2019), as well as complex disorders such as endometriosis, cancer and dilated cardiomyopathy (Bielski & Taylor, 2020; Goumenou et al., 2001; van Beek et al., 2023). Allelic imbalances in *TGFBI* may account for the extreme variances in phenotype that have previously been reported for GCDII patients with the same heterozygous p.R124H mutation (K. E. Han et al., 2012). One family of 21 individuals was investigated for variants in *TGFBI*, the proband carried a homozygous p.R124H mutation, and 4 affected and 7 unaffected individuals carried the heterozygous p.R124H mutation (Cao et al., 2009). Following exclusion of a late disease onset, variable expressivity or non-penetrance of GCDII was concluded for this family. Given the novel findings of allelic skewing described in this chapter, the mechanism underlying this variation in phenotype may be the allelic imbalance of *TGFBI*. Specifically, the p.R124H carriers who presented with no penetrance (Cao et al., 2009) may only be expressing the mutant allele at low levels suppressed in the cornea by *cis*-regulatory mechanisms.

Much of the research exploring allelic imbalance has focused on the monoallelic expression of certain genes. A recent study which used bulk RNA sequencing to profile random monoallelic expression (RAE) in human tissues reported that RAE is enriched for genes that are non-essential, more tolerant of loss of function mutations and linked to later-onset diseases (Kravitz et al., 2023). Furthermore, these genes had a significantly higher intragenic density, absolute number and diversity of *cis*-regulatory elements than the biallelic genes tested (Kravitz et al., 2023). It is clear from the targeted NGS data that both alleles of *TGFBI* are expressed by the four patients included in the current study and it is not expressed in a monoallelic manner. Importantly, *TGFBI* appears to be tolerant of loss of function mutations, as mentioned above. Furthermore, the targeted NGS data (Figure 6.16) shows relative expression of the two alleles of each individual in a cell context appropriate to the corneal dystrophies under investigation such that *TGFBI* polymorphisms in the *cis*-regulatory promotor or enhancer regions of *TGFBI* may have tissue specific effects, leading to the patient-patient differences in allelic expression that we observe.

TGFBI is found on chromosome 5, one of the largest human chromosomes which displays one of the lowest gene densities (Schmutz et al., 2004). This provides support for the allelic imbalance of *TGFBI* as genes that reside in gene-dense regions are less likely to exhibit allelic imbalance than those in less dense regions of the genome (Tung et al., 2009). Furthermore, genes that are pleiotropic and are unevenly expressed in the human body are more likely to have allelic imbalance than those evenly expressed (Tung et al., 2009). The pleiotropy of *TGFBI* has been documented, particularly for its role in cancer, where it has been reported to act as both a tumour promotor and tumour suppressor, depending on the tumour microenvironment (Ween et al., 2012). Thus, taking into account the past reports that define genes susceptible to allelic imbalance, along with the data presented here (Figure 6.16), *TGFBI* appears to be a fitting candidate for a gene subjected to allelic imbalance. The allelic skewing defined in this chapter could have important implications for these cancer studies. Genetic variants affecting gene regulation act predominantly in a cell type-specific manner, with an estimate of 69-80% of regulatory variants being cell type-specific (Dimas et al., 2009). The cell type-specific regulation of genes may contribute to the corneal specificity of TGFBI CD, as *TGFBI* is highly expressed in the human cornea. Therefore, it would be interesting to investigate the allelic imbalance of *TGFBI* in other tissues including the corneal tissue of CD patients to assess whether this is the case for *TGFBI*, while also providing information on the complexity of *TGFBI* gene regulation.

Polymorphisms in the *cis*-regulatory region of *TGFBI* would alter its expression in an allele-specific manner, whereas genetic effects acting in *trans* to the gene would influence both alleles (Cheung et al., 2005; Morloy et al., 2004). This corresponds to the CEpi data, as overall expression levels of *TGFBI*/TGFBIp (Figure 6.5) do not correspond to the presence or direction of allelic imbalance (Figure 6.16). In the case that the WT allele is expressed more than the mutant allele or vice versa, no correlation was observed with total *TGFBI*/TGFBIp levels.

Future research could identify key polymorphisms in the *cis*-regulatory regions of *TGFBI* so that these polymorphisms could be screened alongside the pathogenic *TGFBI* variants in families with TGFBI CD. It would also be ideal to explore this further by assessing the allelic imbalance of *TGFBI* in a large sample size. Locating and defining polymorphisms responsible for allelic imbalance is a challenge, due to the wide spectrum of *cis*-acting regulatory mechanisms, the inconsistent effects of regulatory polymorphisms in different tissues and the difficulty in isolating the causal polymorphisms that are in linkage disequilibrium with many other variants (Pastinen & Hudson, 2004). In the case of *TGFBI*, non-coding regions of the gene, in particular the promoter regions,

located 1 kb upstream of the 5' translation site (Yuan et al., 2004), as well as the 3'UTR miRNA binding sites (C. Liu et al., 2011) should be investigated for elucidation of *TGFBI* gene regulation. Additionally, studies into linkage disequilibrium could identify other polymorphisms that segregate with the pathogenic mutation, potentially indicating candidates responsible for the allelic imbalance. Furthermore, the possibility that the allelic imbalance is not due to Mendelian inheritance patterns may be worth exploring, by investigating epigenetic mechanisms that regulate allelic expression.

Collectively, the data presented in this chapter provide evidence that the ASOs reduce *TGFBI*/TGFBIp in a mutant allele-specific manner, with minimal or no influence on the expression of WT *TGFBI*. These findings support the further evaluation of the ASOs as a promising treatment for TGFBI CDs. A more thorough understanding of the differences between fragmented or multimerised forms of mutant and WT TGFBIp may help to identify potential biomarkers that could provide a functional readout following ASO treatment *in vitro* and *in vivo*. Further knowledge of the influence of *TGFBI* allelic imbalance in disease severity would facilitate more accurate dosing to achieve appropriate ASO-mediated reduction of the mutant *TGFBI* allele.

Chapter 7: General discussion

CDs are a diverse group of conditions that can range from causing mild or no symptoms, to severe visual impairment. The heterogeneity of TGFBI CDs underscores the pronounced specificity of the role of TGFBIp in the cornea where it is highly expressed. Many patients with TGFBI CDs experience severe visual impairment and require therapy for its correction, with therapeutic interventions such as laser ablation for anteriorly-located corneal lesions and corneal transplantation representing available options. However, due to the underlying genetic cause of CDs, symptoms do reoccur so there is a need to develop therapeutic approaches that address the underlying genetic cause of disease. The accessibility and immuneprivilege of the cornea make it an exceptional model for the development of gene silencing therapeutics, which with progress in research, could lead to future clinical trials for numerous autosomal dominant conditions that are caused by missense mutations. With the aim of addressing this need for TGFBI CDs, the current thesis has focused its investigation on establishing new models of disease using TGFBI CD patient cell lines, the implementation of an *in vitro* CEpi cell model, the transcriptomic signatures of WT and mutant TGFBI CEpi samples and the development of an allele-specific gene silencing therapy.

Through the genetic screening of the MEH patient cohort by the Hardcastle laboratory, patients with the p.R124C and p.R124H TGFBI CD-causative mutations were recruited to this study. Four patients (two p.R124C and two p.R124H) donated skin biopsies enabling the establishment of TGFBI CD patient-derived iPSC lines, representing the first report describing p.R124 TGFBI CD iPSC lines, which hold immense value for disease modelling and therapeutic screening. As evidenced by the MEH patient cohort and numerous other reports (Chao-Shern et al., 2019; Evans et al., 2016; Jozaei et al., 2022; Y. Song et al., 2017; J. Yang et al., 2010), the p.R124 hotspot mutations that are of focus in the current study are two of the most common in TGFBIp. Both of these mutations cause an amino acid change at the same codon, however, as in the patient clinical images and profiles presented in **Chapter 3**, LCDI caused by p.R124C and GCDII caused by p.R124H, present with strikingly different phenotypes. The two LCDI patients recruited to this study have both undergone multiple therapeutic interventions for the treatment of their condition, with both suffering from severe and prominent recurrence of symptoms. Treatment complications also arose, such as the development of glaucoma or cataracts due to post-operative corticosteroid application and graft rejection. These cases clearly demonstrate the need for a more effective treatment that targets the underlying genetic cause of TGFBI CDs, while also highlighting the value of genetic screening of patients in the identification of this need. As is characteristic of GCDII

caused by heterozygous p.R124H TGFBIp mutations, patients with this diagnosis recruited to the current study had a slower progression of TGFBIp+ deposition and corneal opacification. The later age of onset of GCDII and the contraindication of LASIK for this condition reinforces the significance of routine genetic screening prior to undergoing such treatments, especially because in numerous countries, GCDII accounts for the highest number of TGFBI CD cases and LASIK is proven to exacerbate symptoms (Banning et al., 2006; Chao-Shern et al., 2018; Jiang & Zhang, 2021; T. I. Kim, Kim, et al., 2008; Poulsen et al., 2016; Roh, Grossniklaus, et al., 2006a, 2006b). It is also important to note that genetic screening is necessary even in the absence of a positive family history, as both patient 2 (LCDI) and patient 3 (GCDII) had no known or reported positive family history.

CD-causative mutations in *TGFBI* affect different tissues of the cornea depending on the mutation and the severity of the condition. Nonetheless, it is expected that a substantial proportion of TGFBIp is produced by the corneal epithelium and secreted into underlying tissues (Chapter 4, Section 4.1.1). The initial examination of publicly available scRNAseq data in **Chapter 4** revealed a prominent co-expression pattern between *TGFBI* and corneal epithelial-specific transcripts at a single cell resolution, indicating that the corneal epithelium plays a crucial role in TGFBIp synthesis in both healthy and diseased conditions. This finding validates the strategy of utilising a patient-derived iPSC-CEpi model for the purpose of disease modelling and screening for a potential therapeutic intervention. The implementation of the iPSC-CEpi model provides a more accurate representation of the actual disease state in comparison to the commonly used *in vitro* overexpression models. Yet the corneal epithelium, being a highly specialised tissue, poses significant challenges in terms of accurately recapitulating its complex characteristics and functions *in vitro*. Thus, the model would still benefit from optimisation, in order to facilitate the recapitulation of corneal-specific characteristics that cause pathological TGFBIp deposition.

The *in vitro* CEpi cell model was used for the assessment of transcriptomic differences between WT and TGFBI CD; and WT and TGFBI KO lines **(Chapter 5)**. The analysis prompted questions about the corneal specific-protein interactions of TGFBIp. As an ECM protein that is known to play different roles in different microenvironments, evidenced by research into its role in cancer, it is of particular importance to define its role and protein interactions in the cornea in the understanding of CD pathophysiology. TGFBIp possesses the ability to interact with other proteins through its RGD domain and FAS1 domains (J. E. Kim, Jeong, et al., 2002; Son et al., 2013), facilitating molecular interactions and potentially influencing various biological processes in a context-specific

manner. As the specific microenvironment of the cornea is necessary for the formation of mutant TGFBIp+ deposits, it is likely that TGFBIp undergoes cornea-specific protein interactions, and the pathogenic mutations may affect these interactions.

The patient-derived *in vitro* model was also used for the development of an ASO treatment for TGFBI CD. Gapmer ASOs were successful in reducing *TGFBI* expression in a mutant allele-specific manner, presenting a promising therapeutic avenue for these conditions **(Chapter 6)**. The success of the ASO in selectively silencing the mutant allele highlights the potential of this approach as a precise and tailored strategy for treating genetic disorders. Currently available CD treatments only provide temporary symptom relief, can exacerbate symptoms, are subject to tissue availability and can cause severe complications. Consequently, the ASO therapy developed holds significant potential in the fundamental transformation of the prevention and treatment of these conditions.

7.1 Addressing Challenges and Considerations of Model Systems in TGFBI Research

Understanding of the role of TGFBIp in healthy and diseased tissue remains limited due to various factors, many of which are relevant to other disease-related proteins. To comprehensively investigate disease mechanisms and evaluate potential therapeutic interventions, the utilisation of appropriate disease models is crucial. However, existing animal models fail to faithfully replicate the precise phenotype of human TGFBI CD. Additionally, the study of ECM proteins such as TGFBIp, poses challenges, as does the replication of the highly specialised microenvironments present in the human cornea, which is particularly challenging within *in vitro* settings.

As previously discussed (Chapter 1, Section 1.5.3), the limited replication of human disease in TGFBI CD mouse models can be attributed to interspecies differences. Human CD disease samples have also been used to provide insight into TGFBIp species and other proteins expressed in corneal aggregates (Courtney et al., 2015; Venkatraman et al., 2017, 2019). However, such samples are not always readily available for research and only allow for investigation of late disease stages. Overexpression cell models have previously been used to investigate TGFBIp (Y. P. Han et al., 2011, 2012). However, such methods disrupt the delicate balance of protein expression, spatiotemporal expression patterns and protein-protein interactions; and do not accurately reflect normal physiological conditions. Other impactful research in the field of TGFBIp pathology includes biophysical studies utilising methods such as mass spectrometry and chromatography techniques (Andersen et al., 2004; Basaiawmoit et al., 2011; García-Castellanos et al., 2017; Underhaug et al., 2013). Such reports have provided knowledge

on the structure and potential protein interaction domains of TGFBIp. Some of these studies have provided information on the amyloidogenic properties of mutant TGFBIp peptides (Schmitt-Bernard et al., 2000, 2002), although they fail to account for full length and secreted mutant TGFBIp. Nevertheless, the *in vitro* replication of an environment that sufficiently recapitulates the *in vivo* characteristics of the cornea would be essential in understanding the specific pathogenic TGFBIp interactions in the cornea.

The *in vitro* model employed in the current study demonstrated clear limitations and would benefit from optimisation. The mixed population of cells that result from the CEpi differentiation could confound downstream experiments in various ways. Differences in proportions of cell types present between cell culture wells would likely cause variance in *TGFBI*/TGFBIp expression levels, affecting comparisons of TGFBI expression between cell lines and causing variation within cell lines when repeating experiments. Further, the different cell populations of the cultures may confer differences in ASO transfection efficiency between different cell types, confounding the analysis of *TGFBI*/TGFBIp downregulation following ASO treatment experiments, leading to inconsistences and inaccuracy of experimental replicates. Additionally, transcriptomic analyses such as the bulk RNAseq data presented in the current thesis can easily be confounded by mixed cell populations, resulting in the obtainment of data that is not relevant to the questions being asked. For these reasons, and taking into account the lack of *KRT12* expression of the model used in the current study, future work conducted to build on the findings of the current study, should prioritise the optimisation of the CEpi differentiation and the FACS purification of the CEpi cells.

The aggregation of mutant TGFBIp either intracellularly or extracellularly has not been observed in *in vitro* models. In the human cornea, approximately 60% of TGFBIp is associated with insoluble components of the ECM (Andersen et al., 2004). In the diseased cornea, TGFBIp preferentially aggregates in the ECM as demonstrated by histopathology studies (Dighiero et al., 2001; Gruenauer-Kloevekorn et al., 2009; Qiu et al., 2016; Santo et al., 1995) and its role in facilitating ECM protein interactions (Billings et al., 2002; Gibson et al., 1997; Hanssen et al., 2003; Reinboth et al., 2006) is likely related to its pathological deposition. This provides indication that abnormal TGFBIp-protein interactions may be contributing to pathophysiology and that the ECM component is key for TGFBI CD disease modelling. *In vitro* models do not currently facilitate the investigation of secreted ECM proteins, due to lack of tissue structure and requirements for regular media changes, thus compromising the length of time required for secreted protein accumulation and the resulting protein-protein interactions. Nonetheless, whether or not the CEpi cultures used in the current study were capable of laying down

their own ECM was not assessed, and could have been assessed through the ICC staining of ECM components such as collagen IV.

To address the need for an appropriate ECM structure *in vitro* and to evaluate phenotypic differences between WT and mutant or KO TGFBI samples, the generation of corneal organoids offers an alternative valuable approach. Corneal organoids have a comparable transcriptomic profile to the developing cornea and exhibit ECM structures composed of collagen microfibrils (Foster et al., 2017; Maiti et al., 2022). Along with the utilisation of the p.R124 iPSC lines generated in the current study, this method holds promise for investigating the formation and characteristics of the ECM in a controlled environment, enabling a deeper understanding of TGFBI-associated pathologies. On the other hand, assessing the efficacy of an ASO treatment is more challenging when using 3D model structures such as organoids. Nonetheless, all models employed to investigate disease possess strengths and limitations, emphasising the requirement of considering multiple complementary systems to gain a more comprehensive understanding of TGFBIp, its involvement in disease and for the development of a prospective treatment.

7.2 Challenges and prospects of gene directed therapeutics for TGFBI CD

The corneal epithelium synthesises a substantial amount of *TGFBI* transcript, indicating that it is responsible for a considerable portion of TGFBIp secretion (Chapter 5, Section 4.2.1). This is mirrored by reports that show, following corneal transplantation, corneal deposits initially reoccur in close proximity to the corneal epithelium, with minimal or no deposition observed in the corneal stroma (Chapter 6, Section 6.1.1.2). The constant turnover of the epithelial cells results in the continuous production of TGFBIp in the anterior cornea. Due to the lengthy recovery process, lack of donor tissue availability and complications such as graft rejection, corneal transplantations are not an appropriate treatment to receive more than once. In order to address the need for an alternative treatment, a gene directed ASO-based treatment was developed for the purpose of reducing expression of the mutant allele of *TGFBI* (Chapter 6). Theoretically, gene directed therapies for TGFBI CDs would allow for the direct targeting of *TGFBI* expression only, whilst also avoiding side effects that may be caused by treatment of pharmacological compounds that do not act directly and solely on TGFBIp.

Other groups have also focused on the reduction of *TGFBI* expression by gene directed therapy as a potential treatment for TGFBI CDs, employing siRNA (Courtney et al., 2014; Yellore et al., 2011) or CRISPR techniques (Christie et al., 2017; Taketani et al., 2017b) to decrease *TGFBI* expression, either in an allele-specific or non-allele-specific manner.

CRISPR/Cas9 is a promising therapeutic approach with significant potential, but it also faces limitations and challenges that need to be addressed before its clinical implementation. Such limitations include off-target modifications, autoimmune reactions and limited target options. ASOs and siRNAs are two of the most commonly used strategies for RNA silencing. Both share important similarities although they assert gene silencing by different intracellular molecular mechanisms. One of the main differences is that siRNAs are double-stranded, whereas ASOs are single stranded. ASOs are more versatile overall, as they can exert different mechanisms of target modulation (Chapter 6, Section 6.1.4) whereas siRNAs can only work to reduce target gene expression. ASOs are also amenable to varied chemical modifications to improve efficacy and specificity, whereas siRNAs are more limited in this aspect (Y. Kim, 2023).

Several studies have compared the efficacy of siRNAs compared to ASOs, with most of the reports concluding that the *in vitro* efficacy of the former seems to surpass the latter (Bertrand et al., 2002; Grünweller et al., 2003; Kretschmer-Kazemi Far & Sczakiel, 2003; Miyagishi et al., 2003). One study however, reported that siRNAs and RNase H-dependent ASOs exhibited similar levels of potency, maximal effects, specificity and duration of action *in vitro*; although ASOs were able to target both pre-mRNA and coding mRNA, whereas siRNAs only targeted coding mRNA (Vickers et al., 2003). Nevertheless, *in vivo* studies directly comparing the efficacy of siRNAs and ASOs are currently lacking. Different animal models of Huntington's disease have been used to test siRNAs or ASOs. siRNAs infused into the monkey brain only reached brain tissue up to around 12 mm from the infusion site (A. E. Ross et al., 2019), whereas ASOs infused into the cerebral spinal fluid of mice exhibited a wide distribution (Gagnon, 2010). As it currently stands, siRNA vs ASO efficacy *in vivo* is debateable, although research will continue to evolve as these therapies are increasingly entering clinical trial testing phases.

Relative to other tissues that are implicated in disease, the cornea is easily accessible for therapeutic intervention, however its treatment still poses challenges in the field of ophthalmology. The ideal ASO delivery method of choice would be topical application perhaps in the form of eye drops, which would be a non-invasive and convenient method of administering ASO treatment to the anterior cornea. Topical eye drop application to the cornea of the FDA-approved ASO drug Aganirsen which targets the insulin substrate-1 receptor has shown efficacy in clinical trial (Cursiefen et al., 2014), providing support for the topical application of ASOs to the cornea. However, the bioavailability of the therapeutic eyedrops is likely to be negatively affected by precorneal factors such as solution drainage, blinking, tear film and lacrimation that may also confound accurate

dosing (Gaudana et al., 2010). For ASO treatments to function effectively as a topical treatment, strategies must be implemented to increase the resident time of drugs in the precorneal region. Topical drug delivery could be enhanced by the use of therapeutic contact lenses or corneal patches loaded with the drug. Contact lens drug delivery systems have been shown to increase drug bioavailability to the anterior eye by increasing the residence time of the therapeutic (Desai et al., 2020; Franco & De Marco, 2021; Rykowska et al., 2021; Sartini et al., 2021; H. Zhang et al., 2014). This drug delivery method has received attention in the treatment of glaucoma, with one study demonstrating that drug loaded lenses were superior in reducing intraocular pressure compared to eye drops while requiring a much lower dosage overall (Hsu et al., 2015). Additionally, delivery of dexamethasone by contact lens to the rabbit eye achieved sustained drug delivery to the retina at therapeutic levels, with retinal drug concentrations being 200 times greater than those treated with drops (A. E. Ross et al., 2019). Furthermore, epidermal application of topical ASOs has proven effective in achieving target effects in models of mice (Venuganti et al., 2015), rat (Özbaş-Turan et al., 2010), 3D human skin tissue and in human clinical studies (Y. I. Lee et al., 2023).

Lipid nanoparticle (LNP) delivery systems offer a promising approach for enhancing intracellular ASO delivery to the cornea. Nanotechnology has dramatically impacted the field of ocular drug delivery by enabling the cellular internalisation and enhancing the bioavailability of therapeutic molecules (Kamaleddin, 2017; Saraiva et al., 2017; Srinivasarao et al., 2019; Weng et al., 2017). A hybrid silicon-lipid nanoparticle delivery system has shown the ability to complex with siRNAs and enhance delivery to all layers of the cornea in mice following topical application (Baran-Rachwalska et al., 2020). Furthermore, research has demonstrated that LNP-gapmer ASO formulations significantly improved silencing of the *Pten* gene in mice compared to non-formulated gapmer ASOs (Prakash et al., 2013), demonstrating the efficacy of LNP-ASO formulations. The development of a gene-directed topical ocular treatment would be a ground-breaking advance in the treatment of genetic ocular diseases, by providing a convenient and effective preventative therapeutic. Overall, topical LNP-ASO administration to the cornea by therapeutic contact lenses is a very attractive prospect that should receive attention for the treatment of CDs.

Other more conventional drug delivery methods include intraocular injections such as intracameral or intravitreal injection. An ASO designed to reduce the expression of the noncoding nuclear RNA, Metastasis-Associated Lung Adenocarcinoma Transcript 1 (*MALAT1*) was shown to achieve a dose-dependent reduction in the mouse cornea following intravitreal or intracameral injection (Chau et al., 2020). This report

demonstrates that *in vivo* ASO delivery to the cornea through intraocular injection is feasible and effective. However, intraocular injections are not considered pleasant for patients and can cause discomfort, pain, and the potential risk of infection or damage to ocular structures. Common side effects include increased intraocular pressure, inflammation, and the potential for retinal detachment.

For conditions such as TGFBI CDs, where genetic mutations affect cells with a high turnover rate, long-term management and repeated treatments are necessary. Thus, topical drug delivery holds significant advantages for the patient and also for reducing the medical burden of side effects associated with intraocular injections. Taking the different factors into account, focus of a potential CD therapeutic delivery mechanism should prioritise topical application.

The ASO treatment developed in this study demonstrated effectiveness in the CEpi model, providing initial evidence of ASO efficacy. However, multiple cell types and tissue structures are involved in TGFBI CD pathogenesis. *In vitro* models cannot replicate the complexity and three-dimensional architecture of the eye and ASO efficacy is reliant on targeting the cells of the limbus, corneal epithelium and stroma. Furthermore, ASO safety must be assessed. Progression of ASO efficacy evaluation would involve the administration of ASOs to mouse models, which would provide a more realistic representation of the ocular environment. Testing in mouse models would enable further investigations of allele specific *TGFBI* reduction as well as assessment of the safety and appropriate delivery methods enabling further progression of ASO validation as a therapeutic. However, due to interspecies differences between mice and humans, accurate assessment of alleviating symptoms or biomarkers of disease such as TGFBIp aggregates is currently not possible.

It is important to note that the ASO therapies designed in the current study are for the purpose of prevention of developing the symptoms, as they work intracellularly using an RNase-H dependent mechanism and are not capable of influencing the clearance of extracellular insoluble protein deposits. Therefore, genetic screening in conjunction with ASO administration would enable prevention of loss of vision, although for patients at more advanced stages of disease, ASOs could be prescribed following corneal transplantation to avoid the recurrence of symptoms. Other factors to consider prior to a clinical trial for ASOs include the timing of intervention and frequency of administration.

The ASOs designed as part of this study offer promising therapeutic prospects in the treatment of TGFBI CD, and the delivery methods reviewed may be appropriate for drug administration. However, the main barrier to progressing towards *in vivo* studies and the

development of appropriate delivery methods is obtaining funding. As TGFBI CDs are rare, and considered treatable through surgical methods, funding is more difficult to secure. The lack of funding for such rare diseases prevents the progression of breakthrough therapies from reaching patients and their families who would benefit greatly from such treatments. Furthermore, TGFBI disease onset and the side effects of conventional treatments, such as graft rejection, place a substantial burden on the medical system. Additionally, the significance of ASO therapy for specific TGFBI CDs extends beyond treatment of these genetic disorders, owing to the shared molecular mechanisms and potential ASO applicability across different genetic disorders. By understanding and overcoming the challenges associated with developing ASO therapies for TGFBI CDs, such as optimising ASO design, delivery methods, and safety profiles, researchers can expand their knowledge and expertise in developing ASO-based treatments for other genetic disorders. Therefore, advancements made in the development of ASO therapies for TGFBI CD can serve as a valuable blueprint and contribute to the progress of treatments for many other diseases, potentially improving the lives of patients affected by different genetic disorders.

7.3 Limitations and future prospects

In order to acknowledge the importance of a comprehensive and varied approach to scientific research, it is necessary to consider the limitations of every study.

At least 78 different mutations (Table 9.1, Appendix B) in *TGFBI* lead to subtypes of TGFBI CDs, this study developed a gene-directed treatment for two of these mutations. The approach to developing *in vitro* models and method of ASO development described in this study could be replicated to generate ASOs for other common *TGFBI* hotspot mutations (p.R124L, p.R124S, p.R555W and p.R555Q) which are responsible for a substantial proportion of cases worldwide (Chao-Shern et al., 2019; Y. Song et al., 2017). However, this approach may not be practical for the ASO development for all pathogenic *TGFBI* mutations. In this case, the construction of different pathogenic variants of *TGFBI* genetically fused to a luciferase reporter may enable a high throughput method of screening multiple ASOs for each mutation by luciferase assay, prior to testing *in vitro*.

Other potential treatment strategies could employ a mutation-dependent approach such as the one demonstrated by Christie et al. (2020), where an array of SNPs that were located within the mutant *TGFBI* allele were targeted by CRISPR/Cas9 editing. This offers a strategy that could be applied to TGFBI CD patients irrespective of the specific disease-causing mutation, but would require whole genome sequencing and perhaps long-read NGS to be carried out on a wide range of patients to identify SNPs in *cis* with

the mutated allele. Another treatment strategy was described by Venkatraman et al. (2020) whereby 2500 compounds were screened using weak affinity chromatography to identify molecules able to bind to mutant TGFBIp, two lead compounds able to delay/prevent the generation of amyloidogenic peptides caused by the p.H572R mutation in *TGFBI* were identified.

As highlighted in Chapter 6 (Section 6.1.1), differences in autophagy and mitochondrial function have been observed between WT and GCDII corneal keratocytes. Autophagy function could be explored using the CEpi model employed in the current study, by subcellular detection of the autophagy protein LC3 by ICC. Co-staining of TGFBIp, using the antibody identified as specific through the data presented in Chapter 4 (Section 4.2.5), and LC3 might also help to elucidate whether there are differences in subcellular localisation of TGFBIp between WT and mutant CEpi cells. Seahorse assays can be used to assess mitochondrial function of the CEpi model. Future work conducting these experiments would contribute to the question of whether autophagy and mitochondrial dysfunction play a role in TGFBI CD pathogenesis.

The current study did not conclude whether all iPSC lines used for CEpi differentiation were able to differentiate into cells the three germ layers. This is easily done through experiments such as the TaqMan hPSC Scorecard Panel assay and should ideally by assessed before differentiations are carried out. Nonetheless, future work should address this issue. In addition, differences in differentiation capacity between cell lines should be investigated. As discussed in Chapter 4 (Section 4.3), the WT1 line did not demonstrate positive expression of K5 and K14, which could be due to poor differentiation capacity of this line, or a poor differentiation batch. In order to address this, comparison of relevant CEpi marker expression between cell lines should be carried out.

One of the main limitations in the current study is the confounding effect caused by using controls with a different genomic profile than the patient lines. The use of gene editing in the generation of isogenic controls for each patient line would provide a critical baseline for comparison by minimising genetic variation and background effects such as those posed by mutation-independent environmental conditions, age, sex and physiological differences between individuals while also enhancing the reproducibility of results. This would greatly assist in gene expression analyses in WT vs mutant experiments such as the DEG analysis on bulk RNAseq data carried out in Chapter 5, and should be the focus for future work.

Furthermore, the ASO treatments in the current study used lipofectamine transfection which greatly enhances transfection efficiency. This method was useful in assessing the

potential of the ASO to knockdown *TGFBI*, but it is not translational to a clinical setting. Thus, a gymnotic approach to ASO delivery should be investigated, as this would correlate much better to *in vivo* activity. Effective gymnotic ASO delivery *in vitro* has been demonstrated for the ASO screening of disorders such as retinitis pigmentosa (Dulla et al., 2021) and amyotrophic lateral sclerosis (Tran et al., 2022).

Additionally, the model utilised in the current study should be optimised in order to thoroughly assess corneal epithelial-specific differences between WT and control (discussed in Chapter 4 Section 4.3). The implementation of a more appropriate model, such as corneal organoids, may allow for a more relevant assessment of transcriptomic or phenotypic differences between mutant, KO and isogenic control cell lines, nevertheless differentiation of corneal organoids is technically much more challenging with a lengthy protocol that may also need to be optimised. The generation of corneal organoids from the *TGFBI* KO iPSC line could provide invaluable knowledge of the corneal-specific function and protein interactions of TGFBIp. Generating corneal organoids from mutant *TGFBI* lines would potentially help to elucidate biomarkers of disease and allow for assessment of phenotypic rescue following ASO treatment through methods such immunohistochemistry, mass spectrometry and proteomics and RNAseq (singe cell and bulk), to progress our knowledge of TGFBI CD pathogenesis while also providing support for the ASO therapeutic. This is of significant importance, as previously mentioned, mouse models have proven ineffective in recapitulating the human disease phenotype and ASO treatment of an *in vitro* model representative of the *in vivo* disease conditions could guide future preclinical studies. Data obtained from scRNAseq or bulk RNAseq of healthy vs TGFBI CD corneas would also be highly valuable in attaining information on over-represented/enriched molecular processes and disease biomarkers, assisting in the development of a functional disease-prevention assay of ASO treatment. scRNAseq has been useful in providing molecular insights into keratoconus, revealing dysregulation of genes involved in collagen biogenesis, proteoglycans and ECM degradation, as well as genes involved in the TGFβ and WNT signalling pathways in keratoconus corneas compared to WT (J. Collin et al., 2021).

7.4 Concluding remarks

TGFBI CDs are caused by various autosomal dominant mutations in the *TGFBI* gene (Table 9.1, Appendix B), which cause an accumulation of TGFBIp+ deposits in the cornea. Protein deposition pattern, location and disease progression are dependent on the specific *TGFBI* mutation and the age of onset is usually within the first two decades of life. The current study demonstrated the implementation of an iPSC-corneal epithelial-

like cell model for the context-specific disease modelling and therapeutic screening of the p.R124 hotspot TGFBI CDs, lattice corneal dystrophy type I (p.R124C) and granular corneal dystrophy type II (p.R124H).

p.R124-variant iPSCs were reprogrammed from patient-derived fibroblasts to enable the differentiation of corneal epithelial-like cells (Chapter 3). The differentiated mutant samples, as well as differentiated WT control samples, expressed TGFBI and corneal epithelial cell markers (Chapter 4), enabling the study of mutant TGFBI in an appropriate genetic and physiological context. The transcriptomic signatures of the mutant and KO lines were compared to the WT lines (Chapter 5), which reinforced the necessity of elucidating TGFBIp cornea specific functions and protein-interactions.

The prospect of developing a mutant allele-specific treatment working to downregulate pathogenic TGFBI expression was investigated (Chapter 6). The ASOs designed successfully reduced expression of the mutant allele of TGFBI utilising the in vitro disease model, providing powerful proof of principle that ASOs are effective in the allele-specific reduction of the p.R124C and p.R124H mutant TGFBI transcripts. This therapeutic mechanism can also be applied to other TGFBI CD mutations as well as, other disease-causing missense variants of other genes.

Nonetheless, continued scientific research is necessary for unravelling the complex molecular mechanisms underlying TGFBI CD and identifying specific disease signatures both in the native cornea and through the utilisation of appropriate corneal models. The potential demonstrated by patient-derived disease models and gene-directed ASO therapeutics in the current thesis offers therapeutic prospects for patients suffering from TGFBI CD. Further advancements in scientific research, collaboration among researchers and clinicians, and the integration of cutting-edge technologies will be vital in bringing these therapies to fruition and improving the lives of those in need.

This thesis presents proof-of-concept of the implementation of an iPSC-corneal epithelial-like cell model for the context-specific disease modelling and therapeutic screening of gene and mutation directed therapies. ASOs were effective for allele-specific targeting of the mutant *TGFBI* p.R124C and p.R124H transcripts. The prospect of developing a mutant allele-specific treatment has been experimentally realised, and the anticipated outcome if this treatment reached the clinic, would be prevention of the toxic build-up of aggregated TGFBIp and vision loss.

Future research and knowledge gained should address the limitations described, so that biomarkers of disease can be identified that would represent outcome measures of efficacy. This proof-of-concept study could be readily expanded to include more or all

TGFBI CD mutations, and to address therapeutic needs for other epithelial-stromal CDs caused by mutations in other genes. Further advancements in scientific research, collaborations between researchers, clinicians, and industrial partners, together with the integration of cutting-edge technologies will be vital in bringing these therapies to fruition and improving the lives of those individuals with rare disease in need of new therapies.

Chapter 8: References

Aartsma-Rus, A., & Krieg, A. M. (2017). FDA Approves Eteplirsen for Duchenne Muscular Dystrophy: The Next Chapter in the Eteplirsen Saga. In *Nucleic Acid Therapeutics* (Vol. 27, Issue 1). https://doi.org/10.1089/nat.2016.0657

Aartsma-Rus, A., van Vliet, L., Hirschi, M., Janson, A. A. M., Heemskerk, H., de Winter, C. L., de Kimpe, S., van Deutekom, J. C. T., 't Hoen, P. A. C., & van Ommen, G. J. B. (2009). Guidelines for antisense oligonucleotide design and insight into splice-modulating mechanisms. *Molecular Therapy*, *17*(3). https://doi.org/10.1038/mt.2008.205

Aberdam, D., Gambaro, K., Rostagno, P., Aberdam, E., De La Forest Divonne, S., & Rouleau, M. (2007). Key role of p63 in BMP-4-induced epidermal commitment of embryonic stem cells. In *Cell Cycle* (Vol. 6, Issue 3). https://doi.org/10.4161/cc.6.3.3800

Abhari, S., Eisenback, M., Kaplan, H. J., Walters, E., Prather, R. S., & Scott, P. A. (2018). Anatomic Studies of the Miniature Swine Cornea. *Anatomical Record*, *301*(11). https://doi.org/10.1002/ar.23890

Adachi, K., & Schöler, H. R. (2012). Directing reprogramming to pluripotency by transcription factors. In *Current Opinion in Genetics and Development* (Vol. 22, Issue 5). https://doi.org/10.1016/j.gde.2012.07.001

Afanasyeva, T. A. V., Corral-Serrano, J. C., Garanto, A., Roepman, R., Cheetham, M. E., & Collin, R. W. J. (2021). A look into retinal organoids: methods, analytical techniques, and applications. In *Cellular and Molecular Life Sciences* (Vol. 78, Issues 19–20). https://doi.org/10.1007/s00018-021-03917-4

Afshari, N. A., Mullally, J. E., Afshari, M. A., Steinert, R. F., Adamis, A. P., Azar, D. T., Talamo, J. H., Dohlman, C. H., & Dryja, T. P. (2001). Survey of patients with granular, lattice, avellino, and Reis-Bücklers corneal dystrophies for mutations in the BIGH3 and gelsolin genes. *Archives of Ophthalmology*, *119*(1).

Ahlfeld, S. K., Wang, J., Gao, Y., Snider, P., & Conway, S. J. (2016). Initial suppression of transforming growth factor-β signaling and loss of TGFBI causes early alveolar structural defects resulting in bronchopulmonary dysplasia. *American Journal of Pathology*, *186*(4). https://doi.org/10.1016/j.ajpath.2015.11.024

Ahmad, S., Stewart, R., Yung, S., Kolli, S., Armstrong, L., Stojkovic, M., Figueiredo, F., & Lako, M. (2007). Differentiation of Human Embryonic Stem Cells into Corneal

Epithelial-Like Cells by In Vitro Replication of the Corneal Epithelial Stem Cell Niche. *Stem Cells*, *25*(5). https://doi.org/10.1634/stemcells.2006-0516

Ahmed, A. A., Mills, A. D., Ibrahim, A. E. K., Temple, J., Blenkiron, C., Vias, M., Massie, C. E., Iyer, N. G., McGeoch, A., Crawford, R., Nicke, B., Downward, J., Swanton, C., Bell, S. D., Earl, H. M., Laskey, R. A., Caldas, C., & Brenton, J. D. (2007). The Extracellular Matrix Protein TGFBI Induces Microtubule Stabilization and Sensitizes Ovarian Cancers to Paclitaxel. *Cancer Cell*, *12*(6). https://doi.org/10.1016/j.ccr.2007.11.014

Akiya, S., Takahashi, H., Nakano, N., Hirose, N., & Tokuda, Y. (1999). Granular-lattice (Avellino) corneal dystrophy. *Ophthalmologica*, *213*(1). https://doi.org/10.1159/000027395

Akiyoshi, S., Ishii, M., Nemoto, N., Kawabata, M., Aburatani, H., & Miyazono, K. (2001). Targets of transcriptional regulation by transforming growth factor-β: Expression profile analysis using oligonucleotide arrays. *Japanese Journal of Cancer Research*, *92*(3). https://doi.org/10.1111/j.1349-7006.2001.tb01090.x

Alam, H., Sehgal, L., Kundu, S. T., Dalal, S. N., & Vaidya, M. M. (2011). Novel function of keratins 5 and 14 in proliferation and differentiation of stratified epithelial cells. *Molecular Biology of the Cell*, *22*(21). https://doi.org/10.1091/mbc.E10-08-0703

Aldave, A. J., Rayner, S. A., Kim, B. T., Prechanond, A., & Yellore, V. S. (2006). Unilateral lattice corneal dystrophy associated with the novel His572del mutation in the TGFBI gene. *Molecular Vision*, *12*.

Aldave, A. J., Yellore, V. S., Sonmez, B., Bourla, N., Salem, A. K., Khan, M. A., Rayner, S. A., & Glasgow, B. J. (2008). A novel variant of combined granular-lattice corneal dystrophy associated with the Met619Lys mutation in the TGFBI gene. *Archives of Ophthalmology*, *126*(3). https://doi.org/10.1001/archopht.126.3.371

Ali, M., Raghunathan, V. K., Li, J. Y., Murphy, C. J., & Thomasy, S. M. (2016). Biomechanical relationships between the corneal endothelium and Descemet's membrane. In *Experimental Eye Research* (Vol. 152). https://doi.org/10.1016/j.exer.2016.09.004

Ali, R. R., & Sowden, J. C. (2011). DIY eye. *Nature*, *472*(7341). https://doi.org/10.1038/472042a

Alshaer, W., Zureigat, H., al Karaki, A., Al-Kadash, A., Gharaibeh, L., Hatmal, M. M., Aljabali, A. A. A., & Awidi, A. (2021). siRNA: Mechanism of action, challenges, and

therapeutic approaches. *European Journal of Pharmacology*, *905*. https://doi.org/10.1016/j.ejphar.2021.174178

Altshuler, A., Amitai-Lange, A., Tarazi, N., Dey, S., Strinkovsky, L., Hadad-Porat, S., Bhattacharya, S., Nasser, W., Imeri, J., Ben-David, G., Abboud-Jarrous, G., Tiosano, B., Berkowitz, E., Karin, N., Savir, Y., & Shalom-Feuerstein, R. (2021). Discrete limbal epithelial stem cell populations mediate corneal homeostasis and wound healing. *Cell Stem Cell*, *28*(7). https://doi.org/10.1016/j.stem.2021.04.003

Amano, S., Yamagami, S., Mimura, T., Uchida, S., & Yokoo, S. (2006). Corneal Stromal and Endothelial Cell Precursors. *Cornea*, *25*(Supplement 1). https://doi.org/10.1097/01.ico.0000247218.10672.7e

Amini, S., Fathi, F., Mobalegi, J., Sofimajidpour, H., & Ghadimi, T. (2014). The expressions of stem cell markers: Oct4, Nanog, Sox2, nucleostemin, Bmi, Zfx, Tcl1, Tbx3, Dppa4, and Esrrb in bladder, colon, and prostate cancer, and certain cancer cell lines. *Anatomy and Cell Biology*, *47*(1). https://doi.org/10.5115/acb.2014.47.1.1

Ancsin, J. B. (2003). Amyloidogenesis: Historical and modern observations point to heparan sulfate proteoglycans as a major culprit. In *Amyloid* (Vol. 10, Issue 2). https://doi.org/10.3109/13506120309041728

Andersen, R. B., Karring, H., Møer-Pedersen, T., Valnickova, Z., Thøgersen, I. B., Hedegaard, C. J., Kristensen, T., Klintworth, G. K., & Enghild, J. J. (2004). Purification and structural characterization of transforming growth factor beta induced protein (TGFBIp) from porcine and human corneas. *Biochemistry*, *43*(51). https://doi.org/10.1021/bi048589s

Andreasen, M., Nielsen, S. B., Runager, K., Christiansen, G., Nielsen, N. C., Enghild, J. J., & Otzen, D. E. (2012). Polymorphic fibrillation of the destabilized fourth fasciclin-1 domain mutant A546T of the transforming growth factor-β-induced protein (TGFBIp) occurs through multiple pathways with different oligomeric intermediates. *Journal of Biological Chemistry*, *287*(41). https://doi.org/10.1074/jbc.M112.379552

Ariga, T., Miyatake, T., & Yu, R. K. (2010). Role of proteoglycans and glycosaminoglycans in the pathogenesis of Alzheimer's disease and related disorders: Amyloidogenesis and therapeutic strategies - A review. In *Journal of Neuroscience Research* (Vol. 88, Issue 11). https://doi.org/10.1002/jnr.22393

Arkell, R. M., & Tam, P. P. L. (2012). Initiating head development in mouse embryos: Integrating signalling and transcriptional activity. *Open Biology*, *2*(MARCH). https://doi.org/10.1098/rsob.120030

Awwad, S. T., di Pascuale, M. A., Hogan, R. N., Forstot, S. L., McCulley, J. P., & Cavanagh, H. D. (2008). Avellino Corneal Dystrophy Worsening after Laser In Situ Keratomileusis: Further Clinicopathologic Observations and Proposed Pathogenesis. *American Journal of Ophthalmology*, *145*(4). https://doi.org/10.1016/j.ajo.2007.12.008

Baccetti, B. (1985). Collagen and Animal Phylogeny. In *Biology of Invertebrate and Lower Vertebrate Collagens*. https://doi.org/10.1007/978-1-4684-7636-1_2

Bae, J. S., Lee, S. H., Kim, J. E., Choi, J. Y., Park, R. W., Yong Park, J., Park, H. S., Sohn, Y. S., Lee, D. S., Bae Lee, E., & Kim, I. S. (2002). βig-h3 supports keratinocyte adhesion, migration, and proliferation through α3β1 integrin. *Biochemical and Biophysical Research Communications*, *294*(5). https://doi.org/10.1016/S0006-291X(02)00576-4

Banning, C. S., Kim, W. C., Randleman, J. B., Kim, E. K., & Stulting, R. D. (2006). Exacerbation of Avellino corneal dystrophy after LASIK in North America. *Cornea*, *25*(4). https://doi.org/10.1097/01.ico.0000195949.93695.37

Baran-Rachwalska, P., Torabi-Pour, N., Sutera, F. M., Ahmed, M., Thomas, K., Nesbit, M. A., Welsh, M., Moore, C. B. T., & Saffie-Siebert, S. R. (2020). Topical siRNA delivery to the cornea and anterior eye by hybrid silicon-lipid nanoparticles. *Journal of Controlled Release*, *326*. https://doi.org/10.1016/j.jconrel.2020.07.004

Barbaric, I., Miller, G., & Dear, T. N. (2007). Appearances can be deceiving: Phenotypes of knockout mice. In *Briefings in Functional Genomics and Proteomics* (Vol. 6, Issue 2). https://doi.org/10.1093/bfgp/elm008

Basaiawmoit, R. V., Oliveira, C. L. P., Runager, K., Sørensen, C. S., Behrens, M. A., Jonsson, B. H., Kristensen, T., Klintworth, G. K., Enghild, J. J., Pedersen, J. S., & Otzen, D. E. (2011). SAXS models of TGFBIp reveal a trimeric structure and show that the overall shape is not affected by the Arg124His mutation. *Journal of Molecular Biology*, *408*(3). https://doi.org/10.1016/j.jmb.2011.02.052

Bassett, A. R. (2017). Editing the genome of hiPSC with CRISPR/Cas9: disease models. In *Mammalian Genome* (Vol. 28, Issues 7–8). https://doi.org/10.1007/s00335-017-9684-9

Basso, M., Samengo, G., Nardo, G., Massignan, T., D'Alessandro, G., Tartari, S., Cantoni, L., Marino, M., Cheroni, C., de Biasi, S., Giordana, M. T., Strong, M. J., Estevez, A. G., Salmona, M., Bendotti, C., & Bonetto, V. (2009). Characterization of detergent-insoluble proteins in ALS indicates a causal link between nitrative stress and aggregation in pathogenesis. *PLoS ONE*, *4*(12). https://doi.org/10.1371/journal.pone.0008130

Basu, S., Hertsenberg, A. J., Funderburgh, M. L., Burrow, M. K., Mann, M. M., Du, Y., Lathrop, K. L., Syed-Picard, F. N., Adams, S. M., Birk, D. E., & Funderburgh, J. L. (2014). Human limbal biopsy-derived stromal stem cells prevent corneal scarring. *Science Translational Medicine*, *6*(266). https://doi.org/10.1126/scitranslmed.3009644

Baum, J. L. (1970). Melanocyte and langerhans cell population of the cornea and limbus in the albino animal. *American Journal of Ophthalmology*, *69*(4). https://doi.org/10.1016/0002-9394(70)91637-5

Becker, J., Erdlenbruch, B., Noskova, I., Schramm, A., Aumailley, M., Schorderet, D. F., & Schweigerer, L. (2006). Keratoepithelin suppresses the progression of experimental human neuroblastomas. *Cancer Research*, *66*(10). https://doi.org/10.1158/0008-5472.CAN-05-3049

Benson, M. D., Waddington-Cruz, M., Berk, J. L., Polydefkis, M., Dyck, P. J., Wang, A. K., Planté-Bordeneuve, V., Barroso, F. A., Merlini, G., Obici, L., Scheinberg, M., Brannagan, T. H., Litchy, W. J., Whelan, C., Drachman, B. M., Adams, D., Heitner, S. B., Conceição, I., Schmidt, H. H., … Coelho, T. (2018). Inotersen Treatment for Patients with Hereditary Transthyretin Amyloidosis. *New England Journal of Medicine*, *379*(1). https://doi.org/10.1056/nejmoa1716793

Bertrand, J. R., Pottier, M., Vekris, A., Opolon, P., Maksimenko, A., & Malvy, C. (2002). Comparison of antisense oligonucleotides and siRNAs in cell culture and in vivo. *Biochemical and Biophysical Research Communications*, *296*(4). https://doi.org/10.1016/S0006-291X(02)02013-2

Beuerman, R. W., & Pedroza, L. (1996). Ultrastructure of the human cornea. In *Microscopy Research and Technique* (Vol. 33, Issue 4). https://doi.org/10.1002/(SICI)1097-0029(19960301)33:4<320::AID-JEMT3>3.0.CO;2-T

Bhattacharya, S., Serror, L., Nir, E., Dhiraj, D., Altshuler, A., Khreish, M., Tiosano, B., Hasson, P., Panman, L., Luxenburg, C., Aberdam, D., & Shalom-Feuerstein, R.

(2019). SOX2 Regulates P63 and Stem/Progenitor Cell State in the Corneal Epithelium. *Stem Cells*, *37*(3). https://doi.org/10.1002/stem.2959

Bian, Y., Song, C., Cheng, K., Dong, M., Wang, F., Huang, J., Sun, D., Wang, L., Ye, M., & Zou, H. (2014). An enzyme assisted RP-RPLC approach for in-depth analysis of human liver phosphoproteome. *Journal of Proteomics*, *96*. https://doi.org/10.1016/j.jprot.2013.11.014

Bielski, C. M., & Taylor, B. S. (2020). Mutant Allele Imbalance in Cancer. In *Annual Review of Cancer Biology* (Vol. 5). https://doi.org/10.1146/annurev-cancerbio-051320-124252

Billings, P. C., Charles Whitbeck, J., Adams, C. S., Abrams, W. R., Cohen, A. J., Engelsberg, B. N., Howard, P. S., & Rosenbloom, J. (2002). The transforming growth factor-β-inducible matrix protein βig-h3 interacts with fibronectin. *Journal of Biological Chemistry*, *277*(31). https://doi.org/10.1074/jbc.M106837200

Bischof, J. M., Chiang, A. P., Scheetz, T. E., Stone, E. M., Casavant, T. L., Sheffield, V. C., & Braun, T. A. (2006). Genome-wide identification of pseudogenes capable of disease-causing gene conversion. *Human Mutation*, *27*(6). https://doi.org/10.1002/humu.20335

Bissey, P. A., Law, J. H., Bruce, J. P., Shi, W., Renoult, A., Chua, M. L. K., Yip, K. W., & Liu, F. F. (2018). Dysregulation of the MiR-449b target TGFBI alters the TGFβ pathway to induce cisplatin resistance in nasopharyngeal carcinoma. *Oncogenesis*, *7*(5). https://doi.org/10.1038/s41389-018-0050-x

Biswas, S., Munier, F. L., Yardley, J., Hart-Holden, N., Perveen, R., Cousin, P., Sutphin, J. E., Noble, B., Batterbury, M., Kielty, C., Hackett, A., Bonshek, R., Ridgway, A., McLeod, D., Sheffield, V. C., Stone, E. M., Schorderet, D. F., & Black, G. C. M. (2001). Missense mutations in COL8A2, the gene encoding the α2 chain of type VIII collagen, cause two forms of corneal endothelial dystrophy. *Human Molecular Genetics*, *10*(21). https://doi.org/10.1093/hmg/10.21.2415

Blank, U., & Karlsson, S. (2011). The role of Smad signaling in hematopoiesis and translational hematology. In *Leukemia* (Vol. 25, Issue 9). https://doi.org/10.1038/leu.2011.95

Bloor, B. K., Seddon, S. v., & Morgan, P. R. (2000). Gene expression of differentiation-specific keratins (K4, K13, K1 and K10) in oral non-dysplastic keratoses and lichen

planus. *Journal of Oral Pathology and Medicine*, *29*(8). https://doi.org/10.1034/j.1600-0714.2000.290803.x

Blumenberg, M. (2013). Transcriptional Regulation of Keratin Gene Expression. In *Intermediate Filaments* (pp. 93–109). Springer US. https://doi.org/10.1007/0-387-33781-4_7

Blythe, A. J., Fox, A. H., & Bond, C. S. (2016). The ins and outs of lncRNA structure: How, why and what comes next? In *Biochimica et Biophysica Acta - Gene Regulatory Mechanisms* (Vol. 1859, Issue 1). https://doi.org/10.1016/j.bbagrm.2015.08.009

Boatz, J. C., Whitley, M. J., Li, M., Gronenborn, A. M., & Van Der Wel, P. C. A. (2017). Cataract-associated P23T γ 3D-crystallin retains a native-like fold in amorphous-looking aggregates formed at physiological pH. *Nature Communications*, *8*. https://doi.org/10.1038/ncomms15137

Bock, C., Kiskinis, E., Verstappen, G., Gu, H., Boulting, G., Smith, Z. D., Ziller, M., Croft, G. F., Amoroso, M. W., Oakley, D. H., Gnirke, A., Eggan, K., & Meissner, A. (2011). Reference maps of human es and ips cell variation enable high-throughput characterization of pluripotent cell lines. *Cell*, *144*(3). https://doi.org/10.1016/j.cell.2010.12.032

Bourne, W. M. (2003). Biology of the corneal endothelium in health and disease. In *Eye* (Vol. 17, Issue 8). https://doi.org/10.1038/sj.eye.6700559

Bouyacoub, Y., Falfoul, Y., Ouederni, M., Sayeb, M., Chedli, A., Chargui, M., Sassi, H., Chakroun Chenguel, I., Munier, F. L., El Matri, L., Abdelhak, S., & Cheour, M. (2019). Granular type I corneal dystrophy in a large consanguineous Tunisian family with homozygous p.R124S mutation in the TGFBI gene. *Ophthalmic Genetics*, *40*(4). https://doi.org/10.1080/13816810.2019.1639202

Boye, K., & Mælandsmo, G. M. (2010). S100A4 and metastasis: A small actor playing many roles. In *American Journal of Pathology* (Vol. 176, Issue 2). https://doi.org/10.2353/ajpath.2010.090526

Brachvogel, B., Zaucke, F., Dave, K., Norris, E. L., Stermann, J., Dayakli, M., Koch, M., Gorman, J. J., Bateman, J. F., & Wilson, R. (2013). Comparative proteomic analysis of normal and collagen IX null mouse cartilage reveals altered extracellular matrix composition and novel components of the collagen IX interactome. *Journal of Biological Chemistry*, *288*(19). https://doi.org/10.1074/jbc.M112.444810

Brejchova, K., Dudakova, L., Skalicka, P., Dobrovolny, R., Masek, P., Putzova, M., Moosajee, M., Tuft, S. J., Davidson, A. E., & Liskova, P. (2019). IPSC-Derived corneal endothelial-like cells act as an appropriate model system to assess the impact of SLC4A11 variants on pre-mrna splicing. *Investigative Ophthalmology and Visual Science*, *60*(8). https://doi.org/10.1167/iovs.19-26930

Burrows, C. K., Banovich, N. E., Pavlovic, B. J., Patterson, K., Gallego Romero, I., Pritchard, J. K., & Gilad, Y. (2016). Genetic Variation, Not Cell Type of Origin, Underlies the Majority of Identifiable Regulatory Differences in iPSCs. *PLoS Genetics*, *12*(1). https://doi.org/10.1371/journal.pgen.1005793

Bustamante, M., Tasinato, A., Maurer, F., Elkochairi, I., Lepore, M. G., Arsenijevic, Y., Pedrazzini, T., Munier, F. L., & Schorderet, D. F. (2008). Overexpression of a mutant form of TGFBI/BIGH3 induces retinal degeneration in transgenic mice. *Molecular Vision*, *14*.

Campbell, C. D., Kirby, A., Nemesh, J., Daly, M. J., & Hirschhorn, J. N. (2008). A survey of allelic imbalance in F1 mice. *Genome Research*, *18*(4). https://doi.org/10.1101/gr.068692.107

Campbell, M. A., & Wengel, J. (2011). Locked vs. unlocked nucleic acids (LNA vs. UNA): Contrasting structures work towards common therapeutic goals. *Chemical Society Reviews*, *40*(12). https://doi.org/10.1039/c1cs15048k

Candi, E., Dinsdale, D., Rufini, A., Salomoni, P., Knight, R. A., Mueller, M., Krammer, P. H., & Melino, G. (2007). TAp63 and ΔNp63 in cancer and epidermal development. In *Cell Cycle* (Vol. 6, Issue 3). https://doi.org/10.4161/cc.6.3.3797

Cantor, E. L., Shen, F., Jiang, G., Tan, Z., Cunningham, G. M., Wu, X., Philips, S., & Schneider, B. P. (2022). Passage number affects differentiation of sensory neurons from human induced pluripotent stem cells. *Scientific Reports*, *12*(1). https://doi.org/10.1038/s41598-022-19018-6

Cao, W., Ge, H., Cui, X., Zhang, L., Bai, J., Fu, S., & Liu, P. (2009). Reduced penetrance in familial Avellino corneal dystrophy associated with TGFBI mutations. *Molecular Vision*, *15*.

Carragher, N. O., & Frame, M. C. (2004). Focal adhesion and actin dynamics: A place where kinases and proteases meet to promote invasion. In *Trends in Cell Biology* (Vol. 14, Issue 5). https://doi.org/10.1016/j.tcb.2004.03.011

Casale, J., & Crane, J. S. (2019). Biochemistry, Glycosaminoglycans. In *StatPearls*.

Castanotto, D., Lin, M., Kowolik, C., Wang, L. A., Ren, X. Q., Soifer, H. S., Koch, T., Hansen, B. R., Oerum, H., Armstrong, B., Wang, Z., Bauer, P., Rossi, J., & Stein, C. A. (2015). A cytoplasmic pathway for gapmer antisense oligonucleotide-mediated gene silencing in mammalian cells. *Nucleic Acids Research*, *43*(19). https://doi.org/10.1093/nar/gkv964

Català, P., Groen, N., Dehnen, J. A., Soares, E., van Velthoven, A. J. H., Nuijts, R. M. M. A., Dickman, M. M., & LaPointe, V. L. S. (2021). Single cell transcriptomics reveals the heterogeneity of the human cornea to identify novel markers of the limbus and stroma. *Scientific Reports*, *11*(1). https://doi.org/10.1038/s41598-021-01015-w

Cerritelli, S. M., & Crouch, R. J. (2009). Ribonuclease H: The enzymes in eukaryotes. In *FEBS Journal* (Vol. 276, Issue 6). https://doi.org/10.1111/j.1742-4658.2009.06908.x

Chaerkady, R., Shao, H., Scott, S. G., Pandey, A., Jun, A. S., & Chakravarti, S. (2013). The keratoconus corneal proteome: Loss of epithelial integrity and stromal degeneration. *Journal of Proteomics*, *87*. https://doi.org/10.1016/j.jprot.2013.05.023

Chakrabarty, K., Shetty, R., & Ghosh, A. (2018). Corneal cell therapy: with iPSCs, it is no more a far-sight. *Stem Cell Research & Therapy*, *9*(1). https://doi.org/10.1186/s13287-018-1036-5

Chakravarthi, S. V. V. K., Kannabiran, C., Sridhar, M. S., & Vemuganti, G. K. (2005). TGFBI gene mutations causing lattice and granular corneal dystrophies in Indian patients. *Investigative Ophthalmology and Visual Science*, *46*(1). https://doi.org/10.1167/iovs.04-0440

Chaloin-Dufau, C., Dhouailly, D., & Sun, T. T. (1990). Appearance of the keratin pair K3/K12 during embryonic and adult corneal epithelial differentiation in the chick and in the rabbit. *Cell Differentiation and Development*, *32*(2). https://doi.org/10.1016/0922-3371(90)90103-4

Chaloin-Dufau, C., Pavitt, I., Delorme, P., & Dhouailly, D. (1993). Identification of keratins 3 and 12 in corneal epithelium of vertebrates. *Epithelial Cell Biology*, *2*(3).

Chan, S. Y., Chan, A. K. W., Cheung, B. P. K., Liang, Y., & Leung, M. P. (2003). Identification of genes expressed during myocardial development. *Chinese Medical Journal*, *116*(9).

Chang, L., Zhiqun, W., Shijing, D., Chen, Z., Qingfeng, L., Li, L., & Xuguang, S. (2009). Arg124Cys mutation of the TGFBI gene in 2 Chinese families with Thiel-Behnke corneal dystrophy. *Archives of Ophthalmology*, *127*(5). https://doi.org/10.1001/archophthalmol.2009.71

Chao-Shern, C., DeDionisio, L. A., Jang, J. H., Chan, C. C., Thompson, V., Christie, K., Nesbit, M. A., & McMullen, C. B. T. (2019). Evaluation of TGFBI corneal dystrophy and molecular diagnostic testing. In *Eye (Basingstoke)* (Vol. 33, Issue 6). https://doi.org/10.1038/s41433-019-0346-x

Chao-Shern, C., Me, R., Dedionisio, L. A., Ke, B. L., Nesbit, M. A., Marshall, J., & Moore, C. B. T. (2018). Post-LASIK exacerbation of granular corneal dystrophy type 2 in members of a Chinese family. *Eye (Basingstoke)*, *32*(1). https://doi.org/10.1038/eye.2017.265

Chau, V. Q., Hu, J., Gong, X., Hulleman, J. D., Ufret-Vincenty, R. L., Rigo, F., Prakash, T. P., Corey, D. R., & Vinod Mootha, V. (2020). Delivery of Antisense Oligonucleotides to the Cornea. *Nucleic Acid Therapeutics*, *30*(4). https://doi.org/10.1089/nat.2019.0838

Chen, J., Li, Z., Zhang, L., Ou, S., Wang, Y., He, X., Zou, D., Jia, C., Hu, Q., Yang, S., Li, X., Li, J., Wang, J., Sun, H., Chen, Y., Zhu, Y. T., Tseng, S. C. G., Liu, Z., & Li, W. (2017). Descemet's Membrane Supports Corneal Endothelial Cell Regeneration in Rabbits. *Scientific Reports*, *7*(1). https://doi.org/10.1038/s41598-017-07557-2

Chen, L., Chen, Y. M., Lu, C. J., Chen, M. Y., Lin, S. Y., Hu, F. R., & Chen, W. L. (2017). Effect of air-lifting on the stemness, junctional protein formation, and cytokeratin expression of in vitro cultivated limbal epithelial cell sheets. *Taiwan Journal of Ophthalmology*, *7*(4). https://doi.org/10.4103/tjo.tjo_101_17

Chen, Y., Huang, K., Nakatsu, M. N., Xue, Z., Deng, S. X., & Fan, G. (2013). Identification of novel molecular markers through transcriptomic analysis in human fetal and adult corneal endothelial cells. *Human Molecular Genetics*, *22*(7). https://doi.org/10.1093/hmg/dds527

Chen, Y. J., Chen, J. T., Lu, D. W., & Tai, M. C. (2010). In vivo corneal confocal microscopic findings and gene analysis of three patients with Thiele-Behnke corneal dystrophy. In *British Journal of Ophthalmology* (Vol. 94, Issue 2). https://doi.org/10.1136/bjo.2009.165217

Chen, Z., de Paiva, C. S., Luo, L., Kretzer, F. L., Pflugfelder, S. C., & Li, D. (2004). Characterization of Putative Stem Cell Phenotype in Human Limbal Epithelia. *STEM CELLS*, *22*(3). https://doi.org/10.1634/stemcells.22-3-355

Cheung, V. G., Spielman, R. S., Ewens, K. G., Weber, T. M., Morley, M., & Burdick, J. T. (2005). Mapping determinants of human gene expression by regional and genome-wide association. *Nature*, *437*(7063). https://doi.org/10.1038/nature04244

Ching, T., Huang, S., & Garmire, L. X. (2014). Power analysis and sample size estimation for RNA-Seq differential expression. *RNA*, *20*(11). https://doi.org/10.1261/rna.046011.114

Chiriboga, C. A., Swoboda, K. J., Darras, B. T., Iannaccone, S. T., Montes, J., de Vivo, D. C., Norris, D. A., Bennett, C. F., & Bishop, K. M. (2016). Results from a phase 1 study of nusinersen (ISIS-SMN Rx) in children with spinal muscular atrophy. *Neurology*, *86*(10). https://doi.org/10.1212/WNL.0000000000002445

Chiu, E. K., Lin, A. Y., Folberg, R., & Saidel, M. (2007). Avellino dystrophy in a patient after laser-assisted in situ keratomileusis surgery manifesting as granular dystrophy. *Archives of Ophthalmology*, *125*(5). https://doi.org/10.1001/archopht.125.5.703

Cho, K. J., Mok, J. W., Na, K. S., Rho, C. R., Byun, Y. S., Hwang, H. S., Hwang, K. Y., & Joo, C. K. (2012). TGFBI gene mutations in a Korean population with corneal dystrophy. *Molecular Vision*, *18*.

Choi, S. il, Dadakhujaev, S., Maeng, Y. S., Ahn, S. Y., Kim, T. I., & Kim, E. K. (2015). Disrupted cell cycle arrest and reduced proliferation in corneal fibroblasts from GCD2 patients: A potential role for altered autophagy flux. *Biochemical and Biophysical Research Communications*, *456*(1). https://doi.org/10.1016/j.bbrc.2014.11.073

Choi, S. il, Dadakhujaev, S., Ryu, H., Im Kim, T., & Kim, E. K. (2011). Melatonin protects against oxidative stress in granular corneal dystrophy type 2 corneal fibroblasts by mechanisms that involve membrane melatonin receptors. *Journal of Pineal Research*, *51*(1). https://doi.org/10.1111/j.1600-079X.2011.00866.x

Choi, S. Il, Jin, J. Y., Maeng, Y. S., Kim, T. I., & Kim, E. K. (2016). TGF-β regulates TGFBIp expression in corneal fibroblasts via miR-21, miR-181a, and Smad signaling. *Biochemical and Biophysical Research Communications*, *472*(1). https://doi.org/10.1016/j.bbrc.2016.02.086

Choi, S. il, Kim, B. Y., Dadakhujaev, S., Jester, J. v., Ryu, H., Kim, T. I., & Kim, E. K. (2011). Inhibition of TGFBIp expression by lithium: Implications for TGFBI-linked corneal dystrophy therapy. *Investigative Ophthalmology and Visual Science*, *52*(6). https://doi.org/10.1167/iovs.10-6405

Choi, S. il, Kim, B. Y., Dadakhujaev, S., Oh, J. Y., Kim, T. I., Kim, J. Y., & Kim, E. K. (2012). Impaired autophagy and delayed autophagic clearance of transforming growth factor β-induced protein (TGFBI) in granular corneal dystrophy type 2. *Autophagy*, *8*(12). https://doi.org/10.4161/auto.22067

Choi, S. il, Kim, K. S., Oh, J. Y., Jin, J. Y., Lee, G. H., & Kim, E. K. (2013). Melatonin induces autophagy via an mTOR-dependent pathway and enhances clearance of mutant-TGFBIp. *Journal of Pineal Research*, *54*(4). https://doi.org/10.1111/jpi.12039

Choi, S. il, Kim, T. I., Kyu, S. K., Kim, B. Y., Ahn, S. Y., Cho, H. J., Hyung, K. L., Cho, H. S., & Eung, K. K. (2009). Decreased catalase expression and increased susceptibility to oxidative stress in primary cultured corneal fibroblasts from patients with granular corneal dystrophy type II. *American Journal of Pathology*, *175*(1). https://doi.org/10.2353/ajpath.2009.081001

Choi, S. Il, Lee, E., Akuzum, B., Jeong, J. Bin, Maeng, Y. S., Kim, T. I., & Kim, E. K. (2017). Melatonin reduces endoplasmic reticulum stress and corneal dystrophy-associated TGFBIp through activation of endoplasmic reticulum-associated protein degradation. *Journal of Pineal Research*, *63*(3). https://doi.org/10.1111/jpi.12426

Choi, S. il, Lee, E., Jeong, J. Bin, Akuzum, B., Maeng, Y. S., Kim, T. im, & Kim, E. K. (2016). 4-Phenylbutyric acid reduces mutant-TGFBIp levels and ER stress through activation of ERAD pathway in corneal fibroblasts of granular corneal dystrophy type 2. *Biochemical and Biophysical Research Communications*, *477*(4). https://doi.org/10.1016/j.bbrc.2016.06.146

Choi, S. il, Maeng, Y. S., Kim, K. S., Kim, T. I., & Kim, E. K. (2014). Autophagy is induced by raptor degradation via the ubiquitin/proteasome system in granular corneal dystrophy type 2. *Biochemical and Biophysical Research Communications*, *450*(4). https://doi.org/10.1016/j.bbrc.2014.07.035

Choi, S. Il, Maeng, Y. S., Kim, T. I., Lee, Y., Kim, Y. S., & Kim, E. K. (2015). Lysosomal trafficking of TGFBIp via Caveolae-mediated endocytosis. *PLoS ONE*, *10*(4). https://doi.org/10.1371/journal.pone.0119561

Choi, S. il, Woo, J. H., & Kim, E. K. (2020). Lysosomal dysfunction of corneal fibroblasts underlies the pathogenesis of Granular Corneal Dystrophy Type 2 and can be rescued by TFEB. *Journal of Cellular and Molecular Medicine*, *24*(18). https://doi.org/10.1111/jcmm.15646

Choi, S. il, Yoo, Y. M., Kim, B. Y., Kim, T. im, Cho, H. ju, Ahn, S. yoen, Lee, H. K., Cho, H. S., & Kim, E. K. (2010). Involvement of TGF-β receptor- and integrin-mediated signaling pathways in the pathogenesis of granular corneal dystrophy II. *Investigative Ophthalmology and Visual Science*, *51*(4). https://doi.org/10.1167/iovs.09-4149

Choi, Y., Oh, H., Ahn, M., Kang, T., Chun, J., Shin, T., & Kim, J. (2020). Immunohistochemical analysis of periostin in the hearts of lewis rats with experimental autoimmune myocarditis. *Journal of Veterinary Medical Science*, *82*(10). https://doi.org/10.1292/jvms.20-0225

Christie, K. A., Courtney, D. G., Dedionisio, L. A., Shern, C. C., De Majumdar, S., Mairs, L. C., Nesbit, M. A., & Moore, C. B. T. (2017). Towards personalised allele-specific CRISPR gene editing to treat autosomal dominant disorders. *Scientific Reports*, *7*(1). https://doi.org/10.1038/s41598-017-16279-4

Christie, K. A., Robertson, L. J., Conway, C., Blighe, K., DeDionisio, L. A., Chao-Shern, C., Kowalczyk, A. M., Marshall, J., Turnbull, D., Nesbit, M. A., & Moore, C. B. T. (2020). Mutation-Independent Allele-Specific Editing by CRISPR-Cas9, a Novel Approach to Treat Autosomal Dominant Disease. *Molecular Therapy*, *28*(8). https://doi.org/10.1016/j.ymthe.2020.05.002

Ciryam, P., Kundra, R., Morimoto, R. I., Dobson, C. M., & Vendruscolo, M. (2015). Supersaturation is a major driving force for protein aggregation in neurodegenerative diseases. *Trends in Pharmacological Sciences*, *36*(2), 72–77. https://doi.org/10.1016/j.tips.2014.12.004

Ciryam, P., Tartaglia, G. G., Morimoto, R. I., Dobson, C. M., & Vendruscolo, M. (2013). Widespread Aggregation and Neurodegenerative Diseases Are Associated with Supersaturated Proteins. *Cell Reports*, *5*(3). https://doi.org/10.1016/j.celrep.2013.09.043

Clayton, S. W., Ban, G. I., Liu, C., & Serra, R. (2020). Canonical and noncanonical TGF-β signaling regulate fibrous tissue differentiation in the axial skeleton. *Scientific Reports*, *10*(1). https://doi.org/10.1038/s41598-020-78206-4

Cohen, E., Johnson, C., Redmond, C. J., Nair, R. R., & Coulombe, P. A. (2022). Revisiting the significance of keratin expression in complex epithelia. *Journal of Cell Science*, *135*(20). https://doi.org/10.1242/jcs.260594

Collin, J., Queen, R., Zerti, D., Bojic, S., Dorgau, B., Moyse, N., Molina, M. M., Yang, C., Dey, S., Reynolds, G., Hussain, R., Coxhead, J. M., Lisgo, S., Henderson, D., Joseph, A., Rooney, P., Ghosh, S., Clarke, L., Connon, C., … Lako, M. (2021). A single cell atlas of human cornea that defines its development, limbal progenitor cells and their interactions with the immune cells. *Ocular Surface*, *21*. https://doi.org/10.1016/j.jtos.2021.03.010

Collin, R. W., den Hollander, A. I., der Velde-Visser, S. D. V., Bennicelli, J., Bennett, J., & Cremers, F. P. (2012). Antisense oligonucleotide (AON)-based therapy for leber congenital amaurosis caused by a frequent mutation in CEP290. *Molecular Therapy - Nucleic Acids*, *1*(3). https://doi.org/10.1038/mtna.2012.3

Collinson, J. M., Quinn, J. C., Hill, R. E., & West, J. D. (2003). The roles of Pax6 in the cornea, retina, and olfactory epithelium of the developing mouse embryo. *Developmental Biology*, *255*(2). https://doi.org/10.1016/S0012-1606(02)00095-7

Conesa, A., Madrigal, P., Tarazona, S., Gomez-Cabrero, D., Cervera, A., McPherson, A., Szcześniak, M. W., Gaffney, D. J., Elo, L. L., Zhang, X., & Mortazavi, A. (2016). A survey of best practices for RNA-seq data analysis. In *Genome Biology* (Vol. 17, Issue 1). https://doi.org/10.1186/s13059-016-0881-8

Conway, S., & Molkentin, J. (2008). Periostin as a Heterofunctional Regulator of Cardiac Development and Disease. *Current Genomics*, *9*(8). https://doi.org/10.2174/138920208786847917

Corden, L. D., Swensson, O., Swensson, B., Smith, F. J. D., Rochels, R., Uitto, J., & McLean, W. H. I. (2000). Molecular genetics of Meesmann's corneal dystrophy: Ancestral and novel mutations in keratin 12 (K12) and complete sequence of the human KRT12 gene. *Experimental Eye Research*, *70*(1). https://doi.org/10.1006/exer.1999.0769

Corona, A., & Blobe, G. C. (2021). The role of the extracellular matrix protein TGFBI in cancer. In *Cellular Signalling* (Vol. 84). https://doi.org/10.1016/j.cellsig.2021.110028

Costanza, B., Rademaker, G., Tiamiou, A., De Tullio, P., Leenders, J., Blomme, A., Bellier, J., Bianchi, E., Turtoi, A., Delvenne, P., Bellahcène, A., Peulen, O., &

Castronovo, V. (2019a). TGFBI, an ECM interacting protein, enhances glycolysis and promotes pancreatic cancer cell migration. *International Journal of Cancer*.

Costanza, B., Rademaker, G., Tiamiou, A., De Tullio, P., Leenders, J., Blomme, A., Bellier, J., Bianchi, E., Turtoi, A., Delvenne, P., Bellahcène, A., Peulen, O., & Castronovo, V. (2019b). Transforming growth factor beta-induced, an extracellular matrix interacting protein, enhances glycolysis and promotes pancreatic cancer cell migration. *International Journal of Cancer*, *145*(6). https://doi.org/10.1002/ijc.32247

Cotsarelis, G., Cheng, S. Z., Dong, G., Sun, T. T., & Lavker, R. M. (1989). Existence of slow-cycling limbal epithelial basal cells that can be preferentially stimulated to proliferate: Implications on epithelial stem cells. *Cell*, *57*(2). https://doi.org/10.1016/0092-8674(89)90958-6

Courtney, D. G., Atkinson, S. D., Moore, J. E., Maurizi, E., Serafini, C., Pellegrini, G., Black, G. C., Manson, F. D., Yam, G. H. F., MacEwen, C. J., Allen, E. H. A., Irwin McLean, W. H., & Tara Moore, C. B. (2014). Development of allele-specific gene-silencing siRNAs for TGFBI Arg124Cys in lattice corneal dystrophy type i. *Investigative Ophthalmology and Visual Science*, *55*(2). https://doi.org/10.1167/iovs.13-13279

Courtney, D. G., Moore, J. E., Atkinson, S. D., Maurizi, E., Allen, E. H. A., Pedrioli, D. M. L., Mclean, W. H. I., Nesbit, M. A., & Moore, C. B. T. (2016). CRISPR/Cas9 DNA cleavage at SNP-derived PAM enables both in vitro and in vivo KRT12 mutation-specific targeting. *Gene Therapy*, *23*(1). https://doi.org/10.1038/gt.2015.82

Courtney, D. G., Poulsen, E. T., Kennedy, S., Moore, J. E., Atkinson, S. D., Maurizi, E., Andrew Nesbit, M., Tara Moore, C. B., & Enghild, J. J. (2015). Protein composition of TGFBI-R124C- and TGFBI-R555W-associated aggregates suggests multiple mechanisms leading to lattice and granular corneal dystrophy. *Investigative Ophthalmology and Visual Science*, *56*(8). https://doi.org/10.1167/iovs.15-16922

Couture, C., Zaniolo, K., Carrier, P., Lake, J., Patenaude, J., Germain, L., & Guérin, S. L. (2016). The tissue-engineered human cornea as a model to study expression of matrix metalloproteinases during corneal wound healing. *Biomaterials*, *78*. https://doi.org/10.1016/j.biomaterials.2015.11.006

Cowles, C. R., Hirschhorn, J. N., Altshuler, D., & Lander, E. S. (2002). Detection of regulatory variation in mouse genes. *Nature Genetics*, *32*(3). https://doi.org/10.1038/ng992

Cui, W., Xue, H., Wei, L., Jin, J., Tian, X., & Wang, Q. (2021). High heterogeneity undermines generalization of differential expression results in RNA-Seq analysis. *Human Genomics*, *15*(1). https://doi.org/10.1186/s40246-021-00308-5

Cursiefen, C., Viaud, E., Bock, F., Geudelin, B., Ferry, A., Kadlecová, P., Lévy, M., Al Mahmood, S., Colin, S., Thorin, E., Majo, F., Frueh, B., Wilhelm, F., Meyer-Ter-Vehn, T., Geerling, G., Böhringer, D., Reinhard, T., Meller, D., Pleyer, U., … Seitz, B. (2014). Aganirsen antisense oligonucleotide eye drops inhibit keratitis-induced corneal neovascularization and reduce need for transplantation: The I-CAN study. *Ophthalmology*, *121*(9). https://doi.org/10.1016/j.ophtha.2014.03.038

Dang, X., Zhu, Q., Wang, L., Su, H., Lin, H., Zhou, N., Liang, T., Wang, Z., Huang, S., Ren, Q., & Qi, Y. (2009). Macular corneal dystrophy in a Chinese family related with novel mutations of CHST6. *Molecular Vision*, *15*.

Daniel, S., Renwick, M., Chau, V. Q., Datta, S., Maddineni, P., Zode, G., Wade, E. M., Robertson, S. P., Petroll, W. M., & Hulleman, J. D. (2020). Fibulin-3 knockout mice demonstrate corneal dysfunction but maintain normal retinal integrity. *Journal of Molecular Medicine*, *98*(11). https://doi.org/10.1007/s00109-020-01974-z

Davanger, M., & Evensen, A. (1971). Role of the pericorneal papillary structure in renewal of corneal epithelium. *Nature*, *229*(5286). https://doi.org/10.1038/229560a0

de Paiva, C. S., Chen, Z., Corrales, R. M., Pflugfelder, S. C., & Li, D. (2005). ABCG2 Transporter Identifies a Population of Clonogenic Human Limbal Epithelial Cells. *STEM CELLS*, *23*(1). https://doi.org/10.1634/stemcells.2004-0093

De Paiva, C. S., Pflugfelder, S. C., & Li, D.-Q. (2006). Cell Size Correlates with Phenotype and Proliferative Capacity in Human Corneal Epithelial Cells. *Stem Cells*, *24*(2). https://doi.org/10.1634/stemcells.2005-0148

Deák, F., Mátés, L., Korpos, É., Zvara, Á., Szénási, T., Kiricsi, M., Mendler, L., Keller-Pintér, A., Ózsvári, B., Juhász, H., Sorokin, L., Dux, L., Mermod, N., Puskás, L. G., & Kiss, I. (2014). Extracellular deposition of matrilin-2 controls the timing of the myogenic program during muscle regeneration. *Journal of Cell Science*, *127*(15). https://doi.org/10.1242/jcs.141556

Del Cid, J. S., Reed, N. I., Molnar, K., Liu, S., Dang, B., Jensen, S. A., DeGrado, W., Handford, P. A., Sheppard, D., & Sundaram, A. B. (2019). A disease-associated

mutation in fibrillin-1 differentially regulates integrin-mediated cell adhesion. *Journal of Biological Chemistry*, *294*(48). https://doi.org/10.1074/jbc.RA119.011109

DelMonte, D. W., & Kim, T. (2011). Anatomy and physiology of the cornea. *Journal of Cataract and Refractive Surgery*, *37*(3). https://doi.org/10.1016/j.jcrs.2010.12.037

Desai, A. R., Maulvi, F. A., Desai, D. M., Shukla, M. R., Ranch, K. M., Vyas, B. A., Shah, S. A., Sandeman, S., & Shah, D. O. (2020). Multiple drug delivery from the drug-implants-laden silicone contact lens: Addressing the issue of burst drug release. *Materials Science and Engineering C*, *112*. https://doi.org/10.1016/j.msec.2020.110885

Dhouailly, D., Pearton, D. J., & Michon, F. (2014). The vertebrate corneal epithelium: From early specification to constant renewal. In *Developmental Dynamics* (Vol. 243, Issue 10). https://doi.org/10.1002/dvdy.24179

Dhuri, K., Bechtold, C., Quijano, E., Pham, H., Gupta, A., Vikram, A., & Bahal, R. (2020). Antisense oligonucleotides: An emerging area in drug discovery and development. In *Journal of Clinical Medicine* (Vol. 9, Issue 6). https://doi.org/10.3390/JCM9062004

di Como, C. J., Urist, M. J., Babayan, I., Drobnjak, M., Hedvat, C. v., Teruya-Feldstein, J., Pohar, K., Hoos, A., & Cordon-Cardo, C. (2002). p63 expression profiles in human normal and tumor tissues. *Clinical Cancer Research*, *8*(2).

Di Girolamo, N., Bobba, S., Raviraj, V., Delic, N. C., Slapetova, I., Nicovich, P. R., Halliday, G. M., Wakefield, D., Whan, R., & Lyons, J. G. (2015). Tracing the fate of limbal epithelial progenitor cells in the murine cornea. *Stem Cells*, *33*(1). https://doi.org/10.1002/stem.1769

di Iorio, E., Barbaro, V., Ruzza, A., Ponzin, D., Pellegrini, G., & de Luca, M. (2005). Isoforms of ΔNp63 and the migration of ocular limbal cells in human corneal regeneration. *Proceedings of the National Academy of Sciences of the United States of America*, *102*(27). https://doi.org/10.1073/pnas.0503437102

Di Iorio, E., Kaye, S. B., Ponzin, D., Barbaro, V., Ferrari, S., Böhm, E., Nardiello, P., Castaldo, G., McGrath, J. A., & Willoughby, C. E. (2012). Limbal stem cell deficiency and ocular phenotype in ectrodactyly-ectodermal dysplasia-clefting syndrome caused by p63 mutations. *Ophthalmology*, *119*(1). https://doi.org/10.1016/j.ophtha.2011.06.044

Dias, N., & Stein, C. A. (2002). Antisense oligonucleotides: Basic concepts and mechanisms. In *Molecular Cancer Therapeutics* (Vol. 1, Issue 5).

Dighiero, P., Drunat, S., Ellies, P., D'Hermies, F., Savoldelli, M., Legeais, J. M., Renard, G., Delpech, M., Grateau, G., & Valleix, S. (2000). A new mutation (A546T) of the βig-h3 gene responsible for a French lattice corneal dystrophy type IIIA. *American Journal of Ophthalmology*, *129*(2). https://doi.org/10.1016/S0002-9394(99)00324-4

Dighiero, P., Niel, F., Ellies, P., D'Hermies, F., Savoldelli, M., Renard, G., Delpech, M., & Valleix, S. (2001). Histologic phenotype-genotype correlation of corneal dystrophies associated with eight distinct mutations in the TGFBI gene. *Ophthalmology*, *108*(4). https://doi.org/10.1016/S0161-6420(00)00662-X

Dill, K. A., & Chan, H. S. (1997). From levinthal to pathways to funnels. In *Nature Structural Biology* (Vol. 4, Issue 1). https://doi.org/10.1038/nsb0197-10

Dimas, A. S., Deutsch, S., Stranger, B. E., Montgomery, S. B., Borel, C., Attar-Cohen, H., Ingle, C., Beazley, C., Arcelus, M. G., Sekowska, M., Gagnebin, M., Nisbett, J., Deloukas, P., Dermitzakis, E. T., & Antonarakis, S. E. (2009). Common regulatory variation impacts gene expression in a cell type-dependent manner. *Science*, *325*(5945). https://doi.org/10.1126/science.1174148

Dimitrova, D. G., Teysset, L., & Carré, C. (2019). RNA 2′-O-Methylation (Nm) modification in human diseases. *Genes*, *10*(2). https://doi.org/10.3390/genes10020117

Ding, X. wei, Wu, J. hua, & Jiang, C. ping. (2010). ABCG2: A potential marker of stem cells and novel target in stem cell and cancer therapy. In *Life Sciences* (Vol. 86, Issues 17–18). https://doi.org/10.1016/j.lfs.2010.02.012

Ding, Z., Dong, J., Liu, J., & Deng, S. X. (2008). Preferential gene expression in the limbus of the vervet monkey. *Molecular Vision*, *14*.

Dixon, I. M. C., Landry, N. M., & Rattan, S. G. (2019). Periostin Reexpression in Heart Disease Contributes to Cardiac Interstitial Remodeling by Supporting the Cardiac Myofibroblast Phenotype. In *Advances in Experimental Medicine and Biology* (Vol. 1132). https://doi.org/10.1007/978-981-13-6657-4_4

Djalilian, A. R., Namavari, A., Ito, A., Balali, S., Afshar, A., Lavker, R. M., & Yue, B. Y. J. T. (2008). Down-regulation of Notch signaling during corneal epithelial proliferation. *Molecular Vision*, *14*.

Dobson, C. M. (2003). Protein folding and misfolding. In *Nature* (Vol. 426, Issue 6968). https://doi.org/10.1038/nature02261

Dobson, C. M., Šali, A., & Karplus, M. (1998). Protein folding: A perspective from theory and experiment. In *Angewandte Chemie - International Edition* (Vol. 37, Issue 7). https://doi.org/10.1002/(SICI)1521-3773(19980420)37:7<868::AID-ANIE868>3.0.CO;2-H

Dokmanovic, M., Chang, B. D., Fang, J., & Roninson, I. B. (2002). Retinoid-induced growth arrest of breast carcinoma cells involves co-activation of multiple growth-inhibitory genes. *Cancer Biology and Therapy*, *1*(1). https://doi.org/10.4161/cbt.1.1.35

Dorà, N. J., Hill, R. E., Collinson, J. M., & West, J. D. (2015). Lineage tracing in the adult mouse corneal epithelium supports the limbal epithelial stem cell hypothesis with intermittent periods of stem cell quiescence. *Stem Cell Research*, *15*(3). https://doi.org/10.1016/j.scr.2015.10.016

Dou, S., Wang, Q., Qi, X., Zhang, B., Jiang, H., Chen, S., Duan, H., Lu, Y., Dong, J., Cao, Y., Xie, L., Zhou, Q., & Shi, W. (2021). Molecular identity of human limbal heterogeneity involved in corneal homeostasis and privilege: Single-cell RNA sequencing of human limbus. *Ocular Surface*, *21*. https://doi.org/10.1016/j.jtos.2021.04.010

Draper, J. S., Pigott, C., Thomson, J. A., & Andrews, P. W. (2002). Surface antigens of human embryonic stem cells: Changes upon differentiation in culture. In *Journal of Anatomy* (Vol. 200, Issue 3). https://doi.org/10.1046/j.1469-7580.2002.00030.x

Du, Y., Carlson, E. C., Funderburgh, M. L., Birk, D. E., Pearlman, E., Guo, N., Kao, W. W. Y., & Funderburgh, J. L. (2009). Stem cell therapy restores transparency to defective murine corneas. *Stem Cells*, *27*(7). https://doi.org/10.1002/stem.91

Du, Y., Funderburgh, M. L., Mann, M. M., SundarRaj, N., & Funderburgh, J. L. (2005). Multipotent Stem Cells in Human Corneal Stroma. *STEM CELLS*, *23*(9). https://doi.org/10.1634/stemcells.2004-0256

Dua, H. S., Faraj, L. A., Said, D. G., Gray, T., & Lowe, J. (2013). Human corneal anatomy redefined: A novel pre-descemet's layer (Dua's Layer). *Ophthalmology*, *120*(9). https://doi.org/10.1016/j.ophtha.2013.01.018

Dudley, A. T., & Robertson, E. J. (1997). Overlapping expression domains of bone morphogenetic protein family members potentially account for limited tissue defects

in BMP7 deficient embryos. *Developmental Dynamics*, *208*(3). https://doi.org/10.1002/(SICI)1097-0177(199703)208:3<349::AID-AJA6>3.0.CO;2-I

Duell, P. B., & Jialal, I. (2016). Modern Management of Familial Hypercholesterolemia. In *Metabolic Syndrome and Related Disorders* (Vol. 14, Issue 10). https://doi.org/10.1089/met.2016.29011.due

Dulla, K., Aguila, M., Lane, A., Jovanovic, K., Parfitt, D. A., Schulkens, I., Chan, H. L., Schmidt, I., Beumer, W., Vorthoren, L., Collin, R. W. J., Garanto, A., Duijkers, L., Brugulat-Panes, A., Semo, M., Vugler, A. A., Biasutto, P., Adamson, P., & Cheetham, M. E. (2018). Splice-Modulating Oligonucleotide QR-110 Restores CEP290 mRNA and Function in Human c.2991+1655A>G LCA10 Models. *Molecular Therapy - Nucleic Acids*, *12*. https://doi.org/10.1016/j.omtn.2018.07.010

Dulla, K., Slijkerman, R., van Diepen, H. C., Albert, S., Dona, M., Beumer, W., Turunen, J. J., Chan, H. L., Schulkens, I. A., Vorthoren, L., den Besten, C., Buil, L., Schmidt, I., Miao, J., Venselaar, H., Zang, J., Neuhauss, S. C. F., Peters, T., Broekman, S., … van Wijk, E. (2021). Antisense oligonucleotide-based treatment of retinitis pigmentosa caused by USH2A exon 13 mutations. *Molecular Therapy*, *29*(8). https://doi.org/10.1016/j.ymthe.2021.04.024

Dupont, S., Zacchigna, L., Cordenonsi, M., Soligo, S., Adorno, M., Rugge, M., & Piccolo, S. (2005). Germ-layer specification and control of cell growth by ectodermin, a Smad4 ubiquitin ligase. *Cell*, *121*(1). https://doi.org/10.1016/j.cell.2005.01.033

Dürig, J., Dührsen, U., Klein-Hitpass, L., Worm, J., Hansen, J. B. R., Orum, H., & Wissenbach, M. (2011). The novel antisense Bcl-2 inhibitor SPC2996 causes rapid leukemic cell clearance and immune activation in chronic lymphocytic leukemia. *Leukemia*, *25*(4). https://doi.org/10.1038/leu.2010.322

Dyrlund, T. F., Poulsen, E. T., Scavenius, C., Nikolajsen, C. L., Thøgersen, I. B., Vorum, H., & Enghild, J. J. (2012). Human cornea proteome: Identification and quantitation of the proteins of the three main layers including epithelium, stroma, and endothelium. *Journal of Proteome Research*, *11*(8). https://doi.org/10.1021/pr300358k

Ebeling, M. C., Geng, Z., Stahl, M. R., Kapphahn, R. J., Roehrich, H., Montezuma, S. R., Ferrington, D. A., & Dutton, J. R. (2022). Testing Mitochondrial-Targeted Drugs in iPSC-RPE from Patients with Age-Related Macular Degeneration. *Pharmaceuticals*, *15*(1). https://doi.org/10.3390/ph15010062

Ebert, A. D., Yu, J., Rose, F. F., Mattis, V. B., Lorson, C. L., Thomson, J. A., & Svendsen, C. N. (2009). Induced pluripotent stem cells from a spinal muscular atrophy patient. *Nature*, *457*(7227). https://doi.org/10.1038/nature07677

Eberwein, P., & Reinhard, T. (2015). Concise reviews: The role of biomechanics in the limbal stem cell niche: New insights for our understanding of this structure. In *Stem Cells* (Vol. 33, Issue 3). https://doi.org/10.1002/stem.1886

Eckardt, S., Romby, P., & Sczakiel, G. (1997). Implications of RNA structure on the annealing of a potent antisense RNA directed against the human immunodeficiency virus type 1. *Biochemistry*, *36*(42). https://doi.org/10.1021/bi9707234

Eder, P. S., Devine, R. J., Dagle, J. M., & Walder, J. A. (1991). Substrate Specificity and Kinetics of Degradation of Antisense Oligonucleotides by a 3' Exonuclease in Plasma. *Antisense Research and Development*, *1*(2). https://doi.org/10.1089/ard.1991.1.141

Eghrari, A. O., Riazuddin, S. A., & Gottsch, J. D. (2015). Overview of the Cornea: Structure, Function, and Development. *Progress in Molecular Biology and Translational Science*, *134*. https://doi.org/10.1016/bs.pmbts.2015.04.001

Ehlers, N., & Hjortdal, J. (2005). *The Cornea* (pp. 83–111). https://doi.org/10.1016/S1569-2590(05)10003-2

el Kochairi, I., Letovanec, I., Uffer, S., Munier, F. L., Chaubert, P., & Schorderet, D. F. (2006). Systemic investigation of keratoepithelin deposits in TGFBI/BIGH3-related corneal dystrophy. *Molecular Vision*, *12*.

Elhusseiny, A. M., Soleimani, M., Eleiwa, T. K., Elsheikh, R. H., Frank, C. R., Naderan, M., Yazdanpanah, G., Rosenblatt, M. I., & Djalilian, A. R. (2022). Current and Emerging Therapies for Limbal Stem Cell Deficiency. In *Stem Cells Translational Medicine* (Vol. 11, Issue 3). https://doi.org/10.1093/stcltm/szab028

Ellies, P., Renard, G., Valleix, S., Yves Boelle, P., & Dighiero, P. (2002). Clinical outcome of eight BIGH3-linked corneal dystrophies. *Ophthalmology*, *109*(4). https://doi.org/10.1016/S0161-6420(01)01025-9

Endo, S., Ha, N. T., Fujiki, K., Hotta, Y., Nakayasu, K., Yamaguchi, T., Ishida, N., & Kanai, A. (1999). Leu518Pro mutation of the βig-h3 gene causes lattice corneal dystrophy type I. *American Journal of Ophthalmology*, *128*(1), 104–106. https://doi.org/10.1016/S0002-9394(99)00053-7

Engler, A. J., Sen, S., Sweeney, H. L., & Discher, D. E. (2006). Matrix Elasticity Directs Stem Cell Lineage Specification. *Cell*, *126*(4). https://doi.org/10.1016/j.cell.2006.06.044

Escribano, J., Hernando, N., Ghosh, S., Coca-Prados, M., & Crabb, J. (1994). cDNA from human ocular ciliary epithelium homologous to βig-h3 is preferentially expressed as an extracellular protein in the corneal epithelium. *Journal of Cellular Physiology*, *160*(3). https://doi.org/10.1002/jcp.1041600314

Espana, E. M., & Birk, D. E. (2020). Composition, structure and function of the corneal stroma. In *Experimental Eye Research* (Vol. 198). https://doi.org/10.1016/j.exer.2020.108137

Evans, C. J., Davidson, A. E., Carnt, N., Rojas Lòpez, K. E., Veli, N., Thaung, C. M., Tuft, S. J., & Hardcastle, A. J. (2016). Genotype-phenotype correlation for TGFBI corneal dystrophies identifies p.(G623D) as a novel cause of epithelial basement membrane dystrophy. *Investigative Ophthalmology and Visual Science*, *57*(13). https://doi.org/10.1167/iovs.16-19818

Evers, M. M., Toonen, L. J. A., & van Roon-Mom, W. M. C. (2015). Antisense oligonucleotides in therapy for neurodegenerative disorders. In *Advanced Drug Delivery Reviews* (Vol. 87). https://doi.org/10.1016/j.addr.2015.03.008

Falkenberg, K. D., Braverman, N. E., Moser, A. B., Steinberg, S. J., Klouwer, F. C. C., Schlüter, A., Ruiz, M., Pujol, A., Engvall, M., Naess, K., van Spronsen, F. J., Körver-Keularts, I., Rubio-Gozalbo, M. E., Ferdinandusse, S., Wanders, R. J. A., & Waterham, H. R. (2017). Allelic Expression Imbalance Promoting a Mutant PEX6 Allele Causes Zellweger Spectrum Disorder. *American Journal of Human Genetics*, *101*(6). https://doi.org/10.1016/j.ajhg.2017.11.007

Fändrich, M., Fletcher, M. A., & Dobson, C. M. (2001). Amyloid fibrils from muscle myoglobin. *Nature*, *410*(6825). https://doi.org/10.1038/35065514

Fedor, M. J., & Uhlenbeck, O. C. (1990). Substrate sequence effects on “hammerhead” RNA catalytic efficiency. *Proceedings of the National Academy of Sciences of the United States of America*, *87*(5). https://doi.org/10.1073/pnas.87.5.1668

Feizi, S., Pakravan, M., Baradaran-Rafiee, A. R., & Yazdani, S. (2007). Granular corneal dystrophy manifesting after radial keratotomy. *Cornea*, *26*(10). https://doi.org/10.1097/ICO.0b013e3181450fa8

Ferguson, J. W., Mikesh, M. F., Wheeler, E. F., & LeBaron, R. G. (2003). Developmental expression patterns of Beta-ig (βIG-H3) and its function as a cell adhesion protein. *Mechanisms of Development*, *120*(8). https://doi.org/10.1016/S0925-4773(03)00165-5

Ferguson, J. W., Thoma, B. S., Mikesh, M. F., Kramer, R. H., Bennett, K. L., Purchio, A., Bellard, B. J., & LeBaron, R. G. (2003). The extracellular matrix protein βIG-H3 is expressed at myotendinous junctions and supports muscle cell adhesion. *Cell and Tissue Research*, *313*(1). https://doi.org/10.1007/s00441-003-0743-z

Ferrarotti, I., Thun, G. A., Zorzetto, M., Ottaviani, S., Imboden, M., Schindler, C., von Eckardstein, A., Rohrer, L., Rochat, T., Russi, E. W., Probst-Hensch, N. M., & Luisetti, M. (2012). Serum levels and genotype distribution of α1-antitrypsin in the general population. *Thorax*, *67*(8). https://doi.org/10.1136/thoraxjnl-2011-201321

Fischer, H., Langbein, L., Reichelt, J., Praetzel-Wunder, S., Buchberger, M., Ghannadan, M., Tschachler, E., & Eckhart, L. (2014). Loss of keratin K2 expression causes aberrant aggregation of K10, hyperkeratosis, and inflammation. *Journal of Investigative Dermatology*, *134*(10). https://doi.org/10.1038/jid.2014.197

Folberg, R., Alfonso, E., Croxatto, J. O., Driezen, N. G., Panjwani, N., Laibson, P. R., Boruchoff, S. A., Baum, J., Malbran, E. S., Fernandez-Meijide, R., Morrison, J. A., Bernardino, V. B., Arbizo, V. v., & Albert, D. M. (1988). Clinically Atypical Granular Corneal Dystrophy with Pathologic Features of Lattice-like Amyloid Deposits: A Study of Three Families. *Ophthalmology*, *95*(1). https://doi.org/10.1016/S0161-6420(88)33226-4

Fong, C. Y., Peh, G. S. L., Gauthaman, K., & Bongso, A. (2009). Separation of SSEA-4 and TRA-1-60 labelled undifferentiated human embryonic stem cells from a heterogeneous cell population using magnetic-activated cell sorting (MACS) and fluorescence-activated cell sorting (FACS). *Stem Cell Reviews and Reports*, *5*(1). https://doi.org/10.1007/s12015-009-9054-4

Fossati, V., Jain, T., & Sevilla, A. (2016). The silver lining of induced pluripotent stem cell variation. In *Stem Cell Investigation* (Vol. 2016, Issue DEC). https://doi.org/10.21037/sci.2016.11.16

Foster, J. W., Wahlin, K., Adams, S. M., Birk, D. E., Zack, D. J., & Chakravarti, S. (2017). Cornea organoids from human induced pluripotent stem cells. *Scientific Reports*, *7*. https://doi.org/10.1038/srep41286

Franco, P., & De Marco, I. (2021). Contact lenses as ophthalmic drug delivery systems: A review. In *Polymers* (Vol. 13, Issue 7). https://doi.org/10.3390/polym13071102

Freier, S. M., & Tinoco, I. (1975). Binding of Complementary Oligoribonucleotides to Yeast Initiator Transfer Rna. *Biochemistry*, *14*(15). https://doi.org/10.1021/bi00686a004

Frieden, M., Christensen, S. M., Mikkelsen, N. D., Rosenbohm, C., Thrue, C. A., Westergaard, M., Hansen, H. F., Ørum, H., & Koch, T. (2003). Expanding the design horizon of antisense oligonucleotides with alpha-L-LNA. *Nucleic Acids Research*, *31*(21). https://doi.org/10.1093/nar/gkg820

Frising, M., Wildhardt, G., Frisch, L., & Pitz, S. (2006). Recurrent granular dystrophy of the cornea: An unusual case. *Cornea*, *25*(5). https://doi.org/10.1097/01.ico.0000214202.84081.a5

Fuchs, E., & Green, H. (1980). Changes in keratin gene expression during terminal differentiation of the keratinocyte. *Cell*, *19*(4). https://doi.org/10.1016/0092-8674(80)90094-X

Fuhrmann, S. (2008). Wnt signaling in eye organogenesis. In *Organogenesis* (Vol. 4, Issue 2). https://doi.org/10.4161/org.4.2.5850

Fujiki, K., Nakayasu, K., & Kanai, A. (2001). Corneal dystrophies in japan. In *Journal of Human Genetics* (Vol. 46, Issue 8). https://doi.org/10.1007/s100380170041

Fuller, Z. L., Berg, J. J., Mostafavi, H., Sella, G., & Przeworski, M. (2019). Measuring intolerance to mutation in human genetics. In *Nature Genetics* (Vol. 51, Issue 5). https://doi.org/10.1038/s41588-019-0383-1

Furuta, Y., & Hogan, B. L. M. (1998). BMP4 is essential for lens induction in the mouse embryo. *Genes & Development*, *12*(23), 3764–3775. https://doi.org/10.1101/gad.12.23.3764

Gabison, E. E., Mourah, S., Steinfels, E., Yan, L., Hoang-Xuan, T., Watsky, M. A., De Wever, B., Calvo, F., Mauviel, A., & Menashi, S. (2005). Differential expression of extracellular matrix metalloproteinase inducer (CD147) in normal and ulcerated corneas: Role in epithelio-stromal interactions and matrix metalloproteinase induction. *American Journal of Pathology*, *166*(1). https://doi.org/10.1016/S0002-9440(10)62245-6

Gage, P. J., Kuang, C., & Zacharias, A. L. (2014). The homeodomain transcription factor PITX2 is required for specifying correct cell fates and establishing angiogenic privilege in the developing cornea. *Developmental Dynamics*, *243*(11). https://doi.org/10.1002/dvdy.24165

Gage, P. J., Qian, M., Wu, D., & Rosenberg, K. I. (2008). The canonical Wnt signaling antagonist DKK2 is an essential effector of PITX2 function during normal eye development. *Developmental Biology*, *317*(1). https://doi.org/10.1016/j.ydbio.2008.02.030

Gagnon, K. T. (2010). HD therapeutics-CHDI fifth annual conference. *IDrugs*, *13*(4).

Galloway, C. A., Dalvi, S., Hung, S. S. C., MacDonald, L. A., Latchney, L. R., Wong, R. C. B., Guymer, R. H., Mackey, D. A., Williams, D. S., Chung, M. M., Gamm, D. M., Pébay, A., Hewitt, A. W., & Singh, R. (2017). Drusen in patient-derived hiPSC-RPE models of macular dystrophies. *Proceedings of the National Academy of Sciences of the United States of America*, *114*(39). https://doi.org/10.1073/pnas.1710430114

Gambaro, K., Aberdam, E., Virolle, T., Aberdam, D., & Rouleau, M. (2006). BMP-4 induces a Smad-dependent apoptotic cell death of mouse embryonic stem cell-derived neural precursors. *Cell Death and Differentiation*, *13*(7). https://doi.org/10.1038/sj.cdd.4401799

García-Castellanos, R., Nielsen, N. S., Runager, K., Thøgersen, I. B., Lukassen, M. V., Poulsen, E. T., Goulas, T., Enghild, J. J., & Gomis-Rüth, F. X. (2017). Structural and Functional Implications of Human Transforming Growth Factor β-Induced Protein, TGFBIp, in Corneal Dystrophies. *Structure*, *25*(11). https://doi.org/10.1016/j.str.2017.09.001

Gaudana, R., Ananthula, H. K., Parenky, A., & Mitra, A. K. (2010). Ocular drug delivery. In *The AAPS journal* (Vol. 12, Issue 3). https://doi.org/10.1208/s12248-010-9183-3

Ge, H., Tian, P., Guan, L., Yin, X., Liu, H., Xiao, N., Xiong, Y., Luo, X., Sun, Y., Qi, D., Ni, S., & Liu, P. (2013). A C-terminal fragment BIGH3 protein with an RGDRGD motif inhibits corneal neovascularization invitro and invivo. *Experimental Eye Research*, *112*, 10–20. https://doi.org/10.1016/j.exer.2013.03.014

Ge, J., Apicella, M., Mills, J. A., Garçon, L., French, D. L., Weiss, M. J., Bessler, M., & Mason, P. J. (2015). Dysregulation of the transforming growth factor β pathway in induced pluripotent stem cells generated from patients with Diamond Blackfan anemia. *PLoS ONE*, *10*(8). https://doi.org/10.1371/journal.pone.0134878

Geary, R. S. (2009). Antisense oligonucleotide pharmacokinetics and metabolism. In *Expert Opinion on Drug Metabolism and Toxicology* (Vol. 5, Issue 4). https://doi.org/10.1517/17425250902877680

Gebert, L. F. R., Rebhan, M. A. E., Crivelli, S. E. M., Denzler, R., Stoffel, M., & Hall, J. (2014). Miravirsen (SPC3649) can inhibit the biogenesis of miR-122. *Nucleic Acids Research*, *42*(1). https://doi.org/10.1093/nar/gkt852

Gettins, P. G. W. (2002). Serpin structure, mechanism, and function. *Chemical Reviews*, *102*(12). https://doi.org/10.1021/cr010170+

Ghaffari, L. T., Starr, A., Nelson, A. T., & Sattler, R. (2018). Representing diversity in the dish: Using patient-derived in vitro models to recreate the heterogeneity of neurological disease. In *Frontiers in Neuroscience* (Vol. 12, Issue FEB). https://doi.org/10.3389/fnins.2018.00056

Ghareeb, A. E., Lako, M., & Figueiredo, F. C. (2020). Recent Advances in Stem Cell Therapy for Limbal Stem Cell Deficiency: A Narrative Review. In *Ophthalmology and Therapy* (Vol. 9, Issue 4). https://doi.org/10.1007/s40123-020-00305-2

Gibson, M. A., Kumaratilake, J. S., & Cleary, E. G. (1997). Immunohistochemical and ultrastructural localization of MP78/70 (βig- h3) in extracellular matrix of developing and mature bovine tissues. *Journal of Histochemistry and Cytochemistry*, *45*(12). https://doi.org/10.1177/002215549704501212

Giudice, G. J., & Fuchs, E. (1987). The transfection of epidermal keratin genes into fibroblasts and simple epithelial cells: Evidence for inducing a type I keratin by a type II gene. *Cell*, *48*(3). https://doi.org/10.1016/0092-8674(87)90196-6

Glazier, A. A., Thompson, A., & Day, S. M. (2019). Allelic imbalance and haploinsufficiency in MYBPC3-linked hypertrophic cardiomyopathy. In *Pflugers Archiv European Journal of Physiology* (Vol. 471, Issue 5). https://doi.org/10.1007/s00424-018-2226-9

Gonzalez, G., Sasamoto, Y., Ksander, B. R., Frank, M. H., & Frank, N. Y. (2018). Limbal stem cells: identity, developmental origin, and therapeutic potential. In *Wiley Interdisciplinary Reviews: Developmental Biology* (Vol. 7, Issue 2). https://doi.org/10.1002/wdev.303

González, S., Halabi, M., Ju, D., Tsai, M., & Deng, S. X. (2020). Role of Jagged1-mediated Notch Signaling Activation in the Differentiation and Stratification of the Human Limbal Epithelium. *Cells*, *9*(9). https://doi.org/10.3390/cells9091945

González, S., Oh, D., Baclagon, E. R., Zheng, J. J., & Deng, S. X. (2019). Wnt signaling is required for the maintenance of human limbal stem/progenitor cells in vitro. *Investigative Ophthalmology and Visual Science*, *60*(1). https://doi.org/10.1167/iovs.18-25740

González, S., Uhm, H., & Deng, S. X. (2019). Notch Inhibition Prevents Differentiation of Human Limbal Stem/Progenitor Cells in vitro. *Scientific Reports*, *9*(1). https://doi.org/10.1038/s41598-019-46793-6

Goumenou, A. G., Arvanitis, D. A., Matalliotakis, I. M., Koumantakis, E. E., & Spandidos, D. A. (2001). Microsatellite DNA assays reveal an allelic imbalance in p16Ink4, GALT, p53, and APOA2 loci in patients with endometriosis. *Fertility and Sterility*, *75*(1). https://doi.org/10.1016/S0015-0282(00)01663-0

Gouveia, R. M., Lepert, G., Gupta, S., Mohan, R. R., Paterson, C., & Connon, C. J. (2019). Assessment of corneal substrate biomechanics and its effect on epithelial stem cell maintenance and differentiation. *Nature Communications*, *10*(1). https://doi.org/10.1038/s41467-019-09331-6

Gratchev, A., Guillot, P., Hakiy, N., Politz, O., Orfanos, C. E., Schledzewski, K., & Goerdt, S. (2001). Alternatively activated macrophages differentially express fibronectin and its splice variants and the extracellular matrix protein βIG-H3. *Scandinavian Journal of Immunology*, *53*(4). https://doi.org/10.1046/j.1365-3083.2001.00885.x

Groulx, J. F., Gagné, D., Benoit, Y. D., Martel, D., Basora, N., & Beaulieu, J. F. (2011). Collagen VI is a basement membrane component that regulates epithelial cell-fibronectin interactions. *Matrix Biology*, *30*(3). https://doi.org/10.1016/j.matbio.2011.03.002

Gruber, J. D., & Long, A. D. (2009). Cis-regulatory variation is typically polyallelic in Drosophila. *Genetics*, *181*(2). https://doi.org/10.1534/genetics.108.098459

Gruenauer-Kloevekorn, C., Clausen, I., Weidle, E., Wolter-Roessler, M., Tost, F., Völcker, H. E., Schulze, D. P., Heinritz, W., Reinhard, T., Froster, U., Duncker, G., Schorderet, D., & Auw-Haedrich, C. (2009). TGFBI (BIGH3) gene mutations in German families: Two novel mutations associated with unique clinical and histopathological findings. *British Journal of Ophthalmology*, *93*(7). https://doi.org/10.1136/bjo.2008.142927

Grünweller, A., Wyszko, E., Bieber, B., Jahnel, R., Erdmann, V. A., & Kurreck, J. (2003). Comparison of different antisense strategies in mammalian cells using locked

nucleic acids, 2′-O-methyl RNA, phosphorothioates and small interfering RNA. *Nucleic Acids Research*, *31*(12). https://doi.org/10.1093/nar/gkg409

Guan, Y. Z., Liu, H., Huang, H. J., Liang, D. Y., Wu, S. Y., & Zhang, T. (2022). Identification of the Potential Molecular Mechanism of TGFBI Gene in Persistent Atrial Fibrillation. *Computational and Mathematical Methods in Medicine*, *2022*. https://doi.org/10.1155/2022/1643674

Guldiken, N., Usachov, V., Levada, K., Trautwein, C., Ziol, M., Nahon, P., & Strnad, P. (2015). Keratins 8 and 18 are type II acute-phase responsive genes overexpressed in human liver disease. *Liver International*, *35*(4). https://doi.org/10.1111/liv.12608

Guo, Y.-S., Tang, J., Chen, B., Huang, W., Li, Y., Cui, H.-Y., Zhang, X., Wang, S.-J., Chen, Z.-N., & Jiang, J.-L. (2011). βig-h3 regulates store-operated Ca 2+ entry and promotes the invasion of human hepatocellular carcinoma cells . *Cell Biology International*, *35*(8). https://doi.org/10.1042/cbi20100916

Haddad, A. (2000). Renewal of the rabbit corneal epithelium as investigated by autoradiography after intravitreal injection of 3H-thymidine. *Cornea*, *19*(3). https://doi.org/10.1097/00003226-200005000-00024

Hafez, D., Huang, J. Y., Huynh, A. M., Valtierra, S., Rockenstein, E., Bruno, A. M., Lu, B., DesGroseillers, L., Masliah, E., & Marr, R. A. (2011). Neprilysin-2 is an important β-amyloid degrading enzyme. *American Journal of Pathology*, *178*(1). https://doi.org/10.1016/j.ajpath.2010.11.012

Hamilton, D. W. (2008). Functional role of periostin in development and wound repair: Implications for connective tissue disease. In *Journal of Cell Communication and Signaling* (Vol. 2, Issues 1–2). https://doi.org/10.1007/s12079-008-0023-5

Han, B., Chen, S. Y., Zhu, Y. T., & Tseng, S. C. G. (2014). Integration of BMP/Wnt signaling to control clonal growth of limbal epithelial progenitor cells by niche cells. *Stem Cell Research*, *12*(2). https://doi.org/10.1016/j.scr.2014.01.003

Han, K. E., Choi, S. il, Chung, W. S., Jung, S. H., Katsanis, N., Kim, T. im, & Kim, E. K. (2012). Extremely varied phenotypes in granular corneal dystrophy type 2 heterozygotes. *Molecular Vision*, *18*.

Han, K. E., Choi, S. Il, Kim, T. I., Maeng, Y. S., Stulting, R. D., Ji, Y. W., & Kim, E. K. (2016). Pathogenesis and treatments of TGFBI corneal dystrophies. In *Progress in Retinal and Eye Research* (Vol. 50). https://doi.org/10.1016/j.preteyeres.2015.11.002

Han, Y. P., Sim, A. J., Vora, S. C., & Huang, A. J. W. (2011). Unique TGFBI protein in lattice corneal dystrophy. *Investigative Ophthalmology and Visual Science*, *52*(11). https://doi.org/10.1167/iovs.11-7618

Han, Y. P., Sim, A. J., Vora, S. C., & Huang, A. J. W. (2012). A unique TGFBI protein in granular corneal dystrophy types 1 and 2. *Current Eye Research*, *37*(11). https://doi.org/10.3109/02713683.2012.700752

Hanna, J., Guerra-Moreno, A., Ang, J., & Micoogullari, Y. (2019). Protein Degradation and the Pathologic Basis of Disease. In *American Journal of Pathology* (Vol. 189, Issue 1). https://doi.org/10.1016/j.ajpath.2018.09.004

Hanssen, E., Reinboth, B., & Gibson, M. A. (2003). Covalent and non-covalent interactions of βig-h3 with collagen VI: βig-h3 is covalently attached to the amino-terminal region of collagen VI in tissue microfibrils. *Journal of Biological Chemistry*, *278*(27). https://doi.org/10.1074/jbc.M303455200

Hao, Y., Hao, S., Andersen-Nissen, E., Mauck, W. M., Zheng, S., Butler, A., Lee, M. J., Wilk, A. J., Darby, C., Zager, M., Hoffman, P., Stoeckius, M., Papalexi, E., Mimitou, E. P., Jain, J., Srivastava, A., Stuart, T., Fleming, L. M., Yeung, B., … Satija, R. (2021). Integrated analysis of multimodal single-cell data. *Cell*, *184*(13). https://doi.org/10.1016/j.cell.2021.04.048

Harburger, D. S., & Calderwood, D. A. (2009). Integrin signalling at a glance. *Journal of Cell Science*, *122*(2). https://doi.org/10.1242/jcs.018093

Harding, P. L., Fall, A. M., Honeyman, K., Fletcher, S., & Wilton, S. D. (2007). The influence of antisense oligonucleotide length on dystrophin exon skipping. *Molecular Therapy*, *15*(1). https://doi.org/10.1038/sj.mt.6300006

Hartsock, A., & Nelson, W. J. (2008). Adherens and tight junctions: Structure, function and connections to the actin cytoskeleton. In *Biochimica et Biophysica Acta - Biomembranes* (Vol. 1778, Issue 3). https://doi.org/10.1016/j.bbamem.2007.07.012

Hashimoto, K., Noshiro, M., Ohno, S., Kawamoto, T., Satakeda, H., Akagawa, Y., Nakashima, K., Okimura, A., Ishida, H., Okamoto, T., Pan, H., Shen, M., Yan, W., & Kato, Y. (1997). Characterization of a cartilage-derived 66-kDa protein (RCD-CAP/βig-h3) that binds to collagen. *Biochimica et Biophysica Acta - Molecular Cell Research*, *1355*(3). https://doi.org/10.1016/S0167-4889(96)00147-4

Hasib Sidiqi, M., & Gertz, M. A. (2021). Immunoglobulin light chain amyloidosis diagnosis and treatment algorithm 2021. In *Blood Cancer Journal* (Vol. 11, Issue 5). https://doi.org/10.1038/s41408-021-00483-7

Hayashi, R., Ishikawa, Y., Ito, M., Kageyama, T., Takashiba, K., Fujioka, T., Tsujikawa, M., Miyoshi, H., Yamato, M., Nakamura, Y., & Nishida, K. (2012). Generation of Corneal Epithelial Cells from Induced Pluripotent Stem Cells Derived from Human Dermal Fibroblast and Corneal Limbal Epithelium. *PLoS ONE*, *7*(9). https://doi.org/10.1371/journal.pone.0045435

Hayashi, R., Ishikawa, Y., Katayama, T., Quantock, A. J., & Nishida, K. (2018). CD200 facilitates the isolation of corneal epithelial cells derived from human pluripotent stem cells. *Scientific Reports*, *8*(1). https://doi.org/10.1038/s41598-018-34845-2

Hayashi, R., Ishikawa, Y., Katori, R., Sasamoto, Y., Taniwaki, Y., Takayanagi, H., Tsujikawa, M., Sekiguchi, K., Quantock, A. J., & Nishida, K. (2017). Coordinated generation of multiple ocular-like cell lineages and fabrication of functional corneal epithelial cell sheets from human iPS cells. *Nature Protocols*, *12*(4). https://doi.org/10.1038/nprot.2017.007

Henriksson, J. T., McDermott, A. M., & Bergmanson, J. P. G. (2009). Dimensions and morphology of the cornea in three strains of mice. *Investigative Ophthalmology and Visual Science*, *50*(8). https://doi.org/10.1167/iovs.08-2941

Herschlag, D., & Cech, T. R. (1990). Catalysis of RNA Cleavage by the Tetrahymena thermophila Ribozyme. 2. Kinetic Description of the Reaction of an RNA Substrate That Forms a Mismatch at the Active Site. *Biochemistry*, *29*(44). https://doi.org/10.1021/bi00496a004

Higa, K., Shimmura, S., Miyashita, H., Shimazaki, J., & Tsubota, K. (2005). Melanocytes in the corneal limbus interact with K19-positive basal epithelial cells. *Experimental Eye Research*, *81*(2). https://doi.org/10.1016/j.exer.2005.01.023

Hirano, K., Klintworth, G. K., Zhan, Q., Bennett, K., & Cintron, C. (1996). βig-h3 is synthesized by corneal epithelium and perhaps endothelium in Fuchs' dystrophic corneas. *Current Eye Research*, *15*(9). https://doi.org/10.3109/02713689609017642

Hirate, Y., Okamoto, H., & Yamasu, K. (2003). Structure of the zebrafish fasciclin I-related extracellular matrix protein (βig-h3) and its characteristic expression during

embryogenesis. *Gene Expression Patterns*, *3*(3). https://doi.org/10.1016/S1567-133X(03)00035-8

Ho, M., Thompson, B., Fisk, J. N., Nebert, D. W., Bruford, E. A., Vasiliou, V., & Bunick, C. G. (2022). Update of the keratin gene family: evolution, tissue-specific expression patterns, and relevance to clinical disorders. *Human Genomics*, *16*(1). https://doi.org/10.1186/s40246-021-00374-9

Hogan, M., & Zimmerman, L. (1953). Ophthalmic Pathology: An Atlas and Textbook. *Archives of Ophthalmology*, *49*(2), 278–278. https://doi.org/10.1001/archopht.1953.00920020244015

Hongisto, H., Ilmarinen, T., Vattulainen, M., Mikhailova, A., & Skottman, H. (2017). Xeno- and feeder-free differentiation of human pluripotent stem cells to two distinct ocular epithelial cell types using simple modifications of one method. *Stem Cell Research and Therapy*, *8*(1). https://doi.org/10.1186/s13287-017-0738-4

Horiuchi, K., Amizuka, N., Takeshita, S., Takamatsu, H., Katsuura, M., Ozawa, H., Toyama, Y., Bonewald, L. F., & Kudo, A. (1999). Identification and characterization of a novel protein, periostin, with restricted expression to periosteum and periodontal ligament and increased expression by transforming growth factor β. *Journal of Bone and Mineral Research*, *14*(7). https://doi.org/10.1359/jbmr.1999.14.7.1239

Hovingh, K., Besseling, J., & Kastelein, J. (2013). Efficacy and safety of mipomersen sodium (Kynamro). In *Expert Opinion on Drug Safety* (Vol. 12, Issue 4). https://doi.org/10.1517/14740338.2013.793670

Howden, S. E., Maufort, J. P., Duffin, B. M., Elefanty, A. G., Stanley, E. G., & Thomson, J. A. (2015). Simultaneous Reprogramming and Gene Correction of Patient Fibroblasts. *Stem Cell Reports*, *5*(6). https://doi.org/10.1016/j.stemcr.2015.10.009

Hsu, K.-H., Carbia, B. E., Plummer, C., & Chauhan, A. (2015). Dual drug delivery from vitamin E loaded contact lenses for glaucoma therapy. *European Journal of Pharmaceutics and Biopharmaceutics*, *94*, 312–321. https://doi.org/10.1016/j.ejpb.2015.06.001

Hu, B. Y., Weick, J. P., Yu, J., Ma, L. X., Zhang, X. Q., Thomson, J. A., & Zhang, S. C. (2010). Neural differentiation of human induced pluripotent stem cells follows developmental principles but with variable potency. *Proceedings of the National*

Academy of Sciences of the United States of America, *107*(9). https://doi.org/10.1073/pnas.0910012107

Hu, Q., Friedrich, A. M., Johnson, L. V., & Clegg, D. O. (2010). Memory in induced pluripotent stem cells: Reprogrammed human retinal-pigmented epithelial cells show tendency for spontaneous redifferentiation. *Stem Cells*, *28*(11). https://doi.org/10.1002/stem.531

Huang, A. J. W., & Tseng, S. C. G. (1991). Corneal epithelial wound healing in the absence of limbal epithelium. *Investigative Ophthalmology and Visual Science*, *32*(1).

Hudziak, R. M., Summerton, J., Weller, D. D., & Iversen, P. L. (2000). Antiproliferative effects of steric blocking phosphorodiamidate Morpholino antisense agents directed against c-myc. *Antisense and Nucleic Acid Drug Development*, *10*(3). https://doi.org/10.1089/oli.1.2000.10.163

Hulleman, J. D., Genereux, J. C., & Nguyen, A. (2016). Mapping wild-type and R345W fibulin-3 intracellular interactomes. *Experimental Eye Research*, *153*. https://doi.org/10.1016/j.exer.2016.10.017

Huntington, J. A., Read, R. J., & Carrell, R. W. (2000). Structure of a serpin-protease complex shows inhibition by deformation. *Nature*, *407*(6806). https://doi.org/10.1038/35038119

Hyer, J., Kuhlman, J., Afif, E., & Mikawa, T. (2003). Optic cup morphogenesis requires pre-lens ectoderm but not lens differentiation. *Developmental Biology*, *259*(2). https://doi.org/10.1016/S0012-1606(03)00205-7

I., B., G., T., A., O., & S., D. (2011). Dynamic control of head mesoderm patterning. In *Development* (Vol. 138, Issue 13).

Ichida, J. K., Blanchard, J., Lam, K., Son, E. Y., Chung, J. E., Egli, D., Loh, K. M., Carter, A. C., di Giorgio, F. P., Koszka, K., Huangfu, D., Akutsu, H., Liu, D. R., Rubin, L. L., & Eggan, K. (2009). A Small-Molecule Inhibitor of Tgf-β Signaling Replaces Sox2 in Reprogramming by Inducing Nanog. *Cell Stem Cell*, *5*(5). https://doi.org/10.1016/j.stem.2009.09.012

Ilmarinen, T., Vattulainen, M., Kandhavelu, J., Bremond-Gignac, D., Aberdam, D., & Skottman, H. (2023). Production and Limbal Lineage Commitment of Aniridia Patient-Derived Induced Pluripotent Stem Cells. *Stem Cells*. https://doi.org/10.1093/stmcls/sxad067

Irigoyen, M., Pajares, M. J., Agorreta, J., Ponz-Sarvisé, M., Salvo, E., Lozano, M. D., Pío, R., Gil-Bazo, I., & Rouzaut, A. (2010). TGFBI expression is associated with a better response to chemotherapy in NSCLC. *Molecular Cancer*, *9*. https://doi.org/10.1186/1476-4598-9-130

Irvine, A. D., Corden, L. D., Swensson, O., Swensson, B., Moore, J. E., Frazer, D. G., Smith, F. J. D., Knowlton, R. G., Christophers, E., Rochels, R., Uitto, J., & McLean, W. H. I. (1997). Mutations in cornea-specific keratin K3 or K12 genes cause Meesmann's corneal dystrophy. *Nature Genetics*, *16*(2). https://doi.org/10.1038/ng0697-184

Isla-Magrané, H., Veiga, A., García-Arumí, J., & Duarri, A. (2021). Multiocular organoids from human induced pluripotent stem cells displayed retinal, corneal, and retinal pigment epithelium lineages. *Stem Cell Research and Therapy*, *12*(1). https://doi.org/10.1186/s13287-021-02651-9

Ittner, L. M., Wurdak, H., Schwerdtfeger, K., Kunz, T., Ille, F., Leveen, P., Hjalt, T. A., Suter, U., Karlsson, S., Hafezi, F., Born, W., & Sommer, L. (2005). Compound developmental eye disorders following inactivation of TGFβ signaling in neural-crest stem cells. *Journal of Biology*, *4*. https://doi.org/10.1186/jbiol29

Ivanov, S. V., Ivanova, A. V., Salnikow, K., Timofeeva, O., Subramaniam, M., & Lerman, M. I. (2008). Two novel VHL targets, TGFBI (BIGH3) and its transactivator KLF10, are up-regulated in renal clear cell carcinoma and other tumors. *Biochemical and Biophysical Research Communications*, *370*(4). https://doi.org/10.1016/j.bbrc.2008.03.066

Jabs, D. A., & Griffiths, P. D. (2002). Fomivirsen for the treatment of cytomegalovirus retinitis. In *American Journal of Ophthalmology* (Vol. 133, Issue 4). https://doi.org/10.1016/S0002-9394(02)01325-9

Jester, J. V., Moller-Pedersen, T., Huang, J., Sax, C. M., Kays, W. T., Cavangh, H. D., Petroll, W. M., & Piatigorsky, J. (1999). The cellular basis of corneal transparency: Evidence for "corneal crystallins." *Journal of Cell Science*, *112*(5). https://doi.org/10.1242/jcs.112.5.613

Jiang, X., & Zhang, H. (2021). Deterioration of Avellino corneal dystrophy in a Chinese family after LASIK. *International Journal of Ophthalmology*, *14*(6). https://doi.org/10.18240/ijo.2021.06.02

Johnson, B. L., Brown, S. I., & Zaidman, G. W. (1981). A light and electron microscopic study of recurrent granular dystrophy of the cornea. *American Journal of Ophthalmology*, *92*(1). https://doi.org/10.1016/S0002-9394(14)75907-0

Joseph, R., Srivastava, O. P., & Pfister, R. R. (2016). Modeling keratoconus using induced pluripotent stemcells. *Investigative Ophthalmology and Visual Science*, *57*(8). https://doi.org/10.1167/iovs.16-19105

Joyce, N. C., & Zieske, J. D. (1997). Transforming growth factor-β receptor expression in human cornea. *Investigative Ophthalmology and Visual Science*, *38*(10).

Jozaei, R., Javadi, M. A., Safari, I., Moghaddasi, A., Feizi, S., Kanavi, M. R., Najafi, S., Safdari, B., Salahshourifar, I., Elahi, E., & Suri, F. (2022). Genetic screening of TGFBI in Iranian patients with TGFBI-associated corneal dystrophies and a meta-analysis of global variation frequencies. *Ophthalmic Genetics*. https://doi.org/10.1080/13816810.2022.2068040

Jung, J. W., Kim, S. A., Kang, E. M., Kim, T. I., Cho, H. S., & Kim, E. K. (2014). Lattice corneal dystrophy type IIIA with hyaline component from a novel A620P mutation and distinct surgical treatments. *Cornea*, *33*(12). https://doi.org/10.1097/ICO.0000000000000281

Jurewicz, E., Robaszkiewicz, K., Moraczewska, J., & Filipek, A. (2020). Binding of S100A6 to actin and the actin–tropomyosin complex. *Scientific Reports*, *10*(1). https://doi.org/10.1038/s41598-020-69752-y

Kabza, M., Karolak, J. A., Rydzanicz, M., Szcześniak, M. W., Nowak, D. M., Ginter-Matuszewska, B., Polakowski, P., Ploski, R., Szaflik, J. P., & Gajecka, M. (2017). Collagen synthesis disruption and downregulation of core elements of TGF-β, Hippo, and Wnt pathways in keratoconus corneas. *European Journal of Human Genetics*, *25*(5). https://doi.org/10.1038/ejhg.2017.4

Kadler, K. E., Hill, A., & Canty-Laird, E. G. (2008). Collagen fibrillogenesis: fibronectin, integrins, and minor collagens as organizers and nucleators. In *Current Opinion in Cell Biology* (Vol. 20, Issue 5). https://doi.org/10.1016/j.ceb.2008.06.008

Kadowaki, H., Nishitoh, H., Urano, F., Sadamitsu, C., Matsuzawa, A., Takeda, K., Masutani, H., Yodoi, J., Urano, Y., Nagano, T., & Ichijo, H. (2005). Amyloid β induces neuronal cell death through ROS-mediated ASK1 activation. *Cell Death and Differentiation*, *12*(1). https://doi.org/10.1038/sj.cdd.4401528

Kamaleddin, M. A. (2017). Nano-ophthalmology: Applications and considerations. In *Nanomedicine: Nanotechnology, Biology, and Medicine* (Vol. 13, Issue 4). https://doi.org/10.1016/j.nano.2017.02.007

Kamarudin, T. A., Bojic, S., Collin, J., Yu, M., Alharthi, S., Buck, H., Shortt, A., Armstrong, L., Figueiredo, F. C., & Lako, M. (2018). Differences in the Activity of Endogenous Bone Morphogenetic Protein Signaling Impact on the Ability of Induced Pluripotent Stem Cells to Differentiate to Corneal Epithelial-Like Cells. *Stem Cells*, *36*(3). https://doi.org/10.1002/stem.2750

Kanchan, K., Iyer, K., Yanek, L. R., Carcamo-Orive, I., Taub, M. A., Malley, C., Baldwin, K., Becker, L. C., Broeckel, U., Cheng, L., Cowan, C., D'Antonio, M., Frazer, K. A., Quertermous, T., Mostoslavsky, G., Murphy, G., Rabinovitch, M., Rader, D. J., Steinberg, M. H., … Mathias, R. A. (2020). Genomic integrity of human induced pluripotent stem cells across nine studies in the NHLBI NextGen program. *Stem Cell Research*, *46*. https://doi.org/10.1016/j.scr.2020.101803

Kang, S., Dong, S. M., & Park, N. H. (2010). Frequent promoter hypermethylation of TGFBI in epithelial ovarian cancer. *Gynecologic Oncology*, *118*(1). https://doi.org/10.1016/j.ygyno.2010.03.025

Kannabiran, C., & Klintworth, G. K. (2006). TGFBI gene mutations in coraeal dystrophies. In *Human Mutation* (Vol. 27, Issue 7). https://doi.org/10.1002/humu.20334

Kao, W. W. Y., Liu, C. Y., Converse, R. L., Shiraishi, A., Kao, C. W. C., Ishizaki, M., Doetschman, T., & Duffy, J. (1996). Keratin 12-deficient mice have fragile corneal epithelia. *Investigative Ophthalmology and Visual Science*, *37*(13).

Karring, H., Poulsen, E. T., Runager, K., Thøgersen, I. B., Klintworth, G. K., Højrup, P., & Enghild, J. J. (2013). Serine protease HtrA1 accumulates in corneal transforming growth factor beta induced protein (TGFBIp) amyloid deposits. *Molecular Vision*, *19*.

Karring, H., Runager, K., Thøgersen, I. B., Klintworth, G. K., Højrup, P., & Enghild, J. J. (2012). Composition and proteolytic processing of corneal deposits associated with mutations in the TGFBI gene. *Experimental Eye Research*, *96*(1). https://doi.org/10.1016/j.exer.2011.11.014

Karring, H., Runager, K., Valnickova, Z., Thøgersen, I. B., Møller-Pedersen, T., Klintworth, G. K., & Enghild, J. J. (2010). Differential expression and processing of transforming growth factor beta induced protein (TGFBIp) in the normal human

cornea during postnatal development and aging. *Experimental Eye Research*, *90*(1). https://doi.org/10.1016/j.exer.2009.09.011

Kawakita, T., Higa, K., Shimmura, S., Tomita, M., Tsubota, K., & Shimazaki, J. (2011). Fate of corneal epithelial cells separated from limbus in vivo. *Investigative Ophthalmology and Visual Science*, *52*(11). https://doi.org/10.1167/iovs.11-7984

Kawasaki, H., Mizuseki, K., Nishikawa, S., Kaneko, S., Kuwana, Y., Nakanishi, S., Nishikawa, S. I., & Sasai, Y. (2000). Induction of midbrain dopaminergic neurons from ES cells by stromal cell-derived inducing activity. *Neuron*, *28*(1). https://doi.org/10.1016/S0896-6273(00)00083-0

Kaya, S. G., Inanc-Surer, S., Cakan-Akdogan, G., Oktay, G., Utine, C. A., & Kalyoncu, S. (2021). Roles of matrix metalloproteinases in the cornea: A special focus on macular corneal dystrophy. In *Medicine in Drug Discovery* (Vol. 11). https://doi.org/10.1016/j.medidd.2021.100095

Keiser, M. S., Kordasiewicz, H. B., & McBride, J. L. (2016). Gene suppression strategies for dominantly inherited neurodegenerative diseases: lessons from Huntington's disease and spinocerebellar ataxia. In *Human Molecular Genetics* (Vol. 25, Issue R1). https://doi.org/10.1093/hmg/ddv442

Kent, W. J. (2002). BLAT —The BLAST -Like Alignment Tool . *Genome Research*, *12*(4). https://doi.org/10.1101/gr.229202

Kepchia, D., Huang, L., Dargusch, R., Rissman, R. A., Shokhirev, M. N., Fischer, W., & Schubert, D. (2020). Diverse proteins aggregate in mild cognitive impairment and Alzheimer's disease brain. *Alzheimer's Research and Therapy*, *12*(1). https://doi.org/10.1186/s13195-020-00641-2

Kheir, V., Cortés-González, V., Zenteno, J. C., & Schorderet, D. F. (2019). Mutation update: TGFBI pathogenic and likely pathogenic variants in corneal dystrophies. *Human Mutation*, *40*(6). https://doi.org/10.1002/humu.23737

Khorkova, O., & Wahlestedt, C. (2017). Oligonucleotide therapies for disorders of the nervous system. *Nature Biotechnology*, *35*(3). https://doi.org/10.1038/nbt.3784

Kielty, C. M., Sherratt, M. J., & Shuttleworth, C. A. (2002). Elastic fibres. *Journal of Cell Science*, *115*(14). https://doi.org/10.1242/jcs.115.14.2817

Kilpinen, H., Goncalves, A., Leha, A., Afzal, V., Alasoo, K., Ashford, S., Bala, S., Bensaddek, D., Casale, F. P., Culley, O. J., Danecek, P., Faulconbridge, A.,

Harrison, P. W., Kathuria, A., McCarthy, D., McCarthy, S. A., Meleckyte, R., Memari, Y., Moens, N., … Gaffney, D. J. (2017). Common genetic variation drives molecular heterogeneity in human iPSCs. *Nature*, *546*(7658). https://doi.org/10.1038/nature22403

Kim, B. Y., Olzmann, J. A., Choi, S. Il, Ahn, S. Y., Kim, T. I., Cho, H. S., Suh, H., & Kim, E. K. (2009). Corneal dystrophy-associated R124H mutation disrupts TGFBI interaction with periostin and causes mislocalization to the lysosome. *Journal of Biological Chemistry*, *284*(29). https://doi.org/10.1074/jbc.M109.013607

Kim, E. K., Kim, S., & Maeng, Y. S. (2019). Generation of TGFBI knockout ABCG2+/ ABCB5+ double-positive limbal epithelial stem cells by CRISPR/Cas9-mediated genome editing. *PLoS ONE*, *14*(2). https://doi.org/10.1371/journal.pone.0211864

Kim, H. R., & Ingham, P. W. (2009). The extracellular matrix protein TGFBI promotes myofibril bundling and muscle fibre growth in the zebrafish embryo. *Developmental Dynamics*, *238*(1). https://doi.org/10.1002/dvdy.21812

Kim, I. G., Kim, S. Y., Choi, S. I., Lee, J. H., Kim, K. C., & Cho, E. W. (2014). Fibulin-3-mediated inhibition of epithelial-to-mesenchymal transition and self-renewal of ALDH+ lung cancer stem cells through IGF1R signaling. *Oncogene*, *33*(30). https://doi.org/10.1038/onc.2013.373

Kim, J. E., Jeong, H. W., Nam, J. O., Lee, B. H., Choi, J. Y., Park, R. W., Park, J. Y., & Kim, I. S. (2002). Identification of motifs in the fasciclin domains of the transforming growth factor-β-induced matrix protein βig-h3 that interact with the αvβ5 integrin. *Journal of Biological Chemistry*, *277*(48). https://doi.org/10.1074/jbc.M207055200

Kim, J. E., Kim, S. J., Jeong, H. W., Lee, B. H., Choi, J. Y., Park, R. W., Park, J. Y., & Kim, I. S. (2003). RGD peptides released from βig-h3, a TGF-β-induced cell-adhesive molecule, mediate apoptosis. *Oncogene*, *22*(13). https://doi.org/10.1038/sj.onc.1206269

Kim, J. E., Kim, S. J., Lee, B. H., Park, R. W., Kim, K. S., & Kim, I. S. (2000). Identification of motifs for cell adhesion within the repeated domains of transforming growth factor-β-induced gene, βig-h3. *Journal of Biological Chemistry*, *275*(40). https://doi.org/10.1074/jbc.M002752200

Kim, J. E., Park, R. W., Choi, J. Y., Bae, Y. C., Kim, K. S., Joo, C. K., & Kim, I. S. (2002). Molecular properties of wild-type and mutant βIG-H3 proteins. *Investigative Ophthalmology and Visual Science*, *43*(3).

Kim, K., Doi, A., Wen, B., Ng, K., Zhao, R., Cahan, P., Kim, J., Aryee, M. J., Ji, H., Ehrlich, L. I. R., Yabuuchi, A., Takeuchi, A., Cunniff, K. C., Hongguang, H., McKinney-Freeman, S., Naveiras, O., Yoon, T. J., Irizarry, R. A., Jung, N., … Daley, G. Q. (2010). Epigenetic memory in induced pluripotent stem cells. *Nature*, *467*(7313). https://doi.org/10.1038/nature09342

Kim, K. H., Marchuk, D., & Fuchs, E. (1984). Expression of unusually large keratins during terminal differentiation: Balance of type I and type II keratins is not disrupted. *Journal of Cell Biology*, *99*(5). https://doi.org/10.1083/jcb.99.5.1872

Kim, M. O., Yun, S. J., Kim, I. S., Sohn, S., & Lee, E. H. (2003). Transforming growth factor-β-inducible gene-h3 (βig-h3) promotes cell adhesion of human astrocytoma cells in vitro: Implication of α6β4 integrin. *Neuroscience Letters*, *336*(2). https://doi.org/10.1016/S0304-3940(02)01260-0

Kim, T. I., Choi, S. il, Lee, H. K., Cho, Y. J., & Kim, E. K. (2008). Mitomycin C induces apoptosis in cultured corneal fibroblasts derived form type II granular corneal dystrophy corneas. *Molecular Vision*, *14*.

Kim, T. I., Kim, H., Lee, D. J., Choi, S. il, Kang, S. W., & Kim, E. K. (2011). Altered mitochondrial function in type 2 granular corneal dystrophy. *American Journal of Pathology*, *179*(2). https://doi.org/10.1016/j.ajpath.2011.04.005

Kim, T. I., Kim, T., Kim, S. W., & Kim, E. K. (2008). Comparison of corneal deposits after LASIK and PRK in eyes with granular corneal dystrophy type II. *Journal of Refractive Surgery*, *24*(4). https://doi.org/10.3928/1081597x-20080401-13

Kim, Y. (2023). Drug Discovery Perspectives of Antisense Oligonucleotides. *Biomolecules & Therapeutics*. https://doi.org/10.4062/biomolther.2023.001

Kimura, K., Kawano, S., Mori, T., Inoue, J., Hadachi, H., Saito, T., & Nishida, T. (2010). Quantitative analysis of the effects of extracellular matrix proteins on membrane dynamics associated with corneal epithelial cell motility. *Investigative Ophthalmology and Visual Science*, *51*(9). https://doi.org/10.1167/iovs.09-4380

Kiššová, I., Deffieu, M., Manon, S., & Camougrand, N. (2004). Uth1p is involved in the autophagic degradation of mitochondria. *Journal of Biological Chemistry*, *279*(37). https://doi.org/10.1074/jbc.M406960200

Kitagawa, K., Kojima, M., Sasaki, H., Shui, Y. B., Chew, S. J., Cheng, H. M., Ono, M., Morikawa, Y., & Sasaki, K. (2002). Prevalence of primary cornea guttata and

morphology of corneal endothelium in aging Japanese and Singaporean subjects. *Ophthalmic Research*, *34*(3). https://doi.org/10.1159/000063656

Kitamoto, K., Taketani, Y., Fujii, W., Inamochi, A., Toyono, T., Miyai, T., Yamagami, S., Kuroda, M., Usui, T., & Ouchi, Y. (2020). Generation of mouse model of TGFBI-R124C corneal dystrophy using CRISPR/Cas9-mediated homology-directed repair. *Scientific Reports*, *10*(1). https://doi.org/10.1038/s41598-020-58876-w

Kitazawa, K., Hikichi, T., Nakamura, T., Sotozono, C., Kinoshita, S., & Masui, S. (2017). PAX6 regulates human corneal epithelium cell identity. *Experimental Eye Research*, *154*. https://doi.org/10.1016/j.exer.2016.11.005

Kiuru, S. (1998). Gelsolin-related familial amyloidosis, Finnish type (FAF), and its variants found worldwide. In *Amyloid* (Vol. 5, Issue 1). https://doi.org/10.3109/13506129809007291

Klamer, S. E., Dorland, Y. L., Kleijer, M., Geerts, D., Lento, W. E., Van Der Schoot, C. E., Von Lindern, M., & Voermans, C. (2018). TGFBI expressed by bone marrow niche cells and hematopoietic stem and progenitor cells regulates hematopoiesis. *Stem Cells and Development*, *27*(21). https://doi.org/10.1089/scd.2018.0124

Klenotic, P. A., Munier, F. L., Marmorstein, L. Y., & Anand-Apte, B. (2004). Tissue inhibitor of metalloproteinases-3 (TIMP-3) is a binding partner of epithelial growth factor-containing fibulin-like extracellular matrix protein 1 (EFEMP1): Implications for macular degenerations. *Journal of Biological Chemistry*, *279*(29). https://doi.org/10.1074/jbc.M403026200

Klintworth, G. K. (1999). Advances in the molecular genetics of corneal dystrophies. *American Journal of Ophthalmology*, *128*(6). https://doi.org/10.1016/S0002-9394(99)00358-X

Kobayashi, N., Kostka, G., Garbe, J. H. O., Keene, D. R., Bächinger, H. P., Hanisch, F. G., Markova, D., Tsuda, T., Timpl, R., Chu, M. L., & Sasaki, T. (2007). A comparative analysis of the fibulin protein family: Biochemical characterization, binding interactions, and tissue localization. *Journal of Biological Chemistry*, *282*(16). https://doi.org/10.1074/jbc.M611029200

Kobayashi, Y., Hayashi, R., Shibata, S., Quantock, A. J., & Nishida, K. (2020). Ocular surface ectoderm instigated by WNT inhibition and BMP4. *Stem Cell Research*, *46*. https://doi.org/10.1016/j.scr.2020.101868

Koch, L. (2017). Functional genomics: Screening for lncRNA function. In *Nature Reviews Genetics* (Vol. 18, Issue 2). https://doi.org/10.1038/nrg.2016.168

Koch, M., Schulze, J., Hansen, U., Ashwodt, T., Keene, D. R., Brunken, W. J., Burgeson, R. E., Bruckner, P., & Bruckner-Tuderman, L. (2004). A novel marker of tissue junctions, collagen XXII. *Journal of Biological Chemistry*, *279*(21). https://doi.org/10.1074/jbc.M400536200

Kolter, T., & Wendeler, M. (2003). Chemical chaperones - A new concept in drug research. In *ChemBioChem* (Vol. 4, Issue 4). https://doi.org/10.1002/cbic.200390045

Koroma, B. M., Yang, J. M., & Sundin, O. H. (1997). The Pax-6 homeobox gene is expressed throughout the corneal and conjunctival epithelia. *Investigative Ophthalmology and Visual Science*, *38*(1).

Korpos, É., Deák, F., & Kiss, I. (2015). Matrilin-2, an extracellular adaptor protein, is needed for the regeneration of muscle, nerve and other tissues. *Neural Regeneration Research*, *10*(6). https://doi.org/10.4103/1673-5374.158332

Korvatska, E., Henry, H., Mashima, Y., Yamada, M., Bachmann, C., Munier, F. L., & Schorderet, D. F. (2000). Amyloid and non-amyloid forms of 5q31-linked corneal dystrophy resulting from kerato-epithelin mutations at Arg-124 are associated with abnormal turnover of the protein. *Journal of Biological Chemistry*, *275*(15). https://doi.org/10.1074/jbc.275.15.11465

Korvatska, E., Munier, F. L., Chaubert, P., Wang, M. X., Mashima, Y., Yamada, M., Uffer, S., Zografos, L., & Schorderet, D. F. (1999). On the role of kerato-epithelin in the pathogenesis of 5q31-linked corneal dystrophies. *Investigative Ophthalmology and Visual Science*, *40*(10).

Korvatska, E., Munier, F. L., Djemaï, A., Wang, M. X., Frueh, B., Chiou, A. G. Y., Uffer, S., Ballestrazzi, E., Braunstein, R. E., Forster, R. K., Culbertson, W. W., Boman, H., Zografos, L., & Schorderet, D. F. (1998). Mutation hot spots in 5q31-linked corneal dystrophies. *American Journal of Human Genetics*, *62*(2). https://doi.org/10.1086/301720

Koster, M. I., Kim, S., Mills, A. A., DeMayo, F. J., & Roop, D. R. (2004). p63 is the molecular switch for initiation of an epithelial stratification program. *Genes and Development*, *18*(2). https://doi.org/10.1101/gad.1165104

Kravitz, S. N., Ferris, E., Love, M. I., Thomas, A., Quinlan, A. R., & Gregg, C. (2023). Random allelic expression in the adult human body. *Cell Reports*, *42*(1). https://doi.org/10.1016/j.celrep.2022.111945

Kreslova, J., Machon, O., Rusickova, J., Lachova, J., Wawrousek, E. F., Kemler, R., Krauss, S., Piatigorsky, J., & Kozmik, Z. (2007). Abnormal lens morphogenesis and ectopic lens formation in the absence of β-catenin function. *Genesis (United States)*, *45*(4). https://doi.org/10.1002/dvg.20277

Kretschmer-Kazemi Far, R., & Sczakiel, G. (2003). The activity of siRNA in mammalian cells is related to structural target accessibility: A comparison with antisense oligonucleotides. *Nucleic Acids Research*, *31*(15). https://doi.org/10.1093/nar/gkg649

Krishnan, N., Dickman, M. B., & Becker, D. F. (2008). Proline modulates the intracellular redox environment and protects mammalian cells against oxidative stress. *Free Radical Biology and Medicine*, *44*(4). https://doi.org/10.1016/j.freeradbiomed.2007.10.054

Kruger, W. D. (2017). Cystathionine β-synthase deficiency: Of mice and men. In *Molecular Genetics and Metabolism* (Vol. 121, Issue 3). https://doi.org/10.1016/j.ymgme.2017.05.011

Kruzynska-Frejtag, A., Wang, J., Maeda, M., Rogers, R., Krug, E., Hoffman, S., Markwald, R. R., & Conway, S. J. (2004). Periostin Is Expressed Within the Developing Teeth at the Sites of Epithelial-Mesenchymal Interaction. *Developmental Dynamics*, *229*(4). https://doi.org/10.1002/dvdy.10453

Kubota, K., Ohashi, A., Imachi, H., & Harada, H. (2006). Improved in situ hybridization efficiency with locked-nucleic-acid- incorporated DNA probes. *Applied and Environmental Microbiology*, *72*(8). https://doi.org/10.1128/AEM.03039-05

Kulesh, D. A., Ceceña, G., Darmon, Y. M., Vasseur, M., & Oshima, R. G. (1989). Posttranslational regulation of keratins: degradation of mouse and human keratins 18 and 8. *Molecular and Cellular Biology*, *9*(4). https://doi.org/10.1128/mcb.9.4.1553

Kulesh, D. A., & Oshima, R. G. (1988). Cloning of the human keratin 18 gene and its expression in nonepithelial mouse cells. *Molecular and Cellular Biology*, *8*(4). https://doi.org/10.1128/mcb.8.4.1540-1550.1988

Kulkarni, B. B., Tighe, P. J., Mohammed, I., Yeung, A. M., Powe, D. G., Hopkinson, A., Shanmuganathan, V. A., & Dua, H. S. (2010). Comparative transcriptional profiling of the limbal epithelial crypt demonstrates its putative stem cell niche characteristics. *BMC Genomics*, *11*(1). https://doi.org/10.1186/1471-2164-11-526

Kwak, J. J., Yoon, S. H., Seo, K. Y., Kim, T. I., Lee, H. K., Stulting, R. D., & Kim, E. K. (2021). Exacerbation of Granular Corneal Dystrophy Type 2 After Small Incision Lenticule Extraction. *Cornea*, *40*(4). https://doi.org/10.1097/ICO.0000000000002655

Kyttälä, A., Moraghebi, R., Valensisi, C., Kettunen, J., Andrus, C., Pasumarthy, K. K., Nakanishi, M., Nishimura, K., Ohtaka, M., Weltner, J., Van Handel, B., Parkkonen, O., Sinisalo, J., Jalanko, A., Hawkins, R. D., Woods, N. B., Otonkoski, T., & Trokovic, R. (2016). Genetic Variability Overrides the Impact of Parental Cell Type and Determines iPSC Differentiation Potential. *Stem Cell Reports*, *6*(2). https://doi.org/10.1016/j.stemcr.2015.12.009

Labat-Robert, J. (2012). Cell-Matrix interactions, the role of fibronectin and integrins. A survey. *Pathologie Biologie*, *60*(1). https://doi.org/10.1016/j.patbio.2011.10.003

Lamarre, S., Frasse, P., Zouine, M., Labourdette, D., Sainderichin, E., Hu, G., Le Berre-Anton, V., Bouzayen, M., & Maza, E. (2018). Optimization of an RNA-seq differential gene expression analysis depending on biological replicate number and library size. *Frontiers in Plant Science*, *9*. https://doi.org/10.3389/fpls.2018.00108

Landrum, M. J., Lee, J. M., Benson, M., Brown, G., Chao, C., Chitipiralla, S., Gu, B., Hart, J., Hoffman, D., Hoover, J., Jang, W., Katz, K., Ovetsky, M., Riley, G., Sethi, A., Tully, R., Villamarin-Salomon, R., Rubinstein, W., & Maglott, D. R. (2016). ClinVar: Public archive of interpretations of clinically relevant variants. *Nucleic Acids Research*, *44*(D1). https://doi.org/10.1093/nar/gkv1222

Lane, E. B., & McLean, W. H. I. (2004). Keratins and skin disorders. In *Journal of Pathology* (Vol. 204, Issue 4). https://doi.org/10.1002/path.1643

Latorra, D., Campbell, K., Wolter, A., & Hurley, J. M. (2003). Enhanced allele-specific PCR discrimination in SNP genotyping using 3′ locked nucleic acid (LNA) primers. *Human Mutation*, *22*(1). https://doi.org/10.1002/humu.10228

LeBaron, R. G., Bezverkov, K. I., Zimber, M. P., Pavelec, R., Skonier, J., & Purchio, A. F. (1995). βIG-H3, a novel secretory protein inducible by transforming growth factor-β, is present in normal skin and promotes the adhesion and spreading of dermal

fibroblasts in vitro. *Journal of Investigative Dermatology*, *104*(5). https://doi.org/10.1111/1523-1747.ep12607024

Lee, C. T., Bendriem, R. M., Wu, W. W., & Shen, R. F. (2017). 3D brain Organoids derived from pluripotent stem cells: Promising experimental models for brain development and neurodegenerative disorders Julie Y.H. Chan. In *Journal of Biomedical Science* (Vol. 24, Issue 1). https://doi.org/10.1186/s12929-017-0362-8

Lee, J. H., Chung, S. H., Stulting, R. D., Kim, W. C., Lee, H. K., & Kim, E. K. (2006). Effects of corneal neovascularization on the manifestations of Avellino corneal dystrophy (granular corneal dystrophy type II). *Cornea*, *25*(8). https://doi.org/10.1097/01.ico.0000224645.89342.55

Lee, J. H., Gao, C., Peng, G., Greer, C., Ren, S., Wang, Y., & Xiao, X. (2011). Analysis of transcriptome complexity through RNA sequencing in normal and failing murine hearts. *Circulation Research*, *109*(12). https://doi.org/10.1161/CIRCRESAHA.111.249433

Lee, J., Ji, Y. W., Park, S. Y., Seo, K. Y., Kim, T. I., & Kim, E. K. (2016). Delayed onset of lattice corneal dystrophy type IIIA due to a novel T621P mutation in TGFBI. In *Journal of Refractive Surgery* (Vol. 32, Issue 5). https://doi.org/10.3928/1081597X-20160225-01

Lee, J. M., Lee, E. H., Kim, I. S., & Kim, J. E. (2015). Tgfbi deficiency leads to a reduction in skeletal size and degradation of the bone matrix. *Calcified Tissue International*, *96*(1). https://doi.org/10.1007/s00223-014-9938-4

Lee, R. C., Feinbaum, R. L., & Ambros, V. (1993). The C. elegans heterochronic gene lin-4 encodes small RNAs with antisense complementarity to lin-14. *Cell*, *75*(5). https://doi.org/10.1016/0092-8674(93)90529-Y

Lee, S. H., Bae, J. S., Park, S. H., Lee, B. H., Park, R. W., Choi, J. Y., Park, J. Y., Ha, S. W., Kim, Y. L., Kwon, T. H., & Kim, I. S. (2003). Expression of TGF-β-induced matrix protein βig-h3 is up-regulated in the diabetic rat kidney and human proximal tubular epithelial cells treated with high glucose. *Kidney International*, *64*(3). https://doi.org/10.1046/j.1523-1755.2003.00158.x

Lee, W. B., Himmel, K. S., Hamilton, S. M., Zhao, X. C., Yee, R. W., Kang, S. J., & Grossniklaus, H. E. (2007). Excimer laser exacerbation of Avellino corneal dystrophy. *Journal of Cataract and Refractive Surgery*, *33*(1). https://doi.org/10.1016/j.jcrs.2006.09.024

Lee, Y. I., Lee, S. G., Jung, I., Suk, J., Baeg, C., Han, S.-Y., Seo, J. Y., Jung, D., Jeon, Y., & Lee, J. H. (2023). Topical Application of Peptide Nucleic Acid Antisense Oligonucleotide for MMP-1 and Its Potential Anti-Aging Properties. *Journal of Clinical Medicine*, *12*(7), 2472. https://doi.org/10.3390/jcm12072472

Lehrer, M. S., Sun, T. T., & Lavker, R. M. (1998). Strategies of epithelial repair: modulation of stem cell and transit amplifying cell proliferation. *Journal of Cell Science*, *111*(19), 2867–2875. https://doi.org/10.1242/jcs.111.19.2867

Levy, S. G., Moss, J., Sawada, H., Dopping-Hepenstal, P. J. C., & McCartney, A. C. E. (1996). The composition of wide-spaced collagen in normal and diseased Descemet's membrane. *Current Eye Research*, *15*(1). https://doi.org/10.3109/02713689609017610

Lewis, P. N., White, T. L., Young, R. D., Bell, J. S., Winlove, C. P., & Meek, K. M. (2016). Three-dimensional arrangement of elastic fibers in the human corneal stroma. *Experimental Eye Research*, *146*. https://doi.org/10.1016/j.exer.2015.12.006

Li, D. Q., Kim, S., Li, J. M., Gao, Q., Choi, J., Bian, F., Hu, J., Zhang, Y., Li, J., Lu, R., Li, Y., Pflugfelder, S. C., Miao, H., & Chen, R. (2021). Single-cell transcriptomics identifies limbal stem cell population and cell types mapping its differentiation trajectory in limbal basal epithelium of human cornea. *Ocular Surface*, *20*. https://doi.org/10.1016/j.jtos.2020.12.004

Li, G. G., Chen, S. Y., Xie, H. T., Zhu, Y. T., & Tseng, S. C. G. (2012). Angiogenesis potential of human limbal stromal niche cells. *Investigative Ophthalmology and Visual Science*, *53*(7). https://doi.org/10.1167/iovs.11-9414

Li, G., Han, D., Wei, S., Wang, H., & Chen, L. (2019). Multiorgan involvement by amyloid light chain amyloidosis. *Journal of International Medical Research*, *47*(4). https://doi.org/10.1177/0300060518814337

Li, G., Xu, F., Zhu, J., Krawczyk, M., Zhang, Y., Yuan, J., Patel, S., Wang, Y., Lin, Y., Zhang, M., Cai, H., Chen, D., Zhang, M., Cao, G., Yeh, E., Lin, D., Su, Q., Li, W. W., Sen, G. L., … Ouyang, H. (2015). Transcription factor PAX6 (paired box 6) controls limbal stem cell lineage in development and disease. *Journal of Biological Chemistry*, *290*(33). https://doi.org/10.1074/jbc.M115.662940

Li, J. M., Kim, S., Zhang, Y., Bian, F., Hu, J., Lu, R., Pflugfelder, S. C., Chen, R., & Li, D. Q. (2021). Single-cell transcriptomics identifies a unique entity and signature

markers of transit-amplifying cells in human corneal limbus. *Investigative Ophthalmology and Visual Science*, *62*(9). https://doi.org/10.1167/iovs.62.9.36

Li, J., Qi, C., Liu, X., Li, C., Chen, J., & Shi, M. (2018). Fibulin-3 knockdown inhibits cervical cancer cell growth and metastasis in vitro and in vivo. *Scientific Reports*, *8*(1). https://doi.org/10.1038/s41598-018-28906-9

Li, J., Riau, A. K., Setiawan, M., Mehta, J. S., Ti, S. E., Tong, L., Tan, D. T. H., & Beuerman, R. W. (2011). S100A expression in normal corneal-limbal epithelial cells and ocular surface squamous cell carcinoma tissue. *Molecular Vision*, *17*.

Li, Q., Zhang, D., Wang, Y., Sun, P., Hou, X., Larner, J., Xiong, W., & Mi, J. (2013). MiR-21/Smad 7 signaling determines TGF-β1-induced CAF formation. *Scientific Reports*, *3*. https://doi.org/10.1038/srep02038

Li, R., Liang, J., Ni, S., Zhou, T., Qing, X., Li, H., He, W., Chen, J., Li, F., Zhuang, Q., Qin, B., Xu, J., Li, W., Yang, J., Gan, Y., Qin, D., Feng, S., Song, H., Yang, D., … Pei, D. (2010). A mesenchymal-to-Epithelial transition initiates and is required for the nuclear reprogramming of mouse fibroblasts. *Cell Stem Cell*, *7*(1). https://doi.org/10.1016/j.stem.2010.04.014

Li, W., Chen, Y. T., Hayashida, Y., Blanco, G., Kheirkah, A., He, H., Chen, S. Y., Liu, C. Y., & Tseng, S. C. G. (2008). Down-regulation of Pax6 is associated with abnormal differentiation of corneal epithelial cells in severe ocular surface diseases. *Journal of Pathology*, *214*(1). https://doi.org/10.1002/path.2256

Li, W., Wei, W., & Ding, S. (2016). TGF-β signaling in stem cell regulation. In *Methods in Molecular Biology* (Vol. 1344). https://doi.org/10.1007/978-1-4939-2966-5_8

Li, X., Bykhovskaya, Y., Canedo, A. L. C., Haritunians, T., Siscovick, D., Aldave, A. J., Szczotka-Flynn, L., Iyengar, S. K., Rotter, J. I., Taylor, K. D., & Rabinowitz, Y. S. (2013). Genetic association of COL5A1 variants in keratoconus patients suggests a complex connection between corneal thinning and keratoconus. *Investigative Ophthalmology and Visual Science*, *54*(4). https://doi.org/10.1167/iovs.13-11601

Li, Y., Inoue, T., Takamatsu, F., Kobayashi, T., Shiraishi, A., Maeda, N., Ohashi, Y., & Nishida, K. (2014). Differences between niche cells and limbal stromal cells in maintenance of corneal limbal stem cells. *Investigative Ophthalmology and Visual Science*, *55*(3). https://doi.org/10.1167/iovs.13-13698

Li, Z., Dang, J., Chang, K. Y., & Rana, T. M. (2014). MicroRNA-mediated regulation of extracellular matrix formation modulates Somatic cell reprogramming. *RNA*, *20*(12). https://doi.org/10.1261/rna.043745.113

Lian, X., Selekman, J., Bao, X., Hsiao, C., Zhu, K., & Palecek, S. P. (2013). A Small Molecule Inhibitor of Src Family Kinases Promotes Simple Epithelial Differentiation of Human Pluripotent Stem Cells. *PLoS ONE*, *8*(3). https://doi.org/10.1371/journal.pone.0060016

Liang, Q., Pan, Z., Sun, X., Baudouin, C., & Labbé, A. (2014). Reis-bücklers corneal dystrophy: A reappraisal using in vivo and ex vivo imaging techniques. *Ophthalmic Research*, *51*(4). https://doi.org/10.1159/000358805

Ligocki, A. J., Fury, W., Gutierrez, C., Adler, C., Yang, T., Ni, M., Bai, Y., Wei, Y., Lehmann, G. L., & Romano, C. (2021). Molecular characteristics and spatial distribution of adult human corneal cell subtypes. *Scientific Reports*, *11*(1). https://doi.org/10.1038/s41598-021-94933-8

Lisch, W., & Seitz, B. (2011). The clinical landmarks of corneal dystrophies. In *Corneal Dystrophies* (Vol. 48). https://doi.org/10.1159/000324075

Lisch, W., & Seitz, B. (2014). Lattice corneal dystrophy type 1: An epithelial or stromal entity? *Cornea*, *33*(10). https://doi.org/10.1097/ICO.0000000000000202

Liu, C., Li, B., Cheng, Y., Lin, J., Hao, J., Zhang, S., Mitchel, R. E. J., Sun, D., Ni, J., Zhao, L., Gao, F., & Cai, J. (2011). MiR-21 plays an important role in radiation induced carcinogenesis in BALB/c mice by directly targeting the tumor suppressor gene Big-h3. *International Journal of Biological Sciences*, *7*(3). https://doi.org/10.7150/ijbs.7.347

Liu, J. J., Kao, W. W. Y., & Wilson, S. E. (1999). Corneal epithelium-specific mouse keratin K12 promoter. *Experimental Eye Research*, *68*(3). https://doi.org/10.1006/exer.1998.0593

Liu, M., Iosef, C., Rao, S., Domingo-Gonzalez, R., Fu, S., Snider, P., Conway, S. J., Umbach, G. S., Heilshorn, S. C., Dewi, R. E., Dahl, M. J., Null, D. M., Albertine, K. H., & Alvira, C. M. (2021). Transforming growth factor–induced protein promotes NF-kB–mediated angiogenesis during postnatal lung development. *American Journal of Respiratory Cell and Molecular Biology*, *64*(3), 318–330. https://doi.org/10.1165/rcmb.2020-0153OC

Liu, S., Yang, W., Li, Y., & Sun, C. (2023). Fetal bovine serum, an important factor affecting the reproducibility of cell experiments. *Scientific Reports*, *13*(1). https://doi.org/10.1038/s41598-023-29060-7

Liu, W., Lagutin, O. V., Mende, M., Streit, A., & Oliver, G. (2006). Six3 activation of Pax6 expression is essential for mammalian lens induction and specification. *EMBO Journal*, *25*(22). https://doi.org/10.1038/sj.emboj.7601398

Liu, Y., Zhou, J., & White, K. P. (2014). RNA-seq differential expression studies: More sequence or more replication? *Bioinformatics*, *30*(3). https://doi.org/10.1093/bioinformatics/btt688

Lloyd, C., Yu, Q. C., Cheng, J., Turksen, K., Degenstein, L., Hutton, E., & Fuchs, E. (1995). The basal keratin network of stratified squamous epithelia: Defining K15 function in the absence of K14. *Journal of Cell Biology*, *129*(5). https://doi.org/10.1083/jcb.129.5.1329

Lo, C. M., Wang, H. B., Dembo, M., & Wang, Y. L. (2000). Cell movement is guided by the rigidity of the substrate. *Biophysical Journal*, *79*(1). https://doi.org/10.1016/S0006-3495(00)76279-5

Love, M. I., Huber, W., & Anders, S. (2014). Moderated estimation of fold change and dispersion for RNA-seq data with DESeq2. *Genome Biology*, *15*(12). https://doi.org/10.1186/s13059-014-0550-8

Lu, H., Hesse, M., Peters, B., & Magin, T. M. (2005). Type II keratins precede type I keratins during early embryonic development. *European Journal of Cell Biology*, *84*(8). https://doi.org/10.1016/j.ejcb.2005.04.001

Lu, H., Lu, Q., Zheng, Y., & Li, Q. (2012). Notch signaling promotes the corneal epithelium wound healing. *Molecular Vision*, *18*.

Lu, H., Zimek, A., Chen, J., Hesse, M., Büssow, H., Weber, K., & Magin, T. M. (2006). Keratin 5 knockout mice reveal plasticity of keratin expression in the corneal epithelium. *European Journal of Cell Biology*, *85*(8). https://doi.org/10.1016/j.ejcb.2006.04.001

Lu, J., Tan, L., Li, P., Gao, H., Fang, B., Ye, S., Geng, Z., Zheng, P., & Song, H. (2009). All-trans retinoic acid promotes neural lineage entry by pluripotent embryonic stem cells via multiple pathways. *BMC Cell Biology*, *10*. https://doi.org/10.1186/1471-2121-10-57

Lu, P., Takai, K., Weaver, V. M., & Werb, Z. (2011). Extracellular Matrix degradation and remodeling in development and disease. *Cold Spring Harbor Perspectives in Biology*, *3*(12). https://doi.org/10.1101/cshperspect.a005058

Lu, X., & Lane, E. B. (1990). Retrovirus-mediated transgenic keratin expression in cultured fibroblasts: Specific domain functions in keratin stabilization and filament formation. *Cell*, *62*(4). https://doi.org/10.1016/0092-8674(90)90114-T

Lukassen, M. V., Poulsen, E. T., Donaghy, J., Mogensen, E. H., Christie, K. A., Roshanravan, H., DeDioniso, L., Nesbit, M. A., Moore, T., & Enghild, J. J. (2020). Protein Analysis of the TGFBIR124H Mouse Model Gives Insight into Phenotype Development of Granular Corneal Dystrophy. *Proteomics - Clinical Applications*, *14*(6). https://doi.org/10.1002/prca.201900072

Lukassen, M. V., Scavenius, C., Thøgersen, I. B., & Enghild, J. J. (2016). Disulfide Bond Pattern of Transforming Growth Factor β-Induced Protein. *Biochemistry*, *55*(39). https://doi.org/10.1021/acs.biochem.6b00694

Lundin, K. E., Gissberg, O., & Smith, C. I. E. (2015). Oligonucleotide Therapies: The Past and the Present. In *Human Gene Therapy* (Vol. 26, Issue 8). https://doi.org/10.1089/hum.2015.070

Lüningschrör, P., Hauser, S., Kaltschmidt, B., & Kaltschmidt, C. (2013). MicroRNAs in pluripotency, reprogramming and cell fate induction. In *Biochimica et Biophysica Acta - Molecular Cell Research* (Vol. 1833, Issue 8). https://doi.org/10.1016/j.bbamcr.2013.03.025

Luo, C., Li, Y., Wang, H., Feng, Z., Li, Y., Long, J., & Liu, J. (2013). Mitochondrial accumulation under oxidative stress is due to defects in autophagy. *Journal of Cellular Biochemistry*, *114*(1). https://doi.org/10.1002/jcb.24356

Luo, J., Qu, L., Gao, F., Lin, J., Liu, J., & Lin, A. (2021). LncRNAs: Architectural Scaffolds or More Potential Roles in Phase Separation. In *Frontiers in Genetics* (Vol. 12). https://doi.org/10.3389/fgene.2021.626234

Lužnik, Z., Bertolin, M., Breda, C., Ferrari, B., Barbaro, V., Schollmayer, P., & Ferrari, S. (2016). Preservation of ocular epithelial limbal stem cells: The new frontier in regenerative medicine. In *Advances in Experimental Medicine and Biology* (Vol. 951). https://doi.org/10.1007/978-3-319-45457-3_15

Lyons, C. J., McCartney, A. C., Kirkness, C. M., Ficker, L. A., Steele, A. D. M. G., & Rice, N. S. C. (1994). Granular Corneal Dystrophy: Visual Results and Pattern of

Recurrence after Lamellar or Penetrating Keratoplasty. *Ophthalmology*, *101*(11). https://doi.org/10.1016/S0161-6420(94)31096-7

Ma, A., Boulton, M., Zhao, B., Connon, C., Cai, J., & Albon, J. (2007). A role for notch signaling in human corneal epithelial cell differentiation and proliferation. *Investigative Ophthalmology and Visual Science*, *48*(8). https://doi.org/10.1167/iovs.06-1373

Ma, C., Rong, Y., Radiloff, D. R., Datto, M. B., Centeno, B., Bao, S., Cheng, A. W. M., Lin, F., Jiang, S., Yeatman, T. J., & Wang, X. F. (2008). Extracellular matrix protein βig-h3/TGFBI promotes metastasis of colon cancer by enhancing cell extravasation. *Genes and Development*, *22*(3). https://doi.org/10.1101/gad.1632008

Macdonald, P. R., Lustig, A., Steinmetz, M. O., & Kammerer, R. A. (2010). Laminin chain assembly is regulated by specific coiled-coil interactions. *Journal of Structural Biology*, *170*(2). https://doi.org/10.1016/j.jsb.2010.02.004

Maeng, Y. S., Lee, G. H., Lee, B., Choi, S. il, Kim, T. I., & Kim, E. K. (2017). Role of TGFBIp in wound healing and mucin expression in corneal epithelial cells. *Yonsei Medical Journal*, *58*(2). https://doi.org/10.3349/ymj.2017.58.2.423

Magin, T. M., Schröder, R., Leitgeb, S., Wanninger, F., Zatloukal, K., Grund, C., & Melton, D. W. (1998). Lessons from keratin 18 knockout mice: Formation of novel keratin filaments, secondary loss of keratin 7 and accumulation of liver-specific keratin 8-positive aggregates. *Journal of Cell Biology*, *140*(6). https://doi.org/10.1083/jcb.140.6.1441

Maherali, N., & Hochedlinger, K. (2009). Tgfβ Signal Inhibition Cooperates in the Induction of iPSCs and Replaces Sox2 and cMyc. *Current Biology*, *19*(20). https://doi.org/10.1016/j.cub.2009.08.025

Maiti, G., Monteiro de Barros, M. R., Hu, N., Dolgalev, I., Roshan, M., Foster, J. W., Tsirigos, A., Wahlin, K. J., & Chakravarti, S. (2022). Single cell RNA-seq of human cornea organoids identifies cell fates of a developing immature cornea. *PNAS Nexus*, *1*(5). https://doi.org/10.1093/pnasnexus/pgac246

Majo, F., Rochat, A., Nicolas, M., Jaoudé, G. A., & Barrandon, Y. (2008). Oligopotent stem cells are distributed throughout the mammalian ocular surface. *Nature*, *456*(7219). https://doi.org/10.1038/nature07406

Malmos, K. G., Stenvang, M., Sahin, C., Christiansen, G., & Otzen, D. E. (2017). The Changing Face of Aging: Highly Sulfated Glycosaminoglycans Induce Amyloid

Formation in a Lattice Corneal Dystrophy Model Protein. *Journal of Molecular Biology*, *429*(18). https://doi.org/10.1016/j.jmb.2017.07.014

Mamuya, F. A., & Duncan, M. K. (2012). αV integrins and TGF-β-induced EMT: A circle of regulation. In *Journal of Cellular and Molecular Medicine* (Vol. 16, Issue 3). https://doi.org/10.1111/j.1582-4934.2011.01419.x

Mandai, M., Watanabe, A., Kurimoto, Y., Hirami, Y., Morinaga, C., Daimon, T., Fujihara, M., Akimaru, H., Sakai, N., Shibata, Y., Terada, M., Nomiya, Y., Tanishima, S., Nakamura, M., Kamao, H., Sugita, S., Onishi, A., Ito, T., Fujita, K., … Takahashi, M. (2017). Autologous Induced Stem-Cell–Derived Retinal Cells for Macular Degeneration. *New England Journal of Medicine*, *376*(11). https://doi.org/10.1056/nejmoa1608368

Marchant, J. K., Zhang, G., & Birk, D. E. (2002). Association of type XII collagen with regions of increased stability and keratocyte density in the cornea. *Experimental Eye Research*, *75*(6). https://doi.org/10.1006/exer.2002.2058

Marfurt, C. F., Cox, J., Deek, S., & Dvorscak, L. (2010). Anatomy of the human corneal innervation. *Experimental Eye Research*, *90*(4). https://doi.org/10.1016/j.exer.2009.12.010

Marrosu, E., Ala, P., Muntoni, F., & Zhou, H. (2017). Gapmer Antisense Oligonucleotides Suppress the Mutant Allele of COL6A3 and Restore Functional Protein in Ullrich Muscular Dystrophy. *Molecular Therapy - Nucleic Acids*, *8*. https://doi.org/10.1016/j.omtn.2017.07.006

Mashima, Y., Yamamoto, S., Inoue, Y., Yamada, M., Konishi, M., Watanabe, H., Maeda, N., Shimomura, Y., & Kinoshita, S. (2000). Association of autosomal dominantly inherited corneal dystrophies with BIGH3 gene mutations in Japan. *American Journal of Ophthalmology*, *130*(4). https://doi.org/10.1016/S0002-9394(00)00571-7

Massagué, J., & Wotton, D. (2000). Transcriptional control by the TGF-β/Smad signaling system. *EMBO Journal*, *19*(8).

Mátés, L., Nicolae, C., Mörgelin, M., Deák, F., Kiss, I., & Aszódi, A. (2004). Mice lacking the extracellular matrix adaptor protein matrilin-2 develop without obvious abnormalities. *Matrix Biology*, *23*(3). https://doi.org/10.1016/j.matbio.2004.05.003

Mathers, P. H., Grinberg, A., Mahon, K. A., & Jamrich, M. (1997). The Rx homeobox gene is essential for vertebrate eye development. *Nature*, *387*(6633). https://doi.org/10.1038/42475

Matveeva, O. v., Mathews, D. H., Tsodikov, A. D., Shabalina, S. A., Gesteland, R. F., Atkins, J. F., & Freier, S. M. (2003). Thermodynamic criteria for high hit rate antisense oligonucleotide design. *Nucleic Acids Research*, *31*(17). https://doi.org/10.1093/nar/gkg710

Mayshar, Y., Ben-David, U., Lavon, N., Biancotti, J. C., Yakir, B., Clark, A. T., Plath, K., Lowry, W. E., & Benvenisty, N. (2010). Identification and classification of chromosomal aberrations in human induced pluripotent stem cells. *Cell Stem Cell*, *7*(4). https://doi.org/10.1016/j.stem.2010.07.017

Mecham, R. P. (2012). Overview of extracellular matrix. *Current Protocols in Cell Biology*, *SUPPL.57*. https://doi.org/10.1002/0471143030.cb1001s57

Medawar, A., Virolle, T., Rostagno, P., de la Forest-Divonne, S., Gambaro, K., Rouleau, M., & Aberdam, D. (2008). ΔNp63 is essential for epidermal commitment of embryonic stem cells. *PLoS ONE*, *3*(10). https://doi.org/10.1371/journal.pone.0003441

Medeiros, C. S., Saikia, P., De Oliveira, R. C., Lassance, L., Santhiago, M. R., & Wilson, S. E. (2019). Descemet's membrane modulation of posterior corneal fibrosis. *Investigative Ophthalmology and Visual Science*, *60*(4). https://doi.org/10.1167/iovs.18-26451

Meek, K. M. (2009). Corneal collagen-its role in maintaining corneal shape and transparency. In *Biophysical Reviews* (Vol. 1, Issue 2). https://doi.org/10.1007/s12551-009-0011-x

Menasche, M., Savoldelli, M., & Pouliquen, Y. (1992). The keratocyte or fibroblast of the cornea: morphological and biochemical characteristics in normal stroma and a few cases of corneal dystrophies. In *Pathologie-biologie* (Vol. 40, Issue 9).

Merjava, S., Neuwirth, A., Tanzerova, M., & Jirsova, K. (2011). The spectrum of cytokeratins expressed in the adult human cornea, limbus and perilimbal conjunctiva. *Histology and Histopathology*, *26*(3). https://doi.org/10.14670/HH-26.323

Merlini, G., Dispenzieri, A., Sanchorawala, V., Schönland, S. O., Palladini, G., Hawkins, P. N., & Gertz, M. A. (2018). Systemic immunoglobulin light chain amyloidosis. *Nature Reviews Disease Primers*, *4*(1). https://doi.org/10.1038/s41572-018-0034-3

Metallo, C. M., Ji, L., de Pablo, J. J., & Palecek, S. P. (2008). Retinoic Acid and Bone Morphogenetic Protein Signaling Synergize to Efficiently Direct Epithelial

Differentiation of Human Embryonic Stem Cells. *Stem Cells*, *26*(2). https://doi.org/10.1634/stemcells.2007-0501

Michelacci, Y. M. (2003). Collagens and proteoglycans of the corneal extracellular matrix. *Brazilian Journal of Medical and Biological Research*, *36*(8). https://doi.org/10.1590/S0100-879X2003000800009

Mihelčić, M., Šimić, G., Leko, M. B., Lavrač, N., Džeroski, S., & Šmuc, T. (2017). Using redescription mining to relate clinical and biological characteristics of cognitively impaired and Alzheimer's disease patients. *PLoS ONE*, *12*(10). https://doi.org/10.1371/journal.pone.0187364

Mikhailova, A., Ilmarinen, T., Uusitalo, H., & Skottman, H. (2014). Small-molecule induction promotes corneal epithelial cell differentiation from human induced pluripotent stem cells. *Stem Cell Reports*, *2*(2). https://doi.org/10.1016/j.stemcr.2013.12.014

Mikkelsen, T. S., Hanna, J., Zhang, X., Ku, M., Wernig, M., Schorderet, P., Bernstein, B. E., Jaenisch, R., Lander, E. S., & Meissner, A. (2008). Dissecting direct reprogramming through integrative genomic analysis. *Nature*, *454*(7200). https://doi.org/10.1038/nature07056

Mills, A. A., Zheng, B., Wang, X. J., Vogel, H., Roop, D. R., & Bradley, A. (1999). p63 is a p53 homologue required for limb and epidermal morphogenesis. *Nature*, *398*(6729). https://doi.org/10.1038/19531

Miyagishi, M., Hayashi, M., & Taira, K. (2003). Comparison of the suppressive effects of antisense oligonucleotides and siRNAs directed against the same targets in mammalian cells. *Antisense and Nucleic Acid Drug Development*, *13*(1). https://doi.org/10.1089/108729003764097296

Moll, R., Divo, M., & Langbein, L. (2008). The human keratins: Biology and pathology. In *Histochemistry and Cell Biology* (Vol. 129, Issue 6). https://doi.org/10.1007/s00418-008-0435-6

Moll, R., Franke, W. W., Schiller, D. L., Geiger, B., & Krepler, R. (1982). The catalog of human cytokeratins: Patterns of expression in normal epithelia, tumors and cultured cells. In *Cell* (Vol. 31, Issue 1). https://doi.org/10.1016/0092-8674(82)90400-7

Møller, H. U. (1990). Granular corneal dystrophy Groenouw type I: Clinical aspects and treatment. *Acta Ophthalmologica*, *68*(4). https://doi.org/10.1111/j.1755-3768.1990.tb01665.x

Møller, H. U., & Weiss, J. S. (2011). IC3D classification of corneal dystrophies. In *Corneal Dystrophies* (Vol. 48). https://doi.org/10.1159/000324074

Monia, B. P., Lesnik, E. A., Gonzalez, C., Lima, W. F., McGee, D., Guinosso, C. J., Kawasaki, A. M., Cook, P. D., & Freier, S. M. (1993). Evaluation of 2'-modified oligonucleotides containing 2'-deoxy gaps as antisense inhibitors of gene expression. *Journal of Biological Chemistry*, *268*(19). https://doi.org/10.1016/s0021-9258(19)85268-7

Moon, J. W., Kim, S. W., Kim, T. I., Cristol, S. M., Chung, E. S., & Kim, E. K. (2007). Homozygous granular corneal dystrophy type II (Avellino corneal dystrophy): Natural history and progression after treatment. *Cornea*, *26*(9). https://doi.org/10.1097/ICO.0b013e3181484013

Moretti, A., Bellin, M., Welling, A., Jung, C. B., Lam, J. T., Bott-Flügel, L., Dorn, T., Goedel, A., Höhnke, C., Hofmann, F., Seyfarth, M., Sinnecker, D., Schömig, A., & Laugwitz, K.-L. (2010). Patient-Specific Induced Pluripotent Stem-Cell Models for Long-QT Syndrome. *New England Journal of Medicine*, *363*(15). https://doi.org/10.1056/nejmoa0908679

Morikawa, M., Derynck, R., & Miyazono, K. (2016). TGF- β and the TGF-β family: Context-dependent roles in cell and tissue physiology. In *Cold Spring Harbor Perspectives in Biology* (Vol. 8, Issue 5). https://doi.org/10.1101/cshperspect.a021873

Morishige, N., Petroll, W. M., Nishida, T., Kenney, M. C., & Jester, J. V. (2006). Noninvasive corneal stromal collagen imaging using two-photon-generated second-harmonic signals. *Journal of Cataract and Refractive Surgery*, *32*(11). https://doi.org/10.1016/j.jcrs.2006.08.027

Morloy, M., Molony, C. M., Weber, T. M., Devlin, J. L., Ewens, K. G., Spielman, R. S., & Cheung, V. G. (2004). Genetic analysis of genome-wide variation in human gene expression. *Nature*, *430*(7001). https://doi.org/10.1038/nature02797

Mosher, D. F., Johansson, M. W., Gillis, M. E., & Annis, D. S. (2015). Periostin and TGF-β-induced protein: Two peas in a pod? In *Critical Reviews in Biochemistry and Molecular Biology* (Vol. 50, Issue 5). https://doi.org/10.3109/10409238.2015.1069791

Moumné, L., Marie, A. C., & Crouvezier, N. (2022). Oligonucleotide Therapeutics: From Discovery and Development to Patentability. In *Pharmaceutics* (Vol. 14, Issue 2). https://doi.org/10.3390/pharmaceutics14020260

Moustakas, A., & Heldin, C. H. (2005). Non-Smad TGF-β signals. In *Journal of Cell Science* (Vol. 118, Issue 16). https://doi.org/10.1242/jcs.02554

Mukhopadhyay, M., Gorivodsky, M., Shtrom, S., Grinberg, A., Niehrs, C., Morasso, M. I., & Westphal, H. (2006). Dkk2 plays an essential role in the corneal fate of the ocular surface epithelium. *Development*, *133*(11). https://doi.org/10.1242/dev.02381

Munier, F. L., Frueh, B. E., Othenin-Girard, P., Uffer, S., Cousin, P., Wang, M. X., Héon, E., Black, G. C. M., Blasi, M. A., Balestrazzi, E., Lorenz, B., Escoto, R., Barraquer, R., Hoeltzenbein, M., Gloor, B., Fossarello, M., Singh, A. D., Arsenijevic, Y., Zografos, L., & Schorderet, D. F. (2002). BIGH3 mutation spectrum in corneal dystrophies. *Investigative Ophthalmology and Visual Science*, *43*(4).

Munier, F. L., Korvatska, E., Djemaï, A., Le Paslier, D., Zografos, L., Pescia, G., & Schorderet, D. F. (1997). Kerato-epithelin mutations in four 5q31-linked corneal dystrophies. *Nature Genetics*, *15*(3). https://doi.org/10.1038/ng0397-247

Munishkina, L. A., Fink, A. L., & Uversky, V. N. (2004). Conformational prerequisites for formation of amyloid fibrils from histones. *Journal of Molecular Biology*, *342*(4). https://doi.org/10.1016/j.jmb.2004.06.094

Murphy, C., Alvarado, J., & Juster, R. (1984). Prenatal and postnatal growth of the human Descemet's membrane. *Investigative Ophthalmology and Visual Science*, *25*(12).

Murray-Zmijewski, F., Lane, D. P., & Bourdon, J. C. (2006). p53/p63/p73 isoforms: An orchestra of isoforms to harmonise cell differentiation and response to stress. In *Cell Death and Differentiation* (Vol. 13, Issue 6). https://doi.org/10.1038/sj.cdd.4401914

Musch, D. C., Niziol, L. M., Stein, J. D., Kamyar, R. M., & Sugar, A. (2011). Prevalence of corneal dystrophies in the United States: Estimates from claims data. *Investigative Ophthalmology and Visual Science*, *52*(9). https://doi.org/10.1167/iovs.11-7771

Naba, A., Clauser, K. R., Hoersch, S., Liu, H., Carr, S. A., & Hynes, R. O. (2012). The matrisome: In silico definition and in vivo characterization by proteomics of normal

and tumor extracellular matrices. *Molecular and Cellular Proteomics*, *11*(4). https://doi.org/10.1074/mcp.M111.014647

Naessens, S., Ruysschaert, L., Lefever, S., Coppieters, F., & de Baere, E. (2019). Antisense oligonucleotide-based downregulation of the G56R pathogenic variant causing NR2E3-associated autosomal dominant retinitis pigmentosa. *Genes*, *10*(5). https://doi.org/10.3390/genes10050363

Nakagawa, M., Koyanagi, M., Tanabe, K., Takahashi, K., Ichisaka, T., Aoi, T., Okita, K., Mochiduki, Y., Takizawa, N., & Yamanaka, S. (2008). Generation of induced pluripotent stem cells without Myc from mouse and human fibroblasts. *Nature Biotechnology*, *26*(1). https://doi.org/10.1038/nbt1374

Nakagawa, M., Takizawa, N., Narita, M., Ichisaka, T., & Yamanaka, S. (2010). Promotion of direct reprogramming by transformation-deficient Myc. *Proceedings of the National Academy of Sciences of the United States of America*, *107*(32). https://doi.org/10.1073/pnas.1009374107

Nakamura, M., Nishida, T., Hikida, M., & Otori, T. (1994). Combined effects of hyaluronan and fibronectin on corneal epithelial wound closure of rabbit in vivo. *Current Eye Research*, *13*(5). https://doi.org/10.3109/02713689409167303

Nakamura, T., Ohtsuka, T., Sekiyama, E., Cooper, L. J., Kokubu, H., Fullwood, N. J., Barrandon, Y., Kageyama, R., & Kinoshita, S. (2008). Hes1 Regulates Corneal Development and the Function of Corneal Epithelial Stem/Progenitor Cells. *Stem Cells*, *26*(5). https://doi.org/10.1634/stemcells.2007-1067

Nakatsu, M. N., Ding, Z., Ng, M. Y., Truong, T. T., Yu, F., & Deng, S. X. (2011). Wnt/β-catenin signaling regulates proliferation of human cornea epithelial stem/progenitor cells. *Investigative Ophthalmology and Visual Science*, *52*(7). https://doi.org/10.1167/iovs.10-6486

Nakatsu, M. N., Vartanyan, L., Vu, D. M., Ng, M. Y., Li, X., & Deng, S. X. (2013). Preferential Biological Processes in the Human Limbus by Differential Gene Profiling. *PLoS ONE*, *8*(4). https://doi.org/10.1371/journal.pone.0061833

Nam, E. J., Sa, K. H., You, D. W., Cho, J. H., Seo, J. S., Han, S. W., Park, J. Y., Kim, S. Il, Kyung, H. S., Kim, I. S., & Kang, Y. M. (2006). Up-regulated transforming growth factor β-inducible gene h3 in rheumatoid arthritis mediates adhesion and migration of synoviocytes through αvβ3 integrin: Regulation by cytokines. *Arthritis and Rheumatism*, *54*(9). https://doi.org/10.1002/art.22076

Nam, J. O., Kim, J. E., Jeong, H. W., Lee, S. J., Lee, B. H., Choi, J. Y., Park, R. W., Park, J. Y., & Kim, I. S. (2003). Identification of the αvβ3 integrin-interacting motif of βig-h3 and its anti-angiogenic effect. *Journal of Biological Chemistry*, *278*(28). https://doi.org/10.1074/jbc.M300358200

Nandhu, M. S., Kwiatkowska, A., Bhaskaran, V., Hayes, J., Hu, B., & Viapiano, M. S. (2017). Tumor-derived fibulin-3 activates pro-invasive NF-κB signaling in glioblastoma cells and their microenvironment. *Oncogene*, *36*(34). https://doi.org/10.1038/onc.2017.109

Nasser, W., Amitai-Lange, A., Soteriou, D., Hanna, R., Tiosano, B., Fuchs, Y., & Shalom-Feuerstein, R. (2018). Corneal-Committed Cells Restore the Stem Cell Pool and Tissue Boundary following Injury. *Cell Reports*, *22*(2). https://doi.org/10.1016/j.celrep.2017.12.040

Nguyen, H. T., Geens, M., Mertzanidou, A., Jacobs, K., Heirman, C., Breckpot, K., & Spits, C. (2014). Gain of 20q11.21 in human embryonic stem cells improves cell survival by increased expression of Bcl-xL. *Molecular Human Reproduction*, *20*(2). https://doi.org/10.1093/molehr/gat077

Nguyen, Q., & Yokota, T. (2019). Antisense oligonucleotides for the treatment of cardiomyopathy in duchenne muscular dystrophy. *American Journal of Translational Research*, *11*(3).

Nie, D., Liu, X., Wang, Y., He, W., Li, M., Peng, Y., Zhang, J., Sun, L., Yan, Z., & Ye, L. (2020). Involvement of the JNK signaling in granular corneal dystrophy by modulating TGF-β-induced TGFBI expression and corneal fibroblast apoptosis. *In Vitro Cellular and Developmental Biology - Animal*, *56*(3). https://doi.org/10.1007/s11626-019-00424-6

Nie, D., Peng, Y., Li, M., Liu, X., Zhu, M., & Ye, L. (2018). Lithium chloride (LiCl) induced autophagy and downregulated expression of transforming growth factor β-induced protein (TGFBI) in granular corneal dystrophy. *Experimental Eye Research*, *173*. https://doi.org/10.1016/j.exer.2018.04.008

Niel-Butschi, F., Kantelip, B., Iwaszkiewicz, J., Zoete, V., Boimard, M., Delpech, M., Bourges, J. L., Renard, G., D'Hermies, F., Pisella, P. J., Hamel, C., Delbosc, B., & Valleix, S. (2011). Genotype-phenotype correlations of TGFBI p.Leu509Pro, p.Leu509Arg, p.Val613Gly, and the allelic association of p.Met502Val-p.Arg555Gln mutations. *Molecular Vision*, *17*.

Nielsen, N. S., Poulsen, E. T., Lukassen, M. V., Chao Shern, C., Mogensen, E. H., Weberskov, C. E., DeDionisio, L., Schauser, L., Moore, T. C. B., Otzen, D. E., Hjortdal, J., & Enghild, J. J. (2020). Biochemical mechanisms of aggregation in TGFBI-linked corneal dystrophies. In *Progress in Retinal and Eye Research* (Vol. 77). https://doi.org/10.1016/j.preteyeres.2020.100843

Nielsen, S. B., Yde, P., Giehm, L., Sundbye, S., Christiansen, G., Mathiesen, J., Jensen, M. H., Jensen, P. H., & Otzen, D. E. (2012). Multiple roles of heparin in the aggregation of p25α. *Journal of Molecular Biology*, *421*(4–5). https://doi.org/10.1016/j.jmb.2012.01.050

Nishida, K., Kinoshita, S., Yokoi, N., Kaneda, M., Hashimoto, K., & Yamamoto, S. (1994). Immunohistochemical localization of transforming growth factor-β1, -β2, and -β3 latency-associated peptide in human cornea. *Investigative Ophthalmology and Visual Science*, *35*(8).

Nishida, T. (2005). Neurotrophic mediators and corneal wound healing. *Ocular Surface*, *3*(4). https://doi.org/10.1016/S1542-0124(12)70206-9

Niu, J. Y., Liu, J., Liu, L., Lü, Y. Y., Chen, J. S., Xu, J. T., & Zhong, J. X. (2012). Construction of eukaryotic plasmid expressing human TGFBI and its influence on human corneal epithelial cells. *International Journal of Ophthalmology*, *5*(1). https://doi.org/10.3980/j.issn.2222-3959.2012.01.08

Norris, R. A., Kern, C. B., Wessels, A., Moralez, E. I., Markwald, R. R., & Mjaatvedt, C. H. (2004). Identification and Detection of the Periostin Gene in Cardiac Development. *Anatomical Record - Part A Discoveries in Molecular, Cellular, and Evolutionary Biology*, *281*(2). https://doi.org/10.1002/ar.a.20135

Nowell, C. S., & Radtke, F. (2017). Corneal epithelial stem cells and their niche at a glance. *Journal of Cell Science*, *130*(6). https://doi.org/10.1242/jcs.198119

Oberemok, V. v., Laikova, K. v., Repetskaya, A. I., Kenyo, I. M., Gorlov, M. v., Kasich, I. N., Krasnodubets, A. M., Gal'chinsky, N. v., Fomochkina, I. I., Zaitsev, A. S., Bekirova, V. v., Seidosmanova, E. E., Dydik, K. I., Meshcheryakova, A. O., Nazarov, S. A., Smagliy, N. N., Chelengerova, E. L., Kulanova, A. A., Deri, K., … Kubyshkin, A. v. (2018). A half-century history of applications of antisense oligonucleotides in medicine, agriculture and forestry: we should continue the journey. In *Molecules* (Vol. 23, Issue 6). https://doi.org/10.3390/molecules23061302

Ohno, S., Doi, T., Fujimoto, K., Ijuin, C., Tanaka, N., Tanimoto, K., Honda, K., Nakahara, M., Kato, Y., & Tanne, K. (2002). RGD-CAP (βig-h3) exerts a negative regulatory function on mineralization in the human periodontal ligament. *Journal of Dental Research*, *81*(12). https://doi.org/10.1177/154405910208101205

Ohno, S., Noshiro, M., Makihira, S., Kawamoto, T., Shen, M., Yan, W., Kawashima-Ohya, Y., Fujimoto, K., Tanne, K., & Kato, Y. (1999). RGD-CAP (βig-h3) enhances the spreading of chondrocytes and fibroblasts via integrin α1β1. *Biochimica et Biophysica Acta - Molecular Cell Research*, *1451*(1). https://doi.org/10.1016/S0167-4889(99)00093-2

Okada, M., Yamamoto, S., Tsujikawa, M., Watanabe, H., Inoue, Y., Maeda, N., Shimomura, Y., Nishida, K., Quantock, A. J., Kinoshita, S., & Tano, Y. (1998). Two distinct kerato-epithelin mutations in Reis-Bucklers corneal dystrophy. *American Journal of Ophthalmology*, *126*(4). https://doi.org/10.1016/S0002-9394(98)00135-4

Okada, Y., Shimazaki, T., Sobue, G., & Okano, H. (2004). Retinoic-acid-concentration-dependent acquisition of neural cell identity during in vitro differentiation of mouse embryonic stem cells. *Developmental Biology*, *275*(1). https://doi.org/10.1016/j.ydbio.2004.07.038

Okita, K., Matsumura, Y., Sato, Y., Okada, A., Morizane, A., Okamoto, S., Hong, H., Nakagawa, M., Tanabe, K., Tezuka, K. I., Shibata, T., Kunisada, T., Takahashi, M., Takahashi, J., Saji, H., & Yamanaka, S. (2011). A more efficient method to generate integration-free human iPS cells. *Nature Methods*, *8*(5). https://doi.org/10.1038/nmeth.1591

Ortuño-Costela, M. D. C., Cerrada, V., García-López, M., & Gallardo, M. E. (2019). The challenge of bringing iPSCs to the patient. In *International Journal of Molecular Sciences* (Vol. 20, Issue 24). https://doi.org/10.3390/ijms20246305

Oshima, A., Tanabe, H., Yan, T., Lowe, G. N., Glackin, C. A., & Kudo, A. (2002). A novel mechanism for the regulation of osteoblast differentiation: Transcription of periostin, a member of the fasciclin I family, is regulated by the bHLH transcription factor, Twist. *Journal of Cellular Biochemistry*, *86*(4). https://doi.org/10.1002/jcb.10272

Ouyang, H., Xue, Y., Lin, Y., Zhang, X., Xi, L., Patel, S., Cai, H., Luo, J., Zhang, M., Zhang, M., Yang, Y., Li, G., Li, H., Jiang, W., Yeh, E., Lin, J., Pei, M., Zhu, J., Cao, G., … Zhang, K. (2014a). WNT7A and PAX6 define corneal epithelium homeostasis and pathogenesis. *Nature*, *511*(7509). https://doi.org/10.1038/nature13465

Ouyang, H., Xue, Y., Lin, Y., Zhang, X., Xi, L., Patel, S., Cai, H., Luo, J., Zhang, M., Zhang, M., Yang, Y., Li, G., Li, H., Jiang, W., Yeh, E., Lin, J., Pei, M., Zhu, J., Cao, G., … Zhang, K. (2014b). WNT7A and PAX6 define corneal epithelium homeostasis and pathogenesis. *Nature*, *511*(7509), 358–361. https://doi.org/10.1038/nature13465

Özbaş-Turan, S., Akbuğa, J., & Sezer, A. D. (2010). Topical application of antisense oligonucleotide-loaded chitosan nanoparticles to rats. *Oligonucleotides*, *20*(3). https://doi.org/10.1089/oli.2009.0222

Pacella, E., Pacella, F., de Paolis, G., Parisella, F. R., Turchetti, P., Anello, G., & Cavallotti, C. (2015). Glycosaminoglycans in the Human Cornea: Age-Related Changes. *Ophthalmology and Eye Diseases*, *7*. https://doi.org/10.4137/oed.s17204

Page-McCaw, A., Ewald, A. J., & Werb, Z. (2007). Matrix metalloproteinases and the regulation of tissue remodelling. In *Nature Reviews Molecular Cell Biology* (Vol. 8, Issue 3). https://doi.org/10.1038/nrm2125

Paliwal, P., Sharma, A., Tandon, R., Sharma, N., Titiyal, J. S., Sen, S., Kaur, P., Dube, D., & Vajpayee, R. B. (2010). TGFBI mutation screening and genotype-phenotype correlation in north Indian patients with corneal dystrophies. *Molecular Vision*, *16*.

Paniza, T., Deshpande, M., Wang, N., O Neil, R., Zuccaro, M. V., Smith, M. E., Madireddy, A., James, D., Ecker, J., Rosenwaks, Z., Egli, D., & Gerhardt, J. (2020). Pluripotent stem cells with low differentiation potential contain incompletely reprogrammed DNA replication. *Journal of Cell Biology*, *219*(9). https://doi.org/10.1083/jcb.201909163

PANSKY, B. (1982). Review of MEDICAL EMBRYOLOGY. In *McGraw-Hill,*.

Pantanelli, S. M., Herzlich, A., Yeaney, G., & Ching, S. T. (2014). Recurrence of granular corneal dystrophy type I deposits within host stroma after non-Descemet baring anterior lamellar keratoplasty. *Cornea*, *33*(12). https://doi.org/10.1097/ICO.0000000000000267

Parfitt, D. A., Lane, A., Ramsden, C. M., Carr, A. J. F., Munro, P. M., Jovanovic, K., Schwarz, N., Kanuga, N., Muthiah, M. N., Hull, S., Gallo, J. M., da Cruz, L., Moore, A. T., Hardcastle, A. J., Coffey, P. J., & Cheetham, M. E. (2016). Identification and Correction of Mechanisms Underlying Inherited Blindness in Human iPSC-Derived Optic Cups. *Cell Stem Cell*, *18*(6). https://doi.org/10.1016/j.stem.2016.03.021

Park, J. E., Yun, S. A., Roh, E. Y., Yoon, J. H., Shin, S., & Ki, C. S. (2021). Prevalence of granular corneal dystrophy type 2-related TGFBI p.R124H variant in a South Korean population. *Molecular Vision*, *27*.

Park, J., Wetzel, I., Marriott, I., Dréau, D., D'Avanzo, C., Kim, D. Y., Tanzi, R. E., & Cho, H. (2018). A 3D human triculture system modeling neurodegeneration and neuroinflammation in Alzheimer's disease. *Nature Neuroscience*, *21*(7). https://doi.org/10.1038/s41593-018-0175-4

Pasquale, L. R., Dorman-Pease, M. E., Lutty, G. A., Quigley, H. A., & Jampel, H. D. (1993). Immunolocalization of TGF-β1, TGF-β2, and TGF-β3 in the anterior segment of the human eye. *Investigative Ophthalmology and Visual Science*, *34*(1).

Pastinen, T., & Hudson, T. J. (2004). Cis-acting regulatory variation in the human genome. In *Science* (Vol. 306, Issue 5696). https://doi.org/10.1126/science.1101659

Patel, D. A., Chang, S. H., Harocopos, G. J., Vora, S. C., Thang, D. H., & Huang, A. J. W. (2010). Granular and lattice deposits in corneal dystrophy caused by R124C mutation of TGFBIp. *Cornea*, *29*(11). https://doi.org/10.1097/ICO.0b013e3181d4f737

Pellegrini, G., Dellambra, E., Golisano, O., Martinelli, E., Fantozzi, I., Bondanza, S., Ponzin, D., McKeon, F., & de Luca, M. (2001). p63 identifies keratinocyte stem cells. *Proceedings of the National Academy of Sciences of the United States of America*, *98*(6). https://doi.org/10.1073/pnas.061032098

Peng, P., Zhu, H., Liu, D., Chen, Z., Zhang, X., Guo, Z., Dong, M., Wan, L., Zhang, P., Liu, G., Zhang, S., Dong, F., Hu, F., Cheng, F., Huang, S., Guo, D., Zhang, B., Yu, X., & Wan, F. (2022). TGFBI secreted by tumor-associated macrophages promotes glioblastoma stem cell-driven tumor growth via integrin αvβ5-Src-Stat3 signaling. *Theranostics*, *12*(9), 4221–4236. https://doi.org/10.7150/THNO.69605

Persa, C., Osmotherly, K., Chao-Wei Chen, K., Moon, S., & Lou, M. F. (2006). The distribution of cystathionine β-synthase (CBS) in the eye: Implication of the presence of a trans-sulfuration pathway for oxidative stress defense. *Experimental Eye Research*, *83*(4). https://doi.org/10.1016/j.exer.2006.04.001

Peters, B., Kirfel, J., Büssow, H., Vidal, M., & Magin, T. M. (2001). Complete cytolysis and neonatal lethality in keratin 5 knockout mice reveal its fundamental role in skin

integrity and in epidermolysis bullosa simplex. *Molecular Biology of the Cell*, *12*(6). https://doi.org/10.1091/mbc.12.6.1775

Petersen, M., & Wengel, J. (2003). LNA: A versatile tool for therapeutics and genomics. In *Trends in Biotechnology* (Vol. 21, Issue 2). https://doi.org/10.1016/S0167-7799(02)00038-0

Pinnamaneni, N., & Funderburgh, J. L. (2012). Concise review: Stem cells in the corneal stroma. In *Stem Cells* (Vol. 30, Issue 6). https://doi.org/10.1002/stem.1100

Pires, C., Schmid, B., Petræus, C., Poon, A., Nimsanor, N., Nielsen, T. T., Waldemar, G., Hjermind, L. E., Nielsen, J. E., Hyttel, P., & Freude, K. K. (2016). Generation of a gene-corrected isogenic control cell line from an Alzheimer's disease patient iPSC line carrying a A79V mutation in PSEN1. *Stem Cell Research*, *17*(2). https://doi.org/10.1016/j.scr.2016.08.002

Pitts, M. W., & Hoffmann, P. R. (2018). Endoplasmic reticulum-resident selenoproteins as regulators of calcium signaling and homeostasis. In *Cell Calcium* (Vol. 70). https://doi.org/10.1016/j.ceca.2017.05.001

Polisetti, N., Schlunck, G., & Reinhard, T. (2023). PAX6 Expression Patterns in the Adult Human Limbal Stem Cell Niche. *Cells*, *12*(3). https://doi.org/10.3390/cells12030400

Popp, B., Krumbiegel, M., Grosch, J., Sommer, A., Uebe, S., Kohl, Z., Plötz, S., Farrell, M., Trautmann, U., Kraus, C., Ekici, A. B., Asadollahi, R., Regensburger, M., Günther, K., Rauch, A., Edenhofer, F., Winkler, J., Winner, B., & Reis, A. (2018). Need for high-resolution Genetic Analysis in iPSC: Results and Lessons from the ForIPS Consortium. *Scientific Reports*, *8*(1). https://doi.org/10.1038/s41598-018-35506-0

Poulsen, E. T., Nielsen, N. S., Jensen, M. M., Nielsen, E., Hjortdal, J., Kim, E. K., & Enghild, J. J. (2016). LASIK surgery of granular corneal dystrophy type 2 patients leads to accumulation and differential proteolytic processing of transforming growth factor beta-induced protein (TGFBIp). *Proteomics*, *16*(3). https://doi.org/10.1002/pmic.201500287

Poulsen, E. T., Runager, K., Nielsen, N. S., Lukassen, M. V., Thomsen, K., Snider, P., Simmons, O., Vorum, H., Conway, S. J., & Enghild, J. J. (2018a). Proteomic profiling of TGFBI-null mouse corneas reveals only minor changes in matrix composition supportive of TGFBI knockdown as therapy against TGFBI-linked corneal dystrophies. *FEBS Journal*, *285*(1), 101–114. https://doi.org/10.1111/febs.14321

Poulsen, E. T., Runager, K., Nielsen, N. S., Lukassen, M. V., Thomsen, K., Snider, P., Simmons, O., Vorum, H., Conway, S. J., & Enghild, J. J. (2018b). Proteomic profiling of TGFBI-null mouse corneas reveals only minor changes in matrix composition supportive of TGFBI knockdown as therapy against TGFBI-linked corneal dystrophies. *FEBS Journal*, *285*(1). https://doi.org/10.1111/febs.14321

Poulsen, E. T., Runager, K., Risør, M. W., Dyrlund, T. F., Scavenius, C., Karring, H., Praetorius, J., Vorum, H., Otzen, D. E., Klintworth, G. K., & Enghild, J. J. (2014). Comparison of two phenotypically distinct lattice corneal dystrophies caused by mutations in the transforming growth factor beta induced (TGFBI) gene. *Proteomics - Clinical Applications*, *8*(3–4). https://doi.org/10.1002/prca.201300058

Prakash, T. P., Lima, W. F., Murray, H. M., Elbashir, S., Cantley, W., Foster, D., Jayaraman, M., Chappell, A. E., Manoharan, M., Swayze, E. E., & Crooke, S. T. (2013). Lipid nanoparticles improve activity of single-stranded siRNA and gapmer antisense oligonucleotides in animals. *ACS Chemical Biology*, *8*(7). https://doi.org/10.1021/cb4001316

Przepiorski, A., Vanichapol, T., Espiritu, E. B., Crunk, A. E., Parasky, E., McDaniels, M. D., Emlet, D. R., Salisbury, R., Happ, C. L., Vernetti, L. A., MacDonald, M. L., Kellum, J. A., Kleyman, T. R., Baty, C. J., Davidson, A. J., & Hukriede, N. A. (2022). Modeling oxidative injury response in human kidney organoids. *Stem Cell Research and Therapy*, *13*(1). https://doi.org/10.1186/s13287-022-02752-z

Qiu, W. Y., Zheng, L. Bin, Pan, F., Wang, B. B., & Yao, Y. F. (2016). New histopathologic and ultrastructural findings in Reis-Bücklers corneal dystrophy caused by the Arg124Leu mutation of TGFBI gene. *BMC Ophthalmology*, *16*(1). https://doi.org/10.1186/s12886-016-0325-y

R., L., E.N., V., S.-M., C., S.S., C., P., S., A., V., C., R., D., V., D., T., T., A., & R.W., B. (2011). A novel mutation in transforming growth factor-beta induced protein (TGFbetaIp) reveals secondary structure perturbation in lattice corneal dystrophy. In *British Journal of Ophthalmology* (Vol. 95, Issue 10).

Radner, W., Zehetmayer, M., Aufreiter, R., & Mallinger, R. (1998). Interlacing and cross-angle distribution of collagen lamellae in the human cornea. *Cornea*, *17*(5). https://doi.org/10.1097/00003226-199809000-00012

Raj, A., Dhasmana, R., & Bahadur, H. (2017). Unilateral lattice corneal dystrophy in a young female: A unique case report. *Nepalese Journal of Ophthalmology*, *9*(1). https://doi.org/10.3126/nepjoph.v9i1.17537

Ramos-Mejia, V., Mũoz-Lopez, M., Garcia-Perez, J. L., & Menendez, P. (2010). IPSC lines that do not silence the expression of the ectopic reprogramming factors may display enhanced propensity to genomic instability. In *Cell Research* (Vol. 20, Issue 10). https://doi.org/10.1038/cr.2010.125

Ran, F. A., Hsu, P. D., Wright, J., Agarwala, V., Scott, D. A., & Zhang, F. (2013). Genome engineering using the CRISPR-Cas9 system. *Nature Protocols*, *8*(11). https://doi.org/10.1038/nprot.2013.143

Rangel-Huerta, E., & Maldonado, E. (2017). Transit-Amplifying Cells in the Fast Lane from Stem Cells towards Differentiation. In *Stem Cells International* (Vol. 2017). https://doi.org/10.1155/2017/7602951

Ravasi, T., Suzuki, H., Cannistraci, C. v., Katayama, S., Bajic, V. B., Tan, K., Akalin, A., Schmeier, S., Kanamori-Katayama, M., Bertin, N., Carninci, P., Daub, C. O., Forrest, A. R., Gough, J., Grimmond, S., Han, J. H., Hashimoto, T., Hide, W., Hofmann, O., … Hayashizaki, Y. (2010). An Atlas of Combinatorial Transcriptional Regulation in Mouse and Man. *Cell*, *140*(5). https://doi.org/10.1016/j.cell.2010.01.044

Rawe, I. M., Zhan, Q., Burrows, R., Bennett, K., & Cintron, C. (1997). Beta-Ig: Molecular cloning in situ hybridization in corneal tissues. *Investigative Ophthalmology and Visual Science*, *38*(5).

Rayner, S. A., Gallop, J. L., George, A. J. T., & Larkin, D. F. P. (1998). Distribution of integrins α(v)β5, α(v)β3 and α(v) in normal human cornea: Possible implications in clinical and therapeutic adenoviral infection. *Eye*, *12*(2). https://doi.org/10.1038/eye.1998.63

Reinboth, B., Thomas, J., Hanssen, E., & Gibson, M. A. (2006). βig-h3 interacts directly with biglycan and decorin, promotes collagen VI aggregation, and participates in ternary complexing with these macromolecules. *Journal of Biological Chemistry*, *281*(12). https://doi.org/10.1074/jbc.M511316200

Ricard-Blum, S. (2011). The Collagen Family. *Cold Spring Harbor Perspectives in Biology*, *3*(1). https://doi.org/10.1101/cshperspect.a004978

Ridgway, A. E. A., Akhtar, S., Munier, F. L., Schorderet, D. F., Stewart, H., Perveen, R., Bonshek, R. E., Odenthal, M. T. P., Dixon, M., Barraquer, R., Escoto, R., & Black, G. C. M. (2000). Ultrastructural and molecular analysis of Bowman's layer corneal

dystrophies: An epithelial origin? *Investigative Ophthalmology and Visual Science*, *41*(11).

Roh, M. I., Chung, S. H., Stulting, R. D., Kim, W. C., & Kim, E. K. (2006). Preserved peripheral corneal clarity after surgical trauma in patients with Avellino corneal dystrophy [2]. In *Cornea* (Vol. 25, Issue 4). https://doi.org/10.1097/01.ico.0000214236.59356.43

Roh, M. I., Grossniklaus, H. E., Chung, S. H., Kang, S. J., Kim, W. C., & Kim, E. K. (2006a). Avellino corneal dystrophy exacerbated after LASIK: Scanning electron microscopic findings. *Cornea*, *25*(3). https://doi.org/10.1097/01.ico.0000183536.07275.9a

Roh, M. I., Grossniklaus, H. E., Chung, S.-H., Kang, S. J., Kim, W. C., & Kim, E. K. (2006b). Avellino Corneal Dystrophy Exacerbated After LASIK. *Cornea*, *25*(3). https://doi.org/10.1097/01.ico.0000183536.07275.9a

Romano, A. C., Espana, E. M., Yoo, S. H., Budak, M. T., Wolosin, J. M., & Tseng, S. C. G. (2003). Different Cell Sizes in Human Limbal and Central Corneal Basal Epithelia Measured by Confocal Microscopy and Flow Cytometry. *Investigative Ophthalmology and Visual Science*, *44*(12). https://doi.org/10.1167/iovs.03-0628

Rosdy, M., & Clauss, L. C. (1990). Terminal epidermal differentiation of human keratinocytes grown in chemically defined medium on inert filter substrates at the air-liquid interface. *Journal of Investigative Dermatology*, *95*(4). https://doi.org/10.1111/1523-1747.ep12555510

Rosen, D. R., Siddique, T., Patterson, D., Figlewicz, D. A., Sapp, P., Hentati, A., Donaldson, D., Goto, J., O'Regan, J. P., Deng, H. X., Rahmani, Z., Krizus, A., McKenna-Yasek, D., Cayabyab, A., Gaston, S. M., Berger, R., Tanzi, R. E., Halperin, J. J., Herzfeldt, B., … Brown, R. H. (1993). Mutations in Cu/Zn superoxide dismutase gene are associated with familial amyotrophic lateral sclerosis. *Nature*, *362*(6415). https://doi.org/10.1038/362059a0

Rosenwasser, G. O. D., Sucheski, B. M., Rosa, N., Pastena, B., Sebastiani, A., Sassani, J. W., & Perry, H. D. (1993). Phenotypic Variation in Combined Granular-Lattice (Avellino) Corneal Dystrophy. *Archives of Ophthalmology*, *111*(11). https://doi.org/10.1001/archopht.1993.01090110112035

Ross, A. E., Bengani, L. C., Tulsan, R., Maidana, D. E., Salvador-Culla, B., Kobashi, H., Kolovou, P. E., Zhai, H., Taghizadeh, K., Kuang, L., Mehta, M., Vavvas, D. G.,

Kohane, D. S., & Ciolino, J. B. (2019). Topical sustained drug delivery to the retina with a drug-eluting contact lens. *Biomaterials*, *217*. https://doi.org/10.1016/j.biomaterials.2019.119285

Ross, C. A., & Tabrizi, S. J. (2011). Huntington's disease: From molecular pathogenesis to clinical treatment. In *The Lancet Neurology* (Vol. 10, Issue 1). https://doi.org/10.1016/S1474-4422(10)70245-3

Ross, S., & Hill, C. S. (2008). How the Smads regulate transcription. In *International Journal of Biochemistry and Cell Biology* (Vol. 40, Issue 3). https://doi.org/10.1016/j.biocel.2007.09.006

Rozario, T., & DeSimone, D. W. (2010). The extracellular matrix in development and morphogenesis: A dynamic view. In *Developmental Biology* (Vol. 341, Issue 1). https://doi.org/10.1016/j.ydbio.2009.10.026

Rozzo, C., Fossarello, M., Galleri, G., Sole, G., Serru, A., Orzalesi, N., Serra, A., & Pirastu, M. (1998). A common beta ig-h3 gene mutation (delta f540) in a large cohort of Sardinian Reis Bücklers corneal dystrophy patients. Mutations in brief no. 180. Online. *Human Mutation*, *12*(3).

Ruan, K., Bao, S., & Ouyang, G. (2009). The multifaceted role of periostin in tumorigenesis. In *Cellular and Molecular Life Sciences* (Vol. 66, Issue 14). https://doi.org/10.1007/s00018-009-0013-7

Runager, K., Basaiawmoit, R. V., Deva, T., Andreasen, M., Valnickova, Z., Sørensen, C. S., Karring, H., Thøgersen, I. B., Christiansen, G., Underhaug, J., Kristensen, T., Nielsen, N. C., Klintworth, G. K., Otzen, D. E., & Enghild, J. J. (2011). Human phenotypically distinct TGFBI corneal dystrophies are linked to the stability of the fourth FAS1 domain of TGFBIp. *Journal of Biological Chemistry*, *286*(7). https://doi.org/10.1074/jbc.M110.181099

Runager, K., García-Castellanos, R., Valnickova, Z., Kristensen, T., Nielsen, N. C., Klintworth, G. K., Gomis-Rüth, F. X., & Enghild, J. J. (2009). Purification, crystallization and preliminary X-ray diffraction of wild-type and mutant recombinant human transforming growth factor β-induced protein (TGFBIp). *Acta Crystallographica Section F: Structural Biology and Crystallization Communications*, *65*(3). https://doi.org/10.1107/S1744309109005016

Runager, K., Klintworth, G. K., Karring, H., & Enghild, J. J. (2013). The insoluble TGFBIp fraction of the cornea is covalently linked via a disulfide bond to type XII collagen. *Biochemistry*, *52*(16). https://doi.org/10.1021/bi400212m

Runyon, S. T., Zhang, Y., Appleton, B. A., Sazinsky, S. L., Wu, P., Pan, B., Wiesmann, C., Skelton, N. J., & Sidhu, S. S. (2007). Structural and functional analysis of the PDZ domains of human HtrA1 and HtrA3. *Protein Science*, *16*(11). https://doi.org/10.1110/ps.073049407

Russell, S. R., Drack, A. v., Cideciyan, A. v., Jacobson, S. G., Leroy, B. P., van Cauwenbergh, C., Ho, A. C., Dumitrescu, A. v., Han, I. C., Martin, M., Pfeifer, W. L., Sohn, E. H., Walshire, J., Garafalo, A. v., Krishnan, A. K., Powers, C. A., Sumaroka, A., Roman, A. J., Vanhonsebrouck, E., … Girach, A. (2022). Intravitreal antisense oligonucleotide sepofarsen in Leber congenital amaurosis type 10: a phase 1b/2 trial. *Nature Medicine*, *28*(5), 1014–1021. https://doi.org/10.1038/s41591-022-01755-w

Rykowska, I., Nowak, I., & Nowak, R. (2021). Soft contact lenses as drug delivery systems: A review. In *Molecules* (Vol. 26, Issue 18). https://doi.org/10.3390/molecules26185577

Saika, S., Saika, S., Liu, C. Y., Azhar, M., Sanford, L. P., Doetschman, T., Gendron, R. L., Kao, C. W. C., & Kao, W. W. Y. (2001). Tgfβ2 in corneal morphogenesis during mouse embryonic development. *Developmental Biology*, *240*(2). https://doi.org/10.1006/dbio.2001.0480

Samavarchi-Tehrani, P., Golipour, A., David, L., Sung, H. K., Beyer, T. A., Datti, A., Woltjen, K., Nagy, A., & Wrana, J. L. (2010). Functional genomics reveals a BMP-Driven mesenchymal-to-Epithelial transition in the initiation of somatic cell reprogramming. *Cell Stem Cell*, *7*(1). https://doi.org/10.1016/j.stem.2010.04.015

Santo, R. M., Yamaguchi, T., Kanai, A., Okisaka, S., & Nakajima, A. (1995). Clinical and Histopathologic Features of Corneal Dystrophies in Japan. *Ophthalmology*, *102*(4). https://doi.org/10.1016/S0161-6420(95)30982-7

Saraiva, S. M., Castro-López, V., Pañeda, C., & Alonso, M. J. (2017). Synthetic nanocarriers for the delivery of polynucleotides to the eye. *European Journal of Pharmaceutical Sciences*, *103*. https://doi.org/10.1016/j.ejps.2017.03.001

Sartini, F., Menchini, M., Posarelli, C., Casini, G., & Figus, M. (2021). In vivo efficacy of contact lens drug-delivery systems in glaucoma management. A systematic review.

In *Applied Sciences (Switzerland)* (Vol. 11, Issue 2). https://doi.org/10.3390/app11020724

Sasaki, H., Kobayashi, Y., Nakashima, Y., Moriyama, S., Yukiue, H., Kaji, M., Kiriyama, M., Fukai, I., Yamakawa, Y., & Fujii, Y. (2002). βIGH3, a TGF-β inducible gene, is overexpressed in lung cancer. *Japanese Journal of Clinical Oncology*, *32*(3). https://doi.org/10.1093/jjco/hyf021

Schadt, E. E., Lamb, J., Yang, X., Zhu, J., Edwards, S., Thakurta, D. G., Sieberts, S. K., Monks, S., Reitman, M., Zhang, C., Lum, P. Y., Leonardson, A., Thieringer, R., Metzger, J. M., Yang, L., Castle, J., Zhu, H., Kash, S. F., Drake, T. A., … Lusis, A. J. (2005). An integrative genomics approach to infer causal associations between gene expression and disease. *Nature Genetics*, *37*(7). https://doi.org/10.1038/ng1589

Schaefer, M. H., Yang, J. S., Serrano, L., & Kiel, C. (2014). Protein Conservation and Variation Suggest Mechanisms of Cell Type-Specific Modulation of Signaling Pathways. *PLoS Computational Biology*, *10*(6). https://doi.org/10.1371/journal.pcbi.1003659

Scharenberg, C. W., Harkey, M. A., & Torok-Storb, B. (2002). The ABCG2 transporter is an efficient Hoechst 33342 efflux pump and is preferentially expressed by immature human hematopoietic progenitors. *Blood*, *99*(2). https://doi.org/10.1182/blood.V99.2.507

Schmidt, R., & Plath, K. (2012). The roles of the reprogramming factors Oct4, Sox2 and Klf4 in resetting the somatic cell epigenome during induced pluripotent stem cell generation. In *Genome biology* (Vol. 13, Issue 10). https://doi.org/10.1186/gb-2012-13-10-251

Schmitt-Bernard, C. F., Chavanieu, A., Derancourt, J., Arnaud, B., Demaille, J. G., Calas, B., & Argiles, À. (2000). In vitro creation of amyloid fibrils from native and Arg124Cys mutated βIGH3((110-131)) peptides, and its relevance for lattice corneal amyloid dystrophy type I. *Biochemical and Biophysical Research Communications*, *273*(2). https://doi.org/10.1006/bbrc.2000.2955

Schmitt-Bernard, C. F., Chavanieu, A., Herrada, G., Subra, G., Arnaud, B., Demaille, J. G., Calas, B., & Argilés, Á. (2002). BIGH3 (TGFBI) Arg124 mutations influence the amyloid conversion of related peptides in vitro. Implications in the BIGH3-linked corneal dystrophies. *European Journal of Biochemistry*, *269*(21). https://doi.org/10.1046/j.1432-1033.2002.03205.x

Schmittgen, T. D., & Livak, K. J. (2001). Analysis of relative gene expression data using real-time quantitative PCR and the 2(-Delta Delta C(T)) Method. *Methods*, *25*(4).

Schmutz, J., Martin, J., Terry, A., Couronne, O., Grimwood, J., Lowry, S., Gordon, L. A., Scott, D., Xie, G., Huang, W., Hellsten, U., Tran-Gyamfi, M., She, X., Prabhakar, S., Aerts, A., Altherr, M., Bajorek, E., Black, S., Branscomb, E., … Rubin, E. M. (2004). The DNA sequence and comparative analysis of human chromosome 5. *Nature*, *431*(7006). https://doi.org/10.1038/nature02919

Schneider, D., Kleeff, J., Berberat, P. O., Zhu, Z., Korc, M., Friess, H., & Büchler, M. W. (2002). Induction and expression of ßig-h3 in pancreatic cancer cells. *Biochimica et Biophysica Acta - Molecular Basis of Disease*, *1588*(1). https://doi.org/10.1016/S0925-4439(02)00052-2

Schoch, K. M., & Miller, T. M. (2017). Antisense Oligonucleotides: Translation from Mouse Models to Human Neurodegenerative Diseases. In *Neuron* (Vol. 94, Issue 6). https://doi.org/10.1016/j.neuron.2017.04.010

Schorderet, D. F., Menasche, M., Morand, S., Bonnel, S., Büchillier, V., Marchant, D., Auderset, K., Bonny, C., Abitbol, M., & Munier, F. L. (2000). Genomic characterization and embryonic expression of the mouse Bigh3 (Tgfbi) gene. *Biochemical and Biophysical Research Communications*, *274*(2). https://doi.org/10.1006/bbrc.2000.3116

Schulze, K. V., Hanchard, N. A., & Wangler, M. F. (2020). Biases in arginine codon usage correlate with genetic disease risk. *Genetics in Medicine*, *22*(8). https://doi.org/10.1038/s41436-020-0813-6

Schurch, N. J., Schofield, P., Gierliński, M., Cole, C., Sherstnev, A., Singh, V., Wrobel, N., Gharbi, K., Simpson, G. G., Owen-Hughes, T., Blaxter, M., & Barton, G. J. (2016). How many biological replicates are needed in an RNA-seq experiment and which differential expression tool should you use? *RNA*, *22*(6). https://doi.org/10.1261/rna.053959.115

Schwanekamp, J. A., Lorts, A., Sargent, M. A., York, A. J., Grimes, K. M., Fischesser, D. M., Gokey, J. J., Whitsett, J. A., Conway, S. J., & Molkentin, J. D. (2017). TGFBI functions similar to periostin but is uniquely dispensable during cardiac injury. *PLoS ONE*, *12*(7). https://doi.org/10.1371/journal.pone.0181945

Schwartzentruber, J., Foskolou, S., Kilpinen, H., Rodrigues, J., Alasoo, K., Knights, A. J., Patel, M., Goncalves, A., Ferreira, R., Benn, C. L., Wilbrey, A., Bictash, M.,

Impey, E., Cao, L., Lainez, S., Loucif, A. J., Whiting, P. J., Gutteridge, A., & Gaffney, D. J. (2018). Molecular and functional variation in iPSC-derived sensory neurons. *Nature Genetics*, *50*(1). https://doi.org/10.1038/s41588-017-0005-8

Sen, K. (2013). Relevance of Pseudogenes to Human Genetic Disease. In *eLS*. https://doi.org/10.1002/9780470015902.a0025002

Serre, D., Gurd, S., Ge, B., Sladek, R., Sinnett, D., Harmsen, E., Bibikova, M., Chudin, E., Barker, D. L., Dickinson, T., Fan, J. B., & Hudson, T. J. (2008). Differential allelic expression in the human genome: A robust approach to identify genetic and epigenetic Cis-acting mechanisms regulating gene expression. *PLoS Genetics*, *4*(2). https://doi.org/10.1371/journal.pgen.1000006

Shah, J. N., Shao, G., Hei, T. K., & Zhao, Y. (2008). Methylation screening of the TGFBI promoter in human lung and prostate cancer by methylation-specific PCR. *BMC Cancer*, *8*. https://doi.org/10.1186/1471-2407-8-284

Shalom-Feuerstein, R., Lena, A. M., Zhou, H., De La Forest Divonne, S., Van Bokhoven, H., Candi, E., Melino, G., & Aberdam, D. (2011). Δnp63 is an ectodermal gatekeeper of epidermal morphogenesis. *Cell Death and Differentiation*, *18*(5). https://doi.org/10.1038/cdd.2010.159

Shao, G., Berenguer, J., Borczuk, A. C., Powell, C. A., Hei, T. K., & Zhao, Y. (2006). Epigenetic inactivation of Betaig-h3 gene in human cancer cells. *Cancer Research*, *66*(9). https://doi.org/10.1158/0008-5472.CAN-05-2130

Sharma, A., & Coles, W. H. (1989). Kinetics of corneal epithelial maintenance and graft loss: A population balance model. *Investigative Ophthalmology and Visual Science*, *30*(9).

Shi, Y., Inoue, H., Wu, J. C., & Yamanaka, S. (2017). Induced pluripotent stem cell technology: A decade of progress. In *Nature Reviews Drug Discovery* (Vol. 16, Issue 2). https://doi.org/10.1038/nrd.2016.245

Shiju, T. M., Carlos de Oliveira, R., & Wilson, S. E. (2020). 3D in vitro corneal models: A review of current technologies. In *Experimental Eye Research* (Vol. 200). https://doi.org/10.1016/j.exer.2020.108213

Shimazaki, M., Nakamura, K., Kii, I., Kashima, T., Amizuka, N., Li, M., Saito, M., Fukuda, K., Nishiyama, T., Kitajima, S., Saga, Y., Fukayama, M., Sata, M., & Kudo, A. (2008). Periostin is essential for cardiac healing after acute myocardial infarction. *Journal of Experimental Medicine*, *205*(2). https://doi.org/10.1084/jem.20071297

Shurman, D. L., Glazewski, L., Gumpert, A., Zieske, J. D., & Richard, G. (2005). In vivo and in vitro expression of connexins in the human corneal epithelium. *Investigative Ophthalmology and Visual Science*, *46*(6). https://doi.org/10.1167/iovs.04-1364

S.-I., C., B.-Y., K., S., D., J.-Y., O., T.-I., K., J.Y., K., & E.K., K. (2012). Impaired autophagy and delayed autophagic clearance of transforming growth factor beta-induced protein (TGFBI) in granular corneal dystrophy type 2. *Autophagy*, *8*(12).

Simões-Wüst, A. P., Hopkins-Donaldson, S., Sigrist, B., Belyanskaya, L., Stahel, R. A., & Zangemeister-Wittke, U. (2004). A functionally improved locked nucleic acid antisense oligonucleotide inhibits Bcl-2 and Bcl-xL expression and facilitates tumor cell apoptosis. *Oligonucleotides*, *14*(3). https://doi.org/10.1089/1545457042258297

Sivak, J. M., & Fini, M. E. (2002). MMPs in the eye: Emerging roles for matrix metalloproteinases in ocular physiology. In *Progress in Retinal and Eye Research* (Vol. 21, Issue 1). https://doi.org/10.1016/S1350-9462(01)00015-5

Skonier, J., Bennett, K., Rothwell, V., Kosowski, S., Plowman, G., Wallace, P., Edelhoff, S., Disteche, C., Neubauer, M., Marquardt, H., Rodgers, J., & Purchio, A. F. (1994). βig-h3: A Transforming Growth Factor-β-Responsive Gene Encoding a Secreted Protein That Inhibits Cell Attachment In Vitro and Suppresses the Growth of CHO Cells in Nude Mice. *DNA and Cell Biology*, *13*(6). https://doi.org/10.1089/dna.1994.13.571

Skonier, J., Neubauer, M., Madisen, L., Bennett, K., Plowman, G. D., & Purchio, A. F. (1992). cDNA Cloning and Sequence Analysis of βig-h3, a Novel Gene Induced in a Human Adenocarcinoma Cell Line after Treatment with Transforming Growth Factor-β. *DNA and Cell Biology*, *11*(7). https://doi.org/10.1089/dna.1992.11.511

Slijkerman, R., Kremer, H., & van Wijk, E. (2018). Antisense Oligonucleotide Design and Evaluation of Splice-Modulating Properties Using Cell-Based Assays. In *Methods in Molecular Biology* (Vol. 1828). https://doi.org/10.1007/978-1-4939-8651-4_34

Smith, A. N., Miller, L. A. D., Song, N., Taketo, M. M., & Lang, R. A. (2005). The duality of β-catenin function: A requirement in lens morphogenesis and signaling suppression of lens fate in periocular ectoderm. *Developmental Biology*, *285*(2). https://doi.org/10.1016/j.ydbio.2005.07.019

Smith, Z. D., Nachman, I., Regev, A., & Meissner, A. (2010). Dynamic single-cell imaging of direct reprogramming reveals an early specifying event. *Nature Biotechnology*, *28*(5). https://doi.org/10.1038/nbt.1632

Snead, D. R. J., & Mathews, B. N. (2002). Differences in amyloid deposition in primary and recurrent corneal lattice dystrophy type 1. *Cornea*, *21*(3). https://doi.org/10.1097/00003226-200204000-00014

Snider, P., Standley, K. N., Wang, J., Azhar, M., Doetschman, T., & Conway, S. J. (2009). Origin of cardiac fibroblasts and the role of periostin. In *Circulation Research* (Vol. 105, Issue 10). https://doi.org/10.1161/CIRCRESAHA.109.201400

Snow, A. D., Mar, H., Nochlin, D., Kimata, K., Kato, M., Suzuki, S., Hassell, J., & Wight, T. N. (1988). The presence of heparan sulfate proteoglycans in the neuritic plaques and congophilic angiopathy in Alzheimer's disease. *American Journal of Pathology*, *133*(3).

Son, H. N., Nam, J. O., Kim, S., & Kim, I. S. (2013). Multiple FAS1 domains and the RGD motif of TGFBI act cooperatively to bind αvβ3 integrin, leading to anti-angiogenic and anti-tumor effects. *Biochimica et Biophysica Acta - Molecular Cell Research*, *1833*(10). https://doi.org/10.1016/j.bbamcr.2013.06.012

Song, B., Estrada, K. D., & Lyons, K. M. (2009). Smad signaling in skeletal development and regeneration. *Cytokine and Growth Factor Reviews*, *20*(5–6). https://doi.org/10.1016/j.cytogfr.2009.10.010

Song, J. (2013). Why do proteins aggregate? "Intrinsically insoluble proteins"? And "dark mediators"? Revealed by studies on "insoluble proteins"? Solubilized in pure water. *F1000Research*, *2*. https://doi.org/10.12688/f1000research.2-94.v1

Song, X., Cai, L., Li, Y., Zhu, J., Jin, P., Chen, L., & Ma, F. (2014). Identification and characterization of transforming growth factor β induced gene (TGFBIG) from Branchiostoma belcheri: Insights into evolution of TGFBI family. *Genomics*, *103*(1). https://doi.org/10.1016/j.ygeno.2013.10.002

Song, Y., Sun, M., Wang, N., Zhou, X., Zhao, J., Wang, Q., Chen, S., Deng, Y., Qiu, L., Chen, Y., Aldave, A. J., & Zhang, F. (2017). Prevalence of transforming growth factor β–induced gene corneal dystrophies in Chinese refractive surgery candidates. *Journal of Cataract and Refractive Surgery*, *43*(12). https://doi.org/10.1016/j.jcrs.2017.07.038

Sperber, H., Mathieu, J., Wang, Y., Ferreccio, A., Hesson, J., Xu, Z., Fischer, K. A., Devi, A., Detraux, D., Gu, H., Battle, S. L., Showalter, M., Valensisi, C., Bielas, J. H., Ericson, N. G., Margaretha, L., Robitaille, A. M., Margineantu, D., Fiehn, O., … Ruohola-Baker, H. (2015). The metabolome regulates the epigenetic landscape

during naive-to-primed human embryonic stem cell transition. *Nature Cell Biology*, *17*(12). https://doi.org/10.1038/ncb3264

Sridhar, M. S. (2018). Anatomy of cornea and ocular surface. In *Indian Journal of Ophthalmology* (Vol. 66, Issue 2). https://doi.org/10.4103/ijo.IJO_646_17

Sridhar, M. S., Laibson, P. R., Eagle, R. C., Rapuano, C. J., & Cohen, E. J. (2001). Unilateral corneal lattice dystrophy. *Cornea*, *20*(8). https://doi.org/10.1097/00003226-200111000-00014

Srinivasarao, D. A., Lohiya, G., & Katti, D. S. (2019). Fundamentals, challenges, and nanomedicine-based solutions for ocular diseases. In *Wiley Interdisciplinary Reviews: Nanomedicine and Nanobiotechnology* (Vol. 11, Issue 4). https://doi.org/10.1002/wnan.1548

Stadtfeld, M., Maherali, N., Breault, D. T., & Hochedlinger, K. (2008). Defining Molecular Cornerstones during Fibroblast to iPS Cell Reprogramming in Mouse. *Cell Stem Cell*, *2*(3). https://doi.org/10.1016/j.stem.2008.02.001

Stenvang, M., Schafer, N. P., Malmos, K. G., Pérez, A. M. W., Niembro, O., Sormanni, P., Basaiawmoit, R. V., Christiansen, G., Andreasen, M., & Otzen, D. E. (2018). Corneal Dystrophy Mutations Drive Pathogenesis by Targeting TGFBIp Stability and Solubility in a Latent Amyloid-forming Domain. *Journal of Molecular Biology*, *430*(8). https://doi.org/10.1016/j.jmb.2018.03.001

Stewart, H. S., Ridgway, A. E., Dixon, M. J., Bonshek, R., Parveen, R., & Black, G. (1999). Heterogeneity in granular corneal dystrophy: Identification of three causative mutations in the TGFBI (BIGH3) genes - Lessons for corneal amyloidogenesis. *Human Mutation*, *14*(2). https://doi.org/10.1002/(SICI)1098-1004(1999)14:2<126::AID-HUMU4>3.0.CO;2-W

Stix, B., Leber, M., Bingemer, P., Gross, C., Rüschoff, J., Fändrich, M., Schorderet, D. F., Vorwerk, C. K., Zacharias, M., Roessner, A., & Röcken, C. (2005). Hereditary lattice corneal dystrophy is associated with corneal amyloid deposits enclosing C-terminal fragments of keratoepithelin. *Investigative Ophthalmology and Visual Science*, *46*(4). https://doi.org/10.1167/iovs.04-1319

Stocum, D. L. (2006). Regenerative Biology and Medicine. In *Regenerative Biology and Medicine*. https://doi.org/10.1016/B978-0-12-369371-6.X5017-5

Stone, E. M., Lotery, A. J., Munier, F. L., Héon, E., Piguet, B., Guymer, R. H., Vandenburgh, K., Cousin, P., Nishimura, D., Swiderski, R. E., Silvestri, G., Mackey,

D. A., Hageman, G. S., Bird, A. C., Sheffield, V. C., & Schordere, D. F. (1999). A single EFEMP1 mutation associated with both Malattia Leventinese and Doyne honeycomb retinal dystrophy. *Nature Genetics*, *22*(2). https://doi.org/10.1038/9722

Stone, E. M., Mathers, W. D., Rosenwasser, G. O. D., Holland, E. J., Folberg, R., Krachmer, J. H., Nichols, B. E., Gorevic, P. D., Taylor, C. M., Streb, L. M., Fishbaugh, J. A., Daley, T. E., Sucheski, B. M., & Sheffield, V. C. (1994). Three autosomal dominant corneal dystrophies map to chromosome 5q. *Nature Genetics*, *6*(1). https://doi.org/10.1038/ng0194-47

Straarup, E. M., Fisker, N., Hedtjärn, M., Lindholm, M. W., Rosenbohm, C., Aarup, V., Hansen, H. F., Ørum, H., Hansen, J. B. R., & Koch, T. (2010). Short locked nucleic acid antisense oligonucleotides potently reduce apolipoprotein B mRNA and serum cholesterol in mice and non-human primates. *Nucleic Acids Research*, *38*(20). https://doi.org/10.1093/nar/gkq457

Sugita, S., Mandai, M., Hirami, Y., Takagi, S., Maeda, T., Fujihara, M., Matsuzaki, M., Yamamoto, M., Iseki, K., Hayashi, N., Hono, A., Fujino, S., Koide, N., Sakai, N., Shibata, Y., Terada, M., Nishida, M., Dohi, H., Nomura, M., … Takahashi, M. (2020). HLA-matched allogeneic IPS cells-derived rpe transplantation for macular degeneration. *Journal of Clinical Medicine*, *9*(7). https://doi.org/10.3390/jcm9072217

Suk, J. Y., Zhang, F., Balch, W. E., Linhardt, R. J., & Kelly, J. W. (2006). Heparin accelerates gelsolin amyloidogenesis. *Biochemistry*, *45*(7). https://doi.org/10.1021/bi0519295

Sunde, M., & Blake, C. (1997). The structure of amyloid fibrils by electron microscopy and x-ray diffraction. In *Advances in Protein Chemistry* (Vol. 50). https://doi.org/10.1016/s0065-3233(08)60320-4

Sunny, S. S., Lachova, J., Dupacova, N., & Kozmik, Z. (2022). Multiple roles of Pax6 in postnatal cornea development. *Developmental Biology*, *491*. https://doi.org/10.1016/j.ydbio.2022.08.006

Susaimanickam, P. J., Maddileti, S., Kumar Pulimamidi, V., Boyinpally, S. R., Naik, R. R., Naik, M. N., Reddy, G. B., Sangwan, V. S., & Mariappan, I. (2017). Generating minicorneal organoids from human induced pluripotent stem cells. *Development (Cambridge)*, *144*(13). https://doi.org/10.1242/dev.143040

Swain, N., Thakur, M., Pathak, J., & Swain, B. (2020). SOX2, OCT4 and NANOG: The core embryonic stem cell pluripotency regulators in oral carcinogenesis. *Journal of Oral and Maxillofacial Pathology*, *24*(2). https://doi.org/10.4103/jomfp.jomfp_22_20

Szalai, E., Felszeghy, S., Hegyi, Z., Módis, L., Berta, A., & Kaarniranta, K. (2012). Fibrillin-2, tenascin-C, matrilin-2, and matrilin-4 are strongly expressed in the epithelium of human granular and lattice type I corneal dystrophies. *Molecular Vision*, *18*.

Taapken, S. M., Nisler, B. S., Newton, M. A., Sampsell-Barron, T. L., Leonhard, K. A., McIntire, E. M., & Montgomery, K. D. (2011). Karyotypic abnormalities in human induced pluripotent stem cells and embryonic stem cells. *Nature Biotechnology*, *29*(4), 313–314. https://doi.org/10.1038/nbt.1835

Tabrizi, S. J., Leavitt, B. R., Landwehrmeyer, G. B., Wild, E. J., Saft, C., Barker, R. A., Blair, N. F., Craufurd, D., Priller, J., Rickards, H., Rosser, A., Kordasiewicz, H. B., Czech, C., Swayze, E. E., Norris, D. A., Baumann, T., Gerlach, I., Schobel, S. A., Paz, E., … Lane, R. M. (2019). Targeting Huntingtin Expression in Patients with Huntington's Disease. *New England Journal of Medicine*, *380*(24). https://doi.org/10.1056/nejmoa1900907

Takács, L., Boross, P., Tözsér, J., Módis, L., Tóth, G., & Berta, A. (1998). Transforming growth factor-β induced protein, βIG-H3, is present in degraded form and altered localization in lattice corneal dystrophy type I. *Experimental Eye Research*, *66*(6). https://doi.org/10.1006/exer.1998.0471

Takács, L., Csutak, A., Balázs, E., & Berta, A. (1999). Immunohistochemical detection of βIG-H3 in scarring human corneas. *Graefe's Archive for Clinical and Experimental Ophthalmology*, *237*(7). https://doi.org/10.1007/s004170050275

Takahashi, J. (2020). iPS cell-based therapy for Parkinson's disease: A Kyoto trial. *Regenerative Therapy*, *13*. https://doi.org/10.1016/j.reth.2020.06.002

Takahashi, K., Tanabe, K., Ohnuki, M., Narita, M., Ichisaka, T., Tomoda, K., & Yamanaka, S. (2007). Induction of Pluripotent Stem Cells from Adult Human Fibroblasts by Defined Factors. *Cell*, *131*(5). https://doi.org/10.1016/j.cell.2007.11.019

Takahashi, K., & Yamanaka, S. (2006). Induction of Pluripotent Stem Cells from Mouse Embryonic and Adult Fibroblast Cultures by Defined Factors. *Cell*, *126*(4). https://doi.org/10.1016/j.cell.2006.07.024

Takamiya, M., Stegmaier, J., Kobitski, A. Y., Schott, B., Weger, B. D., Margariti, D., Delgado, A. R. C., Gourain, V., Scherr, T., Yang, L., Sorge, S., Otte, J. C., Hartmann, V., Van Wezel, J., Stotzka, R., Reinhard, T., Schlunck, G., Dickmeis, T., Rastegar, S., … Strahle, U. (2020). Pax6 organizes the anterior eye segment by guiding two distinct neural crest waves. *PLoS Genetics*, *16*(6). https://doi.org/10.1371/journal.pgen.1008774

Takeshige, K., Baba, M., Tsuboi, S., Noda, T., & Ohsumi, Y. (1992). Autophagy in yeast demonstrated with proteinase-deficient mutants and conditions for its induction. *Journal of Cell Biology*, *119*(2). https://doi.org/10.1083/jcb.119.2.301

Taketani, Y., Kitamoto, K., Sakisaka, T., Kimakura, M., Toyono, T., Yamagami, S., Amano, S., Kuroda, M., Moore, T., Usui, T., & Ouchi, Y. (2017a). Repair of the TGFBI gene in human corneal keratocytes derived from a granular corneal dystrophy patient via CRISPR/Cas9-induced homology-directed repair. *Scientific Reports*, *7*(1). https://doi.org/10.1038/s41598-017-16308-2

Taketani, Y., Kitamoto, K., Sakisaka, T., Kimakura, M., Toyono, T., Yamagami, S., Amano, S., Kuroda, M., Moore, T., Usui, T., & Ouchi, Y. (2017b). Repair of the TGFBI gene in human corneal keratocytes derived from a granular corneal dystrophy patient via CRISPR/Cas9-induced homology-directed repair. *Scientific Reports*, *7*(1). https://doi.org/10.1038/s41598-017-16308-2

Tang, J., Zhou, H. W., Jiang, J. L., Yang, X. M., Li, Y., Zhang, H. X., Chen, Z. N., & Guo, W. P. (2007). βig-h3 is involved in the HAb18G/CD147-mediated metastasis process in human hepatoma cells. *Experimental Biology and Medicine*, *232*(3).

Tanhehco, T. Y., Eifrig, D. E., Schwab, I. R., Rapuano, C. J., & Klintworth, G. K. (2006). Two cases of Reis-Bücklers corneal dystrophy (granular corneal dystrophy type III) caused by spontaneous mutations in the TGFBI gene. *Archives of Ophthalmology*, *124*(4). https://doi.org/10.1001/archopht.124.4.589

Taylor, M. A., Sossey-Alaoui, K., Thompson, C. L., Danielpour, D., & Schiemann, W. P. (2013). TGF-β upregulates miR-181a expression to promote breast cancer metastasis. *Journal of Clinical Investigation*, *123*(1). https://doi.org/10.1172/JCI64946

ten Asbroek, A. L. M. A., van Groenigen, M., Nooij, M., & Baas, F. (2002). The involvement of human ribonucleases H1 and H2 in the variation of response of cells to antisense phosphorothioate oligonucleotides. *European Journal of Biochemistry*, *269*(2). https://doi.org/10.1046/j.0014-2956.2001.02686.x

Tennent, G. A. (1999). Isolation and characterization of amyloid fibrils from tissue. *Methods in Enzymology*, *309*. https://doi.org/10.1016/S0076-6879(99)09004-7

Thapa, N., Kang, K. B., & Kim, I. S. (2005). βig-h3 mediates osteoblast adhesion and inhibits differentiation. *Bone*, *36*(2). https://doi.org/10.1016/j.bone.2004.08.007

Thomas, P. B., Liu, Y. H., Zhuang, F. F., Selvam, S., Song, S. W., Smith, R. E., Trousdale, M. D., & Yiu, S. C. (2007). Identification of Notch-1 expression in the limbal basal epithelium. *Molecular Vision*, *13*.

Tian, H., Liu, J., Chen, J., Gatza, M. L., & Blobe, G. C. (2015). Fibulin-3 is a novel TGF-β pathway inhibitor in the breast cancer microenvironment. *Oncogene*, *34*(45). https://doi.org/10.1038/onc.2015.13

Tian, X., Fujiki, K., Wang, W., Murakami, A., Xie, P., Kanai, A., & Liu, Z. (2005). Novel mutation (V505D) of the TGFBI gene found in a Chinese family with lattice corneal dystrophy, type I. *Japanese Journal of Ophthalmology*, *49*(2). https://doi.org/10.1007/s10384-004-0167-7

Tocharus, J., Tsuchiya, A., Kajikawa, M., Ueta, Y., Oka, C., & Kawaichi, M. (2004). Developmentally regulated expression of mouse HtrA3 and its role as an inhibitor of TGF-β signaling. *Development Growth and Differentiation*, *46*(3). https://doi.org/10.1111/j.1440-169X.2004.00743.x

Tonner, P., Srinivasasainagendra, V., Zhang, S., & Zhi, D. (2012). Detecting transcription of ribosomal protein pseudogenes in diverse human tissues from RNA-seq data. *BMC Genomics*, *13*(1). https://doi.org/10.1186/1471-2164-13-412

Torricelli, A. A. M., Singh, V., Santhiago, M. R., & Wilson, S. E. (2013). The corneal epithelial basement membrane: Structure, function, and disease. In *Investigative Ophthalmology and Visual Science* (Vol. 54, Issue 9). https://doi.org/10.1167/iovs.13-12547

Torricelli, A. A. M., & Wilson, S. E. (2014). Cellular and extracellular matrix modulation of corneal stromal opacity. In *Experimental Eye Research* (Vol. 129). https://doi.org/10.1016/j.exer.2014.09.013

Tran, H., Moazami, M. P., Yang, H., McKenna-Yasek, D., Douthwright, C. L., Pinto, C., Metterville, J., Shin, M., Sanil, N., Dooley, C., Puri, A., Weiss, A., Wightman, N., Gray-Edwards, H., Marosfoi, M., King, R. M., Kenderdine, T., Fabris, D., Bowser, R., … Brown, R. H. (2022). Suppression of mutant C9orf72 expression by a potent

mixed backbone antisense oligonucleotide. *Nature Medicine*, *28*(1). https://doi.org/10.1038/s41591-021-01557-6

Troy, T. C., & Turksen, K. (1999). In vitro characteristics of early epidermal progenitors isolated from keratin 14 (K14)-deficient mice: Insights into the role of keratin 17 in mouse keratinocytes. *Journal of Cellular Physiology*, *180*(3). https://doi.org/10.1002/(SICI)1097-4652(199909)180:3<409::AID-JCP12>3.0.CO;2-V

Tsujikawa, K., Tsujikawa, M., Watanabe, H., Maeda, N., Inoue, Y., Fujikado, T., & Tano, Y. (2007). Allelic homogeneity in Avellino corneal dystrophy due to a founder effect. *Journal of Human Genetics*, *52*(1). https://doi.org/10.1007/s10038-006-0083-4

Tumbarello, D. A., Andrews, M. R., & Brenton, J. D. (2016). SPARc regulates transforming growth factor beta induced (tgfbi) extracellular matrix deposition and paclitaxel response in ovarian cancer cells. *PLoS ONE*, *11*(9). https://doi.org/10.1371/journal.pone.0162698

Tung, J., Fédrigo, O., Haygood, R., Mukherjee, S., & Wray, G. A. (2009). Genomic features that predict allelic imbalance in humans suggest patterns of constraint on gene expression variation. *Molecular Biology and Evolution*, *26*(9). https://doi.org/10.1093/molbev/msp113

Tuori, A., Uusitalo, H., Burgeson, R. E., Terttunen, J., & Virtanen, I. (1996). The immunohistochemical composition of the human corneal basement membrane. *Cornea*, *15*(3). https://doi.org/10.1097/00003226-199605000-00010

Tutar, Y. (2012). Pseudogenes. In *Comparative and Functional Genomics* (Vol. 2012). https://doi.org/10.1155/2012/424526

Ueberham, U., & Arendt, T. (2013). The Role of Smad Proteins for Development, Differentiation and Dedifferentiation of Neurons. In *Trends in Cell Signaling Pathways in Neuronal Fate Decision*. https://doi.org/10.5772/54532

Ünal, M., Arslan, O. S., Atalay, E., Mangan, M. S., & Bilgin, A. B. (2013). Deep anterior lamellar keratoplasty for the treatment of stromal corneal dystrophies. *Cornea*, *32*(3). https://doi.org/10.1097/ICO.0b013e31825718ca

Underhaug, J., Koldsø, H., Runager, K., Nielsen, J. T., Sørensen, C. S., Kristensen, T., Otzen, D. E., Karring, H., Malmendal, A., Schiøtt, B., Enghild, J. J., & Nielsen, N. C. (2013). Mutation in transforming growth factor beta induced protein associated with granular corneal dystrophy type 1 reduces the proteolytic susceptibility through local

structural stabilization. *Biochimica et Biophysica Acta - Proteins and Proteomics*, *1834*(12). https://doi.org/10.1016/j.bbapap.2013.10.008

Upender, M. B., Habermann, J. K., McShane, L. M., Korn, E. L., Barrett, J. C., Difilippantonio, M. J., & Ried, T. (2004). Chromosome transfer induced aneuploidy results in complex dysregulation of the cellular transcriptome in immortalized and cancer cells. *Cancer Research*, *64*(19). https://doi.org/10.1158/0008-5472.CAN-04-0474

Vahsen, B. F., Gray, E., Candalija, A., Cramb, K. M. L., Scaber, J., Dafinca, R., Katsikoudi, A., Xu, Y., Farrimond, L., Wade-Martins, R., James, W. S., Turner, M. R., Cowley, S. A., & Talbot, K. (2022). Human iPSC co-culture model to investigate the interaction between microglia and motor neurons. *Scientific Reports*, *12*(1). https://doi.org/10.1038/s41598-022-16896-8

van Beek, D., Verdonschot, J., Derks, K., Brunner, H., de Kok, T. M., Arts, I. C. W., Heymans, S., Kutmon, M., & Adriaens, M. (2023). Allele-specific expression analysis for complex genetic phenotypes applied to a unique dilated cardiomyopathy cohort. *Scientific Reports*, *13*(1). https://doi.org/10.1038/s41598-023-27591-7

Van Caam, A., Aarts, J., Van Ee, T., Vitters, E., Koenders, M., Van De Loo, F., Van Lent, P., Van Den Hoogen, F., Thurlings, R., Vonk, M. C., & Van Der Kraan, P. M. (2020). TGFβ-mediated expression of TGFβ-activating integrins in SSc monocytes: Disturbed activation of latent TGFβ? *Arthritis Research and Therapy*, *22*(1). https://doi.org/10.1186/s13075-020-2130-5

van der Valk, J. (2022). Fetal bovine serum—a cell culture dilemma. In *Science* (Vol. 375, Issue 6577). https://doi.org/10.1126/science.abm1317

Varlamova, E. G., Goltyaev, M. v., & Turovsky, E. A. (2022). The Role of Selenoproteins SELENOM and SELENOT in the Regulation of Apoptosis, ER Stress, and Calcium Homeostasis in the A-172 Human Glioblastoma Cell Line. *Biology*, *11*(6). https://doi.org/10.3390/biology11060811

Venkatraman, A., Duong-Thi, M. D., Pervushin, K., Ohlson, S., & Mehta, J. S. (2020). Pharmaceutical modulation of the proteolytic profile of Transforming Growth Factor Beta induced protein (TGFBIp) offers a new avenue for treatment of TGFBI-corneal dystrophy. *Journal of Advanced Research*, *24*. https://doi.org/10.1016/j.jare.2020.05.012

Venkatraman, A., Dutta, B., Murugan, E., Piliang, H., Lakshminaryanan, R., Sook Yee, A. C., Pervushin, K. V., Sze, S. K., & Mehta, J. S. (2017). Proteomic Analysis of Amyloid Corneal Aggregates from TGFBI-H626R Lattice Corneal Dystrophy Patient Implicates Serine-Protease HTRA1 in Mutation-Specific Pathogenesis of TGFBIp. *Journal of Proteome Research*, *16*(8). https://doi.org/10.1021/acs.jproteome.7b00188

Venkatraman, A., Hochart, G., Bonnel, D., Stauber, J., Shimmura, S., Rajamani, L., Pervushin, K., & Mehta, J. S. (2019). Matrix-Assisted Laser Desorption Ionization Mass Spectrometry Imaging of Key Proteins in Corneal Samples from Lattice Dystrophy Patients with TGFBI-H626R and TGFBI-R124C Mutations. *Proteomics - Clinical Applications*, *13*(1). https://doi.org/10.1002/prca.201800053

Venkatraman, A., Murugan, E., Lin, S. J., Peh, G. S. L., Rajamani, L., & Mehta, J. S. (2020). Effect of osmolytes on in-vitro aggregation properties of peptides derived from TGFBIp. *Scientific Reports*, *10*(1). https://doi.org/10.1038/s41598-020-60944-0

Venuganti, V. V. K., Saraswathy, M., Dwivedi, C., Kaushik, R. S., & Perumal, O. P. (2015). Topical gene silencing by iontophoretic delivery of an antisense oligonucleotide-dendrimer nanocomplex: The proof of concept in a skin cancer mouse model. *Nanoscale*, *7*(9). https://doi.org/10.1039/c4nr05241b

Vickers, T. A., Koo, S., Bennett, C. F., Crooke, S. T., Dean, N. M., & Baker, B. F. (2003). Efficient reduction of target RNAs by small interfering RNA and RNase H-dependent antisense agents. A comparative analysis. *Journal of Biological Chemistry*, *278*(9). https://doi.org/10.1074/jbc.M210326200

Vickers, T. A., Wyatt, J. R., & Freier, S. M. (2000). Effects of RNA secondary structure on cellular antisense activity. *Nucleic Acids Research*, *28*(6). https://doi.org/10.1093/nar/28.6.1340

Vitart, V., Benčić, G., Hayward, C., Škunca Herman, J., Huffman, J., Campbell, S., Bućan, K., Navarro, P., Gunjaca, G., Marin, J., Zgaga, L., Kolčić, I., Polašek, O., Kirin, M., Hastie, N. D., Wilson, J. F., Rudan, I., Campbell, H., Vatavuk, Z., … Wright, A. (2010). New loci associated with central cornea thickness include COL5A1, AKAP13 and AVGR8. *Human Molecular Genetics*, *19*(21). https://doi.org/10.1093/hmg/ddq349

Volk, S. W., Wang, Y., Mauldin, E. A., Liechty, K. W., & Adams, S. L. (2011). Diminished type III collagen promotes myofibroblast differentiation and increases scar

deposition in cutaneous wound healing. *Cells Tissues Organs*, *194*(1). https://doi.org/10.1159/000322399

Volpato, V., Smith, J., Sandor, C., Ried, J. S., Baud, A., Handel, A., Newey, S. E., Wessely, F., Attar, M., Whiteley, E., Chintawar, S., Verheyen, A., Barta, T., Lako, M., Armstrong, L., Muschet, C., Artati, A., Cusulin, C., Christensen, K., … Lakics, V. (2018). Reproducibility of Molecular Phenotypes after Long-Term Differentiation to Human iPSC-Derived Neurons: A Multi-Site Omics Study. *Stem Cell Reports*, *11*(4). https://doi.org/10.1016/j.stemcr.2018.08.013

Wahlestedt, C., Salmi, P., Good, L., Kela, J., Johnsson, T., Hökfelt, T., Broberger, C., Porreca, F., Lai, J., Ren, K., Ossipov, M., Koshkin, A., Jakobsen, N., Skouv, J., Oerum, H., Jacobsen, M. H., & Wengel, J. (2000). Potent and nontoxic antisense oligonudeotides containing locked nucleic acids. *Proceedings of the National Academy of Sciences of the United States of America*, *97*(10). https://doi.org/10.1073/pnas.97.10.5633

Wang, F., Hu, W., Xian, J., Ohnuma, S. ichi, & Brenton, J. D. (2013). The Xenopus Tgfbi is required for embryogenesis through regulation of canonical Wnt signalling. *Developmental Biology*, *379*(1). https://doi.org/10.1016/j.ydbio.2012.11.010

Wang, H., Yu, H., Zhou, X., Zhang, J., Zhou, H., Hao, H., Ding, L., Li, H., Gu, Y., Ma, J., Qiu, J., & Ma, D. (2022). An Overview of Extracellular Matrix-Based Bioinks for 3D Bioprinting. In *Frontiers in Bioengineering and Biotechnology* (Vol. 10). https://doi.org/10.3389/fbioe.2022.905438

Wang, M. X., Munier, F. L., Araki-Saski, K., & Schorderet, D. F. (2002). TGFBI gene transcript is transforming growth factor-β1-responsive and cell density-dependent in a human corneal epithelial cell line. *Ophthalmic Genetics*, *23*(4). https://doi.org/10.1076/opge.23.4.237.13884

Wang, Y., Mahesh, P., Wang, Y., Novo, S. G., Shihan, M. H., Hayward-Piatkovskyi, B., & Duncan, M. K. (2018). Spatiotemporal dynamics of canonical Wnt signaling during embryonic eye development and posterior capsular opacification (PCO). *Experimental Eye Research*, *175*. https://doi.org/10.1016/j.exer.2018.06.020

Wang, Y., & Nie, G. (2021). Overview of human HtrA family proteases and their distinctive physiological roles and unique involvement in diseases, especially cancer and pregnancy complications. In *International Journal of Molecular Sciences* (Vol. 22, Issue 19). https://doi.org/10.3390/ijms221910756

Wang, Z., Zheng, H., Zhou, H., Huang, N., Wei, X., Liu, X., Teng, X., Hu, Z., Zhang, J., Zhou, X., Li, W., & Li, J. (2019). Systematic screening and identification of novel psoriasis-specific genes from the transcriptome of psoriasis-like keratinocytes. *Molecular Medicine Reports*, *19*(3). https://doi.org/10.3892/mmr.2018.9782

Warden, B. A., & Duell, P. B. (2018). Volanesorsen for treatment of patients with familial chylomicronemia syndrome. *Drugs of Today*, *54*(12). https://doi.org/10.1358/dot.2018.54.12.2899384

Watanabe, H., Hashida, Y., Tsujikawa, K., Tsujikawa, M., Maeda, N., Inoue, Y., Yamamoto, S., & Tano, Y. (2001). Two patterns of opacity in corneal dystrophy caused by the homozygous BIG-H3 R124H mutation. *American Journal of Ophthalmology*, *132*(2). https://doi.org/10.1016/S0002-9394(01)00962-X

Watanabe, T. A., Geary, R. S., & Levin, A. A. (2006). Plasma protein binding of an antisense oligonucleotide targeting human ICAM-1 (ISIS 2302). *Oligonucleotides*, *16*(2). https://doi.org/10.1089/oli.2006.16.169

Watanabe, T., Frost, D. A. B., Mlakar, L., Heywood, J., Da Silveira, W. A., Hardiman, G., & Feghali-Bostwick, C. (2019). A human skin model recapitulates systemic sclerosis dermal fibrosis and identifies COL22A1 as a TGFβ early response gene that mediates fibroblast to myofibroblast transition. *Genes*, *10*(2). https://doi.org/10.3390/genes10020075

Watanabe, Y., Usada, N., Minami, H., Morita, T., Tsugane, S., Ishikawa, R., Kohama, K., Tomida, Y., & Hidaka, H. (1993). Calvasculin, as a factor affecting the microfilament assemblies in rat fibroblasts transfected by src gene. *FEBS Letters*, *324*(1). https://doi.org/10.1016/0014-5793(93)81530-D

Ween, M. P., Lokman, N. A., Hoffmann, P., Rodgers, R. J., Ricciardelli, C., & Oehler, M. K. (2011). Transforming growth factor-beta-induced protein secreted by peritoneal cells increases the metastatic potential of ovarian cancer cells. *International Journal of Cancer*, *128*(7). https://doi.org/10.1002/ijc.25494

Ween, M. P., Oehler, M. K., & Ricciardelli, C. (2012). Transforming growth factor-beta-induced protein (TGFBI)/(βig-H3): A matrix protein with dual functions in ovarian cancer. In *International Journal of Molecular Sciences* (Vol. 13, Issue 8). https://doi.org/10.3390/ijms130810461

Weiss, J. S., Møller, H. U., Aldave, A. J., Seitz, B., Bredrup, C., Kivelä, T., Munier, F. L., Rapuano, C. J., Nischal, K. K., Kim, E. K., Sutphin, J., Busin, M., Labbé, A., Kenyon,

K. R., Kinoshita, S., & Lisch, W. (2015). IC3D classification of corneal dystrophies-edition 2. *Cornea*, *34*(2). https://doi.org/10.1097/ICO.0000000000000307

Weiss, J. S., Møller, H. U., Lisch, W., Kinoshita, S., Aldave, A. J., Belin, M. W., Kivelä, T., Busin, M., Munier, F. L., Seitz, B., Sutphin, J., Bredrup, C., Mannis, M. J., Rapuano, C. J., Van Rij, G., Kim, E. K., & Klintworth, G. K. (2008). The IC3D classification of the corneal dystrophies | La Clasificación IC3D de las distrofias corneales. *Cornea*, *27*(SUPPL. 2). https://doi.org/10.1097/ICO.0b013e31817780fb

Wen, G., Hong, M., Li, B., Liao, W., Cheng, S. K., Hu, B., Calaf, G. M., Lu, P., Partridge, M. A., Tong, J., & Hei, T. K. (2011). Transforming growth factor-β-induced protein (TGFBI) suppresses mesothelioma progression through the Akt/mTOR pathway. *International Journal of Oncology*, *39*(4). https://doi.org/10.3892/ijo.2011.1097

Wen, G., Partridge, M. A., Li, B., Hong, M., Liao, W., Cheng, S. K., Zhao, Y., Calaf, G. M., Liu, T., Zhou, J., Zhang, Z., & Hei, T. K. (2011). TGFBI expression reduces in vitro and in vivo metastatic potential of lung and breast tumor cells. *Cancer Letters*, *308*(1). https://doi.org/10.1016/j.canlet.2011.04.010

Weng, Y., Liu, J., Jin, S., Guo, W., Liang, X., & Hu, Z. (2017). Nanotechnology-based strategies for treatment of ocular disease. In *Acta Pharmaceutica Sinica B* (Vol. 7, Issue 3). https://doi.org/10.1016/j.apsb.2016.09.001

Wenk, J., Brenneisen, P., Meewes, C., Wlaschek, M., Peters, T., Blaudschun, R., Ma, W., Kuhr, L., Schneider, L., & Scharffetter-Kochanek, K. (2001). UV-induced oxidative stress and photoaging. In *Current problems in dermatology* (Vol. 29). https://doi.org/10.1159/000060656

Wernig, M., Meissner, A., Cassady, J. P., & Jaenisch, R. (2008). c-Myc Is Dispensable for Direct Reprogramming of Mouse Fibroblasts. In *Cell Stem Cell* (Vol. 2, Issue 1). https://doi.org/10.1016/j.stem.2007.12.001

West, J. D. (2015). Evaluating alternative stem cell hypotheses for adult corneal epithelial maintenance. *World Journal of Stem Cells*, *7*(2). https://doi.org/10.4252/wjsc.v7.i2.281

West, M. D., Labat, I., Li, J., Sim, P., Janus, J., Mangelson, H., Sullivan, S., Liachko, I., Labhart, P., Craske, M., Egan, B., Chapman, K. B., Malik, N. N., Larocca, D., & Sternberg, H. (n.d.). *Differential Expression of a, b, and g Protocadherin Isoforms During Differentiation, Aging, and Cancer*. https://doi.org/10.1101/2021.03.07.434314

Wheeldon, C. E., de Karolyi, B. H., Patel, D. V., Sherwin, T., McGhee, C. N. J., & Vincent, A. L. (2008). A novel phenotype-genotype relationship with a TGFBI exon 14 mutation in a pedigree with a unique corneal dystrophy of Bowman's layer. *Molecular Vision*, *14*.

White, T. L., Lewis, P. N., Young, R. D., Kitazawa, K., Inatomi, T., Kinoshita, S., & Meek, K. M. (2017). Elastic microfibril distribution in the cornea: Differences between normal and keratoconic stroma. *Experimental Eye Research*, *159*. https://doi.org/10.1016/j.exer.2017.03.002

Wittebol-Post, D., van der Want, J. J. L., & van Bijsterveld, O. P. (1987). Granular dystrophy of the cornea (groenouw's Type I): Is the keratocvte the primary source after all? *Ophthalmologica*, *195*(4). https://doi.org/10.1159/000309808

Wittebol-Post, D., van der Want, J. J. L., & van Bijsterveld, O. P. (2010). Granular Dystrophy of the Cornea (Groenouw's Type I). *Ophthalmologica*, *195*(4). https://doi.org/10.1159/000309808

Wittkopp, P. J., Haerum, B. K., & Clark, A. G. (2004). Evolutionary changes in cis and trans gene regulation. *Nature*, *430*(6995). https://doi.org/10.1038/nature02698

Wolynes, P. G., Onuchic, J. N., & Thirumalai, D. (1995). Navigating the folding routes. In *Science* (Vol. 267, Issue 5204). https://doi.org/10.1126/science.7886447

Wood, V. H. J., O'Neil, J. D., Wei, W., Stewart, S. E., Dawson, C. W., & Young, L. S. (2007). Epstein-Barr virus-encoded EBNA1 regulates cellular gene transcription and modulates the STAT1 and TGFβ signaling pathways. *Oncogene*, *26*(28). https://doi.org/10.1038/sj.onc.1210496

Woreta, F. A., Davis, G. W., & Bower, K. S. (2015). LASIK and surface ablation in corneal dystrophies. In *Survey of Ophthalmology* (Vol. 60, Issue 2). https://doi.org/10.1016/j.survophthal.2014.08.003

Worthen, D. M. (1972). Histology of the Human Eye. *Archives of Ophthalmology*, *88*(2). https://doi.org/10.1001/archopht.1972.01000030236034

Wu, C. (2007). Focal Adhesion. *Cell Adhesion & Migration*, *1*(1). https://doi.org/10.4161/cam.4081

Wu, H., Lima, W. F., & Crooke, S. T. (1999). Properties of cloned and expressed human RNase H1. *Journal of Biological Chemistry*, *274*(40). https://doi.org/10.1074/jbc.274.40.28270

Wu, J., Du, Y., Watkins, S. C., Funderburgh, J. L., & Wagner, W. R. (2012). The engineering of organized human corneal tissue through the spatial guidance of corneal stromal stem cells. *Biomaterials*, *33*(5). https://doi.org/10.1016/j.biomaterials.2011.10.055

-Xaver Kober, F., Koelmel, W., Kuper, J., Drechsler, J., Mais, C., Hermanns, H. M., & Schindelin, H. (2013). The crystal structure of the protein-disulfide isomerase family member ERp27 provides insights into its substrate binding capabilities. *Journal of Biological Chemistry*, *288*(3). https://doi.org/10.1074/jbc.M112.410522

Xiu, H. W., Hyun, C. L., Stulting, R. D., Kim, T., Seung, E. J., Moon, J. K., & Eung, K. K. (2002). Exacerbation of Avellino corneal dystrophy after laser in situ keratomileusis. *Cornea*, *21*(2). https://doi.org/10.1097/00003226-200203000-00021

Xu, X., Tay, Y., Sim, B., Yoon, S. I., Huang, Y., Ooi, J., Utami, K. H., Ziaei, A., Ng, B., Radulescu, C., Low, D., Ng, A. Y. J., Loh, M., Venkatesh, B., Ginhoux, F., Augustine, G. J., & Pouladi, M. A. (2017). Reversal of Phenotypic Abnormalities by CRISPR/Cas9-Mediated Gene Correction in Huntington Disease Patient-Derived Induced Pluripotent Stem Cells. *Stem Cell Reports*, *8*(3). https://doi.org/10.1016/j.stemcr.2017.01.022

Yam, G. H. F., Wang, K., Jhanji, V., Choy, K. W., Baum, L., & Pang, C. P. (2012). In vitro amyloid aggregate forming ability of TGFBI mutants that cause corneal dystrophies. *Investigative Ophthalmology and Visual Science*, *53*(9). https://doi.org/10.1167/iovs.11-9068

Yamanaka, S. (2020). Pluripotent Stem Cell-Based Cell Therapy—Promise and Challenges. In *Cell Stem Cell* (Vol. 27, Issue 4). https://doi.org/10.1016/j.stem.2020.09.014

Yamazoe, K., Yoshida, S., Yasuda, M., Hatou, S., Inagaki, E., Ogawa, Y., Tsubota, K., & Shimmura, S. (2015). Development of a transgenic mouse with R124H human TGFBI mutation associated with granular corneal dystrophy type 2. *PLoS ONE*, *10*(7). https://doi.org/10.1371/journal.pone.0133397

Yan, H., Yuan, W., Velculescu, V. E., Vogelstein, B., & Kinzler, K. W. (2002). Allelic variation in human gene expression. *Science*, *297*(5584). https://doi.org/10.1126/science.1072545

Yang, A., Schweitzer, R., Sun, D., Kaghad, M., Walker, N., Bronson, R. T., Tabin, C., Sharpe, A., Caput, D., Crum, C., & McKeon, F. (1999). p63 is essential for

regenerative proliferation in limb, craniofacial and epithelial development. *Nature*, *398*(6729). https://doi.org/10.1038/19539

Yang, J., Han, X., Huang, D., Yu, L., Zhu, Y., Tong, Y., Zhu, B., Li, C., Weng, M., & Ma, X. (2010). Analysis of TGFBI gene mutations in Chinese patients with corneal dystrophies and review of the literature. *Molecular Vision*, *16*.

Yang, Q. N., Zhao, Y. W., Guo, L. H., Yan, N. H., Liu, X. Y., & Cai, S. P. (2011). Arg124Cys mutation of the TGFBI gene in a Chinese pedigree of Reis-Bücklers corneal dystrophy. *International Journal of Ophthalmology*, *4*(3). https://doi.org/10.3980/j.issn.2222-3959.2011.03.03

Yao, M., Nguyen, T. V. V., & Pike, C. J. (2005). β-Amyloid-induced neuronal apoptosis involves c-Jun N-terminal kinase-dependent downregulation of Bcl-w. *Journal of Neuroscience*, *25*(5). https://doi.org/10.1523/JNEUROSCI.4736-04.2005

Yasuhara, H., Yoshida, T., Sasaki, K., Obika, S., & Inoue, T. (2022). Reduction of Off-Target Effects of Gapmer Antisense Oligonucleotides by Oligonucleotide Extension. *Molecular Diagnosis and Therapy*, *26*(1). https://doi.org/10.1007/s40291-021-00573-z

Yellore, V. S., Rayner, S. A., & Aldave, A. J. (2011). TGFB1-induced extracellular expression of TGFBIP and inhibition of TGFBIP expression by RNA interference in a human corneal epithelial cell line. *Investigative Ophthalmology and Visual Science*, *52*(2). https://doi.org/10.1167/iovs.10-5362

Ying, S. Y., Fang, W., & Lin, S. L. (2018). The miR-302-mediated induction of pluripotent stem cells (iPSC): Multiple synergistic reprogramming mechanisms. In *Methods in Molecular Biology* (Vol. 1733). https://doi.org/10.1007/978-1-4939-7601-0_23

Yoshida, S., Shimmura, S., Nagoshi, N., Fukuda, K., Matsuzaki, Y., Okano, H., & Tsubota, K. (2006). Isolation of Multipotent Neural Crest-Derived Stem Cells from the Adult Mouse Cornea. *STEM CELLS*, *24*(12). https://doi.org/10.1634/stemcells.2006-0156

Yoshinaga, Y., Soma, T., Azuma, S., Maruyama, K., Hashikawa, Y., Katayama, T., Sasamoto, Y., Takayanagi, H., Hosen, N., Shiina, T., Ogasawara, K., Hayashi, R., & Nishida, K. (2022). Long-term survival in non-human primates of stem cell-derived, MHC-unmatched corneal epithelial cell sheets. *Stem Cell Reports*. https://doi.org/10.1016/j.stemcr.2022.05.018

Young, B. B., Zhang, G., Koch, M., & Birk, D. E. (2002). The roles of types XII and XIV collagen in fibrillogenesis and matrix assembly in the developing cornea. *Journal of Cellular Biochemistry*, *87*(2). https://doi.org/10.1002/jcb.10290

Yu, H., Wergedal, J. E., Zhao, Y., & Mohan, S. (2012). Targeted disruption of TGFBI in mice reveals its role in regulating bone mass and bone size through periosteal bone formation. *Calcified Tissue International*, *91*(1). https://doi.org/10.1007/s00223-012-9613-6

Yu, J., Vodyanik, M. A., Smuga-Otto, K., Antosiewicz-Bourget, J., Frane, J. L., Tian, S., Nie, J., Jonsdottir, G. A., Ruotti, V., Stewart, R., Slukvin, I. I., & Thomson, J. A. (2007). Induced pluripotent stem cell lines derived from human somatic cells. *Science*, *318*(5858). https://doi.org/10.1126/science.1151526

Yu, S., Levi, L., Siegel, R., & Noy, N. (2012). Retinoic acid induces neurogenesis by activating both retinoic acid receptors (RARs) and peroxisome proliferator-activated receptor β/δ (PPARβ/δ). *Journal of Biological Chemistry*, *287*(50). https://doi.org/10.1074/jbc.M112.410381

Yuan, C., Yang, M. C., Zins, E. J., Boehlke, C. S., & Huang, A. J. W. (2004). Identification of the promoter region of the human βIGH3 gene. *Molecular Vision*, *10*.

Yuksel, H., Ocalan, M., & Yilmaz, O. (2021). E-Cadherin: An Important Functional Molecule at Respiratory Barrier Between Defence and Dysfunction. In *Frontiers in Physiology* (Vol. 12). https://doi.org/10.3389/fphys.2021.720227

Zajchowski, D. A., Bartholdi, M. F., Gong, Y., Webster, L., Liu, H. L., Munishkin, A., Beauheim, C., Harvey, S., Ethier, S. P., & Johnson, P. H. (2001). Identification of gene expression profiles that predict the aggressive behavior of breast cancer cells. *Cancer Research*, *61*(13).

Zamilpa, R., Rupaimoole, R., Phelix, C. F., Somaraki-Cormier, M., Haskins, W., Asmis, R., & LeBaron, R. G. (2009). C-terminal fragment of transforming growth factor beta-induced protein (TGFBIp) is required for apoptosis in human osteosarcoma cells. *Matrix Biology*, *28*(6). https://doi.org/10.1016/j.matbio.2009.05.004

Zarouchlioti, C., Sanchez-Pintado, B., Hafford Tear, N. J., Klein, P., Liskova, P., Dulla, K., Semo, M., Vugler, A. A., Muthusamy, K., Dudakova, L., Levis, H. J., Skalicka, P., Hysi, P., Cheetham, M. E., Tuft, S. J., Adamson, P., Hardcastle, A. J., & Davidson, A. E. (2018). Antisense Therapy for a Common Corneal Dystrophy

Ameliorates TCF4 Repeat Expansion-Mediated Toxicity. *American Journal of Human Genetics*, *102*(4). https://doi.org/10.1016/j.ajhg.2018.02.010

Zechner, E. M., Croxatto, J. O., & Malbran, E. S. (1986). Superficial involvement in lattice corneal dystrophy. *Ophthalmologica*, *193*(4). https://doi.org/10.1159/000309710

Zeng, L., Zhao, J., Chen, Y., Zhao, F., Li, M., Chao-Shern, C., Moore, T., Marshall, J., & Zhou, X. (2017). TGFBI Gene Mutation Analysis of Clinically Diagnosed Granular Corneal Dystrophy Patients Prior to PTK: A Pilot Study from Eastern China. *Scientific Reports*, *7*(1). https://doi.org/10.1038/s41598-017-00716-5

Zenteno, J. C., Correa-Gomez, V., Santacruz-Valdez, C., Suarez-Sanchez, R., & Villanueva-Mendoza, C. (2009). Clinical and genetic features of TGFBI-linked corneal dystrophies in Mexican population: Description of novel mutations and novel genotype-phenotype correlations. *Experimental Eye Research*, *89*(2). https://doi.org/10.1016/j.exer.2009.03.004

Zhang, C., Zeng, G., Lin, H., Li, D., Zhao, L., Zhou, N., & Qi, Y. (2009). A novel mutation I522N within the TGFBI gene caused lattice corneal dystrophy I. *Molecular Vision*, *15*.

Zhang, H., Yang, D., Wigg, J. P., Unger, H., Unger, M., & Crowston, J. G. (2014). Ultrasound-mediated transscleral delivery of Avastin to the posterior segment of rabbit eye in vivo. *Investigative Ophthalmology and Visual Science*, *55*(13).

Zhang, S., Peng, J., Guo, Y., Javidiparsijani, S., Wang, G., Wang, Y., Liu, H., Liu, J., & Luo, J. (2014). Matrilin-2 is a widely distributed extracellular matrix protein and a potential biomarker in the early stage of osteoarthritis in articular cartilage. *BioMed Research International*, *2014*. https://doi.org/10.1155/2014/986127

Zhang, Y. E. (2017). Non-Smad signaling pathways of the TGF-β family. *Cold Spring Harbor Perspectives in Biology*, *9*(2). https://doi.org/10.1101/cshperspect.a022129

Zhang, Y., Schmid, B., Nikolaisen, N. K., Rasmussen, M. A., Aldana, B. I., Agger, M., Calloe, K., Stummann, T. C., Larsen, H. M., Nielsen, T. T., Huang, J., Xu, F., Liu, X., Bolund, L., Meyer, M., Bak, L. K., Waagepetersen, H. S., Luo, Y., Nielsen, J. E., … Freude, K. K. (2017). Patient iPSC-Derived Neurons for Disease Modeling of Frontotemporal Dementia with Mutation in CHMP2B. *Stem Cell Reports*, *8*(3). https://doi.org/10.1016/j.stemcr.2017.01.012

Zhang, Y., Wen, G., Shao, G., Wang, C., Lin, C., Fang, H., Balajee, A. S., Bhagat, G., Hei, T. K., & Zhao, Y. (2009). TGFBI deficiency predisposes mice to spontaneous

tumor development. *Cancer Research*, *69*(1). https://doi.org/10.1158/0008-5472.CAN-08-1648

Zhang, Z., Schwartz, S., Wagner, L., & Miller, W. (2000). A greedy algorithm for aligning DNA sequences. In *Journal of Computational Biology* (Vol. 7, Issues 1–2). https://doi.org/10.1089/10665270050081478

Zhao, S., Wu, H., Xia, W., Chen, X., Zhu, S., Zhang, S., Shao, Y., Ma, W., Yang, D., & Zhang, J. (2014). Periostin expression is upregulated and associated with myocardial fibrosis in human failing hearts. *Journal of Cardiology*, *63*(5). https://doi.org/10.1016/j.jjcc.2013.09.013

Zhou, H., Janghra, N., Mitrpant, C., Dickinson, R. L., Anthony, K., Price, L., Eperon, I. C., Wilton, S. D., Morgan, J., & Muntoni, F. (2013). A novel morpholino oligomer targeting ISS-N1 improves rescue of severe spinal muscular atrophy transgenic mice. *Human Gene Therapy*, *24*(3). https://doi.org/10.1089/hum.2012.211

Zhou, S., Schuetz, J. D., Bunting, K. D., Colapietro, A. M., Sampath, J., Morris, J. J., Lagutina, I., Grosveld, G. C., Osawa, M., Nakauchi, H., & Sorrentino, B. P. (2001). The ABC transporter Bcrp1/ABCG2 is expressed in a wide variety of stem cells and is a molecular determinant of the side-population phenotype. *Nature Medicine*, *7*(9). https://doi.org/10.1038/nm0901-1028

Zhu, A., Ibrahim, J. G., & Love, M. I. (2019). Heavy-Tailed prior distributions for sequence count data: Removing the noise and preserving large differences. *Bioinformatics*, *35*(12). https://doi.org/10.1093/bioinformatics/bty895

Zieske, J. D. (2004). Corneal development associated with eyelid opening. In *International Journal of Developmental Biology* (Vol. 48, Issues 8–9). https://doi.org/10.1387/ijdb.041860jz

Zieske, J. D., Hutcheon, A. E. K., Guo, X., Chung, E. H., & Joyce, N. C. (2001). TGF-β receptor types I and II are differentially expressed during corneal epithelial wound repair. *Investigative Ophthalmology and Visual Science*, *42*(7).

Zimmermann, D. R., Trüeb, B., Winterhalter, K. H., Witmer, R., & Fischer, R. W. (1986). Type VI collagen is a major component of the human cornea. *FEBS Letters*, *197*(1–2). https://doi.org/10.1016/0014-5793(86)80297-6

Zoega, G. M., Fujisawa, A., Sasaki, H., Kubota, A., Sasaki, K., Kitagawa, K., & Jonasson, F. (2006). Prevalence and Risk Factors for Cornea Guttata in the Reykjavik Eye Study. *Ophthalmology*, *113*(4). https://doi.org/10.1016/j.ophtha.2005.12.014

Zollinger, A. J., & Smith, M. L. (2017). Fibronectin, the extracellular glue. In *Matrix Biology* (Vols. 60–61). https://doi.org/10.1016/j.matbio.2016.07.011

Zou, J., Huang, R., Li, H., Wang, B., Chen, Y., Chen, S., Ou, K., & Wang, X. (2019). Secreted TGF-beta-induced protein promotes aggressive progression in bladder cancer cells. *Cancer Management and Research*, *11*. https://doi.org/10.2147/CMAR.S208984

Zuker, M. (2003). Mfold web server for nucleic acid folding and hybridization prediction. *Nucleic Acids Research*, *31*(13). https://doi.org/10.1093/nar/gkg595

Chapter 9: Appendices

9.1 Appendix A

All materials used in this thesis are listed below.

0.05 % Trypsin-EDTA – Gibco, 25300-054.

0.2 mL 8-strip PCR tube, individually attached domed caps – StarLab, S1602-2900.

2X LabTAQ hi-rox green – LabTech, LTSHR-1.

4’,6-diamidino-2-phenylindole dilactate (DAPI) dilactate – Sigma, D9564-10MG.

6-well CytoOne plate, TC treated – StarLab, CC7682-7506.

10 % SDS solution – Severn Biotech Ltd, 20-4000-10.

12-well CytoOne plate, TC treated – StarLab, CC7682-7512.

16 % paraformaldehyde (PFA) – ThermoFisher, 28908.

24-well CytoOne plate, TC treated – StarLab, CC7682-7524.

30 % Acrylamide – National diagnostics, EC-890.

90 mm Fisherbrand aseptic petri dish – Fisher scientific – 12664785.

96-well CytoOne plate, TC treated – StarLab, CC7682-7596.

100 % Ethanol – VWR, 20821.310P.

100 % Methanol – VWR, 20847.320.

Ammonium persulfate – Sigma, A3678.

Antibiotic-antimycotic (100X) – Gibco, 15240-062.

B27 supplement – Gibco, 17504-044.

Bambanker freeing medium - Nippon Genetics Europe, BB01#

BD Microlance™ Stainless Steel Needles – Fisher Scientific, BD10201211

Blebbistatin – Sigma, B0560-1MG.

Bone morphogenic protein 4 (BMP4) – Peprotech, AF-120-05ET-50.

Bovine Serum Albumin – Sigma, A7906-100G.

β-mercaptoethanol – Gibco, 21985-023.

Cell Dissociation Buffer, Enzyme free, PBS – Gibco, 13151-014.

Cell Line Nucleofector® Kit R – Lonza, VCA-1001.

Cnt-30 - CellNtec

Collagen IV – Sigma, C5533

CozyHi prestained protein ladder – HighQu, PRL0202

DAKO Fluorescent mounting medium – Dako, S3023.

Dispase II (Sigma, D4693)

DMEM/F12 with GlutaMAX – Gibco, 31331-028.

DMEM with GlutaMAX – Gibco, 41966-029.

Dried skimmed milk powder – Marvel.

Dulbecco Phosphate Buffered Saline (DPBS), pH 7-7.3 – Gibco, 14190-094.

Dulbeccos Phosphate Buffers Saline tablets – Oxoid, BR0014G.

Epithelial growth factor (EGF) – Thermo Fisher, PHG0314

Essential 8 (E8) Flex media – Gibco, A2858501.

Falcon 70 µm cell strainer – Fisher scientific, 10788201.

Falcon cell culture flask 75 cm2 – VWR, 734-0050.

Foetal Bovine Serum (FBS) – Labtech, FCS-SA.

Fisherbrand™ 1 ml sterile syringes – Fisher scientific, 17161936

Gelatin – Sigma, G1393-100ML.

Geltrex LDEV-free reduced growth factor basement membrane matrix – Gibco, A1413202.

Glutamax supplement – Gibco, 35050038

GoTaq green master mix – Promega, M7123

Human Dermal Fibroblast, neonatal – Sigma, 106-05N.

Lipofectamine RNAimax – Thermo Fisher, 13778100

Luminata Forte western HRP substrate – Millipore, WBLUF05000.

MicroAmp Optical 96-well reaction plate – Thermofisher, N8010560.

MultiScreen® PCRμ96 Filter Plate – Millipore, LSKMPCR10.

N2 supplement – Gibco, 17502-048.

N,N,N',N'-Tetramethyl-ethylenediamine (TEMED) – Sigma, T9281.

Nitrocelllose Blotting membrane – GE healthcare, 10600002

Non-Essential Amino Acids (NEAA) – Gibco, 11140-035.

Normal donkey serum (NDS) – Sigma, 09663-10ML.

Penicillin-streptomycin (P/S) – Gibco, 15140122.

Phosphatase inhibitor cocktail 3 – Sigma, P0044

Pierce BCA protein assay kit – ThermoFisher, 23227.

Proteinase inhibitor cocktail (PIC) – Sigma, P8340.

Quick-Load® 1 kb plus DNA ladder – NEB, N0550S.

Recombinant human laminin-521 – Thermofisher, 78060.

RNase-Free DNase Set – Qiagen, 79254.

RNeasy mini kit – Qiagen, 79254.

Safeview nucleic acid stain – NBS Biologicals, NBS-SV.

Sodium bicarbonate – Gibco, 25080094

Sodium butyrate – Sigma, B5887.

Sodium dodecyl sulphate (SDS) – Sigma, L3771.

StemFlex media™ – Invitrogen, A3349401.

Tetro cDNA Synthesis Kit – Bioline, BIO-65043.

Transporter™ 5 Transfection Reagent – Polysciences, 26008-1

Tris-Glycine 10X solution – Severn Biotech Ltd, 20-6300-50.

Tris-Glycine SDS 10X solution – Severn Biotech Ltd, 20-6400-50.

Triton X100 – Sigma, T8787.

Tryple express – Gibco, 12604-013.

TWEEN 20 – Sigma, P9146.

Wizard® SV Genomic DNA purification system – Promega, A2360.

280

Buffers and solutions

10 % acrylamide resolving gels – 370 µM Tris (pH 8.8), 10 % (v/v) acrylamide, 0.1 % (v/v) SDS, 0.1% (v/v) APS, 0.05 % (v/v) TEMED, diluted in ddH2O.

10 % acrylamide stacking gels – 125 µM Tris (pH 6.8), 4 % (v/v) acrylamide, 0.1 % (v/v) SDS, 0.1 % (v/v) APS, 0.2 % (v/v) TEMED, diluted in ddH2O.

Ponceau S stain – 0.5 % (w/v) Ponceau S, 1 % (v/v) acetic acid, diluted in ddH2O.

RIPA – 50 nM Tris (pH 8), 150 mM sodium chloride, 1% (w/v) IGEPAL, 0.5% (w/v) sodium deoxycholate, 0.1% (w/v) SDS, diluted in ddH2O.

Running buffer – 1X Tris-glycine SDS, diluted in ddH2O.

Transfer buffer – 1X Tris-glycine with 20 % (v/v) methanol, diluted in ddH2O.

Sample loading buffer – 150 mM Tris-HCl (pH 7), 25% glycerol, 12% SDS, 0.05% bromophenol blue and 6% b-mercaptoethanol.

9.2 Appendix B

Table 9.1 TGFBI mutations causative of CD as reported in the literature. Adapted from Nielsen et al. (2020).

Exon	Protein domain	Mutation	Corneal Dystrophy	Reference
4	FAS-1-1	p.V113I	GCD1	Zenteno et al. (2006)
4	FAS-1-1	p.V113I/L558P	LCD	Ann et al. (2017)
4	FAS-1-1	p.D123H	GCD (atypical)	Ha et al. (2003)
4	FAS-1-1	p.R124C	LCD1	Munier et al. (1997)
4	FAS-1-1	p.R124C/G470Ter	LCD1	Sakimoto et al. (2003)
4	FAS-1-1	p.R124C/A546D	LCD	Cao et al. (2017)
4	FAS-1-1	p.R124H	GCD2	Munier et al. (1997)
4	FAS-1-1	p.R124H/Y88C	GCD2	Jun et al. (2021)
4	FAS-1-1	p.R124H/P130Ter	GCD2	Yam et al. (2012)
4	FAS-1-1	p.R124H/H174D	Severe GCD2	Jun et al. (2021)
4	FAS-1-1	p.R124H/R179Ter	GCD2	Song et al. (2015)
4	FAS-1-1	p.R124H/I247N	Severe GCD2	Jun et al. (2021)
4	FAS-1-1	p.R124H/R257P	Severe GCD2	Jun et al. (2021)
4	FAS-1-1	p.R124H/N544S	GCD2-LCD	Yamada et al. (2009)
4	FAS-1-1	p.R124L	RBCD	Okada et al. (1998)
4	FAS-1-1	p.R124L/T125-E126del	GCD (atypical)	Dighiero et al. (2000)
4	FAS-1-1	p.R124S	GCD1	Stewart et al. (1999)
4	FAS-1-1	p.E131D	Unknown	Foja et al. (2016)
11	FAS-1-3	p.R496W	LCD4	Kawasaki et al. (2011)
11	FAS-1-3	p.P501T	LCD3a	Yamamoto et al. (1998)
11	FAS-1-3	p.M502V	Unknown	Zenteno et al. (2009)
11	FAS-1-3	p.M502V/R555Q	TBCD (atypical)	Niel-Butschi et al. (2011)
11	FAS-1-4	p.V505D	LCD1	Tian et al. (2005)
11	FAS-1-4	p.L509P	GCD2/LCD1	Gruenauer-Kloevekorn et al. (2009)
11	FAS-1-4	p.L509R	LCD (atypical)	Niel-Butschi et al. (2011)
11	FAS-1-4	p.R514P/F515L	LCD1	Zhong et al. (2010)
11	FAS-1-4	p.S516R	GCD1 (atypical)	Paliwal et al. (2010)
12	FAS-1-4	p.L518P	LCD1	Endo et al. (1999)
12	FAS-1-4	p.L518R	LCD1/3a	Munier et al. (2002)
12	FAS-1-4	p.V519delinsGG	RBCD	Kheir et al., (2019)
12	FAS-1-4	p.I522N	LCD1	Zhang et al. (2009)
12	FAS-1-4	p.S524C	Late onset Bowman's layer CD	Chen et al., (2020)
12	FAS-1-4	p.L527R	LCD4	Fujiki et al. (1998)
12	FAS-1-4	p.T538R	LCD1	Yu et al. (2006)
12	FAS-1-4	p.T538R	LCD1/3a	Munier et al., (2002)
12	FAS-1-4	p.V539D	LCD1	Chakravarthi, et al., (2005)
12	FAS-1-4	p.F540S	LCD3a	Stix et al. (2005)

12	FAS-1-4	p.F540del	RBCD/LCD1/3a	Rozzo et al. (1998)
12	FAS-1-4	p.P542R	LCD	Cho et al. (2012)
12	FAS-1-4	p.N544S	LCD	Mashima et al. (2000)
12	FAS-1-4	p.A546D	LCD (atypical)	Eifrig et al., (2004)
12	FAS-1-4	p.A546D/P551Q	LCD1	Klintworth et al. (2004)
12	FAS-1-4	p.A546T	LCD3a	Dighiero et al. (2000)
12	FAS-1-4	p.F547C	GCD	Foja et al. (2016)
12	FAS-1-4	p.F547S	LCD	Takács et al. (2007)
12	FAS-1-4	p.R548P	LCD	Chae et al. (2016)
12	FAS-1-4	p.A549T/R555W	GCD1	Frising et al., (2006)
12	FAS-1-4	p.L550P	GCD2	Zenteno et al. (2009)
12	FAS-1-4	p.L550P/H626R	GCD2 (atypical)	Zenteno et al. (2009)
12	FAS-1-4	p.R555Q	TBCD	Munier et al. (1997)
12	FAS-1-4	p.R555W	GDC1	Munier et al. (1997)
12	FAS-1-4	p.L558P	LCD (atypical)	Pampukha et al., (2009)
12	FAS-1-4	p.L558R	LCD	Dudakova et al. (2016)
12	FAS-1-4	p.L559V	GCD (atypical)	Paliwal et al. (2010)
13	FAS-1-4	p.L565H	LCD	Zhang et al. (2019)
13	FAS-1-4	p.L565P	LCD	Ołdak et al. (2014)
13	FAS-1-4	p.L569Q	LCD	Song et al., (2015)
13	FAS-1-4	p.L569R	LCD1	Warren et al. (2003)
13	FAS-1-4	p.H572R	LCD1	Atchaneeyasakul et al. (2006)
13	FAS-1-4	p.H572del	LCD	Aldave et al., (2006)
13	FAS-1-4	p.S591Y	TBCD/GCD	Benbouchta et al. (2021)
13	FAS-1-4	p.S591F	LCD	Choo et al., (2022)
13	FAS-1-4	p.G594V	LCD4	Chakravarthi et al., (2005)
14	FAS-1-4	p.V613G	LCD	Niel-Butschi et al. (2011)
14	FAS-1-4	p.V613-P616del	LCD	Yang et al., (2010)
14	FAS-1-4	p.M619L	GCD2	Aldave et al. (2008)
14	FAS-1-4	p.A620D	LCD1/3a	Lakshminarayanan et al. (2011)
14	FAS-1-4	p.A620P	LCD3a	Jung et al. (2014)
14	FAS-1-4	p.T621P	LCD3a	Song et al., (2015)
14	FAS-1-4	p.N622H	LCD1/3a	Stewart et al. (1999)
14	FAS-1-4	p.N622K	LCD3a	Munier et al. (2002)
14	FAS-1-4	p.V624M	LCD (atypical)	Afshari et al. (2008)
14	FAS-1-4	p.V624-V625del	LCD (atypical)	Chakravarthi et al., (2005)
14	FAS-1-4	p.V625D	LCD1	Tian et al. (2007)
14	FAS-1-4	p.H626P	RBCD-TBCD/LCD	Munier et al. (2002)
14	FAS-1-4	p.H626R	LCD1/3a	Stewart et al. (1999)
14	FAS-1-4	p.V627Sfs*44	LCD3a	Munier et al. (2002)
14	FAS-1-4	p.T629insNVP	LCD1/3a	Schmitt–Bernard et al. (2000)
14	FAS-1-4	p.V631D	LCD	Munier et al. (2002)

9.3 Appendix C

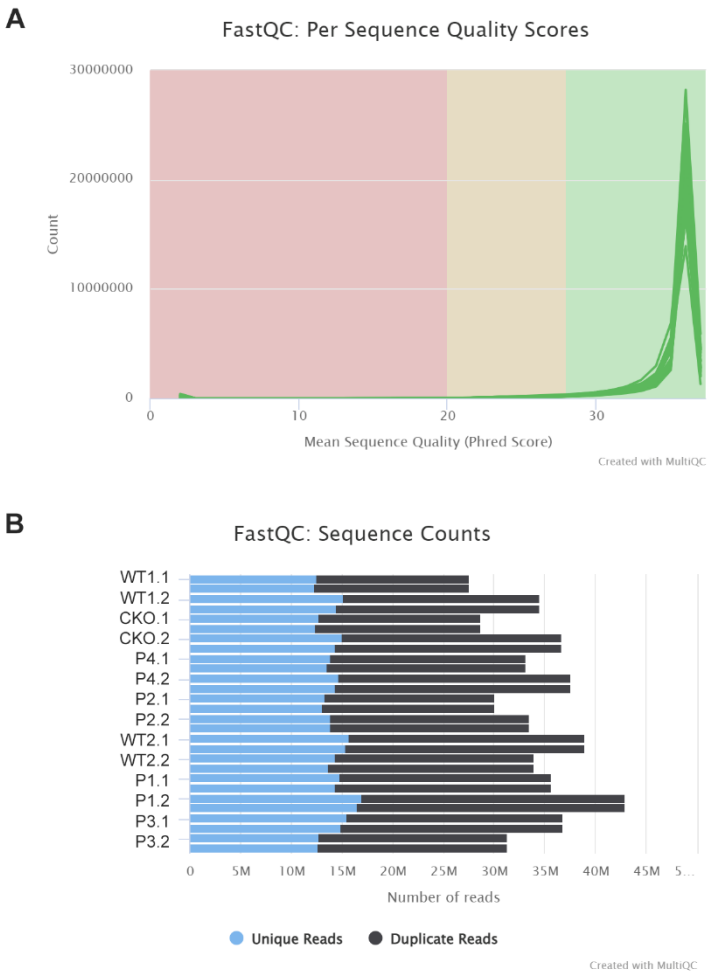

Figure 9.1 FastQC graphs for WT, *TGFBI* mutant and *TGFBI* knockout (CKO) sequencing data. For the 'fastq' file pairs for all 14 samples included in this study **(A)** shows the number of reads against average quality scores and **(B)** shows the sequence counts and number of unique and duplicate reads.

9.4 Appendix D

Code for the analysis of the targeted NGS fastq files, run in Python.

```
import os os.listdir(r'LOCATION ')
for info in os.listdir(r'LOCATION '):
    domain = os.path.abspath(r'LOCATION ') info = os.path.join(domain, info)
    info = open(info, 'r') a = info.read() info.close()
    WT = a.count('WT_SEQUENCE')
    R124C = a.count('MUTANT_SEQUENCE')
    print('WT: ', WT)
    print('MUT: ', MUT)
```

Where:

- *LOCATION* – location of the folder containing the .fastq files generated as a result of the NGS experiment.
- *MUTANT_SEQUENCE* – 11 bp sequence containing the mutation, that would allow for identification
- *WT_SEQUENCE* – equivalent region to the *MUTANT_SEQUENCE,* containing the WT sequence.